Macroevolutionary history of Neotropical vegetation during the Cenozoic: a Palynological perspective from Colombia



Felipe de la Parra Bonilla
Department of Earth Sciences
University of Oxford
Kellogg College

A thesis submitted for the degree of
Doctor of Philosophy

Hilary 2019

Think Horizontally, Work Vertically
Lennart Von Post

Abstract

The Neotropics are the most plant species-rich realm of the Earth. This surprising megadiversity has been studied since times of Darwin and Humboldt, with different mechanisms proposed, not only to explain how such great diversity was produced but also how it is maintained. This system is not completely understood, and will continue being matter of study for a long time. Knowledge of the deep time patterns of diversity and diversification are central to testing hypothesised mechanisms. But the patterns have received much less attention than have the mechanisms proposed to explain them. In this thesis I used an extensive palynological record of Colombia to study the macroevolutionary history of Neotropical vegetation and its relationship with regional and global process occurring during the Cenozoic. The results show a strong correlation between fluctuations in palynological diversity and global changes in temperature. Contrasting responses of vegetation to temperature between the Palaeocene to Eocene and the Oligocene to Present suggest that different mechanisms operated during greenhouse and icehouse intervals. Throughout the Cenozoic, periods of elevated extinction are followed by periods of high origination. This relationship suggests that in the Neotropics when a species become extinct, it is replaced very fast. In contrast, the lack of correlation between origination and extinction suggest that extinction is not controlled by origination. The examination of the taxonomic rates and the global climatic curve indicate a good correspondence between episodes of global climate change and turnover, suggesting that extinction is exacerbated by these episodes. Finally, the palynological record also indicates that the Neotropics experienced several floods during the Cenozoic. These episodes include marine incursions, the development of extensive lacustrine systems and the establishment of mangrove forests. The relationship between floods and the evolution of Neotropical vegetation is challenging due to the uncertainty related to the temporal and geographic range of the floods. The evidence suggest that the floods had a local rather that a regional effect on the evolution of Neotropical vegetation.

Extended Abstract

The Neotropics maintains the highest diversity of plants on Earth (Kricher, 1999). This region, extending from central Mexico in the north to southern Brazil in the south, harbors about 33% of the plant species of the world (Ulloa et al., 2017). The astonishing mega-diversity of the Neotropics has been studied for a long time (Humboldt, 1820) with different mechanisms proposed, not only to explain how such great diversity was produced, but also how it is maintained. These mechanisms have been classified into two major categories, biotic and abiotic (Antonelli and Sanmartin, 2011). Biotic mechanisms include niche conservatism, which suggest that there is most species of plants in the Neotropics because more lineages originated and diversified there due to climatic stability of the region (Wiens, 2007). On the other hand, abiotic mechanisms include the time hypothesis (Mittelbach et al., 2007), which explain the high diversity of plants in the Neotropics as the result of the isolation of South America for nearly 100 Ma. During this period, the continent remained isolated after its breakup from Africa and before its recent connection with North America a couple of million of years ago (3.5 Ma) (ODea et al., 2016) (but see Montes et al. (2015) for a different age interpretation). It is proposed that this isolation, coupled with a stable climate, would have favoured a high speciation and the accumulation of species through time (Mittelbach et al., 2007). Other abiotic mechanisms include climate and the effects produced by the uplift of the Andes Cordillera. Although climate is one of the best predictors of species richness today, its role in producing and maintaining plant diversity in the geological past is still under debate. For example, palynological analysis from the Paleogene of Colombia found a good correlation between diversity and changes in global temperature (Jaramillo et al., 2006). However, this correlation is not evident for the Neogene, where changes in palynological diversity show only a poor correlation with fluctuations in temperature (Hoorn et al., 2010). It is widely accepted that the uplift of the Andes Cordillera brought up deep changes in the paleogeography of South America (Rodazz et al., 2010). This event promoted habitat heterogeneity, created biotic corridors, intensified

the nutrient supply and changed the hydrological regime of the continent (Hoorn et a., 2010). Any of these changes could favour adaptive radiations, produce geographic vicariance, and promote allopatric speciation that may have increases Neotropical plant diversity. The uplift of the Andes Cordillera is a relatively geological young event, with the most intense orogenic pulse occurring during the Miocene (Mora et al., 2010), which could at least partly explain the diversity of plants observed today in the Neotropics. However, this orographic barrier did not exist for most of the Cenozoic and therefore it is likely that different mechanisms have operated through time, and possibly in conjunction, to produce long-term patterns of plant species diversity in the Neotropics.

In summary, several mechanisms have been proposed to explain the high diversity of plants seen today in Neotropics. Their role in producing and maintaining such diversity are not completely understood and surely they will continue being matter of study. However, before attempting to understand those mechanisms, it is crucial to known the macroevolutionary history of the Neotropical vegetation through deep time. In fact, patterns of plant diversification during the Cenozoic have received much less attention than have the mechanisms proposed to explain them. This presents a significant knowledge-gap. Accurate and unbiased estimation of diversity, origination and extinction are therefore pivotal to explaining the high diversity of plants observed in the Neotropics.

In this thesis, I used the palynological record of northern South America (specially from Colombia) Colombia to study the macroevolutionary history of Neotropical vegetation and its relation with regional geological and global climatic processes occurring during the Cenozoic. Palynology provides the best data to study fossil record patterns of diversity in plants. Pollen and spores are recorded in a widely variety of sedimentary environments reflecting therefore local and regional conditions, they are recovered in high quantities allowing the statistical treatment of the information and they offer a higher stratigraphic resolution than any other fossil record of vegetation. The material used in this study corresponds to samples from wells and outcrops located in different sedimentary basins of Colombia, Venezuela, and Brazil, but mainly from the Llanos basin in Colombia. The sediments of this foreland basin preserve the evolutionary history of Neotropical vegetation as well as the geological evolution of the northern Andes. This offers a unique opportunity to study the relationship between the geological and fossil records. The quantitative information used in this study is stored in a relational database owned and managed by the Biostratigraphy Team of the Instituto Colombiano del Petroleo (ECOPETROL S.A). It contains information about the taxonomy, stratigraphic range, geographic distribution and abundance of

thousand of palynomorphs recorded in thousand of samples analyzed from hundred of sites in Colombia.

This thesis is divided in four chapters. The **first chapter** is about Biostratigraphy and its main goal was to establish a biostratigraphic and chronostratigraphic framework, which is the analytical base of the other two chapters. In specific, I used graphic correlation (Shaw 1964; Edwards 1984, 1985) to trace lines of correlation (LOC) for each section and by using the points of calibration in Jaramillo et al. (2011) establish the relationship between stratigraphic depth and age (in Ma). Once the LOC were calibrated with geological time, it was possible to calculate the age of any sample and by extension the age of biostratigraphic events (e.g. first and last appearance datums). The incorporation of new palynological information to the zonation proposed by Jaramillo et al (2011) allowed to include 38 new informal and 11 formal taxa that represent 43 and 15 biostratigraphic events respectively. In annex 1.7 (Systematic Palynology) I described 34 of these new palynomorphs, making emphasis in new forms of particular interest (either rare with a characteristic morphology or, if common, frequent stratigraphically).

In addition to graphic correlation, I explored a technique of data mining known as association rules (AR), which is used in the analysis and discovery of interesting relations between variables in large databases (Hahsler et al., 2005). AR have been mainly used in market basket analysis, where the habits of buying consumers are analysed in order to find associations between different items that consumer buy. In a biostratigraphical context, AR could be used to find which species are frequently found together in a biozone, an environment of deposition or whatever attribute is of interest to the researcher. In specific, I applied this technique to samples of the biozone T6-Spinizioncolpites grandis (Jaramillo et al., 2011) with the aim of refine and increase its resolution. The results show that this biozone is very homogenous in terms of palynological composition, which makes it very difficult for further division. The rules found for T6 are composed by common species that are also very common throughout the Cenozoic. This prevents the use of these rules to identify the biozone T6.

The **second chapter** is about macroevolutionary patterns of Neotropical vegetation in deep time. By using the chronostratigraphic framework obtained in the first chapter, the main aim of chapter two was to produce unbiased estimates of diversity and taxonomic rates (origination, extinction) and compare these estimates with global climate changes occurred during the Cenozoic (Zachos et al., 2008). Because most of the material used in the study corresponds to ditch cutting samples, borehole caving could artificially increase the FAD of the species affecting therefore the macroevolutionary es-

timates. For this reason, several techniques based on Range-through (RTMs) and in-bin occurrence (OBINs) methods were used not only to assess the possible effect of caving but also to standardize by differences in sampling effort. RTMs infer each taxon to be present in all the samples between its first and last occurrence even if the species was not found in any sample in between, while OBINs methods make use of information on taxa that are actually sampled in each interval. The results of the two techniques were compared and complemented to make a complete interpretation of the macroevolutionary estimates.

In terms of diversity, the results show a strong correlation between fluctuations in palynological diversity and global changes in temperature. Contrasting responses of vegetation to temperature between the Palaeocene to Eocene and the Oligocene to present suggest that different mechanisms operated during greenhouse and icehouse intervals. The analysis of the geographic distribution of diversity, represented by choroplet maps, indicate that a high diversity is the result of the contribution of a small proportion of samples belonging to just a few sections rather that the result of a homogeneous high diversity occurring in many samples during those intervals. With respect to the taxonomic rates, the estimated turnover show high and low amplitude fluctuations during green house and icehouse intervals respectively. The results also suggest that throughout the Cenozoic, periods of elevated extinction are followed by periods of elevated origination. This relationship indicates that in the Neotropics when a species become extinct, it is replaced very fast. In contrast, the lack of correlation between origination and extinction suggest that extinction is not controlled by origination. The examination of the taxonomic rates and the global climatic curve indicate a good correspondence between episodes of global climate change and turnover suggesting that extinction is exacerbated by global climate changes.

In the **chapter three** I used the palynological record, in specific the occurrence and abundance of marine palynomorphs (dinoflagellates and microforaminifera), terrestrial palynomorphs (pollen and spores) and algae (*Pediastrum* and *Botryococcus*), to identify and explore the temporal and geographical distribution of floods during the Cenozoic in the Neotropics. The abundance and proportion of these palynomorphs allowed differentiating between episodes of marine influence, the development of lacustrine systems, and the establishment of mangrove forests. The Miocene flood(s) have received special attention from researches because of its possible role in promoting biodiversity in the Amazon (Hoorn et al. 2010 and references there in). However, the palynological evidence reveals that the Miocene floods were just one from several episodes that occurred throughout the Cenozoic and that some of these were not restricted to the western Amazonia but were

spread over wide regions in northern South America.

In this respect, the proportion of marine and lacustrine elements suggests the occurrence of at least seven marine incursions and five episodes of lacustrine influence during the Cenozoic. The proportion of mangrove-related palynomorphs points to at least four intervals in which specific geographic areas exhibited mangrove forests. All the episodes, indistinct of their ecological nature (marine, lacustrine or mangrove) were close related, which suggest a common mechanism. In general, the flooding events were temporary and spatially restricted. The nature of these restrictions may be imposed by the sampling coverage, which is poor in some geographic areas and intervals, and so did not always allow establishing the temporal and geographic range of the events with certainty. In turn, this uncertainty makes it difficult to elucidate the relationship between the floods and the macroevolutionary estimates. It is common to find intervals of marine/lacustrine influence characterized by either low or high diversity. In this sense, the floods seem to have had a local rather than a regional effect on the macroevolution of Neotropical vegetation.

In chapter three I also explore the age of deposition and paleoecology of the Barzalosa Formation. This is a litostratigraphic unit from the Upper Magdalena Valley that has been correlated with the fossiliferous horizons of the Middle Magdalena Valley (Los Corros, Mugrosa, and La Cira) and the members of the Carbonera Formation in the Llanos Basin. The results suggest that the Barzalosa Formation was deposited during the upper Early Miocene (16.5 Ma) and therefore is correlative with the deposits of the La Cira fossiliferous Horizon in the Middle Magdalena Valley, the member C2 of the Carbonera Formation in the Llanos basin, and the Pebas system in western Amazonia. Palynologically, the Barzalosa Formation is dominated by elevated abundances of *Pediastrum* and *Botryococcus*, two algae commonly associated with lacustrine conditions. The proportion of these two algae allowed separating this unit into three intervals, which are interpreted to represent distinct phases of a complex lacustrine system controlled by climate and the input of nutrients. A Markov chain based analysis and differences in palynological composition support the three intervals. The lascustrine system of the Barzalosa Formation, indicates that floods during the Miocene were not restricted to the Llanos Basin (Jaramillo et al., 2017) and western Amazonia (Hoorn 2010) but also reached the Upper and Middle Magdalena Valley Basins that by Miocene times were probably already separated from the Llanos Basin by the Eastern range of the Andes Cordillera.

Finally, in **chapter 4** I make a synthesis of the macroevolutionary history of Neotropical vegetation during the Cenozoic. I propose that on a regional scale, diversity is controlled by global temperature while on a local scale by changes in the environments of deposition. The amplitude of temperature

fluctuations explains the pattern of the diversity curve. Greenhouse and Icehouse climates show high and low amplitude respectively, which is reflected in the diversity curve. Distinctive changes in diversity, like those during the middle Eocene and late Miocene are explained in terms of the climatic curve, paleogeography (flooding events, uplift of the Andes Cordillera) and factors like emigration. The results also show that origination shows a strong correlation with the extinction in the previous 1 Ma interval indicating that when species become extinct in the Neotropics, they are replaced very rapidly. A relationship between extinction and origination was not detected. However, transient climate events seems to have played an important role as a driver of extinction and therefore driving pulses of turnover among Neotropical plants.

Acknowledgements

During my doctoral studies I had the opportunity to meet and interact with different people, specially in the Department of Earth Sciences. This was extremely enriching and I want to thank all of them. Special thanks to Cesar Espinoza, Alfredo Guerrero, May Chung, Viridiana Lizardo, Lilith Espinoza and Felix Castellanos.

I wish to thank my supervisor Roger Benson for his constant support, continuous source of ideas and unconditional help during my studies at Oxford.

This research was founded by Ecopetrol S.A. I am particularly grateful to them for giving me the opportunity to study at Oxford University.

The information used in this study is the result of years of studies by the Biostratigraphy team of the Instituto Colombiano del Petroleo. Without the dedicated and constant effort of its members this work would not have been possible.Special thanks to Omar Bedoya, Maria Carolina Vargas, Guillermo Rodriguez, Milton Rueda, Carlos Jaramillo and Olga Celis and other people who have been part of the team and have helped to produce the most amazing palynological information of the Neotropics.

My family deserves a very special recognition for their support during these years of intense work. To my mother who is always the inspiration. Thanks to Laura Penaranda for her unconditional support and infinite patience during all these years. Muchas Gracias a todos.

Contents

1 Biostratigraphy of Northern South America 1
1.1 Introduction . . . 1
1.1.1 Previous Palynological Zonations . . . 4
1.2 Methods . . . 14
1.2.1 Biostratigraphy . . . 14
1.2.2 Quantitative Biostratigraphy . . . 15
1.2.2.1 Graphic Correlation . . . 16
1.2.2.2 Association Rules Analysis . . . 19
1.3 Materials . . . 24
1.3.1 Biostratigraphy . . . 24
1.3.2 Association Rules Analysis . . . 25
1.4 Results and Discussion . . . 28
1.4.1 Biostratigraphy . . . 28
1.4.2 Association Rules Analysis . . . 37
1.5 Conclusions . . . 41

2 Macroevolution of Neotropical vegetation during the Cenozoic 44
2.1 Introduction . . . 44
2.1.1 Macroevolutionary estimates in the fossil record . . . 49
2.1.2 The fossil record of plants . . . 51
2.1.3 Cenozoic plant diversity in the Neotropics . . . 52
2.2 Materials . . . 57
2.2.1 Biases in Origination and Extinction estimates . . . 59
2.2.1.1 Borehole caving . . . 59
2.2.1.2 Reworking . . . 64
2.2.2 Regional Diversity . . . 64
2.2.2.1 Information from literature . . . 67
2.2.2.2 Information from wells . . . 71
2.3 Methods . . . 71
2.3.1 Estimates based on Range Through Methods . . . 72

2.3.1.1 Diversity and taxonomic rates 72
2.3.1.2 Taxonomic Survivorship analysis 76
2.3.2 Estimates based on In Bin Occurrence Methods 78
2.3.2.1 Shareholder Quorum Subsampling (SQS) . . . 78
2.3.2.2 Taxonomic rates via three timers and gap fillers 80
2.3.3 Diversity in Space 83
2.3.4 Climate and Macroevolution 85
2.4 Results 87
2.4.1 Estimates based on Range Through Methods 87
2.4.1.1 Standing Diversity 87
2.4.1.2 Per-capita 0rigination and Extinction rates . 94
2.4.1.3 Cohort Survivorship Analysis 97
2.4.2 Estimates based on In Bin Occurrence Methods 101
2.4.2.1 Shareholder Quorum Subsampling (SQS) . . . 101
2.4.3 Regional Diversity 109
2.4.3.1 Panama Sections 112
2.4.3.2 Sinu-San Jacinto Basin 114
2.4.3.3 Catatumbo Basin 116
2.4.3.4 Middle Magdalena Valley 117
2.4.3.5 Saltarin Rock Core 118
2.4.3.6 Apaporis Section 120
2.4.3.7 Mariname Section 121
2.4.3.8 1AS-27AM and 1AS-19AM Rock Cores 121
2.4.3.9 1AS-105AM Rock Core 122
2.4.3.10 1AS-33AM Rock Core 123
2.4.3.11 Contamana Section 124
2.4.4 Diversity in Space 126
2.4.4.1 Diversity in space during the Miocene 142
2.4.5 Origination and Extinction using Gap Fillers 146
2.4.5.1 Origination 149
2.4.5.2 Extinction 151
2.4.6 Macroevolutionary Dynamics 153
2.4.7 Climate and Macroevolution of Neotropical plants . . . 160
2.5 Discussion 167
2.5.1 Diversity 169
2.5.2 Taxonomic Rates 182
2.5.3 Macroevolutionary Dynamics 187
2.6 Summary and Conclusions 191

3 Flooding Events during the Cenozoic in the Neotropics 194
3.1 Introduction . . . 194
3.1.1 Evidence of flooding events in the Neotropics . . . 195
3.1.1.1 Neogene Flooding Events . . . 196
3.1.1.2 Paleogene Flooding Events . . . 202
3.2 Materials and Methods . . . 206
3.2.1 Cenozoic Floods . . . 206
3.2.2 Middle and Upper Magdalena Valleys . . . 214
3.3 Results . . . 218
3.3.1 Flooding events in the Magdalena Valleys . . . 218
3.3.2 Flooding events during the Cenozoic . . . 227
3.3.2.1 Marine Events . . . 227
3.3.2.2 Lacustrine Events . . . 236
3.3.2.3 Mangrove Forest . . . 240
3.4 Discussion . . . 243
3.4.1 Flooding events during the Cenozoic . . . 246
3.4.1.1 Paleocene . . . 248
3.4.1.2 Eocene to Oligocene . . . 250
3.4.1.3 Miocene to Present . . . 252
3.4.2 Flooding events in the Magdalena Valleys . . . 260
3.4.3 Macroevolution and Flooding Events . . . 265
3.5 Conclusions . . . 269

4 Synthesis 271

5 Annexes 280

Chapter 1

Biostratigraphy of Northern South America

1.1 Introduction

In sensu-stricto Palynology is defined as the "study of the organic microfossils that are found in maceration preparations of sedimentary rocks" (Traverse, 2007) and therefore includes the study of acritarchs, chitinozoas, scolecodonts, algae, spores, pollen, dinoflagellates, fungi, microforaminifera and palynodebris. The range of organisms studied by palynology makes this discipline very versatile and useful for oil exploration in a country like Colombia, where as a consequence of a complex geological history related mainly with the uplift and evolution of the Andes orogen,the geology is diverse and full of structural and stratigraphic complexity. Each sedimentary basin of the country has their own history and each one keeps record of their own evolution. Two of the most important sedimentary basins in Colombia, from the oil exploration point of view, are the Eastern Cordillera and the Llanos (Figure 1.1).

The Eastern Cordillera Basin is characterized by intense structural complexity as the result of tectonic processes operating during the uplift of the Eastern Andes Cordillera. Exploratory objectives in this basin include Cretaceous and Cenozoic rocks units (Figure 1.2).Cretaceous units include the Une, Gacheta and Guadalupe formations that in general correspond to marine sequences with sporadic episodes of continental deposition.Cenozoic units like the Mirador Formation and some members of the Carbonera Formation (C7 and C5) are considered reservoirs and their deposition took place in continental to transitional environments. The seals of the Cenozoic reservoirs correspond to members of the Carbonera Formation (C8, C6 and C2) (Figure 1.2)

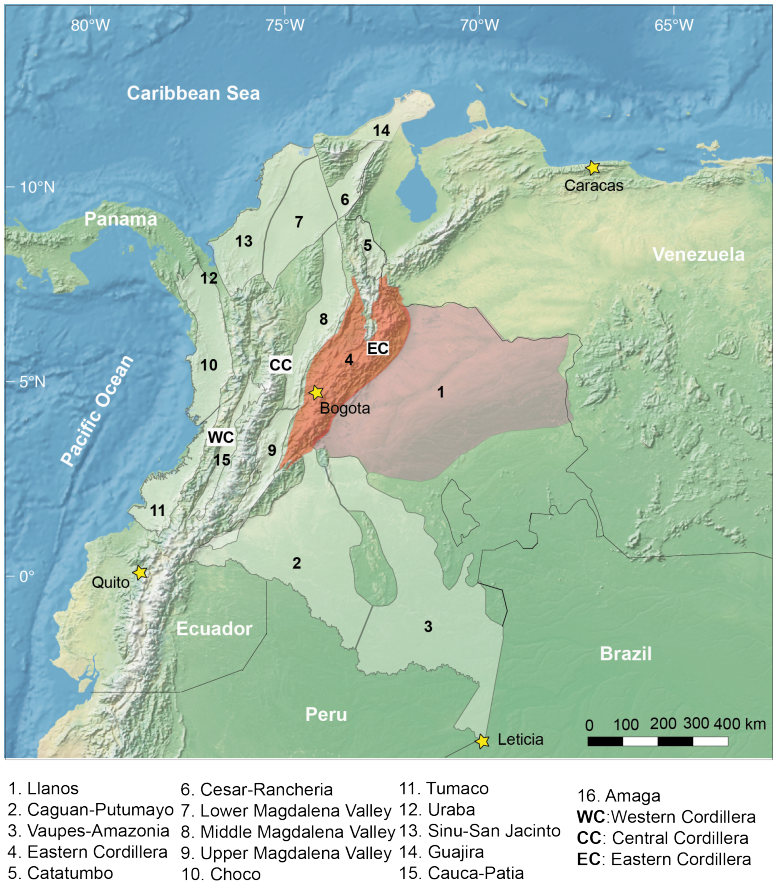

Figure 1.1: Map of northern South America showing the sedimentary basins of Colombia. Highlighted in purple and red the Llanos (1) and Eastern Cordillera (4) basins respectively.

whose deposition has been related with regional episodes of marine incursions (Duarte et al., 2017; Jaramillo et al., 2017, Reyes-Harker et al., 2015). Palynology has proved to be very useful for biostratigraphic correlation of these units. In the marine units, dinoflagellates are used as the main biostratigraphic proxy. In transitional-continental environments, pollen and spores is the main tool (Gonzales-Guzman 1967; Jaramillo et al., 2005; Jaramillo et al., 2004). Current local biostratigraphic schemes developed by the oil industry are resolved to the reservoir scale. This has allowed the identification of faults, repetitions and unconformities that have been used to refine the geological model of the basin (Bayona et al.,2007; Bayona et al., 2008; Mora et al., 2013; Reyes-Harker et al., 2015; Sanchez et al., 2015). Also, during the drilling of exploratory wells, palynology has become an indispensable tool

used in real time (biostering) allowing control the stratigraphic position of the drill.

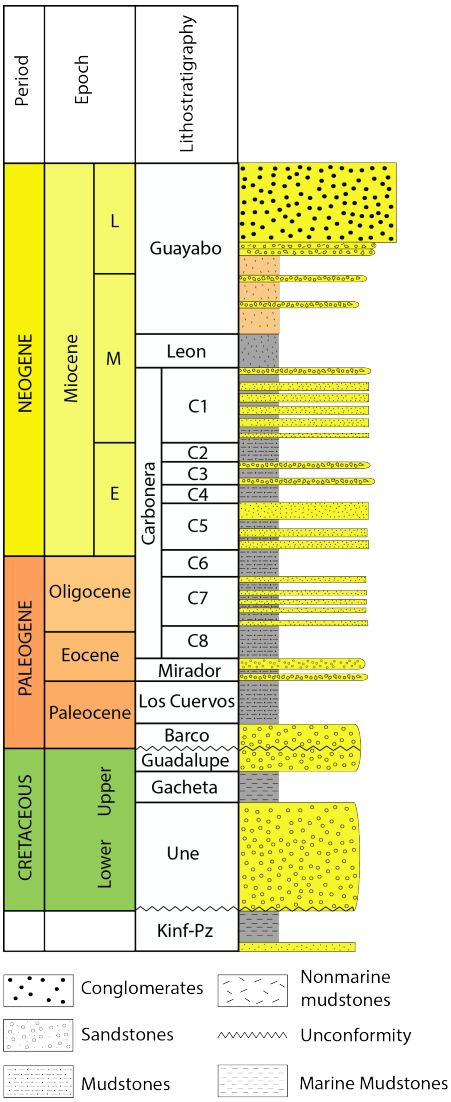

Figure 1.2: Generalized stratigraphic column of the Llanos and Llanos Foothills basins of Colombia.

The Llanos is a foreland basin adjacent to the Eastern Cordillera (Figure 1.1) where rapid lateral changes as well as minor unconformities and vertical truncations (pinchouts) are vey common along the basin. Unlike the Eastern Cordillera Basin, structural complexity in the Llanos basin is low with some minor faults and folds. The target reservoirs are mainly Cenozoic and late Cretaceous. Adjacent to the foothills, the reservoirs correspond to the

Eocene Mirador Formation and some operational units known as K1 and K2 that temporally correspond to the early Paleocene and Late Cretaceous (Figure 1.2). Toward the east of the basin, the age of the reservoirs progressively becomes younger with Oligocene and Miocene units. The environments of deposition correspond mainly to fluvial environments. Minor episodes of marine incursions represented by some members of the Carbonera Formation are generally the seal of the system. In this geological context, palynology has also been very useful. Pollen and spores are very abundant and in spite of the rapid lateral facies changes that prevent rigorous lithostratigraphic correlations, sequence of biostratigraphic events is very consistent along the basin. The Palaeozoic sequence of the Llanos Basin has also been an exploratory target during the past couple of years, and again palynology has proven to be very useful with an extraordinary recovery of acritarchs, conodonts and chitinozoans (Duenas et al., 2006; Hughes et al., 2014).

For all these reasons, palynology has been largely used in Colombia as the main biostratigraphic tool in oil exploration since the past three decades. As a result of this, considerable knowledge of the temporal and geographic distribution of palynomorphs has been acquired. This information has not only allowed increase certainty in oil exploration (Jaramillo, 2009; Jaramillo et al., 2005) but has also established a rigorous temporal framework of research studies across several disciplines including palaeobiology (Gomez et al., 2009; Hoorn et al., 2010b., Jaramillo et al., 2010); tectonostratigraphy (de la Parra et al., 2015; Mora et al., 2010a; Ochoa et al., 2012; Parra 2008); geochemistry (Carvajal-Ortiz et al., 2009) and sedimentology (Bayona et al., 2008b; Caballero et al., 2010; Bayona et al., 2013; Reyes-Harker et al., 2015; Duarte et al., 2017) among others.

1.1.1 Previous Palynological Zonations

Although during the last 60 years a great amount of palynological studies have been conducted in Colombia, only a few formal biostratigraphical schemes have been formally proposed for the Cenozoic (Van der Hammen 1957a, 1957b; Gonzales-Guzman 1967; Germeraad et al., 1968; Muller et al., 1987; Jaramillo et al., 2011). Van der Hammen was the pioneer of palynological studies in northern South America, including Colombia. He used the fluctuations in pollen and spores as a proxy for climatic cycles (Van der Hammen 1957a; 1957b; 1958). He proposed that the abundance peaks of certain groups (*Psilamonocolpites*,*Mauritiidites* and *Psilatriletes*) were indicative of vegetational changes due to regional climate changes. These were assumed to have chronostratigraphic value that could inform stratigraphic correlation. The ages in the pollen diagram are placed based on the changes of relative

proportions of certain groups assuming that climate changes are correlated with key boundaries. However, this line of reasoning and the approaches of Van der Hammen (1957a) have several problems (Jaramillo et al., 2011). In their pollen diagrams, the proportion of each palynomorph group was calculated by counting 200-300 grains and then normalizing the results. This approach have associated the statistical artefact of the "closed sum" (Kovach 1994) in which a significantly increase in the abundance of one group cause a decrease in the abundance of a second group even though their real abundance did not change. The abundance peaks for focal taxa in Van der Hammens diagram could therefore result from the decreases in the abundance of other taxa and not a response of focal taxa to climate variation. The second problem relies on the nature of the samples. Van der Hammen used mainly coal samples, which generally have a unique and restricted flora that is not ideal for biostratigraphic purposes (Traverse, 2007). Finally, correlation based on abundance of specific palynomorph groups probably reflects similar ecological conditions rather than temporal equivalences.

Germeraad et al. (1968) proposed a zonation based on twenty years of palynological studies of Palaeogene sediments in several places of Tropical South America, Africa and Asia. In South America the focus was Colombia, Venezuela, Trinidad and the Guianas. The number of samples used in the analysis is not specified however they claim that a very large number was used. Only samples collected at the surface, cores and sidewalls samples taken in wells were studied (Germeraad et al., 1968). The main purpose of Germeraad's work was to provide a zonation useful to solve problems on a variety of scales. From detailed correlations between wells separated only a few kilometres to correlation between basins in separated continents. As a result, they proposed "marker" species classified into: 1) species that can be found in the tropical region (pantropical); 2) species that occur in both the South American and west African regions and 3) species which are of significance only within a single botanical province (Germeraad et al., 1968). Noticeably, the number of species is much lower in the pantropical category than in the other two categories. On base of this distribution, Germeraad et al. (1968) proposed a broad stratigraphical framework on a pantropical scale that is useful for correlation at intercontinental scales. This scheme was further subdivided in regional zones (Atlantic, Caribbean and Borneo) (Figure 1.3) that are useful for correlation at intra-basin scale. The scheme proposed by Germeraad et al. (1968) was extensively used in Colombia during the last 40 years. However, when oil exploration started to move into more complicated geological areas, the level of resolution was not adequate for the new challenges and a more refined biostratigraphy scheme was necessary. Additionally, Germeraad 's zonation relies on some palynomorph species that

are very common in sediments of Venezuela, but rare or absent in Colombia restricting therefore their use.

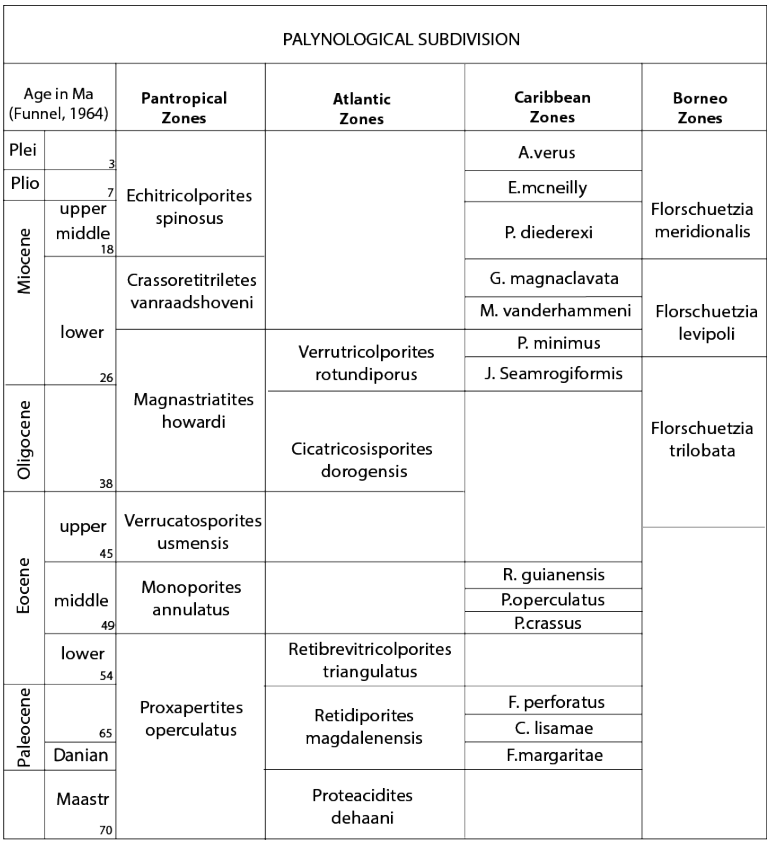

Figure 1.3: Palynological zonation proposed by Germeraad et al. (1968) for the Cenozoic of tropical areas.

Based on the work of Germeraad et al. (1968), Muller et al. (1987) proposed a zonation for northern South America by using additional material and information from Colombia, Venezuela, Trinidad, Guyana, Surinam and Brazil. Muller et al. (1987) proposed 10 superzones (six Cretaceous and four Paleogene/Neogene) and 31 zones (13 Cretaceous and 18 Paleogene-Neogene) (Figure 1.4). Superzones make reference to two or more successive zones characterizing a particular phase in the evolutionary development and succession of terrestrial microfloras. Although Muller's zonation subdivided the Cenozoic in more detail that that of Germeraad et al. (1968), making special emphasis in the division of the Eocene using well-known palynostratigraphic information from Venezuelan formations, the resolution was still low compared to the needs of oil exploration in Colombia. For example, Jaramillo et al. (2005) developed a biostratigraphic framework for the Palaeocene Los

Cuervos Formation based on the study of 14 sections located in the Llanos Basin and Llanos Foothills and found that two of four biozones that they proposed were not identified in either Muller's (Muller et al., 1987) or Germeraad's (Germeraad et al., 1968) zonations. Additionally and similar to Germeraad's zonation, some of the palynomorphs in Muller's scheme are very common in Venezuela but rare or absent in Colombia.

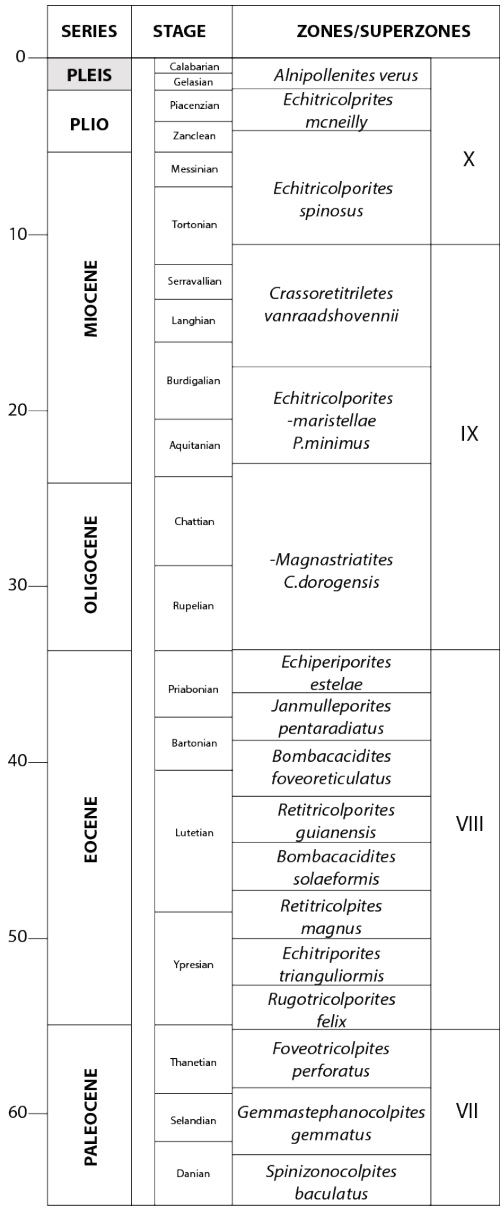

Figure 1.4: Palynological zonation proposed by Muller et al. (1987) for the Cenozoic of northern South America.

In 2011, Jaramillo et al. (2011) proposed the most recent biostratigraphic framework for the Cenozoic of Colombia. Using the most relevant palynological information produced mainly from oil exploration activities, and through the use of Graphic Correlation and Constrained Optimization proposes a palynological zonation for the Llanos Basin and Eastern Cordillera Basin. The scheme of Jaramillo et al. (2011) unifies previously published information (Jaramillo et al., 2009; Jaramillo and Dilcher, 2001; Jaramillo et al., 2005; Jaramillo et al., 2004) and offers a zonation that is calibrated with the standard geological timescale. The calibration used foraminifera, magnetostratigraphy and isotopes that are the proxies commonly used to define the epoch boundaries within the Cenozoic (Gradstein et al., 2012). It is based on information from 70 sites including 16 outcrops; 11 rock cores and 43 sites with ditch cutting samples from oil exploration wells. The zonation is focused in the Llanos Basin and Eastern Cordillera Basin and although most of the information comes from wells drilled in these two basins, information for other sedimentary basins was also used (Table 1.1).

Table 1.1: Number of sections discriminated by sedimentary basin used in Jaramillo et al. (2011) palynological zonation.

Basin	**Number Sections**
Llanos	19
Eastern Cordillera	17
Middle Magdalena Valley	7
Catatumbo	11
Upper Magdalena Valley	9
Guajira	1
Caguan-Putumayo	2
Cesar-Rancheria	2
Urumaco (Venezuela)	2

Jaramillo et al. (2011) analysed 624744 occurrences of more than 2000 palynomorphs taxa in 6707 samples using Graphic Correlation (Shaw 1964) and Constrained Optimization (Sadler 2003). The main goal of both techniques is to find an optimal sequence of events. Optimal makes reference to a sequence that best agrees with the empirical sequence of events found within individual sites and event refers to either a first appearance datum (FAD) or a last appearance datum (LAD) of a fossil taxon. The final result of this work is a composite section with the positions in composite units and Ma (million of years) of approximately 500 events. To assess the degree of confidence of the position of any event, a spreading parameter was calcu-

lated for each event (Jaramillo et al., 2005). Low values of this parameter indicate that an event occurred in a similar position relative to the other events in all the evaluated sections. The 20 events with the lowest spreading parameter and greatest presence among the sites were selected as key zonal events. Jaramillo's scheme comprises 18 biozones (Figure 1.5) tied to the global geological timescale by 18 calibration points obtained through the analysis of carbon isotopes, magnetostratigraphy and Foraminifera (Table 1.2). Each section has its own line of correlation and through the points of calibration, describing the relationship stratigraphic depth in that section and stratigraphic depth in the composite section, it is possible to calculate the relationship between stratigraphic depth and age (in Ma) for the composite section and therefore to estimate the age of any event.

Table 1.2: Calibration points for the composite section in Jaramillo et al.(2011) palynological zonation.

Datum	**Proxy**	**Composite units**	**Age (Ma)**
Present	Formation	0	0
Codore Algodones	Formation Top	1332	1.81
La Vela	Formation Top	1332	1.81
Codore Chiguaje	Formation Top	1942	3.6
Codore Jebe	Formation Top	1991	5.33
Caujarao Tara	Formation Top	2087	5.6
Urumaco	Formation Top	2471	6.8
Socorro	Formation Top	3964	12.4
Querales	Formation Top	4492.45	14.5
Cerro Pelado	Formation Top	5017.42	16
Agua Clara	Formation Top	8884.77	17.5
C.dorogensis LAD	Isotopic record	14377	23.03
E.trian var. orbicularis LAD	Isotopic record	16068	33.9
ETM spike LAD	Isotopic record	17372	48.6
PETM spike LAD	Isotopic record	17941.7	55.63
PETM spike FAD	Isotopic record	18077.1	55.8
B. annae FAD	Isotopic record	19113.75	60
E, protofranciscoi LAD	Isotopic record	19842	65.5
Top C4 Ar2r	Magnetostratigraphy	3178.6	8.1

Figure 1.5 is a summary of Jaramillo et al. (2011) zonation and the information that was used to produce it. The first panel, on the left, shows the Geological Time scale (Gradstein et al., 2012) and palynological biozones. Each zone is named by the capital letter "T" followed by a number and the name of one of their most representative species (e.g. T11 - Cicatricosisporites dorogensis). The second panel show the number of events for each biozone with the red-black rectangles indicating the number of LADs (last appearance datum) and FADs (first appearance datum) of palynomorph taxa

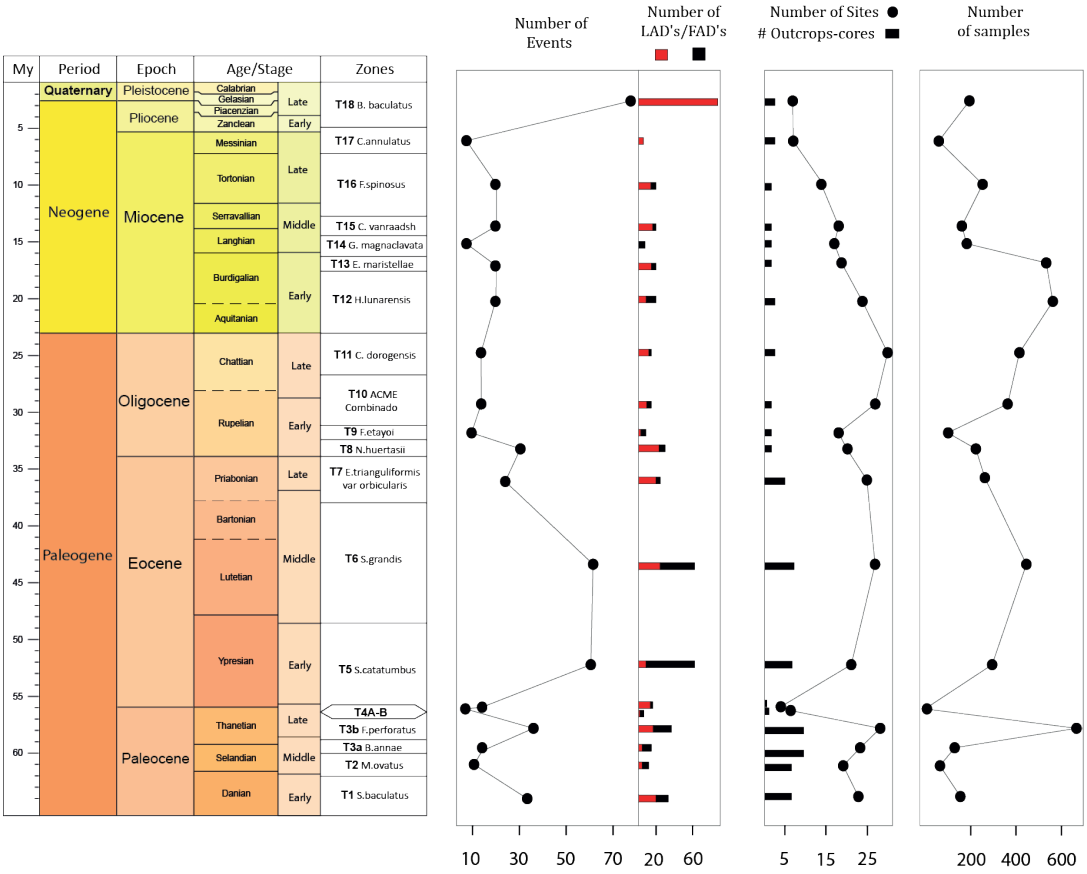

Figure 1.5: Palynological zonation proposed by Jaramillo et al. (2011) for the Cenozoic of northern South America. The right panel show the number of events, number of first and last appearances (FADs and LADs), the number of sites and the number of samples for each biozone.

for each zone. In the third panel, the black dots represents the number of sites used for each biozone and the black rectangles the number of outcrops/rock cores. The final panel represent the number of samples used for each biozone. Hereafter and in order to avoid the repetitive use of the word biozone only the letter and number of the zone will be named.

The durations (in million of years) of biozones are variable, ranging from 0.1 Ma (T4B) to 10 Ma (T6). The number of sites and samples used for each biozone is also variable and are highly correlated (R^2= 0.45). Biozones with a high number of sites usually also have a high number of samples (Figure 1.5). T3b has the highest number of sections and samples analysed and in general those zones encompassing the late Oligocene-early Miocene (T10-T13) also present a high numbers of sections and samples. The zonation comprises 500

events; 294 corresponding to LADs and 206 to FADs. The biozone with the highest number of events is T18, all of them corresponding to LADs.

The correlation between the number of samples and the number of events inferred is evident for some biozones. In order to explore this correlation, a Spearman Rank Correlation was used and supported with a permutation test using 1000 replicates. The test was run to assess the correlation between the number of samples and the total number of events and for the number of samples and the number of FADs and LADs. The correlation was also analysed for the entire dataset (all the biozones) and separately for the biozones T1 to T9 and T10 to T18. The results are presented in Table 1.3. A good correlation between the number of samples and the number of events is observed for the complete dataset. This correlation has better support when the number of samples and number of LADs are compared (Table 1.3). The analysis of T1 through T9, suggests a very strong correlation (rho=0.85, p=0.007) between the number of samples and number of events. For this interval, the number of FADs shows a stronger correlation (rho=0 .71, p=0.013) with the number of samples than the one exhibited by the LADs (rho=0.63, p=0.037).

Table 1.3: Spearman rank correlation test between the number of samples and the total number of events and for the number of samples and the number of FADs and LADs.

Biozone			**rho**	**p-value**	**Perm-test**
All Biozones	Samples	Events	0.58	0.007	0.007
All Biozones	Samples	FADs	0.35	0.12	0.13
All Biozones	Samples	LADs	0.43	0.05	0.05
T1-T9	Samples	Events	0.85	0.007	0.001
T1-T9	Samples	FADs	0.71	0.01	0.01
T1-T9	Samples	LADs	0.63	0.037	0.043
T10-T18	Samples	Events	0.34	0.36	0.36
T10-T18	Samples	FADs	0.41	0.26	0.261
T10-T18	Samples	LADs	0.14	0.73	0.72

From figure 1.5 is also evident that the interval T1-T9 presents the highest number of samples from cores and outcrops. This is something to be expected because most of the FADs should be defined in base of samples from cores or outcrops. The use of information from ditch cutting samples to define FADs is dangerous because this type of sample has problems associated with caving, which potentially can extend artificially the FAD of the species. Another interesting fact is although T5 and T6 after T18 have the

highest number of events, they also are the biozones of greatest durations (7.1 and 10.g Ma respectively). This seems contradictory from a biostratigraphical perspective, because we might expect that it should be possible to subdivide intervals containing high numbers of events into finer subdivisions. Counts of the number of sites in which each event was observed provide a possible explanation.

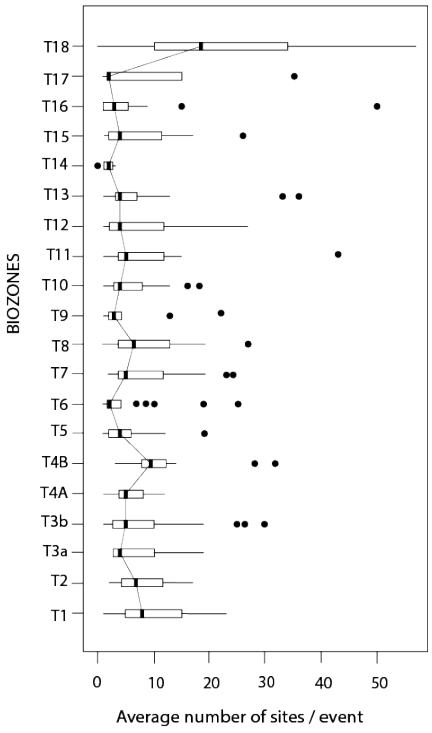

Figure 1.6: Boxplot of the number of sites for the events that define each biozone in Jaramillo's zonation (Jaramillo et al., 2011) (see text for discussion).

Figure 1.6 shows the mean number of sites in which the events (FADs and LADs) observed in each biozone were found as a time series of boxplots. For example the biozone T4A includes seven events and the counts of sites in which each one was found are 4,5,12,4,8,8,1. The mean number of sites per event in T4A is therefore 6. It is evident in Figure 1.6 that the mean number of sites for T5 and T6 is very low (4.7 and 3.7 respectively), meaning that their events are not observed in many sites and demonstrating that there is little information on the relative sequence of events in T5 and T6. Most of the events in these two biozones are FADs that were observed through core or outcrop material (Figure 1.5). This evidence suggest that in order

to subdivide and increase the resolution of T5 and T6, it is necessary to study additional outcrops or rock-cores, and therefore increase the number of sites in which the events (FADs) are observed. It seems that increasing the number of analyses in ditch cutting samples will not allow to find more events because, with this type of material, it is not possible to track the consistency of the FADs and the number of LADs possibly is not going to increase.

For the second interval, corresponding to the zones T10 through T18, no significant support of correlation was found (Table 1.3). It is evident from figure 1.5 that the increase in the number of samples analysed throughout T10-T13, is not accompanied by an increase in the number of events. For this interval the number of ouctrops and cores is low and most of the samples analysed correspond to ditch cuttings from wells. In order to increase the number of events in the biozones covering this interval, it would be necessary to analyse outcrop and/or core samples to detect new FADs. However, because of the absence of statistically significant correlation between the number of samples and the number of events, it is feasible that regardless of an increase in the number of samples analysed, the number of LADs will not change consistently with relative increases in sampling. If the number of FADs increases, then the number of LADs must also increase, unless all the newly discovered taxa extend up until the recent. Also, a further possibility is that FADS do not increase, but do get pushed further back in time by improved sampling of older units.

Since the publication of Jaramillo et al. (2011) and as a result of an intense exploratory program, Ecopetrol S.A have drilled several exploratory wells and rock cores in the Llanos Foothills and Eastern Llanos. As a result, thousand of samples have been analysed for palynology by the Biostratigraphy team of the Instituto Colombiano del Petroleo. The main objective of the present chapter is to incorporate and integrate all this new palynological information into a revision of the scheme proposed by Jaramillo et al. (2011) with the objectives of: (1) Adding new biostratigraphic events; (2) Improving the stratigraphical resolution of the zonation; and (3) Establishing the temporal framework for the new sections.

I predominantly used Graphic Correlation to incorporate the new sections to the rounds of correlation performed in the Jaramillo's scheme. Also, a data mining technique known as Association Rules Analysis (AR) was explored in an attempt to subdivide the biozone T6-Spinizonocolpites grandis. This zone spans from 38 to 48 Ma (middle Eocene) (Figure 1.5) and is particularly relevant because the most important oil reservoirs in the Llanos basin and Eastern Cordillera basin were deposited during this time interval (Reyes-Harker et al., 2015), and although this biozone is one with the highest number

of events it is also the largest in duration (Figure 1.5). Subdivision of T6 would allow among other things, a more precise temporal framework for the reservoir units in the Llanos and Eastern Cordillera basins. The aim of the Association Analysis is try to discover interesting and useful patterns hidden in large datasets (Han et al., 2012). This technique has been mainly used in market basket analysis (Hahsler et al., 2011) where the analysis of commercial transactions made by customers has revealed for example which products are buy together by customers. However the concepts of Association Analysis are easily applicable to biostratigraphic data such as those presented here. This is a very promising area of research that may complement of the traditional quantitative biostratigraphic techniques. To my knowledge Association Rules have been not previously applied to biostratigraphic problems.

1.2 Methods

1.2.1 Biostratigraphy

Biostratigraphy is a sub-discipline of stratigraphy that deals with the distribution of fossils in the stratigraphic record and the organization of strata into units on the basis of their contained fossils (Murphy and Salvador, 1999). Its main goal is the study of the geometry, biotic composition and time relations of fossiliferous rocks (Foote and Miller, 2006). The fundamental data for many approaches in biostratigraphy are the First and Last appearance data (FAD and LAD respectively), which represent events of appearance and disappearance of a taxon in a specific stratigraphic section. In this sense, FADs and LADs represent local events. The main objective of biostratigraphy is to determine the most likely sequence or order of events by using information from multiple taxa across multiple sections. Because fossil events are the result of the evolution of life on Earth, they reflect actual biological events and differ from most physical events in that they are unique, non-recurrent and irreversible (Gradstein 2004). For this reason, Biostratigraphy has long been recognized as an important tool in deciphering the temporal relations of rock units (Edwards 1984). One of the most important features to make an event a useful biostratigraphic data is its traceability. It must be recognized in several sections and its position in relation with other events should be consistent. However, most microfossil groups show an inverse relation between the cumulative frequencies of event occurrences versus the number of sections (Gradstein 2004). None of the events generally occur in all the sections and the common situation is that most of the events occur only in a few sections. This behaviour is an indicator of poor traceability. Reasons for

poor traceability also include: inadequate sampling effort (the probability of detecting events increases with the number of samples); the time and experience of the examiner of each sample (a routine examination yields fewer taxa and events than may be detected with a more dedicated approach); lateral variation in sedimentation rate (which influences the relative abundance of taxa in coeval samples); and lateral facies changes (which produce artificial LADs or FADs in stenotypic taxa).

1.2.2 Quantitative Biostratigraphy

Traditionally, biostratigraphic zonations have been produced "by hand", in a mental exercise where the biostratigrapher try to order a sequence of events according to their experience and knowledge. This approach is feasible when only data for a couple of sections is analysed and few events are interpreted. When the number of sections and events increases, this exercise becomes impossible to conduct rigorously. Therefore, several quantitative biostratigraphic methods have been developed during the last 50 years. These methods are essentially statistical in nature because of the large uncertainties commonly associated with positioning of biostratigraphic events (Agterberg et al., 2013). For example, it is common to find that the relative position of two events is interchangeable. Suppose the hypothetic case of two taxa (A and B) found in three sections (1,2 and 3). In this case, it is possible to think at least in three possibilities: (1) In the section 1 the LADs of A and B occur at the same stratigraphic level; (2) In section 2, the LAD of A is stratigraphically higher than the LAD of B; and (3) In section 3, the LAD of B is stratigraphically higher than the LAD of A. In this scenario is difficult to figure out the temporal sequence of events. The chance of finding the LAD of A before the LAD of A is the same that the chance of finding the LAD of B above the LAD of A. The third section does not provide information to break the argument because the LAD of both species was found at the same stratigraphic level. Surely, this situation is even more complicated when the number of taxa and samples increases.

There are two principal approaches in quantitative biostratigraphy: deterministic and probabilistic (Figure 1.7). The deterministic methods such as Graphic Correlation (Edwards 1984) seek the total range of taxa and assume that inconsistencies in the stratigraphic range of a taxon are due to missing data (Figure 1.7). Probabilistic methods such as Ranking and Scaling (RASC) (Agterberg and Gradstein, 1999) calculate the most probable or average range of taxa accompanied by an estimate of its stratigraphic uncertainty. Inconsistencies in the probabilistic approach are explained as the result of random deviations from the average stratigraphic ranges of taxa

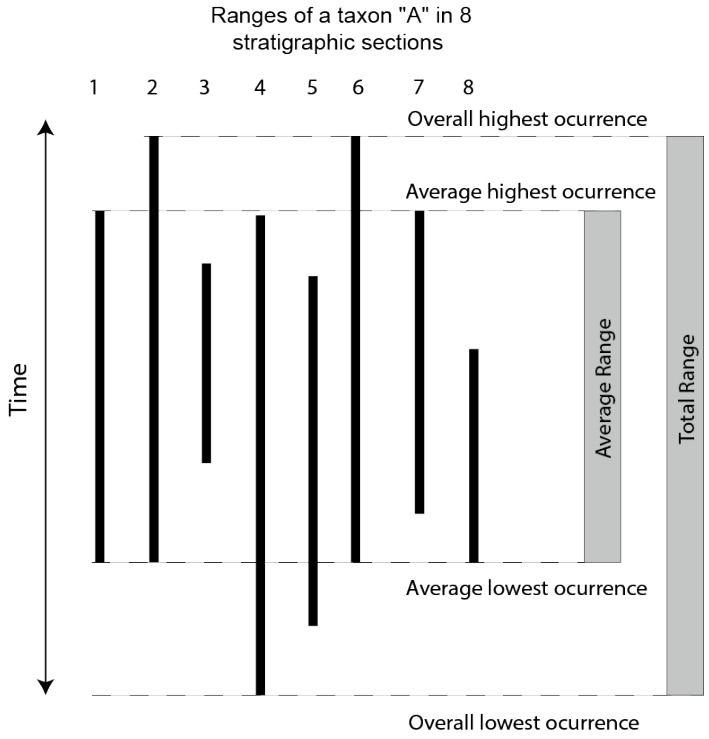

Figure 1.7: Probabilistic and deterministic methods in quantitative Biostratigraphy. Deterministic methods (e.g. Graphic Correlation) seek the total range of taxa while probabilistic methods (e.g. RASC) calculate the most probable range of taxa.

(Gradstein 2004) (Figure 1.7).

1.2.2.1 Graphic Correlation

Among the deterministic methods, graphic correlation (GC) is the best known. GC is used to establish a total composite or composite range for each taxon based on all available stratigraphic sections (Hood 1986). The technique is an extension of the work of Shaw (1964) and involves the representation of biostratigraphic and other data by the two axes of a bivariate graph. Horizons having a unique correspondence between two sections are displayed as points in the graph (Figure 1.8) and generally represent observed biostratigraphic events, although other potential horizons like paleomagnetic reversals, bentonites and lithologically or geochemically distinctive markers can be included. Because the points represent isochronous horizons, their trend defines the correlation between the sections (Hood 1986) (Figure 1.8). This line of trend is called Line of Correlation (LOC) and the placement of this line

is the crucial step in defining the temporal relationships among stratigraphic sequences. This is by far the most important and potentially difficult task of the GC technique. The position and slope of the LOC is totally controlled by the rock record of the sections, and for that reason they will vary depending on stratigraphic completeness and sedimentation rates.

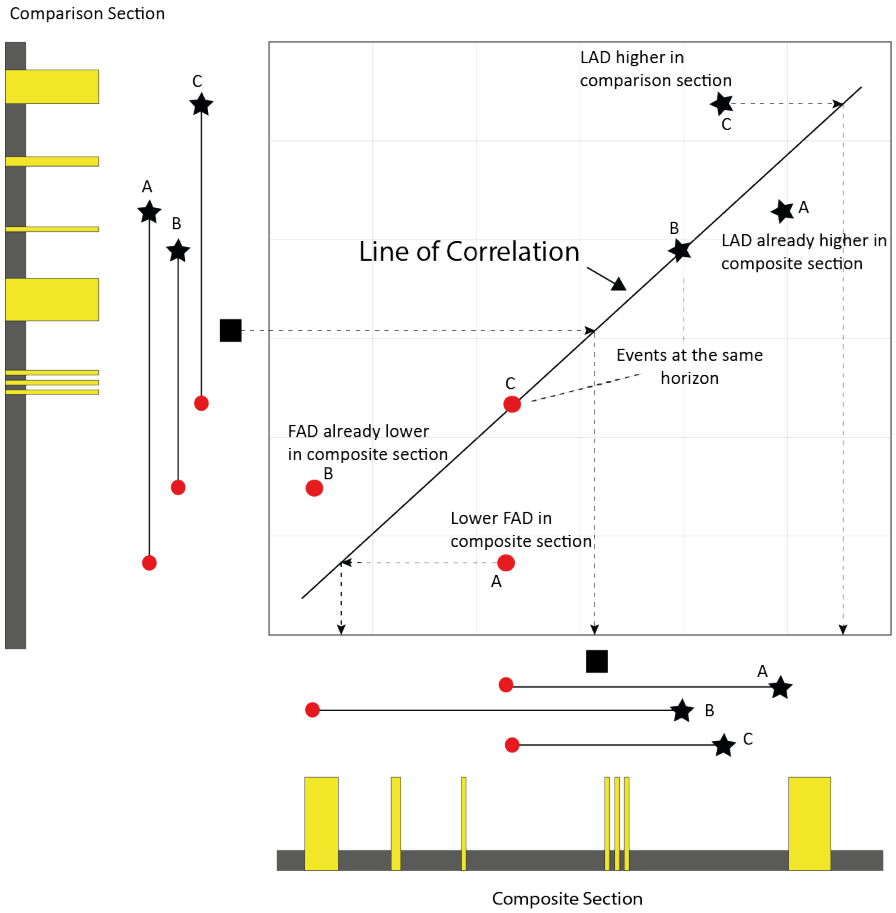

Figure 1.8: In Graphic Correlation two sections are compared using the representation of biostratigraphic and other data by the two axis of bivariate graph. Horizons having a unique correspondence between the two sections are displayed as points in the graph. In this example the FAD and LAD of three shared species are used to trace a line of correlation that define the temporal or stratigraphic relationship between the two sections. New taxa (black square in the comparison section) can be extrapolated to the composite section using the line of correlation.

In cases where only one or two segments are needed, the trace is relatively simple and implies a constant ratio of sediment accumulation between

the two sections. For sections with varying ratios of sedimentation rates or with hiatuses of different lengths, multiple line segments with different slopes (doglegs) are needed. When multiple lines are required, is more difficult to construct the LOC because many alternate choices of line slope and number of lines exist (Edwards 1995). In this case, the use of statistical methods has been suggested to automatically produce the LOC. These methods include principally: Least Squares (Shaw 1964), Constrained Optimization (Kemple et al., 1995) and Genetic Algorithms (Zhang et al, 2007). However, the statistical methods have some problems. The Least Squares methods have problems when doglegs are needed because choosing the position of each line introduces subjectivity (Edwards 1995). In Constrained Optimization, a simulated annealing is used to estimate the optimal position of the LOC that in this case is a piecewise correlation curve instead of a straight line. With this approach, the LADs and FADs position of every taxon on both sections are optimized creating a large number of unknown controlling parameters that makes the method computationally intensive and slow (Zhang et al., 2007). The Genetic Algorithms approach (Zhang 2000) integrates artificial intelligence techniques (Genetic Algorithms) with classic Least Squares Regression to optimize the LOC. In this method it is necessary to specify the start and end points of each line segment as well as the number of segments for the LOC. This technique could be problematic in situations where a high number of events are used in the rounds of correlation. The technique traces the LOCs based on the position of all the events, giving them equal weight in the correlation. Sections influenced by caving and reworking are problematic because FADs and LADs are increased artificially. This increase will be reflected in the correlation.

Additionally and as pointed by Edwards (1984), the proposed statistical methods are inappropriate at least for three reason: (1) Some points on the graph more nearly represent time equivalences than others; (2) The biostratigraphic implications of FAD and LAD events are quite distinct and (3) Sedimentological details may offer insights into the LOC, and therefore constrain its position. For these reasons, some GC users prefer to trace the LOC manually because in this way it is possible to incorporate the experience and geological knowledge into the interpretation. In this study I traced the LOC manually, finding several advantages. In sections with poor information (low number of events) was possible to use information from the nearby sections and by using for example lithological information (from well logs) was possible to establish lithological correlations that were used to support the trace of the LOC.

Once the line of correlation has been established for a pair of sections, the relative sequence of events can be compared and this relationship is used to

build a hypothetical Composite Section (CS). The building of the CS begins with the selection of the most complete section available (Standard reference Section (SRS)) against which all other sections will be compared. The choosing of which axis of the graph (horizontal or vertical) is used for the SRS, and which for the comparison section is simply matter of convenience and the results are geologically and mathematically equivalent (Hood 1986). When the composite section is display on the X-axis (Figure 1.8), the LADs that plot below the LOC are lower in the SRS than in the comparison section. These events are adjusted in the composite section by projecting their position upward the LOC. The LADs that plot above the LOC are already higher in the SRS and are not adjusted. FADs that plot above the LOC are higher in the SRS than in the comparison section and are adjusted in the CS by projecting their position in the LOC. The FADs that plot below the LOC are already lower in the SRS and are not adjusted. Taxa that are in the comparison section but not in the SRS are added into the composite by projecting them to the LOC (Figure 1.8). The positions of the events in the inference section are updated iteratively until a maximum and stable composite section is obtained. After data for all the available sections are incorporated to the SRS it becomes the CS. The CS represents a chronostratigraphic model incorporating the composite ranges of all the taxa included in the project (Hood 1986).

1.2.2.2 Association Rules Analysis

Mining frequent patterns and Association Rules Analysis (AR) are methods used in the analysis and discovery of interesting relations between variables in large databases (Hahsler et al., 2005). AR have been mainly used in market basket analysis, where the habits of buying consumers are analysed in order to find associations between different items that customers buy. The discovery of these associations can help for example to gain insight into which items are frequently purchased together by customers and this knowledge can then be used to design marketing strategies (Han et al., 2012). A typical example corresponds to the analysis of the items or products purchased in different transactions by clients in a supermarket (Table 1.4).

In this case, the first client for example bought Milk, Bread and Cereal (this operation is called a transaction). A second client bought Bread and Eggs (transaction 2), the third client bought Bread and Fruits (transaction 3) and so on (Table 1.4). The manager of the supermarket benefits from learning the buying habits of their clients, for example he might wonder: Which groups of products are customers likely to purchase on a given trip to the supermarket? or What is the frequency in which customers purchase

Table 1.4: Example of market basket analysis in which products (or items) are bought by costumers in different transactions. The first transaction corresponds to a customer buying Milk, Bread and Cereal.

Client	**Transactions**	**List of items**
1	1	Milk,Bread, Cereal
2	2	Bread,Eggs
3	3	Bread, Fruits
4	4	Milk, Bread, Eggs
5	5	Milk, Fruits
6	6	Bread, Fruits
7	7	Milk, Fruits
8	8	Milk, Bread, Bread, Fruits, Cereal
9	9	Milk, Bread, Fruits

Bread, Milk and Cereal in the same transaction? This is the type of question in which association rules and frequent pattern mining methods can help to answer.

The concept of AR in market basket analysis can be easily extrapolated to the information obtained in palaeontological studies and more specifically information from micropalaeontology and biostratigraphy where thousand of samples and species are generally recorded. The example presented in Table 1.4 can be redefined in palaeontological terms. The samples and species recorded in a paleontological study are the equivalent of transactions and items respectively. Table 1.5 shows a hypothetical example of ten samples belonging to the biozone B1, where the sample M1 records the presence of the species A, B and E.

In this case, the sample M1 can be interpreted as a transaction and the presence of the species as the items/products found/purchased on that specific sample/transaction. In this way it is possible to make some correspondences in terminology being transactions the equivalent of samples and items/products the equivalent of species. As in the case of the manager in the market basket example, AR in palaeontological data can help the biostratigrapher or palaeontologist to gain insight into which species are frequently found together in samples that share a common attribute, like for example a biozone, an environment of deposition or whatever attribute is of interest to the researcher.

From the palaeontological point of view, it is possible to think about the statistical universe as the set of species recorded in all the samples and each species is a Boolean variable representing their presence or absence. Each

Table 1.5: Example of market basket analysis in a paleontological context. The samples in the biozone B1 can be seen as the equivalent of transactions and the species recorded in the samples can be seen as the list of items or products.

Biozone	**Sample**	**Transaction**	**List of items (Species)**
B1	M1	1	Sp.A, Sp.B, Sp.E
B1	M2	2	Sp.B, Sp. D
B1	M3	3	Sp.B, Sp.C
B1	M4	4	Sp.A, Sp.B, Sp.D
B1	M5	5	Sp.A, Sp.C
B1	M6	6	Sp.B, Sp.C
B1	M7	7	Sp.A, Sp.C
B1	M8	8	Sp.A, Sp.B,Sp.C, Sp.E
B1	M9	9	Sp.A, Sp.B, Sp.C

sample can then be represented by a Boolean vector of values assigned to these variables (Han et al., 2012). The Boolean vectors can be analysed for association patterns reflecting species that are frequently found together. These patterns can be represented in the form of association rules (Tan et al., 2014). For example, the information that samples with presence of Sp.A also tends to have the presence of Sp.B can be represented by the association rule: $Sp.A => Sp.B$.

The number of rules and patterns from a large transaction data set can be very extensive and therefore computationally expensive. Additionally, some of the discovered patterns can be spurious because they may occur simply by chance (Tan et al, 2014). In order to select interesting and predictive rules from the universe of all the possible rules, three measures of significance and interest can be used.

- **Support** The support supp (X) of an itemset X is defined as the proportion of transactions in the dataset that contain the itemset and reflects therefore the usefulness of the rule (Hahsler et al., 2005). In the example of the Table 1.5, the itemset [Sp.A, Sp.B] has a support of $4/9 = 0.44$. This number means that 44% of the samples under analysis (4 out of 9) show Sp.A and Sp.B occurring together. A rule that has very low support may occur simply by chance.

- **Confidence** The confidence (conf) measures the reliability of the inference made by a rule and determines how frequently items in Y appear

in transactions that contain X (Tan et al., 2014). It is defined as: conf (X => Y)= supp (XUY)/supp (X). In the example of Table 1.5 the confidence for the rule [$Sp.A$] => [$Sp.B$] is 4/6= 0.66, which means that 66% of the samples containing Sp.A also contain Sp.B.

- **Lift** Han et al. (2012) demonstrated that confidence could be deceiving because it does not measure the real strength (or lack of strength) of the correlation between items in a rule. Additionally inferences made by association rules do not necessarily imply causality (Tan et al., 2014). Lift can be regarded as measure of correlation between items. The occurrence of itemset A is independent of the occurrence of itemset B if P(AUB)=P(A)P(B); otherwise itemsets A and B are dependent and correlates as events (Hastie, 2008). The lift between the occurrence of two items A and B can be measured as: *lift* (A,B) = P(AUB)/P(A)P(B). If the value of lift is less than 1, then the occurrence of A is negatively correlated with the occurrence of B, meaning that the presence of one of them likely indicates the absence of the other one. If lift is greater than 1, then A and B are positively correlated, meaning that the presence of one implies the presence of the other. If lift is equal to 1, then A and B are independent (Han et al., 2012). In the example of the Table 1.5, is possible to calculate the lift for the rule $Sp.A$ => $Sp.B$ by constructing a contingence table (Table 1.6), where Sp.B (in italic) refer to samples of the Table 5 that do not contain Sp.B. and Sp.A to those that do not contain Sp.A. From the Table 1.5, the probability of finding Sp.A is P (Sp.A)= 0.60; the probability of finding Sp.B is P([Sp.B])=0.70; and the probability of finding both is P([Sp.A, Sp.B])=0.40. By Eq. (1), the lift of the rule $Sp.A$ => $Sp.B$ is P ([Sp.A, Sp.B])/(P ([Sp.A]) X P ([Sp.B])) = 0.40/(0.60x 0.70)= 0.95. Because this value is less than 1, there is a negative correlation between the occurrences of [Sp.A] and [Sp.B].

Table 1.6: Contingency table to calculate the lift of the rule $Sp.A$ => $Sp.B$ (see text for explanation).

	Sp.A	*Sp.A*	**Sum row**
Sp.B	4	3	7
Sp.B	2	0	2
Sum col	6	3	9

Typically, association rules are considered interesting if they satisfy both a minimum support threshold and a minimum confidence threshold (Leskovec

et al., 2014). Lift on the other hand assesses the degree to which the occurrence of one item lifts or increases the likelihood of the occurrence of another item.

The basic algorithm for mining the simplest form of frequent patterns is called Apriori. This is a seminal algorithm proposed by Agrawal et al.(1994) for mining frequent item sets. Its name is based on the fact that the algorithm uses prior knowledge of frequent item sets properties (Han et al., 2012). It employs an iterative approach known as level-wise search, where k-itemsets are used to explore (k+1)-itemsets. The basic operation of Apriori is very well explained in Han (2012) and the example is partially reproduced in Figure 1.9 by using the data of Table 1.5.

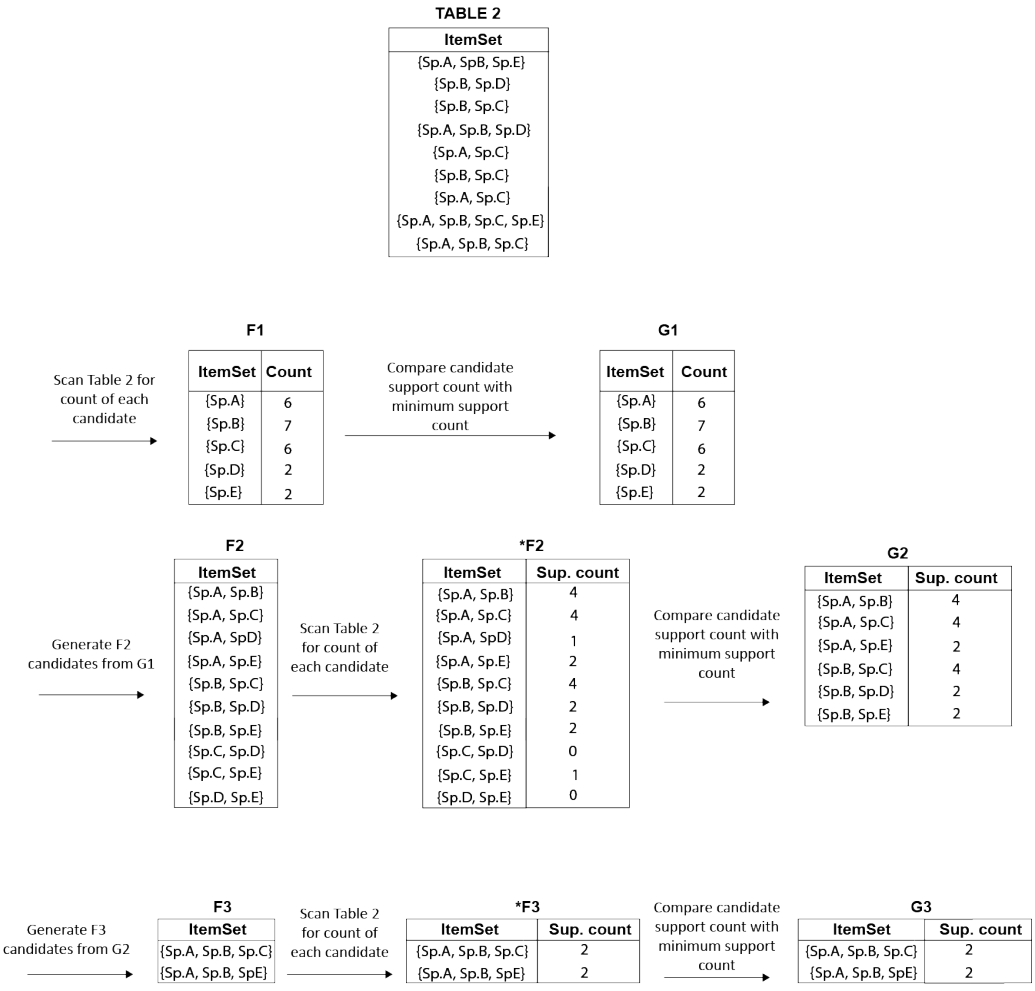

Figure 1.9: Example of the approach used by the Apriori algorithm (Agrawal et al., 1994) for the mining of frequent item sets (see text for details).

The first step in Apriori is to calculate the accumulative count for each item by scanning the data in the Table 1.5 as is presented in F1 (Figure 1,9). Those items that satisfy the minimum support are then collected in G1. In this example the minimum support was set in 0.2 meaning that only the items found in 20% of the transactions are used in the analysis. Because all items satisfy the minimum support, F1 is equal to G1 and represents the set of frequent 1-itemsets. To discover the set of frequent 2-itemsets, the transactions in Table 1.5 are scanned and the support count of each candidate item set in F2 is accumulated as is shown in *F2. The set of frequent 2-itemsets consist of those candidates in *F2 having minimum support. The same operation is repeated until no more frequent k-items can be found. In order to improve the efficiency of the generation of frequent itemsets, a property called the Apriori is used to reduce the search space (Han et al., 2012). This is an anti-monotocity property in the sense that if a set cannot pass a test, all of its supersets will fail the same test as well. If an item set L does not satisfy the minimum support threshold, then L is not frequent. If an item A is added to L, then the resulting item set cannot occur more frequently than L.

1.3 Materials

1.3.1 Biostratigraphy

Forty-seven new sites were incorporated to the 63 sites previously analysed in the Jaramillo 's Graphic Correlation project (included in the Annex 2 of the supplementary material of Jaramillo et al. (2011)) (Table 1.14) (Figure 1.10). The new sites are located along the Llanos, Llanos foothills and Catatumbo basins. Forty-five of them correspond to oil wells with different types of samples used in the analyses (ditch-cuttings, sidewall cores, cores, and core-chips) (Annex 1.1). The other two sections (Cano las Blancas and Cano Sagu) were measured at outcrops in the Llanos foothills close to the towns of Akacias and Villavicencio. The master taxonomic dictionary used in the Jaramillo 's zonation was updated by adding the new species found in the new sections. In addition to the 372 taxa used by Jaramillo et al. (2011), 58 additional taxa were included, of which 43 are new species and 15 are formal taxa that were already in the Jaramillo 's dictionary but were not included in their zonation because they were present only in one sample prior to the addition of new sites here. The selection of the new taxa followed the same line of reasoning of the Jaramillo's scheme: they are morphologically distinct, relatively common and have ranges that are constrained stratigraphically.

Ideally they should be present in more than one sample, however some taxa found in one single sample were very morphologically distinct, such that it is noteworthy to include them in the zonation in order to track their record in future new sites. Informal species are denoted by quotation marks (e.g. *Bombacacidites "gemmatus"*) and they are described in the Systematic Palynology Section (Annex 1.7). The Graphic Correlation analysis was done using the software GraphCor (Hood 1986). The spreading parameter (SP) was recalculated for species occurring into two or more sections (including wells and outcrops). This parameter evaluates the degree of confidence in the position of a datum in the composite section (Jaramillo et al., 2005). For each FAD, the spreading parameter = (oldest FAD in composite units − youngest FAD in composite units) / 50. For each LAD, the SP = (oldest LAD in composite units − youngest LAD in composite units) /50. The number 50 in the denominator represents 50 feet in the reference section and is indicative of the level of precision expected when drillers are trying to determine the top of a formation in the Llanos Foothills (Jaramillo et al., 2011). The calibration of the new sequence with the standard geological timescale was done by using the calibration points used by Jaramillo et al. (2011) (Table 1.2).

1.3.2 Association Rules Analysis

The AR was done in samples corresponding to the Biozone T6 (38-48.6 Ma). Thirty-three (33) sites with a total of 551 samples (Table 1.7) were used in the analysis. As a first approach, all the samples were analysed together and then the analysis was applied to the same group of samples but divided in two groups. The first group was made up of samples with ages between 38 and 43.3 Ma and the second one with ages between 43.3 and 48.6 Ma. The objective was to determine if it is feasible to find different rules for each group. If a different set of rules were found in each group, such rules could be used to separate and increase the biostratigraphic resolution of the Biozone T6.

Of the 773 taxa recorded in all the samples, 198 were selected for analysis, leaving out of the analysis, informal taxa and those that were not present in at least 3 sites. Each sample was considered as a transaction and the species recorded in the samples as items. The data was represented as a sparse matrix and organized in a horizontal data format following the recommendations in Hahsler et al. (2011). The Apriori algorithm included in the R package arules (Hahsler et al., 2015) was used for the analysis. For exploration and visualization purposes, a matrix-based visualization technique included in the R package arulesViz (Hahsler et al., 2015) was used.

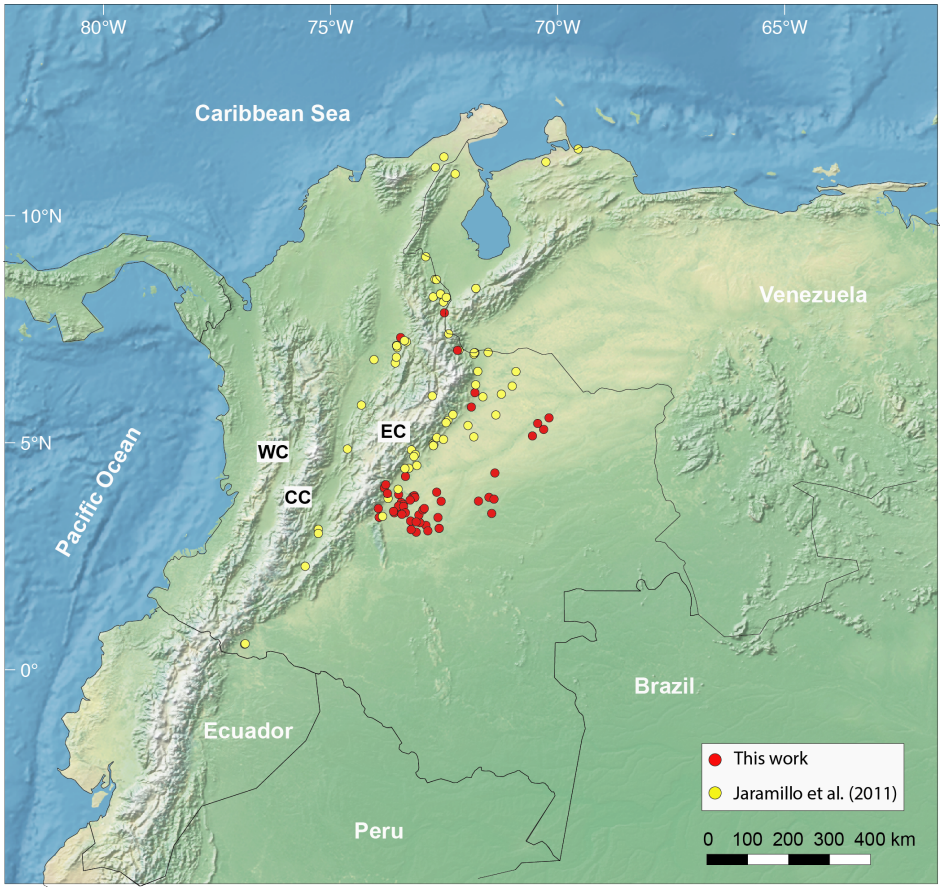

Figure 1.10: Map of sections (wells and outcrops) incorporated to the sites previously analysed in Jaramillo's Graphic Correlation project (Jaramillo et al., 2011).WC: Western Cordillera; CC: Central Cordillera; EC: Eastern Cordillera.

This technique organises the antecedent and consequent itemsets (species in this case) on the x and y axes respectively. The antecedent and consequent makes reference to the right and left side of a rule respectively. A selected interest measure (in this case support) is displayed at the intersection of the antecedent and consequent of a given rule. If no rule is available for the antecedent/consequent combination the intersection area is left blank.

Table 1.7: List of sites, number of samples and age of the samples used in the Association Rules Analysis.

Section	**Samples**	**From Age**	**To Age**
Aga-1	28	44.43	38.10
Bue-3Cor	33	46.70	41.11
Cano las Blancas	19	42.40	38.02
Cano Sagu	32	42.43	38.11
Chac-1	22	40.62	38.08
Concentracion	3	42.08	38.51
Cop-1	4	48.47	47.23
Cor-1	5	48.6	42.08
Cus-5	35	47.43	41.9
Flo-C3	9	47.70	38.26
Fon-1	4	40.74	38.77
Gib	22	47.36	38.09
Gon-1	11	48.51	41.33
Gonzales	12	46.50	38.42
Gua-2	14	47.83	38.56
Medina	24	48.37	38.11
Muc-3	13	47.76	38.59
Nuesp-1	8	44.14	38.71
Pac-1	1	38.14	38.14
Past-4	29	42.15	38.08
Pau-C2Fz	1	44.16	44.16
Pum-1	37	45.26	38.06
Regadera	4	45.44	41.37
Reg-1	36	48.6	38.09
RieMacheRull	7	48.148	39.96
RioCh-1	34	45.42	38.20
Rio Loro	2	39.20	38.46
Ros-1	5	48.31	38.85
S-17	11	41.00	38.03
SanJ-1	3	39.70	38.52
Tib-182/187	18	47.95	38.92
Uribe	18	48.02	38.19
Zul-1	47	48.57	42.84

1.4 Results and Discussion

1.4.1 Biostratigraphy

The complete session of the Graphic Correlation includes Jaramillo 's section (Jaramillo et al., 2011) and the ones used in this work. The equations of the lines of correlation (LOC) versus the composite section are presented in Annex 1.2. Each pair of points corresponds to the end points of a segment of the LOC with the first column corresponding to comparison section and the second column to the composite section. An example for Rub-79 is presented in Figure 1.11.

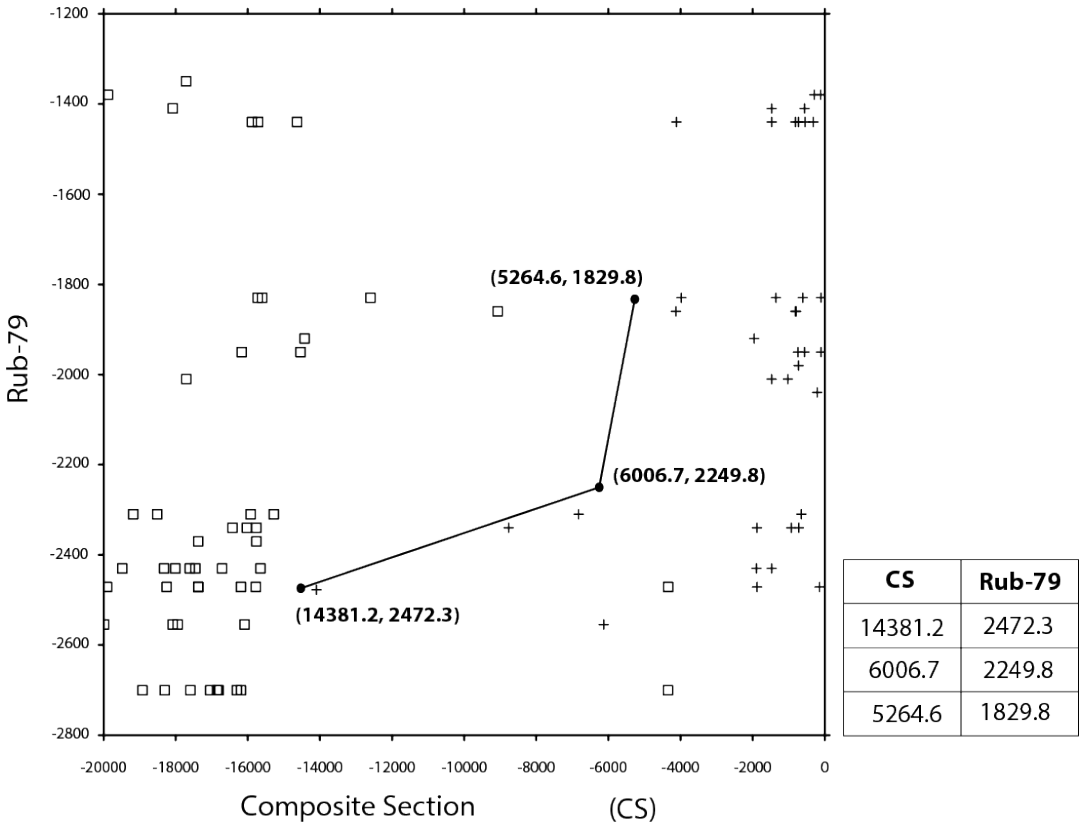

CS	Rub-79
14381.2	2472.3
6006.7	2249.8
5264.6	1829.8

Figure 1.11: Equations of the line of correlation (LOC) for Rub-79. Each pair of points corresponds to the end points of a segment of the LOC. The first column corresponds to the comparison section (Rub-79) and the second column to the composite section (CS).Squares and crosses represent FADs and LADs respectively.

The final sequence of events can be found in the Annex 1.3 with taxa

separated into three categories. The first category contains 515 events already present in Jaramillo's zonation (Jaramillo et al., 2011). The second category contains information about 38 new informal taxa representing 43 events and the third category contains information about 11 formal species representing 15 events that were included in this work. Information about the position of each event in composite units and million of years is presented, as well as the number of sites where the event was found and their spreading parameter. In order to track changes in the positions of the events as a consequence of the inclusion of the new sections and taxa, the values from Jaramillo's original work and the values obtained based on this study are both presented and the differences highlighted. Annex 1.4 contains the list of all the events presented in chronological order. The taxa in categories two and three are highlighted with one and two asterisk respectively to easily visualize their position in the final sequence of events. Annex 1.5 includes the FAD and LAD of each taxon in every section used in the analysis (Annex 1.5 can be solicited to the author).

The composite section obtained in this work was compared with the sequence obtained by Jaramillo et al. (2011) (Figure 1.12).

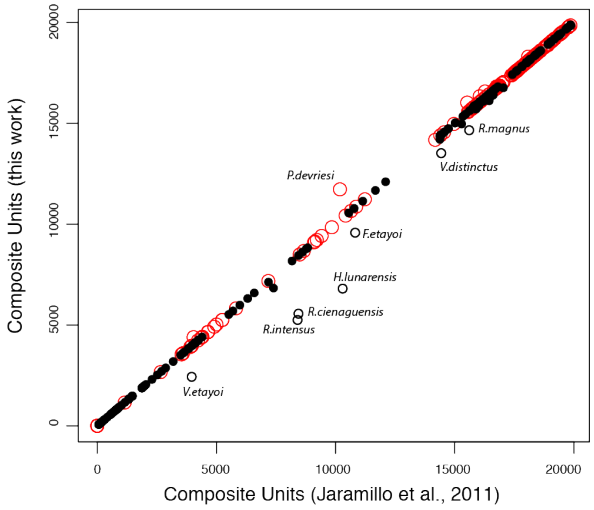

Figure 1.12: Comparison between the Graphic Correlation sequence produced by Jaramillo et al. (2011)(black points) and the Graphic Correlation sequence obtained in this work (red points).

Aside from the new taxa, there is an almost perfect correspondence in the position of the events, with exception of 32 from a total of 502 events whose ranges changed very little. For LADs, the largest difference was found in the position of *Retitrescolpites magnus* with a difference of 6.1 Ma, and the

smallest was found for event dinocyst acme C2 with a difference of 0.02 Ma. For the FADs the largest difference was found for *Bombacacidites echinatus* with a difference of 3.45 Ma, and the smallest was found for *Multimarginites vanderhammenii* with a difference of 0.05 Ma. The complete list of changes is presented in Table 1.8.Of the 32 events, only 10 change their position to a new biozone, however these changes were not very significant since all the events only change from their original biozone to the previous or the next one (Figure 1.13). The results can be considered a good indicator of the reliability of the events used in Jaramillo 's zonation because despite adding a considerable number of new sections (47 in total) and thousand of new samples, the majority of events did not change their position in the composite section.

The new taxa incorporated into this work include 11 formal species representing 15 events (Table 1.9) (Figure 1.14). Three of these species (*Bombacacidites araracuarensis*, *Psilatriletes peruanus* and *Retitricolpites caquetanus*) were originally described by (Hoorn 1994a; Hoorn 1994b). *B. araracuarensis* and *R. caquetanus* were found in sediments of the Caqueta River area (Amazonas Basin, Colombia) while *P. peruanus* was found in sediments from the upper Amazon River area. All three were interpreted as a part of the Retitricolporites and Psiladiporites-Crototricolpites pollen zones that correspond to the early Miocene and early to middle Miocene (Hoorn 1993). In the present study, *Bombacacidites aracuarensis* occurs in eight sites (Annex 1.5) and its range is between 17.41 and 2.22 Ma. *Psilatriletes peruanus* is present in six sites (Annex 1.5) with a range of 13.3-7.15 Ma and *R. caquetanus* is reported in 17 sites (Annex 1.5) with a LAD interpreted as occurring at 12.44 Ma (Figure 1.14).

It was not possible to establish the FAD of *R. caquetanus* because it was recorded only in ditch cutting samples. Six species, *Polypodiisporites amazonensis*, *Cingulatisporites laevigatus*, *Pteriadicites gemmatus*, *Margocolporites fastigiatus*, *Polypodiisporites planus* and *Ctenolophonidites suigeneris* were originally described by Silva-Caminha et al. (2009) in a study of two cores drilled east of the Iquitos Arch (northwestern Brazil).

Although the age of the two cores was interpreted as late Miocene-early Pliocene, Silva-Caminha et al. (2009) suggested an age of Miocene to lower Pliocene in their systematics chapter, without any further reference about the chronostratigraphic range of the species. In this study, all but one of these species (*Margocolporites fastigiatus*) were reported in more than four sites (Annex 1.5). The LAD of five of the species falls within the biozone T18 that encompass the Pliocene and Pleistocene (Figure 1.14), and the range of *C. suigeneris* extends from T6 to T12 (middle Eocene-early Miocene) (Figure 1.14). Finally, *Psilatricolporites venezuelanus* and *Psilastephanocolporites*

Table 1.8: Change in the position of biostratigraphic events (composite units and million of years (Ma)) between the scheme of Jaramillo et al. (2011) (Jm) and the analysis in this work (tw).

Sp	**Event**	**UC (Jm)**	**UC (tw)**	**Ma (Jm)**	**Ma (tw)**	**Diff (Ma)**
B.echinatus	FAD	16265.8	16572.2	36.1	39.5	3.4
C.fossulats	FAD	16046.3	16336.0	33.7	36.9	3.1
F.spinosus	FAD	4039.3	4392.4	12,7	14,1	1,4
L.colombianensis	FAD	16755.3	16825	41.6	42.4	0.79
M.vanderhammenii	FAD	5001.3	5021.1	15.9	16	0.05
P.devriesi	FAD	10181.6	11722.4	18.8.	20.3	1.5
P.pachydermatus	FAD	15521.1	16022.8	30.38	33.61	3.23
R.simplex	FAD	18077.2	18302.4	55.8	57.1	1,3
C.dorogensis	LAD	14377	14197	23.03	22.8	0.18
C.eocenicus	LAD	16442.3	16113.5	38.1	34.4	3.7
C.undulatus	LAD	15285	14964	28.8	26.8	2
C.scabrata	LAD	7393.4	6826.6	16.9	16.7	0.2
dinocyst acme C2	LAD	7184	7122.3	16.8	16.8	0,02
E.trianguliformis	LAD	16068	16046	33.9	33.7	0.14
F.etayoi	LAD	10819.2	9572.4	19.4	18.1	1.2
H.lunarensis	LAD	10294	6800.1	18.9	16.6	2.2
L.vaneendenburgi	LAD	17038	16754.7	44.8	41.6	3.1
L.colombianensis	LAD	16194	16084.5	35.3	34.0	1.2
N.huertasii	LAD	15786	15774.8	32.09	32.02	0.07
P.perfectus	LAD	15999.2	15858.1	33.4	32.5	0.9
R.facilis	LAD	16278.5	16143.4	36.2	34.7	1.5
R.triangulatus	LAD	15794	15717.9	32.1	31.6	0.4
R.speciosus	LAD	16609.9	16394.6	40	37.5	2.4
R.baculatus	LAD	15896.5	15708.2	32.8	31.5	1.2
R.magnus	LAD	15604	14653.9	30.9	24.8	6.1
R.cienaguensis	LAD	8440.8	5556.5	17.3	16.2	1.1
R.intensus	LAD	8404.4	5244.9	17.3	16	1.2
S.grandis	LAD	16426	16384.8	37.9	37.4	0.4
V? distinctus	LAD	14429.1	13515.5	23.3	22.1	1.2
V. etayoi	LAD	3962	2426.5	12.3	6,6	5.7
V. reticulatus	LAD	16024.1	15927	33.6	32.9	0.6
Z. minor	LAD	16528.2	16339.5	39	36.9	2.1

Table 1.9: New taxa and events incorporated to the zonation (CU= Composite Units; SP=spreading parameter).

Sp	**Event**	**CU**	**Age (Ma)**	**Sites**	**SP**	**Author**
Bombacacidites araracuarensis	LAD	1471.5	2.2	7	131	Hoorn(1994)
Bombacacidites araracuarensis	FAD	8663.1	17.4	1	uncertain	Hoorn(1994)
Cingulatisporites laevigatus	LAD	102.5	0.14	4	90	Silva-Caminha et al.(2010)
Ctenolophonidites suigeneris	FAD	16805.6	42.2	1	uncertain	Silva-Caminha et al.(2010)
Ctenolophonidites suigeneris	LAD	6548.2	16.5	19	205	Silva-Caminha et al.(2010)
Margocolporites fastigiatus	LAD	204.9	0.28	1	uncertain	Silva-Caminha et al.(2010)
Polypodiisporites amazonensis	LAD	71.7	0,10	7	246	Silva-Caminha et al.(2010)
Polypodiisporites planus	LAD	1878.1	3.4	10	272	Silva-Caminha et al.(2010)
P. brevicolpatus	LAD	16346,9	37.04	5	8	Jaramillo and Dilcher (2001)
P. brevicolpatus	FAD	16849.7	42.7	2	5	Jaramillo and Dilcher (2001)
Psilatriletes peruanus	LAD	2661	7.1	6	259	Hoorn(1994b)
Psilatriletes peruanus	FAD	4148.4	13.1	1	uncertain	Hoorn(1994b)
Psilatricolporites venezuelanus	LAD	4114.9	13	14	239	Lorente (1986)
Pteridaceoisporis gemmatus	LAD	174.2	0.2	8	304	Silva-Caminha et al.(2010)
Retitricolpites caquetanus	LAD	3973.6	12.4	17	154	Hoorn (1994)

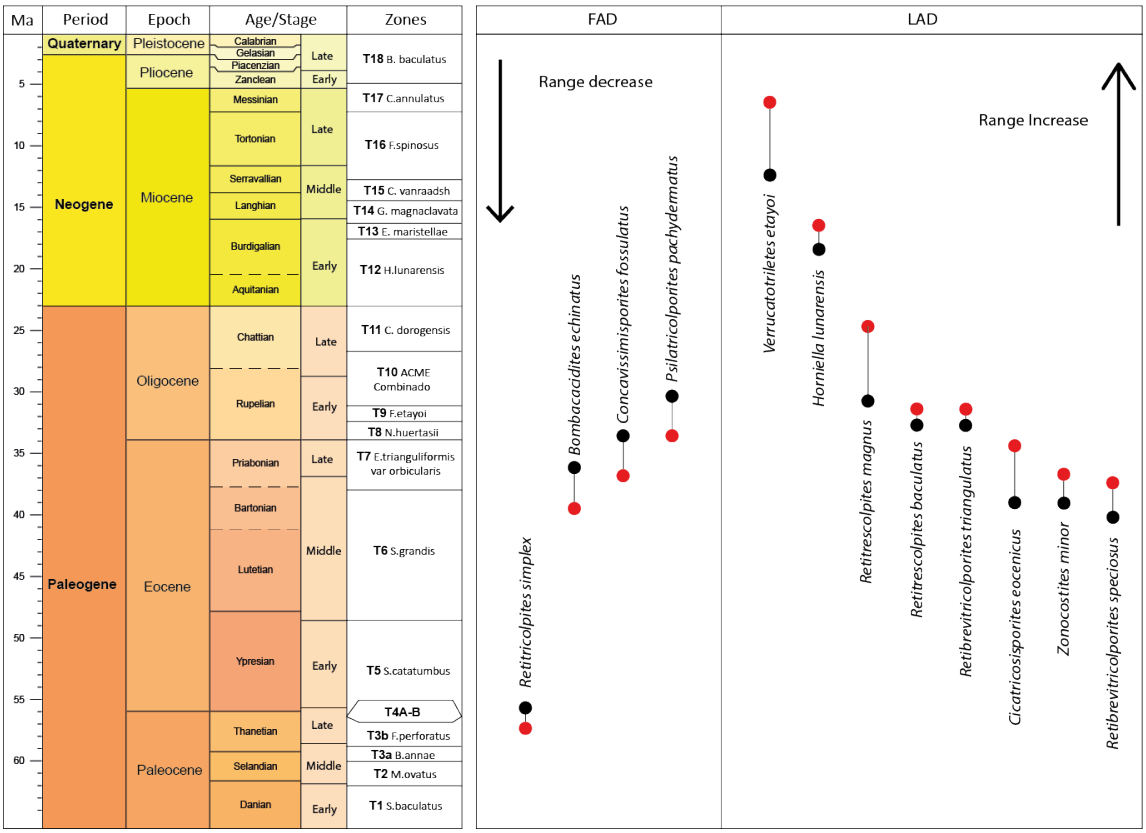

Figure 1.13: Change in the range of species from their position in Jaramillo's zonation (Jaramillo et al., 2011) to the previous or next biozone as estimated in this work. The low number of species showing small changes in their ranges is a good indicator of the reliability of events used in the zonation.

brevicolpatus were originally described by Lorente (1986) and Jaramillo and Dilcher (2001), respectively. The range of *P. venezuelanus* spans from the late Palaeocene (Rull, 1999) to the Miocene (Lorente 1986). In this study, *P. venezuelanus* was reported in 16 sites and its LAD was interpreted at 13 Ma. *P. brevicolpatus* was reported in five sites and their range spans from 42.7-37 Ma (Figure 1.14).

The new informal taxa correspond to 38 species representing 43 events (Annex 1.3 - Category 2). Twenty-two events were reported only in one site; however these species are morphologically very distinct and so are suitable to be recognized in new sites. The new events by biozone are:

- **Biozone T4B-PETM Interval**: 55.8 to 55.7 Ma
  - LAD of *Tetracolpites "quadrangularis"*: 18005.23 composite units

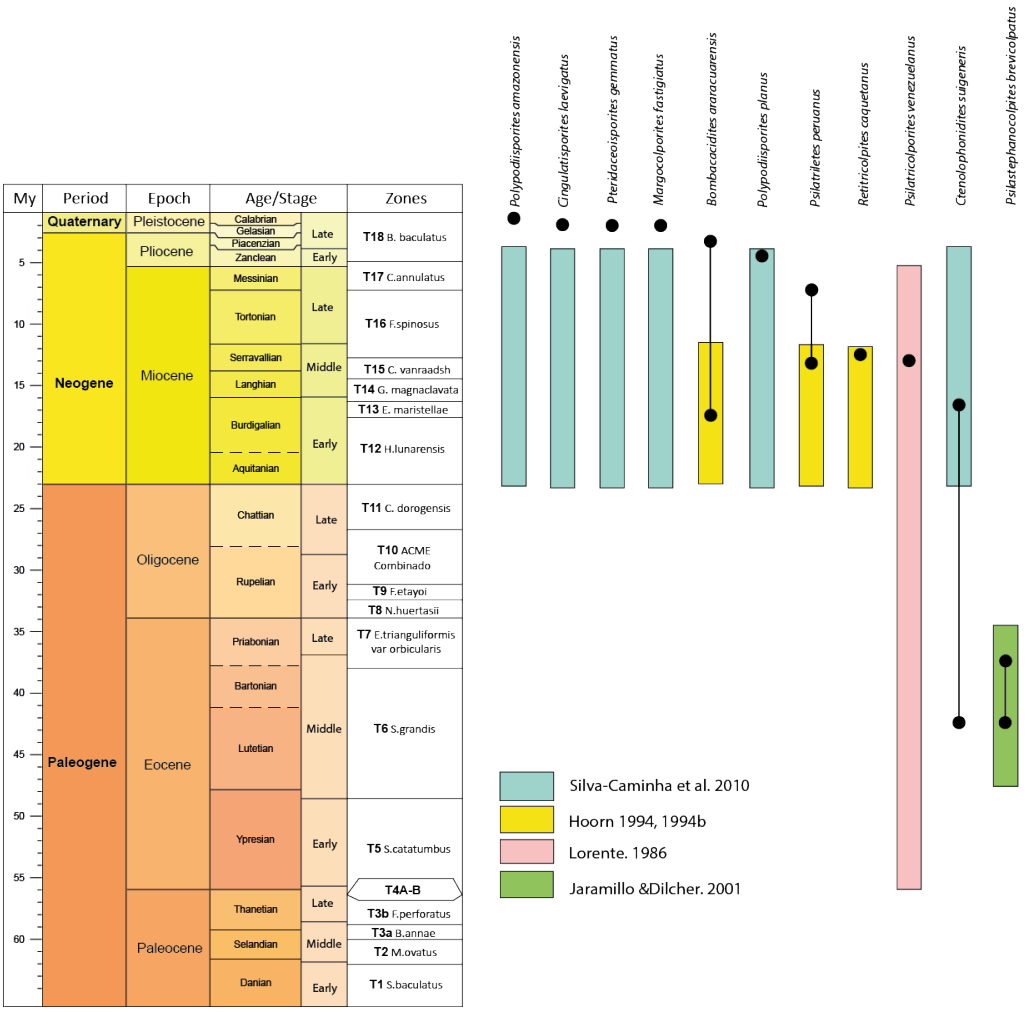

Figure 1.14: Range of the new taxa incorporated in this work (black dots). The boxes indicate the ranges estimated from the literature.

(CU), 55.7 Ma

- **Biozone T6-Spinizonocolpites grandis**: 48.6 to 38 Ma
  - LAD of *Retistephanocolpites "araucaensis"*: 16426.5 CU, 37.94 Ma
  - FAD of *Retitricolporites "magnificus"*: 16549.16 CU, 39.32 Ma
  - FAD of *Retitricolporites "uwaeorum"*: 17038 CU, 44.84 Ma
- **Biozone T7-E.trianguliformis var. orbicularis**: 38 to 33.9 Ma

  - LAD of *Clavatriporites "spicatus"*: 16113.5 CU, 34.41 Ma
  - LAD of *Gemmaperprolatoporis "teresitae"*: 16151.9 CU, 34.85 Ma
  - LAD of *Bombacacidites "gemmatus"*: 16259.8 CU, 36.06 Ma
  - LAD of *Retitricolporites "magnificus"*: 16383 CU, 37.45 Ma
- **Biozone T9-Foveotricolporites etayoi**: 32.1 to 31.5 Ma
  - LAD of *Psilabrevitricolporites "hoornii"*: 15727.24 CU, 31.71 Ma
  - LAD of *Bombacacidites "pulcherrimus"*: 15745 CU, 31.82 Ma
- **Biozone T10-Combined ACME**: 31.5 to 26.8 Ma
  - LAD of *Verrustephanocolporites "pastinensis"*: 15189.6 CU, 28.25 Ma
- **Biozone T11-Cicatricosisporites dorogensis**: 26.8 to 23 Ma
  - LAD of *Hexaporotricolpites "striatus"*: 14510 CU, 23.89 Ma
  - LAD of *Bombacacidites "verrucatus"*: 14547.3 CU, 24.13 Ma
- **Biozone T12-Horniella lunarensis**: 23 to 17.7 Ma
  - LAD of *Chomotriletes "zenueorum"*: 9572.3 CU, 18.19 Ma
  - LAD of *Echipollenites "magnificus"*: 10093.7 CU, 18.72 Ma
  - LAD of *Bombacacidites "concavoides"*: 10964.9 to 19.59 Ma
  - LAD of *Concavissimisporites "rugulatus"*: 13967.1 CU, 22.62 Ma
  - LAD of *Brevitricolporites "uwaeorum"*: 14132.47 CU, 22.78 Ma
  - LAD of *Clavainaperturites "grimsdaleoides"*: 14171 CU, 22.82 Ma
- **Biozone T13-Echitricolporites maristellae**: 17.7 to 16.1 Ma
  - LAD of *Echitricolporites "clipoechinatus"*: 5511.76 to 16.19 Ma
  - LAD of *Retistephanoporites "yariguensis"*: 6979.1 CU, 16.76 Ma

  - LAD of *Retitricolporites "magnoguianensis"*: 8404.38 CU, 17.31 Ma
  - LAD of *Zlivisporis "gibraltarensis"*: 8439.9 CU, 17.33 Ma

- **Biozone T14-Grimsdalea magnaclavata**: 16.1 to 14.2 Ma
  - FAD of *Echiperiporites "psilatus"*: 5021.1 CU, 16 Ma

- **Biozone T15- Crassoretitriletes vanraadshooveni**: 14.2 to 12.7 Ma
  - LAD of *Trichotomosulcites "scabrata"*: 4038.9 CU, 12.7 Ma
  - LAD of *Echiperiporites "psilatus"*: 4126 CU, 13.04 Ma
  - FAD of *Trichotomosulcites "clavatus"*: 4243.6 CU, 13.51 Ma
  - LAD of *Fossulotriletes "hermosus"*: 4314.63 CU, 13.79 Ma

- **Biozone T16- Fenestrites spinosus**: 12.7 to 7.1 Ma
  - LAD of *Rugutricolporites "etayoi"*: 2390.6 CU, 7.64 Ma
  - FAD of *Crassosporites "baculatus"*: 3537 CU, 10 Ma
  - FAD of *Liliacidites "titanicus"*: 3600.8 CU, 10.41 Ma
  - LAD of *Echiperiporites "magnoexinatus"*: 3884.6 CU, 11.97 Ma

- **Biozone T17- Cyatheacidites annulatus**: 7.1 to 4.8 Ma
  - LAD of *Trichotomosulcites "clavatus"*: 2063 CU, 5.53 Ma

- **Biozone T18- Bombacacidites baculatus**: 4.8 to 0 Ma
  - LAD of *Crassosporites "baculatus"*: 102.47 CU, 0.14 Ma
  - LAD of *Verrutriletes "ampullatus"*: 265.1 CU, 0.35 Ma
  - LAD of *Cingulatisporites "lorentae"*: 420.12 CU, 0.57 Ma
  - LAD of *Scabratriletes "bacataensis"*: 543.08 CU, 0.74 Ma
  - LAD of *Kuylisporites? "bicostatus"*: 563.57 CU, 0.77 Ma

- LAD of *Polypodiaceoisporites "verrucatus"*: 758.2 CU, 1.03 Ma
- LAD of *Psiladiporites "ecopetrolis"*: 866.3 CU, 1.18 Ma
- LAD of *Polypodiaceoisporites "interruptus"*: 892.19 CU, 1.21 Ma
- LAD of *TPolypodiaceoisporites "murilloi"*: 917.9 CU, 1.25 Ma
- LAD of *Polypodiaceoisporites "projectoradialis"*: 943.78 CU, 1.28 Ma

1.4.2 Association Rules Analysis

A total of 515 samples (transactions, by analogy with market basket analysis) and 186 species (items) were used in the analysis. Table 1.10 shows the element (species/samples) length distribution of the data, in which 31% of the samples (161) have 18 species, and 9.3% (48) are represented by only one species. The mean number of species per sample is 11.1. The total number of possible rules that can be extracted from a data set that contains f items is : $R = 3^f 2^{f+1} + 1$ (Tan, 2014).

Table 1.10: Number of samples and species in the Association Rules Analysis.

# Species	1	2	3	4	5	6	7	8	9	10	11	12	13	14	15	16	17	18
# Samples	48	27	18	15	18	25	20	17	10	12	19	11	15	8	12	18	61	161

This requires computation of support and confidence for $31982199 + 1 = 2.91e94$ rules in biozone T6, for example. Table 1.11 shows the number of rules remaining after applying different combinations of minimum support (minsup) and minimum confidence (minconf) thresholds. More than 95% of the rules are discarded after applying a minsup=10% and minconf=10% and the number of rules remaining is almost zero (with a few exceptions) for all the minconf values when the minsup is between 50% and 90% meaning that possible interesting associations rules only occur in 40% of the transactions (188 samples).

With a minsup= 20% and minconf=50% the number of rules is reduced to 79 and the lift of all of them are greater than 1 (Figure 1.15). A lift greater than 1 indicate a positive correlation in the sense that the occurrence of one species implies the occurrence of the other. Tables 1.12 and 1.13 presents the summary statistics of the 79 rules. The rule length distribution (Table 1.12) indicates the distribution of the number of species contained in each rule (e.g. 34 rules are composed by the interactions between exactly two species)

Table 1.11: Number of rules obtained by using different combinations of minimum support and minimum confidence thresholds.

		Support								
		90	80	70	60	50	40	30	20	10
Confidence	90	0	0	0	0	0	3	8	21	200
	80	0	0	0	0	0	4	9	31	352
	70	0	0	1	1	1	5	18	49	467
	60	0	0	1	1	1	6	26	63	567
	50	0	0	1	1	2	10	31	79	672
	40	0	0	1	1	2	13	34	89	775
	30	0	0	1	1	2	13	38	96	867
	20	0	0	1	1	2	13	38	107	940
	10	0	0	1	1	2	13	38	107	969

and the summary of quality measures indicates the quartile, minimum, maximum, median and mean of the support, confidence and lift (Table 1.13). The medians of the support and confidence are 0.26 and 0.76 respectively, suggesting that although the rules are fulfilled only by a small fraction of the samples (1/4 approximately) they are reliable. The species with a support equal to 20% (occurring at least in 101 of the 515 samples) are *Cicatricosisporites dorogensis*, Fungi spp., *Laevigatosporites tibuensis*, *Lanagiopollis crassa*, *Mauritiidites franciscoi var. franciscoi*, *Mauritiidites franciscoi var. minutus*, *Polypodiisporites* spp., *Psilamonocolpites medius*, *Psilatriletes* sp. 25, *Retistephanocolpites minutiporus*, *Retritrescolpites magnus*, *Rhoipites guianensis*, *Spinizonocolpites grandis* and *Spirosyncolpites spiralis* (Figure 1.16). It is interesting to note that from 61 species whose events (FAD and LAD) occur within the biozone T6 (Annex 1.4) only *Rhoipites guianensis* and *Spinizonocolpites grandis* have a minsupport = 20%; meaning that 95% of the species that characterize the biozone have a support lower than 20% (the support for those species is in fact $< 2\%$). The FAD and LAD of the other species with support = 20% are beyond the range of the biozone T6, however they seem to be relatively common in samples dated as T6.

Table 1.12: Summary of the 79 rules selected for the data from the biozone T6. Number of species used for each rule.

# Species	1	2	3	4
# Rules	2	34	35	8

The association rules with a minsup = 20% and conf = 50% and their

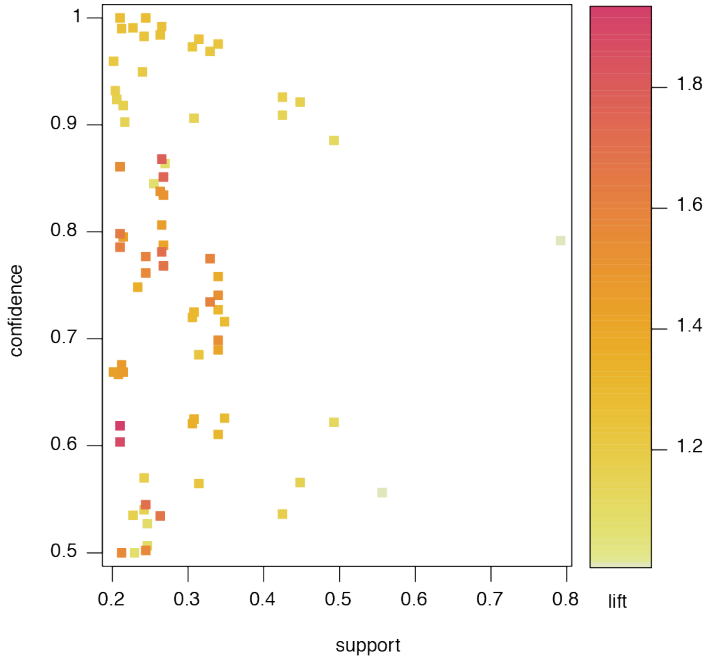

Figure 1.15: Support vs. Confidence for rules with a minimum support of 20% and minimum confidence of 50%. The colors represent the lift of the rule (see text for explanation).

respective support, confidence and lift are presented in the Annex 1.6. The matrix-based visualization presented in the Figure 1.17 shows in the X and Y-axis respectively the antecedent and consequent of each rule. Since there is not much space for long labels in the X-axis only numbers are show as labels and the complete list of antecedents is presented in the Table 1.14. The colour in the intersection of each antecedent and consequent shows the support of the rule with warmer colours indicating higher support. The two more common taxa are *Psilatriletes* sp. 25 and *Polypodiisporites* spp. and the rules with the highest support and confidence involves *Psilatriletes* sp. 25, *Polypodiisporites* sp., *Laevigatosporites tibuensis*, *Psilamonocolpites medius* and Fungi sp. (Figure 1.17). This association is far of being exclusive of the biozone T6 and their presence and co-occurrence is very common in almost all the Cenozoic sequence of Colombia. For species that define the biozone T6 (Jaramillo et al., 2011) (*Spinizonocolpites grandis*, *Retibrevitricolporites speciosus*, *Ranunculacidites operculatus*, *Retistephanoporites crassiannulatus*, *Jandufouria minor*, *Janduforia seamrogiformis*, *Rhoipites guianensis* and *Perisyncolporites pokornyi*) it was only possible to determine rules for *Spinizonocolpites grandis*. With a minsup=10%, this species is found with

Table 1.13: Summary of the 79 rules selected for the data from the biozone T6. Summary of quality measures indicating the quartile, minimum, maximum, median and mean of the support, confidence and lift.

Statistic	**Support**	**Confidence**	**Lift**
Min	0.20	0.5	1
1st Q	0.22	0.62	1.16
Median	0.26	0.76	1.28
Mean	0.29	0.75	1.34
3rd Q	0.32	0.9	1.51
Max	0.79	1	1.93

Retitrescolpites magnus and *Psilatriletes* sp.25 (support= 0.12, confidence = 0.59 and lift =2.8). Association analysis for the other species require a minsup=1%, which is not practical from the point of view of biostratigraphy because the discovered rules would apply only in small portion of the samples.

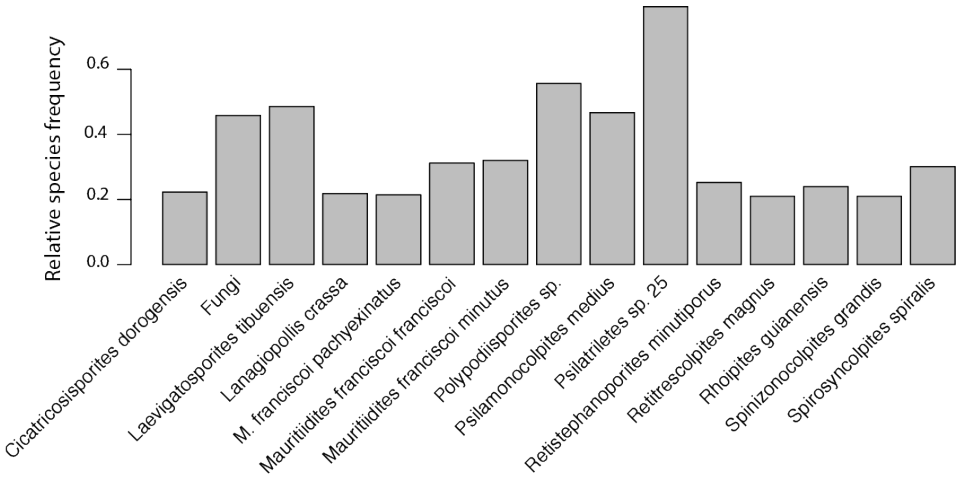

Figure 1.16: Relative species frequency with a support greater than 20% in samples from the biozone T6 (Jaramillo et al., 2011).

The procedure explained above was also applied to the same groups of samples but divided into two groups. The first group made up of samples with ages between 38 and 43.3 Ma and the second one with ages between 43.3 and 48.6 Ma. The objective was to determine if it is feasible to find different rules for each group. The results were pretty similar to the ones obtained for the entire group of samples and no significant difference in rules

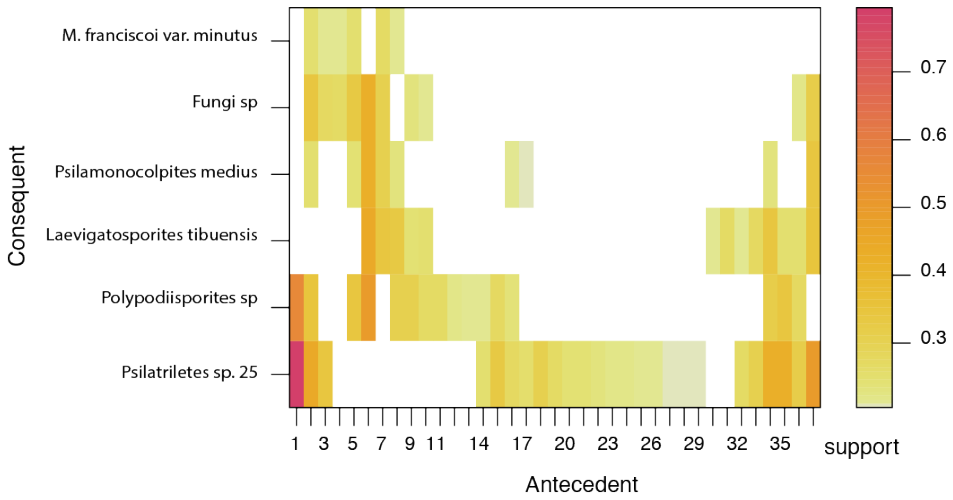

Figure 1.17: Relative species frequency with a support greater than 20%.

or their components were found between the groups.

These results supports the idea explained in the introduction about the difficulty of subdividing biozone T6. Although this is one of the zones with the largest number of events, the number of sites where they were found is very low and most of the events correspond to FADs. This probably suggests endemism and high origination rates for this time interval (although this is possibly an artifacts caused by the high number of outcrops analysed in comparison with the other biozones) making the events restricted in space and time. A possible solution is to study rock cores or outcrop samples of this age in order to increase the number of sites where events (mainly FADs) are observed. This will increase the support of the species (for the association analysis) and the spreading parameter of the events (for the Graphic correlation analysis).

1.5 Conclusions

- The integration of new palynological information to the zonation scheme proposed by Jaramillo et al. (2011) allowed to include 38 new informal taxa representing 43 biostratigraphic events (FADs and LADs) and 11 formal species representing 15 biostratigraphic events.

- The comparison between the composite section obtained in this work and the sequence obtained by Jaramillo et al.(2011) show a very good correspondence in the position the of events (Figure 1.12). Only 32

Table 1.14: Complete list of antecedents that are represented by numbers in Figure 1.17 (see text for explanation).

Number	**Itemset**
1	
2	*Laevigatosporites tibuensis*
3	*Laevigatosporites tibuensis, Polypodiisporites sp.*
4	*Laevigatosporites tibuensis, Polypodiisporites sp., Psilatriletes 25-50*
5	*Laevigatosporites tibuensis, Psilatriletes 25-50*
6	*Psilatriletes 25-50*
7	*Polypodiisporites sp., Psilatriletes 25-50*
8	*Fungi, Psilatriletes 25-50*
9	*Psilamonocolpites medius,Psilatriletes 25-50*
10	*M.franciscoi var. minutus,Psilatriletes 25-50*
11	*Fungi,Laevigatosporites tibuensis, Psilatriletes 25-50*
12	*M.franciscoi franciscoi,Psilatriletes 25-50*
13	*Laevigatosporites tibuensis,M.franciscoi franciscoi, Psilatriletes 25-50*
14	*Laevigatosporites tibuensis,M.franciscoi franciscoi*
15	*Fungi,Laevigatosporites tibuensis*
16	*M.franciscoi franciscoi*
17	*Spirosyncolpites spiralis*
18	*Polypodiisporites sp.,Psilamonocolpites medius*
19	*Fungi,Laevigatosporites tibuensis, Polypodiisporites sp.*
20	*Laevigatosporites tibuensis,Psilamonocolpites medius*
21	*Retistephanoporites minutiporus*
22	*Fungi, Psilamonocolpites medius*
23	*Rhoipites guianensis*
24	*M.franciscoi franciscoi,Polypodiisporites sp.*
25	*Fungi, M. franciscoi minutus*
26	*Laevigatosporites tibuensis, M. franciscoi minutus, Polypodiisporites sp.*
27	*Cicatricosisporites dorogensis*
28	*Lanagiopollis crassa*
29	*Retitrescolpites magnus*
30	*M.franciscoi minutus,Polypodiisporites sp., Psilatriletes sp.25*
31	*Fungi,Polypodiisporites sp., Psilatriletes sp.25*
32	*M.franciscoi minutus,Polypodiisporites sp.*
33	*Fungi,Polypodiisporites sp.*
34	*Fungi*
35	*Psilamonocolpites medius*
36	*M.franciscoi minutus*
37	*Polypodiisporites sp*

events changed their ranges very little (Table 1.8). This result is a good indicator of the reliability of the events in Jaramillo's zonation because despite adding a considerable number of new sections (47 in total) and thousand of new samples, most of the events did not change their position in the composite section.

- For LADs, the largest difference in position was found for *Retitrescolpites magnus* with 6.1 Ma and the smallest was found for the dynocyst acme C2 event with 0.02 Ma. For FADs, the largest difference was found for *Bombacacidites echinatus* with 3.45 Ma, and the smallest was found for *Multimarginites vanderhammenii* with 0.05 Ma (Figure 1.13).

- From the new 38 informal taxa included in the zonation, 23 events were reported only in one site. Because they are morphologically very distinct, they are susceptible to be identified in new sites, increasing therefore their biostratigraphic usefulness. 34 of these species are described in Annex 1.7.

- The biozone T6 (Jaramillo et al., 2011) is very homogeneous in terms of palynological composition and this homogeneity makes it difficult for further subdivision.

- The species that are common (with high support) are also very common in the rest of the Cenozoic sequence of Colombia restricting therefore their usefulness in biostratigraphy and the same applies to the rules because them are composed by the common species.

- Almost all the species that define the biozone T6 (Jaramillo et al 2011 and this work) have very low support (< 0.02) indicating that they are rare, and for this reason it is also very difficult to establish association rules for them.

- Although the results of the Association Rules Analysis did not allow to separate the biozone T6, this is a powerful technique with great potential in Biostratigraphy and Paleontology that deserve further exploration. It can be used to discover association of species found together in a biozone, geographic area, environment of deposition or whatever attribute is of interest.

Chapter 2

Macroevolution of Neotropical vegetation during the Cenozoic

2.1 Introduction

The Neotropics maintains the highest diversity of plants on Earth (Gentry 1992; Kricher 1999). This region, extending from central Mexico in the north to southern Brazil in the south, harbors about 33% of global plant species (Ulloa et al., 2017). The surprising mega diversity of the Neotropics has been recognised for almost two centuries (Humboldt 1820). Mechanisms have been proposed not only to explain how such great diversity was produced, but also how it is maintained through time. Although the processes and events that have allowed the increase in diversity over geological time scales may not be the same than those that maintain it, it is reasonable to assume that they are closely related.

Explanations of the evolution of Neotropical hyper-diversity are closely linked to one of the most remarkable large-scale patterns in biological diversity, the dramatic increase in the number of species and higher taxa from the poles to the tropics. This pattern, called the latitudinal diversity gradient (LDG), has been documented in the biotas of forest, grasslands, wetlands, continental shelves, oceans and characterizes fungi, invertebrates, vertebrates and plants (Hillebrand 2004). The LDG has roots extending back into the Palaeozoic and Mesozoic (Crame 2001, Alroy et al., 2008; Mannion et al., 2014). Although its magnitude was less pronounced than today, the evidence suggests a substantial increase of the LDG throughout the Cenozoic when most of the modern components of the Earths flora and fauna diversified (Mittelbach et al., 2007, Marcot et al., 2016).

The two simplest models of LDG assume that taxa are static in their ge-

ographic distribution, with scarce interchange of species between the tropics and the extra-tropics.These two models, "tropics as a cradle" and "tropics as a museum" (Stebbins 1974), explain the enormous species richness of the tropics as the result of either higher tropical origination rates (cradle) or lower extinction rates (museum) compared to the extra-tropics. A third model called "out of the tropics" (Jablonski et al.,2006) breaks this dichotomy; based on a study of marine invertebrates, Jablonski et al. (2006) demonstrated that at least for the last 11 Ma the tropics have acted both as a cradle and museum, with taxa preferentially originating in the tropics and expanding into high latitudes without losing their initial tropical distribution.

In the case of tropical vegetation, Antonelli et al. (2015) found compelling evidence that supports the "out of the tropics" mechanism proposed by Jablonski et al. (2006). They compared origination and extinction rates of angiosperms inferred from the phylogeny of living species between tropical and non-tropical regions, as well as among tropical regions (tropical Asia, tropical, Africa and tropical America).They found no significant differences between tropics and extra tropics but did find prominent differences among the tropical regions of different continents, suggesting that the LDG, at least in plants, derived from other factors than differential rates of diversification. They also estimated the timing and direction of range shifts of extant angiosperms between tropical and non-tropical zones, and into and out of the major tropical regions of the world. The results indicate that range shifts out of tropical America were more frequent that those entering in. With this evidence, Antonelli et al. (2015) propose that neotropical plant species are being formed and replaced by one another at unparalleled rates and that tropical America stands out from other continents by having pumped out more species than it received through most of the Cenozoic. In words of Antonelli et al. (2015, page 1): "the Neotropics have acted as a engine for global plant diversity".

When it comes to explaining how diversity in the neotropics is maintained, the proposed mechanisms have been generally classified in two major categories, abiotic and biotic (Antonelli et al., 2015). These mechanisms may also help to explain how this diversity was produced in the first place. The distinction between abiotic and biotic is subtle and some mechanisms are impossible to frame within one single category. The general idea behind the classification is only to facilitate the organization and explanation of the proposed mechanisms.

Biotic Mechanisms

The most frequently cited of the biotic mechanisms is the *tropical conservatism hypothesis.*This hypothesis suggests that there are more species of plants in the neotropics because more lineages originated and diversified there due to the climatic stability of the region, and because species tend to retain their niches over evolutionary time (Wiens and Donoghue, 2004). The evidence supporting this hypothesis is however contradictory.

At a broad scale, it is clear that many higher plant clades are widely distributed in the Neotropics (e.g. modern cycads, palms) but have never invaded temperate regions. The reason for this is neither the lack of time or limited dispersal ability but instead climate and niche conservatism, which act as barrier to prevent their expansion into higher latitudes. Regional-scale studies focused on floristic zonation of the Amazon basin indicate that the forest is partitioned into broad scale floristic units on the basis of their geology and edaphic conditions (ter Steege et al., 2006; Pitman et al; 2008; Higgins et al., 2011). A comparison of functional traits between different geological units in the Amazon of Peru also indicates strong habitat filtering as the main driver of tree composition in the area (Fortunel et al., 2014). Other studies (Duque et al., 2002) have also demonstrated that the number of species, and even counts of higher taxa such as genera and families, is lower on cratonic units (the oldest geological units in the Amazon basin) than on the younger Neogene and Quaternary sedimentary units. All these studies suggest that niche conservatism has shaped the ecological structure of trees communities in the Amazon basin, and suggest that environmental conditions play an important role in determining which species occupy which areas.

Other studies, however, have found contrasting results. Cardenas et al. (2017) compared tree communities located in three different geological units of the Amazonas in Colombia. The aim of the study was to evaluate whether differences in substrate age and environmental conditions determine the phylogenetic structure and spatial turnover of the tree communities. The results give support for both environmental filtering (niche conservatism) and dispersal as important drivers of the distribution of the tree communities in the Amazon basin. The authors suggest that dispersal limitation appears to actively drive phylogenetic turnover at distances equal to or lower than 20 km, beyond this distance abiotic factors have a significant complementary effect (Cardenas et al., 2017). In a regional study comprising 12 regions distributed over the entire the Amazon basin and Panama, Dexter et al. (2017) interpreted the lack of geographic phylogenetic structure in species of the genus *Inga* as indicator that in evolutionary timescales the metacommunity for the

local or regional tree communities in the Amazon is the entire Amazon basin. According to this study, speciation is therefore the result of the isolation of peripheral populations by dispersal rather than a result of geological bedrock-driven phenomenon that isolates regions and promotes diversification due to niche conservatism. However, in the same study Dexter et al. (2017) also cite studies (Pennington et al., 2010; Sarkinen et al., 2012) that indicate that some species of woody plants are confined to single regions of dry forest, like the Brazilian catingas or the seasonally dry Andean valleys. The differences in distribution between species of woody plants and the species of the genus *Inga* reflect, according to Dexter et al. (2017), the scattered nature of the dry forest that limits the dispersal ability, and also ecological factors specific of the dry forest that affect the ability of the propagules to establish after dispersal.

Abiotic Mechanisms

Among the abiotic mechanisms, the "time hypothesis" argues that the Neotropics have accumulated species over a longer period of time than temperate regions (Mittelbach et al., 2007). The South American continent remained isolated from other continents during almost 100 Ma after its breakup from Africa (Pitman et al., 1993) and before its geological recent connection with North America via the Isthmus of Panama during the Pliocene (ODea et al., 2016; but see Montes et al., 2015 for an alternative dating of the closure). During this long period, the Neotropics maintained about the same geographic latitude resulting, theoretically, in a long interval of climatic stability. According to the time hypothesis, the geological isolation and climatic stability of South America would have favoured the gradual accumulation and preservation of lineages over time (Raven et al., 1974; Young et al., 2002). However, this model has been considered too simplistic because molecular phylogenetic studies have demonstrate that the South American flora has received immigrant taxa throughout the Cenozoic from Laurasia, Africa and Australia (Renner et al., 2001; Renner 2004; Pennington et al., 2004).

Other abiotic mechanisms include climate and the uplift of the Andes Cordillera. Although climate is one of the best predictors of species diversity today, its role in producing and maintain plant diversity in the geological past is still under debate. Palynological analysis from the Paleogene of Colombia found a good correlation between fluctuations in diversity and changes in global temperature (Jaramillo et al., 2006). Especially during the Palaeocene-Eocene thermal maximum (PETM) (56 Ma) when the temperature in the northern neotropics seems to have increased 3-5 C (Jaramillo et al., 2013). Based on the palynological records of three terrestrial sections

located in northern South America, the PETM transition is characterized by an abrupt but short-lived increase in origination rate, and the resulting increase in plant diversity was driven by the addition of new taxa, mainly angiosperms, to a pre-existing low diversity Palaeocene flora (Jaramillo et al., 2010). Nevertheless, a correlation between diversity and temperature is not very evident in the Neogene, where the changes in palynological diversity reveal a poor relation with fluctuations in temperature (Hoorn et al., 2010). In a recent palynological study, D'Apolito (2016) used of a rock-core drilled in the Amazon basin of Brazil to investigate changes in diversity across the middle Miocene Climatic Optimum (MMCO). The MMCO was a global warming event that occurred between 17 and 14.5 Ma in which the temperatures could have risen 3 to 4 degree Celsius in comparison with today (Goldner et al., 2014). Analysis of the core suggests an increase in diversity and high origination rates overlapping the duration of the MMCO. These results therefore open the possibility that global temperature could have played important role in promoting neotropical plant diversification during the Neogene.

Other authors have proposed a recent geological origin for the Amazon mega-diversity through the Pleistocene refugia hypothesis. According to this hypothesis, the climatic changes during the Pleistocene produced periods of aridity in which the vegetation contracted and created isolated forest remnants or refugia (Haffer 1969). In the lowland Amazonas basin, the arid climate would have resulted in the replacement of forest by savannah. The refuges acted as centers of speciation, producing endemism and geographic barriers that prevented the dispersion of plants (Bueno et al., 2017; Cheng et al., 2013). The palaeoenvironmental record, however, shows no such forest contraction or fragmentation of the Amazon lowlands during the Pleistocene (Benett et al., 2012; Bush et al., 2002), neither the establishment of savannahs even during the coldest stages of the Quaternary (Colinvaux et al., 2001). Additionally, in the 1990s the centers of diversification or refugia were shown to be sampling artifacts resulting from the concentration of botanical studies in collecting centers (Nelson et al., 1990). The theory of refugia has therefore been gradually abandoned (Hoorn et al., 2010).

In relation to the uplift of the Andes Cordillera,it is clear that this was a very complex geological event, involving multiple pulses that occurred throughout the entire Cenozoic (Dengo and Covey, 1993; Bayona et al., 2008; Parra et al., 2009; Horton et al., 2010). One of the most intense pulses occurred during the Miocene (Mora et al., 2010). It is believed that this Miocene pulse resulted in substantial changes to the paleogeography of South America and especially to the Amazon basin (Roddaz et al., 2010; Leite et al., 2016; Mora et al., 2010; Bermudez et al., 2015). This pulse promoted habitat heterogeneity, created biotic corridors, intensified the nu-

trient supply and changed the hydrological and climate regime of the entire continent (Mora et al., 2008; Hoorn et al., 2010 and references therein). Any of these changes could favour adaptive radiations, produce geographic vicariance, and promote allopatric speciation that may have increased the plant diversity of the region. The uplift of the Andes, and specifically the events of the Miocene, could potentially explain the high diversity of plants observed today in the region. However, the evidence is still scarce and fragmented.

The palynological diversity curve presented by Jaramillo et al. (2006) is restricted to the interval between 65 and 20 Ma, preventing therefore any interpretation with regard to the Miocene. Other palynological studies in the Amazon basin of Brazil (Silva-Caminha et al., 2009; Leite et al., 2016; D'Apolito, 2016) covers only parts of the Miocene (from 19 Ma to 3 Ma). An intriguing question that arises is if the intense orogenic activity and related changes in paleogeography during the Miocene are responsible for the high diversity of plants observed today, what then explains the high diversity estimated for the middle Eocene, knowing that the orogenic activity during the Eocene was minimal? Although the paleogeographic reconstruction of the middle Eocene suggests the exposure of isolated rock units, this is a very small proportion in comparison with the areas exposed during the Miocene (Reyes-Harker et al., 2015). It is likely that different mechanisms have operated through time, and possibly in conjunction, to produce long-term patterns of plant species diversity in the neotropics.

2.1.1 Macroevolutionary estimates in the fossil record

The fossil record offers a unique and extraordinary opportunity to study macroevolutionary patterns in the geological past. Indeed, one of the main objectives in paleobiology is to determine the number of taxa that were extant during successive geological time intervals. In this respect, diversity curves and measures of taxonomic rates (extinction and origination) have been widely used to study the evolutionary history of organisms including marine invertebrates (Sepkoski 1996; Foote 1998; Alroy et al.,2008,2010); mammals (Alroy 2009); marine microorganisms (Lazarus et al., 2014; Fraass et al., 2015; Lloyd et al., 2011) and tetrapods (Benton 1995; Benson et al., 2016). Although the counts of fossils, and the methods used in paleobiological research, can be distorted by factors like sampling bias, the pull of the recent and the Signor-Lipps effect (Raup 1972; Foote and Miller, 2006) there is substantial evidence that for a broad perspective on global and regional diversity trends, the methods and compendia of fossils have now matured sufficiently to capture the main biotic transitions preserved in the geological record (Alroy 2010; Foote and Miller, 2006; Quental and Marshal, 2010).

As a consequence, several approaches and methods to estimate diversity and taxonomic rates from the fossil record are now available (Alroy 2000; Foote 2000; Foote and Miller, 2006; Alroy 2010b; Alroy 2014).

In the specific case of diversity, the choice of the method is constrained by the available information. When the presence/absence of the species in a time interval is the only data available, diversity is generally estimated by counting the number of species found in each sample or collection. However, because this metric is positively correlated with many measurements of sampling effort (e.g. number of specimens, samples, collections, formation, etc.), differences in diversity between samples or collections may be due to differences in the sampling effort and not to biological or ecological factors. On the other hand, when information is restricted to the time of first and last occurrences, most methods have adopted the range through assumption in which every species is considered present in all the samples between its first and last occurrence, even if the species was not detected in intermediate samples (Boltoskoy 1988). The range through assumption has the advantage of interpolating taxon ranges through poorly-sampled intervals and decreases the effect of environmental influences that potentially prevent the preservation of taxa (Hazel 1970) but introduces undesirable bias, like the Signor-Lips effect (Signor and Lipps, 1982), the pull of the recent and the edge effect, that are difficult to quantify and remove (Foote and Miller, 2006). The first and best-known database that compiled information about the global first and last occurrences of marine animals at family and genus level was developed by Jack Sepkoski (Sepkoski 2002). Sepkoski' s database started as a compilation of information extracted from the Treatise of Invertebrate Palaeontology. Subsequently, Sepkoski incorporated information from the literature to expand and refine his compendia. Several studies have used information from Sepkoski 's database to estimate Phanerozoic global marine diversity curves (Sepkoski 1978, 1979, 1996; Foote and Sepokoski, 1999, Foote 2000; Smith and McGowan, 2007).

Finally, when information about abundance is available, the range of possibilities opens. Abundance can refer to both the number of specimens counted within a locality or sample and to the number of localities in which a taxon is found. With abundance data it is possible to use quantitative metrics that are applied mainly in Ecology, like diversity indices (e.g. Shannon, Simpson, among many others) (Magurran 2003) to metrics that allow standardizing, like rarefaction (Hayek and Buzas, 1997), shareholder quorum subsampling (Alroy 2010) as well as other forms of subsampling (Chao and Lost, 2015; Chao et al., 2014).

2.1.2 The fossil record of plants

In comparison with other groups like mammals, invertebrates and vertebrates, macroevolutionary studies of vegetation are scarce and even more when it comes to neotropical vegetation. In a recent phylogenetic study of global plant diversification, Antonelli et al. (2015) discussed the utility of the plant fossil record to infer diversity trends in the tropics, arguing that the macrofossil record of plants, in this case angiosperms, is temporal and spatial biased, and potentially uninformative. The information considered by Antonelli et al. (2015) comes from a global dataset of plant macrofossil occurrences downloaded from the Paleobiology Database. The data show that the fossil record of angiosperms in the northern hemisphere (USA and Europe) is continuous through the lower Cretaceous to the Quaternary, whereas the fossil record of the tropics for the same interval is patchy and characterized by a low to null number of occurrences. Nevertheless, plant macrofossils have been informative to paleodiversity studies on longer time intervals and when the focus of the study is wider and includes other vascular plants. For example, pioneering work by Niklas et al. (1983) identified four evolutionary phases of terrestrial plant diversification: first, a Silurian-Devonian proliferation of early vascular plants; second, a subsequent late Devonian-Carboniferous radiation of derived pteridophytic lineages; third, the appearance of seed plants in the late Devonian culminating in a gymnosperm-dominated Mesozoic flora; and fourth, the appearance and rise of flowering plants in the Cretaceous and Tertiary (Niklas et al., 1983). More recently, the macrofossil record of plants as represented in the Paleobiological database (https://paleobiodb.org) has been used been used to test different macroevolutionary hypothesis. Examples include the origin and diversification of vascular plants (Silvestro et al., 2015), the dispersal and extinction rates across continents during the Cenozoic (Silvestro et al., 2016) and the role of biotic and abiotic mechanisms in controlling species diversification in ferns (Lehtonen et al., 2017).

Microfossils provide another source of information for vegetation dynamics in the geological past, specifically pollen and spores. Pollen is the microspore wall of seed plants plus the microgametophyte that develops within the wall (Traverse 2007). Spores are the unicellular, asexual or sexual reproductive units of cryptogams and fungi (Punt, 2007), which are primitive for land plants. Both pollen and spores have a wall composed mainly by a substance called sporopollenin, which is one of the most refractory organic compounds in nature (Traverse 2007). The strong nature of the wall is necessary because in pollen grains it has the function of protecting the male gametophyte during its journey between the anther and the stigma. Sporopollenin also plays a protective role in spores, but in this case during the dispersal

from the sporophyte to a moist location suitable for germination (Moore 1994). Because of their resistance to decay, both pollen and spores fossilize readily. Furthermore, due to their role in reproduction, plants tend to produce large amounts of pollen and spores as a strategy to secure offspring. Due to their resistance and elevated production, pollen and spores are found in a widely variety of sedimentary environments. All these characteristics make palynology (the study of pollen, spores and other acid resistant biological materials) a very powerful proxy of vegetation in the geological past. It has been argued that because pollen and spores lack of sufficient amount of diagnostic synapomorphies that prevent and accurate taxonomic classification, they are not reliable source of information in evolutionary studies of plants (Silvestro et al., 2015). However, it has been also demonstrated that diversity in pollen rain follows trends in vegetation diversity over ecological gradients (Weng et al., 2006; Birks et al., 2016; Felde et al., 2016) and reflect local to regional vegetation conditions well (Jantz et al., 2013, Gosling et al., 2009; Julier et al., 2017; Mathias et al., 2015).

In spite of its potential, only a few studies have used palynology to approach the macroevolutionary history of neotropical vegetation. These studies have focused in local geographic areas and relatively short time intervals (Hoorn et al., 2010; Leite et al., 2016, D'Apolito, 2016). One exception is the work of Jaramillo et al. (2006), which to date is unique in presenting a diversity curve and taxonomic rates for vegetation based on palynomorphs over a long time interval, spanning most of the Cenozoic. A detailed description of Jaramillo's work is presented below.

2.1.3 Cenozoic plant diversity in the Neotropics

Jaramillo et al. (2006) used palynological information from 1530 samples distributed among 15 stratigraphic sections corresponding to rock-cores, wells and outcrops located in Colombia and Venezuela. A total of 1411 morphospecies represented by 287.736 occurrences were used in Jaramillo's analysis. The samples from all the sections were integrated into a single composite section (SCS) by using graphic correlation (Shaw 1964). The final SCS range between 0 and 66 Ma, although data from the oldest 17 Ma and the youngest 3.3 Ma were eliminated to avoid the edge effect. In the SCS, the FAD of each species was interpreted regardless of whether it was estimated from ditch cutting samples or rock cores. To justify this, Jaramillo et al. (2006) suggested that caving of ditch cutting samples was not expected to produce a systematic bias affecting the record of FADs in any particular interval. The final SCS is presented in the supplemental material as a presence-absence matrix, and assuming that each species is present in all the samples between its FAD and

LAD (range through assumption). The range-through assumption is valid, and has been widely used in studies of the marine invertebrate fossil record (Sepkoski 1978; Foote 2000). However, it is problematic when it is already incorporated in the original dataset, because it is then impossible to evaluate sampling probabilities or the influence of borehole caving in the range of the species, among other things. Jaramillo et al. (2006) estimated diversity for each time horizon of their SCS using the boundary crossers approach (Foote 2000). A reproduction of the original diversity curve is presented in the panel C of Figure 2.1 (black line).

To explore if there is a correlation between diversity reported by Jaramillo et al. (2006) and the density of palynological samples in time, here, their SCS was divided into 1 Ma time intervals, and the number of samples and diversity was calculated for each interval (Figure 2.1-A). With the original data it would be not possible because each diversity estimate corresponds to a time horizon composed by only one sample.

When the original curve and the curve based on the pooled section are compared, their similarity is evident (panel C, Figure 2.1). The only and subtle difference is the higher resolution obtained when all the samples are used. In this sense, it is fair to use the pooled version of the diversity curve to discuss the results. The pooled diversity and the number of samples (panel A, Figure 2.1) were compared using a Spearman rank correlation test. These were performed for both the raw data and detrended data using the first differences (Smith and McGowan, 2007; Lloyd et al., 2011). The test was also applied independently to each geological epoch (Paleocene, Eocene, Oligocene, Miocene). The raw correlation between the number of samples and standing diversity is statistically significant but negative (p= 0.02; rho =-0.32). Figure 2.2 shows the raw correlation for each geological epoch. All the correlations are statistically non-significant except for the Oligocene (p=0.03; rho=-0.64)

Figure 2.3 shows the first difference in absolute rise or fall over time of number of samples (red line) and standing diversity (black line). When all the data is compared the correlation is non significant (p=0.24; rho=0.17). When the data is discriminated by geological epochs, the correlation is only significant for the Paleocene (p = 0.012; rho=0.8). A visual inspection of the two curves (panel A, Figure 2.1) reveals a positive correlation for specific intervals. From the Palaeocene to the middle Eocene, the increase in the number of samples is accompanied by an increase in diversity. In fact, the interval between 58.5 and 59.5 Ma presents the largest number of samples, and is also characterized by a prominent peak in diversity. The subsequent and abrupt decrease in the number of samples in the late Palaeocene is characterized by a decline in diversity. During the middle Eocene, diversity and

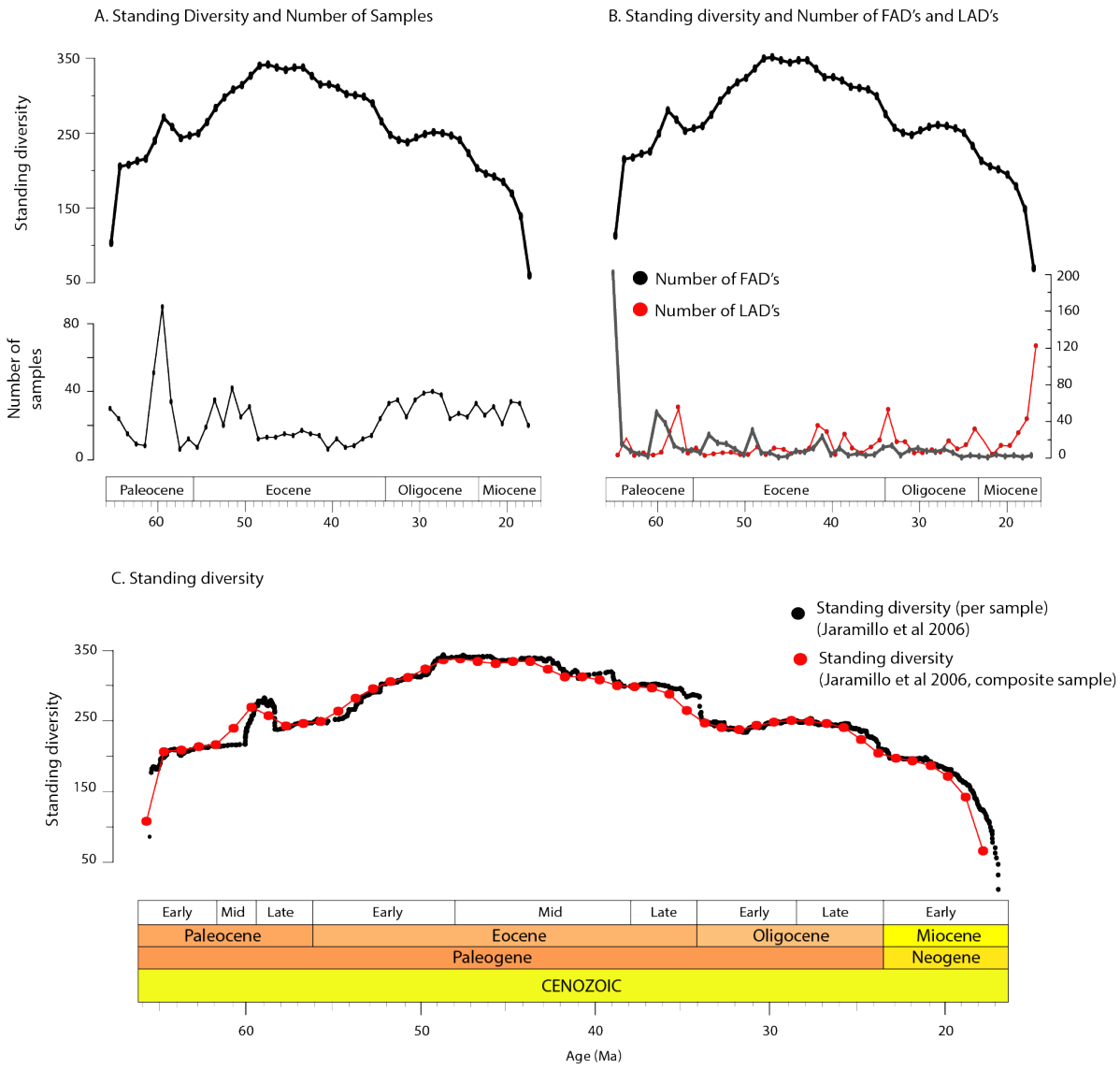

Figure 2.1: Standing diversity, number of samples and number of FADs and LADs estimated from the information presented in the supplemental material by Jaramillo et al (2006). Panel A: standing diversity and number of samples; Panel B: standing diversity and number of FADs and LADs; Panel C: standing diversity calculated for each individual samples (black line) as in the original work by Jaramillo et al (2006) and standing diversity calculated at 1 Ma intervals (red line).

the number of samples both show a decreasing trend. The Eocene-Oligocene boundary is the only interval where the two curves exhibit opposite trends.

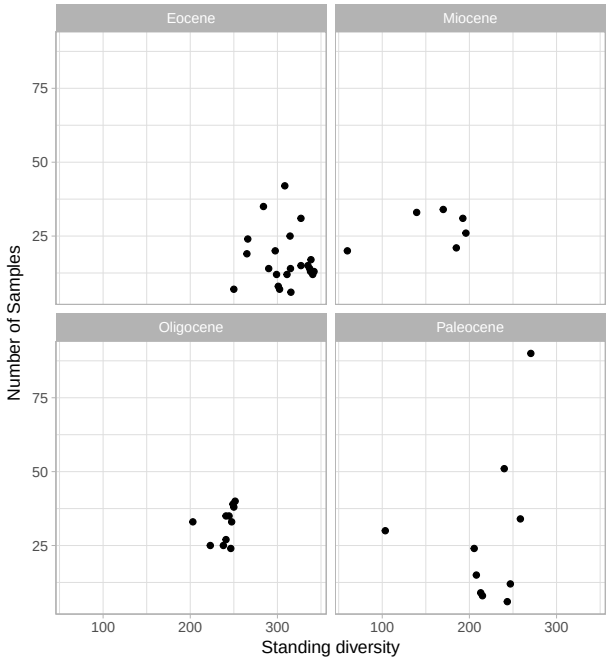

Figure 2.2: Raw correlation between the number of samples and standing diversity (data from Jaramillo et al., 2006) separated by geological epochs.

In this short interval, the number of samples increases, but the diversity declines. In the early Oligocene, the number of samples progressively increases and the diversity also shows a tendency to increase. In the late Oligocene (approx. 26 Ma) the number of samples and diversity both decrease. During the Miocene, the number of samples fluctuates while diversity decreases.

Another concern in Jaramillo 's work is that ditch cutting samples contribute most of the material used for the study. The use of this type of samples is problematic because borehole caving can contaminate them. Borehole caving refers to pieces of rock that came from the wellbore but that were not removed directly by the action of the drill bit and when it occurred the FAD of species could be artificially increased. Put in other words, the origination of a species would seem older than it really is. The effect of contamination by caving was discarded by Jaramillo et al. (2006), who argued that caving is not expected to produce a systematic bias in any particular time period (Jaramillo et al., 2006, supplemental material). However an inspection of the number of FADs (panel B, Figure 2.1) indicates that 31% of them (207 out of 665) are concentrated in the first interval (64.5 - 65.5 Ma). Because most of the material in this interval corresponds to ditch cuttings samples,it is possible that the elevated number of FADs is a by-product of caving. Establishing

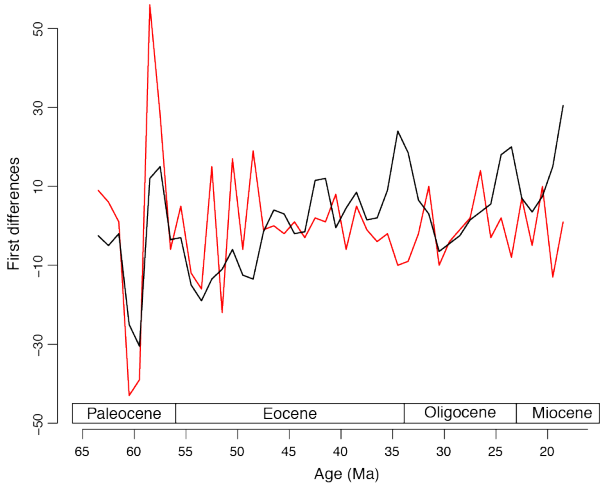

Figure 2.3: First difference of number of samples (red) and standing diversity (black line) (data from Jaramillo et al., 2006) separated by geological epochs.

the veracity of FADs is crucial to estimating diversity and the dynamics of diversification, and even more so when the range-through assumption is incorporated. Evidently, the accumulation of FADs in the youngest interval may reflect factors other than contamination. However, because the dataset presented in the supplemental material of Jaramillo et al. (2006) has already incorporated the range through assumption, it is impossible to know the real stratigraphic ranges of the species. This unfortunately prevents to explore the possible role of caving in the accumulation of FADs observed in the first interval.

In summary, several mechanisms have been proposed to explain the high diversity of plants seen today in the Neotropics. Their role in producing and maintaining such diversity are not completely understood and it is likely that they will continue to be debated and studied for a long time. However, before attempting to understand those mechanisms, it is crucial to known the macroevolutionary history of the neotropical vegetation through deep time. In fact, patterns of plant diversification during the Cenozoic have received much less attention than have the mechanisms proposed to explain them. This presents a significant knowledge gap.

Accurate and unbiased estimation of diversity, origination and extinction are therefore pivotal to explaining the high diversity of plants observed in the Neotropics. Previous macroevolutionary studies in the Neotropics have been based on global compilations of plant macrofossils. However it been show that the macrofossil record of plants is temporal and spatially biased in substantial ways. Also, because data compilations are global in scope, the

stratigraphic resolution of these studies is in general very low. Palynology provides a useful complementary tool to study past vegetation. Pollen and spores reflect local to regional conditions and in general they also offer a higher stratigraphic resolution than macrofossils. As with other fossil data of past diversity, estimates based on palynology are potentially affected by sampling effort and extrinsic factors such as borehole caving and reworking.

In this chapter, I use the most complete compilation of palynological data from northern South America to date in order to explore the macroevolutionary history of neotropical vegetation during the Cenozoic. Different methods were used to estimate diversity and taxonomic rates (origination and extinction) and to explore their distribution and changes through time and space. Several protocols were also used to standardize and reduce the effects imposed by differences in the collection effort and to control the effects produced by extrinsic factors as caving and reworking.

2.2 Materials

One hundred and thirteen sections (113), including both wells and outcrops, were used in the analysis presented here (Annex 2.1, Figure 2.4). Of these, 106 correspond to sections presented in the first chapter of this work. The remaining 7 sections correspond to five wells drilled in the Middle Magdalena Valley basin (MMVB) and two wells drilled in the Catatumbo basin (Annex 2.1). The lines of correlation (LOC) of the new sections were traced using the same approach described in Chapter 1 and are presented in Annex 2.2.

For the MMVB, a standard reference section (SRS) was constructed by using information from Aga-1, Mon-1A, Rega-1 and Uribe. These sections were used in Jaramillo 's zonation and they are already calibrated with the geological time scale (Jaramillo et al., 2011). In the SRS, composite units were used as a measure of the stratigraphic positions of the events. Four additional biostratigraphic events were added to the SRS to facilitate the trace of the LOC. These events have been recognized regionally and are commonly used for intra-basin correlations. The first event is the superabundance (ACME) of the palynomorph *Proxapertites operculatus*. The end of the *P. operculatus* ACME corresponds to the top of the biozone T03b (Jaramillo et al., 2011) and is related to the late Palaeocene Lisama Formation. The other events correspond to three rich fossiliferous deposits regionally known as the Los Corros, Mugrosa and La Cira horizons (Pilsbry and Olsson, 1935). Stratigraphically, these are located at the top of the Esmeraldas, Mugrosa and Colorado formations respectively. Palaeontologically, a rich association of fresh water molluscs characterizes these deposits. In ditch cutting samples,

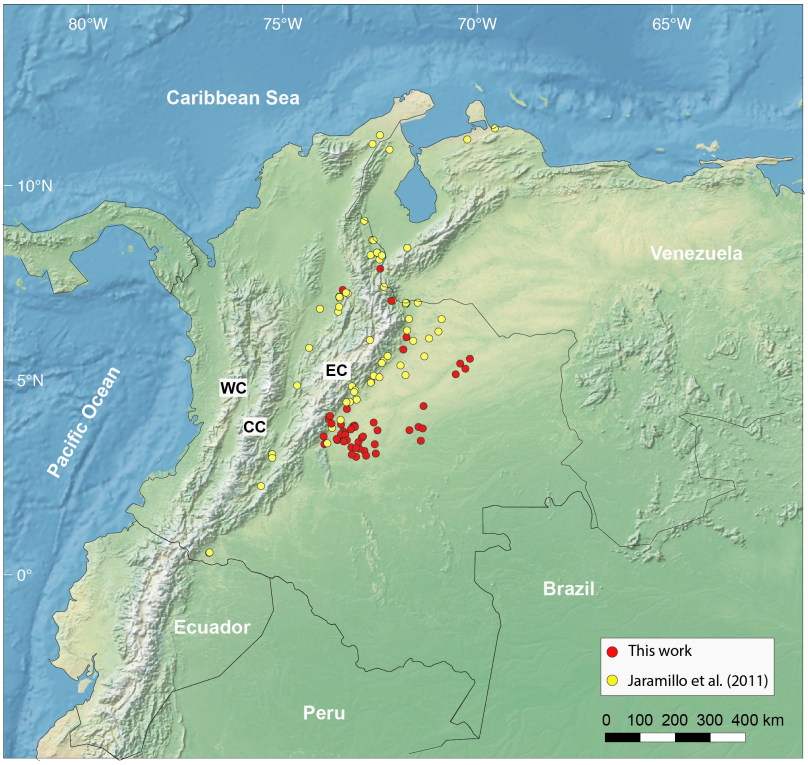

Figure 2.4: Sections (outcrops and wells) used in the Macroevolutionary analysis. Yellow circles correspond to sections previously studied by Jaramillo et al. (2011) and the red circles correspond to sections studied in this work. WC: Western Cordillera; CC: Central Cordillera; EC: Eastern Cordillera.

the recovery of small fragments of shells is used by the well loggers to locate the three horizons and to establish regional correlations. In the SRS, the three horizons were interpreted as follow. The La Cira horizon was positioned at 6490 CU due to the presence of shell fragments reported in Mon-1A at a depth of 7000 feet. The Mugrosa horizon was interpreted at 14393 CU because of the presence of shell fragments at 3190 in Reg-1. The Los Corros horizon was interpreted at 16164 CU in the CS based on the presence of shell fragments at 7250 in Reg-1.

The two wells located in the Catatumbo basin were compared against the composite section presented in the Chapter-1 (Anexx-3). The coordinates of the lines of correlation are presented in Annex 2.2.

The composite Section

A total of 2777 species distributed in 6098 samples were used for the macroevolutionary analysis. The age in million years of each sample was calculated by using the lines of correlation and the calibration points of the graphic correlation project presented in Chapter 1 as well as the lines of correlation of the seven new sections discussed above (MMVB and Catatumbo). The individual samples from all the sections were combined to form a single composite section. The species of the composite section were classified in one of four categories. The first category corresponds to formal species already described in the literature (e.g. *Cicatricosisporites dorogensis*). The second category makes reference to informal species (denoted with quotation marks; e.g. *Echitricolpites 'clipoechinatus'*). The third category includes those taxa with non-specific name (e.g. *Spinizonocolpites* sp.) and the fourth category includes species with affinity or conferred to other species (e.g. *Rhoipites aff. guianensis*; *Malvacipolloides cf. maristellae*). The number of species reported between one and 100 samples are presented as an occurrence count-frequency histogram in the Figure 2.5. The distribution of the number of species reported in more than 100 samples is not presented because the number of species is very low. From figure 2.5, the number of species found in only one sample is 1325 (48% of the total). The number of species reported between one and ten samples is 2228, which represents almost 80% of the total number of species. In contrast, 417 species (15% of the total) are reported between ten and 100 samples and only 132 species (5%) are reported in more than 100 samples. These results indicate that most of the species in the composite section correspond to rare species.

2.2.1 Biases in Origination and Extinction estimates

2.2.1.1 Borehole caving

A trustworthy interpretation of the time of origination and extinction of the species is the basis of any macroevolutionary study. Any artificial increase in the range of a species could bias the estimation of diversity and taxonomic rates. This is true for many of the methods used to calculate standing diversity, which make use of the range-through convention that each taxon ranges through the entire stratigraphic interval between its origination and extinction (Foote and Miller 2006). Because most of the material used in this study corresponds to ditch cutting samples, borehole caving (henceforth called caving) can artificially increase the FAD of the species (making the apparent time of origination of the species older than the actual time of origination). This could act as a systematic bias if caving is concentrated in

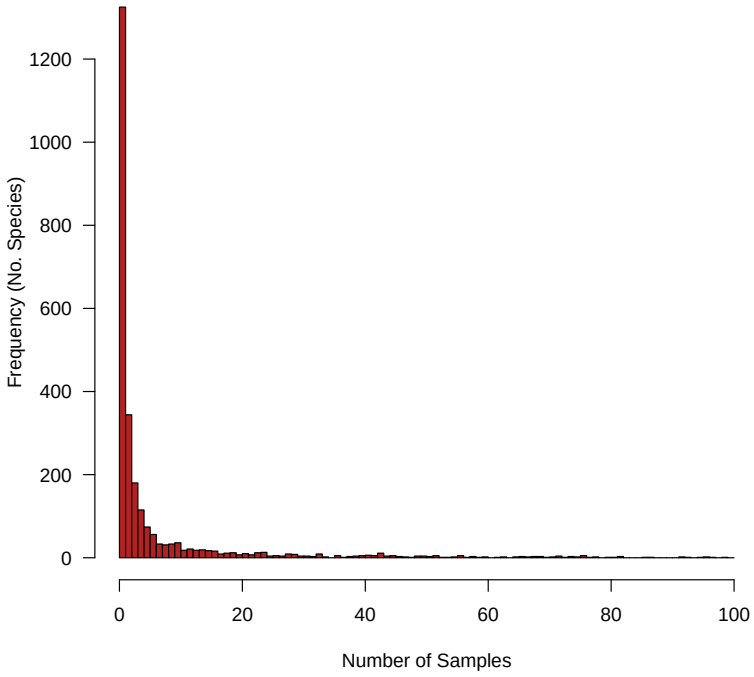

Figure 2.5: Species occurrence frequency for the dataset used in the macroevolutionary analysis.

a particular time interval, in which case the estimated diversity would be inflated toward that interval.

The effect of caving may therefore be similar to the phenomenon known as Pull of the Recent (Foote and Miller 2006), in which an artificial increase in range-through diversity estimates, particularly in the Cenozoic, in the amount of sedimentary rock and hence the number of fossils available for sampling increase the possibility of finding more recent representatives for young species than for old ones, even for rare taxa. This bias is particularly acute if observations of extant species are used as LADs, a practise that substantially inflates diversity of younger geological strata above the level that would be achieved if no data from the recent were available. Caving can induce a similar effect.

In the palynological zonation presented in the first chapter of this work, originations (FADs) were only interpreted for those species whose oldest presence was found in outcrop or core sample material, and not in ditch cuttings,

thereby avoiding the possible effect of caving. However, most of the samples in the composite section (approx. 70%) correspond to ditch cuttings, which make it difficult to interpret the time of origination for the most of the species (84%). In Jaramillo's work (Jaramillo et al., 2006) the effect of caving was discarded, arguing that there is not reason to expect a systematic bias in any particular period of time (Jaramillo et al., 2006-supplemental material). However, no evidence was provided in support of this assumption.Additionally, the analysis presented in the introduction of the present work suggest that in fact there is a suspicious accumulation of FADs toward the oldest interval.

To assess the possible effect of caving in this study, the distribution of the number of FADs through time was analyzed (Figure 2.6). The histogram in the panel A shows data for N=192 species, for all of which FADs were defined using information from cores or outcrops material. This is the most reliable approach to the distribution of FADs because it explicitly avoids the effect of caving. The histogram shows a very pronounced peak (approximately 70 FADs) between 50 and 60 Ma while the remaining FADs are evenly distributed over the other time intervals. The histogram in the panel B (Figure 2.6) shows data for N= 1014 species whose FADs were interpreted as the age of the oldest sample where the species was recorded regardless whether the sample correspond to a ditch cutting. A peak in the number of FADs (approx. 400) is observed between 50 and 60 Ma while the remaining FADs are evenly distributed over the other time intervals. It is evident that the two histograms are very similar (Figure 2.6). Both are highly skewed to the left and exhibit a prominent peak between 50 and 60 Ma. If caving were artificially increasing the number of FADs in any specific time period, it would be expected that the two data samples came from two different statistical populations. A Mann-Whitney-Wilcoxon test suggests that is not possible to reject the null hypothesis that the two samples come from the same statistical population (p=0.98).

Although this evidence suggests that caving is not concentrated in any particular interval a second possible undesirable effect may occur. From the total 1014 species that are represented in the histogram B (Figure 2.6) 327 were reported in two samples while 687 were reported in more than two samples (Figure 2.7-A). For those species reported in only two samples, 212 (65%) of them were detected in only one well, indicating that their ranges could be potentially being affected by caving. The remaining 114 species (35%) were found in more that one well indicating that their estimated stratigraphic ranges were based on information from two sites. This would reduce the probability of affectation by caving in these species (Figure 2.7-A). In the other hand, for those 687 species recorded in more than two samples,

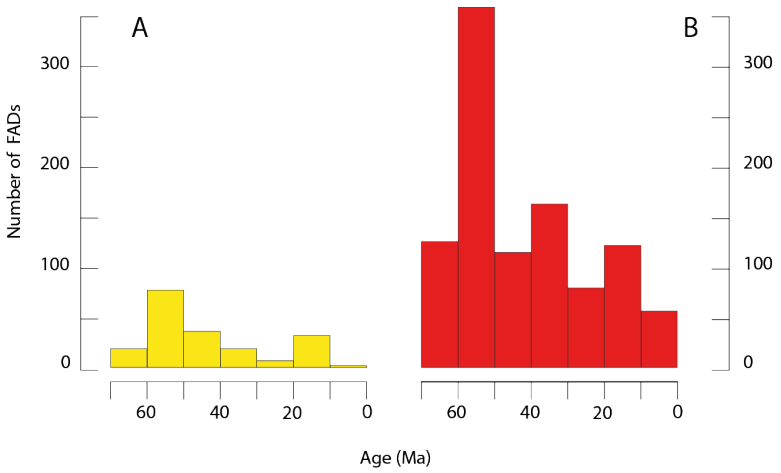

Figure 2.6: Histograms showing the number of FADs in 10 Ma time intervals. Panel A: species with FAD defined from core or outcrop material. Panel B: species with FAD defined from ditch cutting material. Note the similarity between both histograms and the pronounced peak between 50 and 60 Ma.

209 (30%) of them were found in only one well, indicating that their ranges could be potentially being affected by caving. The remaining 478 species (70%) were found in more than one well, implying that their ranges were estimated based on information from more than two sites. This would reduce the probability of an influence of caving on the ranges of these species (Figure 2.7-A).The temporal range of the species that are possible affected by caving based on the above criteria is 1-5 Ma (mean=1.7 Ma, standard deviation= 8 Ma) and 4-10 Ma (median=2.3 Ma; standard deviation=7 Ma) for the species found in two and more than two samples respectively (Figure 2.7-B).

The analysis above suggests that if caving is influencing the chronostratigraphic ranges, it may affect at least 421 of the 1014 species (41.5%). This proportion is represented with grey crossed lines in Figure 2.7-A. Based on the temporal range of the caving-susceptible species, the effect of caving would be to artificially produce taxa with unreliable temporal ranges. The use of these taxa could be problematic when diversity and taxonomic rates are estimated under the range through assumption because they can introduce several biases. For example, the rates of turnover could be overestimated because the presence of species with apparently short ranges that would otherwise be singletons and not considered in the analysis. Also, standing diversity calculated using boundary crossers (Foote 2000) could be overestimated in those intervals with artificial accumulation of short-range taxa.

As discussed, determining whether the stratigraphic ranges of species are

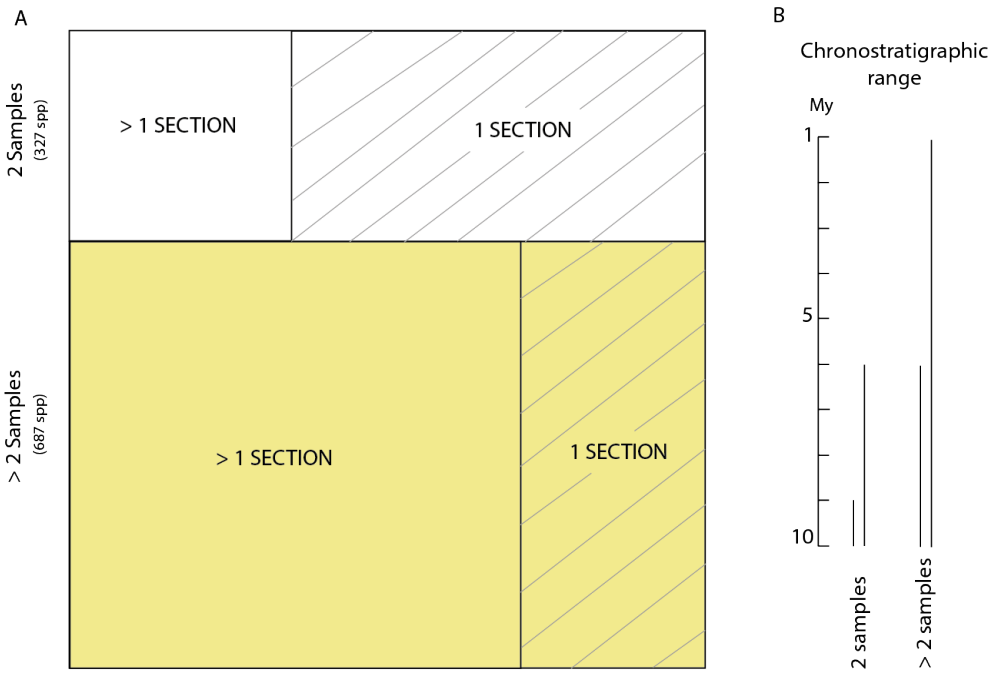

Figure 2.7: Distribution of 1014 species, with FADs estimated regardless if the sample corresponds to ditch cuttings, among the number of samples and wells in which they were detected. In the panel A, the complete square represents all the species (1014). The white and yellow areas represent respectively the proportion of species reported in only 2 samples (327 spp.) and the proportion of species reported in more than two samples (687 spp.). The sub-areas with diagonal stripes indicate the proportion of species with FADs estimated from samples of the same well. The FADs of these species are susceptible to be affected by caving. The plain colour represents the proportion of species reported in more than one section. The FADs of these species are less susceptible to be affected by caving. The panel B show the mean chronostratigraphic range of the species reported in 2 or more than 2 samples.

systematically biased by caving is important, but is not an easy task. On the one hand, there is not conclusive evidence that shows the existence of a systematic bias on the number of FADs in a specific time interval, but on the other hand, the evidence suggests that the ranges of a great proportion of taxa are potentially susceptible of being affected by caving.

To identify the potential influence of caving on the ranges of the species, and therefore on the diversity and taxonomic rates estimates, two versions of the composite sections were used in all the analysis involving the range

through assumption. One version including all the species independently of the type of samples from which the FADs were interpreted and the other version only includes those taxa with FADs determined from core or outcrop samples. If caving did not affecting the ranges of the species, we would expect to find similar results with both datasets.

2.2.1.2 Reworking

Opposite to the effect of caving, that artificially increases the FAD of the species, reworking is a process that has the potential of artificially increase the extinction (LAD) of the species. In other words, reworking makes the apparent time of extinction of a species younger than it really is. Because palynomorphs are strongly resistant to physical and chemical degradation, they often survive multiple cycles of erosion and sedimentation (Traverse 2007). Intense periods of reworking, associated with orogenic pulses of the Andes Cordillera, have been identified during the Miocene and to less of an extent during the Eocene in Colombia (de la Parra et al., 2015). Intervals with high concentrations of reworking artificially increase the LAD of the species and this effect has the potential to inflate the diversity in the younger intervals. To avoid the effect of reworking, the approach suggested by de la Parra et al (2015) was applied to the species of the composite section. The LAD of each species recorded in each section was compared with the LAD of the species calculated using the biozonation proposed in the first chapter of this work. The datum of the zonation represents the regional LAD. If the LAD in a specific section is younger than its regional LAD the presence of the species in that specific sample is considered as reworked. The LAD is then reinterpreted and reconciled with the datum of the zonation.

2.2.2 Regional Diversity

In the diversity analysis presented in this chapter, most of the material comes from samples obtained from the Llanos basin of Colombia. It is therefore possible that the diversity signals reported reflected only local-scale patterns. Although several palynological studies have been carried out in Cenozoic sequences of different regions of the Neotropics, direct comparisons among samples analyzed by different authors has been challenging for several reasons.

- First, the heterogeneity in the palynological nomenclature impedes comparison of samples analyzed by different authors, even if the samples are from the same geographic area.

- Second, differences in the standard numbers of palynomorphs counted per sample potentially makes raw estimations of diversity (e.g., richness) non-comparable.

- Third, the comparison of isolated samples with global or even regional diversity estimates is difficult because many of the techniques used to produce the diversity curves (e.g. standing diversity) use the total range of the species. This requires registration of the samples to a unique composite section. Once the composite section is constructed and the range-through assumption is made, it is very difficult to discern the individual contribution of each sample to the regional diversity curve. Furthermore, there is no way to compare an individual sample that is not part of the composite section with the regional curve.

- Fourth, calculations of ages of a samples based on palynological content can be subjective. Palynologists working in the Neotropics have used at least four regional biostratigraphic zonations (Lorente 1986; Germeraad et al., 1968; Muller et al., 1987 and Jaramillo et al., 2011) and two local schemes (Silva-Caminha, 2009; Hoorn 1993) to compare and establish the biostratigraphic and chronostratigraphic framework for their analysis. Use of zonation varies depending on: (1) which zonations were published and available at the time of the study; and (2) different zonations have higher resolution and greater utility for different geographic areas. To determine the age of a series of samples, the palynologists compares the stratigraphic range of the species in the zonation with the interpreted range of the same species found in their studies. With this information, they make inferences about the possible position of the samples with respect to the zonation. This interpretation is highly subjective, because the results are dependent of the expertise and yardstick of the analyst as well as the zonation used. The problem is more complex in situations where isolated samples are analyzed. In this case, the palynologist does not have a stratigraphic series long enough to capture the origination and extinction of the species that are the events generally used to define the boundaries of the biozones. Biostratigraphic assessments of such samples are usually reported with a broad and relatively inaccurate age (e.g., middle Miocene), rendering their significance for diversity dynamics on shorter timescales uncertain

To compare the diversity estimates in the present work with regional information extracted from the literature, different strategies were used to solve the problems mentioned above.

- Heterogeneity in palynological nomenclature is a potential problem only if the objective of the analysis is to compare of the palynological compositions of the samples. However, in the estimation of diversity, this problem could be disregarded because the aim of the analysis is to compare the number of species between samples and not their palynological similarity.

- Differences in the standard numbers of palynomorphs counted per sample, and the resulting difficulties comparing individual samples with the regional diversity curves could be addressed using subsampling. A satisfactory solution to this problem can be achieved by using the shareholder quorum-subsampling estimator (SQS) proposed by Alroy (2010) (discussed further below, in Methods). Because this method of diversity estimation does not rely on the range-through assumption, it is possible to estimate standing diversity either within individual samples (abundance-based subsampling: using individual palynomorphs as units of subsampling) or across a pool of samples (occurrence-based subsampling: using the presence/absence of species within samples as units of subsampling). In this way it is not only possible to compare regional estimates with individual samples but also establish the contribution of individual samples to the regional estimates.

- Subjectivity among estimates of the ages of the samples was addressed using the following criteria. If the age of the samples to compare were estimated using the zonation proposed in the first chapter of this work, or the compatible zonation proposed by Jaramillo et al. (2011), then the reported age was assumed without any further analysis. On the other hand, for those sections where the age of the samples is not reported or their interpretation is doubtful two strategies were used: (1) graphic correlation, and (2) a probabilistic approach. Graphic correlation was extensively explained in the first chapter of this work. The sections from the literature were compared against the composite section produced in the first chapter of this work and the age of the samples were calculated using the interpreted lines of correlation and the calibration points. The probabilistic approach makes reference to a methodology that uses a maximum likelihood approach to estimate the age of an individual sample or group of samples (Punyasena et al., 2012). This technique uses the relative abundance of microfossils (in this case palynomorphs) to provide shape to the known stratigraphic ranges of taxa based on the changing abundance of a taxon through time and to weigh the relative influence of a taxon in an isolated sample.

> The first step to apply the technique is to produce a baseline model that represents the changes in abundance over time to which a single sample or set of samples can be compared. This baseline model represents the entire priori knowledge of all known taxa and their abundance data for all time slices. Changes in abundance in the model can be described in absolute measures of time (e.g., million of years), as relative measures of time (e.g., older or younger) or as any significant measure of change through time or another gradient of interest (e.g., stratigraphic position). The taxon abundances of the model provide the comparative data against which all single sample estimates are matched. Once the individual samples are compared with the model, the final result is a likelihood distribution describing the position of the sample in the gradient as a range of probabilities. For the purposes of this work, the baseline model corresponds to the same composite section used to produce the diversity curve. This model represents the best current knowledge of the changing abundance of thousands of palynomorphs species during the Cenozoic in the area of study. The gradient of the baseline model uses the ages of each sample calculated through the lines of correlations and calibration points of the graphic correlation presented in the first chapter of this work. The comparison of each sample with the baseline model produces a probabilistic estimate of its age. Because each sample is compared against the same baseline model, this approach reduces the subjectivity involved in the age estimation. A downloadable version of the software used to complete the analysis is available in the personal webpage of one of the authors (http://publish.illinois.edu/punyasena/).

The diversity estimated in this work was compared with the diversity of several samples located in different areas of northern South America. Two sources of information were used. (1) Information of 39 sections from seven publications in Panama, Brazil, Peru y Colombia (Jaramillo et al., 2014; Leite et al., 2016; Silva-Caminha et al., 2009; Jaramillo et al., 2017; Antoine et al., 2016; Hoorn 2006; Salamanca et al., 2016); (2) Palynological information obtained from nine wells drilled in the Sinu-San Jacinto, Catatumbo and Middle Magdalena Valley sedimentary basins of Colombia (de la Parra et al., 2018). The information about the sections and their geographic location is presented in the Annex 2.3 and Figure 2.8 and summarised below.

2.2.2.1 Information from literature

Palynological information was extracted from seven publications (Hoorn 2006; Jaramillo et al., 2014; Antoine et al., 2016; Leite et al., 2016; Silva-Caminha

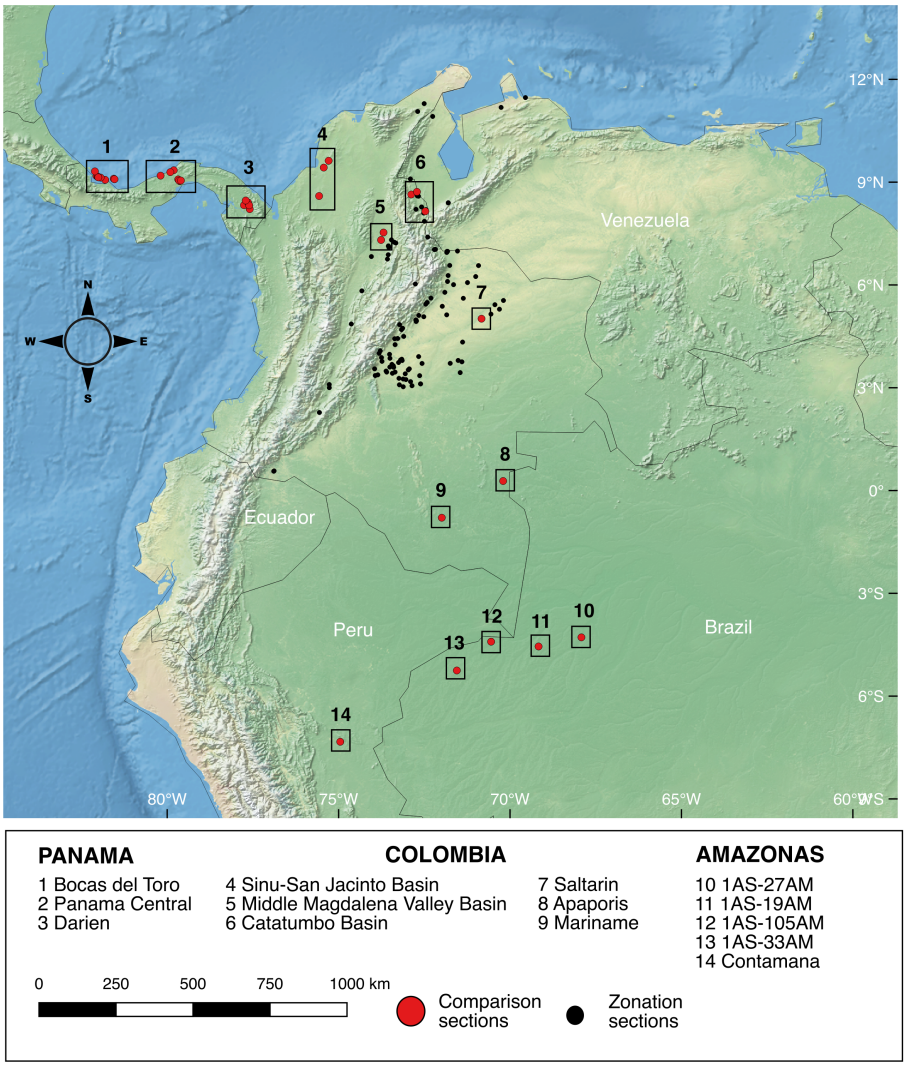

Figure 2.8: Map of localities with palynological information extracted from literature and wells (red dots). Localities were grouped in 14 areas for comparison purposes. Black dots correspond to localities (wells and surface sections) used to construct the regional diversity curve. For information about the localities refer to Annex 2.3.

et al., 2009; Jaramillo et al., 2017 and Salamanca et al., 2016). Quantitative counts for five of them can be found in their respective supplemental materials while the counts for Leite et al.(2016) and Silva-Caminha et al.(2009) are presented as tables in the manuscript and were digitized in the present

work.

- **Hoorn (2006)**: *Mangrove Forests and Marine Incursions in the Neogene Amazonia (Lower Apaporis River, Colombia).* This study describes the palynological and sedimentological results of eight sections measured along the lower Apaporis and Pira Parana Rivers (Hoorn, 2000b). The two rivers are located in the southwest edge of the Guiana Shield (Figure 2.8-number 8). Approximately 175 meters of sediments were described in the two sections. The unit described by the author, known informally as the Apaporis Sand Unit, is characterized by alternation of sandstones and sporadically organic rich clay. As a part of the study, a total of 25 samples were analyzed for palynology. The raw counts were downloaded on March-2017 from the repository mentioned in the publication and correspond to an excel file where the two first rows indicates the sample code and the stratigraphic position of each sample.

- **Jaramillo (2014)**:*Palynological Record of the Last 20 Million Years in Panama.* This study describes the palynological results of 282 samples from a large number of outcrops exposed during the new expansion of the Panama Canal. The samples came from three different sources. (1) Fifty-five samples from a new exposed stratigraphic section covering the Culebra and Cucaracha formations. (2) Two hundred samples collected by the Panama Palaeontology Project that were processed and analyzed by the authors. (3) Twenty-seven samples previously published by Alan Graham in different years (Graham 1988a; Graham 1988b; Graham 1991a; Graham 1991b). The sections are located in three areas of Panama: Bocas del Toro, central Panama and Darien (#1,2,3, Figure 2.8). A summary of the sections is presented in the Annex 2.3. The raw counts were downloaded on March-2017 from the repository mentioned in the publication and correspond to a single Excel sheet with the counts of all the samples.

- **Antoine (2016)**: *A 60-million-year Cenozoic history of western Amazonian ecosystems in Contamana Peru.* In this study the authors provide a survey of the Cenozoic deposits along the Quebrada Cachiyacu, located near the town of Contamana in the Peruvian Amazonia (#14, Figure 2.8). The authors visited 34 fossil localities where they found a rich and diverse association of fossil remains, including vertebrates, molluscs, arthropods, plant fossils and microorganisms. The palynological analysis is restricted to seven samples, three of them corresponding

to the lower part of the Pozo Formation and four samples to the Pebas Formation. The raw counts were downloaded on March-2017 from the repository mentioned in the publication and correspond to a single Excel sheet with the counts of all the samples.

- **Leite (2016)**:*The effects of the inception of Amazonian transcontinental drainage during the Neogene on the landscape and vegetation of the Solimoes Basin, Brazil*. In this work, the authors study the Neogene palynology of the Solimoes basin using 32 samples from a rock core (1AS-33-AM) drilled in the Amazonas basin of Brazil (#13, Figure 2.8). The core recovered 405 meters of sediments from the Solimoes Formation. The raw palynological counts are presented as a table in the manuscript and were manually digitalized for the purposes of this work.

- **Silva-Camhina (2009)**: *Neogene palynology of the Solimoes Basin, Brazilian Amazonia*. This study presents the pollen and spore record of two rock-cores of the Solimoes Formation drilled in northwestern Brazil, east of the Iquitos Arch (#10-11, Figure 2.8). The two cores (1AS-27-AM and 1AS-19AM) are 1320 feet and 839 feet in thickness respectively. A total of 41 palynological samples were analyzed from the two cores. The raw palynological counts are presented as tables in the manuscript. A digitalized version of the counts was requested from the main author.

- **Salamanca et al. (2016)**:*Amazon Forest dynamics under changing abiotic conditions in the early Miocene (Colombian Amazonia)*. This study presents a palynological and geochemical analysis of a 60m thick sedimentary succession situated along the Caqueta River in Colombia Amazonia (#9, Figure 2.8). Fifty-two samples were analyzed for palynology, with 43 of them previously analyzed by Hoorn (1994). All the samples with palynomorphs counts below 100 specimens were excluded, leaving a total of 47 samples (Salamanca et al., 2016). The raw counts were downloaded on March-2017 from the repository mentioned in the publication and correspond to a single Excel sheet with the counts for all the samples.

- **Jaramillo (2017)**:*Miocene-Flooding events of Western Amazonia*. This study analyzed the age, fossil record (including palynology), geochemistry and depositional environments of two Miocene rock cores drilled in the Llanos and Amazonas/Solimoes basins. The main objective of the study was to identify the timing, duration and frequency of the

marine flooding events that occurred during the Miocene in the western Amazonia. One of the cores, called Saltarin, was drilled in the northeastern part of the Llanos Basin in Colombia (#7, Figure 2.8). The core recovered approximately 671 meters of sediments from the Carbonera, Leon and Guayabo Formations and 138 samples were analyzed for palynology. The second core, called 1-AS-105AM, was drilled in the Amazonas Basin (#12, Figure 2.8). This core recovered a total of 405 meters of sediments from the Solimoes and Ramon Formations, from which 95 samples were analyzed for palynology. The raw palynological counts for both cores were downloaded on March-2017 from the repository cited in the publication.

2.2.2.2 Information from wells

Palynological information from nine wells drilled in three different basins of Colombia was used to produce additional estimates of diversity. These wells were not included in the biostratigraphic analysis of the Chapter 1, neither were they included in the diversity estimates presented in this chapter because the number of samples and the resolution is very low. The palynological information from these wells comes from both ditch cutting samples and rock-core samples. The counts are presented in the internal reports of the Biostratigraphy Team at Ecopetrol S.A. Because the information is confidential, the original names of the wells were codified. The wells were grouped by sedimentary basin (Annex 2.3, Figure 2.8):

- **Sinu-San Jacinto Basin (# 5, Figure 2.8)**: The information from this geographic area corresponds to 24 samples distributed in four rock-cores (SSJ-3, SSJ-15, SSJ-4, SSJ-8) (Annex 2.3).

- **Catatumbo basin (#6, Figure 2.8)**: The information from this geographic area corresponds to 35 ditch cutting samples distributed in three wells (In1, Ti, Tr1) (Annex 2.3).

- **Middle Magdalena Valley Basin (#5, Figure 2.8)**: The Information from this geographic area corresponds to 73 samples distributed in two wells (Bo3 and Cr7) (Annex 2.3).

2.3 Methods

Various methods were used to produce regional diversity estimates and to calculate taxonomic rates (origination and extinction rates) from palynomorphs

assemblages from northern South America. Because caving could artificially increase the FAD of the species, the composite section was constructed in two different ways. One version including all the species regardless of whether their FADs were interpreted based on ditch cutting samples. This version is referred to as the complete composite section. The second version includes only those taxa whose FADs were estimated from rock-core or outcrop samples. This version is referred to as the restricted-FAD composite section. The results obtained from both interpretations were compared.

One of the most important differences between the methods used to calculate diversity and taxonomic rates is between Range-Through Methods (RTMs) and In-Bin Occurrence Methods (OBINs). RTMs infer each taxon to be present in all the samples between its first and last occurrence even if the species was not found in any sample in between (Cheetham and Debo 1963). This approach have been mainly used for compilations that only record first and last occurrences of taxa (Sepkoski 1978; Foote 1993), and has been justified as a mean of smooth spotty data sets (Boltovskoy 1988) and to counteract the effects of environmental influences (Hazel 1970). However, RTMs also introduce a series of biases, like the Signor-lips effect, the Pull of the Recent and other edge effects, that are difficult to quantify and remove (Alroy 2010; Signor and Lipps, 1982; Raup 1972). For example, the origination rates are likely to be too high at the beginning of a time series because of the edge effect while the extinction rates are likely to be too low at the end a the time series because of the Pull of the Recent (Alroy 2010).

OBINs methods make use of information on taxa that are actually sampled in each interval. This approach makes the assumptions of RTMs methods unnecessary, removing the problems of edge effects. The present study compares both RTMs (standing diversity, taxonomic rates using boundary crossers and cohort survivorship analysis) and OBINs methods (shareholder quorum subsampling (SQS) and taxonomic rates using three timers and gap fillers).

2.3.1 Estimates based on Range Through Methods

2.3.1.1 Diversity and taxonomic rates

In a paleontological context, diversity can be defined as an estimate of the number of taxa that were extant from interval to interval (Foote and Miller, 2006). Taxonomic rates make reference to the rates at which new lineages originate and existing lineages become extinct (Foote 2000). Both approaches assumes the so-called Range-Through Method (RTM) in which every species is considered to be present in all the intervals between its first and last

occurrence, even if the species was not found in any sample in between. Following Foote (2000), any taxon known from or inferred to be present in a stratigraphic interval can be classified into one of four mutually exclusive categories (Figure 2.9):

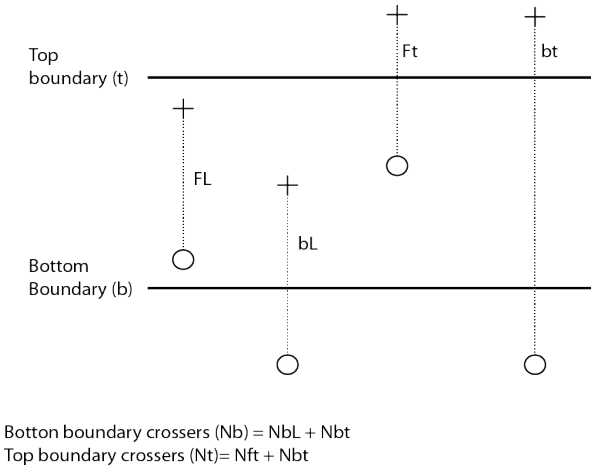

Figure 2.9: Illustration of the four fundamental categories of taxa present during a stratigraphic interval. FL: species with both their FAD and LAD occurring during the interval, bL: species with FAD occurring before the bottom of the interval and LAD occurring during the interval; Ft: species with FAD within the interval and LAD occurring afterwards; bt: species with FAD before the interval and LAD afterwards.Circles and crosses denote FAD and LAD respectively (modified from Foote 2000).

- **FL:** taxa confined to the interval, with first appearance datum (FAD) and last appearance datum (LAD) both falling within the interval
- **bL:** taxa crossing the bottom boundary, with FAD before the interval and LAD occurring during the interval.
- **Ft:** taxa with FAD during the interval and crossing the top boundary and LAD in a younger interval.
- **bt:** taxa that range through the entire interval, crossing both the bottom and top boundaries. With FAD before the interval and LAD after it.

In this nomenclature, b and t make reference to the bottom and top boundaries of a stratigraphic interval and F and L refer to FAD and LAD

within the interval. The numbers of taxa in the four categories are denoted as NFL, NbL, NFt, and Nbt (Foote 2000). Several measures of diversity and taxonomic rates can be derived by the combination of the number of taxa in the four fundamental classes. For taxonomic rates, the two simplest and most intuitive metrics are the Intensity of Extinction (NL) and the Proportional Extinction (PE) (Foote 2000). The metric NL is simply the total number of last appearances in an interval (e.g. for extinction is number of taxa of the categories bL and FL (Figure 2.9)). This metric is however problematic when the objective is to compare taxonomic rates among different intervals of time because it may be expected that the number of extinction/originations to be greater when the standing diversity is higher because there are more species at risk (Foote and Miller, 2006). The metric PE solves this problem by dividing NL by the total number of taxa in the interval. However, if extinction occurs continuously throughout a time interval, then more extinctions are expected in longer time intervals. Dividing the metric PE by the length of the time interval can solve the problem. However and despite the corrections, the metrics NL and PE still have undesirable properties related to the way in which they account for diversity. Because not all the taxa present during a time interval exist throughout the entire interval, the total diversity could overestimates the number of taxa at risk (Foote and Miller,2006).

Foote (2000) and Foote and Miller (2006) addressed this problem by proposing extinction and origination rate measures that take a census of taxa at two precise moments in time, the beginning and end of the interval, and which are based on model of exponential survivorship. These two rates are essentially exponential decay coefficients (where origination can be perceived as a decay process operating in reversed time) (Alroy 2014).

The per-capita extinction rate (q) is the natural log of the proportion of taxa crossing the lower boundary of an interval that are still extant across its upper boundary (Table 2.1). The per-capita origination rate (p) is the reverse survivorship of lineages alive at the end of the interval (origination can be viewed as extinction in reversed time). It is calculated as the natural log of the proportion of taxa that were already extant at the start of the interval (Table 2.1). The taxonomic rates p and q are expressed on a per-capita basis, meaning that the number of originations/extinctions is scaled to the number of taxa at risk and the amount of time they are on risk.

There are many different ways to count the number of taxa present in an interval, which is the final goal of any diversity estimate. Most of them rest on the convention that each taxon ranges across any time horizon occurring between its FAD and LAD. These methods have been largely used in studies involving global diversity curves because they do not require detailed information about the occurrences of taxa within individual intervals

Table 2.1: Equations to calculate mean standing diversity and per capita extinction (q) and origination (p) rates for intervals of length (dt). Measurements are expressed in terms of the number of taxa classified into the four fundamental categories (Figure 2.9) (modified from Foote 2000).

Measure	**Symbol**	**Equation**
Bottom boundary crossers	Nb	Nb = NbL + Nbt
Top boundary crossers	Nt	Nt = Nft + Nbt
Mean Standing Diversity	Sd	Sd = (Nb + Nt) / 2
Per-capita origination rate	p	p = -ln (Nbt/Nt) /dt
Per-capita extinction rate	q	p= -ln(Nbt/Nb)/dt

or fossil localities, but only information about their FADs and LADs (Raup 1972; Sepkoski et al.,1981; Alroy 1996). Two of the most basic approaches, the standard and the boundary crossers methods, use the number of FADs and LADs in each interval for the estimation. The standard method estimates diversity within the interval as a whole, while the boundary crossers method estimates the diversity at an instantaneous time horizon (the boundary between consecutive intervals; Foote and Miller,2006). A complementary method proposed by Foote (2000), called mean standing diversity (Sd), measures the relative changes in diversity using the proportional difference between the number of taxa crossing into an interval and the number crossing out. In terms of the four fundamental classes of taxa (Figure E-1), Sd is defined as the sum of the bottom boundary crossers (Nb) and top boundary crossers (Nt) divided by two (Table 2.1). In Sd, singletons are irrelevant in the calculation. Also, Sd offers a good control to the effects produced by incomplete preservation and variation in interval length (Foote 2000).

The fossil record is incomplete, and this incompleteness affects diversity estimates. Importantly, completeness of taxon sampling varies among intervals, biasing estimates of relative change in diversity through time. Quantifying and compensating for this incompleteness is not a trivial task in part because fossil preservation varies in both time and space (Foote et al., 1999; Raup 1979). A useful approach to quantifying and compensating for the incompleteness of the fossil record is to calculate the sampling probability within each stratigraphic interval (Rbin) and then use this metric to compensate the diversity (Quental et al., 2010). Rbin is the proportion of range through taxa that have been sampled within an interval compared with the total number of taxa that range through the interval. This is an estimate of the probability that a taxon that was actually present in an interval would be sampled. Diversity can be estimated by dividing the number of taxa actually

sampled in the interval (Nbtsamp) by its preservation probability (Rbin).

To estimate diversity and taxonomic rates (per-capita extinction and origination rates), the two versions of the composite section (the complete composite section and the restricted-FAD composite section) were analyzed. The mean standing diversity (Sd) and the diversity compensated by the preservation probability (Rbin) were also calculated. Confidence intervals for the taxonomic rates were constructed using bootstrapping.

Singletons and boundaries

Following the definition of Foote (2000), a singleton is any taxon confined to a single stratigraphic interval at the given level of resolution (any member of the FL category (Figure 2.9)). Other authors have used the term making reference to those species represented by a single occurrence (e.g., Buzas and Culver, 1998; Alroy 2010). The boundary of the stratigraphic intervals can be established in at least two different ways (Figure 2.10) and here is where the definition of singleton becomes important. The first approach is to define the boundaries as the mid point between every consecutive pair of samples (Figure 2.10-A). In this case a singleton is any taxon present in only one sample or what it is equivalent, in the interval. When boundaries are defined in this way, diversity can be estimated for the time at which the sample occurred. The second approach is to divide the stratigraphic section into equal-length time intervals. In this context, all the samples within a defined time interval are merged to form a composite sample (Figure 2.10-B). In this case, although a taxon could be present in several samples within an interval, it is considered a singleton in the sense of Foote (2000; i.e. a single-interval taxon). This information can be used to estimate the diversity of each time interval.

The complete and the restricted-FAD composite sections were divided into 1Ma time intervals and standing diversity and taxonomic rates were calculated. Additionally, standing diversity was also calculated for the two versions of the composite section by defining the boundaries of the intervals as the mid point between consecutive pairs of samples.

2.3.1.2 Taxonomic Survivorship analysis

Taxonomic survivorship analysis makes reference to the statistical study of the durations of taxa (Foote and Miller, 2006). Although several techniques of survivorship analysis have been developed in the field of population dynamics and demography, two of them have shown to be very useful in studies of macroevolution (Kurten 1954; Van Valen 1973) and especially in the esti-

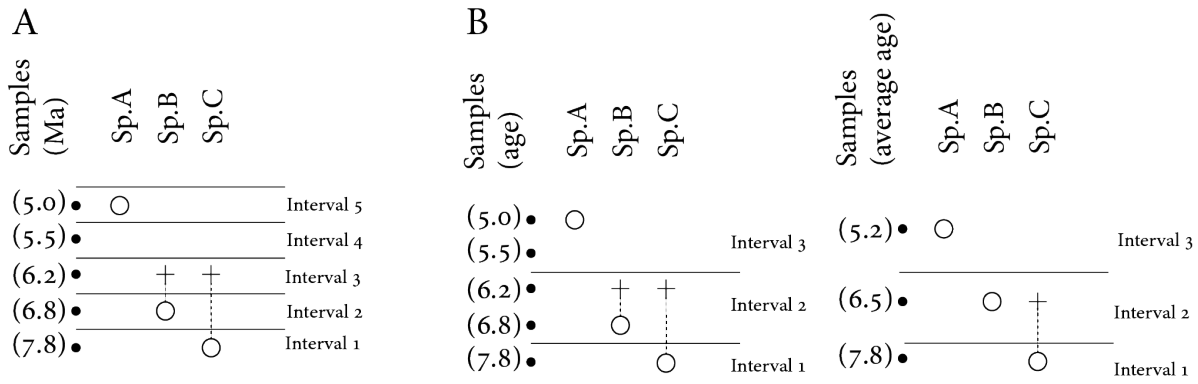

Figure 2.10: Definition of stratigraphic intervals and singletons. This hypothetical example show the distribution of three species (A, B, C) in 5 samples with ages 5,5.5,6.2,6.8 and 7.8 Ma. In the panel A, the mid point between consecutive samples defines the boundary of each interval. A taxon found in only one sample is considered a singleton (e.g. Sp. A). The Panel B shows the same distribution of taxa that A but in this case the section is divided in equal intervals of 1 Ma. The interval 2 for example, ranges between 6 and 7 Ma. Because two samples (6.2 and 6.8) fall within this interval, they are merged and represented by one single sample (6.5). In this case, the species B is considered a singleton even though is recorded in two samples.

mation of origination and extinction rates (Raup 1977; Levinton 1974; Jones 1986; Arnold 1995). The first is termed dynamic survivorship analysis and was originally described in a paleontological context by Kurten (1954). In this approach, all the taxa with a given duration are classed together, regardless of when they lived. The species durations are calculated and a table with the observed frequency distributions is produced. This table, called survivorship table, depicts the number of taxa with a given duration and the cumulative number with at least that duration (Foote and Miller,2006). When the frequencies of the survivorship table are plotted on a logarithmic scale, the slope of the line fitting the cumulative distribution is an estimate of the mean extinction rate. Dynamic survivorship analysis assumes that the full distribution of durations of fossil groups can be sampled. A violation of this assumption occurs when the origination of a taxonomic group is young. A group that originated 7 Ma ago, for example, can only have species with durations between 0 and 7 Ma (Foote and Miller, 2006). Because dynamic survivorship estimates a single extinction rate for the entire species pool, it assumes that extinction rates show little variation through time (temporal stability in the age distribution of species) (Raup 1978). If the age distribu-

tion changed over time (i.e. due to variation in extinction rates), something common in most paleontological situations, this represents a problem in the dynamic method (Foote and Miller,2006).

The second approach, called cohort survivorship analysis, is nearly assumption-free with regard to the stability of age distributions. In this approach, cohorts of taxa that originated in the same interval are analysed independently of other cohorts. Each cohort is then followed forward in time and the number of taxa remaining is monitored as a function of elapsed time (Foote and Miller, 2006). Because the cohort analysis is confined to monitoring the decay of each cohort, it makes no assumptions about origination rates (Raup 1975). As with the dynamic survivorship analysis, the slope of a straight line fitting a cohort curve on a semi-log graph gives an estimate of the extinction rate for a cohort. It is assumed that the external factors causing mortality remain the same throughout the entire duration of the cohort (Raup 1978). An abrupt change in the probability of death caused by environmental change will show up as an inflection in the survivorship curve (Raup 1978). If several cohorts show inflection of their curves during the same interval, this could be interpreted as an external event occurring at that time.

The cohort survivorship analysis was performed for both the complete composite section and the restricted-FAD composite section binned into 1 Ma intervals. Single-occurrence taxa were eliminated, as they do not provide information in survivorship analysis. Four cohorts from the Maastrichtian were included in the analysis of the complete composite section for comparison purposes. The composite sections were separated into cohorts (cohort number), each representing a 1 Ma time interval (interval). The cohort size column refers to the number of species originating during each time interval. The rows indicate the number of species surviving at the end of each interval. The percentage of survivors was calculated and plotted on a semi log graph. Only those cohorts with an initial size bigger than 10 species were used in the analysis.

2.3.2 Estimates based on In Bin Occurrence Methods

2.3.2.1 Shareholder Quorum Subsampling (SQS)

An accurate estimate of diversity should statistically remove biases imposed by the counting method and by the amount of fossil data sampled in each interval. Variation in the quantity of sampling is problematic because estimated differences in diversity between two samples can be explained by differences in sampling effort and not to biological factors. The goal of most resampling methods is obtain an empirical approximation of a sampling dis-

tribution of a statistic of interest and can be used to standardize samples, test statistical hypothesis, estimate standard errors and confidence limits and carry out other types of statistical evaluations of empirical data sets (Kowalewski and Novack-Gottshall 2010). In the specific case of diversity estimation, randomized subsampling protocols seek to hold each time interval to a quota of data items. This quota may be expressed in terms of: (1) number of taxonomic occurrences; (2) number of fossil collections; (3) occurrences represented by the collections (Alroy 2010). Most methods proposed so far, including classic rarefaction, subsample the data from each interval to attain an entirely uniform and fixed quota of data items (i.e., counts of specimens, counts of occurrences or counts of fossil collections) (Alroy et al., 2001; Bush et al., 2004; Alroy 2010a). However, uniform-sampling schemes tend to flatten out variation in diversity through time because they are designed to count items and kind of items, ignoring systematically two prominent features of the fossil record, rarity and commonness (Alroy 2010b). Uniform subsampling is therefore different to fair or representative subsampling. As pointed by Alroy (2010b), when the actual richness of the species pool is low, it is not necessary to sample very hard, but when richness is high and many taxa are rare, it may be necessary to subsample more intensively to achieve comparable coverage of the species pool. In this case, uniform sampling schemes fail by under-sampling the richer species pool. Shareholder Quorum Subsampling (SQS) attempts to estimate diversity by means of fair sampling, rather than uniform subsampling. In contrast to uniform sampling, SQS tracks not the number of items that are drawn but the coverage of each species pool represented by the species that have been drawn.

Coverage is the proportion of the entire frequency distribution represented by the species found so far (i.e., if one species represent 35% of occurrences within an interval, then the species contributes a proportional frequency of 0.35 when it is sampled during subsampling draws). The coverage of observed data is modified to estimate the coverage of the real taxon distribution for each sample pool (Alroy 2010a; Alroy 2010b). This is achieved by multiplying the coverage of the observed data by Goods u; the proportion of occurrences representing non-singleton taxa, which is a measure of sample completeness (Alroy 2010). Standardization in SQS is achieved therefore by drawing enough collections in each time interval to generate the same coverage level (Alroy 2010b). The quorum (q) refer to a certain amount of coverage, if q=0.30 sampling stops when 30% of the distribution is covered. Alroy (2010a,b) proposed that a quorum of 0.4 was the minimum required to recover consistent relative estimates of diversity and how it has changed through time.

Two approaches were used to estimate diversity using SQS. First, diver-

sity was estimated for each sample of the complete composite section and the restricted-FAD composite section by subsampling based on abundance of species within each sample. The complete composite section includes the abundance information from 2688 species distributed among 6812 samples. The restricted-FAD composite section includes the abundance information from 192 species, with FADs interpreted from core or outcrop material, distributed among 6137 samples. The difference in the number of samples represents the elimination in the restricted-FAD composite section of ditch cutting samples recording FADs. Only samples with counts greater than 50 palynomorphs were included in the analysis. This level was chosen because is the level used by other authors in their analysis (Jaramillo et al., 2006; Jaramillo et al., 2015; Leite et al., 2016) which facilitate further comparisons. The total number of samples fulfilling this condition is 3978 and 3620 for the complete and the restricted-FAD composite section respectively. The result is a cloud of points representing the estimated diversity of all the samples through the Cenozoic.

In the second approach, the two versions of composite section were divided into 1 Ma time intervals. All the samples falling within each interval were grouped and combined to form a single sampling pool (composite sample). The aim was to produce a unique set of composite samples representing the regional composition of the vegetation within each interval. Two approximations were used to represent the regional contribution of each species. First, the total abundance of each species calculated as the sum of the abundances reported in all the samples where the species was found. Second, the abundance was calculated as the total number of samples in which each species was reported (i.e. occurrence-based subsampling). SQS was calculated for both approximations and for each one of the 65 intervals. The result is two diversity curves in which each point represents the standardized regional diversity for each time interval.

2.3.2.2 Taxonomic rates via three timers and gap fillers

A practical impact of estimate origination and extinction rates by using the equations presented in Table 2.1 (Foote 2000) is that those metrics consider entire age ranges (the range-through assumption). As explained before, this introduces a series of biases, such as the Signor-Lipps effect, the Pull of the Recent and other edge effects, which are difficult to quantify and remove. To correct some of these problems, Alroy (2008, 2010, 2014) introduced a series of equations to estimate origination (μ) and extinction (λ) that do not make use of the range-through assumption, and instead focused on occurrence data that indicate which taxa are sampled in which time interval. These equa-

tions involve examining only a limited sampling window consisting of four consecutive time intervals (Figure 2.11). Similar to the approach proposed by Foote (2000), Alroys method counts the number of taxa sampled in each one of four different categories (Figure 2.11).

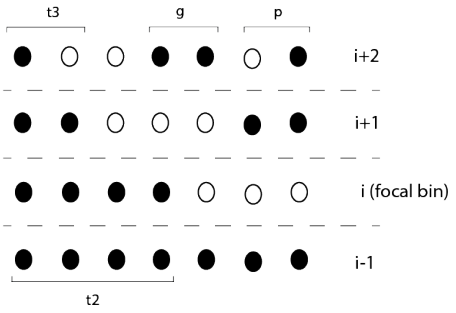

Figure 2.11: Sampling patterns across a four interval-moving window. The stratigraphic intervals are denoted as i-1, i, i+1 and i+2. The black and white circles represent absence and presence respectively. In this example, i is the focal interval, meaning the one for a which a rate will be computed; t2 = two timers taxa; t3= three timers taxa; g=gap fillers taxa; p= part timers taxa (modified from Alroy 2014).

- **Two-timers (t2)**: make reference to those taxa sampled immediately before and within the focal bin (forward two-timers; t2i) or within and immediately after the focal bin (backward two-timers t2i+1).

- **Three-timers (t3)**: refer to those taxa sampled in the focal bin and immediately before (i-1) and after (i+1).

- **Part-timers (p):** those taxa sampled before and after but not in the focal interval.

- **Gap-fillers (g):** are those taxa sampled in intervals i-1 and i+2 but not within interval i+1 (forward gap-fillers) or in interval i-2 and i+1 (backward gap-fillers). May or may not be found in the focal interval (Figure 2.11).

The first set of rate equations described by Alroy (2008) termed three-timers equations, use a per-taxon and per-interval sampling probability computed from three- timers (t3) and part-timers (p) to correct that many apparent two-timers taxa (t2) have not been resampled before the focal (for origination) or afterwards (for extinction) (Alroy 2008, 2014). In these equations, extinction is estimated comparing forward two-timers with three-timers and part timers while origination is estimated comparing backward two-timers with three timers. The three-timer equations are presented in the Table 2.2. A second pair of equations, denominated gap-fillers (Alroy 2014) also work with four interval-moving windows. The equations not only consider t2, t3 and p, but also count of taxa found in intervals i-1 and i+2 and not within the interval i+1. These taxa, called forward gap- fillers (g in figure 2.11), may or may not be found in the focal interval, but in any case they are excluded from the t3 and p counts. They are called gap-fillers because the forward gaps they fill are crucial to distinguish real extinction from sampling failures (Alroy 2014). When origination is estimated, t2 applies to top two timers and the g class taxa must be sampled in i+1 and not i-1. For the extinction estimates, t2 applies to bottom two-timers and g must be sampled in i-1 and not i+1. Although the gap-filler origination and extinction equations use some of the same counts, there is not spurious correlation between them (Alroy 2014). The gap-filler equations are presented in the Table 2.2.

Table 2.2: Nomenclature and equations to calculate origination and extinction rates using the fundamental sampling patterns presented in Figure 2.11 (Three Timers and Gap Fillers equations, Alroy 2008, 2014).

Source	**Metric**	**Symbol**	**Equation**
Three Timers (Alroy 2008)	sampling probability	Ps	Ps = t3 / (t3 + p)
Three Timers (Alroy 2008)	extinction rate	μ	u = log(t2i/t3) + log (Ps)
Three Timers (Alroy 2008)	origination rate	λ	λ = log (t2i+1/t3) + log(Ps)
Gap Fillers (Alroy 2014)	gap-filler equation	μ/λ	log [(t2+p)/(t3+p+g)]

Simulations performed by Alroy (2014) suggest that the three-timers and gap-fillers equations produce similar results. Simulations also suggested that all the methods (including the boundary crossers) might yield different values depending on whether the data are sampling standardized (Alroy 1996; Alroy 2010b; Foote 2000). Three-timers might produce noisier values when the subsamples are small; gap-fillers might produce less noisy values if sampling probabilities are made more uniform; and boundary crossers (Foote 2000) should produce lower values whenever turnover rates and sampling probabilities covary strongly (Alroy 2014). The most commonly employed standard-

ization methods are classic rarefaction of taxonomic occurrences (CR) (Miller and Foote, 2006) and SQS (Alroy 2010). Although CR is nearly useless for reconstructing diversity, the three-timers and gap-fillers methods build in assumptions about the equality of sampling probabilities from one interval to the next, they are better met by data that is previously standardized by CR (Alroy 2014). In this sense, in the present study the turnover rates using the three-timer and gap-filler methods are based on CR data.

Occurrences on both the complete composite section and the restricted-FAD composite section were used to calculate the origination and extinction rates. The data of the restricted-FAD composite section consists of 65 intervals of 1 Ma in duration. The counts are derived from 45597 occurrences of 192 species distributed among 6137 samples that were sampling standardized using classical rarefaction (CR), by random drawing entire collections up to a quota of 39 collections per time interval. The resampling was repeated 1000 times and taxonomic rates were calculated for each one of the iterations. Three bins (64-65, 63-64, 55-56) did not reach the quota of 39 occurrences and were not used in the analysis. This has a knock-on effect that excludes adjacent intervals whose moving-windows include those bins.

Data of the complete composite section consist of 65 intervals of 1Ma in duration. The counts are derived from 110213 occurrences of 2688 species distributed among 6812 samples that were sampling standardized by random drawing entire collections up to a quota of 137 collections per bin. The resampling protocol was repeated 1000 times and taxonomic rates were calculated for each one of the iterations. Only one bin (55-56) did not reach the quota of 137 occurrences and was therefore removed of the analysis.

2.3.3 Diversity in Space

In spite of its importance to understand macroevolutionary patterns in deep time, spatial patterns of diversity are not frequently discussed in the paleontological literature. This could be explained by the fact that the scale of most of the macroevolutionary analysis is global in scope, which make difficult to compare very separate geographical regions. In the specific case of this study, the scope of the analysis is regional and spatial coordinates are available for each locality. This offers a great opportunity to explore spatial patterns in diversity through time.

To investigate the geographic distribution of diversity into successive time intervals, the complete composite section was divided in 5 Ma intervals (bins). For each one of the bins, the samples belonging to the same section were grouped to form a unique sample (composite sample). The composite sample represents therefore the palynological composition of a specific site in a

determined bin. Diversity was then calculated using SQS for each one of the composite samples for all the bins. Once the diversity was estimated, statistical analysis including a t-test and ANOVA were used to test for differences in diversity between geographic areas.

To visualize the results, 12 choropleth maps (one for each 5 Ma bin) were produced. These maps are a useful and intuitive way to visualize and understand how a measurement varies across a geographic area. Each region of the map is coloured on the basis of some metric of interest and a specific colour progression is used to capture the spatial variation of the data.

In general, choropleth maps are based on data aggregated over previously defined regions or areas (e.g. countries, political divisions, etc.) (Carr et al., 2005; Cromley et al., 2009). In the case of the diversity maps there are not such previously defined regions. In fact, the sections to be represented are not even areas but points in the space. To define the areas of the diversity choropleth maps, a Dirichlet tessellation around each one of the sites was calculated. A Dirichlet tessellation, also known as Thiessen polygons or Voronoi diagrams, is a mosaic of polygons constructed around a set of points where each polygon represents the geometric zone of influence of the respective point on a map (Legendre 1988). The zone of influence of a specific point X (in this case a section) includes all the other points in the surface that are close to X than to any other point in the area of study.

The construction of the tessellation for each bin was restricted to the areas with active depositional systems at the specific time of the reconstruction; excluding therefore areas considered as a rock units exposed in the source areas. Also, the external boundaries of the tessellations were truncated according with the paleogeographic configuration of the basin at the respective time interval. The paleogeographic information and reconstructions were obtained from Reyes-Harker et al. (2015). These authors used biostratigraphy, core descriptions, petrography, seismic information and thermochronology to build nine Cenozoic paleogeographic reconstructions (represented as a maps) of the Andean retro arc region of Colombia, including the ancestral Central Cordillera, the Middle Magdalena Valley, the Eastern Cordillera and the Llanos basin. The reconstruction used for each one of the 12 intervals is presented in the Table 2.3.

Because of a special interest in exploring the diversity pattern during the Miocene, the same methodology explained above was applied to the interval between 4 and 24 Ma. For this analysis, the composite section was subdivided in 2 Ma intervals producing therefore 10 choropleth diversity maps. Because for this interval the paleogeographic reconstruction of the area is very similar (Reyes-Harker et al., 2015) the same configuration (early Miocene) was used to construct a unique tessellation for the 10 intervals. All the sections with

Table 2.3: Age of the paleogeographic reconstruction (Reyes-Harker et al., 2015) used to produce the choropleth diversity maps.

Age Reconstruction	**Time Interval in Map (Ma)**
early Paleocene	60-65
late Paleocene	55-60
early-middle Eocene	50-55
early-middle Eocene	45-50
early-middle Eocene	40-45
late Eocene	35-40
early Oligocene	30-35
late Oligocene	25-30
early Miocene	20-25
early Miocene	15-20
middle Miocene	10-15
late Miocene	5-10

information in at least one interval were used to produce the tessellation. If one specific section does not have palynological information in an interval, their representative polygon is empty in the choropleth map. The paleogeographic maps in Reyes-Harker et al (2015) were digitalized and converted to shape files by using QGIS (QGIS Development team, 2017). The Dirichlet tessellations were also produced in QGIS by using the geometric tool of the vector menu.

2.3.4 Climate and Macroevolution

The work of Jaramillo et al. (2006) suggested a good correlation, at least for the interval between 65 and 20 Ma, between Neotropical plant diversity fluctuations and changes in global temperature. D'Apolito (2016) has also suggested a good correlation between diversity and temperature for the interval covering the Mid Miocene Climatic Optimum (14 to 17 Ma approximately). Diversity in Jaramillo's work (Jaramillo et al., 2006) was estimated using the cross boundary equations of Foote (2000) using the range through assumption. D'Apolito (2016) used rarefaction to estimate diversity. For the comparisons, these authors used a composite curve of isotopic values for benthic foraminifera as a proxy of climate (Zachos et al., 2008). This benthic oxygen isotope ($\delta O18$) curve has been used as a proxy for global temperature in studies of climate change in deep time (Zachos et al., 2001; Zachos et al., 2008; Foster et al., 2012; Anagnostou et al., 2016) and biotic response

to climate change (Prothero et al., 1996; Alroy et al., 2000;Jaramillo et al., 2006; Lazarus et al., 2014; Pound et al., 2017).

To study the relationship with climate, the regional diversity curve and the taxonomic and diversification rates estimated in this work were compared with the composite isotopic curve of Zachos et al. (2001, 2008). Three methods were used to test these correlations: First Fifferencing (FD) followed by correlation tests, Generalized Least Squares Regression (GLS), incorporating an Autoregressive Model and Critical Intervals (CIN). FD is a simple treatment for minimizing autocorrelation in the data (McKinney 1990) and it means that comparisons between time series focus on short term patterns of variation. FD is calculated as the value of one time interval minus the value of the preceding interval. The correlation between the data was estimated using Pearson's product moment and the non-parametric Spearman's rank correlation tests. GLS is a regression technique that incorporates covariance among data points (Chatfield 2003). This is particularly relevant to time series that may present serial correlation between variables independently of the presence/absence of serial correlation in the variables themselves. GLS incorporates an autoregressive model to account for potential non-independence of successive data points in a time series. The autoregressive models were compared using orders of one, two and three.

GLS have been applied to paleontological time series data by Hunt et al. (2005), Marx and Uhen (2010), Benson and Mannion (2011), and Benson et al. (2011), among others. GLS was implemented in R version 3.4.2 (R Development Core Team 2018) with the packages nlme version 3.1-96 (Pinheiro et al., 2009). Finally, the critical intervals approach (Alroy 1998, 1999; Prothero 1999) examines the state of the macroevolutionary estimates during critical intervals documented in the climatic curve. It is based on the possibility that climate has an influence on macroevolution but only in the form of occasionally and unpredictably producing unique, one-time- only biotic responses (Alroy 2000). Several histograms were constructed to summarise the climatic curve. Those intervals with climatic parameters values more than two standard deviations from mean Cenozoic values were considered intervals of climate change. Then, the intervals of climate change were compared with the taxonomic rates to identify correspondences.

To produce the climatic curve, the isotopic data was extracted from the supplemental material in Zachos et al. (2008) (https://websites.pmc.ucsc.edu/ jzachos/Publications.html) and represent information about the site, the age (Ma), the genus of the foraminifera and the adjusted 18C value of 17694 points. To facilitate comparisons with the macroevolutionary estimates, the isotopic data was divided in 1 Ma intervals and the mean and standard deviation of the $\delta O18$ values were calculated for each interval.

2.4 Results

2.4.1 Estimates based on Range Through Methods

2.4.1.1 Standing Diversity

Standing diversity was calculated for the complete and the restricted-FAD composite sections (Figure 2.12). The black points represent the diversity calculated for each individual sample and the red points connected by the red line represent the diversity calculated from the composite samples in 1 Ma intervals. It is evident that both estimates are very similar. There are small differences especially at the beginning and at the end of the section. In the other hand, the differences between the diversity curves calculated from the complete composite section and the restricted-FAD composite section are evident.

The two curves show a convex-upwards pattern, with lowest diversity at the start and end of the data series (Figure 2.12). Because of the range-through assumption, this may be largely explained by edge effects. Nevertheless, it is difficult to asses the durations of the initial and terminal intervals for which the edge effect is affecting the curve. A visual inspection of the youngest part of the curve show a change in the slope nearly to the Pliocene-Pleistocene boundary suggesting that from this point to the present the curves could be affected by the edge effect. At the oldest part of the curve, the change is more difficult to identify. However is possible to suggest a subtle change in the slope between 65 and 63 Ma (Figure 2.12).

Both curves reveal continuous increase in diversity in the early Palaeocene but the increase is much steeper in the complete composite section. The Palaeocene-Eocene boundary is marked by an abrupt and short-term decrease. Both curves show the decrease. Furthermore, the diversity calculated per-sample in the complete composite section shows not just one but two declines occurring just before and the after the Palaeocene-Eocene boundary (Figure 2.12). This pattern is not evident in the restricted-FAD composite section or in the 1 Ma-binned data for the complete composite section.

Both curves show a continuous and constant increase in diversity during the early Eocene. This culminates in the high diversity during the middle Eocene, which is maintained for approximately 2 to 3 Ma (39-41 Ma) and represents the highest diversity of the Cenozoic. Subsequently, both curves show a constant decline up to the early Oligocene (approx. 32 Ma). During the Oligocene, diversity is stable with a subtle decreasing trend. This behaviour is evidenced in both curves (Figure 2.12)

The most striking discrepancy between the two curves occurs between

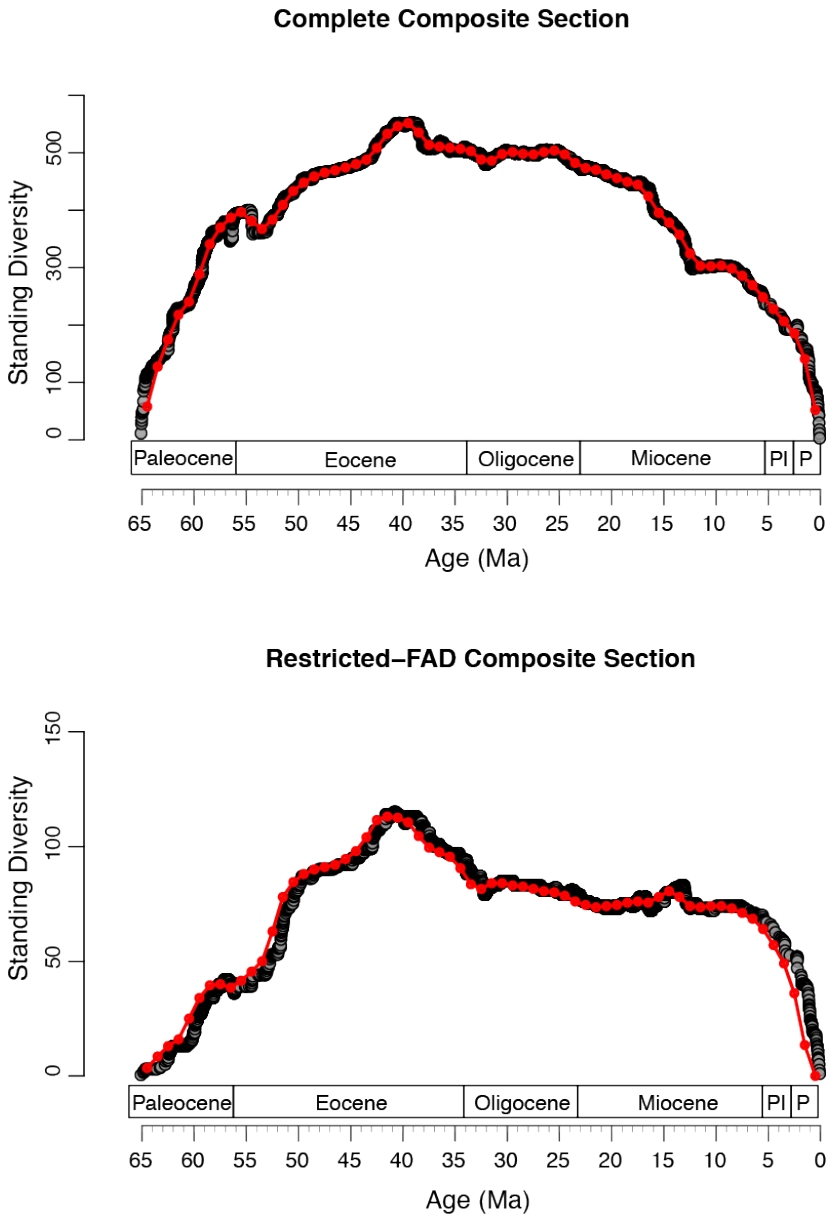

Figure 2.12: Standing diversity for the complete and restricted-FAD composite sections. The black points represent diversity calculated for each individual samples. The red points connected by the red line represent diversity calculated for the pooled versions of the composite sections. Each red point represents therefore the diversity for 1 Ma time intervals.

the late Oligocene and the end of the time series (the recent). The complete composite section shows a continuous decline with differences in magnitude that are evidenced by changes in the slope of the curve. The decline is only interrupted by a brief period of stability in the late Miocene, between 9 and 12 Ma (Figure 2.12). In contrast, the restricted FAD-FAD composite section prolongs the stability observed during the Oligocene up to the end of the Miocene. The period of stability is only interrupted by a minor increase occurring at 13 Ma and lasting for approximately 3 Ma. From the late Miocene (approx. 8 Ma) to the end of the time series, the diversity exhibits an abrupt decline.

In summary, the differences between the diversity curves from the complete composite section and the restricted-FAD composite section are especially pronounced during the Miocene. The complete composite section shows the Miocene as a period characterized by a continuous and rapid decline in diversity with important changes in magnitude while the restricted-FAD composite section suggests that the Miocene was an stable period punctuated by at least one short period of subtle increase in diversity.

Preservation probability (Rbin)

Preservation probability (Rbin) allows the incompleteness of the fossil record to be quantified. Values of Rbin close to 0 indicate that few of the taxa ranging through the interval have actually been sampled in that interval. This could be indicative of an interval with low preservation potential and/or poor sampling. It could also suggest change in taxon ranges, so a species was actually absent in the studied region during that interval. On the other hand, Rbin values close to 1.0 suggest that most of the taxa that range through the interval have been sampled in the interval, and that the assemblage may therefore be well sampled and exhibit good preservation. Rbin was calculated for the pooled versions (1 Ma bins) of the complete and the restricted-FAD composite sections (Figure 2.13). The red and green lines represent the values for the restricted-FAD and the complete composite sections respectively. Both curves exhibit very similar behaviour, and the most notable difference is their absolute magnitudes: Rbin is on average higher in the restricted-FAD composite section than in the complete composite section (Figure 2.13). This difference could be explained by the fact that the restricted-FAD composite section contains mainly common taxa with well-defined stratigraphic ranges, which increases Rbin.

Preservation probability is relatively high during the Palaeocene, with a drastic fall occurring at the Palaeocene-Eocene boundary. Preservation potential is variable during the first half of the Eocene, with two outstanding

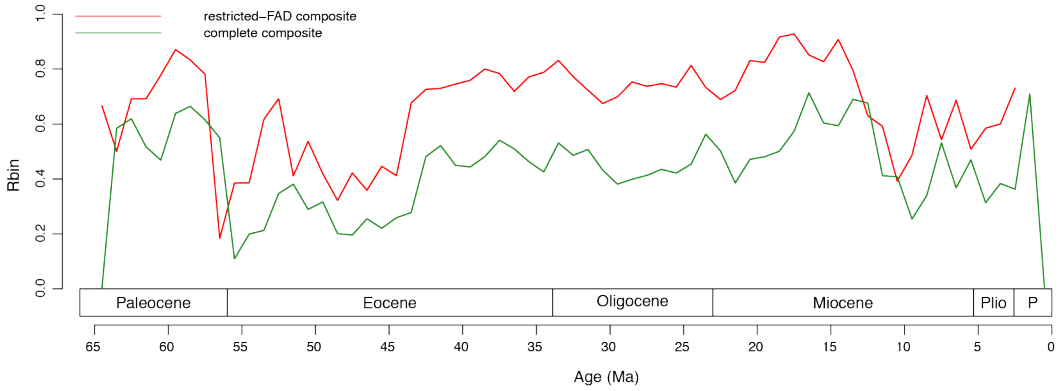

Figure 2.13: Preservation potential (Rbin) calculated as the proportion of range through taxa present in the interval in relation with the number of taxa that range through the interval. Red and green lines represent the restricted-FAD and the complete composite sections respectively.

peaks occurring at 53 Ma and 51 Ma. Rbin increases abruptly during the middle Eocene (44 to 45 Ma), and remains high up to the Oligocene-Miocene boundary. Sporadic short-term peaks are also observed in this interval. Rbin increases and reaches the highest level of the Cenozoic during the first half of the Miocene (13-21 Ma). These high values are maintained for approximately 7 Ma. From this point (12 Ma), the preservation probability drastically falls to the level observed at 9 Ma. The interval between the second half of the Miocene (approx. 8 Ma) and the end of section is characterized by fluctuations without apparent trend (Figure 2.13).

When Rbin is compared with the number of samples, the restricted-FAD composite section shows a significant positive correlation (spearman correlation test, p =7.5e-10, rho=0.68) (panel A, Figure 2.14). However when the first difference is calculated, this correlation is not significant (panel B, Figure 2.14) (p = 0.78, rho=-0.03).In the complete composite section the correlation between Rbin and the number of samples (panel A, Figure 2.15) is significant (p=8.2e-05, rho=0.46). When the first difference is calculated (panel B, Figure 2.15) the correlation is significant but negative (p=0.08, rho=-0.21)

Figure 2.16 present the the preservation potential (Rbin) and the number of samples for the restricted-FAD composite section, but the same pattern is also observed in the complete composite section. The correlation between the two curves is very clear in the Palaeocene-Eocene boundary and the middle Miocene where the Rbin and the number of samples decrease almost simultaneously. Other intervals, like the early Eocene (53-54 Ma) and middle

Eocene (approx. 46 Ma), exhibit abrupt changes in Rbin that, however, are not accompanied by considerable changes in the number of samples. Furthermore, in the first half of the Eocene (55 to 45 Ma) the number of samples is constant while Rbin fluctuates.

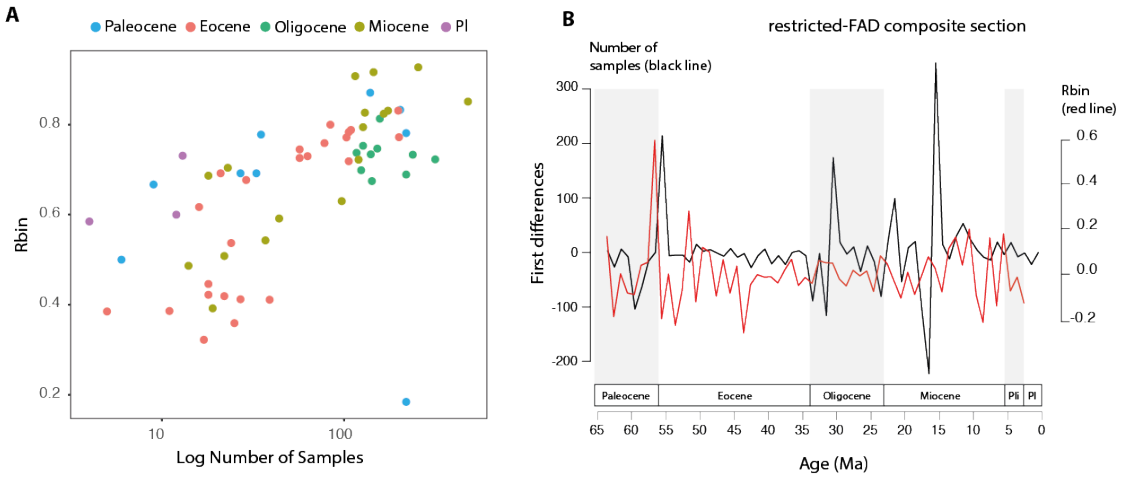

Figure 2.14: A. Correlation between the number of samples and preservation probability (Rbin) for the restricted-FAD composite section differentiated by Geological epochs.PL= Pliocene and Pleistocene. The spearman correlation test suggests a significant correlation (p=7.5e-10, rho=0.68). B. First differences of the number of samples (black line) and Rbin (red line)

Diversity corrected by Rbin

Diversity was also estimated by dividing the number of taxa actually sampled in the interval (Nbt.samp) by its preservation potential (Rbin) (Figures 2.17 and 2.18 for the complete and the restricted-FAD composite sections respectively). Nbt.samp represents an uncorrected estimation of the diversity because it only counts the number of range through taxa that were sampled. A corrected version is obtained when Nbt.samp is divided by the preservation potential (Rbin). When Rbin is high, the corrected and uncorrected estimation of diversity are similar. If the two curves are superimposed, the area between them is small. In the other extreme, when Rbin is low, the diversity of the interval is compensated and the difference between the uncorrected and corrected estimates is high. In this case the area between the curves is wide.

When the uncorrected estimates (Nbt.samp) of the complete and the restricted-FAD composite sections are compared, they reveal two of the most

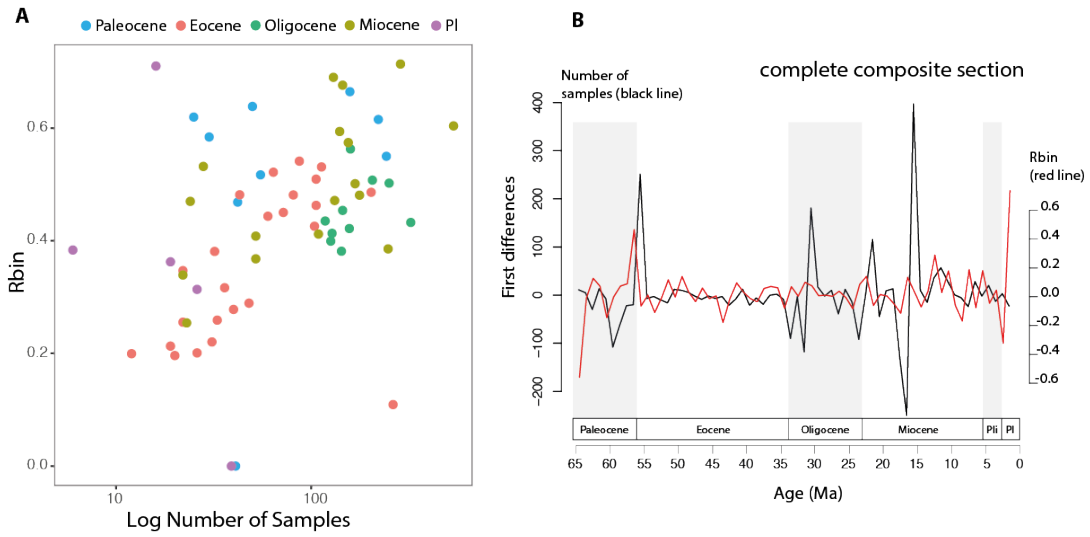

Figure 2.15: A. Correlation between the number of samples and preservation probability (Rbin) for the complete composite section differentiated by Geological epochs. PL= Pliocene and Pleistocene. The spearman correlation test suggests a significant correlation (p=7.5e-10, rho=0.68). B. First differences of the number of samples (black line) and Rbin (red line).

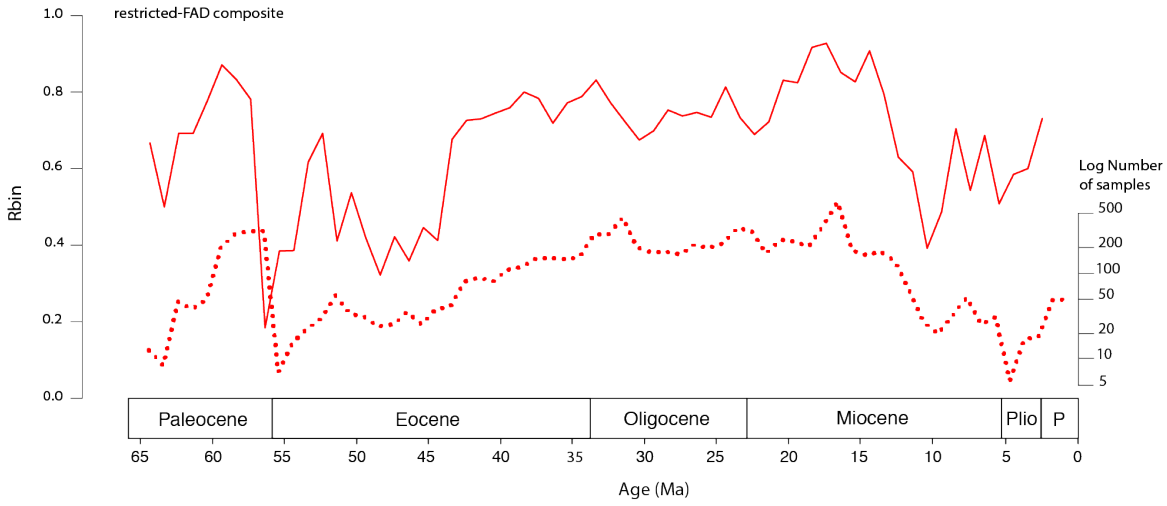

Figure 2.16: Preservation potential (Rbin) and Logarithm (log) of the number of samples for the restricted-FAD composite section.

prominent features of the diversity curve, abrupt decrease in diversity at Palaeocene-Eocene boundary and during middle Miocene, and an interval of elevated diversity extending from the middle Eocene to the middle Miocene

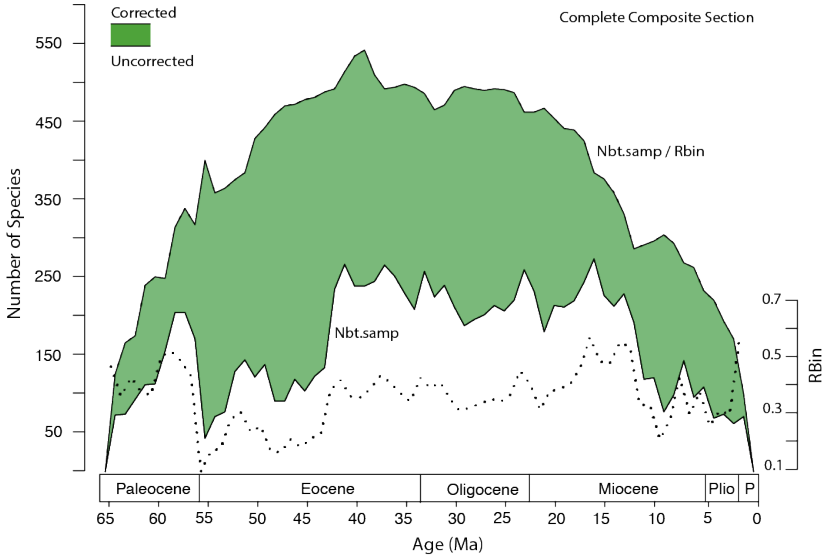

Figure 2.17: Uncorrected and corrected diversity curves calculated for the complete composite section. The uncorrected curve (Nbt.samp) corresponds to the number of range through taxa that were actually sampled in each interval. The corrected curve is estimated by dividing Nbt.samp by the preservation potential (Rbin) which is also presented in the figure.

(Figures 2.17 and 2.18). The most noticeable difference occurs in the interval between the middle Eocene and Oligocene. During this period, the complete composite section shows a plateau of fluctuating diversity, whereas the restricted-FAD composite exhibits a dramatic decline in the late Eocene from maximal diversity, followed by a period of stability during most of the Oligocene.

When the uncorrected (Nbt.samp) and the corrected (Nbt.samp/Rbin) diversity curves are compared, the area between them is much larger in the complete composite section (Figure 2.17) than in the restricted-FAD composite section (Figure 2.18). This difference is especially pronounced during the Eocene to middle Miocene interval and could be explained by the differences in Nbt.samp and Rbin between the two versions of the composite section. On the one hand, Nbt.samp and Rbin are very fluctuating in the complete composite section (Figure 2.17) while in the restricted-FAD composite section Rbin present higher values that additionally are very stable (Figure 2.18).

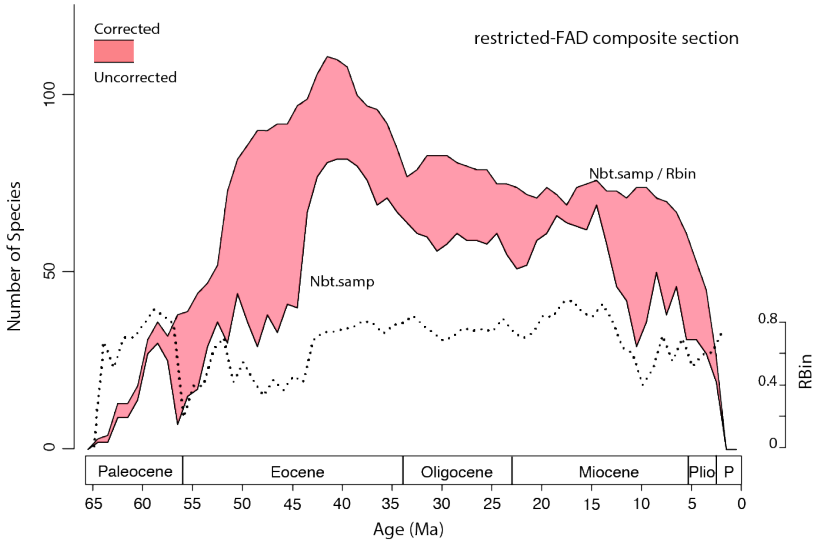

Figure 2.18: Uncorrected and corrected diversity curves calculated for the restricted-FAD composite section. The uncorrected curve (Nbt.samp) corresponds to the number of range through taxa that were actually sampled in each interval. The corrected curve is estimated by dividing Nbt.samp by the preservation potential (Rbin) which is also presented in the figure.

2.4.1.2 Per-capita 0rigination and Extinction rates

The per-capita origination (p) and per-capita extinction (q) rates were calculated for the pooled (1 Ma) versions of the complete and the restricted-FAD composite sections. The equations used in the calculations are presented in the Table 2.1. Because the composite sections were divided into equal length 1 Ma intervals, the denominator in the two equations (time) can be ignored. The two metrics (p and q) were calculated for each one of 1000 bootstrapped replicates produced from the interpreted FADs and LADs. The grey circles represent the values for the iterations (Figures 2.19 and 2.20). The green and red circles represent, respectively, the median of the origination and extinction rates of each interval. The green and red lines in the panels A and B of Figure 2.21 are the five-point moving average calculated from all the estimates (the complete and restricted-FAD composite sections). The upper right figure in the panels A and B show the difference between the complete and the restricted-Fad composite sections. For comparison purposes, the differences were also plotted at the same scale in the panel C of Figure 2.21.

In the case of the per-capita origination rate, the most prominent changes are revealed by the two versions of the composite section (Figure 2.19). The Palaeocene exhibit the highest origination rates of the Cenozoic but also

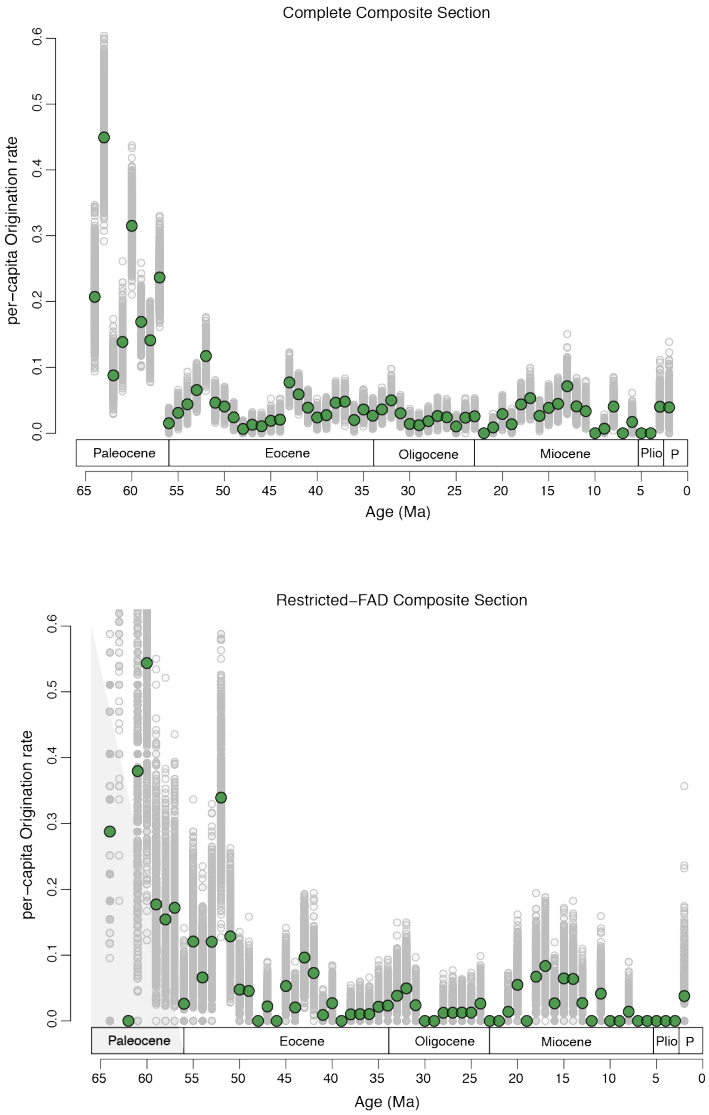

Figure 2.19: per-capita Origination rate calculated from the pooled versions of the complete composite and the restricted-FAD composite sections. The grey circles represent the per-capita origination rate calculated for each bootstrapped replicate produced from the interpreted FADs and LADs. The green circles represent the median of the per-capita origination rate of each bin.

the highest variability (Figure 2.19). The major differences between the two versions are also found through this interval (upper right panel, Figure 2.21).

During the Eocene the variability decreases and two prominent peaks at 42-43 Ma and 51-52 Ma are detected in both versions. The differences are still high during the early Eocene, but from the middle Eocene to the late Eocene, the difference decreases and is close to zero at the end of the interval (upper right panel, Figure 2.21). During the Oligocene, the differences between the two estimates are minimal. The origination rates are in general very low and exhibit low variability (Figure 2.21). There is no evident trend or peaks during this interval. During the early Miocene the origination rate rapidly increases and reaches a point around 17 Ma where it is stabilized and remain constant for approximately 3 to 4 Ma. From this point (13 Ma) the rate declines to finally reach the low values observed during the late Miocene. The estimates based on the complete and the restricted-FAD composite section exhibit very small differences (upper right panel, Figure 2.21). Finally, during the Pliocene-Pleistocene the origination rate seems to increase again. However the low number of estimations during this time period prevents a reliable interpretation.

The most prominent changes in the per-capita extinction rate are evidenced in the two versions of the composite section (Figure 2.20). The differences between the values obtained from the complete and the restricted-FAD composite sections are greater than those observed for the origination rates. These differences are more evident in the Palaeocene, the late Eocene and the mid to late Miocene (panel B, Figure 2.21). Using the information from the moving average is possible to suggest that during the Palaeocene the extinction rate is variable with a distinct peak occurring between 53 and 54 Ma approximately. The early and middle Eocene is characterized by a low extinction rate that abruptly begin to increase at approximately 45 Ma and result in the two peaks observed at the end of the Eocene. Near to the Eocene-Oligocene boundary the extinction rate dramatically falls. From this point (approx. 30 Ma) until the middle Miocene there is a general trend of the extinction rate to increase. Two peaks are especially prominent during the late-early Miocene and middle Miocene (panel B, Figure 2.21). Finally, in the transition between the middle Miocene and the late Miocene the extinction rate abruptly falls. Low values are observed in the following 3 Ma after which the extinction again increases to finally reach the high values observed at the Pliocene (Figure 2.21). When origination and extinction are compared at the same scale (panel C, Figure 2.21) is evident that the differences between the complete composite and restricted-FAD composite sections for the extinction are much greater than those for origination.

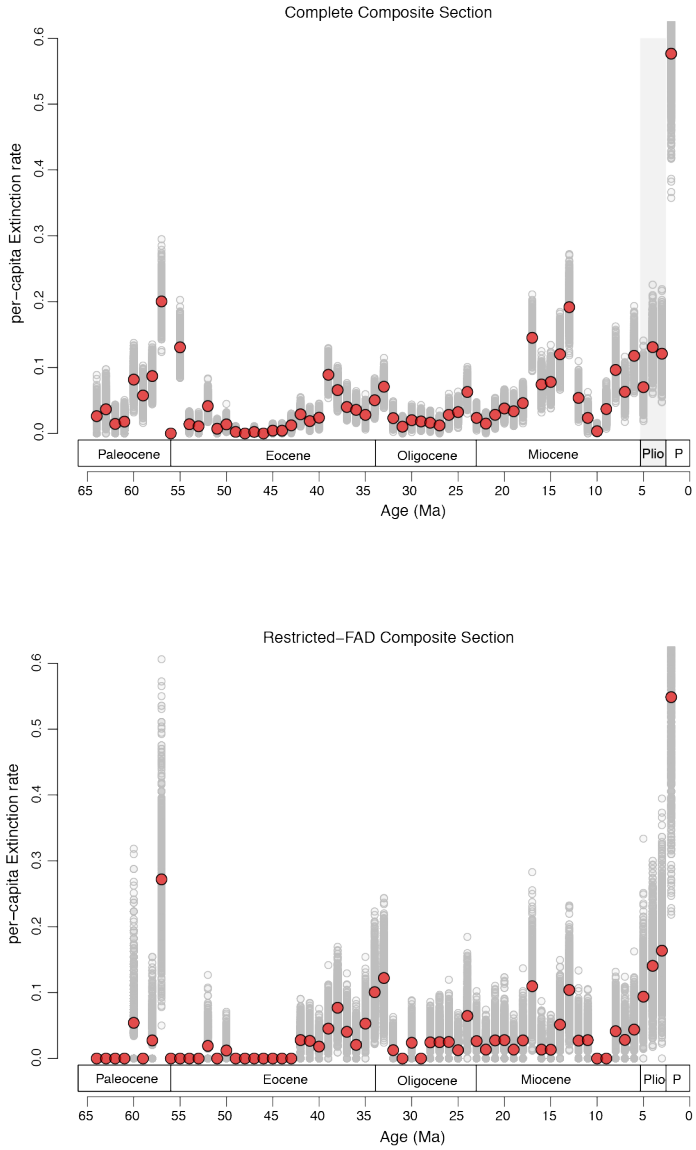

Figure 2.20: per-capita Extinction rate calculated from the pooled versions of the complete composite and the restricted-FAD composite sections. The grey circles represent the per-capita extinction rate calculated for each bootstrapped replicate produced from the interpreted FADs and LADs. The red circles represent the median of the per-capita extinction rate of each bin.

2.4.1.3 Cohort Survivorship Analysis

For the cohort survivorship analysis the pooled versions (1Ma) of the two composite sections were used. The number of cohorts obtained from the com-

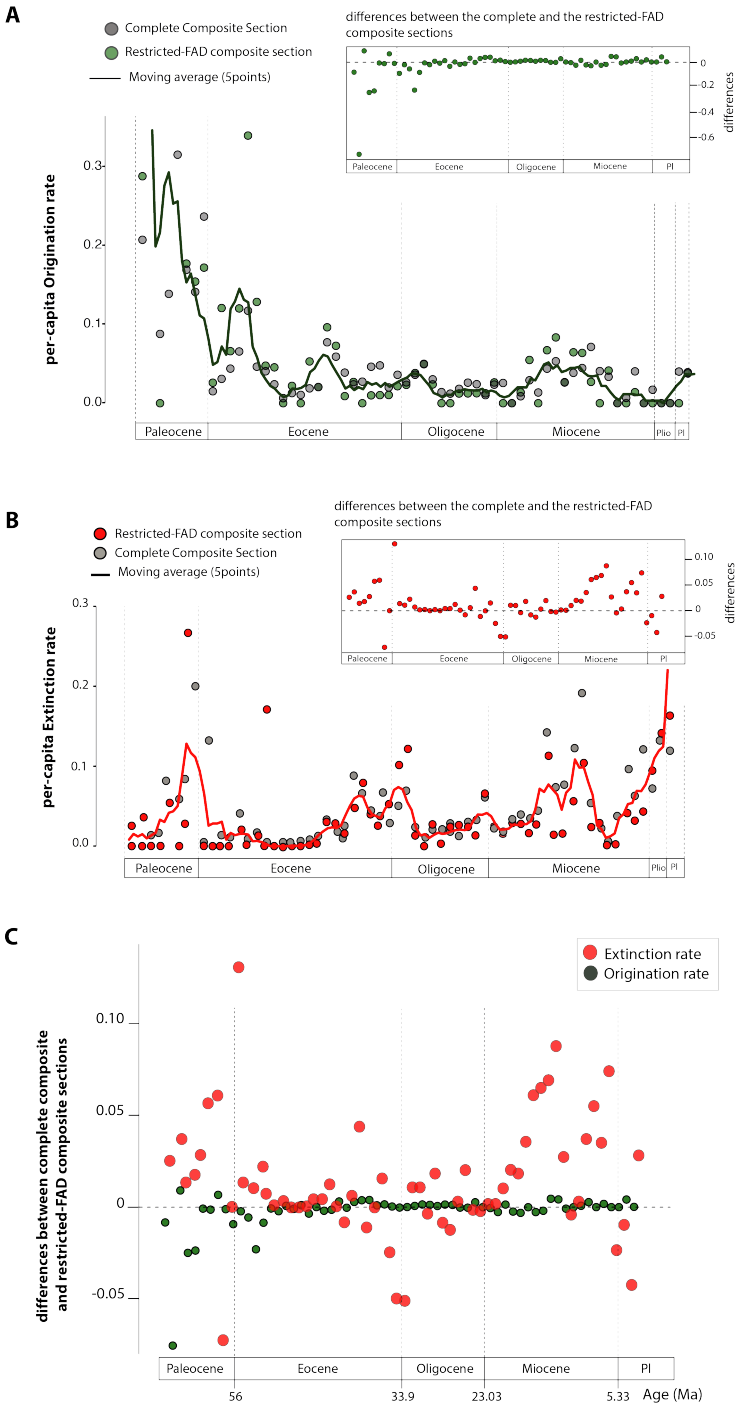

Figure 2.21: per-capita Origination (panel A) and Extinction (panel B) rates calculated from the 1 Ma-pooled version of both versions of the composite section. The grey circles represent the complete composite section and the green circles represent the restricted-FAD composite section. The black line is a five point moving average calculated from the all the points. The upper right panel in A and B shows the difference between the two versions of the composite section. The panel C show these differences at the same scale.

plete composite section (Figures 2.22 and 2.23) is higher than those obtained for the restricted-FAD composite section (Figures 2.24 and 2.25) because in the complete composite section all the species are included in the analysis. Although it increases the resolution of the analysis, the use of the complete composite section can be problematic because of the potential effects introduced by the borehole caving.

The Figures 2.22 and 2.24 represent the trajectories of the cohorts for the two versions of the composite section. Groups of cohorts that originated in the same geological epoch are represented in the same colour (e.g. the cohorts originating in the Eocene are coloured in yellow). To facilitate the interpretation, each group of cohorts originating in the same epoch were represented individually (Figures 2.23 and 2.25 for the complete and the restricted-FAD composite sections respectively). The slope of a straight line fitting a cohort curve on a semi-log graph gives an estimate of the extinction rate. A change in the slope therefore represents a change in the extinction rate. When several cohorts show inflection of their curves at the same point, this could be interpreted as an external event occurring at that specific time and is reflecting an increase in the extinction rate.

A close inspection of the figures 2.22 and 2.23 suggest at least four intervals in which several cohorts show concurrent inflections and/or abrupt changes in their slopes. These intervals are numbered from 1 to 4 in the corresponding figures. The interval 1 is located in the early Palaeocene (62-64 Ma) and is characterized by the inflection of the three Maastrichtian cohorts (Figures 2.22 and 2.23). The interval 2 is located near the Palaeocene-Eocene boundary (56-58 Ma) and is marked by the inflection of the Palaeocene cohorts and the abrupt change of slope in the Maastrichtian cohorts. Between the intervals 1 and 2, which correspond almost to the entire Palaeocene, the slope of the cohorts suggest medium to high extinction levels.

Interval 3, located close to the Eocene-Oligocene boundary (34-38 Ma), is characterized by the concurrent inflection of the Eocene cohorts. The change is less evident in the Maastrichtian and Palaeocene cohorts, where only a subtle change in the slope of the cohorts is observed (Figure 2.23). Between intervals 2 and 3, which roughly correspond to the Eocene, the cohorts exhibit low angles indicating that extinction during this interval was in general low. This observation is valid for all the cohorts coinciding during this interval independent of their ages.

Interval 4, located in the middle Miocene (11-14 Ma), is the most prominent of the four events. The change is especially evident in the Palaeocene, Eocene and Oligocene cohorts and less obvious in the Maastrichtian and Miocene cohorts (Figure 2.22). Between the events 3 and 4, the Maastrichtian and Palaeocene cohorts exhibit low slopes in comparison with the Eocene and

Oligocene cohorts. Form the interval 4 to the present, the slope of the cohorts suggest medium to high extinction levels (Figure 2.22).

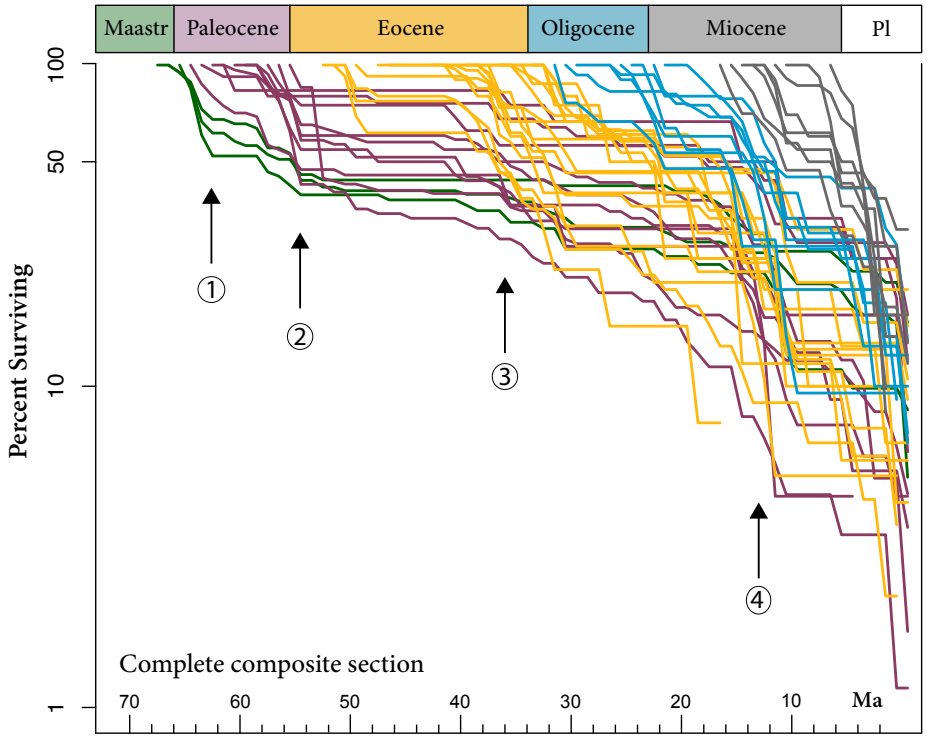

Figure 2.22: Cohort survivorship curves for the species of the complete composite section. The numbers identify intervals where several cohorts show concurrent inflections or identifiable changes of their slopes.

Although the number of cohorts is lower in the restricted-FAD composite section, it is still possible to distinguish three of the previously described events (Figures 2.24 and 2.25). Event 1 is not identifiable because of the absence of Maastrichtian cohorts. Event 2 is only evident in the Palaeocene cohorts while the events 3 and 4 are recognizable in the Palaeocene and Eocene cohorts. The Oligocene and Miocene are characterized by a low number of cohorts, making any interpretation difficult.

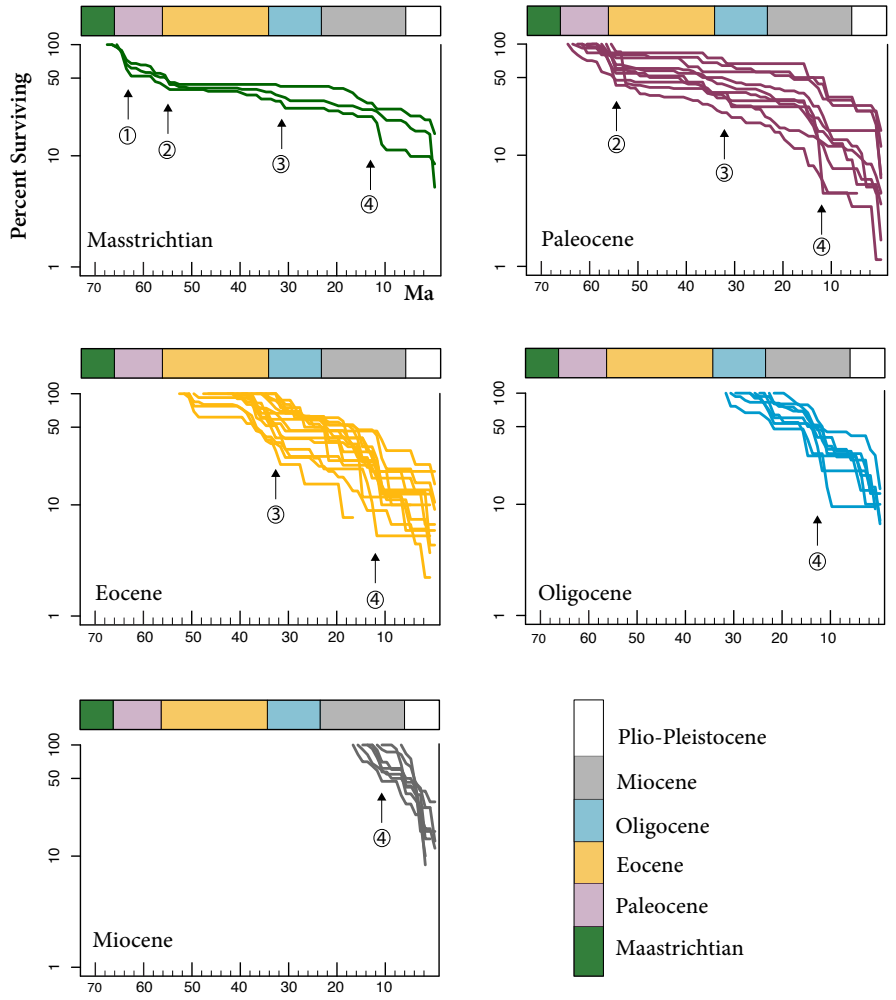

Figure 2.23: Cohort survivorship curves for the species of the complete composite section discriminated by geological epochs. The numbers identify intervals where several cohorts show concurrent inflections or identifiable changes of their slopes.

2.4.2 Estimates based on In Bin Occurrence Methods

2.4.2.1 Shareholder Quorum Subsampling (SQS)

One of the most important considerations taken into account during the development of this work is the possible effect of borehole caving. Caving could artificially increase the chronostratigraphic range of the species (by pushing back their FADs) and this would be reflected in the macroevolutionary esti-

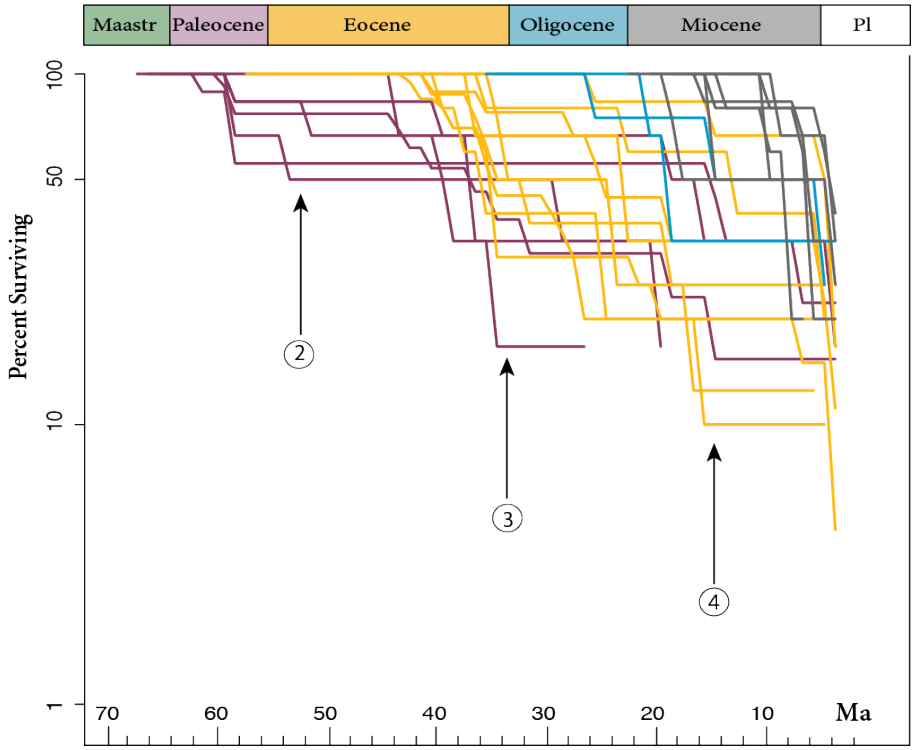

Figure 2.24: Cohort survivorship curves for the species of the restricted-FAD composite section. The numbers identify intervals where several cohorts show concurrent inflections or identifiable changes in their slopes.

mates. This is particularly true when the metrics used to estimate diversity or taxonomic rates operate under the range- through assumption. However, when diversity is estimated using SQS, the range- through assumption is not longer needed because diversity is estimated by counting directly the number of species detected in a sample or collection. This approach allows therefore diminishes the possible effect introduced by caving.

When the abundance-based SQS for pooled samples is estimated for the complete and the restricted-FAD composite sections, the two curves exhibit the same general pattern (Figure 2.26). Diversity in the Figure 2.26 was estimated using a quorum level of 0.6, although similar results were obtained using different levels. The most prominent changes in diversity, like the drastic decline observed during the early and middle Eocene, are evidenced in both curves. A closer inspection reveals however subtle differences. The most remarkable occurring between 8 Ma and 14 Ma. During this interval, the estimates from the restricted-FAD composite section (red line, Figure 2.26) suggest a continuous and sustained increase in diversity while the estimates

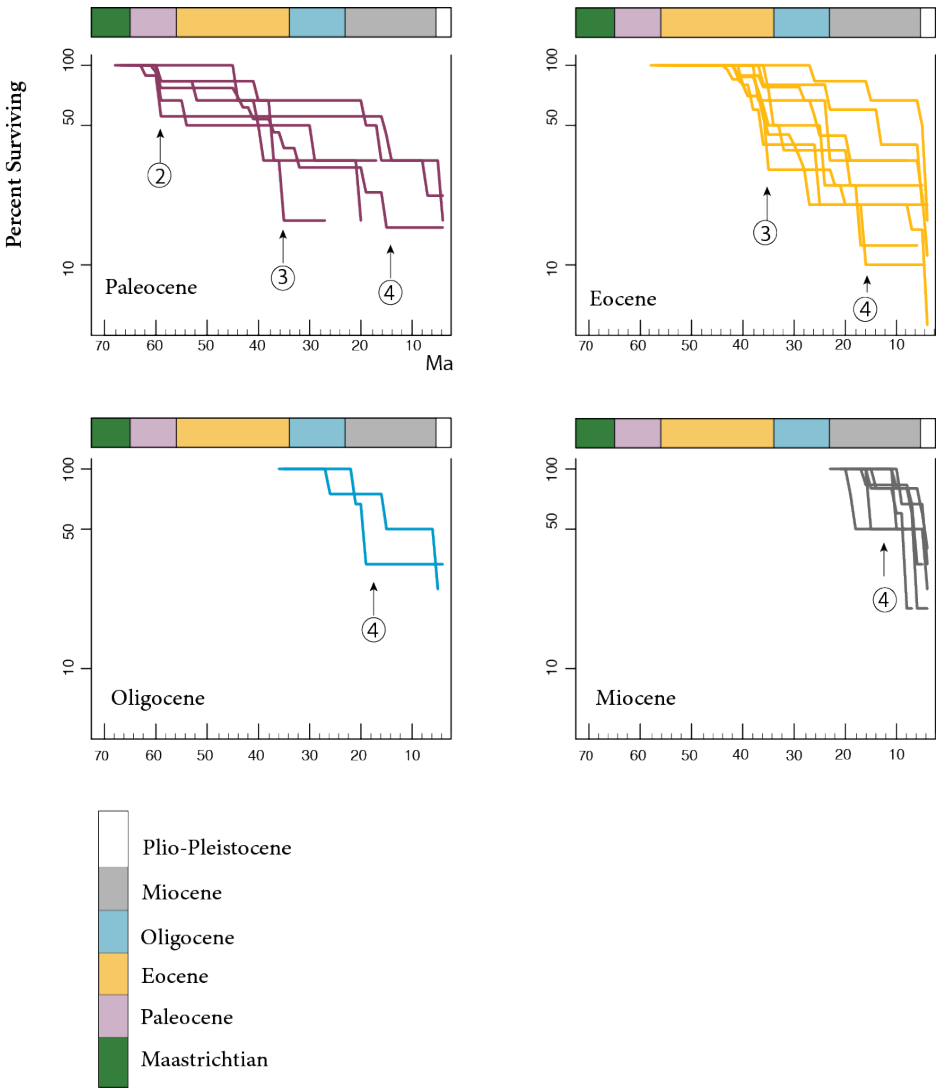

Figure 2.25: Cohort survivorship curves for the species of the restricted-FAD composite section discriminated by geological epochs. The numbers identify intervals where several cohorts show concurrent inflections or identifiable changes in their slopes.

from the complete composite section (black line, Figure 2.26) suggest that posterior to the high values reached at 14 Ma, the diversity abruptly drop and start to increase again after 8 Ma. The difference between the two estimates could be explained by the low number of samples analyzed in this interval, which may introduce uncertainty in the number of detected species. The discrepancy between the two curves is partially solved when later in this

chapter new information from the literature is incorporated into this interval.

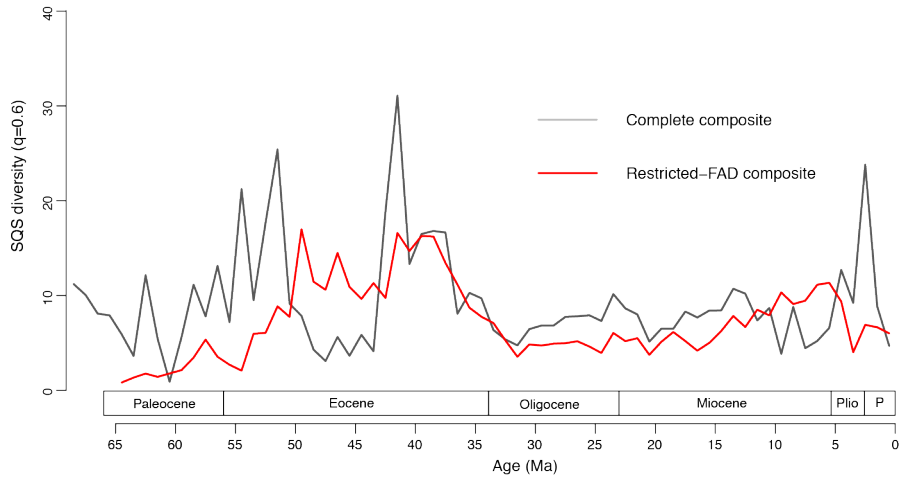

Figure 2.26: Abundance-based SQS for pooled samples estimated for the complete composite section (grey line) and the restricted-FAD composite section (red line) (q=0.6).

Because in general the pattern of diversity estimated from the two version of the composite section is similar (Figure 2.26), the following discussion will focus on the results obtained from the complete composite section. The reason to choose the complete composite section is that incorporates information from a greater number of species in comparison with the restricted-FAD composite section (2689 spp. vs. 193 spp.). In spite of the significant difference in the number of species, the similarity between the two diversity curves is clear (Figure 2.26). This might reinforce the idea that if caving is affecting the complete composite section, its effect is almost undetectable when diversity is estimated using SQS. This is opposite to the results obtained using the standing diversity range-through approach where both versions of the composite section exhibit marked differences (Figure 2.12).

Three different approaches were used to produce the diversity estimate from the complete composite section. In the first approach, the composite section was subdivided into 1 Ma intervals. Each interval or bin is therefore composed by multiple samples from different localities. The contribution of each species to the bin was estimated as the sum of all the abundances reported across all samples. This is the abundance version of the composite section. In the second approach, the composite section was also subdivided in 1 Ma intervals, but this time the contribution of each species was estimated as the number of samples where the species was reported. This is the occurrence version of the composite section. In the third approach, diversity

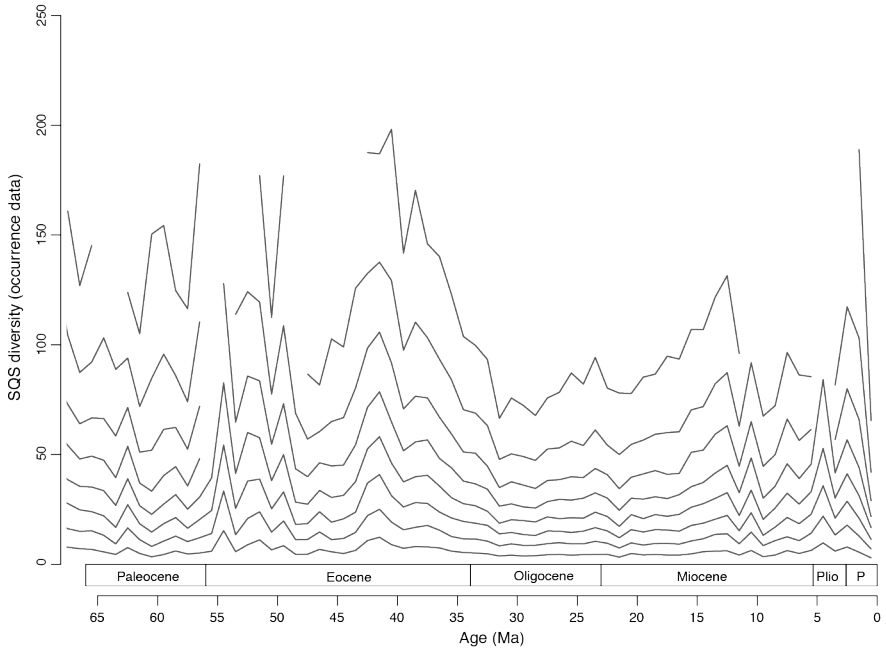

Figure 2.27: SQS diversity curves based on occurrence of the binned complete composite section. Quorum level from 0.1 (bottom curve) to 0.9 (top curve).

was calculated for each individual sample of the complete composite section. In all the approaches diversity was estimated using quorum levels between 0.1 and 0.9.

When the occurrence version is used, only quorum levels between 0.1 and 0.4 produce diversity estimates for all the intervals. With a quorum level greater than 0.4 is not possible to estimate diversity in some intervals of the Eocene and the Miocene (Figure 2.27). On the other hand, when the abundance version is used all but one quorum level produce diversity estimates for all the intervals. The exception is an interval close to the Palaeocene-Eocene boundary for which is not possible to estimate diversity even with a quorum level of 0.9 (Figure 2.28). A comparison between the diversity curves obtained from the occurrence and abundance- based subsampling approaches to pooled 1 Ma samples, using quorum level of 0.9, indicates that the two curves agree on the most prominent changes in diversity (Figure 2.29). However SQS identifies that in the occurrence version the sampled coverage of the underlying taxon pool is insufficient for several bins of the Eocene and Miocene and does not provide information of diversity (black line, Figure 2.29). For this reason, the discussion about diversity will be based on the results obtained from the abundance version of the complete composite section

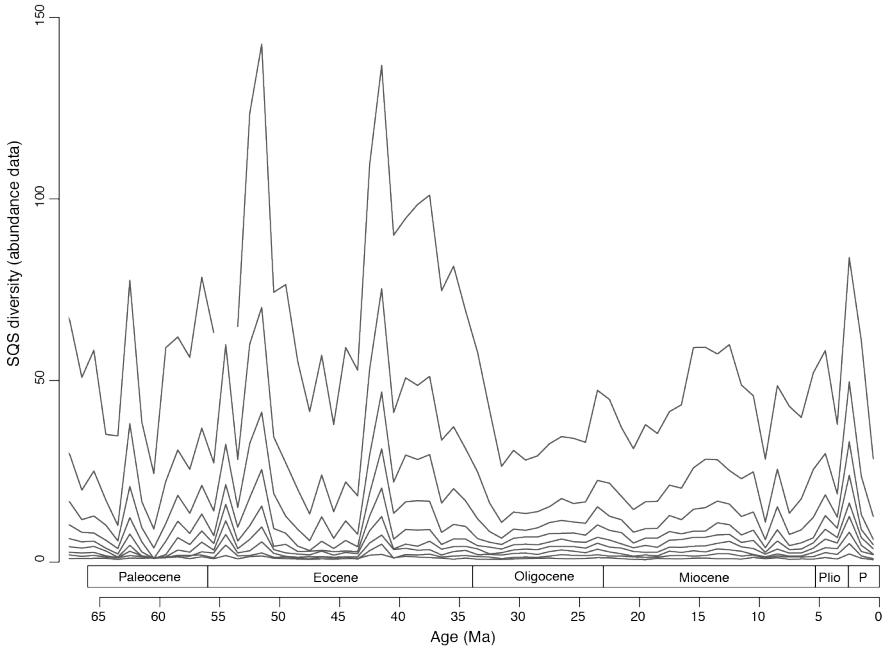

Figure 2.28: SQS diversity curves based on the abundance version of the binned complete composite section. Quorum level from 0.1 (bottom curve) to 0.9 (top curve).

and specifically the results obtained using a quorum level of 0.6.

For the sample-by-sample, abundance-based analysis, only samples with counts higher than 50 palynomorphs were used to estimate diversity. The number of samples meeting this condition is 3978. SQS diversity was estimated using a quorum level of 0.6. The result is a cloud of points where the first thing to notice is the difference in the number of samples analyzed through the Cenozoic (Figure 2.30). The Paleocene is characterized by an elevated number of samples. Sample counts are much lower at the Paleocene-Eocene boundary, and remain very low during the early and middle Eocene. From the middle Eocene (43 Ma) to the middle-late Miocene (11 Ma) the number samples is again very high. Finally, a reduction in the number of samples is observed between 11 Ma to the end of the section. This change is however subtle in comparison with the abrupt change observed at the Palaeocene-Eocene boundary (Figure 2.30).

From the cloud of points it is also evident the differences in diversity among samples of the same interval. In others words, diversity estimates made from samples within each interval can show substantial variation (Figure 2.30). This observation applies for the whole Cenozoic and may reflect

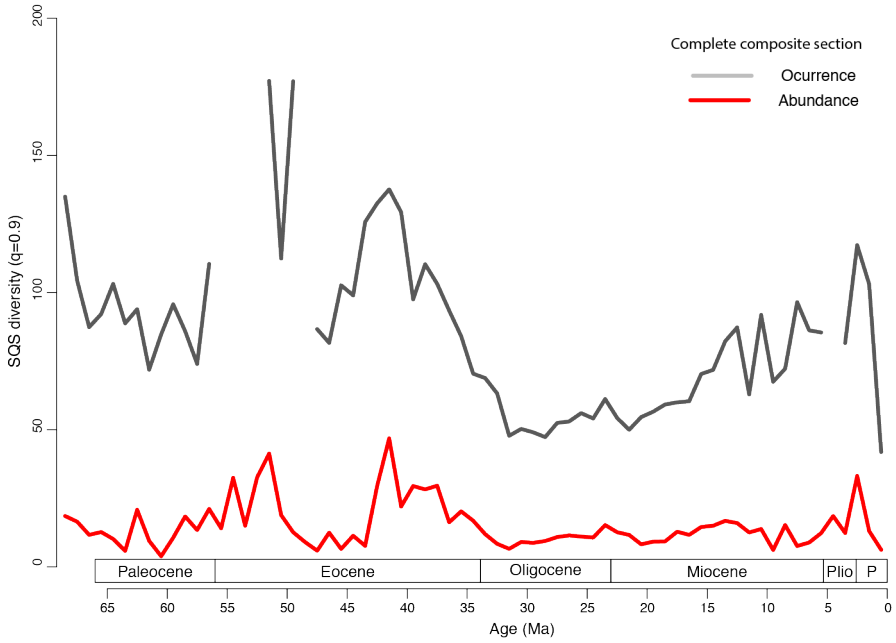

Figure 2.29: SQS diversity curves based on the occurrence and abundance versions of the complete composite section using a quorum level of 0.9.

geographic differences in diversity, which in turn could be related to differences in the environment of deposition between the sites. In fact, 80% of the samples (3176 of 3926) have SQS diversity estimate ranging between 0 and 10, while only 20% of them (785) present values higher than 10 (histogram, Figure 2.31). The previous percentages were calculated for the complete Cenozoic. If this percentage is calculated for all samples grouped in 5 Ma intervals, most of intervals are dominated by samples with low diversity (upper right panel, Figure 2.31). An exception occurs in three intervals of the Eocene where 30-40% of the samples have diversities higher than 10 (upper right panel, Figure 2.31).

Two approaches were used to produce a diversity curve based on abundance-subsampling of individual samples. In the first approach, the section was divided in 1 Ma intervals and diversity was estimated as the mean of the SQS diversity of the samples that compose each interval. Their respective confidence intervals were also calculated (red line, Figure 2.30). Because the difference in the number of samples between the intervals could be influencing the calculated mean diversity (upper right panel, Figure 2.32), bootstrapping was used to standardize the number of samples through time. A fixed number of samples (5, 10 and 20) were randomly selected in each interval and diversity was calculated as the mean of the SQS diversity of the selected set

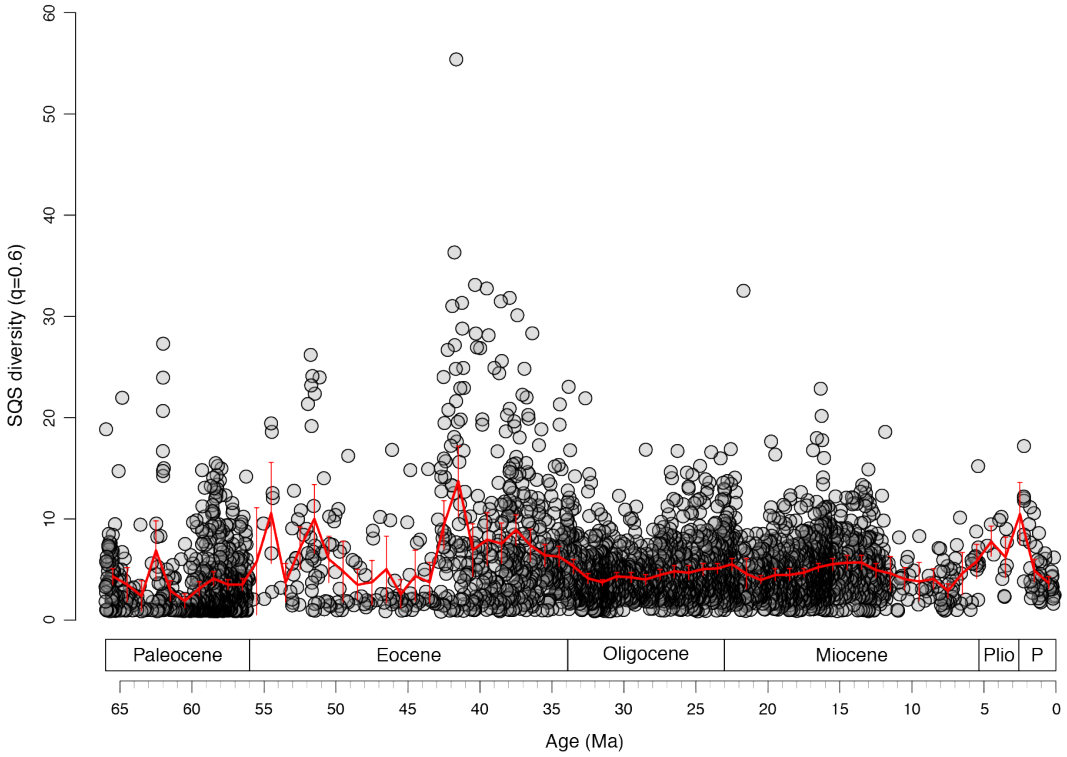

Figure 2.30: Diversity calculated for each sample of the complete composite section using a quorum level of 0.6 (grey points). The red line represents the diversity calculated as the average of the samples than compose each interval. Confidence intervals for each bin are also presented.

of samples. This procedure was repeated 1000 times and the mean of all the subsamples was calculated (lower panel, Figure 2.32). When five samples are used, all but two intervals produced an estimate. These intervals correspond to 55-56 Ma and 5-6 Ma in which the number of samples is two and three respectively. When the mean SQS diversity estimated in each bin without sample-standardisation (upper left panel, Figure 2.32) and the bootstrapped curves (lower panel, Figure 2.32) are compared, they are very similar with only very subtle differences.

In the second approach, the samples from each 1 Ma interval were pooled forming a composite sample.The abundance of each species was calculated adding the abundance where the species was recorded. Diversity was then estimated for each interval using SQS with a quorum level of 0.6 (Figure 2.33). When this curve is compared with curve estimated as the mean of the samples in each bin (Figure 2.30) the similarity is evident. In a broad scale, both curves reveal the same trends and the most perceivable changes. The

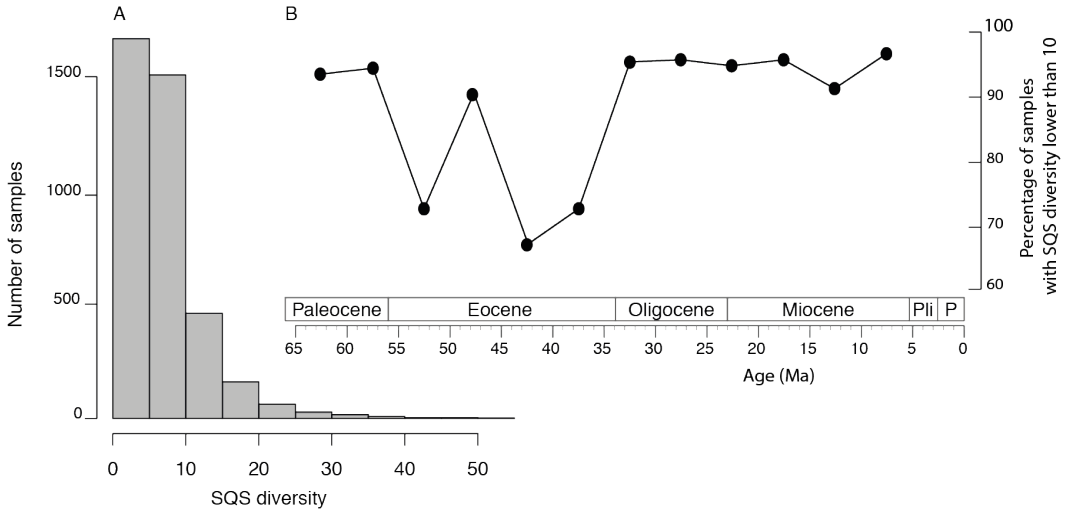

Figure 2.31: Histogram of the number of samples and SQS diversity. Approximately 80% of the samples (3176) present diversity values below 10. Panel B. Percentage of the number of samples with SQS diversity values below 10 in intervals of 5 Ma.

couple of peaks during the early Palaeocene, the peak near the Palaeocene-Eocene boundary, the low values during the middle Eocene, the peak at the middle Eocene, the abrupt fall during the late Eocene, the increasing trend from the Oligocene to the middle Miocene that ends with a drop at approximately 13 Ma and the sustained increase observed during the last 10 Ma. The main difference between the two curves is the magnitude of the changes, which are better revealed by the curve where the samples of each interval were pooled (Figure 2.33). This difference is especially noticeable in the interval between the Oligocene and Miocene.

2.4.3 Regional Diversity

To compare the diversity estimated from the composite section with information from the literature, the SQS diversity from the pooled version was used (Figure 2.33). As explained before, both approaches (the mean of the samples and pooling the section) produced very similar results even when sample size is standardized. From now on the diversity estimation based on the pooled section will be named the regional diversity curve (Figure 2.33). When talking about information from the literature, it makes reference to both the publications and the internal reports of the Biostratigraphy Team of Ecopetrol S.A (Figure 2.8 and Annex 2.3).

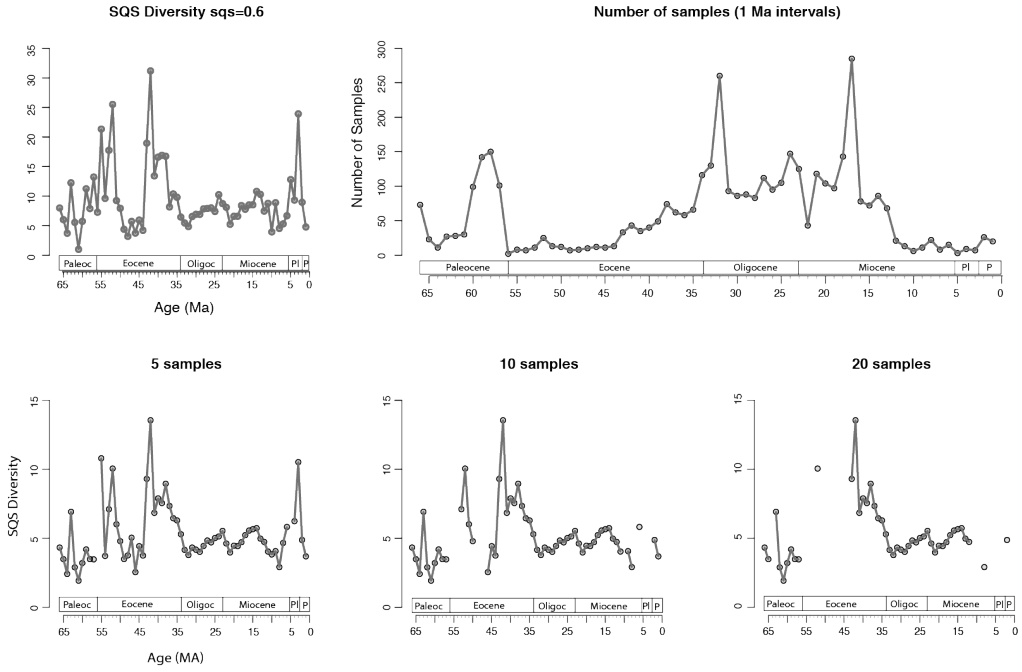

Figure 2.32: The upper left panel show the SQS diversity calculated as the average of all the samples present in each interval; the upper right panel show number of samples in each interval; the lower panel show the diversity calculated by resampling at 5, 10 and 20 samples.

Although most of these studies have a biostratigraphic and temporal interpretation, the age of the samples was reinterpreted in order to have a common chronostratigraphic framework. This is especially true for some publications, where the age was interpreted based on not base on up-to-date biostratigraphic schemes (Hoorn 2006). Graphic correlation (Shaw 1964; Edwards 1984) and the maximum likelihood approach (Punyasena et al., 2012) were used to make the new interpretations. The resulting chronostratigraphy and the geographic location of the sections is presented in the Figure 2.34.

When the estimated SQS diversity from all the samples from the literature (colour points in Figure 2.35) is plotted with the regional SQS diversity estimated in this work (grey points and black line in Figure 2.35), is clear the over representation of samples from the literature in the Miocene and the Pliocene (Figure 2.35). The Oligocene is less well represented while the Eocene and Palaeocene present the lowest number of samples. It is also clear that the variation in SQS diversity that characterizes most intervals. This is particularly evident in the Miocene-Pliocene where the elevated number of samples from different localities exhibits a wide range of values. During this

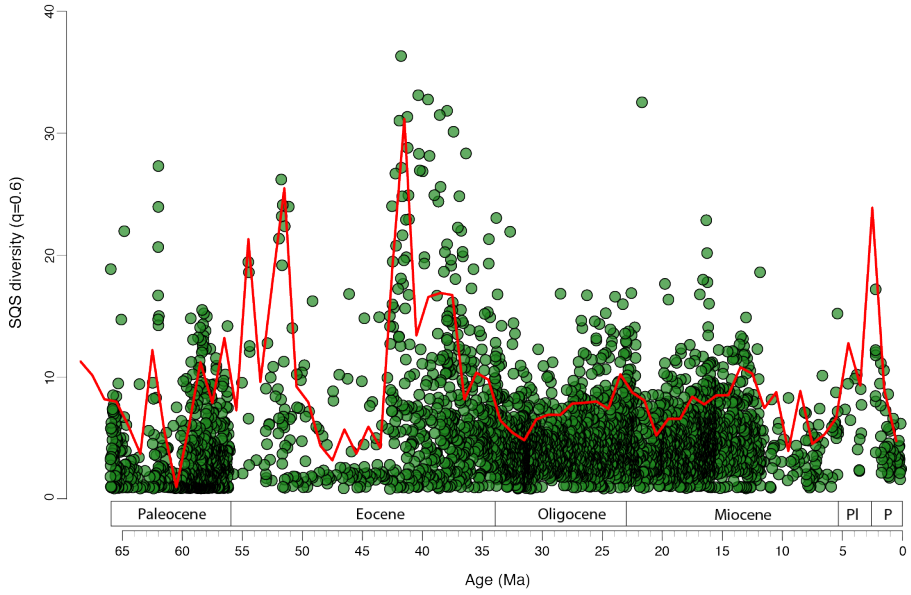

Figure 2.33: Diversity calculated for the samples of the complete composite section using a quorum level of 0.6 (green dots). The samples of each bin were grouped to form a single sample. Diversity was then calculated for each bin using a quorum level of 0.6 and is represented by the red line.

interval, from 1.8Ma to 19.5Ma, only 15% of the samples (420 out of 504) have SQS diversities greater than 10. This percentage is quite similar to the to the percentage obtained from the samples of the complete composite section (Figure 2.31). When the samples from the literature are compared with the regional diversity curve (black line, Figure 2.35), most of the samples fall below and only a small proportion exceeds the values of the curve.

In order to compare not only the SQS diversity of the samples (Figure 2.35), but also the trend of the regional diversity curve with the information from the literature, the same approach used to produce the regional diversity curve was used to produce estimates for the new sections. All the samples within a specific bin were grouped forming a unique sample. Diversity was then calculated using SQS with a quorum level of 0.6. This comparison is however not balanced because the number of samples used to estimate the regional diversity curve exceeds by far, in most of the intervals, the number of samples used to produce the estimates from the literature. The results for each section are presented below.

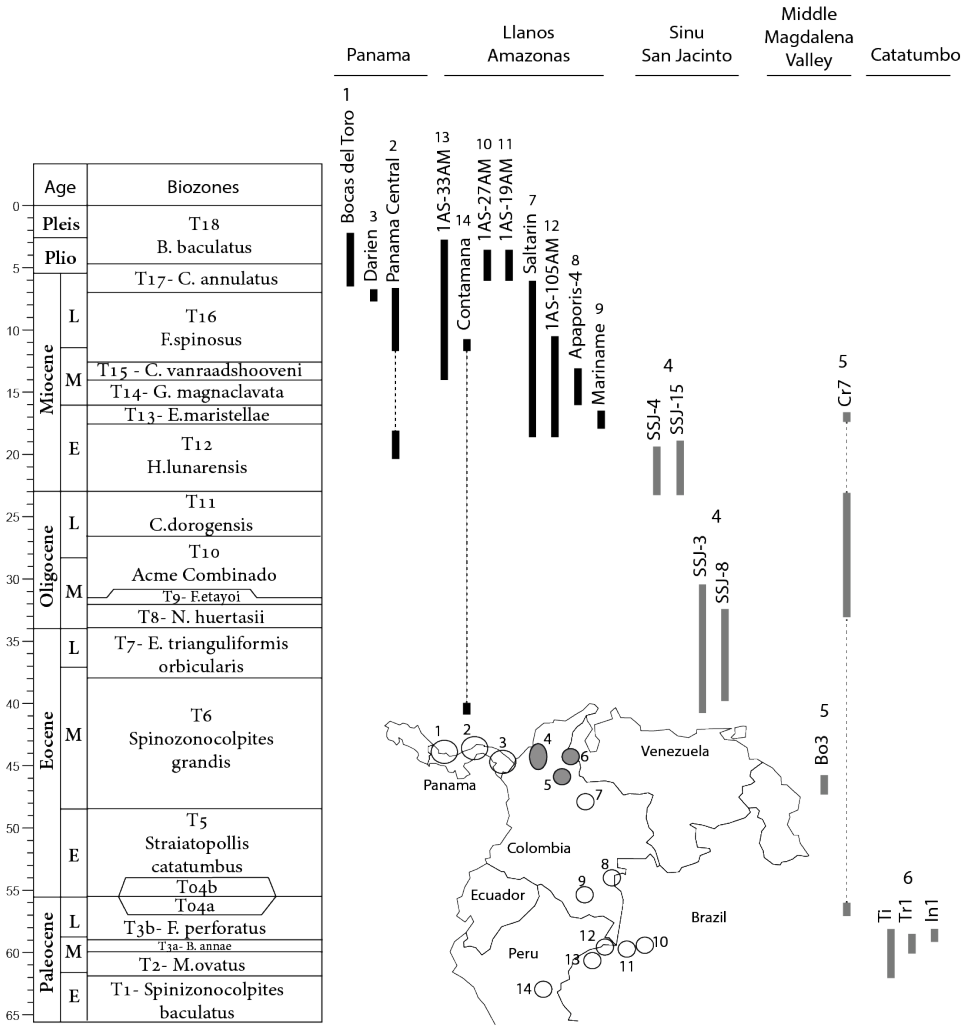

Figure 2.34: Chronostratigraphic framework and geographic location of the sections (outcrops, rock-cores and ditch cutting samples) from the literature used to compare the diversity estimates. The locations in grey correspond to wells drilled by Ecopetrol S.A.(Sections 1,2,3: Jaramillo et al., 2014; sections 4,5,6: Internals reports of the Biostratigraphy Team-Ecopetrol S.A; sections 7, 12: Jaramillo et al., 2017; section 8: Hoorn 2006; section 9: Salamanca et al., 2016; sections 10, 11: Silva-Caminha et al., 2009).

2.4.3.1 Panama Sections

Jaramillo et al.(2014)(areas 1,2,3 in Figures 2.34 and 2.8)

In this study, 282 samples from several sections located in three areas

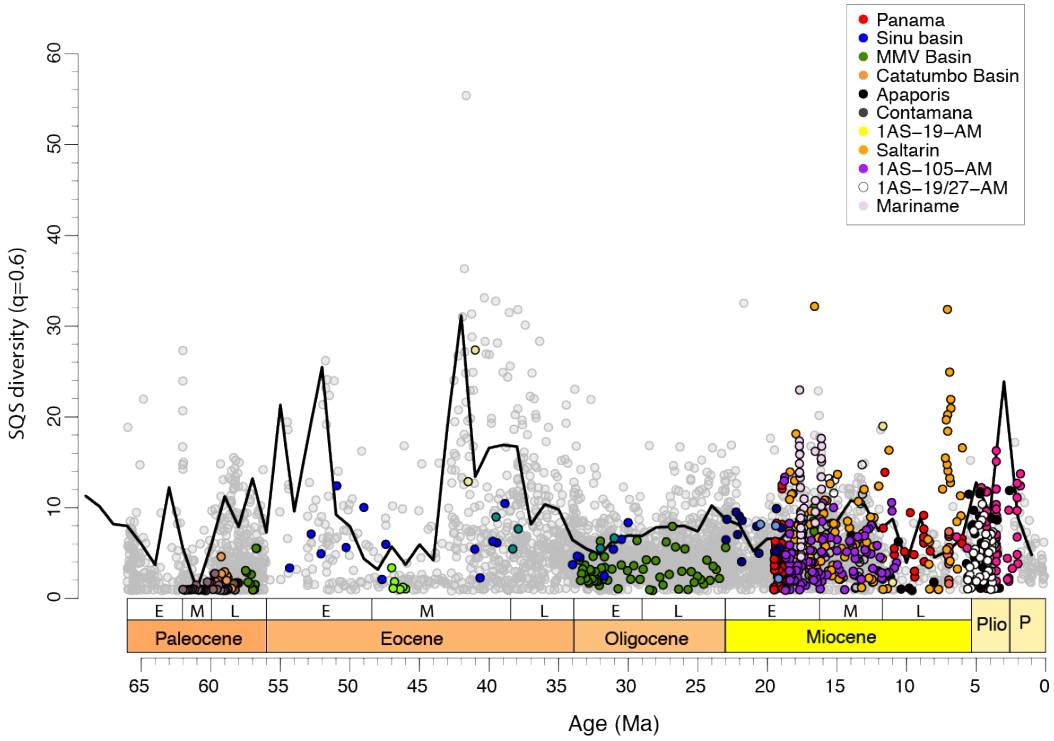

Figure 2.35: Diversity curve (black line) and per sample diversity (grey dots) calculated for the complete composite section compared with the SQS diversity estimated in samples from the literature (colour dots). Diversity was estimated using SQS with a quorum level of 0.6.

of Panama were analyzed. The ages of the samples can be found in the supplemental material of the publication (Jaramillo et al., 2014) and were calculated by using the ages of the formations from which the samples were collected. The methods used to estimate the ages of the formations include U-Pb geochronology, magnetostratigraphy, planktonic foraminifera, nannofossils, and molluscan biostratigraphy (Jaramillo et al., 2014). From the total of 282 samples, only 140 were used for the diversity analysis and correspond to the samples with counts higher than 50 specimens. Diversity was estimated using SQS with a quorum level of 0.6. The results are presented in the Annex 2.4.

The left panel in Figure 2.36 show the SQS diversity of the samples discriminated by geographic regions (Bocas del Toro, Panama Central and Darien). Two intervals are covered by the samples (1-12Ma and 18-19Ma). The interval between 18 and 19 Ma is especially important because in the regional estimates, this interval present a low number of samples (Figure

2.33). Almost all the samples have diversities lower than those of the diversity curve. In the few exceptions in which a sample exceeds the value of the curve, the diversity of that sample is always within the range imposed by the samples of the regional diversity estimates (grey dots, Figure 2.36). This also applies for the interval between 1 Ma and 12 Ma, indicating that the samples from of Panama support the pattern observed from the regional diversity curve.

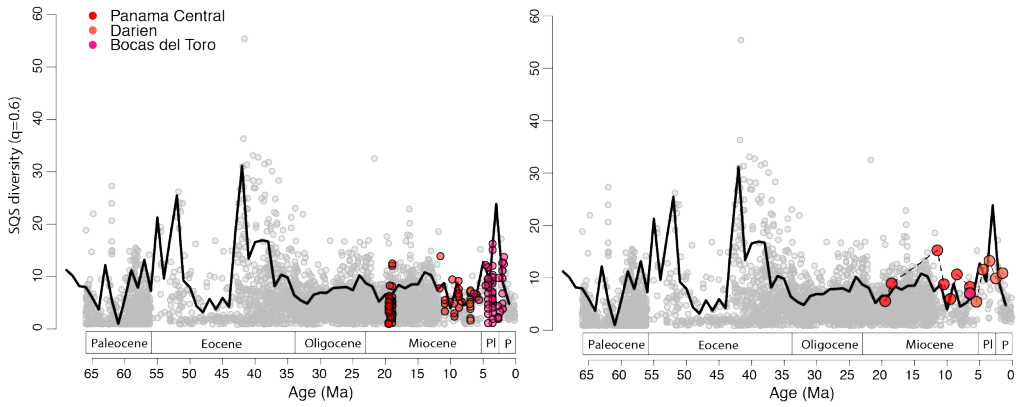

Figure 2.36: Diversity calculated for the samples of the Panama sections (Jaramillo et al., 2014). Left panel: diversity of the individual samples discriminated by geographic regions. Right panel: diversity of the 1 Ma bins. All diversity estimates using SQS with a quorum level of 0.6.

When the SQS diversity is estimated for the 1 Ma pooled samples (right panel, Figure 2.36), the oldest interval (18-20 Ma) only includes two bins. The two estimates however follow the pattern observed from the regional diversity curve. The youngest interval (1-11 Ma) includes information of 11 bins. The bin at 11 Ma has a higher SQS diversity than the regional diversity curve. However this points represents the diversity peak observed at 11 Ma in the regional diversity curve. The following six estimates show a decline in diversity between 10 Ma and 6 Ma while the youngest 3 estimates indicate an increase between 1 and 4 Ma. In general, the two curves reveal the same pattern. The only difference, which is very subtle, is the magnitude of the change.

2.4.3.2 Sinu-San Jacinto Basin

Internal report, Ecopetrol S.A (area 4 in Figures 2.34 and 2.8)

Palynological information from four cores was obtained from confidential reports of the Biostratigraphy Team of Ecopetrol S.A. A total of 46 samples

with counts higher than 50 specimens were used in the analysis. The samples are distributed between the Palaeocene and early Miocene (Figure 2.37).

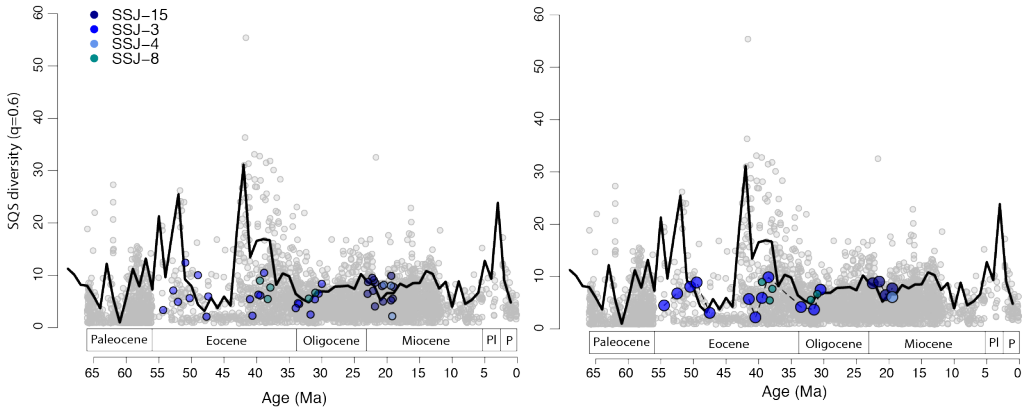

Figure 2.37: Diversity calculated for the samples of the Sinu-San Jacinto cores (Internal reports-Biostratigraphy Team-Ecopetrol S.A). Left panel: diversity of the individual samples discriminated by geographic regions. Right panel: diversity of the 1 Ma bins. All diversity estimates using SQS with a quorum level of 0.6.

The ages of the samples were estimated as follows. First, all samples were compared with the complete composite section using the maximum likelihood approach (Punyasena et al., 2012). The samples with the most confident age estimates were used as a correlation points. Assuming a constant sedimentation rate between these samples and the stratigraphic position of the samples, the age of each sample was calculated by interpolation (Annex 2.4).

The left panel in the Figure 2.37 show the diversity of the samples discriminated by sections (rock core). Almost all the samples are below the regional diversity curve and the few exceptions are within the range of values imposed by the samples of the regional estimates (grey circles, Figure 2.37). When SQS diversity is estimated for the 1 Ma pooled samples, three intervals can be interpreted (right panel, Figure 2.37). The first interval covers the early Eocene and is represented by four points. In terms of magnitude, the values are below the regional diversity curve but exhibiting the same pattern, an increase during the early Eocene followed by an abrupt decline at 48 Ma (Figure 2.37). The second interval covers between 30 and 41 Ma and is represented by two cores (SSJ-3 and SSJ-8). The main difference with the regional diversity curve is again the magnitude. However, the two cores resemble the pattern of the regional diversity curve, an increase between 39 and 34 Ma followed by an abrupt decline and again an increase between 33 and 30 Ma (Figure 2.37). Finally, the interval between 23 and 18 Ma is rep-

resented by two cores (SSJ-15 and SSJ4). In this case both the magnitude and the pattern are very similar to the regional diversity curve.

2.4.3.3 Catatumbo Basin

Internal report, Ecopetrol S.A (area 6 in Figures 2.34 and 2.8)

Palynological information from three wells was obtained from confidential reports of the Biostratigraphy Team of Ecopetrol S.A. A total of 50 samples with counts higher than 50 specimens were used in the analysis. The samples cover an interval between the early and the late Palaeocene (62 to 58 Ma)(Figure 2.38).

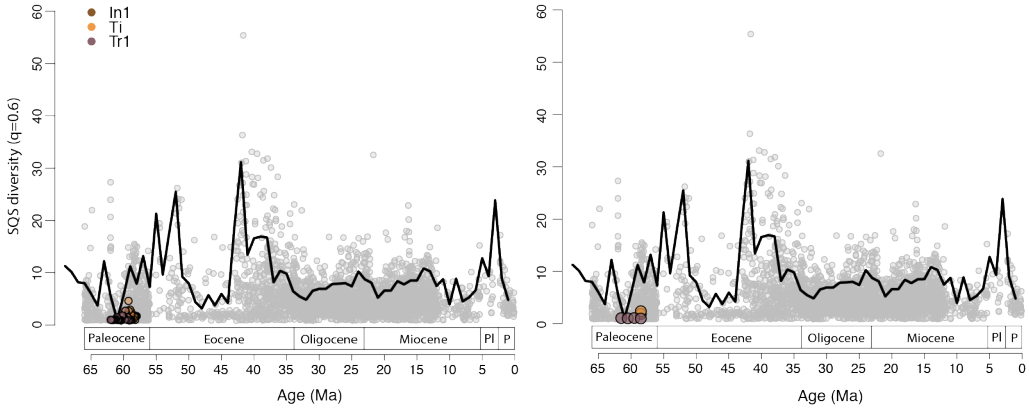

Figure 2.38: Diversity calculated for the samples of the Catatumbo basin (Internal report Biostratigraphy Team-Ecopetrol S.A.) Left panel: diversity of the individual samples discriminated by geographic regions. Right panel: diversity of the 1 Ma bins. All diversity estimates using SQS with a quorum level of 0.6.

The ages of the samples were estimated as follows. First, all samples were compared with the complete composite section using the maximum likelihood approach (Punyasena et al., 2012). The samples with the most confident age estimation were used as a correlation points. The age of each sample was calculated by interpolation and assuming constant sedimentation rate between the correlation points. The ages of the samples are presented in Annex 2.4. The left panel in the Figure 2.38 show the estimated SQS diversity of the samples discriminated by wells. All the samples are below the regional diversity curve. When SQS diversity is estimated for the 1 Ma pooled samples, the increase observed in regional diversity curve is not evident in the estimation from the wells (right panel, Figure 2.38). However,

a closer inspection of the per-sample estimates reveals a subtle increase in diversity in the younger samples of the interval (left panel, Figure 2.38).

2.4.3.4 Middle Magdalena Valley

Internal report, Ecopetrol S.A (area 5 in Figures 2.34 and 2.8)

Palynological information of two wells drilled in the Middle Magdalena Valley was obtained from confidential reports of the Biostratigraphy Team of Ecopetrol S.A. A total of 98 samples with counts higher than 50 specimens were used in the analysis. The samples are distributed in several intervals (left panel, Figure 2.39). The Oligocene is the interval with the most extensive coverage, while the samples in the other intervals (Paleocene, Eocene and Miocene) only covers between 1 and 2 Ma.

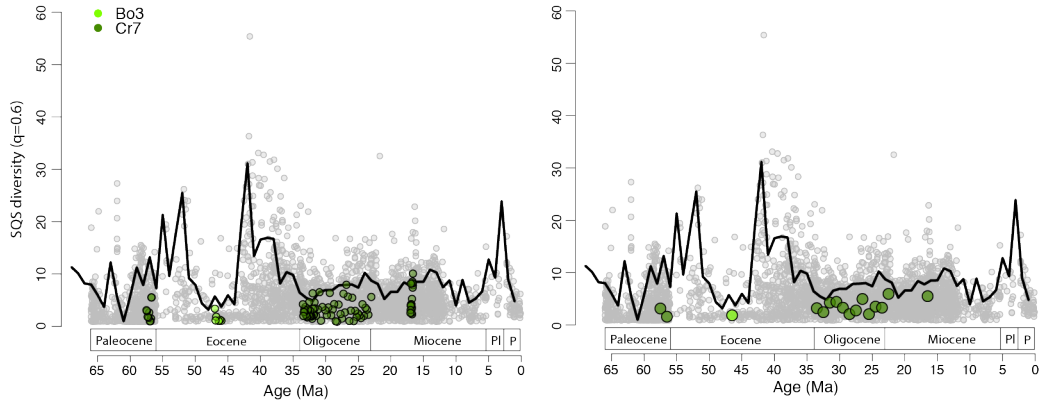

Figure 2.39: Diversity calculated for the samples of the Middle Magdalena Valley basin (Internal report Biostratigraphy Team-Ecopetrol S.A.). Left panel: diversity of the individual samples discriminated by geographic regions. Right panel: diversity of the 1 Ma bins. All estimates using SQS with a quorum level of 0.6.

The ages of the samples was estimated as follows. First, all samples were compared with the complete composite section using the maximum likelihood approach (Punyasena et al., 2012). The samples with the most reliable age estimation were used as a correlation points. The age of each sample was calculated by interpolation and assuming a constant sedimentation rate between the correlation points. The ages of the samples are presented in Annex 2.4. The left panel in the Figure 2.39 show the SQS diversity of the samples discriminated by wells. All the samples as well as the estimates based on the pooled intervals are below the regional diversity curve (right panel, Figure 2.39). For the Oligocene, the regional diversity curve suggests an increasing

trend, which is not reflected by the pooled values of the wells, which rather exhibit a fluctuating pattern (right panel, Figure 2.39).

2.4.3.5 Saltarin Rock Core

Jaramillo et al. (2017) (area 7 in Figures 2.34 and 2.8)

In this study the authors analyzed 138 samples from a rock core drilled in the Llanos basin of Colombia. The age of the samples was estimated using biostratigraphy and this information is included in the supplemental material of the publication (Jaramillo et al., 2017). From the total of 282 samples, 112 were used for the diversity analysis and correspond to the samples with counts higher than 50 specimens. Diversity was estimated using SQS using at a quorum level of 0.6. The results are presented in Annex 2.4. The samples are distributed almost throughout the entire Miocene (21-5 Ma) but interrupted by three gaps (Figure 2.40, red boxes). These gaps are not due to the lack of samples but are the result of the very low recovery of palynomorphs that prevent a reliable estimate of diversity.

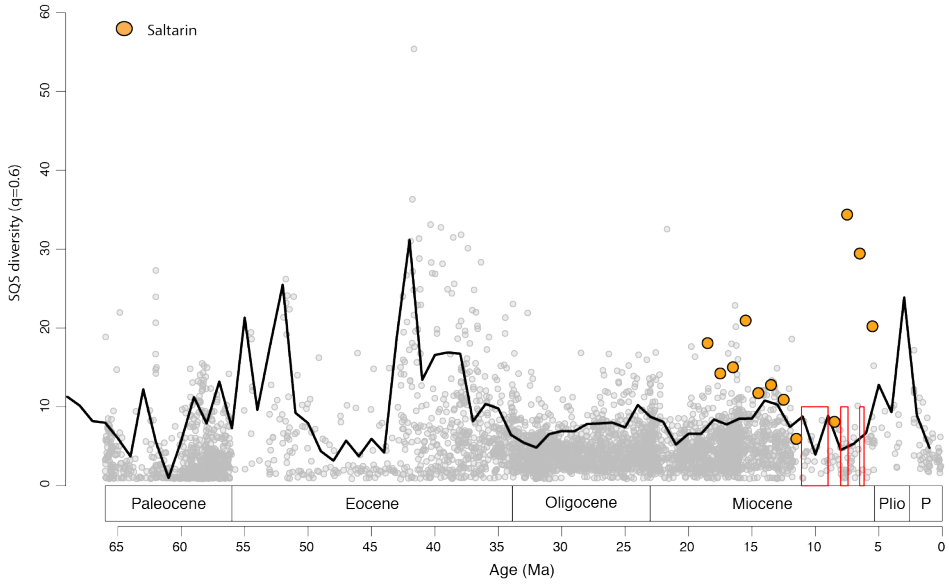

Figure 2.40: Diversity calculated for the samples of the Saltarin core. The red boxes indicate the three time intervals where palynological samples were analyzed (Jaramillo et al., 2017) but the recovery of palynomorphs was very low. Note the low diversity of this interval in the regional estimates (grey dots and black line).

The more evident gap occurs between 11.2 and 8.4 Ma and although nine samples were analyzed in this interval, their counts were extremely low

(between 0 and 5 specimens). In the other two gaps (6.16 - 6.3 Ma and 7.43 - 8.01 Ma) five and 13 samples were analyzed respectively but their counting was again very low (between 0 and 17 specimens) (Figure 2.40). The poor recovery in these intervals is particularly relevant because the regional diversity curve in those intervals is also characterized by a low number of samples with low diversity (Figure 2.40).

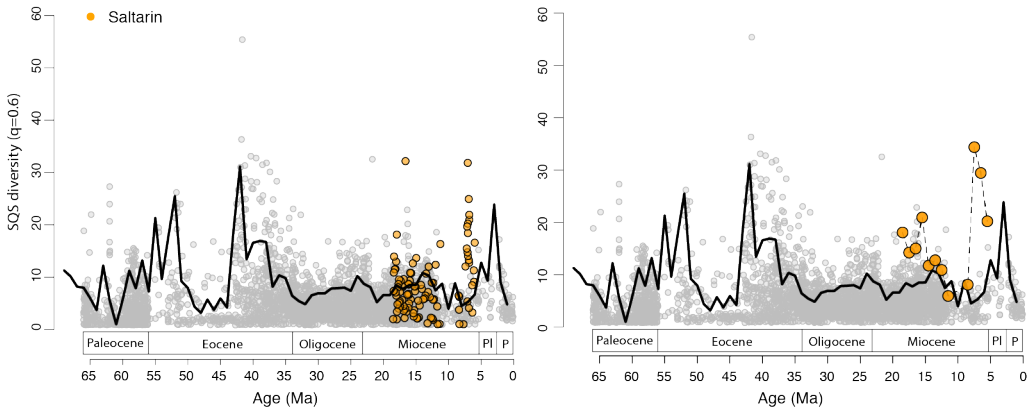

Figure 2.41: Diversity calculated for the samples of the core Saltarin-1 (Jaramillo et al., 2017). Left panel: diversity of individual samples. Right panel: diversity of the 1 Ma bins. All estimates using SQS with a quorum level of 0.6.

The left panel in the Figure 2.41 show the diversity calculated for the individual samples. Most of them present values that are below the regional diversity curve with the clear exception of the interval between 6 and 7 Ma where most of the samples exceed the values of the curve. In this respect, the high variability in diversity of the samples in this interval is very intriguing since they are restricted to an interval not longer than 1 Ma in duration.

When diversity is estimated for the pooled samples, the oldest four and youngest three estimates exceed the values of the regional diversity curve, while the intermediate intervals exhibit similar values to the regional diversity curve (right panel, Figure 2.41). Despite of the differences in magnitude, the diversity curve and the estimates from Saltarin reveal similar patterns. A peak in diversity between 13 and 14 Ma followed by a sustained decrease that results in the low values observed between 11 and 8 Ma. This interval of low diversity is represented in Saltarin by a unique estimate with low diversity and is confirmed by the 27 samples whose recovery was very poor. Finally, an outstanding peak in diversity is registered in Saltarin between 7 and 8 Ma, which is followed by two intervals with lower diversity. A similar pattern is observed in the regional diversity curve but with clear differences

in magnitude (right panel, Figure 2.41).

2.4.3.6 Apaporis Section

Hoorn 2006(area 8 in Figures 2.34 and 2.8)

In this work, the author analyzed 25 samples from two sections measured along the lower Apaporis and Pira Rivers located in Colombia. All the samples were used in the diversity analysis because they present counts higher than 50 specimens. The author dated the sediments as middle to late Miocene based on the presence of the species *Grimsdalea magnaclavata*, which is indicative of the Grimsdalea zone of Germeraad et al. (1968). Here, to estimate the age of the samples, the palynological results were compared with the complete composite section using the maximum likelihood approach (Punyasena et al., 2012). The samples with the most reliable age estimation were used as a correlation points. The age of each sample was calculated by interpolation and assuming a constant sedimentation rate between the correlation points. The age of the samples is presented in Annex 2.4.

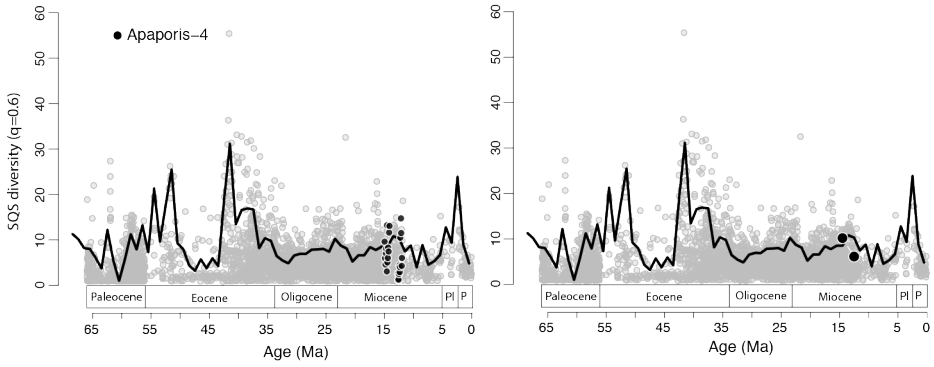

Figure 2.42: Diversity calculated for the samples of the Apaporis section (Hoorn 2006). Left panel: diversity of individual samples. Right panel: diversity of the 1 Ma bins. All estimates using SQS with a quorum level of 0.6.

The samples are distributed in two narrow intervals of the Miocene (left panel, Figure 2.42). Most of the estimates for the samples are below the regional diversity curve and the few exceptions are within the range of values imposed by the individual samples of the regional estimates. When SQS diversity is estimated for the pooled samples, the two intervals show the decrease recorded by the regional diversity curve.

2.4.3.7 Mariname Section

Salamanca et al. (2016) (area 9 in Figures 2.34 and 2.8)

In this work, the authors analyzed 47 samples from a stratigraphic section measured along the Caqueta River in Colombia. All the samples present counts higher than 50 specimens and therefore all of them were used in the diversity analysis. According to the authors, the age of the succession is early Miocene based on biostratigraphy (17.7-16.1 Ma, T-13-Echitricolporites maristellae zone, sensu Jaramillo et al., 2011). The age of the individual samples was calculated by interpolation, using the age of the biozone and assuming a constant accumulation rate between the extreme points (Annex 2.4).

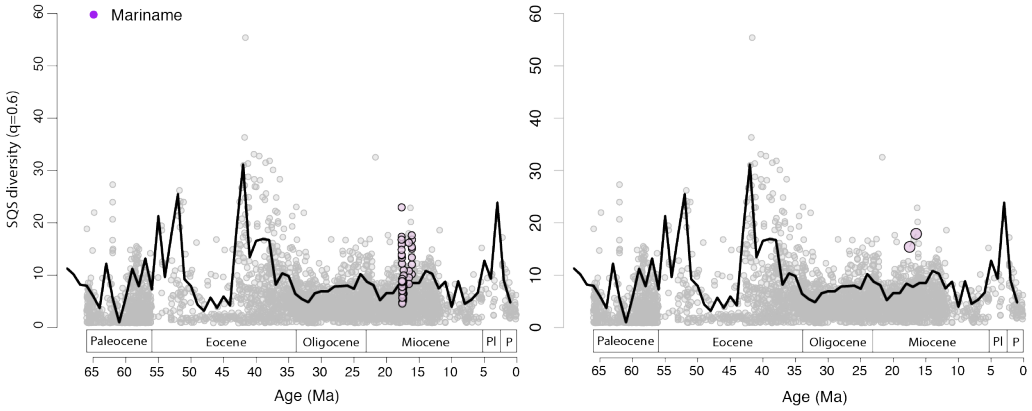

Figure 2.43: Diversity calculated for the samples of the Mariname section (Salamanca et al., 2016). Left panel: diversity of individual samples. Right panel: diversity of the 1 Ma bins. All estimates using SQS with a quorum level of 0.6.

The samples are distributed in two narrow intervals within the early Miocene (left panel, Figure 2.43). The SQS diversity for most of the samples as well as the estimates for the two 1 Ma pooled intervals exceed the regional diversity curve but are within the range of values imposed by the samples of the regional estimates (Figure 2.43). The two estimates suggest an increase in diversity between 16 and 17 Ma.

2.4.3.8 1AS-27AM and 1AS-19AM Rock Cores

Silva-Caminha et al. (2009)(area 10 and 11 in Figures 2.34 and 2.8)

In this work, 41 samples from two rock-cores drilled in the northwestern of Brazil were analyzed. The authors used Unitary Associations (Guex 1991)

to establish a zonation for the sequence and compared their results with the zonation proposed by Lorente (1986). According to the continuous presence of *Cichoreacidites longispinosus* and *Ladakhipollenites? caribbiensis*, the authors correlated their biozones with the palynological zone of Fenestrites longispinosus, subzone of Psilatricolporites caribbiensis of Lorente (1986). The age of this zone is interpreted as late Miocene to early Pliocene (nannofosil zone NN15 to NN9), which corresponds to the interval between 5.6 and 3.7 Ma (Lorente 1986). These two ages were interpreted as the oldest and youngest age of the cores. The age of the individual samples was calculated by interpolation between these the points and assuming constant accumulation rates between them (Annex 2.4).

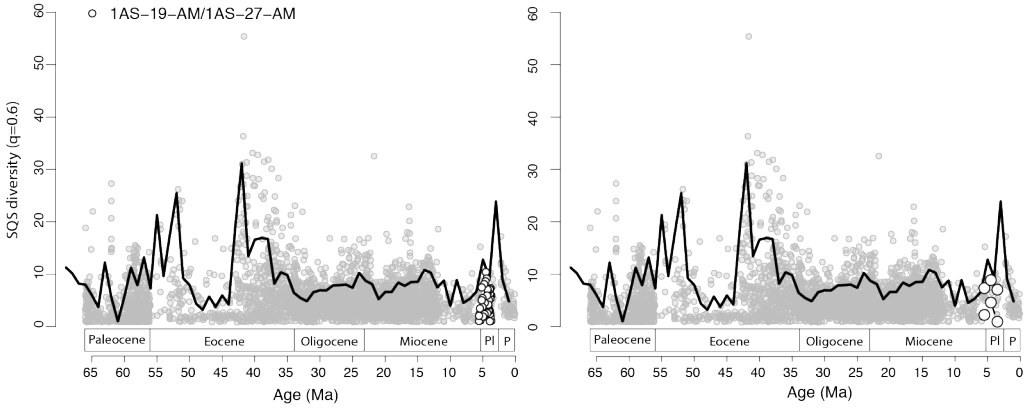

Figure 2.44: Diversity calculated for the samples of the cores 1AS-27AM and 1AS-19AM (Silva-Caminha et al., 2009). Left panel: diversity of individual samples. Right panel: diversity of the 1 Ma bins. All estimates using SQS with a quorum level of 0.6.

Samples of the two cores are indistinctively distributed in a narrow interval in the Pliocene. The SQS diversity of all the samples is below the values of the regional diversity curve (left panel, Figure 2.44). When diversity is estimated for the 1 Ma pooled intervals, the two cores resemble the pattern observed from the diversity curve (right panel, Figure 2.44).

2.4.3.9 1AS-105AM Rock Core

Jaramillo et al.(2017) (area 12 in Figures 2.34 and 2.8)

In this work, the authors analyzed 95 samples from a rock core drilled in the Amazon basin of Brazil. Thirteen samples with counts lower than 50 specimens were excluded of the diversity analysis. The age of the samples was estimated using biostratigraphy and can be found in the supplemental

material of the publication (Jaramillo et al., 2017). The samples are distributed continuously between 18.78 and 10.72 Ma and almost all of them present SQS diversities below the regional diversity curve and the few exceptions are within the range of the samples of the regional estimates (left panel, Figure 2.45). The SQS diversity of the 1 Ma pooled intervals is also below the values of the regional diversity curve (right panel, Figure 2.45). In the oldest interval of the core (19-13 Ma) the diversity fluctuates while the regional diversity curve suggest an increasing trend. The youngest interval (13-10 Ma) shows a decreasing trend that is also evidenced in the regional diversity curve (right panel, Figure 2.45).

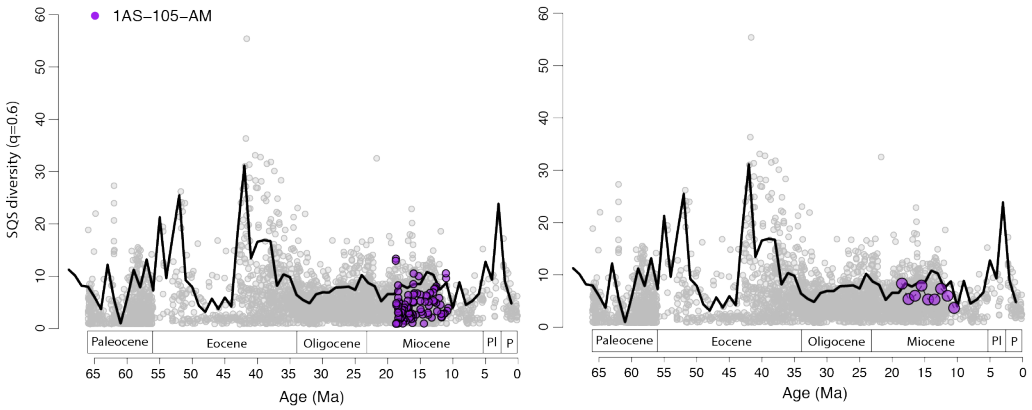

Figure 2.45: Diversity calculated for the samples of the core 1AS-105AM (Jaramillo et al., 2017). Left panel: diversity of individual samples. Right panel: diversity of the 1 Ma bins. All estimates using SQS with a quorum level of 0.6.

2.4.3.10 1AS-33AM Rock Core

Leite et al. (2016) (area 13 in Figures 2.34 and 2.8)

In this work, the authors analyzed 32 samples from a rock core drilled in the Amazon basin of Brazil. All the samples have counts higher than 50 specimens and therefore all of them were used in the diversity analysis.

The authors compared their palynological results with the zonation proposed by Lorente (1986) and Jaramillo et al. (2011) to establish a chronostratigraphic framework for the sequence. The base of the core was interpreted as being within the palynological zone of Crassoretitriletes (Lorente 1986) and the top of the core within the palynological zone Fenestrites longispinosus; subzone Echitricolporites-Alnipollenites (Lorente 1986). According to this interpretation the base of the core correspond to 14 Ma and

the top to 2.6 Ma. These two ages were used as correlation points to calculate the age of each individual sample (Annex 2.4).

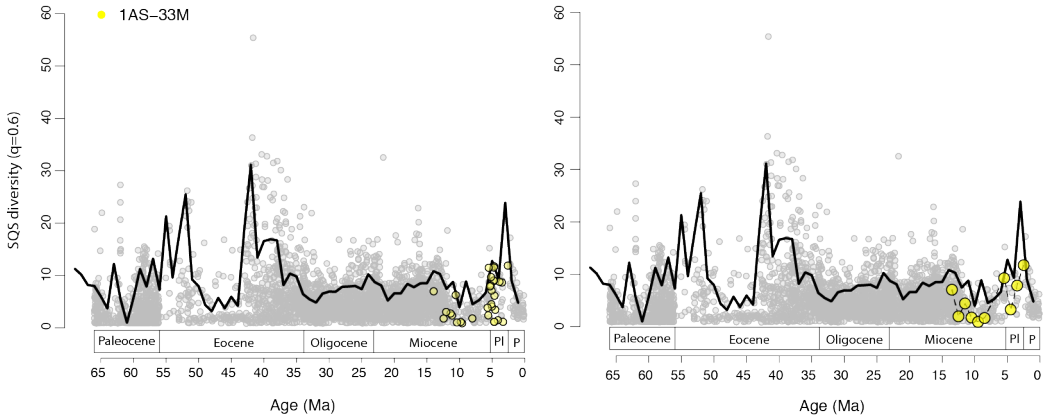

Figure 2.46: Diversity calculated for the samples of the core 1AS-33AM (Leite et al., 2016). Left panel: diversity of individual samples. Right panel: diversity of the 1 Ma bins. All estimates using SQS with a quorum level of 0.6.

The samples are distributed in two intervals of the late Miocene and the Pliocene and all of them have SQS diversities below the values of the regional diversity curve (left panel, Figure 2.46). When diversity is estimated for the 1 Ma pooled intervals they show the same pattern of the regional diversity curve (right panel, Figure 2.46). Elevated values at 14 Ma followed by a dramatic fall and low values up to 8 Ma. From 5 to 2 Ma, the two estimates suggest an increasing trend punctuated by sporadic falls (right panel, Figure 2.46).

2.4.3.11 Contamana Section

Antoine et al. (2016)(area 14 in Figures 2.34 and 2.8)

In this work, the authors analyzed seven samples from a stratigraphic section measured along the Quebrada Cachiyacu located near the town of Contamana in Peruvian Amazonia. Three samples have counts lower than 50 specimens and were excluded of the diversity analysis. In the supplemental material, the authors give a very general interpretation of the age of the sequences (e.g. middle to late Miocene). Here, a more precise age of the four samples was interpreted by using information from the publication. The samples CTA 47 (CTA-3-2) and CTA-27 were taken in the lower member of the Pozo Formation. Based on mammalian biostratigraphy and isotope analysis this formation is assigned to the late middle Eocene (42.8 to 37.8

Ma) (Antoine et al., 2016). The locality CTA-27 coincides with the early Bartonian age indicating therefore an age of approximately 41 Ma. The sample CT-47 is stratigraphically located below the locality CTA-27 so its age is interpreted as 42.5 Ma. The samples CT-44Middle and CTA-10 were taken in the Pebas Formation. The association of molluscs found in the locality CT-44 indicate latest middle Miocene (11.7 Ma) while a mammalian fauna documents the earliest late Miocene. With this evidence, the age of the sample CT-44Middle was interpreted as 11.6 Ma. The locality CTA-10 is considered not to be significantly younger than the locality CTA-43 (earliest late Miocene), for this reason the age of the sample CTA-10 was interpreted as 11 Ma (Annex 2.4).

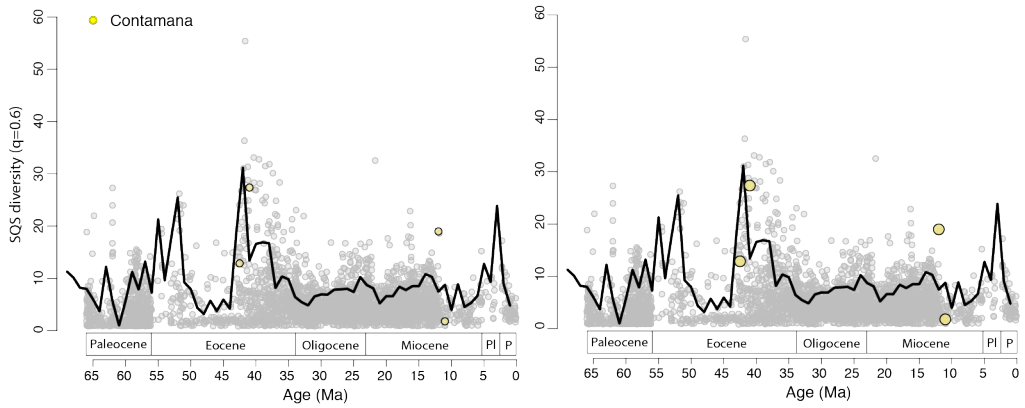

Figure 2.47: Diversity calculated for the samples of the Contamana section (Antoine et al., 2016). Left panel: diversity of individual samples. Right panel: diversity of the 1 Ma bins. All estimates using SQS with a quorum level of 0.6.

Even though only four samples were used to estimate SQS diversity, it is clear that they reveal the same pattern of the regional diversity curve (Figure 2.47). In the middle Eocene the samples from Contamana show an increase that is also evident in the regional diversity curve. The magnitude of this change is very similar in the two estimates (Figure 2.47). On the other hand, the samples of the Miocene record the abrupt fall in diversity between 12 and 11 Ma, which is also evident in the diversity curve. The magnitude of the change for this interval is however very different in the two estimates (Figure 2.47). With only four 4 samples, it was not possible to estimate the SQS diversity of the pooled intervals, so the two panels of the Figure 2.47 are identical and reflect the SQS diversity of the individual samples.

2.4.4 Diversity in Space

The regional diversity curve is the product of the contribution of samples from sections distributed throughout the area of study. When the sections and samples are differentiated by geographic region it is possible therefore to explore the contributions of those regions to the diversity estimates.

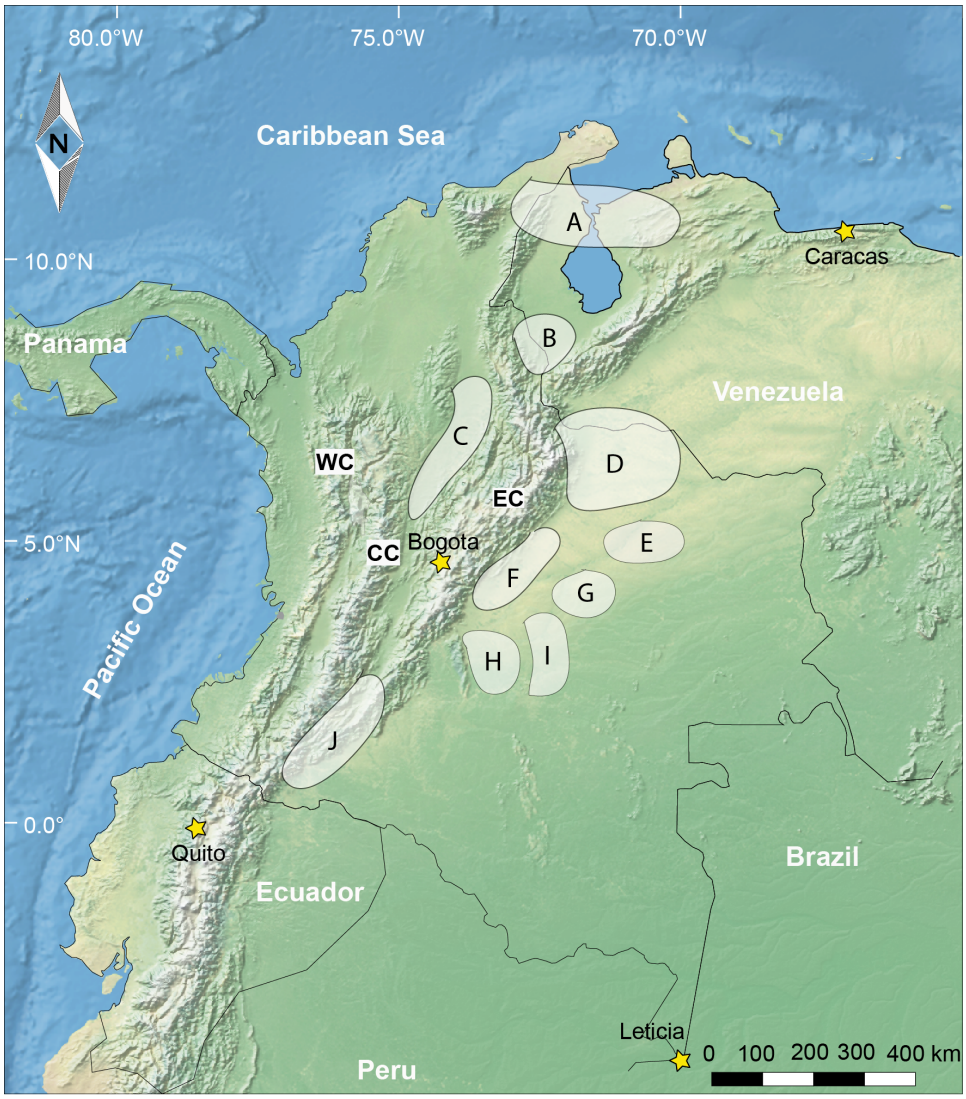

Figure 2.48: Map of Colombia showing the 10 areas (A to J) used to group the sections for the spatial analysis of diversity. WC: Western Cordillera, CC: Central Cordillera, EC: Eastern Cordillera. The area assigned to each section is presented in the Annex 2.5.

The 116 sections and 3978 samples used in the SQS diversity analysis were grouped in 10 geographic regions identified with letters from A to J (Figure 2.48). The delimitation of the 10 areas did not follow any specific criteria and was done visually. The objective was to group nearby sections and gets a general idea of the diversity changes by latitude and longitude. The SQS diversity estimated for the individual samples, discriminated by geographic region is presented in Figure 2.49. Each colour represents a letter, from A to J, which in turn correspond to a specific geographic area (Figure 2.48). From the cloud of points it is clear that two intervals are characterized by extremely low numbers of samples. The first correspond to the interval between 56 and 43 Ma and the second to the interval between 11 and 2.5 Ma. Not only are the numbers of samples very low in these two intervals, but also the numbers of sections. From Figure 2.49 the contribution of specific regions to the high SQS diversity values observed in different intervals is also evident. Two clear examples are the intervals 50-55 Ma and 40-45 Ma, from which the samples with the highest SQS diversity belong only to two regions (areas D and F respectively).

To better investigate the geographic distribution of diversity through time, the Cenozoic was subdivided in 5 Ma intervals, starting at 5 Ma. For each interval (12 in total), a choropleth map of diversity was produced (Figure 2.51-2.56). The number of sections and samples that are part of each interval are presented in the Figure 2.50. A significant correlation (spearman correlation test) between the number of sections and the number of samples was found (rho = 0.84, $p < 0.0005$). In general, a concurrent increase in the number of samples and sections is observed from the early Palaeocene (interval 50-55) to the early Miocene (interval 15-20) (Figure 2.50). In the corresponding figures, each choropleth map is accompanied by the paleogeographic reconstruction (Reyes-Harker et al 2015) that encompasses the interval (Table 2.3). In the maps, the sections are numbered according to the nomenclature in the Annex 2.5. To estimate the SQS diversity for each tessellation, the samples that compose each geographic region were combined forming a composite sample by adding the abundance of their constitutive species. Diversity was then estimated for the composite sample of each tessellation using SQS with a quorum level of 0.6.

An ANOVA test was used to find significant differences in diversity among the sites of each interval. When the test rejects the null hypothesis of no difference, Tukeys test was used to identify which sites are different. For the ANOVA, the information of all the samples with counts higher than 50 specimens was used instead of the diversity calculated for the tessellations on the choropleth maps. Because a whole-tessellation SQS diversity estimate would provide a single value representing the SQS diversity of a composite

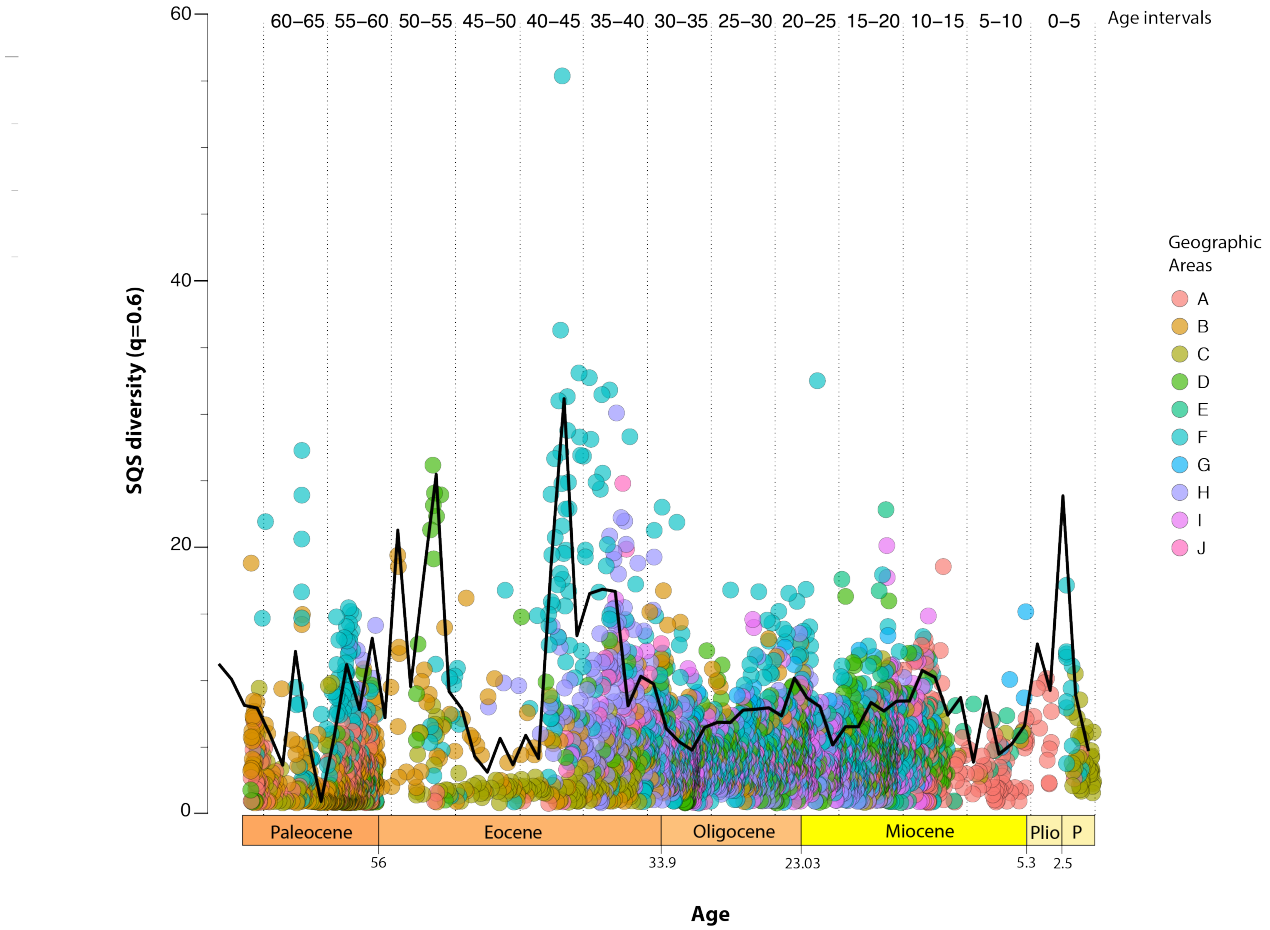

Figure 2.49: Diversity estimated for all the samples of the complete composite section for the entire Cenozoic. Diversity was calculated using SQS with a quorum level of 0.6. The colours represent the geographic location of the samples defined in the map of Figure 2.48.

sample, it would not give information about the variance among samples that is required to test for differences among tessellations. However, because the tessellations on the choropleth maps are coloured according to the whole-composite sample diversity estimate, it is possible that the results from the ANOVA may not be exactly reflected on the maps as shown. However, these differences are expected to be minor because (as explained in the results of the SQS (Results, section 2.46)), both the diversity estimated as the mean of the SQS diversity of each sample and the diversity estimated for the pooled intervals produce similar results. The main reasons of choosing to represent diversity on the maps using the whole tessellation composite sample, instead

of the mean of the samples, is that for several sections the number of samples with counts higher than 50 specimens is very low or zero, which would have prevented the use of several sections in the maps. Also the difference in the number of samples between the sections would have made difficult to make realistic comparisons of the diversity among sites.

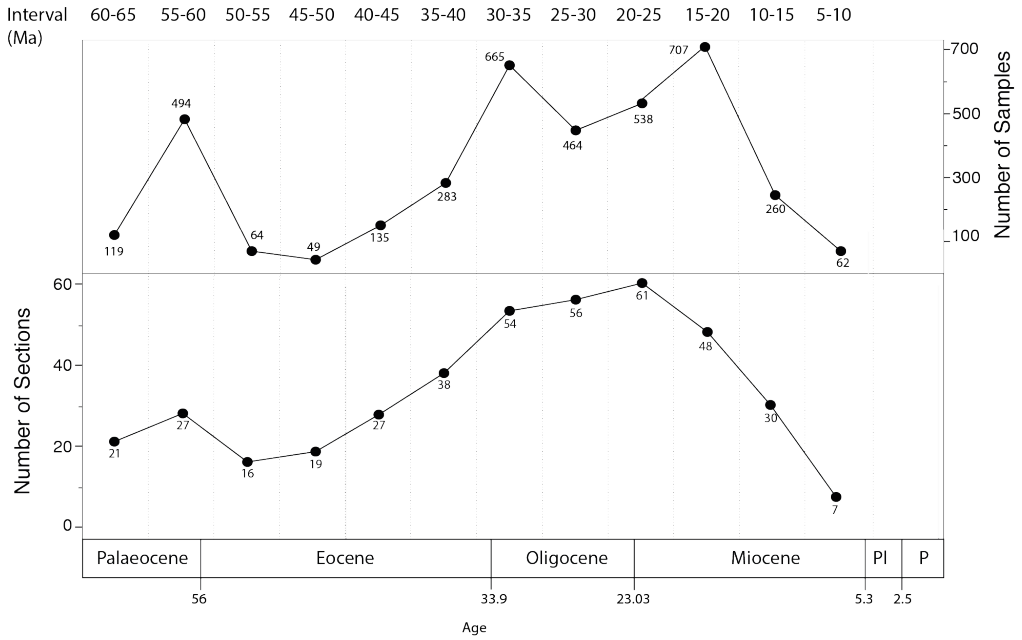

Figure 2.50: Number of sections and samples for the 5Ma time intervals in which the Cenozoic was subdivided.

The information about the sections that compose each interval is presented in the Annex 2.6. This information includes: the diversity of each section calculated from the composite sample (used to produce the choropleth maps), the mean diversity estimated from the samples (used for the ANOVA) and the number of samples in each section. When all the samples of a section present count levels lower than 50 specimens, the section was not used in the ANOVA but is represented in the maps. In the Annex 2.6 these sections are labelled as N/A in the cell where the number of samples is recorded. The result of the ANOVA is presented in the Annex 2.8 and explained for each interval below.

Interval 65-60 (early Palaeocene)

This interval comprises 119 samples distributed in 21 sections (Figure 2.50). Most of the samples (94%) have SQS diversity below 10 and only eight sam-

ples (6%) exceed this value (Figure 2.49). Five of these eight samples belong to Rioch-1 (#86) and the other three belong to Medina (#62) and Cer-3 (#18). For the ANOVA, 11 sections with more than three samples were used in the comparison. The remaining 10 sections were discarded because of their low number of samples and/or counts (Annex 2.6). The ANOVA suggest a significant difference among the sections (Annex 2.8, p = 8.8e-15). Tukeys test indicates that the diversity in Rioch-1 (#86) is significantly higher than the diversity in the other 10 sections (Annex 2.7). The choropleth map supports this difference and for the remaining areas suggests homogeneous values (bottom, Figure 2.51). From the choropleth map high SQS diversity is also apparent in Medina (#62) and Cas-1 (#16). The section number 16 was not included in the ANOVA due to the low counting. Although Medina (#62) was included in the ANOVA, a non-significant difference with the other sections was found. The paleogeographic reconstruction used for this interval corresponds to the early Palaeocene (Figure 2.51). Sequences of the basement as well as the Palaeozoic and Cretaceous were exposed while two depositional systems (coastal plain and continental) were active during this time period (Figure 2.51).

Interval 60-55 Ma (late Palaeocene)

This interval comprises 494 samples distributed among 27 sections (Figure 2.50). The SQS diversity in this interval ranges between 0 and 16 with a few samples from Bue-3Cor (#8) and Cano Sagu (#13) (areas F and H) exceeding this range (Figure 2.49). For the ANOVA, 21 sections with more than 3 and less than 30 samples were used (Annex 2.6). The results show a significant difference among the sections (Annex 2.8, p= 2e-16) with Tukeys test indicating that the SQS diversities in Bue-3Cor (#8), Bue-H15 (#9), Cano Sagu (#13) and Medina (#62) are significantly higher that in the other sections (Annex 2.9). The choropleth map supports this difference and suggests higher diversity toward the south of the area (top Figure 2.51). In comparison with the previous interval (60-65 Ma) the estimates are essentially similar.

The paleogeographic reconstruction for this interval corresponds to the late Palaeocene (upper panel, Figure 2.51). Marked differences with the previous reconstruction (early Palaeocene) are evident. New sequences of Jurassic and Paleogene are exposed in this interval. Toward the south, the exposed area of Cretaceous and Palaeozoic sequences seem to have increased reducing the available area for the development of depositional systems. It is also noticeable the increasing of area covered by the coastal plain and the establishment of several fluvial fans in the foothills of the lower Cretaceous

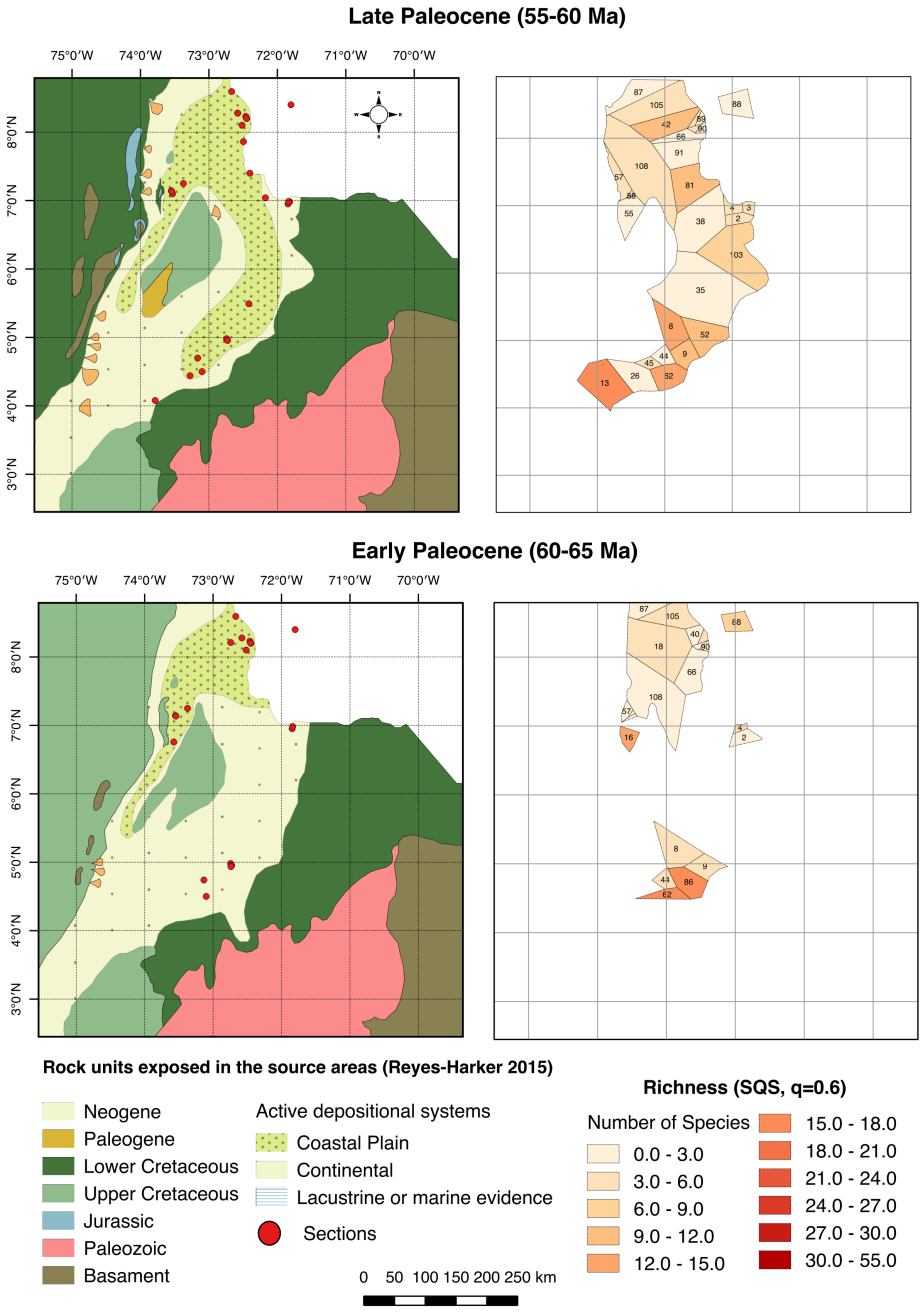

Figure 2.51: **Figures 2.51-2.56** Choropleth and paleogeographic maps for consecutive 5 Ma intervals starting at 5 Ma. Left panel, paleogeographic reconstruction, according with Reyes-Harker (2015) that best fits each interval. The red points in the map represent the exact position of the sections. Right panel, choropleth map representing the diversity of the sections. The Thiessen polygons were truncated and delineated according to the interpretation of the units exposed in the source area for each respective interval and according with the paleogeographic reconstruction. The numbers in the choropleth map are the codes used to identify the sections (Annex 2.4). The diversity was calculated using SQS with a quorum level of 0.6.

exposures.

Interval 55-50 Ma (early middle Eocene)

A low number of samples characterize this interval with only 64 samples distributed in 16 sections (Figure 2.50). This is the result of the abrupt decrease in the number of samples observed at the end of the previous interval. Seventeen of the 64 samples present SQS diversities higher than 10: this one of three intervals with a high proportion of samples with SQS diversities above 10 (Figure 2.31). The 17 samples with elevated SQS diversities are distributed between Regadera (#81) (eight samples); GonOut (#42) (four samples); Bue-3Cor (#8) (three samples) and Tib-182/187 (#105) (two samples). Six sections with more than three samples were used in the ANOVA (Annex 2.6). The results suggest a significant difference among the sections (Annex 2.8, p=1.5e-06) with Tukeys test indicating that SQS diversity in Regadera (#81) is significantly higher than in the other sections, except GonOut (#42) (Annex 2.10).

The choropleth map support this difference and also suggest a low SQS diversity for the areas in the centre of the map (lower panel, Figure 2.52) in comparison with the previous (55-60 Ma) and next interval (45-50 Ma). According with the paleogeographic reconstruction for this interval, that correspond to the early Miocene (lower panel, Figure 2.52), toward the East there is a substantial decrease in the area occupied by exposed lower Cretaceous units that now is occupied by continental depositional systems. The absence of coastal plain depositional systems that were present and widely distributed during the two previous intervals is notable.

Interval 50-45 Ma (early middle Eocene)

This is the interval with the lowest number of samples, only 49 from 19 sections (Figure 2.50). The SQS diversity of several of these is very low ($<$ 3) and only four samples exhibit SQS diversity values greater than 10 (Figure 2.49). Only four sections were used for the ANOVA and correspond to the sections with more than three samples analyzed (Annex 2.6). According to Tukeys test, the diversity in Tib-182/187 (#105) is significantly higher than the diversity in Reg-1 (#82), Li4 (#58) and Muc-3 (#66). The choropleth map however suggests than at least 6 sections exceed the diversity of Tib-182/187 (upper panel, Figure 2.52). These sections were excluded from the ANOVA because of their low number of samples. It is interesting to note that Regadera (#81) is the section in the choropleth map with the highest diversity. Although nine samples were analyzed in this section, only one

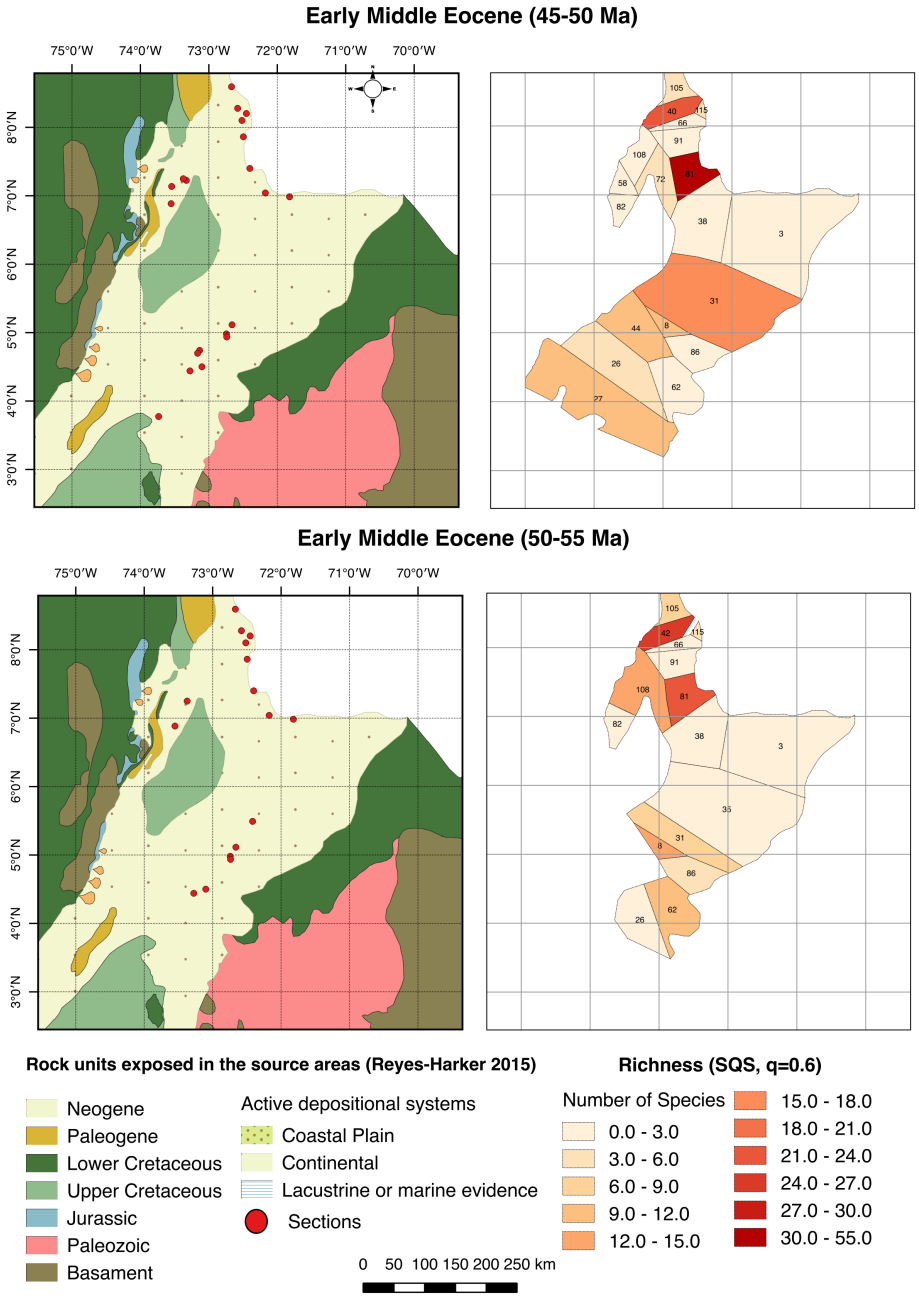

Figure 2.52: see caption Figure 2.51

sample has specimen count higher than 50. However, when all the samples are combined, their estimated diversity is very high. The paleogeographic reconstruction corresponds to the one used in the previous interval (early middle Eocene).

Interval 45-40 Ma (early middle Eocene)

This interval contains 135 samples from 27 sections (Figure 2.50). The youngest part of the interval (43-45 Ma) is characterized by a low number of samples that can be interpreted as the continuation of the pattern observed in the two previous intervals. At 43 Ma the number of samples abruptly increases (Figure 2.50). This is another of the three intervals characterized by a high proportion of samples with SQS diversities above 10 (Figure 2.31). In fact, 42 samples (31% of the total) exceed this value and belong to sections located in position F (Figure 2.48) and specifically to Bue-3Cor (#8) (22 samples); RioCh-1 (#86) (eight samples); Medina (#62) (six samples); Cano Sagu (#13) (two samples); Nuesp-1 (#71) (two samples); Cus-5 (#31) (one sample) and Regadera (#81) (one sample). For the ANOVA, 13 sections with more than 3 samples were used (Annex 2.6). The results suggest a significant difference among the sections (Annex 2.8, r= 1.9 e-07) with Tukeys test indicating that SQS diversity in Bue-3Cor, RioCh-1, and Medina is significantly higher than in the other sections used in the comparison (Annex 2.11). These results are supported by the choropleth map, from which it is evident that sections 86, 31 and 8 have elevated SQS diversity (lower panel, Figure 2.53). The paleogeographic reconstruction correspond to the one used in the previous interval (early middle Eocene).

Interval 40-35 Ma (late Eocene)

This interval comprises 283 samples from 38 sections (Figure 2.50). This is another of the three intervals characterized by a high proportion of samples with SQS diversities above 10 (Figure 2.31). In fact, 75 samples (26% of the total) exceed this value. These 75 samples are distributed among 25 sections. The sections with the largest number of samples are RioCh-1 (#86) (ten samples), Past-4 (#77) (seven samples) and Pum-1 (#80, not shown in the map) (seven samples). The remaining 51 samples are distributed among the other 22 sections. Is important to note, that those samples with high SQS diversities represent a small proportion of the total number of samples analyzed in the section (Annex 2.6). For example, in RioCh-1 and Past-4 a total of 14 and 18 samples were analyzed respectively and only in ten and seven samples the SQS diversity was above 10. The sections with less than

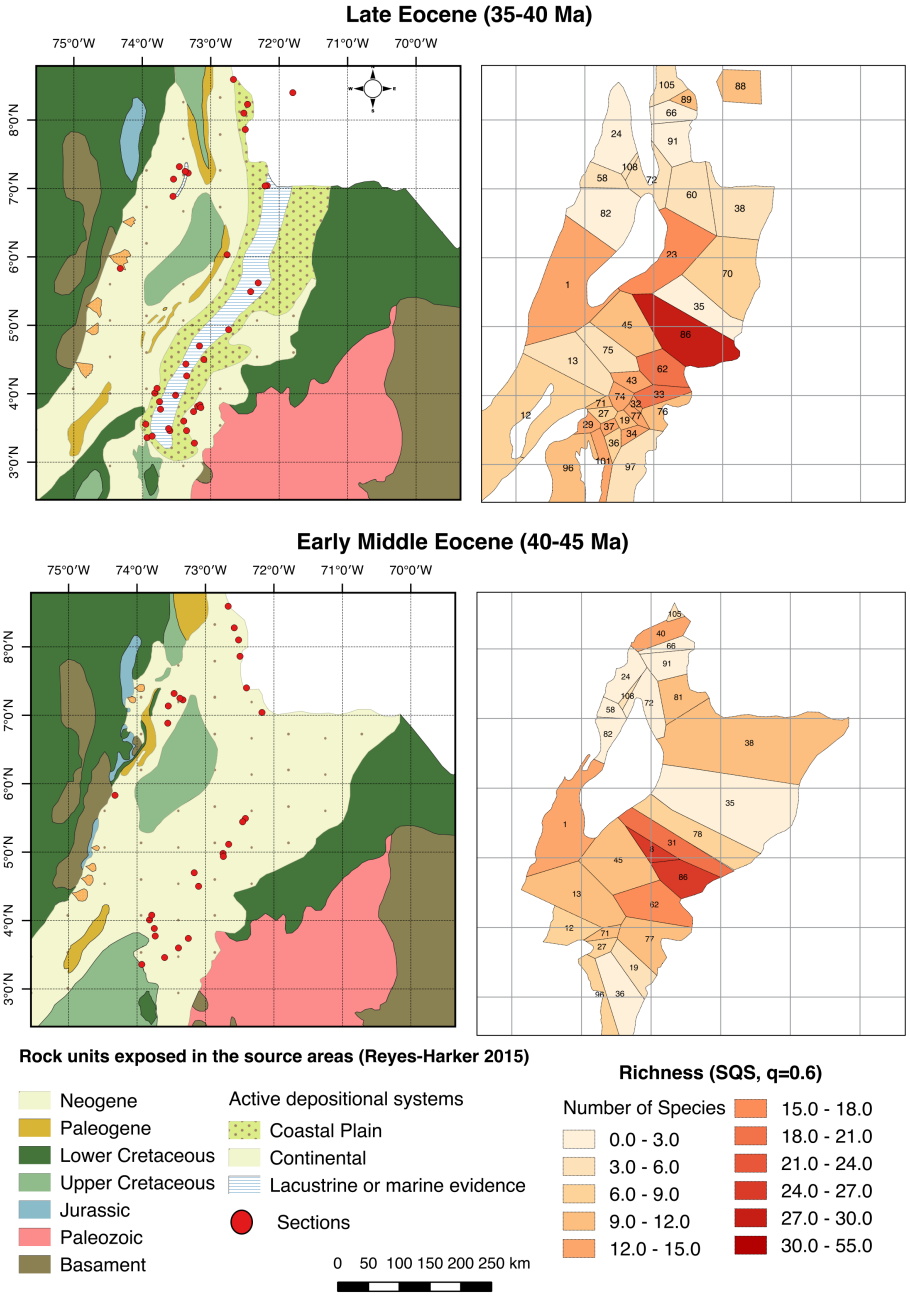

Figure 2.53: see caption Figure 2.51

four samples were discarded for the ANOVA, leaving a total of 20 samples for this analysis (Annex 2.6). The results suggest a significant difference

among the sections (p= 2e-16). According to Tukeys test, the SQS diversity in RioCh-1 (#86), Past-4 (#77), Pum-1 (#80), Medina (#62) and SanJ-1 (#101) is significantly higher than in the other sections (Annex 2.12). The choropleth map supports the results of the ANOVA and reveals that the highest diversity is concentrated in RioCh-1 (#86), Medina (#62) and Cusu-2 (#33) (upper panel, Figure 2.53). Although Cusu-2 was not included in the ANOVA, because of its low number of samples, it is clear from the choropleth map that this section exhibits one of the highest diversities of this interval (upper panel, Figure 2.53).

The paleogeographic reconstruction for this interval corresponds to the late Eocene (upper panel, Figure 2.53). The main differences with the previous reconstruction (early middle Eocene) are the increase to the east of the area occupied by exposed lower Cretaceous units and the development of an extensive active depositional system that includes continental, coastal plain and marine/lacustrine systems. Indeed this is the first interval where a marine/lacustrine system is reported (Reyes-Harker et al., 2015).

Interval 35-30 Ma (early Oligocene)

This interval comprises 665 samples from 54 sections (Figure 2.50). Most of the samples (96%) have SQS diversities below 10 while 27 samples (4%) exceed this value. The samples with the highest diversity are concentrated toward the youngest part of the interval, with 15 of them distributed in three sections, Nis-E1 (#69) (six samples), Tib-182/187 (#105) (six samples) and Medina (#62)(three samples). The other 12 samples are distributed in an equal number of sections (Figure 2.50).

For the comparison, 40 sections with more than four samples were used in the ANOVA (Annex 2.6). The results suggest a significant difference among the sections (Annex 2.8, p=2e-16). According to Tukeys test, the SQS diversities of the samples from Tib-182/187 (#105) are significantly higher than those of the other 19 sections while the SQS diversity of the samples from Nis-E1 (#70) and Medina (#62) are significantly higher than those of another 10 sections (Annex 2.13). From the choropleth map, it is evident that the sections with the highest diversity are LaMar-1 (#52), Pac-1 (#74) and Medina (#62) (lower panel, Figure 2.54). The first two were not included in the ANOVA because of their low specimens counts.

The paleogeographic reconstruction for this interval corresponds to the early Oligocene (lower panel, Figure 2.54). The only difference from the previous reconstruction (late Eocene) is the slightly increase of exposed Palaeogene units. There is not evident change in the distribution and amount of area covered by the active depositional systems.

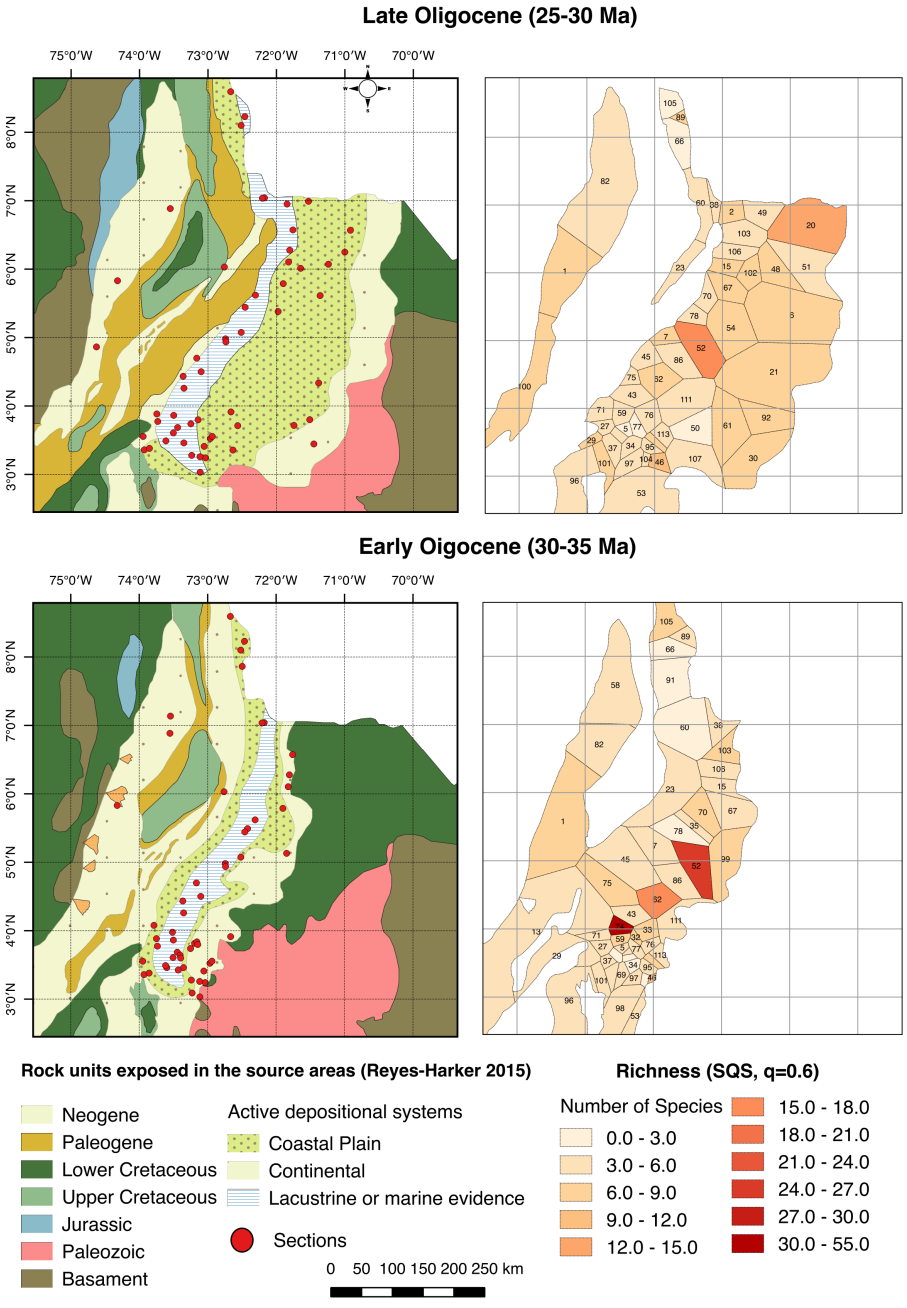

Figure 2.54: see caption Figure 2.51

Interval 30-25 Ma (late Oligocene)

This interval comprises 464 samples from 56 sections (Figure 2.50). Most of the samples (96%) have SQS diversities below 10 and only 20 of them (4%)

exceed this value (Figure 2.49). Eight of these 20 samples belong to Nis-E1 (#70) while 12 are distributed among eight other sections. For the comparison, 30 sections with more than four samples were used in the ANOVA (Annex 2.6). The results suggest a significant difference among the sections (Annex 2.8, p=1.54e-12). According to Tukeys test, the SQS diversity of the samples in ZuW2 (#89) and Bue-3Carb (#7) is significantly higher than the diversity of the samples from other sections (Annex 2.14). In the choropleth map the sections LaMar-1 (#52) and Chig-1 (#20) exhibit the highest SQS diversity (upper panel, Figure 2.54) however those sections were not used in the ANOVA because of their low counts of palynomorphs.

The paleogeographic reconstruction corresponds to the late Oligocene (upper panel, Figure 2.54). The main differences from the previous reconstruction (early Oligocene) are the increase of Palaeogene units exposed at the surface, the decrease toward the east of the area occupied by the exposed lower Cretaceous units, and the increase of the area occupied by the costal plain depositional system (upper panel, Figure 2.54).

Interval 25-20 Ma (early Miocene)

This interval comprises 538 samples from 61 sections (Figure 2.50). Most of the samples (95%) have SQS diversities below 10 and only 29 samples (5%) exceed this value. One sample belonging to Pal-1 (#75) presents the highest SQS diversity, with a value close to 33 (Figure 2.49). The other 28 high SQS diversity samples are distributed between Medina (#62) (eight samples) and Nis-E1 (#70) (five samples) while the remaining 15 are distributed among the other sections.

The 37 sections with more than four samples were used in the ANOVA (Annex 2.6). The results of the analysis suggest a significant difference between the sections (Annex 2.8, p=2e-16) with the Tukeys test suggesting that the SQS diversity of the samples in Nis-E1 (#70) is significantly higher than the diversity of the samples in all the other sections while the sections Pal-1 (#75) and Tib-182.187 (#105) show significant differences with specific sections (Annex 2.15).

The choropleth map support the high diversity in Nis-E1 (#70) and suggests homogeneity in the other areas. (lower panel, Figure 2.55). The paleogeographic reconstruction corresponds to the early Miocene (lower panel, Figure 2.55). The most noticeable difference with the previous reconstruction (late Oligocene) is the change in position of the lacustrine/marine depositional system. In the late Oligocene was located adjacent to the exposed Palaeogene units while in the early Miocene apparently it migrated toward the center of the basin (upper panel, Figure 2.54).

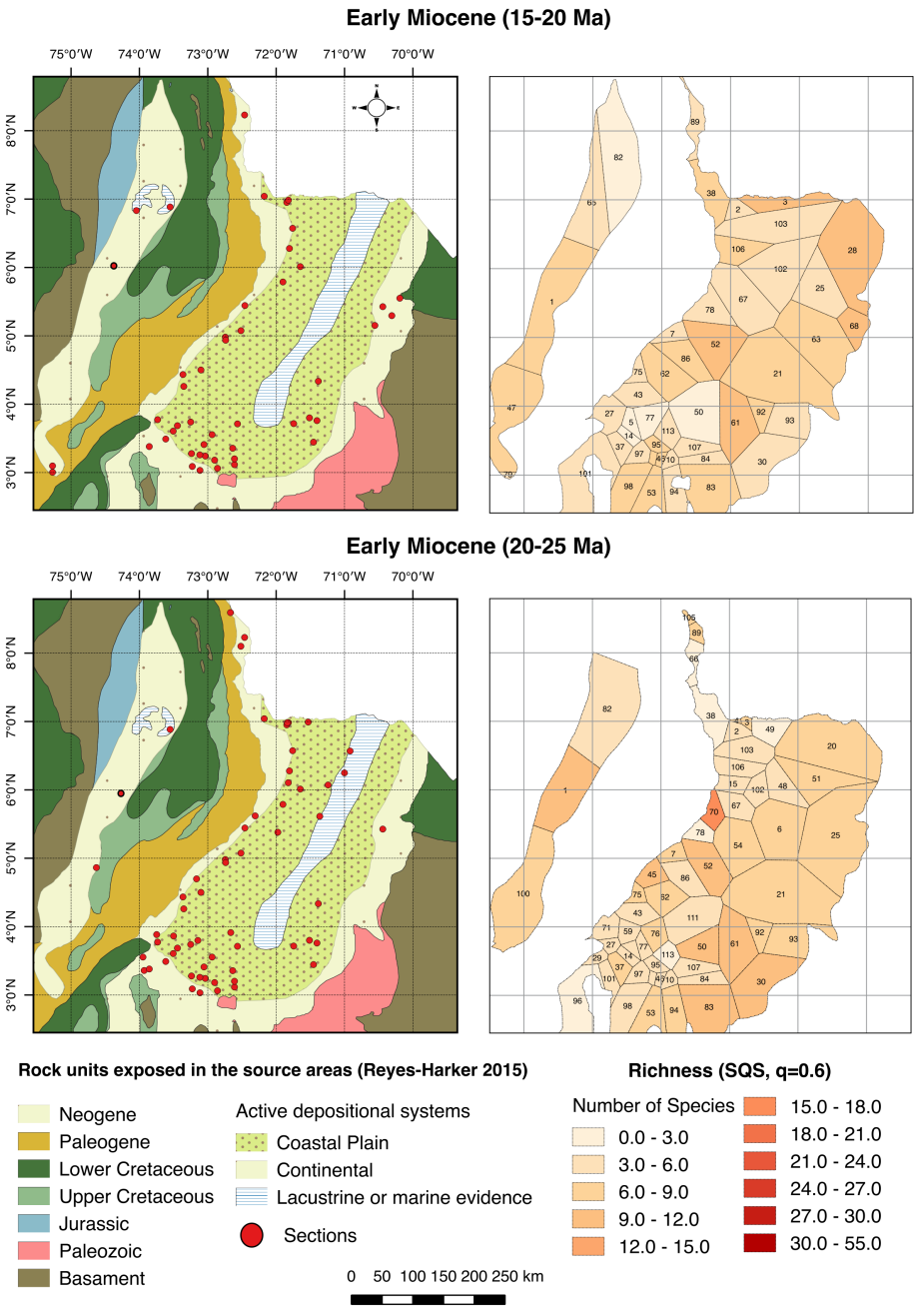

Figure 2.55: see caption Figure 2.51

Interval 20-15 Ma (early Miocene)

This interval comprises 707 samples from 48 sections (Figure 2.50). Most of the samples (96%) have SQS diversities values below ten and only 32 samples

(4%) exceed this value (Figure 2.49). Eight and five of the 32 samples belong to Medina (#62) and Toc-1 (#106) respectively while the remaining 19 are from other 12 sections. The 26 sections with more than nine samples analyzed were used in the ANOVA (Annex 2.6). The results indicate a significant difference among the sections (Annex 2.8, p=8.4e-12). Tukeys test shows that the SQS diversity of the samples in Toc-1 (#106) is significantly higher that the SQS diversity of the samples in eight other sections used for the comparison (Annex 2.16). The choropleth map suggests that SQS diversity in this interval is homogeneous. The differences detected in the ANOVA and Tukeys test are not evident in the map (upper panel, Figure 2.55). The paleogeographic reconstruction corresponds to the one used in the previous interval (early Miocene) (lower panel, Figure 2.55).

Interval 15-10 (middle Miocene)

This interval comprises 260 samples from 30 sections (Figure 2.50). There is an abrupt decrease in the number of samples toward the end of the interval (11 Ma) (Figure 2.49). Most of the samples (93%) present SQS diversity values between 0 and 10 and only 22 samples (7%) exceed this range (Figure 2.50). Nine of the 22 samples belong to Urumaco West (not shown in the map) and the remaining 13 samples are from eight other sections. For the ANOVA, only 17 of the 30 sections were compared and correspond to those sections where between three and 50 samples were analyzed. Seven sections were additionally discarded because all of their samples contained fewer than 50 specimens (Annex 2.6).

The ANOVA suggest significant differences among the sections (Annex 2.8, p=1.8 e-05). According to Tukeys test, the SQS diversity of the samples in S-14 (#95) is significantly higher than the SQS diversity of the samples of four of the sections used in the comparison (Annex 2.17). It is interesting to note that although the sections Fue182 (#37), LaMar-1 (#52) and Ara-3 (#3) show the highest SQS diversity in the choropleth map (10.5, 9.9 and 9.9 respectively), these sections were not compared in the ANOVA because their individual samples have counts below 50 specimens. The choropleth map support the results of the ANOVA and suggest that the diversity in this interval is homogeneous (lower panel, Figure 2.56). The paleogeographic reconstruction for this interval corresponds to the middle Miocene (bottom panel, Figure 2.56). The main difference with the previous reconstruction (early Miocene) is the increase toward the east of the area occupied by coastal plain depositional systems.

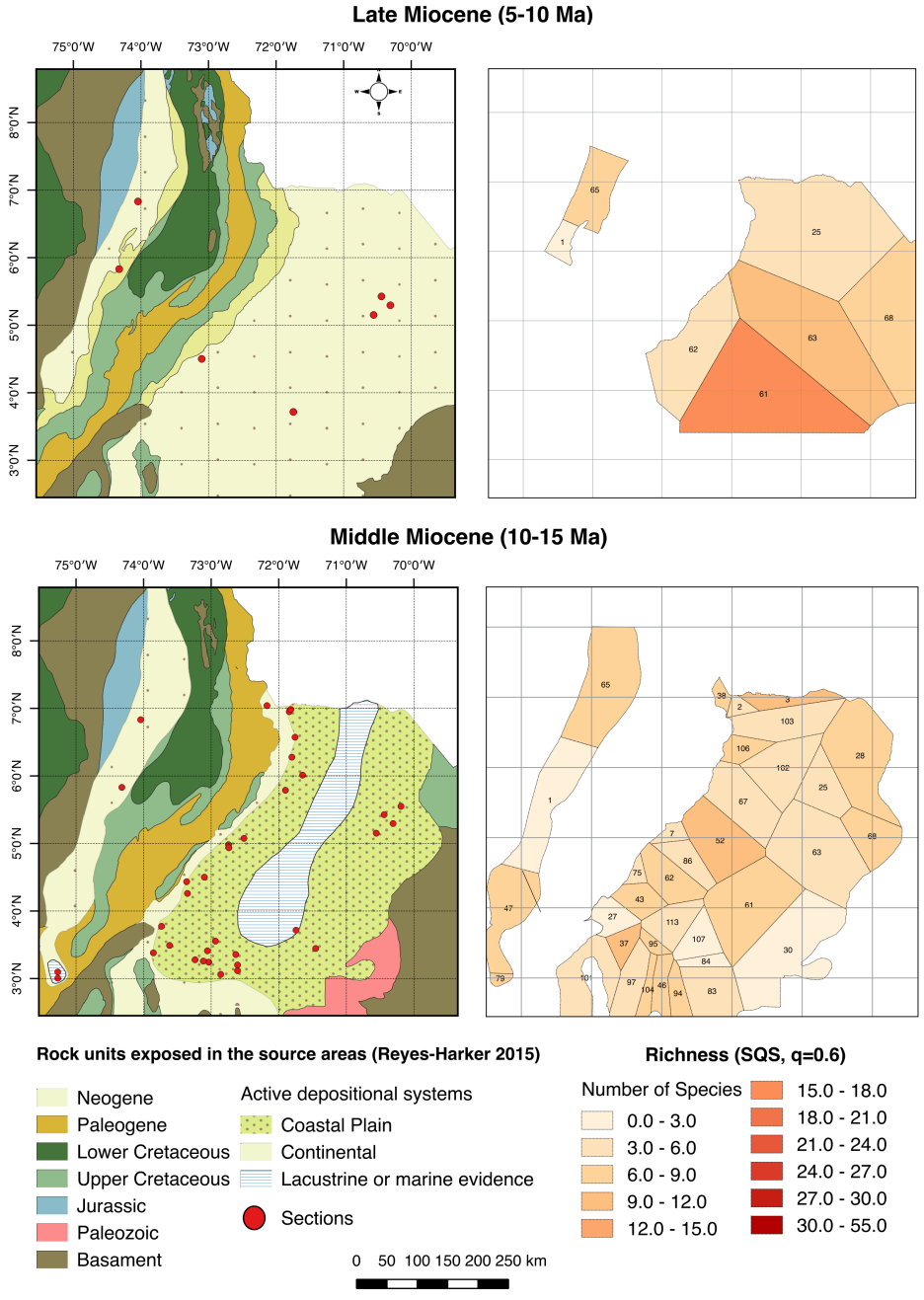

Figure 2.56: see caption Figure 2.51

Interval 10-5 Ma

This interval comprises 62 from seven sections (Figure 2.50). Only two samples from Mag-1 (#60) present SQS diversities higher than 10 (Figure 2.49).

For the ANOVA, only three sections were compared and correspond to those with more than two samples analyzed. The results of the ANOVA support the null hypothesis of no differences in diversity among the three sites (Annex 2.8, p=0.06)

The paleogeographic reconstruction corresponds to the late Miocene and indicates that only the continental depositional system was active during this time (upper panel, Figure 2.56). From the reconstruction, it is also evident that several units were exposed during time, including the basement, the Jurassic, the Cretaceous, the Palaeogene and the Neogene. This configuration is very similar to the Recent configuration of the area.

2.4.4.1 Diversity in space during the Miocene

The Miocene was a special period of time from a macroevolutionary and geological point of view. Several authors (Hoorn 2010 and references therein) have suggest that profound geological, climatic and biological events that occurred globally and regionally during the Miocene were responsible of the mega-diversity observed today in the Amazon basin. In order to explore the patterns of diversity during the Miocene the same methodology used to produce the choropleth maps for the Cenozoic was applied to the time interval between 23.04 and 4 Ma. To gain more detail, the composite section was divided in 2 Ma. The sections were grouped in the same geographic areas that were defined for the analysis of the Cenozoic (Figure 2.48). A total of 1244 samples distributed in 65 sections were used in this analysis.

In terms of coverage, there are differences in the number of sections and samples analyzed throughout the Miocene with more sections and samples analyzed during the early Miocene than during in the middle-late Miocene (Figure 2.57). The change in the number of sections is gradual, but is punctuated by three major episodes. The first occurs at the Oligocene-Miocene boundary where almost 30% of the sections analyzed in the interval 22-24 Ma are not represented in the following interval (20-22 Ma). The other two episodes occur from 16-18 Ma to 14-16 Ma and from 12-14 Ma to 10-12 Ma. In those intervals the number of sections represented decreases by 21% and 55% respectively (lower panel, Figure 2.57).

In contrast, changes in the number of samples are more gradual than changes in the number of sections, but are also punctuated by three major episodes (upper panel, Figure 2.57). The first episode occurs from 18-20 Ma to 16-18 Ma, during which the number of samples more than doubles. The other two changes occur from 16-18 Ma to 14-16 Ma and from 12-14 Ma to 10-12 Ma, during which intervals the number of samples decreases by 64% and 77% respectively.

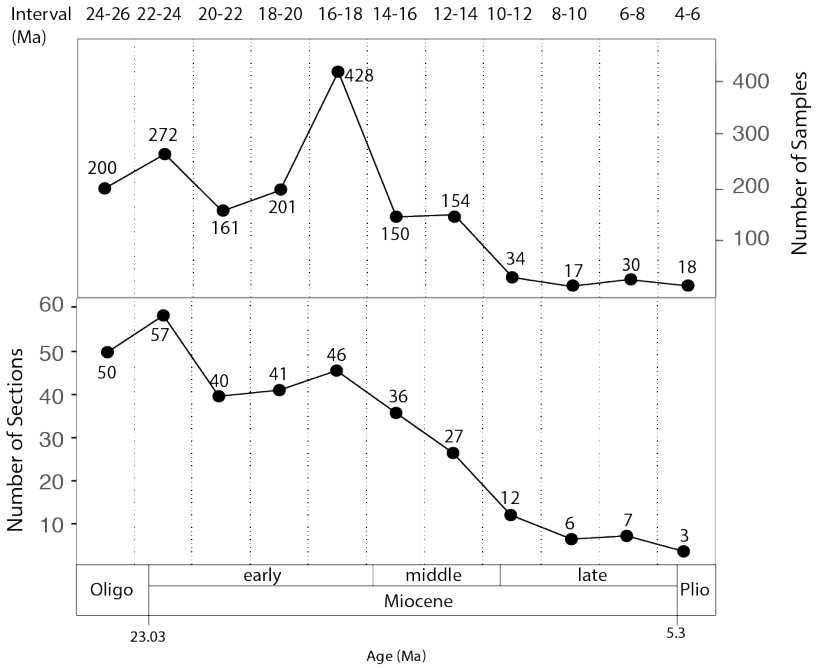

Figure 2.57: Number of sections and samples for the 2 Ma time intervals in which the Miocene was subdivided.

The SQS diversity of the individual samples is presented in Figure 2.58. The colours indicate the geographic areas from which samples were taken, and the black line is the SQS diversity curve for the interval (Figure 2.58). To complement the discussion of these results, the samples from Saltarin (Jaramillo et al., 2017) and the core 1AS-33M (Leite et al., 2016) were included and are represented by white and yellow circles respectively (Figure 2.58).

During the early and middle Miocene (23.03- 11.63 Ma) the SQS diversity of 96% of the 1244 samples is lower than 10 (Figure 2.58). Only 65 samples exceed this value and belong to sections located mainly in the areas F, D and A with 19, 11 and ten samples respectively (Figure 2.48). The change in the number of sections/samples during this interval (from 18-20 Ma to 16-18 Ma and from 16-18 Ma to 14-16 Ma) does not seem to have a pronounced effect on the regional diversity pattern. During this interval, most of the samples from Saltarin also have SQS diversities below 10 and only a small proportion exceeds this value.

The choropleth maps for the early to middle Miocene includes the intervals 22-24 Ma, 20-22 Ma, 18-20 Ma, and 16-18 Ma, 14-16 Ma and 12-14 Ma (Figures 2.60 and 2.61). The maps support the results of the individual

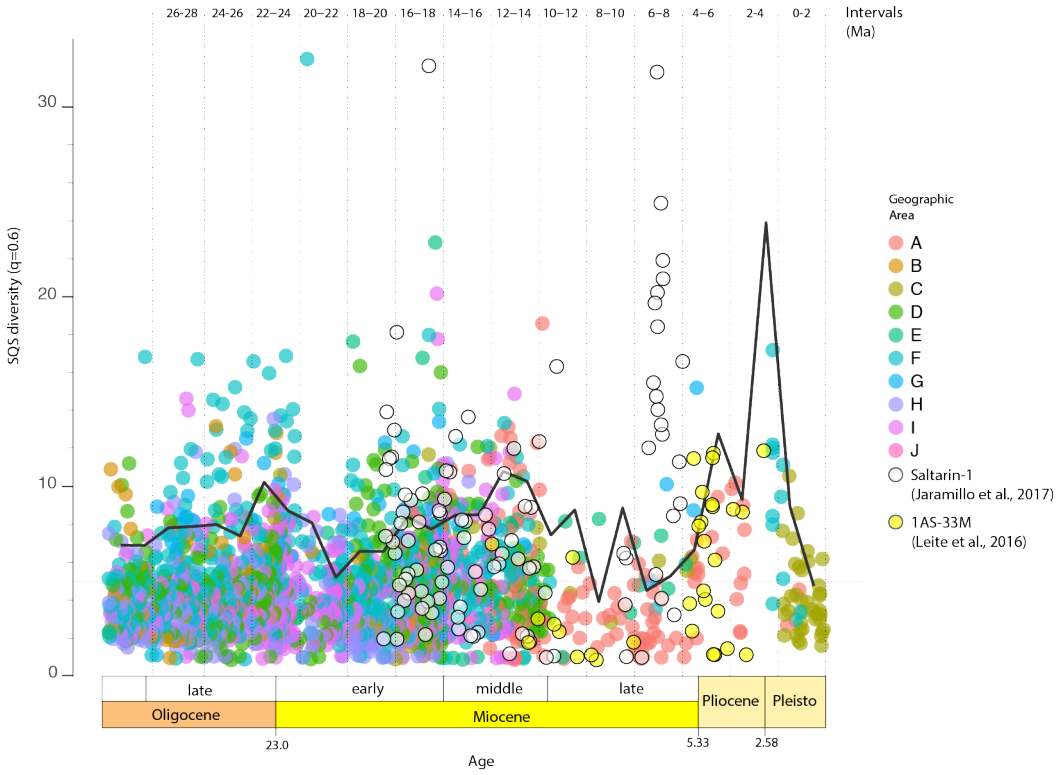

Figure 2.58: Diversity estimated for all the samples of the complete composite section for the interval between 32 Ma and the present. Diversity was calculated using SQS with a quorum level of 0.6. The colours represent the geographic location of the samples defined in the map of the Figure 2.48.

samples (Figure 2.58) in the sense that no differences are evident between the intervals, and reinforce the idea that the high SQS diversity is concentrated in just a few specific sites. It is also evident from the maps that SQS diversity is not static and the sites with the highest SQS diversity change from interval to interval (Figures 2.60 and 2.61).

An abrupt change in the number of sections and samples occurs during the late Miocene (Figure 2.58). During this period, corresponding to the intervals 10-12 Ma, 8-10 Ma and 6-8 Ma in Figure 2.58, only 79 samples were analyzed. The SQS diversity is very low with 68% of the samples showing SQS diversities below 10 while 29% of the samples present values ranging from 5-10. Only one sample exceeds 10 (Figure 2.58). Fifty-six of the samples belong to Urumaco West and Urumaco East and the remaining 27 are distributed in nine different sections.

During the Pliocene-Pleistocene interval, corresponding to the intervals

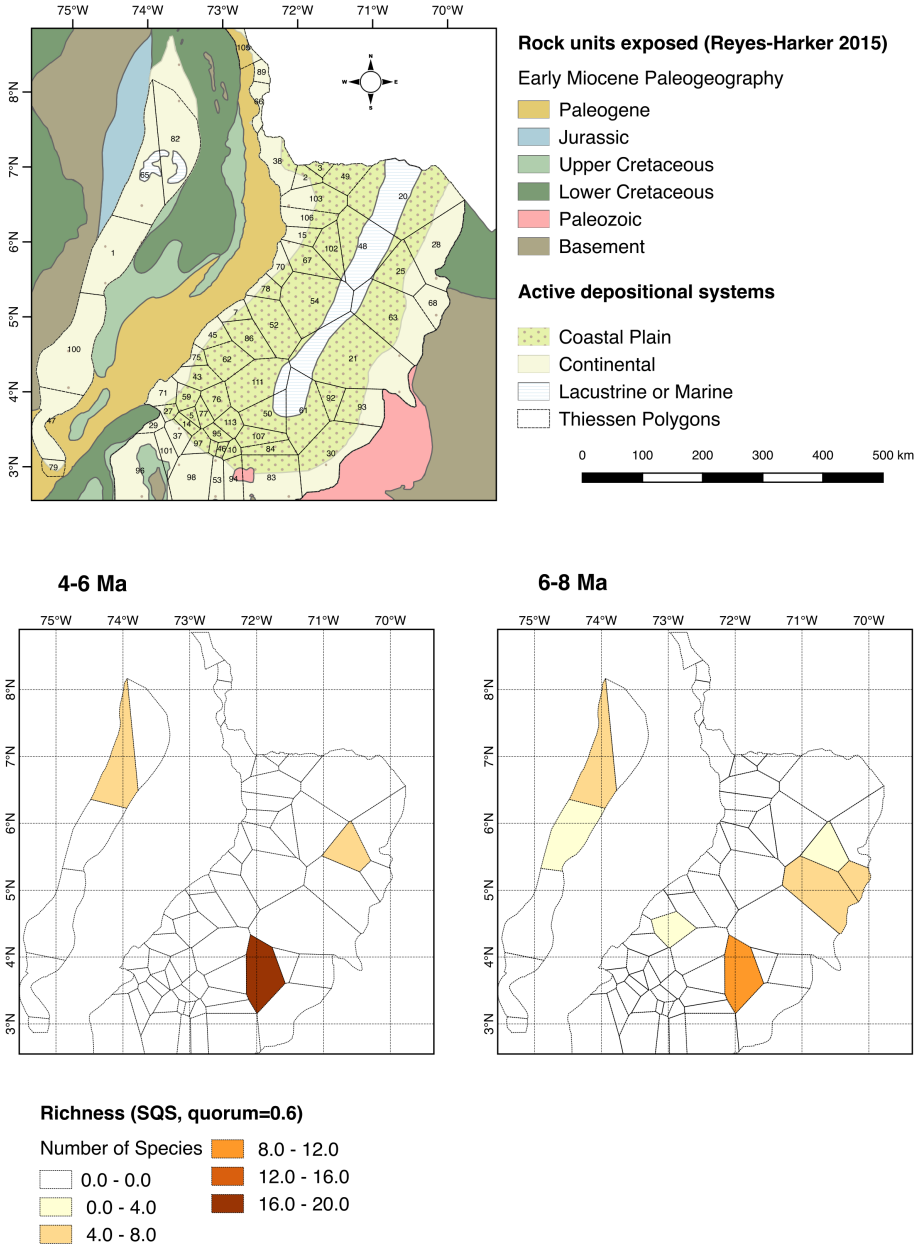

Figure 2.59: Choropleth maps for consecutive 2 Ma intervals starting at 4 Ma. The paleogeographic reconstruction in the upper panel of the Figure 2.59 corresponds to the early Miocene (Reyes-Harker 2015). This reconstruction was used to produce the tessellation framework used in all the maps. The numbers in the paleogeographic reconstruction correspond to the codes to identify the sections (Annex 2.4). The diversity in the choropleths maps was calculated using SQS with a quorum level of 0.6.

4-6 Ma, 2-4 Ma and 0-2 Ma in Figure 2.58, only 65 samples were analyzed. The SQS diversity is also very low but slightly higher than during the late Miocene (Figure 2.49). In total 58% of the samples have SQS diversities lower than 5, while 30% of them range from 5 -10. Only 9% of the samples exhibit values higher than 10 (Figure 2.58). Most of the samples (60%) belong to Mont-1 while the remaining 40% are distributed between Urumaco West (14 samples) and Medina (12 samples).

The samples from the core 1AS-33M are mainly distributed in the intervals 10-12 Ma and 4-6 Ma (yellow dots, Figure 2.58). The standing diversities of both intervals are within the range of the other geographic areas. This is especially true in the interval 4-6 Ma, during which all the samples are below the regional diversity curve but supporting the increasing trend observed for this interval (Figure 2.58).

The samples from Saltarin are distributed between 6 and 20 Ma (white dots, Figure 2.58). The samples between 12 and 20 Ma present SQS diversities that are within the range of the other geographic areas and most of them are below the regional diversity curve. Between 8 and 12 Ma the few samples available are also within the range of the other sections and below the regional diversity curve. Although the number of samples in this interval is very low, from the supplemental material in Jaramillo et al. (2017) is known that nine additional samples were analyzed between 8.4 Ma and 11.2 Ma. Most of the samples were sterile or their recovery was very poor, which made impossible to estimate their SQS diversities. The low recovery in this interval is consistent with the low diversity observed between 8 Ma and 12 Ma from the regional diversity curve (Figure 2.58).

In contrast, the SQS diversities of most of the 27 samples analyzed from 6-8 Ma by Jaramillo et al. (2017) exceed the range of values of the other areas as well as the regional diversity curve (Figure 2.58). This is interesting and demonstrates that even in a short time interval of less than 2 Ma (from 5.48 to 7.49 Ma), diversity may fluctuate considerably.

The choropleth maps for the early to late Miocene (Figures 2.59 and 2.60) support the results obtained from the individual samples. In this interval only a few sections were analyzed and most of them exhibit low SQS diversity. The section #61(Mag-1) is however characterized by relatively high values in the four reconstructions.

2.4.5 Origination and Extinction using Gap Fillers

Origination (o) and Extinction (e) rates were calculated using the gap-fillers equations proposed by Alroy (2014). To assess the possible effect produced by the borehole caving, o and e were calculated for both the complete composite

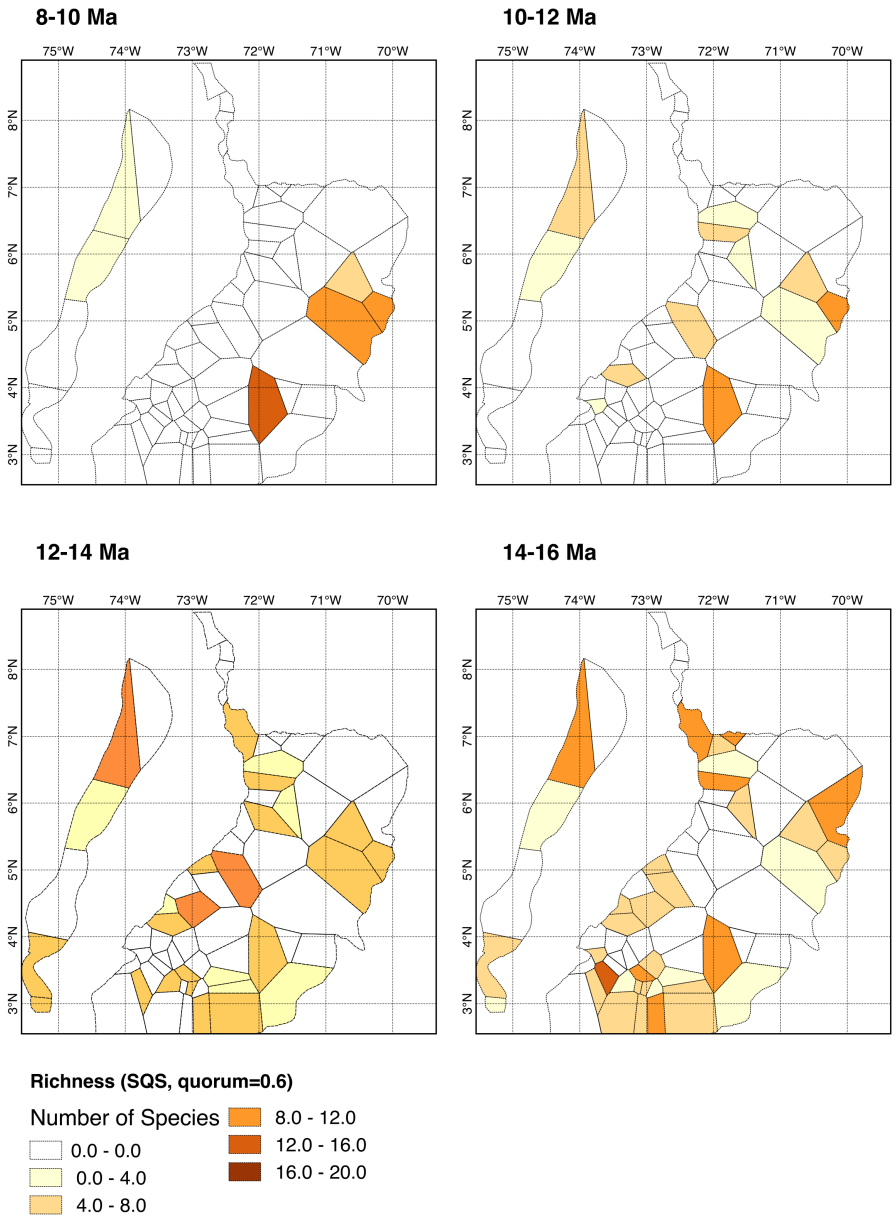

Figure 2.60: see caption Figure 2.59

sections and the restricted-FAD composite section. The two versions were divided into 1 Ma time intervals and standardized by randomly drawing

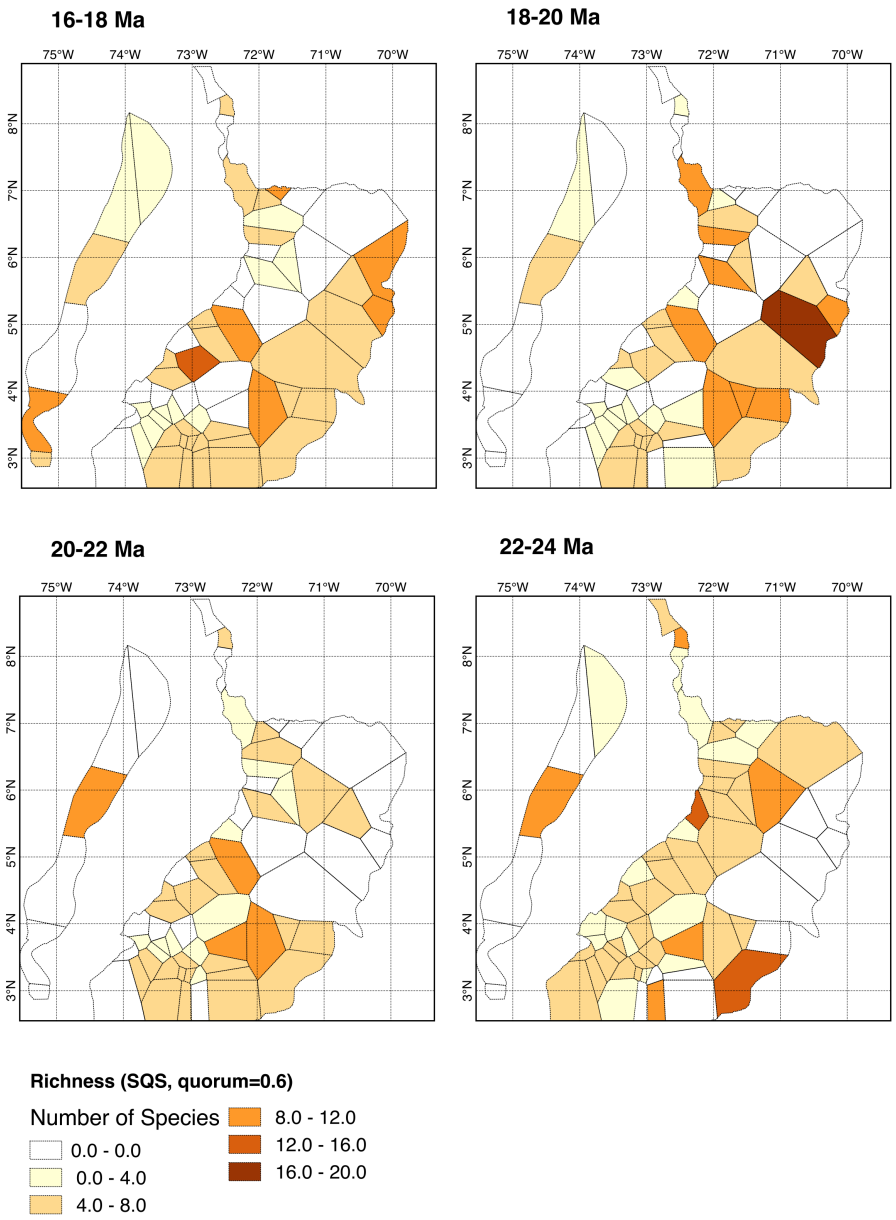

Figure 2.61: see caption Figure 2.59

entire collections up to a uniform quota of 137 occurrences for the complete composite section, and 39 for the restricted-FAD composite section. The

intervals that did not reach the respective quota were eliminated from the analysis. These intervals correspond to 64-65 Ma, 63-64 Ma and 55-56 Ma for the restricted-FAD composite section and 55-56 Ma for the complete composite section. The resampling was repeated 1000 times and o and e were calculated for each one of the iterations. The median for each interval was calculated from the iterations. The estimate for the iterations is represented by grey and the median is represented by green and red (origination and extinction) in the respective figures (Figures 2.62 and 2.64).

2.4.5.1 Origination

The origination rates estimated for the complete and the restricted-FAD composite sections are in general very similar (Figure 2.62). A significant positive correlation of the medians indicates that the two estimates exhibit the same pattern (rho = 0.82; p= 3.1e-15). When the difference between the two estimates is calculated is clear that the major dissimilarity is found in the Palaeocene and early Eocene (Figure 2.63). In the Palaeocene (66-56 Ma) the two estimates differ the most. The elimination in the restricted-FAD composite section of the intervals 64-65 Ma and 63-64 Ma could explain this disparity. Because the gap-fillers equation requires information from the two previous and the subsequent intervals, the elimination of these prevent the estimation of the origination rate for the intervals 64-65 Ma, 63-64 Ma, 62-63 Ma, 61-62 Ma and 56-57 Ma (Figure 2.62). This leaves the restricted-FAD composite with only four data points, which are disperse and interrupted by intervals containing no information. On the other hand, in the complete composite section only the first two intervals lack estimates of origination rate.

When compared with the other epochs of the Cenozoic, the Palaeocene and early Eocene exhibit in general high origination rates (Figure 2.62). The differences between the estimates from the composite and the restricted-FAD composite sections are great during this interval (Figure 2.63).

During the middle and late Eocene the origination rate in both the complete and the restricted-FAD composite sections show the same pattern and their differences are small (Figure 2.63). The early Eocene is characterized by a trend of decreasing origination rates, which is observed in both versions of the composite section. During the middle and late Eocene, the origination rate is highly fluctuating, but restricted to a range of values lower than those observed during the early Eocene. An exception occurs in the interval between 42 and 43 Ma of the complete composite section when origination rates exceed almost all the values of the Cenozoic. High origination rates are also observed in the restricted-FAD composite section but occurring at 44-45

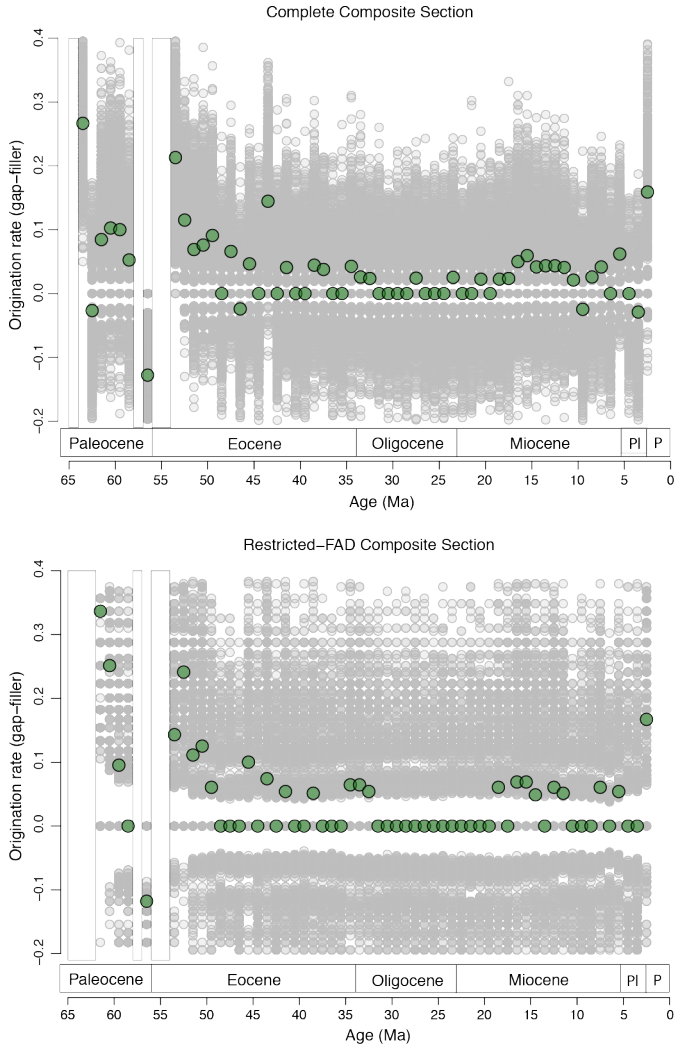

Figure 2.62: Origination rate calculated using the gap-filler equation (Alroy 2014) for the complete and the restricted-FAD composite sections .The grey circles represent the origination for each one of the 1000 iterations and the green circles are the median for each time interval.

Ma (Figure 2.62).

During the Oligocene, both the complete composite section and the restricted-FAD composite section exhibit the same pattern. The differences between the two estimates are minimal (Figure 2.63). Most of the intervals during the Oligocene have an origination rate equal or very close to zero except for the three younger intervals (33-34 Ma, 32-33 Ma and 31-32 Ma), during which the origination rate is a little bit higher and seems to follow the trend observed

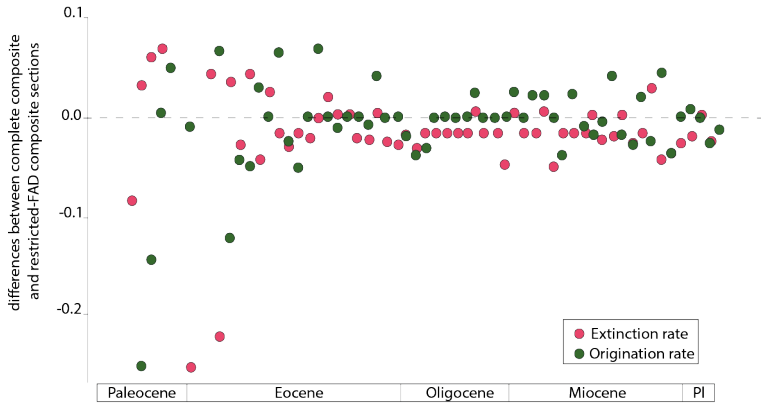

Figure 2.63: Differences between the origination rate and extinction rate estimated from the complete and the restricted-FAD composite sections. The major differences in both are concentrated in the Palaeocene and early-middle Eocene.

during the mid-late Eocene (Figure 2.62). In the Miocene, both versions of the composite section show a similar pattern. The differences between them are more pronounced in the middle and late Miocene (Figure 2.63). The early Miocene exhibits a fluctuating pattern, between low and zero origination. This pattern is very evident in the complete composite section while, whereas for most of the Miocene intervals of the restricted-FAD composite section the origination rates is zero. During the middle Miocene, the origination rate increases and stays high until the beginning of the late Miocene. In the early late Miocene (approx. 10.5 Ma) the origination rate dramatically falls and from this point until the last interval of the time series (present) it shows again a fluctuating pattern that this time is wider in comparison with the pattern observed in middle-late Eocene and early Miocene.

2.4.5.2 Extinction

The extinction rates estimated for the complete and the restricted-FAD composite sections are in general very similar (Figure 2.64). A significant positive correlation of the medians indicates that the two estimates exhibit the same pattern (rho = 0.69, p= 1.69e-09). When the differences between the two estimates are calculated most of the dissimilarities are concentrated in the Palaeocene and early Eocene (Figure 2.63)

Similar to origination, the extinction rate for the Palaeocene of the restricted-FAD composite section is scattered and interrupted by intervals of no information. The lack of information may explain the big differences observed

between the two versions of the composite section during this interval (Figure 2.63).

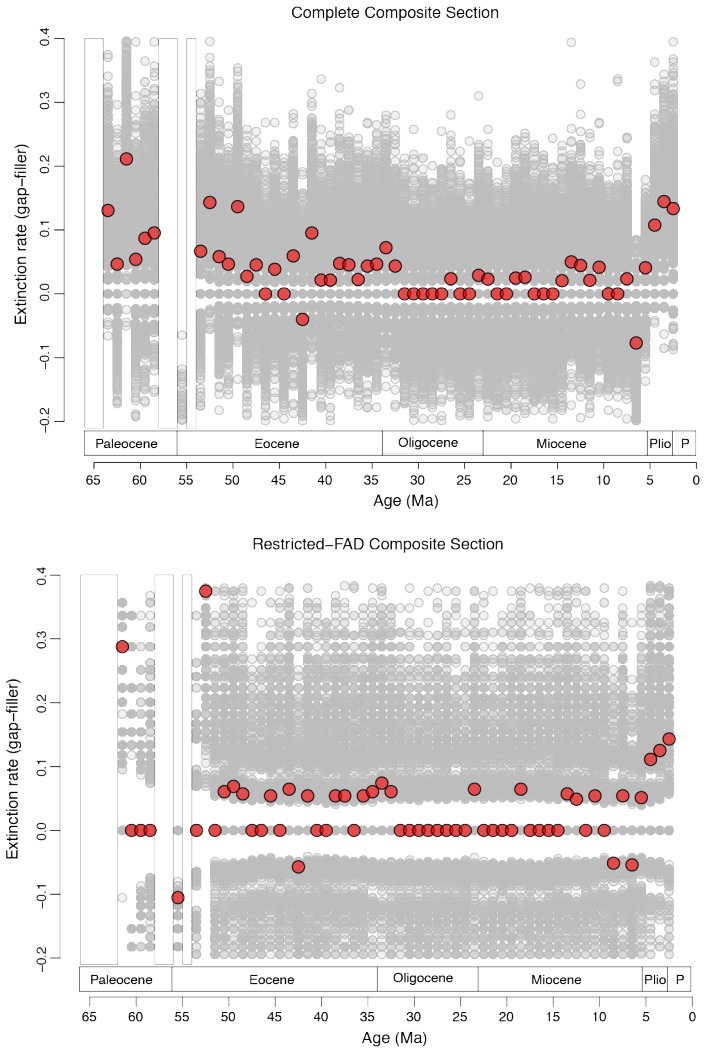

Figure 2.64: Extinction rate calculated using the gap-filler equation (Alroy 2014) for the complete and the restricted-FAD composite sections. The grey circles represent the extinction for each one of the 1000 iteration and the red circles are the median for each time interval.

From the early Eocene to the end of the middle Eocene, the differences between the complete and restricted-FAD composite sections are still significant but less than those observed during the Palaeocene. During this interval the extinction rates exhibits a decreasing trend imposed over a fluctuating

pattern. This behaviour is very clear in the complete composite section, while in the restricted-FAD composite section; the fluctuation is evident but lacks any trend. The fluctuation is in general wide with sporadic peaks standing out (Figure 2.64). Indeed, this period presents the intervals with the highest extinction rates of the entire Cenozoic. The fluctuations continue from the end of the middle Eocene until the late Eocene, but are no longer accompanied by a decreasing trend. The extinction rate abruptly falls at the Eocene-Oligocene boundary, and from the Oligocene to the late Miocene a fluctuating pattern is observed again, but this time is concentrated over a narrower set of values (between zero and low extinction) in comparison with the previous interval. During the Oligocene the differences between the estimates from the complete and the restricted-FAD composite sections are close to zero. During the early and late Miocene these differences are zero or very minimal (Figure 2.63). At the beginning of the middle Miocene the extinction rate increases and remains relatively high and stable until the early late Miocene. During the late Miocene the extinction rate is very close to zero. The last four intervals, corresponding to the Pliocene, are characterized by high extinction rates comparable to those observed in the early Eocene (Figure 2.64).

Finally, the complete composite section was divided into 2 and 5 Ma time intervals and the origination and extinction rates were calculated using the same approach explained before (Figures 2.65 and 2.66). This approach allows knowing if the origination and extinction patterns observed at 1 Ma (Figure 2.63 and 2.64) are specific to this temporal scale or if the patterns are reproducible at other temporal scales. The analysis was restricted to 5 Ma because at higher intervals (e.g. 10 Ma) the number of estimates is too small to make a reliable interpretation.

The origination rates at 2 Ma and 5 Ma shows the same pattern that is obtained when the section is pooled at 1 Ma intervals (Figure 2.65). For the extinction rates the results are also similar (Figure 2.66). The version of the origination and extinction rates at 5 Ma, despite of having only 10 estimates, is also successful detecting the most prominent peaks observed when the section is pooled at 1 Ma intervals (Figures 2.65 and 2.66).

2.4.6 Macroevolutionary Dynamics

As an initial test of the occurrence of diversity dependent diversification, the origination and extinction rates calculated using the gap-fillers equations (Figures 2.62 and 2.64) were compared to the estimated SQS diversity from the abundance data of the complete composite section (Figure 2.33). Because two autocorrelated time series could show strong cross-correlation due

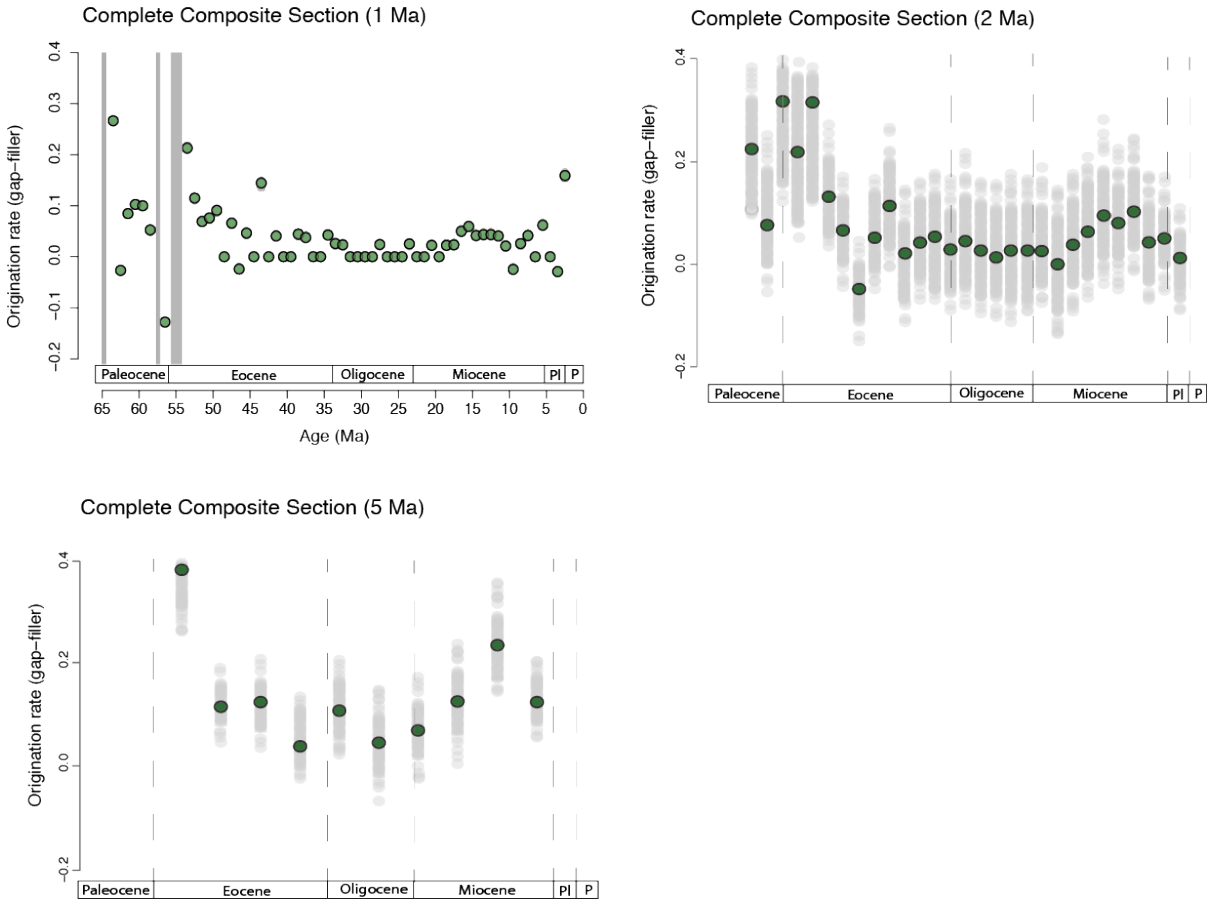

Figure 2.65: Origination rates calculated using the gap-filler equation (Alroy 2014) for the complete composite section pooled at 1 Ma, 2 Ma and 5 Ma time intervals. The grey circles represent the origination for each one of the 1000 iterations and the green represent the median for each time interval.

to expected random walks and no because common causal factors (McKinney 1990) the taxonomic rates and diversity were tested for autocorrelation. In the case of SQS diversity a serial correlation is detected at a lag of 1 (Figure 2.67) while for origination and extinction rates serial correlations were detected at lags 11 and seven respectively (Figure 2.67). Each one of the three time series was detrended by taking the residuals of the regression line fitted to the data. The slopes of the estimated regression lines are very small (SQS diversity = -0.023; origination rate= -0.0009; extinction rate= -0.0004) suggesting a lack of long-term trend. The three detrended time series also shows a lack of autocorrelation (Figure 2.67).

The lack of serial correlation in the origination and extinction rates does

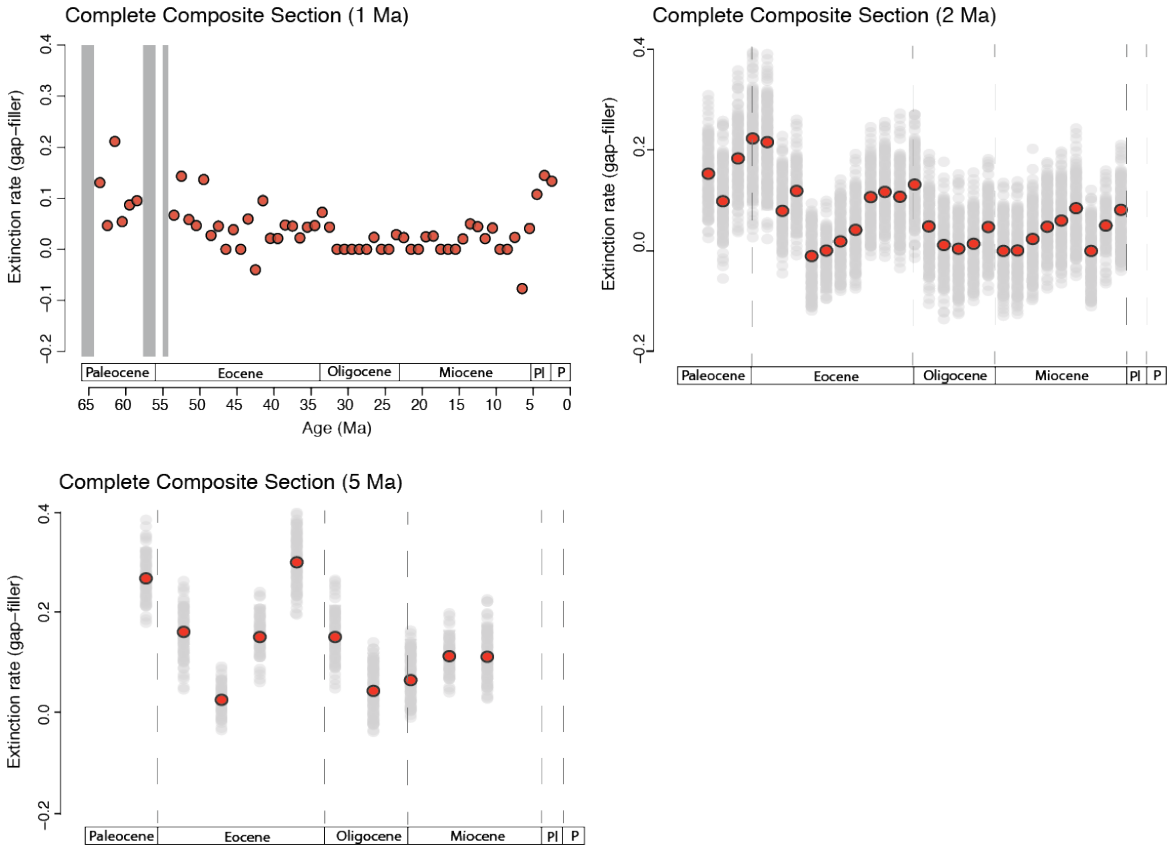

Figure 2.66: Extinction rates calculated using the gap-filler equation (Alroy 2014) for the complete composite section pooled at 1 Ma, 2 Ma and 5 Ma time intervals. The grey circles represent the extinction for each one of the 1000 iterations and the red circles are the median for each time interval.

not imply that these rates are random and therefore does not imply that the diversity curve evolves randomly (Alroy 2008). There are at least three causal relationships that might regulate turnover and diversity without producing autocorrelation (Alroy 2008): (1) origination rates may correlate negatively with preceding diversity levels, in the case where speciation rates and/or immigration rates become lower as richness increases; (2) diversity and subsequent extinction rates may correlate positively, in the case where extinction rates increases as richness increases; and (3) origination and extinction may be positively correlated. To test the existence of these relationships, the regional diversity curve was compared with each one of the 1000 time series of estimated origination and extinction rates using a Spearman-rank rank-correlation test. The results show that neither origination nor extinction show a strong correlation with regional richness in the immediately preced-

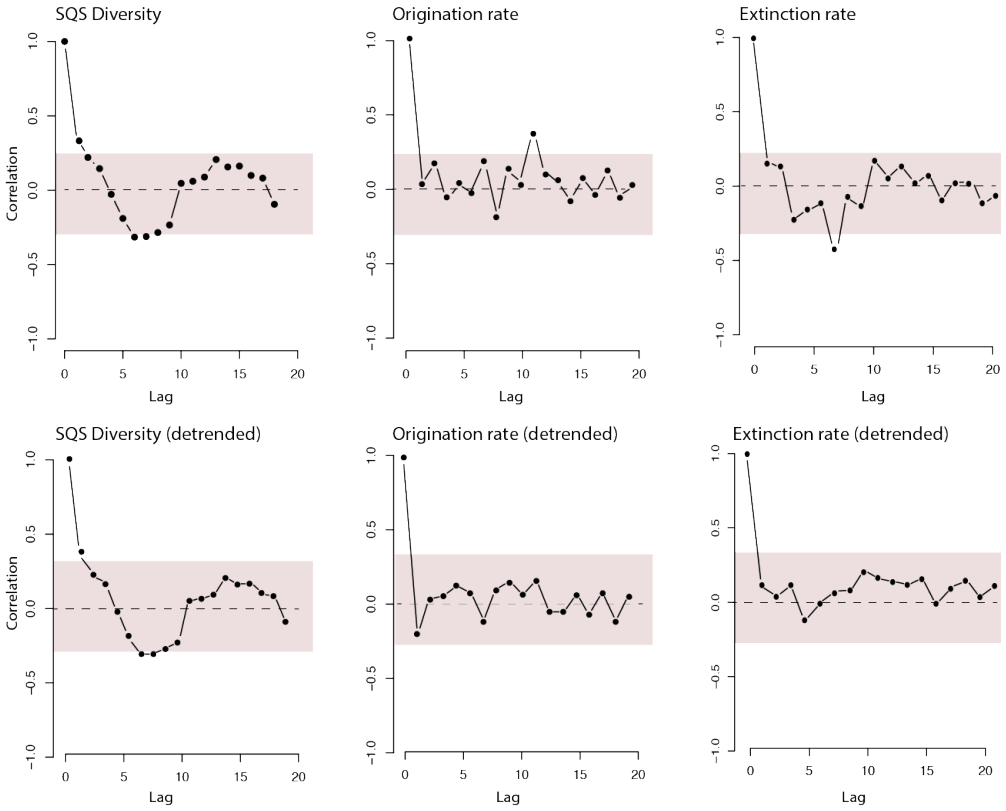

Figure 2.67: Correlograms for SQS diversity, origination and extinction rates. The lower panel show correlograms for the detrended series.

ing, current or succeeding bins (i.e. at time lags of -1, 0 or +1). For the origination rates, from a total of 1000 estimated curves, only 105 (time lag -1), 25 (time lag 0) and 24 (time lag +1) simulations produced significant correlations ($p < 0.05$) and the median rho value of these correlations was 0.13, -0.03 and -0.027 respectively. Figure 2.68 shows the correlations between the regional diversity curve and the median of the origination rates at different lags. In this comparison the correlations were not significant either (time lag-1: p=0.84, rho=-0.02; time lag 0: p=0.19, rho=0.17; time lag+1: p=0.64, rho=-0.025). When the time series of extinction rates were compared with the regional diversity curve, the total number of replicates producing significant correlations was 25 (time lag -1), 106 (time lag 0) and 7 (time lag +1). The median rho value of these correlations was 0.05, 0.12 and 0.046 respectively. Figure 2.69 shows the correlations between the regional diversity curve and the median of the extinction rates at different lags. In this comparison the correlations were not significant either (time lag-1: p=0.3, rho=0.13;

time lag 0: p=0.06, rho=0.24; time lag+1:p=0.23,rho=0.15). When SQS diversity is log transformed and is compared with the origination and extinction rates, the number of significant correlations is similar to the results presented above.

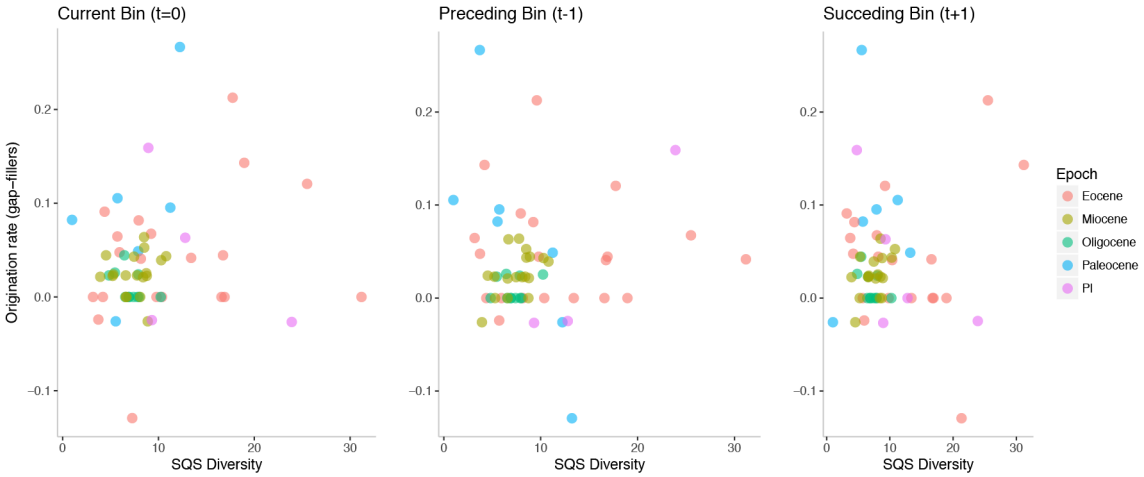

Figure 2.68: Correlation between the SQS diversity (regional diversity curve) and the mean origination rates for the current, preceding and succeeding bins.

To explore the relationship between extinction and origination, the estimates of origination and extinction rates from each one of the 1000 iterations were compared using a Spearman-rank correlation test. For the time lag= 0, only 80 iterations were significant ($p < 0.05$). The median rho value of all the iterations was 0.44. When origination is compared with the extinction during the previous interval (preceding bin (t-1)), 975 of the 1000 simulations (97%) showed a significant correlation ($p < 0.05$). The Spearman correlation coefficient is always positive and exhibits values between 0.17 and 0.795 with a median value of 0.48. Figure 2.70 shows three of the correlations exemplifying the range of coefficients (rho = 0.18, 0.45 and 0.78 from the left to the right panel in Figure 2.70). On the other hand, when the extinction is compared with the origination during the previous interval (preceding bin (t-1)), 486 of the 1000 iterations (48%) showed a significant correlation ($p < 0.005$). The Spearman correlation coefficient can be positive or negative with a median value of 0.26. Figure 2.71 shows three of the correlations exemplifying the range of coefficients (rho=-0.10, 0.31, 0.65 from the left to the right panel in Figure 2.71).

Another way to explore the dynamics of origination and extinction is by estimating the diversification and turnover rates. Diversification is the difference between origination and extinction and turnover is estimated here as the

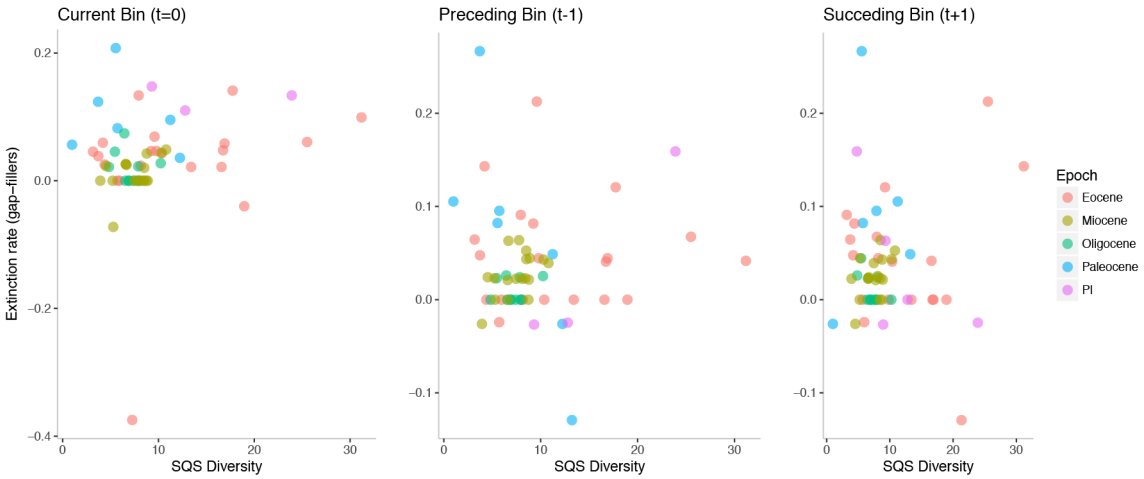

Figure 2.69: Correlation between the SQS diversity (regional diversity curve) and the mean extinction rates for the current, preceding and succeeding bins.

sum of origination and extinction. These two rates were calculated using the origination and extinction estimated using the gap-filler equation from the complete composite section. All the simulations were used in the calculation (grey circles Figure 2.72) and their medians were also estimated (orange and violet circles for the diversification and turnover rates respectively (Figure 2.72).

The diversification rate during the Paleocene is represented by six data points, which are highly dispersed, and are interrupted by intervals containing no information. The gaps are explained by the elimination of several intervals during the estimation of the origination and extinction rates due to the fact that some of them did not reach the number of occurrences used in the iterations. During the early Eocene to the end of the middle Eocene the diversification rates exhibit a decreasing trend imposed over a fluctuating pattern (between -0.1 and 0.1) (upper panel, Figure 2.72). The amplitude of the fluctuation is in generally wide with one peak standing out at approx. 43.5 Ma. Indeed, this interval presents one of the three highest diversification rates of the entire Cenozoic (the two highest are concentrated in the Palaeocene). From the late Eocene and during all the Oligocene, the diversification rates are very stable and concentrated over values close to zero (upper panel, Figure 2.72). During the entire Miocene a fluctuating pattern is observed again with a peak standing out at 7.5 Ma. The fluctuating pattern during the Miocene is no longer accompanied by any apparent trend and is concentrated over a narrower set of values (between zero and 0.5) in comparison with the Eocene. The last four intervals, corresponding to the

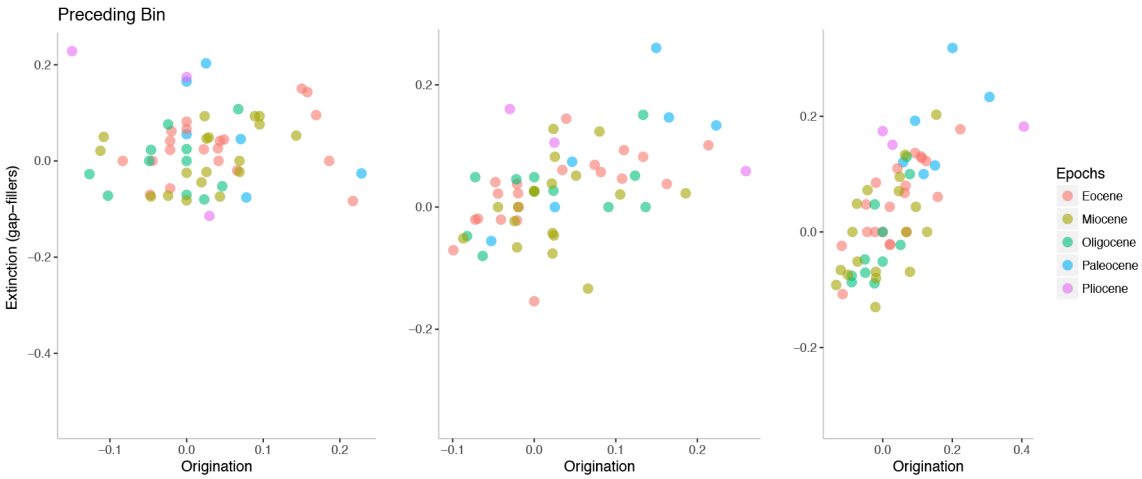

Figure 2.70: Correlation between origination rate in the current interval and extinction rate in the previous interval (preceding bin) differentiated by geological epochs (colors) Each panel represents the lowest, medium and highest correlation coefficients (rho) obtained from 1000 simulations. All the simulations produced positive correlations.

Pliocene, are characterized by low and negative diversification rates (upper panel, Figure 2.72).

The turnover rates during the Palaeocene are restricted to five data points (lower panel, Figure 2.72) that are concentrated over a narrow set of high values. During the early Eocene, the turnover rates show a clear decreasing trend that seems to be the continuation of a pattern started in the Palaeocene. From the middle Eocene to the Eocene-Oligocene boundary the turnover rates show a fluctuating pattern, between zero and 0.1, without any apparent trend. The first four data points of the Oligocene show a decline in the turnover rates. During the Oligocene to the end of the middle late Miocene (10.5 Ma) a fluctuating pattern is observed again, but concentrated in a narrower set of los values (between zero and less than one) in comparison with the fluctuation observed during the Eocene (lower panel, Figure 2.72). From the late Miocene to the Pliocene the turnover rates are highly fluctuating, exceeding the amplitudes observed during the Oligocene-Miocene and even the Eocene.

To summarize, the previous analysis suggest that there is no autocorrelation or apparent trend in the taxonomic rates or in the regional diversity curve (Figure 2.67). The comparisons between the diversity curve and the origination and extinction rates did not show significant correlation, which suggests that diversity is apparently controlled by other factors than taxo-

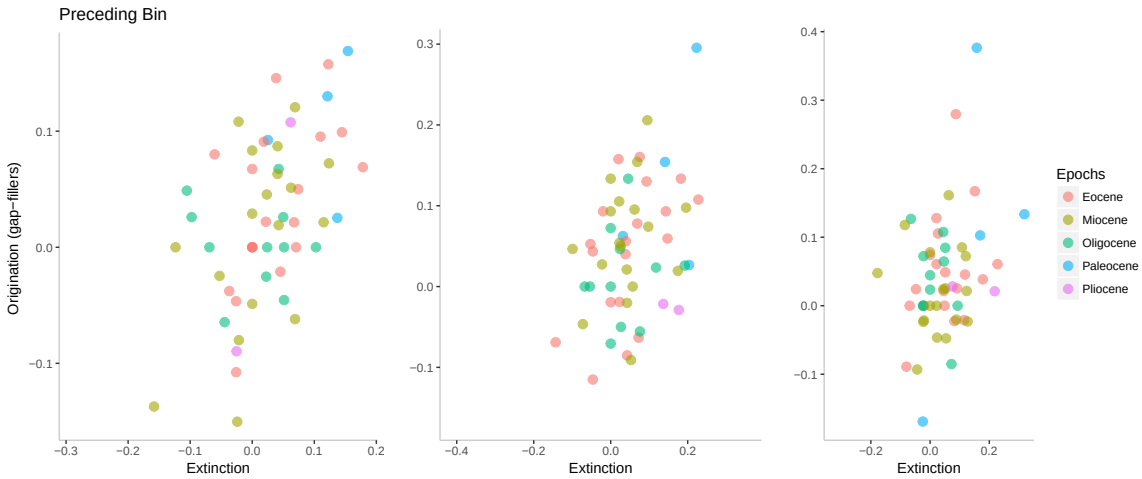

Figure 2.71: Correlations between extinction rate in the current interval and origination rate in the previous interval (preceding bin) differentiated by geological epochs (colors). Each panel represents the lowest, medium and highest correlation coefficients obtained from the 1000 simulations. Note that in the first panel the correlation is negative while in the other two panels the correlation is positive.

nomic rates (Figures 2.68 and 2.69). When origination and extinction rates were compared, only the current extinction and the origination in the following interval showed a significant correlation (Figure 2.70). This result suggests that origination is controlled by extinction but extinction does not seem to be controlled by origination. Finally, three general patterns describe the Cenozoic in terms of diversification and taxonomic rates. (1) A decreasing trend imposed over a wide amplitude fluctuating pattern during the Paleocene to late Eocene interval, (2) A low amplitude fluctuating pattern without apparent trend during the Oligocene, (3) An intermediate amplitude fluctuating pattern without apparent trend during most of the Miocene and, (4) A high amplitude fluctuating pattern during the Pliocene (Figure 2.72).

2.4.7 Climate and Macroevolution of Neotropical plants

To study the relationship with climate, the regional diversity curve and the taxonomic and diversification rates estimated in this work were compared with the composite isotopic curve of Zachos et al. (2001, 2008). The oxygen isotope raw data (from now on called climate curve) is presented together with the SQS regional diversity curve in Figure 2.73. To facilitate comparisons with the macroevolutionary estimates, the isotopic data was divided in

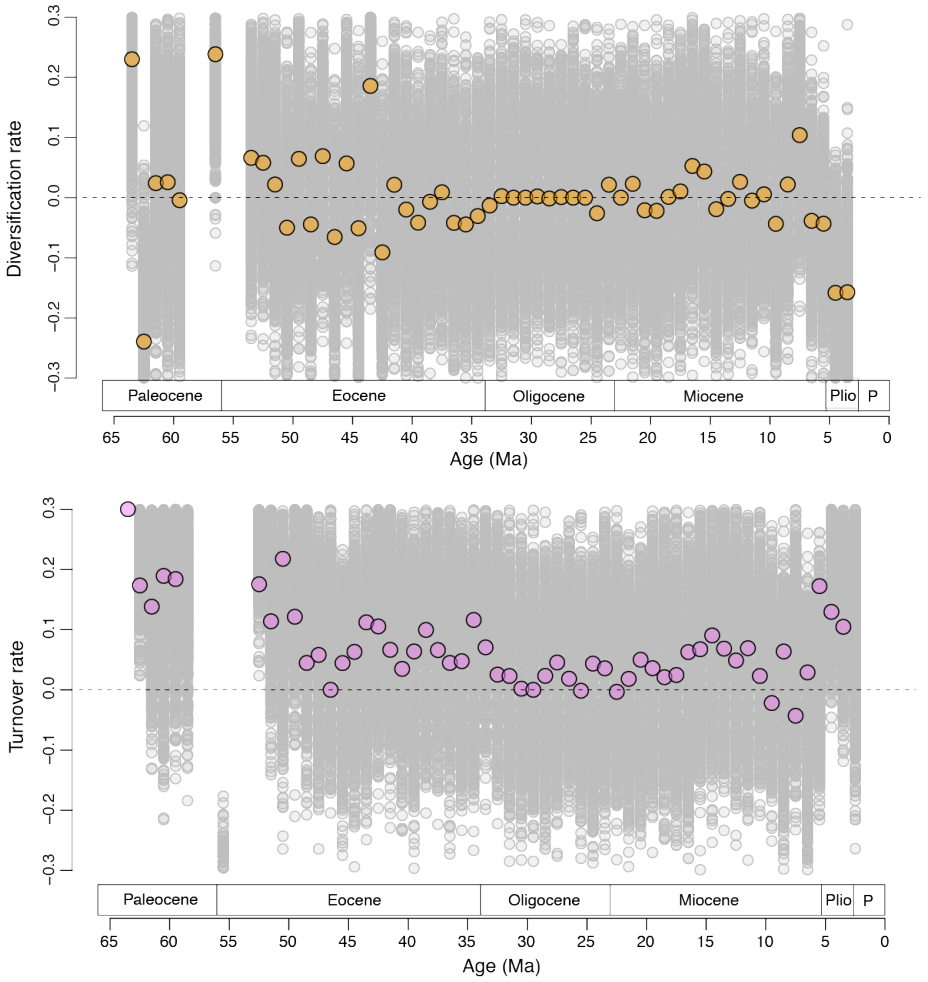

Figure 2.72: Diversification and turnover rates; grey circles corresponds to simulations and orange and violet circles to the median of the diversification and turnover rates respectively.

1 Ma intervals and the mean and standard deviation of the $\delta O18$ values were calculated for each interval (Annex 2.18, left panel Figure 2.74). Three methods were used to tests these correlations: First Differencing (FD) followed by correlation tests, Generalized Least squares Regression (GLS) incorporating an autoregressive model and critical intervals.

First differencing (FD)

The mean $\delta O18$ data (left panel, Figure 2.74) is strongly correlated with time ($r = 0.91$; $p < 0.0001$) and also highly auto correlated (i.e., the correlation

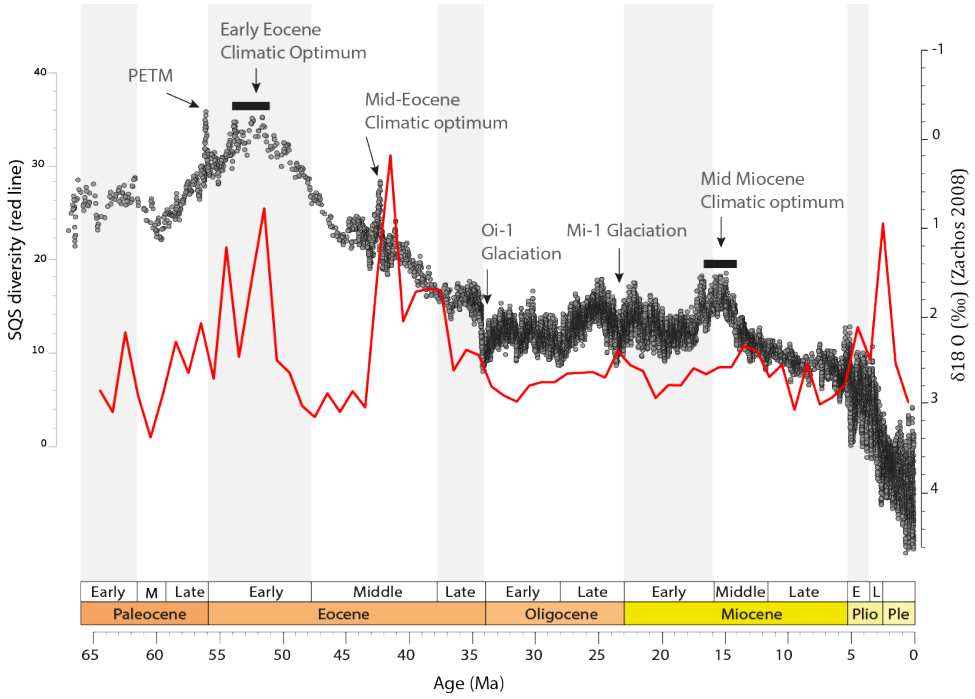

Figure 2.73: Changes in palynological diversity during the Cenozoic. Red line: pollen and spore SQS diversity using a quorum level of 0.6. Black dots: Cenozoic oxygen isotope record for benthic foraminifera showing the most important global climate change events during the Cenozoic (Zachos et al., 2008).

between the current values and the value lagged backwards by one interval is r=0.98; p < 0.0001). On the other hand, the SQS diversity curve is not correlated with time (r=0.07, p=0.5) and also does not show significant autocorrelation (Figure 2.67). The first difference was calculated for both the mean $\delta O18$ values (right panel, Figure 2.74) and the SQS diversity. The resulting data sets exhibit neither significant correlation with time (climatic data: rho=0.21, p=0.09; SQS diversity: rho=0.012, p=0.92) nor a significant autocorrelation. The relationship between diversity and climate was estimated comparing the mean values as well as the first differences.

When the climatic and SQS diversity curves are compared, either using the mean values or the first differences, there is no significant correlation. The results are also not significant when diversity is lagged at one, two or three intervals. The lack of correlation is consistent in both the Pearson and Spearman tests (Annex 2.19). Nevertheless, an inspection of the climatic and regional diversity curves suggests a differential response of the vegeta-

tion to the climatic changes occurring during the Paleocene-Eocene and the Oligocene-present. During the Paleocene to Eocene interval the changes in diversity are abrupt and large. In contrast, during the Oligocene to the present, the changes in diversity are very subtle and appear to follow the shape of the climatic curve. This difference is well evidenced in the early to middle Eocene interval, where the cooling trend is accompanied by an abrupt and almost instantaneous fall of the diversity (Figure 2.73). The differential response of vegetation in the two intervals could be affecting the correlation estimates. For this reason the time series was splitted in two and both intervals were separately tested for correlation between SQS diversity and climate. The SQS diversity estimates between 40.5 and 50.5 Ma were discarded from the analysis because although they correspond with the decline in temperature, the low values suggest that a different mechanism was acting during this interval. The first time series correspond to the interval between 5 and 40 Ma and the second correspond to the interval between 51.5 and 64.5 Ma. Both the mean value and the first differences were used in the comparison. Pearson and Spearman correlation tests were used to establish the significance and degree of correlation (Annex 2.20).

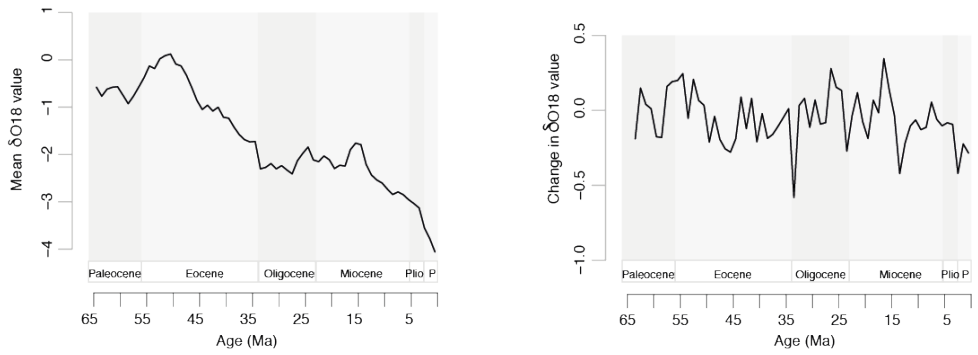

Figure 2.74: Cenozoic oxygen isotope records for benthic foraminifera (Zachos et al., 2008). Mean $\delta O18$ value: estimated mean value in each 1 Ma interval. These data show a strong trend and strong autocorrelation. The y axis is reversed because positive values are correlated with low temperatures. Change in $\delta O18$ values: differences between consecutive bins in mean $\delta O18$ value.

For the interval between 4.5 Ma and 44.5 Ma there is a good correlation between the mean values of the climate and the regional diversity curves. The correlation is still significant ($p < 0.05$) when the diversity is lagged backward one and two intervals. These results are consistent either using Pearson or Spearman correlation tests (upper panel,Annex 2.20). When the

changes in the mean values are used for the comparison, there is no significant correlation (upper panel, Annex 2.20).

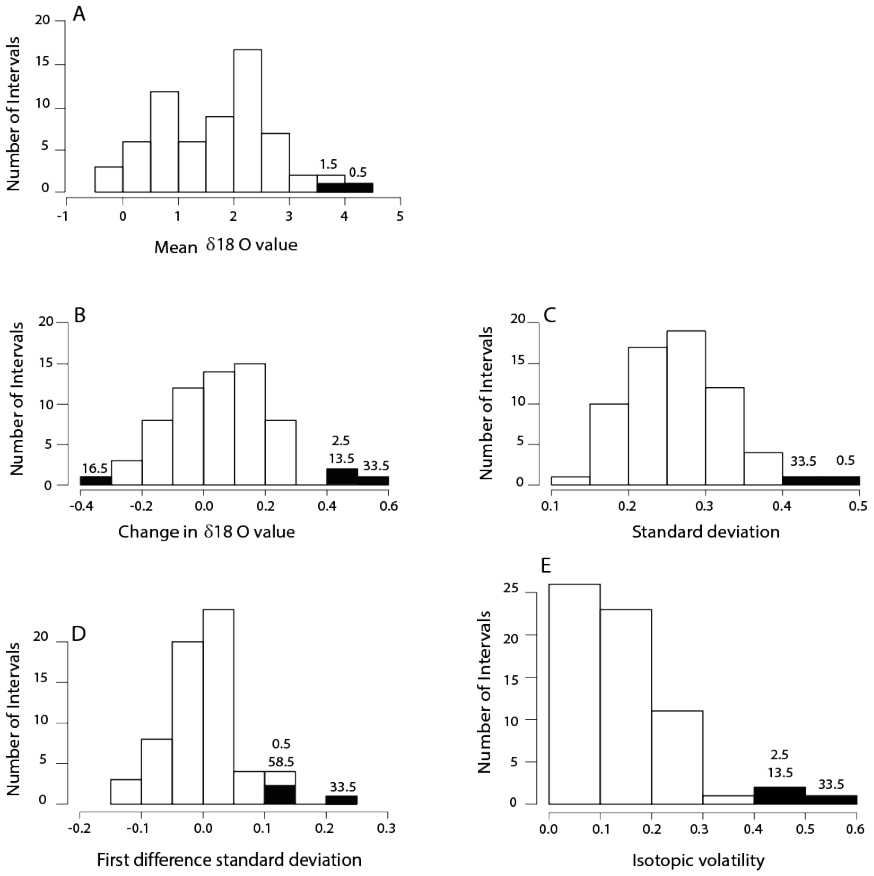

Figure 2.75: Frequency distributions of statistics describing the isotope record. Black boxes and numbers indicate the seven critical intervals of isotopic change discussed in the text. A: estimated mean $\delta O18$ value; B: change in mean $\delta O18$ value from preceding bin to current bin; C: standard deviation of $\delta O18$ values; D: first differences of standard deviations; E: isotopic volatility (absolute value of change).

On the other hand, the interval between 51.5 and 64.5 Ma includes only 14 data points. During this interval the regional diversity curve exhibits an increasing trend imposed over a wide amplitude fluctuating pattern. The climatic curve also exhibit an increasing trend but without any apparent fluctuations (Figure 2.73). When the two curves are compared, the results suggest a significant correlation between the mean values of the current interval. The relationship is only significant using the Pearson's correlation

test. There is no correlation when the changes between the intervals are compared (lower panel,Annex 2.20). It is interesting to note the close correspondence between some isolated but outstanding peaks. The Paleocene-Eocene thermal maximum (PETM) and the early Eocene climatic optimum are two global warming events that are very identifiable in the climatic curve and they match very well with two peaks of high diversity. The same correspondence is observed during the warming event known as the mid-Eocene climatic optimum (Figure 2.73).

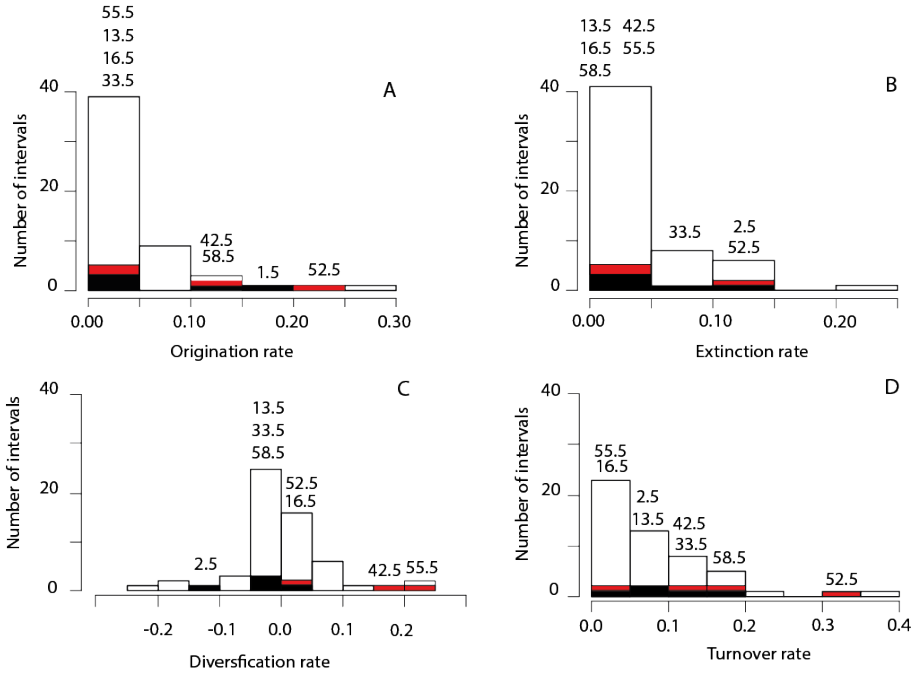

Figure 2.76: Frequency distributions of turnover rates over the Cenozoic. All the rates apply to a single 1 Ma long sampling interval with boxes and numbers indicating intervals of global climate change (black boxes indicating intervals detected using the critical intervals approach, and the red boxes indicating intervals extracted from the literature), A: Origination rate; B: Extinction rate; C: Diversification rate; D: Turnover rate.

Generalized least squares (GLS)

GLS was used to examine the relationship between climate and diversity and between climate and diversification and taxonomic rates. The same two intervals used in the First Differencing (FD) approach were used for the GLS (4.5 to 40.5 Ma and 51.5 to 64.5 Ma). In the interval between 40 and 5

Ma, the mean values of the regional diversity curve are well explained by a regression model including the mean values of the climatic curve. The relationship is significant either using autoregressive models of order one or two. The AIC are very similar in the two models (157.61 and 157.68). This result is consistent with the result from the first difference approach reported above. When the mean turnover and diversification rates from this interval are compared with the mean value of the climatic curve there is no significant relationship. However, the turnover rate is well explained by a regression model including the first difference of the climatic curve. This model is significant either using autoregressive models of order one, two or three (Annex 2.21). On the other hand, the diversification rate is not explained by the mean values or the first difference of the climatic curve (Annex 2.21). Finally, for the interval between 51.5 and 64.5 Ma, the mean values of the regional diversity curve are well explained by a regression model including the mean values of the climatic curve. The relationship is significant either using autoregressive models of order one, two or three (Annex 2.22). This result is consistent with the result from the first difference approach reported above. A model including the mean values of the climatic curve does not explain the mean diversification and taxonomic rates. When the first differences of the climatic curve are used, the diversification rate show a good correlation for the autoregressive models or order two and three (Annex 2.22).

Critical Intervals

To estimate the relationship between taxonomic rates and climate change, the intervals of rapid changes in the climate record were subjectively identified and then the response of vegetation during these intervals was examined. This could be very useful to identify data points characterized by anomalous high values like the interval between the Paleocene and Eocene were the taxonomic rates exhibit abrupt changes rather than any specific trend (Figure 2.72). To identify the intervals of rapid climatic change, four histograms summarizing the climatic curve were constructed (change in $\delta O18$ value, standard deviation of the $\delta O18$ values, first difference of the standard deviation and isotopic volatility (absolute value of the change in $\delta O18$ value)) (Figure 2.75). Those intervals with climatic parameter values more than two standard deviations from average Cenozoic values were considered intervals of rapid climate change. The limits are -0.39 to 3.69 for the mean $\delta O18$ values, -0.29 to +0.40 for change in mean $\delta O18$ values, zero to +0.36 for isotopic volatility, +0.13 to +0.39 for standard deviation of the $\delta O18$ values, and -0.123 to +0.126 for the first difference of the standard deviation (Figure

2.75). By this standard, the identified significant climatic events are: 58.5 Ma (high detrended standard deviation), 33.5 Ma (high change in $\delta O18$, standard deviation, detrended standard deviation and isotopic volatility), 16.5 Ma (low change in $\delta O18$), 13.5 Ma (high change in $\delta O18$ and isotopic volatility), 2.5 Ma (high change in $\delta O18$ and isotopic volatility), 1.5 Ma (high mean $\delta O18$), and 0.5 Ma (high mean $\delta O18$ and standard deviation). Of the seven intervals identified here, only two (0.5 Ma and 33.5 Ma) coincide with those identified by Alroy et al. (2000). The difference in the two versions of the isotopic data set used in the studies could explain this discrepancy. Widely recognized global climatic events, like the Paleocene-Eocene thermal maximum (55.5 Ma), the early Eocene climatic optimum (52.5 Ma) and the mid Eocene climatic optimum (42.5 Ma) (Zachos et al., 2000, 2008) that were not recognized in the above analysis were also included in the comparisons.

When the climatic episodes are compared with the taxonomic rates, only five intervals show correspondence between climatic and biotic change (Figure 2.76). These intervals are: 1.5 Ma for the origination rate, 2.5 Ma for the diversification and extinction rates, 42.5 Ma for the diversification rate, 52.5 Ma for the origination, extinction and turnover rates, and 55.5 Ma for the diversification rate. Other intervals with taxonomic rate values more than two standard deviation from typical Cenozoic values are: 62.5 Ma (origination, diversification and taxonomic rates), 61.5 Ma (extinction and diversification rates), 49.5 Ma (extinction rate) and 3.5 Ma (extinction and diversification rates). However none of these intervals show correspondence with climatic episodes.

Three of five intervals showing correspondence between climatic and biotic change are concentrated in the Paleogene and correspond to well- recognized episodes of global warming (The Palaeocene-Eocene thermal maximum (56 Ma), the early Eocene climatic optimum (52 Ma) and the mid Eocene Climatic optimum (42.5 Ma). These intervals are characterized not only by changes in taxonomic rates but also by short duration peaks of diversity that stands out from the regional diversity curve. In fact, the intervals with the highest diversities of the Cenozoic are the mid Eocene Climatic optimum followed by the early Eocene climatic optimum and the Palaeocene-Eocene thermal maximum (Figure 2.73). The other two intervals of correspondence between climatic and biotic change are 1.5 Ma and 2.5 Ma (Figure 2.76).

2.5 Discussion

Several mechanisms have been proposed to explain the high diversity of plants observed today in the Neotropics and how this diversity was pro-

duced. In contrast, very few studies have provided an understanding about the macroevolutionary history of Neotropical vegetation through deep time. In fact, patterns of plant diversification during the Cenozoic have received much less attention than have the mechanisms proposed to explain them.

One of the principal obstacles to studying macroevolution in the Neotropics has been the difficulty to find fossils, and in general complete sedimentary sequences to extract and study their paleontological record. Also, the elevated rates of weathering that characterize the tropics hinder the preservation of macrofossil. In this context, palynology, and specifically the study of pollen and spores, has become a very useful proxy to study the dynamics of vegetation in the geological past. Pollen and spores are highly resistant to weathering and they also give a good representation of regional and local vegetation. The use of sediment-cores or rock material extracted from drilling activities is a good solution to the scarcity of outcrops in the Neotropics. In regions like the Amazon basin and the foothills of the Andes Cordillera that are covered by dense vegetation, are very difficult to find outcrops, and where they are present are difficult to access. Despite this, palynological analysis of isolated outcrops in the Amazon basin (Hoorn 1993, 1994, 1994b, 2006; Dino et al., 2012; Nogueira et al., 2013; Salamanca et al., 2016; Antoine et al., 2016), the foothills of the Andes Cordillera (Jaramillo and Dilcher, 2001; Jaramillo 2002; Ochoa et al., 2012; Jaramillo et al., 2007; Pardo et al., 2003) and sediment-cores (Jaramillo et al., 2006; Silva-Camhina et al., 2009; Leite et al., 2016; Jaramillo et al., 2017; D'Apolito) have provided important information about the composition and evolution of Neotropical vegetation. However, these studies have been restricted to specific and short intervals of the Cenozoic, giving us only snapshots of how Neotropical plants have evolved throughout time. To date the complete macroevolutionary history of Neotropical vegetation during the Cenozoic has been very difficult to capture.

In this study I took advantage of an extensive compilation of palynological information from northern South America that comes mainly from samples obtained from exploratory wells drilled in Colombia by Ecopetrol S.A and in a smaller proportion samples from outcrops to study the macroevolutionary history of neotropical vegetation during the Cenozoic. The analysis of the palynological information shows that the diversity of plants is highly correlated with changes in global temperature and that there are differential responses of vegetation to the global changes in temperature occurred during greenhouse and icehouse intervals. The relationship between origination and extinction rates suggests that those intervals with high extinction are followed by intervals with high origination. In this sense, it seems that origination is highly controlled by extinction. The opposite, extinction controlled

by origination, is not supported by the data. Below I discuss in detail the results of the different analysis.

2.5.1 Diversity

One of the main concerns to estimate diversity in this work was the possible effect the borehole caving. Caving can artificially increase the ranges of the species, and this can influence estimates of both diversity and diversification (origination and extinction). This is particularly true for those estimates incorporating the range-through assumption. To understand the possible influence of caving, two versions of the data were used. The complete composite section that includes all species regardless of whether their FADs were interpreted from ditch cutting material, and the restricted-FAD composite section that include only those species for which FADs were interpreted from outcrop or sediment-core material. When diversity is calculated using the boundary crossers approach (Foote 2000) the two curves show differences, especially in the Miocene (Figure 2.12). The Miocene in the complete composite section is shown as a period of continuous and rapid decline in diversity, while in the restricted-FAD composite section this interval is shown as a period of stability only punctuated by a short and subtle period of increasing diversity. Apart from the obvious difficulties of making reliable interpretations from two curves that exhibit different patterns, the differences between the two curves are also remarkable at the beginning and end of the data series, which introduces another source of uncertainty to estimate for example edge effects (Foote 2000). On the other hand, when diversity was estimated using the shareholder quorum subsampling protocol (SQS), the two versions of the composite section exhibit similar patterns (Figure 2.26). The only exception is the late Miocene when the two curves show opposite trends (a declining and increasing trend for the complete composite and restricted-FAD composite sections respectively). In the other intervals, the only appreciable difference between the two curves is their magnitude, which is well explained by the difference in the number of species used in each version of the composite section. Although, the analysis of the distribution of the number of the FADs suggest that caving is not concentrated in any particular time interval (Figure 2.6, 2.7) it also suggest that an elevated proportion of taxa is susceptible of being affected for caving. Trying to prove whether caving affects the ranges of the taxa is not a simple task. However, the results suggest that caving exerts a major influence when diversity is estimated using a range-through assumption.

As explained before, the methods incorporating the range-through assumption are more susceptible to be biased by the effect of caving. When

abundance data is available, it is better to use methods like SQS. This not only decreases the possible effect of caving, because it does not use the range-through assumption, but also standardizes richness estimates by sample coverage. In fact, during the last decade many of the paleobiological studies involving diversity have made use of standardization techniques like SQS (Alroy, 2008, 2010; Benson et al., 2016; Close et al., 2018) and it is becoming less common to use the range-through methods such as boundary crossers, or raw richness.

Several approaches were used to produce the regional diversity curve using SQS. Because of the similarities of the curves produced using the complete and the restricted-FAD composite sections (Figure 2.26), the complete composite section was preferred because it includes information from more species. A quota level of 0.6 for the SQS analysis was chosen because at this the level all the intervals discussed later are included and also strongly resembles the patterns obtained using higher quora (0.7-0.9). The SQS diversity was first calculated for each individual sample from the complete composite section presenting counts higher than 50 palynomorphs. The cloud of points reveals that most intervals provide high numbers of samples with exception of the early-middle Eocene and late Miocene-Pliocene where the number of samples is very low (Figure 2.49). The low number of samples in the late Miocene-Pliocene interval is a consequence of the scarce oil-exploratory interest in this sequence. The low number of samples in the early-middle Eocene is a consequence of a regionally diachronous Eocene unconformity (Reyes-Harker et al., 2015) that make it difficult to find sequences of this age, even in drilling operations (Jaramillo et al., 2009). It is also evident from the cloud of points (Figure 2.49) that most of samples during all the intervals present low SQS diversities. In fact, 80% of the samples exhibit SQS diversities lower than 10 (histogram, Figure 2.31). Also, when the samples are grouped in 5 Ma intervals the percentage of them with SQS diversities lower than 10 is more than 90% in all the intervals. An exception occurs in the Eocene, where this percentage is close to 7% in three intervals (Figure 2.31). In this sense, is possible to say that only a small proportion of samples are responsible of the high diversity observed in the intervals. This is an important and clarifying finding. Jaramillo et al. (2006) did not state whether the high diversity observed in specific intervals, e.g. the Eocene, resulted from homogeneous high diversity occurring in many samples during those intervals, or from a small proportion of samples yielding high diversities, but belonging to just a few sections (as shown here).

Analysis of the middle Eocene to late Eocene (36-43 Ma, Figure 2.49), the interval with the highest SQS diversity of the Cenozoic, reveals that only 31% of the samples (105 out of 336) present SQS diversities higher than 10.

The samples from this interval are distributed among 39 sites from which only 26 of them have a small proportion of samples showing high SQS diversities. The question that arises then is: What is controlling the changes in diversity observed within individual sections? A good candidate could be the change in depositional environments that can either exert a control in the preservation of the palynoflora or reflect changes in the composition of the vegetal communities. According to the analysis presented here, the scales at which these changes occurred are in the order of hundreds of thousands of years. At this short temporal scales try to find and test possible mechanisms, like the change in environments, is a difficult task and even more so when the information comes from drilling operations, where sedimentological and stratigraphic interpretations are scarce. This difficulty is exemplified in the rock-core Saltarin-1 (Jaramillo et al., 2017). The diversity analysis of Saltarin-1 shows a short interval (between 6.7 Ma to 7.3 Ma) in which 17 samples exhibit SQS diversities ranging between zero and 31.8 (Figure 2.41). The samples were taken in an interval of 45.83 m (138.5m to 184.33m, stratigraphic column of Jaramillo et al., 2017) that corresponds to the informal member G5 of the Guayabo Formation (Jaramillo et al., 2017). According to the sedimentological and stratigraphic interpretation of Saltarin-1 (Bayona et al., 2008b), the G5 member records a very strong change in the accommodation space that was caused by an increase in the sediment supply produced by either climatic factors (increase in the precipitation) and the influence of the uplifting of tectonic blocks. Although these changes probably play an important role explaining the variation in diversity, it is very difficult to find sedimentological evidence of these processes, even in a rock-core like Saltarin that has a very detailed sedimentological description and stratigraphic interpretation.

Diversity Curve

Several approaches were used to produce the regional diversity curves from the SQS estimates. In a first approach, the samples were grouped in 1Ma intervals and the median and confidence intervals were estimated (Figure 2.30). In a second approach, all the samples that compose each interval were integrated forming a composite sample by either using the abundances (Figure 2.28) or the occurrences (Figure 2.27) of their constituent species. Diversity was then estimated for each composite sample using SQS. An advantage of the estimates based on the composite samples is that they include more information because all the samples, regardless of their counting levels are used in the analysis. On the other hand, the estimates based on some statistics (e.g. mean, median) of the individual samples have less information

because those samples with counting levels less than 50 palynomorphs were previously removed from the analysis.

The curve estimated as the median of the individual samples fails to clearly identify the intervals of high diversity (Figure 2.30). This is because the distribution of SQS diversity values is highly skewed to the left (the lowest values dominate each interval). This skew is evident even using the median as a measure of central tendency. Although there is a clear difference in the number of samples that constitute each interval, the resampling protocol suggests diversity is not controlled by the number of samples (Figure 2.32). This result is relevant because it demonstrates, for example, that the low diversity during the middle Eocene and the late Miocene do not result from the low number of samples in these intervals. On the other hand, the two curves produced by the analysis of the abundance-pooled and occurrence-pooled samples are very similar. The main difference is the magnitude of the changes, which are better reflected in the occurrence-based curve (notice the differences of scale, Figure 2.77).

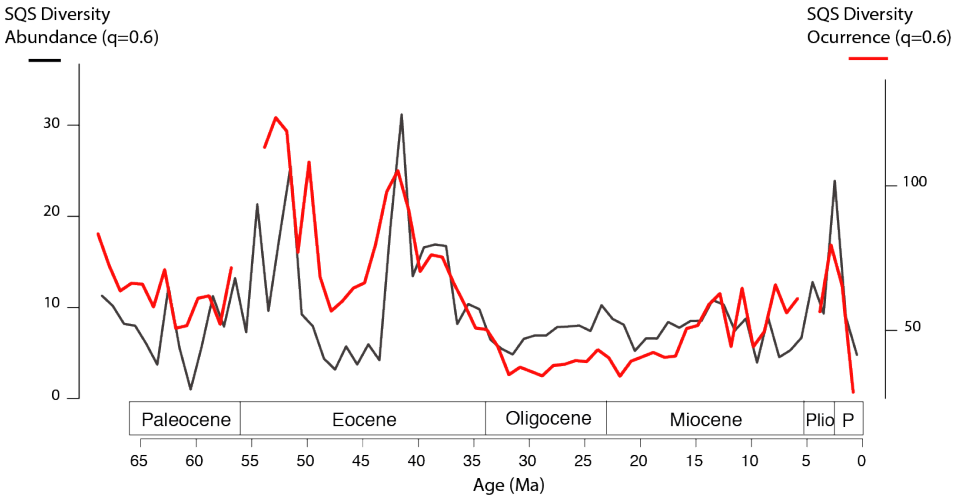

Figure 2.77: SQS diversity curves based in the abundance and occurrence data of the pooled samples (q=0.6).

A spearmans rank test bears out the strong correlation between the two curves (rho=0.48, p=4.1e-05). An important feature of the occurrence-based estimate is that is not biased toward the possible effects imposed by ecological factors like dominance or evenness that in fact can be a source of bias in abundance-based estimates. However, by using the occurrence-based data, it was not possible to estimate diversity in several intervals of the early Eocene and the late Miocene, therefore losing valuable information (Figure 2.77).

Additionally, the occurrence-based curve has the disadvantage that cannot be used to make comparison with the information from the literature in which the estimates are exclusively based of the abundance data recorded in one single section. For these reasons, the abundance-based curve is preferred. The possible effects of dominance and evenness in the abundance-based estimations are mitigated because in the SQS estimates, the single most abundant taxon was removed from each data pool prior subsampling. It is also interesting that when the abundance-based diversity curve is compared with the corrected and uncorrected curves by sampling probability (Rbin) versions of the complete and the restricted-FAD composite sections (Figures 2.17 and 2.18) the only significant correlation is with the uncorrected version (Nbt.samp) of the complete composite section (Figure 2.17) (p=0.03, rho=0.26). This result suggests that caving is not playing a substantial role in the diversity estimates. Also, it indicates that although compensating for the incompleteness of the fossil record is necessary, compensating by sampling probability (Rbin) could be counterproductive. It could overestimate the total standing diversity because not all taxa found in an interval may have co-existed (some may have become extinct before others had originated) (Quental et al., 2010). Rbin also has the undesirable effect of flattening and smoothing the diversity curve. This is evident for example in the Eocene (Figure 2.17) where the uncorrected diversity curve shows a clear decline in diversity during the Palaeocene-Eocene boundary followed by a continuous period of low diversity which is supported by the results of the SQS. On the other hand, the corrected curve and the boundary crossers approach show an increasing trend during this interval.

The SQS abundance-based diversity curve (regional diversity curve) exhibits two distinctive patterns that show correspondence with the global climate curve (Figure 2.73). The first pattern is interpreted to occur through the Paleocene-Eocene interval and the second from the Oligocene to present. Both intervals are discussed below.

Paleocene to Eocene interval

During this interval, the regional diversity curve shows high amplitude fluctuations imposed over two long temporal trends that are separated by a period of sustained low diversity occurred in the youngest half of the middle Eocene (Figure 2.73). During the Paleocene to the early Eocene, the regional diversity curve show an increasing trend that is punctuated by two outstanding peaks in diversity that show a good correspondence with the global warming events of the Palaeocene-Eocene Thermal Maximum (PETM) and the early Climatic Optimum (EECO). The PETM is recognized as a rapid (< 20 Ka)

worldwide warming event that occurred about 56 Ma ago that was possible driven by the destabilization of carbon from surface sedimentary reservoirs such as methane hydrates (Dickens et al., 1995) or by the volcanism associated with the North Atlantic Igneous province (Gutjahr et al., 2017). During the PETM the mean global temperatures increased between 5 and 8C (McInney et al., 2011) causing low to moderate decrease in plant diversity in mid latitudes of North America (Wing et al., 2001).

In northern South America, palynological studies in a section located in Venezuela (Rull 1999) reveal a gradual but significant palynofloral change from late Palaeocene to early Eocene driven by an increase in the origination rates (Rull 1999). Jaramillo (2002) used a composite section from eight localities in Colombia to study the palynological changes through the late Paleocene-middle Eocene transition. By using a variety of methods (rarefaction, standing diversity, diversity indices among others), Jaramillo (2002) concluded that Eocene samples are more diverse on average than Palaeocene samples. Like Rull (1999), Jaramillo (2000) also deduced that because most of the species in the Eocene have been reported consistently only in South America, the increase in diversity in the Eocene was mainly driven by in-situ origination rather than by immigration from other latitudes. Because the works of Rull (1999) and Jaramillo (2000) lack a strong chronostratigraphic framework and in fact they did not precisely identify the PETM, their results can be seen as a rough comparison between the late Palaeocene and early Eocene. Later, Jaramillo et al. (2010) studied the palynological content of three sections from Colombia and Venezuela (including the section analyzed by Rull (1999)). They used one radiometric age, biostratigraphy and carbon isotope biostratigraphy to identify the PETM in the three localities. By using rarefaction and standing diversity they suggested a rapid and distinct increase in plant diversity and origination rates trough the PETM in the three sites. Again, Jaramillo et al. (2010) concluded that the increase in diversity was produced by the addition of many taxa (with some representing new taxa) to the stock of pre-existing Paleocene taxa. The regional diversity curve presented in this work confirms the results of Rull (1999), Jaramillo (2000) and Jaramillo et al. (2010) in the sense that the Paleocene exhibits lower diversity than the early Eocene (Figure 2.73). The low diversity values during the Paleocene are also evident in the information from the literature (Figure 2.35) and specifically in the sections from the Middle Magdalena Valley and Catatumbo Basins (Figures 2.39 and 2.38 respectively). The regional diversity curve also shows that the Paleocene and the early Eocene are characterized by similar high amplitude fluctuating patterns, which suggests that the same mechanism controlling diversity operated in both intervals. The peak in diversity is observed between 54 Ma and 55 Ma (represented

in the regional diversity curve at 54.5 Ma) while the PETM is estimated to have occurred at approximately 56 Ma (McIneney et al., 2010). The offset between the two events could be explained by inaccuracies in the chronology of the composite section or as a time delay on the palynoflora response to the warming event.

The early Eocene Climatic Optimum (EECO) is the culmination of a long period of global warming and represents the highest ocean temperatures of the last 65 Ma (Miller et al., 1987). An increase in plant diversity has been documented in both southern and northern middle to high latitudes (Christopel 1995; Wing et al., 1995). In the Neotropics no palynological work has specifically focused in this interval. The previously discussed works (Rull 1999; Jaramillo 2002 and Jaramillo et al., 2010) concentrated on the Paleocene and early Eocene, and they suggest an increase of diversity during the EECO. The regional diversity curve shows an outstanding peak occurring between 51 and 52 Ma, which is represented in the curve at 51.5 Ma (Figure 2.73). This peak, that in fact is the second with the highest diversity of the entire Cenozoic, corresponds very well with the interval where the EECO is interpreted. It is interesting to note that the number of samples analyzed in both the PETM and EECO is very low and the high SQS diversity values are concentrated on a small proportion of samples from the regions B, C, D and F (Figures 2.48 and 2.49). This is also evidenced in the diversity map for this interval (50-55 Ma) where the areas of high diversity are concentrated toward the north (lower panel, Figure 2.52). Although the climatic curve explains well diversity during this interval (Annex 2.22) it is also possible that changes in the paleogeography have played an important role controlling the diversity. The temporal scale of the paleogeographic maps is too broad to identify changes occurring specifically during the PETM or EECO. However, the palaeographic reconstructions (Figures 2.51 and 2.52) do show a decrease of the area occupied by exposed rocks from the Paleocene to the early Eocene and also a change from coastal plain (shalier facies) and fluvial (sandy facies) environments occurring during the Paleocene to exclusively fluvial (sandy facies) environments during the early to middle Eocene. These changes may have helped to increase diversity via the area-species relationship (Rosenzweig 1995). This relationship proposes that larger regions can support more species, which enhance both regional and local diversity by reducing the risk of extinction and increasing niche opportunities (Fine et al., 2008). The reduction in extinction risk is debatable. Although no specific extinction estimates for the PETM and EECO intervals are available (Figure 2.66), when the extinction estimates (using the gap-filler equation) from the complete Paleocene and early Eocene are compared their differences are not significant ($p=0.5$). The increase in niche opportunities is plausible

because as explained above, there were important paleogeographic changes occurring during this time.

Following the increasing trend observed during the Paleocene to the youngest half of the middle Eocene and the high values reached at the EECO, the regional diversity curve shows an abrupt and almost instantaneous fall. The low values last until the youngest half of the middle Eocene (Figure 2.73). Although the number of samples analyzed is very low, the resampling protocol suggest low diversity during this interval (Figure 2.32). In contrast, when diversity is estimated using boundary crossers and the range through assumption, the curve does not show any decline (Figure 2.12). In fact, the diversity values in the interval follow the increasing trend that continues until the middle Eocene. A similar pattern is observed in Jaramillo's curve (Jaramillo et al., 2006), in which diversity during this interval is the highest of the entire Cenozoic (Figure 2.1). The contrasting pattern between the estimates based on SQS and boundary crossers suggest that the decline in SQS diversity is not the result of an increase in extinction, but rather the result of a short temporal reduction in the presences of several taxa that reappear again toward the youngest half of the middle Eocene. The abrupt fall in regional diversity show a very close correspondence with the decline in the isotopic curve that marks the beginning of the cooling trend of the Cenozoic (Zachos et al., 2001) (panel C, Figure 2.73). The response of plant diversity to this rapid change in global temperature although was abrupt, it seems that did not cause significant extinctions but apparently did cause temporary, regional disappearances. A few samples from the Middle Magdalena Valley and Sinu Basins also indicate low SQS diversity during this interval (Figures 2.39 and 2.37 respectively). Unfortunately, the same paleogeographic reconstruction (early middle Eocene) (Reyes-Harker et al., 2015) represents the interval between 40 and 55 Ma (Figures 2.52 and 2.53). This prevents exploration of the role that paleogeography could have played in determining the low diversity during this interval as well as their relation with the cooling trend. This is a very interesting and important topic that deserves further exploration.

Following the low diversity values of the youngest half of the middle Eocene, the regional diversity curve shows an outstanding peak at 42.5 Ma. Subsequently, the diversity curve exhibits a declining trend that shows a good correspondence with the cooling trend suggested by the isotopic curve (Figure 2.73). The diversity peak at 42.5 Ma represents the highest diversity of the Cenozoic, which is also evident in the diversity curve estimated using boundary crossers (Figure 2.12). The peak match with an episode of transient global warming called the Mid-Eocene Climatic optimum (MECO) that interrupted the long-term middle Eocene cooling trend (Bohaty et al.,

2003). The MECO (approx. 41.4 Ma) has been associated with a globally 4 to 6 degree Celsius warming of both surface and deep oceans that lasted for approximately 600.000 years (Bohaty et al., 2009). The offset between the MECO and the peak in diversity could be explained by inaccuracies in the chronology of the composite section and the event itself. In fact, in several publications reviewed here (Bohaty et al., 2003, 2009; Bijl et al., 2010; Galazzo et al., 2014) the MECO is reported as approximately 40 Ma. However, the isotopic curve in Zachos et al (2008) clearly shows that the anomaly related to the MECO occurred between 42 and 43 Ma (figure 2, Zachos et al., 2008).

Unlike the warming events of the PETM and the EECO, the MECO is represented by a large number of samples (Figure 2.49). It is also the interval with the greatest proportion of samples with diversities higher than 10 (Figure 2.31), which are mainly concentrated in the area F (Figures 2.48 and 2.49). Thus arises the question of why a high diversity is specifically concentrated in this region? Although the choropleth map that encompasses the MECO incorporates information from a 5 Ma interval (40-45 Ma), it also confirms the center of the map (area F, Figure 2.31) as the area with the highest diversity (lower panel Figure 2.53). The paleogeographic reconstruction indicates that continental environments (sandy fluvial facies) dominated during this interval and nothing in particular seems to characterize the central area. This lack of evidence could however be the result of the scale of the paleogeographic reconstruction that prevents interpretations at finer scales. Finally, the regional diversity curve (Figure 2.73) and the estimated of the individual samples (Figure 2.49) indicate that the high diversity values were only maintained for a short time (approx. 1 Ma). This is in concordance with the duration of the MECO estimated in approximately 660.000 years (Bohaty et al., 2009).

Oligocene to Present interval

When diversity is estimated using boundary crossers and the range through assumption, the differences between the complete and the restricted FAD composite section are evident, especially in the Miocene (Figure 2.12). The complete composite section shows the Miocene as a period characterized by a continuous and rapid decline in diversity with important changes in magnitude while the restricted-FAD composite section suggests that the Miocene was an stable period punctuated by at least one short period of subtle increase in diversity. The differences between the two curves highlight the disadvantage of using boundary crossers and the range-through assumption, especially with information from ditch cutting samples.

When diversity is estimated using SQS, following the high values of the MECO, the regional diversity exhibits a declining trend to finally reach low values at the Eocene-Oligocene boundary (Figure 2.73). From the Oligocene to the present, the regional diversity curve show a fluctuating pattern that tracks the pattern of the global climatic curve very well (Figure 2.73). The climatic curve can be separated in two cycless of low frequency and low amplitude. The first covering the Oligocene and the second covering the early to middle Miocene. These two cycles end with the relatively high values observed prior to the M1-1 Glaciation and the Mid Miocene Climatic Optimum respectively (Figure 2.73). Another cycle can be defined from the middle Miocene to the early Pliocene, which is imposed over a declining trend. From the late Pliocene to the present, the climatic curve shows a declining trend.

The regional diversity curve tracks the same climatic cycles with relatively high diversity values ending near the episodes that separate the cycles interpreted for the climatic curve. For instance, high diversities are observed prior to the Mi-1-Glaciation and near to the Mid Miocene Climatic Optimum (Figure 2.73). In fact, the analysis shows a strong correlation between the regional diversity curve and the climatic curve for the interval between 40 Ma and 4.5 Ma (Annexes 2.20 and 2.21). The correlation is significant for the current values and also when diversity is lagged 1 and 2 Ma forward (the 2 Ma lag is only significant in Pearson's correlation test). This could be indicative of a delay on the vegetational response to climate change, especially during cooling events. However, the fact that the correlation is significant both at the current and at lagged intervals also could be indicative a mismatch between the two chronologies. A better chronology for the diversity curve is therefore needed to test these interpretations.

During the Oligocene, the regional diversity curve shows an increasing trend that ends before the Mi-1 Glaciation (Figure 2.73). The samples from other sections exhibit diversities that are below the regional diversity curve (Figure 2.35). The samples from the Middle Magdalena Valley basin (Figure 2.34) do not show the increasing trend that is clearly observed in the regional diversity curve, but they do reflect better the low amplitude fluctuations that are less evident in the regional diversity curve (Figure 2.39). The differences between the regional estimates and the Middle Magdalena Valley Basin could be the result of either the combination of samples from several sections that better reflect regional trends than local fluctuations or paleogeographic differences between the Llanos and Middle Magdalena Basins that were already separated in the earliest Oligocene prior to the onset of the major late Neogene exhumation pulses of the Eastern Cordillera of the Andes (Ochoa et al., 2012; Reyes-Harker et al., 2015) (Figure 2.54). On

the other hand, despite that the Sinu-San Jacinto basin is located toward north of the Llanos basin (Figure 2.34) the samples from these sections show the increase and decline in diversity (Figure 2.37) toward the beginning and end of the Oligocene respectively that are observed in the regional diversity curve and that correspond to important changes in the climate curve (Figure 2.73). This is indicative that the response of vegetation to major changes in temperature is synchronic and not geographically restricted.

Following the high diversity prior to the Mi-1 glaciation, the regional diversity curve shows a gradual decline that last for 3 Ma. Then, an increasing trend ends with the relatively high values observed near to the Mid Miocene Climatic Optimum (MMCO) (Figure 2.73). The peak in diversity shows a mismatch of less than 1Ma with respect to the end of the MMCO. As explained before, this mismatch could reflect discrepancies between the chronologies or a delay of the response of vegetation to the temperature change. Climatically, the MMCO was a transient warming event occurred between 14 and 17 Ma in which temperatures are believed to rise between 3 and 4 degrees Celsius compared to today (Zachos et al., 2008; Goldner et al., 2014). The information from the literature fully supports the results of the diversity curve in the sense that they show a peak in diversity during the MMCO. D'Apolito (2016) using palynological information from a sediment core drilled in the Amazon basin of Brazil (Figure 2.34) suggested an increase in palynological richness starting at 16 Ma and reaching a peak at 13.7 Ma. The changes in diversity are coincident with the beginning and duration of the MMCO and are independent of variables like lithology, flooding events or taphonomic biases (D'Apolito, 2016). The palynological record of Panama (Figure 2.34) (Jaramillo et al., 2014) analyzed here, shows an increase in SQS diversity from early to late Miocene, with a very outstanding peak close to the MMCO (Figure 2.35). Unfortunately a temporal gap covering part of the early Miocene and the complete middle Miocene prevents a detailed understanding of the changes in diversity at this geographic area. Finally, the diversity analysis from the information in Leite et al. (2016) (Figure 2.34) also reveals a peak in diversity close to the MMCO, which is followed by a decline in diversity (Figure 2.46). To conclude, the regional diversity curve and the diversity estimates from the literature show that the increase during the early to middle Miocene and the peak in diversity near the MMCO are not restricted to the Llanos basin but could be considered a regional pattern. Also it reinforces the idea that the link between change in temperature and plant diversity is not restricted to the interval between the Palaeocene and the Oligocene but it also exists for the Miocene.

From the high diversity values of the MMCO the regional diversity curve show a declining trend to finally reach an outstanding peak at the Miocene-

Pliocene boundary. The climatic curve reveals a similar pattern represented by a declining trend that ends with high values at the Miocene-Pliocene boundary (Figure 2.73). The number of samples analyzed during this interval is one of the lowest of the entire Cenozoic (Figure 2.49) with most of the samples belonging to sections located in the geographic area A and few to the areas F and G (Figure 2.58). The low number of samples however does not explain the low diversity observed during this interval. When diversity is estimated by resampling, the diversity is still very low (Figure 2.32). The diversity pattern observed during this interval is well supported by the information from literature analyzed here (Jaramillo et al., 2014, Figure 2.35; Leite et al., 2016, Figure 2.45; Jaramillo et al., 2017, Figures 2.41 and 2.46; Silva-Caminha et al., 2009, Figure 2.44; Antoine et al., 2016, Figure 2.47). The SQS diversity of the samples from the cores Saltarin-1 and 1AS-33M (Jaramillo et al., 2017; Leite et al., 2016) are compared with the regional estimates in Figure 2.58. The interval between 8 and 12 Ma is characterized by a low number of samples in both cores, however the estimates are always below the regional diversity curve. It is important to mention that several additional samples from Saltarin-1 were analyzed in three intervals (Figure 2.40) (Jaramillo et al., 2017, supplemental material). The low recovery of palynomorphs did not allow estimation of diversity in the samples from those intervals. This could be considered as evidence supporting the low diversity observed in the regional diversity curve but also is consistent with either low abundance, or adverse taphonomy. Further detailed sedimentological analysis in several sections is necessary to establish the causes of the low recovery in this interval.

The interval between 6.7 and 7.3 Ma is represented by 17 samples from Saltarin-1 (Figure 2.58). As explained before, these samples exhibit SQS diversities ranging from zero to 31.8. By far, the samples from Saltarin-1 present the greatest variability of all the sections, not only for the Miocene but the complete Cenozoic (Figures 2.49 and 2.58). Despite the detailed sedimentological description of Saltarin -1 (Bayona et al., 2008b; Jaramillo et al., 2017) is difficult to find sedimentological evidences of a mechanism that could explain the changes in diversity. Of the total pool of 287species available in these 17 samples, more than half (52%) correspond to informal species (Jaramillo et al., 2017, supplemental material), which suggest that either this specific area was a center of endemism and therefore populated by species that were not reported in older and/or younger intervals or that these informal species represent morphological variation of formal species and therefore there is a taxonomic bias in the estimates. In any case, the high diversity values represented by the samples of Saltarin-1 are interpreted as reflect the initial phase of the increasing trend observed in the regional

diversity curve that culminates with the peak in diversity observed in the early Pliocene (Figure 2.73). The peak in diversity at the early Pliocene seems to partially coincide with a relative high of the isotope curve that represent the last increase in temperature before the abrupt declining trend observed until the end of the time series (Figure 2.73). A final outstanding peak of elevated diversity is observed near the Pliocene-Pleistocene boundary, which is followed by an abrupt decline that seems to correspond with the declining trend of the climatic curve (Figure 2.73). The estimates for the youngest part of the record, and specially the interval between 2 and 4 Ma, need to be interpreted with caution because all the samples correspond to only one or two sections (Figures 2.58 and 2.59) and therefore reflect a local rather than a regional signal. In fact, these two samples inflate diversity to levels not reached when the curve is estimated using the mean of the samples (Figure 2.30). However, in general both curves show that diversity is higher in the Pliocene and Pleistocene than in the late Miocene, which is further corroborated by information from literature (Jaramillo et al., 2014 (Figure 2.35); Leite et al. (2016) (Figure 2.45); and Silva-Caminha et al., 2009 (Figure 2.44).

The interval between 12.4 and 4.4 Ma is very important because is related to the most active pulses of orogenic activity in the Andes Cordillera (Hoorn et al., 201b). It is clear that the Andes uplift changed the neotropics landscapes by reconfiguring drainage patterns and creating vast influx of sediments that produced a wide mosaic of edaphic conditions in the region (Hoorn et al., 2010b). The edaphic changes and new niches promoted diversification in Amazonia. The pattern of the diversity curve during the most active pulse of orogenic activity in the Andes is in turn characterized by a continuous declining trend in global temperature that started at the end of the MMECO and ended at the early Pliocene (Figure 2.73). This interval exhibits a low diversity and taxonomic rates showing a declining trend. Because both the Andes uplift and climate change occurred contemporaneously, it is difficult to distangle the role played for each one in producing low diversity and declining taxonomic rates. However, it is reasonable to think that in addition to the cooling conditions, during the reconfiguration of the landscape the vegetation did not adjust immediately and only when the intense orogenic activity ceased and the new niches were completely established the vegetation strengthened and diversity increased reaching the values observed at the end of the Pliocene (Figure 3.26). It is also not possible to rule out a preservation bias produced by the reconfiguration of the drainage patterns. The influx of sediments from the Andes Cordillera produced alluvial deposits and scarce fine grained deposits, which are those that preserve palynomorphs. The low number of samples analyzed during this interval gives support to

this interpretation.

The choropleth maps for the Miocene (Figures 2.59-2.61) reveal that during the early Miocene to the middle Miocene (22-12 Ma) diversity is relatively homogenous spatially with specific sites concentrating high diversity values. It is also evident that those sites vary from interval to interval. An example of this variation is the site #63 (Figure 2.59) which reveal low diversity values for the intervals 14-16 Ma and 10-12 Ma (Figure 2.60), intermediate values for the intervals 16-18 Ma, 12-14 Ma and 8-10 Ma (Figures 2.60 and 2.61) and high values for the interval 18-20 Ma (Figure 2.61). Similar to Saltarin-1, the causes of the variation are difficult to establish but are probably related to changes in the environments of deposition. The paleogeographic reconstruction used to construct the 10 choropleth diversity maps for the Miocene corresponds to the early Miocene (Reyes et al., 2015). According with this reconstruction, three depositional systems were active: coastal plain, continental (fluvial) and lacustrine- marine environments (Figure 2.59). However, it is unrealistic to think that this reconstruction could represent accurately the paleogeographic configuration of the entire Miocene, Pliocene and Pleistocene, epochs that are well known by the occurrence of important regional changes like the onset of the Amazon River (Hoorn et al., 2010), the main orogenic pulses of the Andes Cordillera (Mora et al., 2010) and separated regional flooding events (Jaramillo et al., 2017; Hoorn et al., 2010). To understand the role played by environments of deposition in the geographic distribution of diversity is therefore necessary to have paleogeographic reconstructions of higher temporal resolution (1-2 Ma) than those presented here.

2.5.2 Taxonomic Rates

When the origination and extinction rates are estimated using boundary crossers and the range-through assumption (Foote 2000) the differences between the complete composite section and the restricted-FAD composite section are considerably greater for the extinction rates. The differences are more evident in the Paleocene, the late Eocene and the Miocene for the extinction, while for the origination the differences are concentrated exclusively in the Paleocene and the early Eocene (panel C, Figure 2.21). The extinction rates show big differences due to the fact that borehole artificially make younger the LADs of the species. On the other hand, when origination and extinction rates are estimated using gap-fillers (Alroy 2014) the differences between the complete and the restricted-FAD composite sections are minor (Figure 2.63). These differences are mainly concentrated in the Palaeocene and early Eocene in both the origination and extinction rates. These results

suggest that if borehole caving is affecting the ranges of the species, then its effect are more pronounced in those estimates using boundary crossers and the range-through assumption, and especially in the extinction rates. Figure 2.78 compares the origination and extinction rates using the gap filler equation and a five points moving average from the boundary crossers of the complete and restricted-FAD composite sections (Figure 2.21). For the origination rate, both estimates show a similar pattern, however in the early-middle Eocene the boundary crossers show low origination rates while the gap-filler indicate higher rates. From the late Miocene to present, the boundary crossers suggest low origination values while the gap-fillers indicate high origination values, especially at the end of the Pleistocene (Figure 2.78). For extinction rates, the differences are more pronounced. In particular during the Eocene, gap-fillers suggest high variability with extinction rates higher than zero while the boundary crossers show little or null variability and values close to zero (Figure 2.78). The survivorship analysis supports the results of the boundary crossers and shows the Eocene as a period characterized by low extinction rates and almost null variability (Figure 2.22). This result is consistent for the Maastrichtian, Palaeocene and Eocene cohorts (Figure 2.23). The similarities between the boundary crossers and the cohort survivorship estimates are due to the fact that both methods use the range-through assumption. In the specific case of the Eocene, the discrepancies between the results obtained from the range-through based methods and the gap-filler equation (lower panel Figure 2.78) suggest range shifts and local extirpations rather than global extinctions. In this scenario, gap-fillers produce fluctuating extinction rates while the boundary crossers-based methods produce extinction estimates close to zero.

When origination and extinction rates are estimated using the gap-filler approach, four general patterns are recognized in the Cenozoic (Figure 2.79). (1) Wide amplitude fluctuating rates imposed over a declining trend during the Palaeocene to late Eocene interval, (2) low amplitude fluctuating rates without apparent trend during the Oligocene, (3) low to wide amplitude fluctuating rates without apparent trend during the Miocene, and (4) an increasing trend in both rates during the Pliocene- Pleistocene. Similar patterns can be interpreted when the origination and extinction rates are estimated using time windows of 2 Ma and in less extent 5 Ma (Figures 2.65 and 2.66). The comparison between the origination and extinction rates and the climatic curve, suggest that the periods exhibiting wide amplitude fluctuations are related to greenhouse climates (Paleocene-Eocene) while periods with narrow amplitude fluctuations are related to icehouse climates (Oligocene to present) (Scotese 2016).

When the intervals of rapid change in the climate record (Figure 2.75)

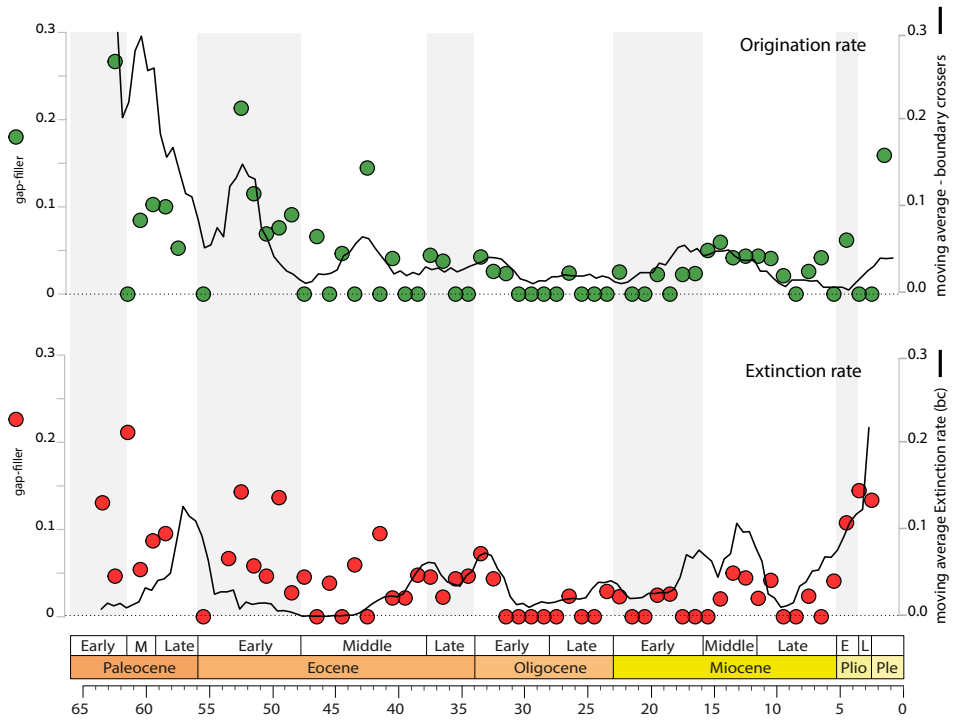

Figure 2.78: Origination and extinction rates using boundary crossers (Foote 2000) (black line) and gap-fillers (Alroy 2014) (colour points). The boundary crosser is represented by a five-point moving average calculated from the estimates of both the complete and restricted-FAD composite sections.

are compared with the taxonomic rates, two of them correspond to intervals of elevated origination (1.5 Ma and 52.5 Ma) while one corresponds to an interval of elevated extinction (52.5 Ma) (Figure 2.38). Other intervals exhibiting high taxonomic rates (62.5 Ma, 61.5 Ma, 49. 5 Ma and 3.5 Ma) apparently are not related to intervals of rapid climate change. However, a closer inspection of the Figure 2.79 reveals that both the origination and extinction rates show important changes near to the global climatic events of the early Eocene climatic optimum (EECO), the mid Eocene climatic optimum (MECO), the onset of the Oi-1 Glaciation, and the Mid Miocene Climatic optimum (MMCO). All these events are characterized by relatively high taxonomic rates (origination and extinction) that drop after the event (Figure 2.79). The reason why these events are not identified in the critical intervals analysis is because there is often a mismatch between the climatic

events and the taxonomic rates, which makes it difficult to identify their correspondence. The mismatch is especially evident in the Mid Miocene Climatic Optimum where the origination and extinction rates as well as the regional diversity curve shows a lag of approximately 1-2 Ma with respect to the climatic curve (Figure 2.79).

As explained before the possible causes of this mismatch could correspond to either discrepancy in the chronostratigraphic frameworks or a delay of the response of vegetation to the climatic events. In any case, the increase in extinction rates during the PETM, EECO and MMCO are supported by the survivorship analysis. The three climatic events are characterized by a concurrent increase in the slope of the individual cohorts (Figure 2.22). The concurrent inflection of cohorts at approximately 36 Ma shows the transition from high extinctions rates in late Eocene to low extinctions rates in the Oligocene, which is also evidenced in the gap-filler estimates (Figure 2.78). The homogeneity in the trajectory of the individual cohorts within each epoch (Figure 2.23) suggests that the response of plants to the mechanism(s) that drives extinction is independent of the age of the cohort. The intervals showing relatively elevated origination rates are well evidenced in the boundary crossers-based estimates (panel A, Figure 2.21) except the middle Eocene where the two estimates show clear discrepancies.

The results presented by Jaramillo et al. (2006) suggest that the extinction rate, estimated using the boundary crossers, is stable through Palaeocene-Miocene interval with an increase over background levels during the Eocene-Oligocene transition. This increase is also evidenced in the gap-fillers and boundary crossers estimates presented here (Figure 2.78). However, the highest extinction rates estimated in the present work are concentrated in intervals of the Paleocene and Eocene and not in the Eocene-Oligocene transition as suggested by Jaramillo et al. (2006). Opposite to the stability proposed by Jaramillo et al. (2006) the extinction rate estimated in the present work show a declining trend imposed over high amplitude variability during the Palaeocene-Eocene.

Jaramillo et al. (2006) suggested a slow, long-term decrease in the origination rate with an increase during the late Palaeocene and the early Eocene. A declining trend is also suggested by the present study, but it is restricted to the Palaeocene-Eocene interval and imposed over a high-amplitude fluctuating pattern (Figure 2.78). By studying the range shift between the tropics and the extra tropics in extant angiosperms, Antonelli et al. (2015) suggested that during the first half of the Cenozoic (from 66 until c. 30 Ma) most of the large range shifts occurring globally took place outside of the tropics. In the specific case of the Neotropics, the Palaeocene and Eocene were the periods with the highest emigration rates of the entire Cenozoic

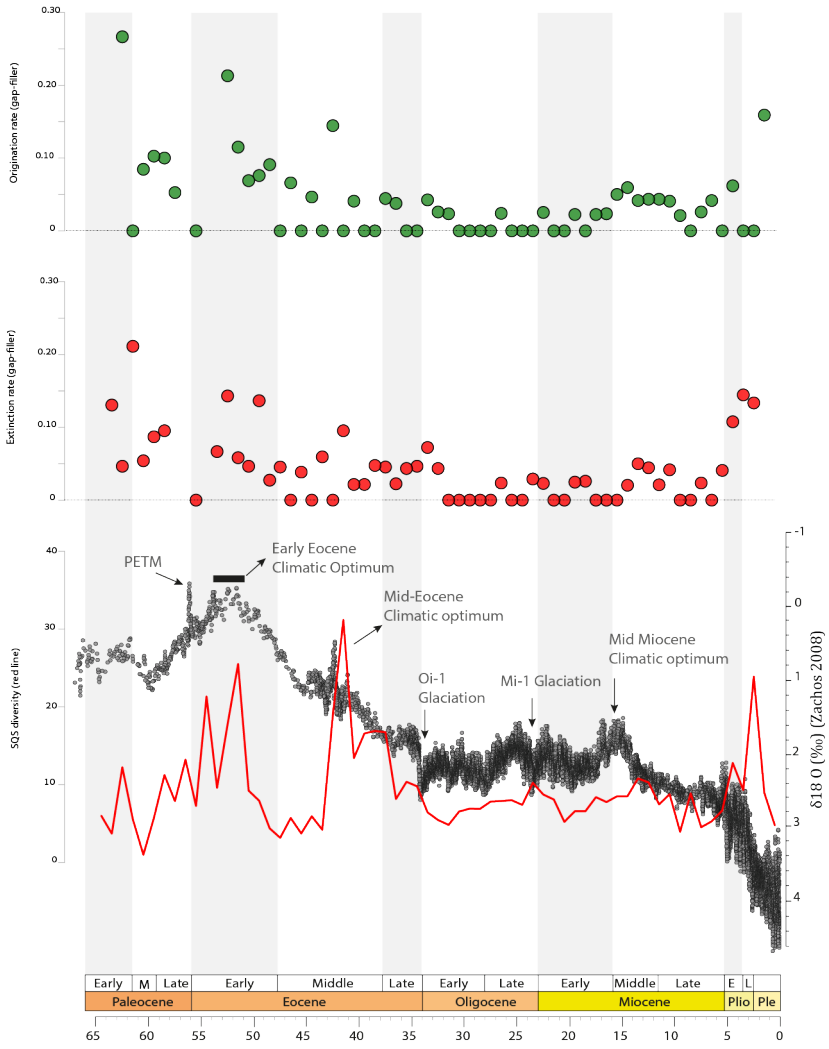

Figure 2.79: Macroevolutionary history of Neotropical vegetation during the Cenozoic. (a). Origination rate estimated using the gap filler equation (Alroy 2010). (b) Extinction rate estimated using the gap-filler equation (Alroy 2010). (c) SQS diversity curve (using the abundance version of the complete composite section (red line)) and $\delta O18$ data (black points) showing the most relevant climatic events occurred during the Cenozoic (modified from Zachos et al., 2008).

with a remarkable peak at 57 Ma.The number of immigration events during the Cenozoic was in general very low, indicating that the Neotropics pumped out more species than it received (Antonelli et al., 2015). The high Neotropical emigration rates during the Paleocene -Eocene inferred by Antonelli et

al. (2015) may be consistent with the inference presented here of apparent local extirpations followed by regional reappearances of taxa that explain the differences in taxonomic rates between the range-through based methods and the gap-filler estimates during the Eocene (Figure 2.78). During this interval, a great proportion of species emigrated out of the Neotropics diminishing temporarily their presence in this area and making therefore difficult their detection. However, these species did not become extinct, as revealed by the range-through based methods.

2.5.3 Macroevolutionary Dynamics

Diversification and turnover rates show similar patterns to those of the origination and extinction rates (Figure 2.72). A period of high-amplitude fluctuations concentrated in the Paleocene and Eocene; low values with null to low variability during the Oligocene and Miocene and a declining trend during the Pliocene-Pleistocene. A noticeable difference however occurs in the Oligocene. The turnover rates exhibit low- amplitude fluctuations, while diversification rates are zero during this interval. Similar to the regional diversity curve and the origination and extinction rates, the pattern of diversification and turnover rates show a good correspondence with the climatic curve (Figure 2.80). When abrupt episodes of global climate change are compared with the diversification and taxonomic rates, a correspondence is detected at 2.5 Ma, 55.5 Ma and 42.5 Ma for the diversification rate, and at 52.5 Ma for the turnover rate (Figure 2.76). The mismatch between the two time series makes it difficult to establish correspondences. However, a close inspection of Figure 2.80 reveals elevated turnover and diversification rates during the mid-Miocene Climatic Optimum and the mid-Eocene Climatic Optimum. The onset of the Oi-1 Glaciation at the Eocene-Oligocene boundary correspond with a fall of the turnover rate and also mark the beginning of the low amplitude fluctuations that characterize the Oligocene to middle Miocene interval. The diversification rates during the Oi-1 reveal a modest increase that is followed by a near-stasis during the entire Oligocene. The transient warming event of the mid-Eocene Climatic Optimum coincide with the highest diversification rate of Cenozoic while the turnover rates show two peaks that represent the culmination of an increasing trend started in the middle Miocene. The long term cooling trend of the early to middle Eocene evidenced by the climatic curve is characterized by a similar declining trend of the turnover rate, while the diversification rate during this interval exhibit high-amplitude fluctuations without any apparent trend. Near the Miocene-Pliocene boundary, the diversification and turnover rates are very high but immediately they fall following the decline trend of the climatic curve. The

diversification and taxonomic rates during the Palaeocene-Eocene thermal maximum are impossible to evaluate because of the lack of estimates in this interval (Figure 2.80).

The comparisons between the macroevolutionary estimates (origination, extinction, diversification, turnover and diversity) allow inferences of the dynamics of neotropical vegetation during the Cenozoic. When the regional diversity curve is compared with the origination and extinction rates (Figures 2.68 and 2.69 respectively) no significant correlation was found. When origination and extinction rates were compared, only current extinction and the origination in the following younger interval showed a significant correlation (Figure 2.70). This result suggests that origination is controlled by extinction, but extinction does not seem to be controlled by origination. In other words, those intervals showing high extinction rates are followed by intervals of high origination rates. The question that then arises is: if extinction is not controlled by origination, what is controlling extinction? Punctuated climatic events, like the EECO, MECO, Oi-1 Glaciation and MMCO show good correspondence with elevated turnover rates. This indicate that climate exert a very important control on both extinction and origination. Outstanding climatic events increase extinction. However, shortly after (less than 1 Ma later) origination also increases replacing those species that went extinct or redetecting those that were temporary absent (e.g. the transition between the early to middle Eocene). These results agree with the idea that Neotropics have acted as engine for global plant diversity with species being formed and replacing each other at unparalleled rates (Antonelli et al., 2015). The engine seems to have run at higher power during the Paleocene and Eocene. The dynamics of neotropical vegetation during the Cenozoic are comparable to the fern diversity dynamics, which is primarily driven by environmentally induced extinctions, with origination being an opportunistic response to diminishing ecospace occupancy (Lehtonen et al., 2017).

It is interesting to note in the early to middle Eocene the coincidence in the declining trends between the taxonomic rates and the number of emigrations from tropical America (Antonelli et al., 2015) (Figure 2.81). This relationship suggests that emigration also play an important role controlling both origination and extinction. When emigration from the Neotropics declines, the origination and extinction stabilized and show no apparent trends or wide amplitude fluctuations (Figure 2.81). The most relevant changes in taxonomic and diversification rates are however not related to appreciable changes in the emigration rates. Why emigration would have influenced taxonomic rates as observed here is puzzling, and may reflect poorly understood vegetational dynamics related with competition and niche occupancy.

The results presented here reveal the close relationship between origi-

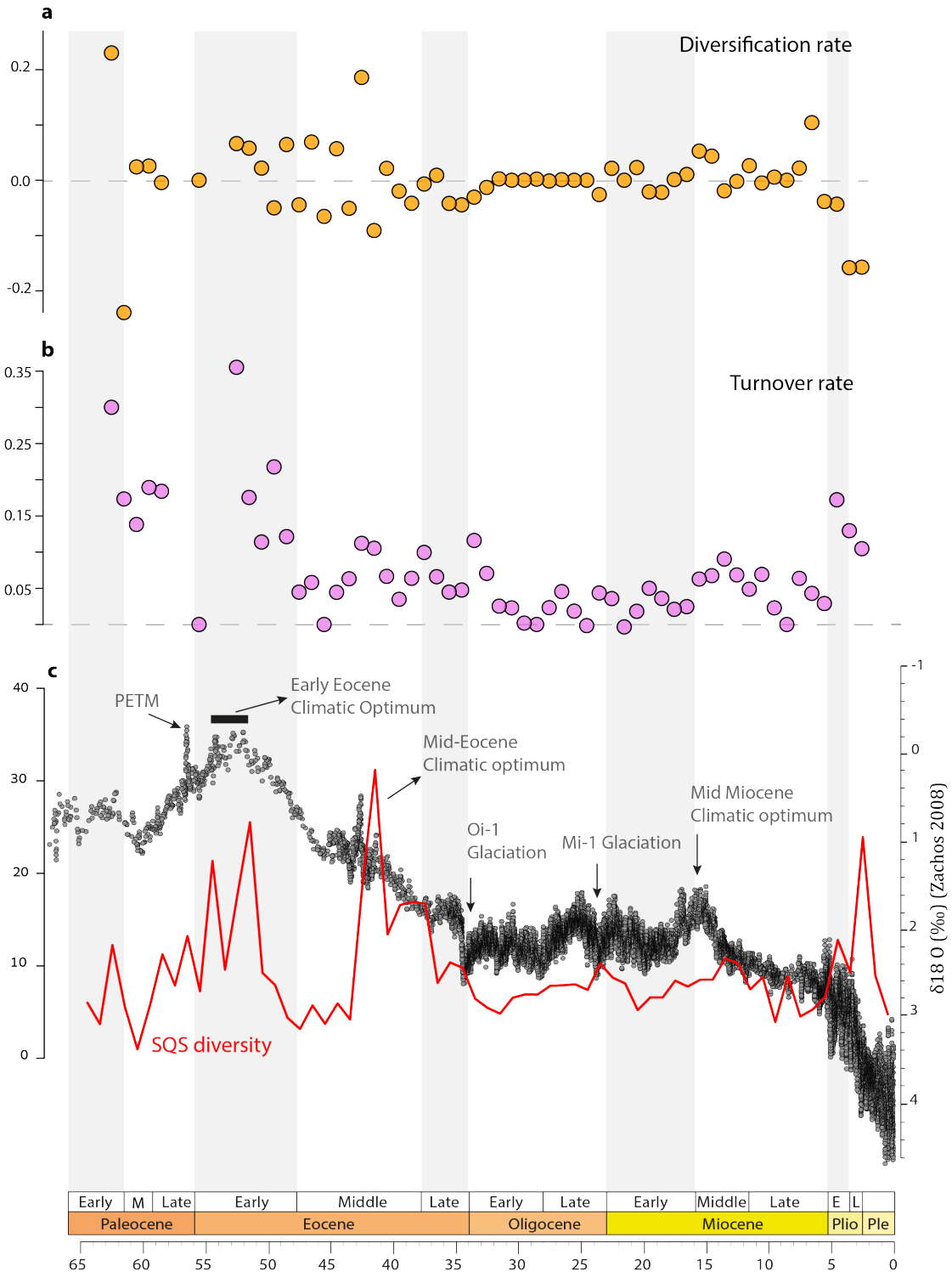

Figure 2.80: Macroevolutionary history of Neotropical vegetation during the Cenozoic. (a) Diversification rate (origination-extinction). (b) Turnover rate (origination+extinction). (c) SQS diversity curve (using the abundance version of the complete composite section (red line)) and $\delta O18$ data (black points) showing the most relevant climatic events occurred during the Cenozoic (modified from Zachos et al., 2008)

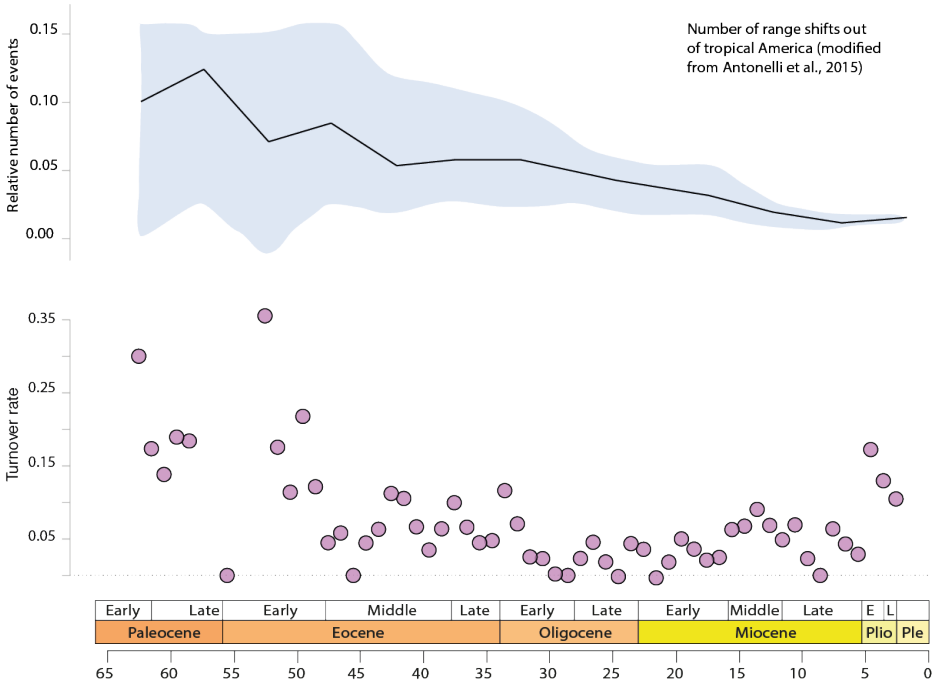

Figure 2.81: Comparison between the number of range shifts from tropical Americas (calculated as the number of events through time relative to the available number of lineages (modified from Antonelli et al., 2015) and turnover rates estimated in this work.The 95% confidence intervals are shown as shaded blue area in the range shifts plot.

nation and extinction, which is ultimately reflected in the taxonomic and turnover rates (Figures 2.79 and 2.80). It is also evident the big difference in macroevolutionary patterns between the Paleocene-Eocene and the Oligocene to present. This results contrast with those hypothesis that link the diversification of the Amazon biota to the substantial changes in landscape during the Neogene (Wesselingh et al., 2010). It is now well established that the onset of the transcontinental Amazon River occurred between 9.4 and 9.0 Ma (Gorini et al., 2013; Hoorn et al., 2017). Also, that the orogenic activity of the Andes Cordillera intensified between 12.4 and 4.4 Ma (Hoorn et al., 2010b) and that several marine-lacustrine incursions occurred during the Miocene (Hoorn 1993; Jaramillo et al., 2017; Linhares et al., 2017). All these events produced environmental and ecological changes that it is believed have helped to produce the mega-diversity of the Amazon basin. However, turnover and diversification rates during the Miocene are very low and exhibit low variability in comparison with those of the Paleocene and Eocene (Figure 2.80). Furthermore, taxonomic rates show a declining trend

from the oldest half of the middle Miocene to the late Miocene, which is precisely the interval when most changes in landscape occurred. The only outstanding peak in taxonomic rates of the Mid Miocene Climatic Optimum occurred a couple of millions before the full development of the Amazon basin (Figure 2.80). These results suggest that the changes occurred during the middle to late Miocene did not promote, but rather depressed taxonomic rates and diversity (Figures 2.79 and 2.80). It is however difficult to assess at what extent changes in landscape controlled macroevolution because this interval also coincides with a very pronounced decline in temperature. Temperature, as it has been shown through this work, exerted a very important control on plant macroevolution. It is possible therefore that the combined effect of cooling and changes in landscape were responsible for the low diversity and taxonomic rates during this interval. The taxonomic rates and diversity exhibit short-temporary outstanding peaks close to the Miocene-Pliocene boundary that are followed by a declining trend during the late Pliocene to Pleistocene. The decline coincides with an abrupt fall in temperature occurred at the Pliocene-Pleistocene boundary (Figure 2.80) showing again the close relationship between climate and macroevolution.

2.6 Summary and Conclusions

The analysis of palynological information from northern South America allowed a reconstruction of the macroevolutionary history of neotropical vegetation during the Cenozoic. The integration, via biostratigraphy, of information from different sections (outcrops and wells) enables us to construct a complete and continuous composite section of the palynological record of northern South America that spans the entire Cenozoic. The integration of results obtained using different techniques gave us a complete idea of how Neotropical vegetation has changed during the last 65Ma and the possible drivers of these changes.

Diversity exhibits a strong correlation with climate. The regional diversity and climatic curves exhibit high-amplitude patterns during the Paleocene-Eocene interval and low-amplitude patterns during the Oligocene to present interval. Episodes of global warming like the Paleocene-Eocene Thermal Maximum, the early Eocene Climatic Optimum, the Mid Eocene Climatic Optimum and the Mid Miocene Climatic Optimum, show elevated diversities. The high diversity during those warming intervals is the result of the contribution of a small proportion of samples belonging to just a few sections and not the result of a homogeneous high diversity occurring in many samples during those intervals. The reason why specific sections and samples

exhibit high diversities is difficult to test. The low temporal and geographic resolution of the paleogeographic reconstructions did not allow establishing concrete differences between the sections in terms of environments of deposition. Regarding to the differences in diversity between samples of the same section, changes in the environments of deposition can be also playing an important role. However, the scarcity of sedimentological information obtained from wells (that is the main source of information used in this study) prevents a deep understanding about the relationship between diversity and environments of deposition. Even in rock cores, where the sedimentological information is abundant, this relationship was difficult to set down.

On the other hand, episodes of global cooling like the long term cooling trends of the early to late Eocene and middle Miocene to Present exhibit severe declines in diversity. The most dramatic occurred during the early to middle Eocene in which the diversity reaches the lowest values of the complete Cenozoic. This interval is associated with a diachronous regional unconformity that makes difficult to find sedimentary sequences of this age. However, when diversity is estimated by resampling the results show that in fact this interval is characterized by low diversities. The extinction rates estimated using boundary crossers and the range-through assumptions indicates that the low diversity during this interval rather than being consequence of regional extinctions was caused by local extirpations followed by regional reappearances of taxa. This temporal disappearance of species can be explained by a high Neotropical emigration rates as inferred by Antonelli et al. (2015). During this early to middle Eocene, a great proportion of species emigrated out of the neotropics diminishing temporarily their presence in this area and making therefore difficult their detection. However, these species did not become extinct. Punctual episodes of global cooling like the onset of the Oi-1 and Mi-1 glaciations, are also characterized by a decline in diversity that however are less severe that those changes related to the long-term cooling trends of the Eocene and middle Miocene.

The Neogene is a very interesting period in the Neotropics because several global and regional changes occurred during this time. This has attracted the attention of investigators from different disciplines, especially those investigating the Amazon basin, that have tried to link these changes with the origin and maintenance of the Amazon biota mega diversity (Hoorn et al., 2010 and references therein). Important changes in climate include the initiation of the glaciations during the Eocene-Oligocene transition and the transient warming event called the Mid Miocene Climatic Optimum (Zachos et al., 2001). On regional scale episodes like the uplift of the Andes Cordillera (Mora et al., 2010; Horton et al., 2010), marine-lacustrine incursions (Hoorn 1993; Jaramillo et al., 2017; Linhares et al., 2017) and the onset of the Ama-

zon River (Figueiredo et al., 2009; Gorini et al., 2013; Hoorn et al., 2017) produced environmental and ecological changes that is believed helped to modulate the mega diversity of the Amazon basin. The results present here suggest a decline in diversity during this interval. The taxonomic rates fluctuate and this is reflected in relatively high turnover and diversification rates (Figure 2.80). Although the change in diversity is subtle, it seems to follow the cooling trend of the middle to late Miocene. In this sense, the evidence suggests that climate exerted a major control on diversity while the paleogeographic changes occurred during this time did not promote, but rather depressed taxonomic rates and diversity.

The taxonomic rates (origination and extinction) during the Cenozoic show a very close relationship. Both rates are especially high during the Paleocene and Eocene. The Oligocene can be considered as a period of stability while the Miocene show small fluctuations. During the Pliocene and Pleistocene an increasing trend is observed, especially in the extinction rate (Figure 2.78). When extinction is high, the origination in the following 1 Ma interval is also high. This relationship suggests that when a species become extinct, it is replaced very fast. In contrast, the lack of correlation between origination and extinction suggest that extinction is not controlled by origination. The examination of the taxonomic rates and the climate curve indicate a good correspondence between episodes of global climate change and turnover (Figure 2.80). These results agree with the idea that the Neotropics have acted as engine for global plant diversity with species being formed and replacing each other at unparalleled rates (Antonelli et al., 2015). The engine seems to have run at higher power during the Paleocene and Eocene.

Chapter 3

Flooding Events during the Cenozoic in the Neotropics

3.1 Introduction

The Cenozoic was a very important period in the history of Neotropical vegetation because the evidence suggests that the high plant diversity observed today in this region has roots going back to the Paleocene (Wing et al., 2009). Important global climatic and regional paleogeographic changes occurred during the Cenozoic, and have attracted the attention of researchers from different disciplines, especially those investigating the Amazon basin, who have tried to link these environmental changes with the origin and maintenance of the mega diversity of the Amazon biota (Hoorn et al., 2010 and references therein; Hoorn et al., 2018 and references there in). Important global climate changes include the transition from a greenhouse world during the Paleocene and Eocene to an icehouse world during the Oligocene to Present and the short-term climate fluctuations that includes the PETM (Paleocene-Eocene Thermal Maximum, the EECO (Early Eocene Climatic Optimum), the MECO (Mid Eocene Climatic Optimum), the MMCO (Mid Miocene Climatic Optimum) and the onset of the glaciations (Oi-1 and Mi-1 Glaciations).

Important regional paleogeographic changes also occurred during the Cenozoic in the Neotropics (Reyes-Harker et al., 2015; Roddaz et al., 2010), including the uplift of the Andes Cordillera (Mora et al., 2010; Horton et al., 2010, Hoorn et al., 2018 and references there in), the onset of the Amazon River (Figueiredo et al., 2009; Gorini et al., 2013; Hoorn et al., 2017) and the occurrence of several marine-lacustrine incursions (Hoorn 1993,1994,2006; Webb 1995; Wesselingh 2006; Boonstra et al., 2015; Jaramillo et al., 2017).

These events produced environmental and ecological changes that are believed to have modulated the mega-diversity of the Amazon basin (Hoorn et al., 2010). In particular, it is believed that the marine incursion(s) occurred during the Miocene played an important role in the biodiversity dynamic of the Amazon by favouring biogeographical isolation and promoting allopatric speciation (Webb 1995; Rasanen et al., 1995; Lovejoy et al., 1998; Hoorn et al., 2010 and references there in). However, the evidence also reveals that the Miocene marine incursions were just one from several flooding episodes that occurred throughout the Cenozoic and that these episodes were not restricted to the western Amazonia but they also spread over wide regions in northern South America. The evidence is also highly fragmented (reviewed below) and therefore the chronology, ecology and lateral distribution of most of the flooding events is very unclear. Without this basic knowledge it is impossible to establish for example the role that the floods could have played in the macroevolutionary history of Neotropical vegetation and the relationship between global climate changes and the occurrence of these episodes.

In this chapter, I make use an extensive palynological dataset from northern South America to explore the occurrence of flooding events during the Cenozoic in the Neotropics, specifically in Colombia. In this work I use the terms flood and flooding to make reference to episodes in which landscapes were covered by water in specific intervals of time. The process that caused these episodes may correspond to marine incursions or the establishment of lacustrine systems. The main goal is to establish a temporal framework for the floods to further explore their paleogeographic significance and its possible relationship with the macroevolutionary estimates obtained in the second chapter of this work (taxonomic rates and diversity) and the global climate changes occurred during the Cenozoic. The paleoecology of the floods is also explored. However, because the analysis is based only on palynological information, the inferences about ecology are limited to the type of information provided by the palynology.

3.1.1 Evidence of flooding events in the Neotropics

The flooding events are generally represented by fine-grained lithologies, identifiable in well logs and relatively easy to follow in seismic lines. They exhibit a very characteristic paleontological content, including among others mollusc and microfossils like foraminifera, ostracods, dinoflagellates and algae. These characteristics and their synchronous nature make flood events a very powerful and important tool for both regional stratigraphic correlations and paleogeographic reconstructions (Bayona et al., 2007; Reyes-Harker et al., 2015; Duarte et al., 2017; Caycedo et al., 2018).

In northern South America, the Cenozoic sedimentary record is predominantly continental. Nevertheless, it reveals the occurrence of several episodes of marine flooding. Studies on different sedimentary basins in Colombia (Hoorn 1993; Hoorn 2006; Santos et al., 2008; Gomez et al., 2009; Jaramillo et al., 2017), Peru (Louterbach et al., 2014; Boonstra et al., 2015), Brazil (D'Apolito 2016; Linhares et al., 2017) and Venezuela (Rull 1997) indicate that some of these events were geographically extensive covering large areas for prolonged intervals of time. For example, the most studied and best known of these events is the Miocene Pebas system, which was a huge (> 1 million km2) system of long-lived lakes and wetlands lakes and swamps that occupied most of western Amazonia between 24 and 7 Ma (Wesselingh 2006; Hoorn et al., 2010b; Hoorn et al., 2010c).

The nature of the Pebas system, as well as for other floods occurred during the Cenozoic in nothern South America, is still intensely debated (Hovikoski et al., 2010; Wesselingh et al., 2010). Several proxies, including sedimentology (Dino et al., 2012; Soares et al., 2017), palaeontology (Wesselingh et al., 2001; Gomez et al, 2009; Wesselingh et al., 2010), micropalaentology (Rull 1998; Boonstra et al., 2015), geochemistry (Roddaz et al., 2005; Villegas et al., 2016), biogeography (Echeverry et al., 2015) and even molecular biology (Lovejoy et al., 1998, 2010) have been used to establish their environments of deposition. Environmental interpretations of these deposits depend largely on the proxy used, but in general they range from marine incursions through tidal and estuarine deposits to continental-scale lake systems. As the environments of deposition have been difficult to establish, the mechanisms and processes involve in the generation and development of the flood events remains still more difficult to clarify. Below is a summary of the main flooding events by geological period recorded in the Neotropics.

3.1.1.1 Neogene Flooding Events

Flooding during the Miocene have received particular interest because of its possible role in the origin and maintenance of the mega diversity of the Amazonia. Jaramillo et al. (2017) provided a complete review and compilation of previously literature, summarising current interpretations of depositional environments in northern South America during the Miocene. In summary, the interpretations compiled by Jaramillo et al. (2017) comes mainly from isolated outcrops and a few rock cores located in western Amazonia and include: (1) an epicontinental shallow sea covering the Amazon basin for million of years (Rasanen et al., 1995); (2) a large freshwater megalake covering almost all of Amazonia (Frailey et al., 1998); (3) a fluvial-lacustrine system with extensive floodplains punctuated by sporadic marine incursions (Hoorn

1993, 1994, 2006); (4) a high frequency intercalation of marginal marine and continental strata (Hovikoski et al., 2007); (5) avulsive fluvial belts in a floodbasin-floodplain environment lacking of marine influence (Latrubesse et al., 2007); (6) a long-lived (8-23 Ma) megalake/wetland system composed of widespread and semi permanent aquatic ecosystems (Wesselingh et al., 2001); (7) a complex series of interconnected mega lakes overlying a regional peneplain (Campbell et al., 2006); and (8) a tidal system covering extensive areas of Amazonia (Roddaz et al., 2006).

Jaramillo et al. (2017) interpreted two distinct marine intervals that were recorded in two cores drilled in the Llanos basin of Colombia (Saltarin) and the Amazon/Solimoes basin of Brazil (105-AM), based on sedimentology and palynology (Figure 3.1). They used the proportion of marine palynomorphs (the sum of Foraminifera and Dinoflagellates) in relation to the total count of palynomorphs (the sum of pollen and spores) as indicator of marine influence. They also used the presence of a tooth of a ground shark (Carcharhiniformes) and remains of a mantis shrimp (Stomatopoda) recovered in one of the cores as further evidence of the occurrence of the two marine incursions in the Llanos basin. According to Jaramillo et al. (2017) the first marine incursion (Early Miocene Incursion (EMI)) occurred during the early Miocene (from 18.1 to 17.2 Ma in the Llanos basin and from 18.0 to 17.8 Ma in the Amazon/Solimoes basin) and the second marine incursion (Middle Miocene Incursion (MMI)) occurred during the middle Miocene (from 16.1 to 12.4 Ma in the Llanos basin and from 14.1 to 13.7 Ma in the Amazon/Solimoes basin). By using the evidence from the two cores and the seismic interpretation of the area (by regionally tracing the seismic reflectors of the floods) Jaramillo et al. (2017) proposed that shallow marine waters covered the western Amazon region at least twice during the Miocene. These two events were short in duration rather that a continuous full-marine occupancy lasting for several million years.

On the other hand, Hoorn et al. (2010c) subdivided the history of the Miocene mega-wetland system in three phases (Figure 3.1). The first correspond to a fluvial-lacustrine precursor phase (24 to 16 Ma) in which lacustrine conditions alternated with episodes of Andean and cratonic fluvial drainage as well as marine influence. The second refers to the mega-wetland or Pebas phase (16 to 11.3 Ma) in which the lacustrine conditions expanded reaching their maximum extension. The third correspond to the fluvio-tidal-dominated wetland or Acre phase (< 11.3 to 7 Ma, which represented the incipient transcontinental Amazon River system (Hoorn et al., 2010c). During its maximum extent the Pebas system covered an area of more that 1.5 X 10 6 Km2 comprising much of the Present western Amazonian lowlands (Hoorn et al., 2010c).

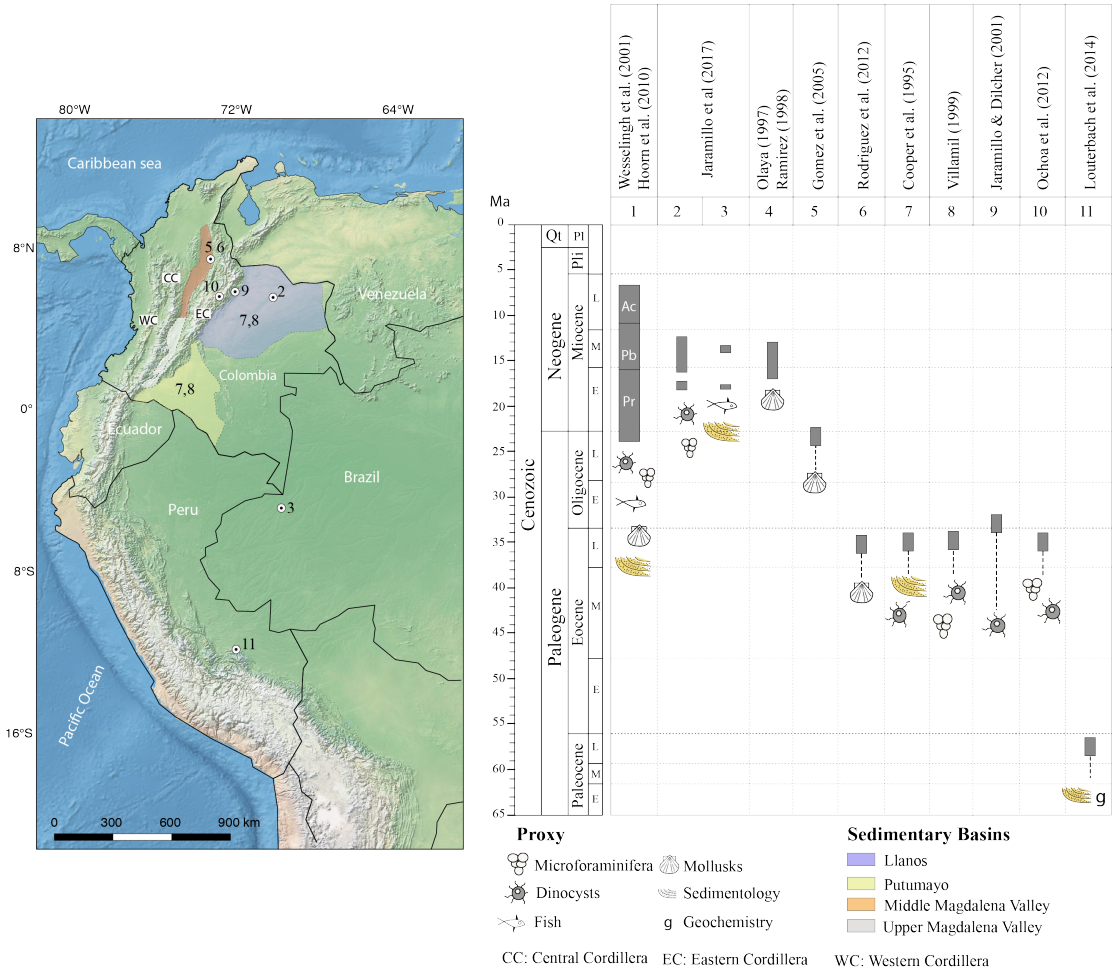

Figure 3.1: Map of northern South America showing areas and sections in which flooding episodes have been reported. On the right is shown the chronology and the type of evidence used to support the floods. Dashed line indicates uncertainty in the chronology. The number 1 represents the three phases of the Pebas system (Pr: Precursor; Pb: Pebas; AC: Acre) (Hoorn et al., 2010).

However, Miocene flooding episodes were not restricted to western Amazonia. There is evidence of marine-lacustrine influence in sediments from the sub-Andean basins of northern South America during the late Eocene and Miocene. The Middle Magdalena Valley (MMV) and Upper Magdalena Valley (UMV) are two sedimentary intramontane basins currently located between the Central and Eastern cordilleras of the Andes in Colombia (Figure 3.2). Geological and paleontological evidence suggest the occurrence of

several flood episodes in these two basins.

Middle Magdalena Valley (MMV): Three rich fossiliferous deposits have been described in the MMV (Pilsbry and Olsson, 1935). These fossil deposits known, as Los Corros, Mugrosa and La Cira are stratigraphically located at the top of the Esmeraldas, Mugrosa and Colorado Formations respectively (Figure 3.2). The fauna reported by Pilsbry and Olsson (1935) consist of fresh-water mollusks with a few slightly brackish water elements for the Los Corros and La Cira fossil horizons, whereas the Mugrosa fauna is composed exclusively by fresh-water mollusks. Pilsbry and Olsson (1935) explain that the three horizons must differ widely in age, although the mollusc association does not allow precise age estimates. Nevertheless, they suggested ages of deposition for the three horizons based on their stratigraphic positions and fauna.

Pilsbry and Olsson (1935) suggested a late upper Eocene age for the Los Corros horizon because of similarity to the fauna of the Saman Formation in northern Peru, the late Jacksonian of Southern United States of America, and the Ludian of Europe. Nuttall (1990) reviewed the palynological zones related with the three fossil horizons, previously calibrated in time with planktonic foraminifera, to suggest an Oligocene age for the Los Corros horizon. A palynological study by Rodriguez et al. (2012) in the Nuevo Mundo Syncline area of the MMV corroborated the late Eocene age proposed by Pilsbry and Olsson (1935) for the Los Corros horizon.

Pilsbry and Olsson (1935) tentatively assigned a middle Oligocene age to the Mugrosa horizon, based on the presence of the freshwater snails genus *Hemisinus*. This genus resembles a group of species that belong to this genus found in Oligocene sequences of Antigua and Cuba. According to Nuttall (1990) the age of the Mugrosa horizon is late Oligocene.

Finally, based on its stratigraphic position, Pilsbry and Olsson (1935) suggested an upper Oligocene or lower Miocene age for the La Cira Fossiliferous horizon while Nuttall (1990) proposed a middle Miocene age. Wesselingh (2001, 2006, 2006a) suggest that the malacofauna of the la Cira Fossiliferous Horizon was the precursor of the Pebas fauna and estimated an early Miocene age. Palynological age determinations place the La Cira in the late Oligocene (Van der Hammen 1957), and early to middle Miocene (Olaya 1997; Ramirez 1988).

Upper Magdalena Valley (UMV): In the Upper Magdalena Valley (UMV) at least two regional flooding events have been recognized in the Barzalosa Formation (Oligocene-Miocene? (De Porta 1974) and the Honda

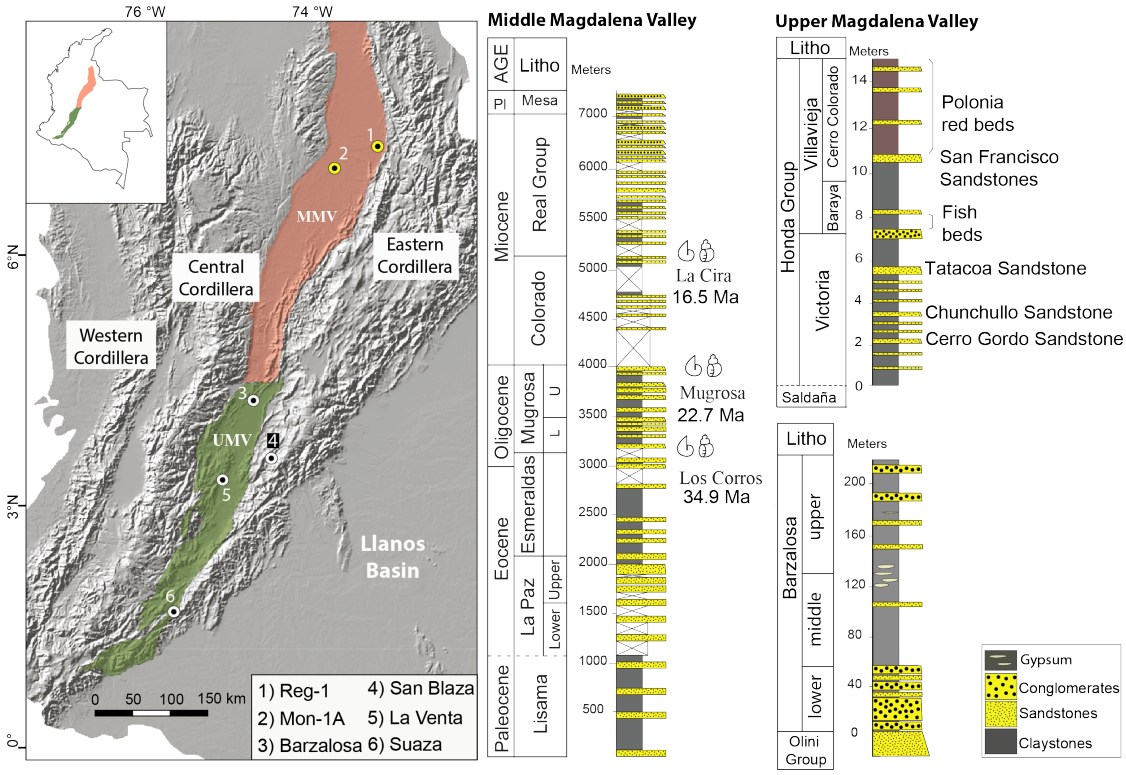

Figure 3.2: Map of Colombia showing the Middle and Upper Magdalena Valleys (MMV and UMV), and wells and sections discussed in the text. On the right, the composite stratigraphic columns of the MMV and UMV. The main lithological characteristics of the MMV were adapted from Gomez et al. (2005). The stratigraphic position and ages of the three fossiliferous horizons (Los Corros, Mugrosa, and La Cira) were estimated from the lines of correlations of the wells Reg-1 and Mon-1A. The main lithological characteristics of the UMV were adapted from an internal report of Ecopetrol and STRI (2012). The information of the Barzalosa Formation and Honda Group correspond to the localities Barzalosa and La Venta respectively. The San Blaza and Suaza are two small outcrops of the Barzalosa Formation with shell fragments.

Group (middle to late Miocene (Guerrero 1997). The evidence for the Honda Group have been largely described in the literature (Kay et al., 1997 and chapters therein) while for the Barzalosa Formation the evidence is very scarce and correspond mainly to confidential reports produced by oil companies.

The Barzalosa Formation was originally described by Scheibe (1934) and

redefined by Caceres and Etayo-Serna (1969). In its type area, the Barzalosa Formation can be informally subdivided into three segments (Ecopetrol-STRI, 2011) (Figure 3.2). The lower segment comprises thick layers of conglomerates intercalated with siltstones and fine-grained sandstones. The middle segment comprised thick layers of siltstones and claystones intercalated with medium thickness layers of fine to medium-grained sandstones. In this segment it is also common to presence of gypsum veins perpendicular to the claystones and siltstones bedding plains. The upper segment corresponds to thick layers of oligomictic conglomerates intercalated with claystones and siltstones. The stratigraphic thickness of the three segments in the type area is 56m, 126m and 45m for the lower, middle and upper segments respectively. No fossils were found in the type area (Ecopetrol-STRI, 2011). However, two isolated outcrops of the Barzalosa Formation located in the Suaza Creek (1.82N, -75.83W; 45 m thick) and San Blaza Creek (3.40N, -74.75W; 1.5m thick) each present one layer 1.3 m thick containing abundant remains of gastropods and bivalves, ranging in size between 0.5 and 1.cm (Ecopetrol-STRI, 2011). Unfortunately the limited exposure of these two outcrops, does not allow a determination of the exact stratigraphic position of the fossil horizons with respect to the informal subdivision of the formation, and the age of deposition of the Barzalosa Formation has not yet been clearly established. Confidential palynological reports from wells drilled in the UMV basin suggest a late Oligocene-early Miocene age for this unit. These reports also indicate the occurrence of important abundances of freshwater algae, specifically *Botryococcus* spp. and *Pediastrum* spp. in specific intervals of the Barzalosa Formation, which suggest lacustrine influence during the deposition of the unit.

The Honda Group is divided in two formal lithostratigraphic units, the La Victoria and the Villavieja formations (Guerrero 1997) (Figure 3.2). The La Victoria Formation is characterized by an alternation of fining upward sequences of grey pebbly volcanic lithoarenites and variegated mudstones deposited between 13.5 and 12.9 Ma (Guerrero 1997b). The mudstones in this formation are very rich in fossil vertebrates, including fish, reptiles, birds and mammals (De Porta 1962;Madden et al., 1997; Villaroel 2000; Zurita et al., 2013). In its type area, the La Victoria Formation varies in thickness from 462 to 570m (Guerrero 1997). The Villavieja Formation is composed mainly of red and grey mudstones with minor layers of medium-grained volcanic litharenites deposited between 12.9 and 11.5 Ma (Guerrero 1997b). In the area type this unit reach 578m thick. Fossil vertebrates are very abundant, especially in the lower part of the formation. Guerrero (1997) subdivided the Villavieja Formation in the Baraya and Cerro Colorado members (Figure 3.2). Toward the base of the Baraya Member, an informal unit between

1.2 and 6 m thick known as the Fish Bed is characterized by the presence of enormous quantities of disarticulated fish remains (spines, vertebrae, and teeth) suggesting lacustrine or swamps environments (Guerrero 1997). Confidential palynological reports from wells drilled in the UMV basin indicate abundant occurrences of algae of the genus *Botryococcus* and *Pediastrum* on specific intervals of the Honda Group. The stratigraphic position of the algae abundances with respect to the litostratigraphic units proposed by Guerrero (1997) is however unclear.

Previous information therefore shows that there are important palaeoecological differences between the areas in which Neogene flooding episodes have been reported (Figure 3.1). The evidence suggests that marine incursions occurred in specific areas of the Llanos Basin (Jaramillo et al., 2017), while lacustrine to swamps environments prevailed in the Middle and Upper Magdalena Valleys and western Amazonia (Hoorn et al., 2010). The single foreland basin integrated by the Middle Magdalena Valley, the Upper Magdalena Valley, the Eastern Cordillera and the Llanos basin was disrupted at least in the late Eocene to earliest Oligocene prior to the onset of the major late Neogene exhumation pulses of the Andes (Ochoa et al., 2012). For late Eocene times, the Eastern Cordillera was already separating the Middle Magdalena Valley and Llanos basin (Parra et al., 2009; Caballero et al., 2010; Nie et al., 2010; Moreno et al., 2011 Nie et al., 2012). The isolation of the UMV from the Llanos is less clear. Using sedimentological information and apatite fission tracks, Guerrero (1997) estimated at approximately 12.9 Ma the initial phase of uplift of the Eastern Cordillera at the latitude of the Upper Magdalena Valley. Other studies (Farris et al., 2011; Horton et al., 2010; Mora et al., 2010a; Moreno et al., 2011) however have suggested a positive relief for the Eastern Cordillera at least since approximately 22 Ma. The uncertainty about when the MMV and UMV were isolated from western Amazonia raise the question if paleogeography played a role in producing the ecological differences observed between the floods in the MMV-UMV and western Amazonia. To gain knowledge that allow approaching this hypothesis, it is necessary to establish first a common chronostratigraphic framework for the flooding events. As seen before, the chronology of the floods, particularly those in the UMV, is still very dubious and therefore the correlation of events between the different geographic areas is speculative.

3.1.1.2 Paleogene Flooding Events

Flooding events in the northern South America were not temporarily restricted to the Neogene. During the Paleogene, several lines of evidence sug-

gest the occurrence of floods. From these, undoubtedly the most recognized event occurred during the late Eocene.

Late Eocene Flooding Event: Sedimentological and paleontological evidence from Colombia indicate the occurrence of deltaic and marine conditions in the Llanos basin during the late Eocene (Cooper et al., 1995; Villamil 1999; Reyes-Harker et al., 2015). Paleogeographic reconstructions based on well log, sedimentology and seismic information (Pindell et al., 1997) suggest that a marine incursion flooded the Llanos basin of Colombia through the Maracaibo Lake. Apparently, the incursion was not restricted to the Llanos basin but also affected the south-western region of Colombia (southern Llanos basin and western Putumayo basin) (Figure 3.1) from which the incursion apparently came from the south, through the Ecuadorian Coast (Osorio et al., 2002).

The late Eocene flooding event has received special attention from researchers in Colombia because it is lithostratigraphically related to the Mirador Formation, which is one of the most important oil reservoir in the Llanos and Llanos foothills basins (Villamil et al., 2004). From the oil exploration point of view, the Mirador formation has been informally divided in two members (Fajardo et al., 2000). The lower member is composed by medium to coarse-grained sandstones, and the upper member is composed by quartzitic-conglomeratic sandstones alternating with light grey massive sandy mudstones and locally laminated organic mudstones (Fajardo et al., 2000). Micropaleontological analysis of the upper member have shown the existence of abundant dinoflagellates and microforaminifera, which have been interpreted as evidence of coastal and marine influence during the deposition (Cazier et al., 1995). Higgs (1997) however interpreted the presence of ichnofossils and microfossils in the upper member of the Mirador Formation as indication of fluvial environments (fluvial channels, overbank paleosols and lakes).

In a study of the upper part of the Mirador Formation, Santos et al. (2008) used palynological information from 80 wells and four sections to determine the paleogeography of the late Eocene marine incursion in Colombia. The analysis focused specifically in the upper part of the palynological zone T-07 that corresponds to the late Eocene (Jaramillo et al., 2011). For each sample interpreted as T07, they estimated a salinity index (SI), which describes the proportion of marine palynomorphs (microforaminifera + dinoflagellates) in relation to the total count of each sample (marine + terrestrial palynomorphs). Santos et al. (2008) used the SI to make a quantitative assessment of the degree of marine influence. For each stratigraphic section

(well or outcrop) the sample with the highest SI value was used as the indicator of the maximum marine influence for that site. According to the SI, marine influence during the late Eocene was geographically concentrated in the central Llanos Foothills and the Putumayo basins, while minimal or no marine influence was recognized in the Catatumbo, Middle Magdalena Valley, and Eastern Cordillera (Figure 3.1). The geographic distribution of the marine incursion proposed by Santos et al. (2008) diverges from the models proposed by Cooper et al. (1995) and Villamil (1999) in which the marine incursion came from the Caribbean Sea and therefore the connection with the Llanos basin must have occurred through southern Maracaibo, Catatumbo and northern Llanos, where according with Santos et al. (2008) the marine influence was minimal or null. To explain the geographic distribution of the late Eocene flooding event, Santos et al. (2008) used the dynamic model for northwestern South America proposed by Montes et al. (2005) in which block rotations during the Eocene could have disrupted and displaced a marine corridor that probably connected the Caribbean Sea with the central Llanos Foothills through the initial opening of the Lower Magdalena Valley.

Paleocene, middle Eocene, and Oligocene Flooding events: Other less investigated flooding episodes in northern South America occurred in the early Oligocene, middle Eocene and late Paleocene (Figure 3.1). The early Oligocene event corresponds to a maximum flooding surface identified in several sites in Colombia and Ecuador including the southern part of the Upper Magdalena Valley and Putumayo basins in Colombia (Osorio et al., 2002) and the Maranon basin in Peru (Christopoul et al., 2002). In the Floresta Syncline, Ochoa et al. (2012) reported the occurrence of three marine episodes litostratigraphically associated to the Concentracion Formation (Figure 3.1). The youngest of these events occurred within the uppermost T7 to the lowest T8 palynological zones of Jaramillo et al. (2011) (latest Priabonian to early Rupelian) and is characterized by salinity indices (SI) between 0.03 and 0.12, and relatively high abundances of palynomorphs related to mangrove vegetation (Ochoa et al., 2012). This event could be related to the marine incursion of the late Eocene (Santos et al., 2008) however the possible relation between the two was not discussed by Ochoa et al. (2012).

The middle Eocene flooding event is litostratigraphically related with the middle part of the Mirador Formation and the palynological zone T06 (Bartonian) of Jaramillo et al. (2011). This event was also recognized in the Concentration Formation by Ochoa et al. (2012) but is represented by a unique sample with a salinity index of approximately 0.14 and moderate abundances of palynomorphs related to mangrove vegetation (Ochoa et al., 2012) (Figure

3.1). A section along the Pialerita Creek in the central Llanos Foothills of Colombia (Jaramillo and Dilcher, 2001; Jaramillo et al., 2011) also recorded the mid Eocene flooding event. In this section, moderate abundances of the dinoflagellates species *Cordosphaeridium inodes*, *Coronifera* sp.1, *Glaphyrocysta* sp. 1, *Homotryblium floripes* were reported along with palynomorphs associated to mangrove vegetation suggesting marine to brackish influence during the deposition (Jaramillo and Dilcher, 2001). The interval of marine influence ranges in age between 43 and 32 Ma, although not all the samples from this interval showed marine or mangrove-related palynomorphs, suggesting sporadic rather than a continuous marine influence in this specific section (Figure 3.1).

For the Palaeocene, Louterbach et al. (2014) reported a marine incursion in the Madre de Dios-Sub-Andean zone of Peru (southern Amazonia) (Figure 3.1). They found evidence from biostratigraphy (foraminifera and ichtiofauna), sedimentology and organic geochemistry which they interpreted as indication of the presence of a tidally influenced shallow marine environment occurring during the Paleocene in this area. The chronology of the flood was interpreted as Danian (early Paleocene) or Thanetian (late Paleocene), with Thanetian being the most probable age (Louterbach et al., 2014) (Figure 3.1). In the Llanos and Llanos foothills of Colombia, the Paleocene lithostratigraphically corresponds to the Barco and the Los Cuervos Formations (Jaramillo et al., 2005). The uppermost segment of the Barco Formation show fluvial influence in the axial Eastern Cordillera, while in the Llanos Foothills, bi-directional cross beds, heterolithic lamination (Cazier et al., 1995) and few dinoflagellates cysts suggest tidally influenced deposition (Bayona et al., 2007). Cooper et al. (1995) also suggest strong marine influence in the deposition of the Barco Formation in the Llanos Foothills area with a relatively abrupt upward transition to coastal plain and alluvial deposits toward the top of the formation. The upper Los Cuervos Formation accumulated in coastal plains with more estuarine influence toward the Llanos foothills (Bayona et al., 2007).

In this chapter two topics are explored and discussed. The first is the temporal and geographic distribution of flooding events occurred during the Cenozoic in northern South America. The second correspond to the comparison between the marine-lacustrine deposits of the Middle and Upper Magdalena Valleys, with emphasis in establishing the age of the Barzalosa Formation and its environments of deposition.

3.2 Materials and Methods

3.2.1 Cenozoic Floods

A total of 120 sites (Annex 3.1) were used in the analysis of the Cenozoic flooding events. The age of each sample was estimated using the lines of correlation obtained from the graphic correlation model and the calibration points as explained in the Chapter-1 of this work. Samples from six wells located in the Upper Magdalena Valley (Br11, Gc1, Ym1, Nd1, Gb1) were not included in the graphic correlation model, and their ages were instead estimated using the maximum likelihood approach of Punyasena et al. (2012) as explained later. Samples with counts lower than 100 palynomorphs were excluded of the analysis to facilitate the comparison with other studies that have used this threshold. The total number of samples after this counting filter is 3066. To facilitate the interpretation of the results and explore the geographic distribution of the floods, each site and therefore their corresponding samples were assigned to a specific geographic region (Annex 3.1 and Figure 3.3).

The delimitation of these 10 geographic regions did not follow any specific criteria and was done visually with the objective to group sections by their geographic proximity to each other. Most of the defined areas (A, B, C, D, E, F, G, H, I, and J) correspond partially with oil prospective sedimentary basins of Colombia (Figure 3.3). Of all the areas, the Llanos basin is the largest and also presents the highest number of sections analyzed. To facilitate its interpretation it was further divided into six subareas (D, E, F, G, H and I) (Figure 3.3).

Palynology is the study of the organic microfossils that are found in maceration preparations of sedimentary rocks and therefore includes the study of acritarchs, chitinozoans, scolecodonts, algae, spores, pollen, dinoflagellates, fungi, microforaminifera and palynodebris (Traverse 2007). Each one of these microfossils offers valuable information about the ecology and environments of deposition. In this study, the palynomorphs were classified into one of the following five categories:

- **Dinocysts** Dinoflagellates are an extant group unicellular eukaryotic phytoplankton, predominantly marine and planktonic in habitat that in general occur as motile cells in surface waters (Head 1996). As a part of their life cycle, some dinoflagellates produce preservable organic-walled hypnozygotic resting cysts (dinocysts) (Traverse 2007). Most dinoflagellates cyst species are known from shallow marine settings. This is because they need to be able to return to the photic zone after excystment, which limits the maximum water depth of the habitat and

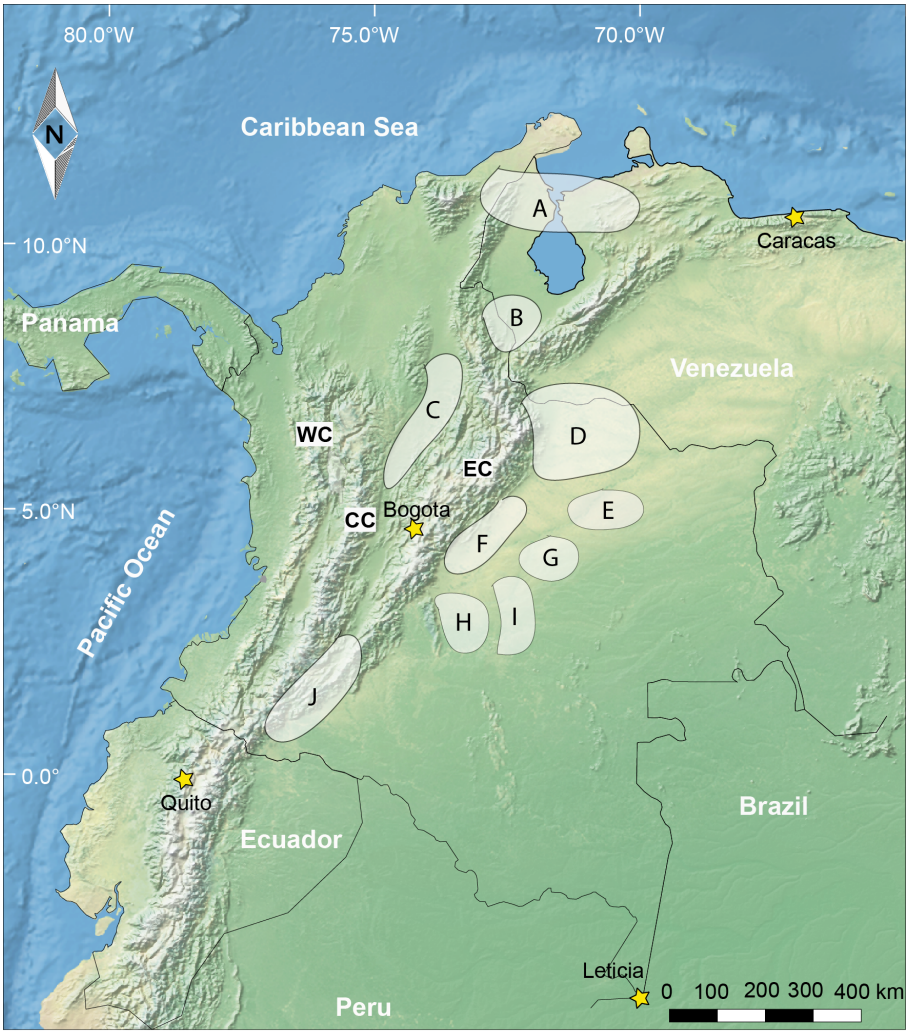

Figure 3.3: Map of Colombia showing the geographic areas (A to J) used in the analysis of the flooding events and discussed throughout the chapter. The delimitation of the areas did not follow any specific criteria and was done visually to group section by their proximity. WC: Western Cordillera; CC: Central Cordillera; EC; Eastern Cordillera.

inhibits occurrences of most cyst-forming species in the open ocean (Sluijs et al., 2005). Together with diatoms and coccolithophorids, dinoflagellates are among the most prominent marine primary producers in the ocean today and therefore they play a very important role in the global carbon cycle (Brasier 1985). In hydrocarbon exploration, biostratigraphy based on dinoflagellates is now a routine tool, yield-

ing even higher stratigraphic resolution than calcareous microfossils in some oil and gas provinces (Gradstein et al., 1992). Dinocysts have been used as sensitive palaeoenvironmental indicators because they are globally distributed, are abundant and diverse, occur continuously in the fossil record from the mid Triassic onwards and their distribution is controlled by different environmental parameters (Zonneveld et al., 2013). Modern biogeographical distribution have shown that organic walled cyst-producing dinoflagellates are highly sensitive to parameters such as nutrient levels, salinity, sea ice cover, temperature and nutrient availability (Sangiorgi et al., 2002, Boessenkool et al., 2001; Boyd et al., 2018). The environmental preferences of modern dinoflagellates cysts can therefore be compared to the Cenozoic record to make inferences about palaeoenvironmental conditions (Head 1996; Zonneveld et al, 2013; Woods et al., 2014; Boyd et al., 2018). Sluijs et al. (2005) presented a comprehensive review of methodologies, and the environmental and climatic signals recognized through Paleogene dinocysts studies. The review includes studies about paleoproductivity, sea surface temperature, salinity, stratification and paleo-oxygenation, oceanic circulation, water mass reconstructions and sequence stratigraphy (Sluijs et al., 2005). In the present study, most of the reviewed dinocysts were identified to genus level and only a minor proportion to species level. The reason for this is that most of the samples are from oil drilling activities where the main objective of the analysis was routine biostratigraphic analysis rather than a detailed taxonomic work. In the present study, the abundance of dinocysts was used as a general indicator of marine depositional conditions. In samples where dinocysts were identified to species level, the ecological preferences of these species were used to complement the palaeoecological interpretation.

- **Microforaminifera** the term microforaminifera refers to the organic remains of microforaminifera found on palynological preparations slides made using the standard palynological preparation procedure (Stanclife 1989). Although, the linings of microforaminifera cannot be positively assigned at the generic level using the foraminifera classification, informal descriptive schemes have been proposed (Stancliffe 1989). A very important morphological feature for the classification of microforaminifera is the relationship of the chambers. The lining types are described under the headings of isolated chamber, uniserial, biserial, coiled and combined. Secondary morphological features include the presence of material inside the chambers, wall structures, secondary degradation level of organic maturation, and the ability of the lin-

ing to accept stains (Stancliffe 1989). Microforaminifera linings have been recovered in sediments from the Permian to the recent (Stancliffe 1989) and are not commonly used in biostratigraphy. Microforaminifera linings are almost certainly exclusively marine in origin (Pawlowski et al., 1993; Decommer, 1982). The highest concentration of microforaminiferal linings recovered from modern environments seems to occur near upwelling currents (Melia, 1984), shallow waters and waters of raised salinity (Cross et al., 1966). In the fossil record they have been found in palynological preparations from marine and brackish sediments (Tappan et al., 1965) and marine Cretaceous palynofacies dominated by amorphous matter (Batten 1982). In the present study the abundance of microforaminiferal linings was used as an indicator of marine depositional conditions.

- **Algae** this category includes all the individuals belonging to species of the genus *Botryococcus* and *Pediastrum*, and its presences is used as evidence of freshwater influence.

  - **Pediastrum** is a genus of the family Hydrodictyaceae (class Chlorophyceae, order Sphaeropleales) that along with three other genera (Euastropsis, Hydrodictyon and Sorastrum) belongs to the coccal green algae with a polynucelar life cycle (Leliaert et al., 2012). Coenobia of the family Hydrodictyaceae are flat, disc-shaped, circular or oval in outline, composed from two up to several hundreds of cells, organized into one layer or arranged radially (Komarek and Jankovska, 2001). The form of coenobia, the morphology of the cells and the sculpture of the outer sporopollenin cell-layer are the main morphological criteria to identify separate species (Ediger et al., 1988; Komarek and Jankovska, 2001). However some species are very variable with numerous morphologically definable and stable varieties. The genus *Pediastrum* presents a worldwide distribution and comprises 24 living species. Some of them are cosmopolitan while others are restricted to cold, temperate or warms regions. In fact, of the 24 species; only four have really worldwide distributions (*Pediastrum simplex*, *Pediastrum boryanum*, *Pediastrum duplex*, and *Pediastrum tetras*) (Komarek and Jankovska, 2001). In the fossil record, 15 species and numerous varieties from the total 24 species have been described (Komarek and Jankovska, 2001). Although *Pediastrum* is not an integral part of routine palynological analysis, the species of the genus are ecologically distinct and has served for ecological identification in both Quaternary (Whiteside 1965; Sarmaja-Korjonen et al., 2006; Weckstrom

et al., 2010; Whitney et al., 2012) and pre-Quaternary studies (Nielsen et al., 1992; Brenner et al., 1994; Jankovska et al., 2000; Tell et al., 2004; Tahoun et al., 2017). Nowadays the genus *Pediastrum* contains only freshwater species. The rare occurrence of the genus in marine settings has been explained as caused by freshwaters influxes (Brenner et al., 1994; Matthiessen et al., 2000). The geographical distribution of the species is mainly determined by two factors: global distribution responds to temperature, whereas regional distribution is better explained by water quality (Tell 2004). In the northern mid latitudes, changes in the abundance of *Pediastrum* have been interpreted to reflect changes in trophic state and erosion in the catchment (Van Geel 2001) while variation in tropical and subtropical regions are thought to reflect changes in temperature (Rull et al., 2008), lake levels (Gosling et al., 2008) and increase or decrease of the macrophyte cover in lakes (Caballero et al., 1999; Lamb et al., 1999). Changes in communities of *Pediastrum* have shown a relationship with nutrient availability (Bradshaw et al., 2005), pH and dissolved organic carbon (Weckstrom et al, 2010), water quality (Jankovska et al., 2002), water level (Whitney et al., 2012), and presence of littoral vegetation (Danielsen 2010). In summary, extant *Pediastrum* is more abundant in tropical to subtropical permanent, low salinity hyper-eutrophic lakes (Reynolds, 1984). Chu (1943) found that the minimum level of nitrate for optimum growth was twice as high for *Pediastrum* cultures as it was for those of *Botryococcus*, which indicate a preference of *Pediastrum* for high nutrient load. In the present study, the occurrence of *Pediastrum* was recognized mainly to the genus level with only few specimens recognized to the specific level. The reason of this is that most of the samples used in this study come from oil industry activities where the main objective of the analysis was to carry on routine biostratigraphic analysis rather than produce a detailed taxonomic identification. In this study, the abundance of *Pediastrum* was used as an indicator of freshwater (lakes and ponds) depositional conditions. In samples where individuals of *Pediastrum* were identified to the species level, the ecological preferences of those species were used to complement the palaeoecological interpretation.

– **Botryococcus** (Kuetzing 1849) (Botryococcaceae, Trebouxiales, Trebouxiophyceae, Chlorophyra) is a green colonial microalga widespread in freshwater and brackish lakes, reservoirs, ponds, or even ephemeral

lakes situated in continental, tropical, alpine and temperate zones (Aaronson et al., 1983). *Botryococcus* occurs as colonies of various sizes with individual cells ranging in size from 5 to 15um and colonies from 10 to 100um (Guy-Ohlson 1992). The taxonomy of the genus is still unclear. Komarek and Marvan (1992) defined 13 species based on morphological characters from light microscopy observations in fixed natural samples. However, diagnostic characters such as color, cell size and colony form had the potential to change within a clonal strain when placed under different culture conditions (Plain et al., 1993). For this reason the taxonomic system proposed by Komarek and Marvan (1992) has not been widely used, and a single species, *Botryococcus braunii*, is currently used in most studies (Kawachi et al., 2012). The oldest putative *Botryococcus* fossil was found in Neoproterozoic sediments (Arouri et al., 2000). Their colonies occur throughout the entire Phanerozoic and they became very widespread especially during the Mesozoic and Cenozoic (Aaronson et al., 1983). *Botryococcus* have received much attention mainly because its high content of alkenes and fatty acids, which can generate important amounts of hydrocarbons (Dubreuil et al., 1989; Metzger et al., 2005; Hou et al., 2014). *Botryococcus* have been identified as an oil source in Mesozoic and Cenozoic sequences of several oil provinces in China (Li-Ming et al., 2010), Cambrian and Precambrian sedimentary basins in Australia, the Ordovician of Estonia (Glikson et al., 1989) and the Eocene of India (Kumar et al., 2016) among others. In spite of its little biostratigraphical significance, *Botryococcus* can be used, by analogy with the modern microalga, to interpret palaeoecological and climatic conditions and for palaeoenvironmental reconstructions (Guy-Ohlson 1998). Modern *Botryococcus* is commonly encountered in terrestrial regions and although it is prevalent in tropical regions, it also tolerates cooling events (Herrmann 2010). It is found in fresh and brackish water lakes, and seawater near river estuaries where is a very important contributor of organic content (kerogen) (Metzger and Largeau, 2005). It is rarely found in lakes deeper than 100m, as it is an autotrophic alga that requires sufficient sunlight and clear water (Li-Ming et al., 2010). *Botryococcus* prefers calm waters with few underwater plants and low sedimentary/nutrient input from the outside. This means it favours oligotrophic to mesotrophic waters but also tolerates eutrophic conditions (Herrmann 2010). In normal lacustrine conditions, *Botryococcus* can bloom and may form floating mats

of several centimetres thick spreading over an area of several hundred square meters (De Decker, 1988). Earlier records indicate that *Botryococcus* colonies flourished in both fresh and brackish water in lake facies of organic rick black mudstone and fine siliceous mudstones, but rarely in near shore and shallow water lake facies (Prasad and Sarkar, 2000; Ji et al., 2010). In summary, extant *Botryococcus* has a cosmopolitan distribution in permanent to semi-permanent ponds, lakes and rivers ranging from tropical to arctic latitudes (Aaronson et al., 1983) and is more characteristic of oligotrophic lakes (Wetzel 1983). Modern day observations show that elevated abundances of *Botryococcus* are found in shallow, often temporary, partly saline lakes located in arid areas subject to climatic extremes (Tyson 1995). *Botryococcus* also occur in unstable salinity regimes characterized by periodic deposition of gypsiferous or other shallow water evaporitic facies (Nagappa 1957). In the present study, the presence and abundance of *Botryococcus* is used as indicator of lacustrine conditions.

- **Mangrove** mangrove forests are important components of the coastal ecosystems associated with intertidal habitats in the tropical and subtropical sheltered shores from approximately 30N to 30S latitude of the world (Tomlinson 1986). Extant mangroves comprise about 70 taxonomically diverse tree, shrub, palm and fern species that share adaptations to saline, anoxic habitats (Tomlinson 1986). The Cenozoic palynological record from Gulf/Caribbean region reflects a trend of increasing diversity of genera adapted to the mangrove environment. They diversified from four or five genera in the Eocene, to about 15 in the Quaternary, and 27 in the present (Graham 1995). According to Graham (1995) the mangrove forest components during the Eocene were different from those today and included *Nypa*, *Pelliciera*, *Acrostichum*, and the parent species of *Brevitricolpites variabilis*, which has been considered the ecological equivalent of Rhizophora (Geermerad et al., 1968). During the Eocene, *Nypa* was distributed almost globally. At present however, it only occurs in the Indo-Malaysian region (Rull 1998; Gee 2001). Germeraad et al. (1968) suggested that its extinction in the Tethys region was caused by a drier, more seasonal climate. In the palynological fossil record, *Nypa* is represented by species of the genus *Spinizonocolpites*, including *Spinizonocolpites grandis*, *Spinizonocolpites baculatus*, and *Spinizonocolpites echinatus* (Graham 1995; Srivastava et al., 2015). In contrast, the genus *Pelliciera* was present in the Caribbean area and the Atlantic coasts of Guyana and Brazil during

Eocene-Oligocene times, but now it is restricted to a small area of Central and Northern South America (Rull 1998). According to Jimenez et al. (1984), the limited distribution of *Pelliciera* today is a consequence of its low tolerance to high salinities caused by increased evaporation in dry climates. In the palynological fossil record, *Pelliciera* is represented by *Lanagiopollis crassa* (van der Hammen and Wijmstra, 1964; Germeraad et al., 1968; Graham 1995; Rull 1998). However, Morley (1982) proposed that *Lanagiopollis* is attributable to the family Alangiaceae. In specific, based on pollen morphological variation, to the botanical sections *Conostigma* and *Marlea*. The palynological material analysed by Morley (1982) correspond to offshore and onshore sections from southeast Asian deposited in a wide range of environments, ranging through supralittoral, littoral and sublittoral. This would suggest that species of *Conostigma* and *Marlea* and therefore those of *Lanagiopollis* were probably associated to environments close to the shore. However, it is still unclear if species of *Lanagiopollis* described for northern South America are comparable to those described in Asia by Morley (1982). This is a very interesting topic that deserves further investigation, but it is beyond the scope of this work. Based on the work by van der Hammen and Wijmstra, 1964; Germeraad et al., 1968; Graham 1995; and Rull 1998, the presence of*Lanagiopollis* is considered here as an indicator of suitable conditions for the development of mangrove forests. Finally, the most common extant mangrove-forming genus of the present is *Rhizophora*, which has been recorded in coastal environments from the late Eocene onwards (Rull 1998), represented in the palynological record by several species like *Zonocostites ramonae* (Germeraad et al., 1968); *Zonocostites equatorialis* (Silva-Caminha et al., 2010); *Zonocostites duquei* (Duenas 1980); and *Zonocostites minor* (Jaramillo and Dilcher, 2001). In the present study the presence and abundance of the species *Lanagiopollis crassa*, *Lanagiopollis* spp., *Zonocostites ramonae*, *Zonocostites* spp., *Spinizinocolpites grandis*, *Spinizonocolpites baculatus* and *Spinizonocolpites echinatus* are used as indicators of mangrove vegetation.

- **Continental** this category includes abundances of formal and informal species of pollen and spores, excluding those categorized in mangrove.

Three indices were estimated for those samples with counts higher than 100 palynomorphs:

- **Salinity index ($SI = M/T$)**:where **M** is the abundance of dinocysts and microforaminifera, and **T** is the total count of the sample, which

includes palynomorphs of the categories; dinocysts, foraminifera, algae, continental and mangrove.

- **Lacustrine index ($LI = L/T$)**:where **L** is the abundance of algae (*Pediastrum* and *Botryococcus*) and **T** is the total count of the sample, which includes palynomorphs of the remaining categories.

- **Mangrove index ($MGI = G/T$)**:where **G** is the abundance of mangrove palynomorphs and **T** is the total count of the sample.

To further explore in more detail the ecology of the **SI** and **LI** indices, the contribution of each of their components was also estimated (microforaminifera vs. dinoflagellates and *Botryococcus* vs.*Pediastrum* for the SI and LI respectively).

3.2.2 Middle and Upper Magdalena Valleys

As explained in the introduction, at least three distinct flooding events have been reported in the Middle Magdalena Valley (MMV) and Upper Magdalena Valley (UMV) (Figure 3.2). However, the sediments recording the flooding in these regions were not included in the wider chronostratigraphic model presented in the Chapter 1. To establish a temporal equivalence among the events in the MMV and UMV, the palynological records of the two basins were compared.

First, for the MMV a standard reference section (SRS) was constructed by using information from the wells Mon-1A and Reg-1. These sections were used in Jaramillo's zonation and they are already calibrated with the geological time scale (Jaramillo et al., 2011). In the SRS, composite units were used as a measure of the stratigraphic positions of the events. Three additional biostratigraphic events were added to the SRS to facilitate the trace of the lines of correlation. These events have been recognized regionally and are commonly used for intra-basin correlations. They correspond to the Los Corros, the Mugrosa and the La Cira Fossiliferous horizons (Pilsbry and Olsson, 1935; described above) located at the tops of the Esmeraldas, Mugrosa and Colorado Formations respectively (Figure 3.2). Palaeontologically, a rich association of fresh water molluscs characterizes these deposits. In ditch cutting samples, the recovery of small fragments of shells is used by the well loggers to locate the three horizons and to establish regional correlations. In the SRS, the three horizons were interpreted as follows. The La Cira Fossiliferous Horizon was positioned at 6490 composite units (16.5 Ma) due to the presence of shell fragments reported in Mon-1A at a depth of 7000 feet. The

Mugrosa Fossiliferous Horizon was positioned at 14393 composite units (22.7 Ma) because of the presence of shell fragments at 3190 in Reg-1. The Los Corros Fossiliferous Horizon was positioned at 16164 composite units (34.9 Ma) in the SRS based on the presence of shell fragments at 7250 in Reg-1 (Figure 3.2).

The palynological content of 128 samples from five wells located in the UMV (Hig-1= 16 samples; Gc1= 29 samples; Gb1= 59 samples; Nd1= 13 samples; Ym1= 11 samples) (Annex 3.1) (Figure 3.4) distributed throughout the Barzalosa Formation and Honda Group were compared with the MMV standard reference section using a probabilistic approach. The probabilistic approach makes reference to a methodology that uses a maximum likelihood to estimate the age of an individual sample or group of samples (Punyasena et al., 2012). This technique uses the relative abundance of microfossils (in this case palynomorphs) to provide shape to the known stratigraphic ranges of taxa based on the changing abundance of a taxon through time and to weigh the relative influence of a taxon in an isolated sample. The first step to apply the technique is to produce a baseline model that represents the changes in abundance over time to which a single sample or set of samples can be compared. This baseline model represents the entire a priori knowledge of all known taxa and their abundance data for all time slices. Changes in abundance in the model can be described in absolute measures of time (e.g., million of years), as relative measures of time (e.g., older or younger) or as any significant measure of change through time or another gradient of interest (e.g., stratigraphic position). The taxon abundances of the model provide the comparative data against which all single sample estimates are matched. Once the individual samples are compared with the model, the final result is a likelihood distribution describing the position of the sample in the gradient as a range of probabilities. In this case the baseline model corresponds to the MMV standard reference section. This model represents the best current knowledge of the changing abundance of palynomorphs species in the MMV for the time when the flooding events occurred. The gradient of the baseline model uses the ages of each sample calculated through the lines of correlations and calibration points of the graphic correlation. The comparison of each sample with the baseline model produces a probabilistic estimate of its age. Because each sample is compared against the same baseline model, this approach reduces the subjectivity involved in the age estimation. A downloadable version of the software used to complete the analysis is available in the personal webpage of one of the authors (http://publish.illinois.edu/punyasena/).

The samples from the UMV as well as the samples associated with the three fossiliferous horizons in the standard reference section are character-

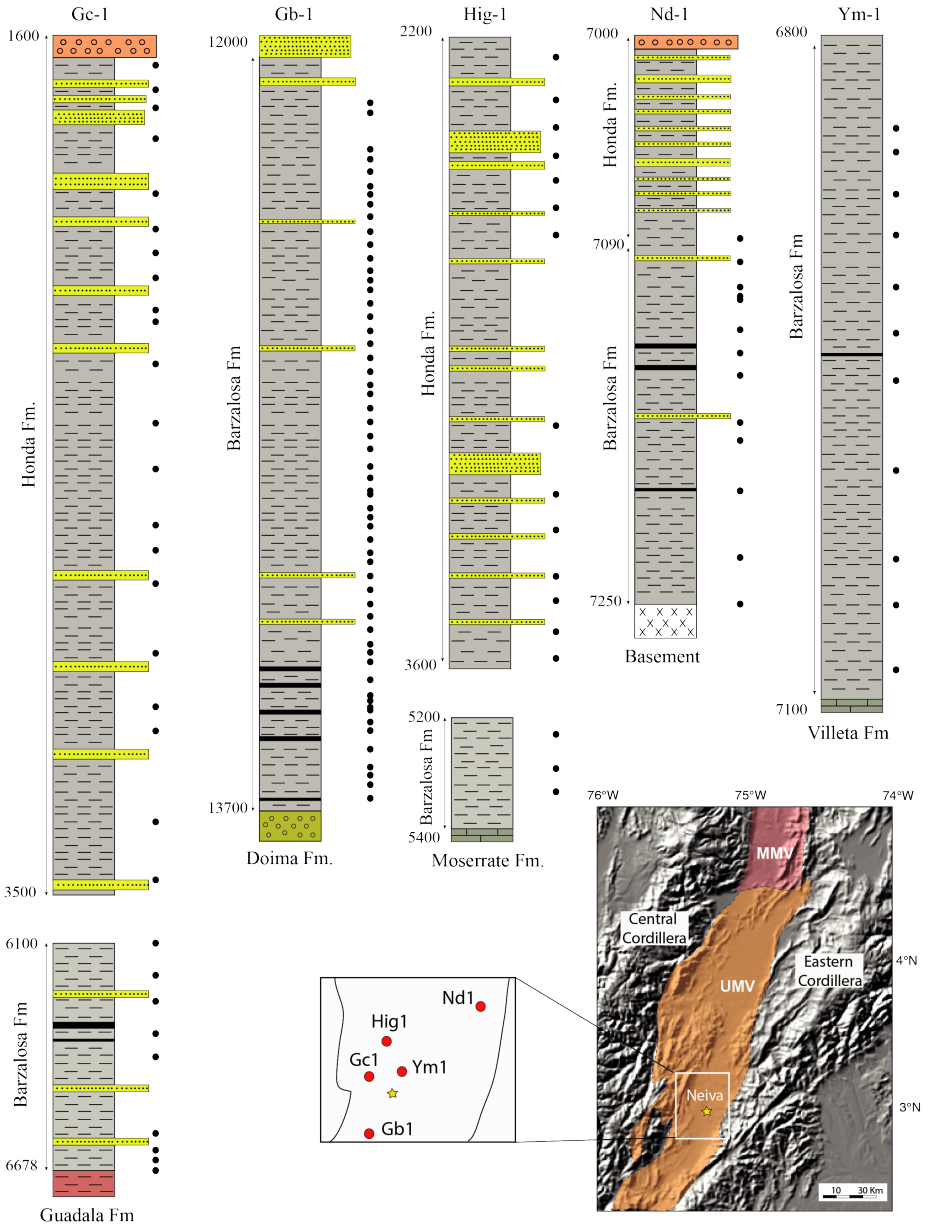

Figure 3.4: Lithology of the Barzalosa Formation and Honda Group in five wells drilled in the Upper Magdalena Valley. The lithological information was extracted from well logs. Scale in Nd-1 and Ym-1 is different from the scale in Gc-1, Gb-1 and Hig-1. Location of the samples for the analysis are indicated. MMV: Middle Magdalena Valley; UMV: Upper Magdalena Valley.

ized by high abundances of the algae *Pediastrum* and *Botryococcus*. Two samples or intervals could exhibit a high probability of correlation simply

because the abundance of the algae and not because they have similar palynological associations. To further explore this possibility, the maximum likelihood estimates were calculated both including and excluding the abundances of *Pediastrum* and *Botryococcus* from the standard reference section and from the samples of the UMV. Only samples with counts higher than 20 palynomorphs were used in the maximum likelihood analysis.

To explore the depositional sequence of the Barzalosa Formation, the lithological information from the well Gb-1 was extracted from the well log. This well was chosen because it presents the most complete section with palynological analysis. The lithology in a well log corresponds to the lithological classification of the ditch cutting samples recovered during the drilling operation. This information is later integrated with information from well logs (e.g. Gamma Ray, Spontaneous Potential) to produce a lithological interpretation of the well. In the case of the Barzalosa Formation in Gb-1, the information corresponds to five lithologies (shale, sandstones, grey claystones, coal, and siltstones) reported between 13480 and 12000 feet. The result is a list depths (from and to) with the lithology associated to each interval (Annex 3.2).

To establish the depositional sequence of the Barzalosa Formation, a transition matrix (TM) method based on Markov chain was used. TM is a method for quantitative stratigraphy (Walker 1979), which supposes that the succession of facies in a set of stratigraphic logs can be considered as a Markov process (Davis 2002). A Markov process is defined as a succession of states or events in which the occurrence of a given state depends on the previous one (Powers et al., 1982). In the case of Gb-1 the states or events represent the changes in lithology. The TM starts with a state transition matrix, which consist of a two-way table that record the number of transitions between every couple of states. The depositional sequence is defined based on the statistically significant transitions (Ndiaye et al., 2014). Three methods, Walker (Walker 1979), Harper (Harper 1984), and Turk (Turk 1979) have been proposed to separate significant transitions from random transitions. In Walker method, the sequence is obtained by comparing the observed probability of transition between states with randomly occurring transitions. In Harper method (Harper 1984) the transitions probabilities greater than random are tested for statistical significance (Harper 1984). For each transition between two states, the probability of having at least the observed number of successions in N trials is computed. This corresponds to the binomial probability. Considering the null hypothesis that a transition occurs at random, it can be rejected if the binomial probability is greater or equal to the chosen level of significance (Ndiaye et al., 2014). In Turk method (Turk 1979) the transition matrix is separated into noise and signal matrix. Several iterations are often necessary to isolate these two disjoint matrices, which are performed

iteratively based on priori hypothesis or posterior hypothesis based on residual analysis (Ndiaye et al., 2014). The final sequence is computed using the difference between the observed and the random matrix. The analysis was executed in the software Strati-Signal (Ndiaye, 2007).

3.3 Results

3.3.1 Flooding events in the Magdalena Valleys

The standard reference section (SRS) for the MMV corresponds to the integration of data from wells Mon-1A and Reg-1 (Figure 3.2). The SRS comprises a total of 288 samples, from which 185 correspond to Mon-1A and 103 to Reg-1. Four different stratigraphic levels characterized by abundant fragments of molluscs were recognized during the drilling of the Mon-1A and Reg-1. These were interpreted to be the Los Corros and the Mugrosa Fossil Horizons in Reg-1, while the La Cira Fossil Horizon was recognized in Mon-1A (Figures 3.2, 3.5). Another stratigraphic level with molluscs was recognized, between the Los Corros and Mugrosa Fossil Horizons, in the well Reg-1 (Figure 3.2). The fragments in this level could be the result of contamination by borehole caving or may be indicative of the stratigraphic range of the La Mugrosa or the Los Corros horizon. The ages of the horizons were estimated using the palynological zonation of Jaramillo et al. (2011) (Figure 3.2).

The palynological analysis of the SRS shows that fossiliferous molluscs horizons present elevated abundances of the two algae *Pediastrum* and *Botryococcus* (Figure 3.5). *Botryococcus* is especially abundant in the La Cira Fossiliferous Horizon and relatively abundant in the Mugrosa and the Los Corros Fossiliferous Horizons (Figure 3.5). On the other hand, *Pediastrum* is only abundant in the La Cira and Mugrosa Fossiliferpus Horizons (Figure 3.5). It is interesting to note that *Pediastrum* is abundant in some samples that are not related to the fossiliferous horizons. These abundances of *Pediastrum* can be the result of contamination by caving.

Along with *Botryococcus* and *Pediastrum*, several species of pollen and spores were recovered in the samples associated with the fossiliferous horizons. The samples related to the La Cira Fossiliferous Horizon exhibit high abundances of Psilatriletes 25-50, *Laevigatosporites tibuensis*, *Verrucatosporites usmensis*, *Polypodiisporites sp.*, *Psilamonocolpites medius*, and *Mauritiidites franciscoi var. minutus*. Other species with lower abundances includes *Magnastriatites grandiosus*, *Retitricolpites simplex*, *Echiperiporites akhantos*, *Rhoipites guianensis*, *Crassiectoapertites colombianus*, *Malvacipol-*

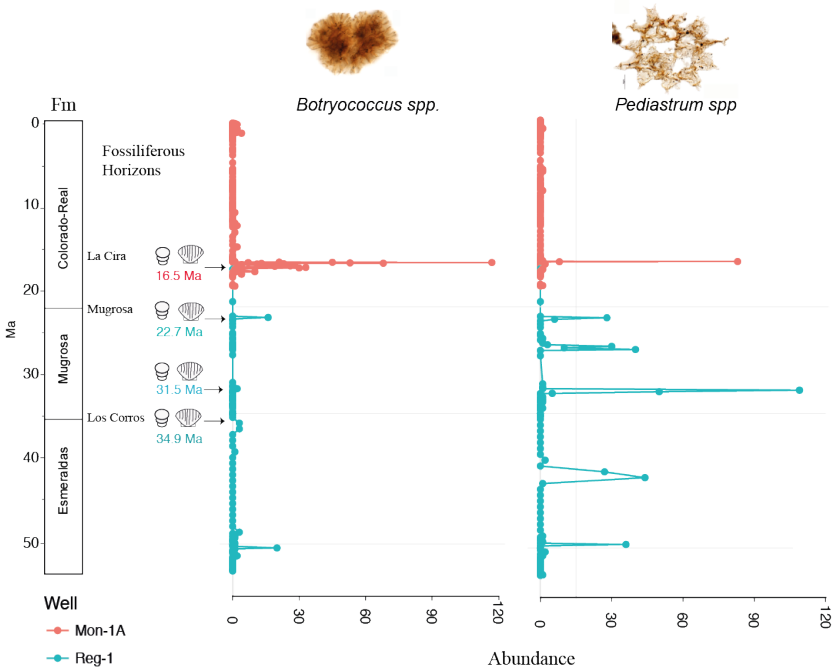

Figure 3.5: Standard reference section (SRS) for the Middle Magdalena Valley using the wells Mon-1A and Reg-1 showing the stratigraphic position and age interpretation of the shell fragments recovered during the drilling of the two wells. The age interpretation corresponds to Jaramillo et al. (2011). Right panel show the raw abundances of *Botryococcus* and *Pediastrum* through the SRS. Red and blue colors in the abundance and age panels, indicate information extracted from Mon-1A and Reg-1 respectively.

loides maristellae, and *Magnaperiporites spinousus* among others. The samples related to the Mugrosa horizon exhibit relatively high abundances of *Magnastriatites grandiosus* and *Psilatriletes 25-50um* and sporadic occurrences of *Retitricolpites simplex*, *Verrutriletes viruelensis*, *Echiperiporites akhantos*, and *Echiperiporites estelae* among others. Finally, the samples related to the Los Corros horizon present high abundances of *Psilatriletes 25-50um* and *Laevigatosporites tibuensis*, and sporadic occurrences of *Psilamonocolpites medius*, *Retitricolpites simplex*, *Rhoipites guianensis*, *Tetracolporopollenites transversalis*, *Psilamonocolpites medius*, and *Rhoipites perprolatus* among others.

A total of 127 samples distributed in five wells (Hig-1= 16 samples; Gc-1= 29 samples; Gb-1= 59 samples; Nd-1= 13 samples; Ym1= 11 samples) (Figure 3.4) from the UMV were compared with the SRS of the MMV (Figure 3.2). The samples are distributed through the Barzalosa Formation

and Honda Group. The Barzalosa Formation is represented by 92 samples distributed in the five wells while the Honda Group is represented by 35 samples distributed in two wells (Gc-1, Hig-1) (Figure 3.4). According to the well logs, the Barzalosa Formation unconformably overlies the Guaduala and Doima Formations (Paleocene and Oligocene in age) in Gc-1 and Gb-1 respectively, the Monserrate and Villeta Formations (Cretaceous in age) in Hig-1 and Ym-1 respectively, and the basement in Nd-1 (Figure 3.4). The Honda Group overlies the Barzalosa Formation in the five wells (Figure 3.4). The lithological information extracted from the well logs indicates that the Barzalosa Formation is dominated by fine grained lithologies (mainly claystones and siltstones) with sporadic intercalations of thin layers of fine grained sandstones (Figure 3.4). All the studied wells, except Hig-1, present thin coal seems that are apparently restricted to the lower part of the formation (Figure 3.4). On the other hand, The Honda Group is also dominated by fine grain lithologies (mainly claystones and siltstones) and presents a greater number of layers of sandstones than those observed in the Barzalosa Formation (Figure 3.4). No coal seams were reported in any of the wells for the Honda Group. Palynologically the samples from the UMV present a very good recovery of palynomorphs, with conspicuous abundances of *Botryococcus* and *Pediastrum* accompanied by a diverse association of pollen and spores including *Crassoretitriletes vanraadshooveni*, *Retitricolpites simplex*, *Crototricolpites annemarie*, *Echiperiporites akhantos*, *Magnastriatites grandiosus*, *Psilatriletes 25-50*, *Ranunculacidites operculatus*, *Malvacipolloides maristellae*, and *Mauritiidites francisoi var. franciscoi*, among others. Interestingly, neither microforaminifera nor dinocysts were found in any of the samples.

In the comparison between the MMV and UMV, *Pediastrum* and *Botryococcus* were discarded from the analysis to avoid the possibility that the correlations are influenced by the abundances of these two algae. However, the analysis was also done using the two algae and the results were almost identical. Only the results discarding the algae are presented. According to the maximum likelihood results (Figure 3.6) the samples related with the Barzalosa Formation present a high probability of correlation with the interval in the standard reference section (SRS) related to the la Cira Fossiliferous Horizon. This is especially evident in wells in which only samples from the Barzalosa Formation were analyzed. In Gb-1, which is the well with the most complete sampling coverage, the samples are concentrated around 16.5 Ma with the highest probabilities exhibited by those samples stratigraphically located at the lower part of the interval (Figure 3.6). In spite of their low probability values, the samples from the upper interval are also concentrated around 16.5 Ma. In the wells Nd-1 and Ym-1 the samples from the Barza-

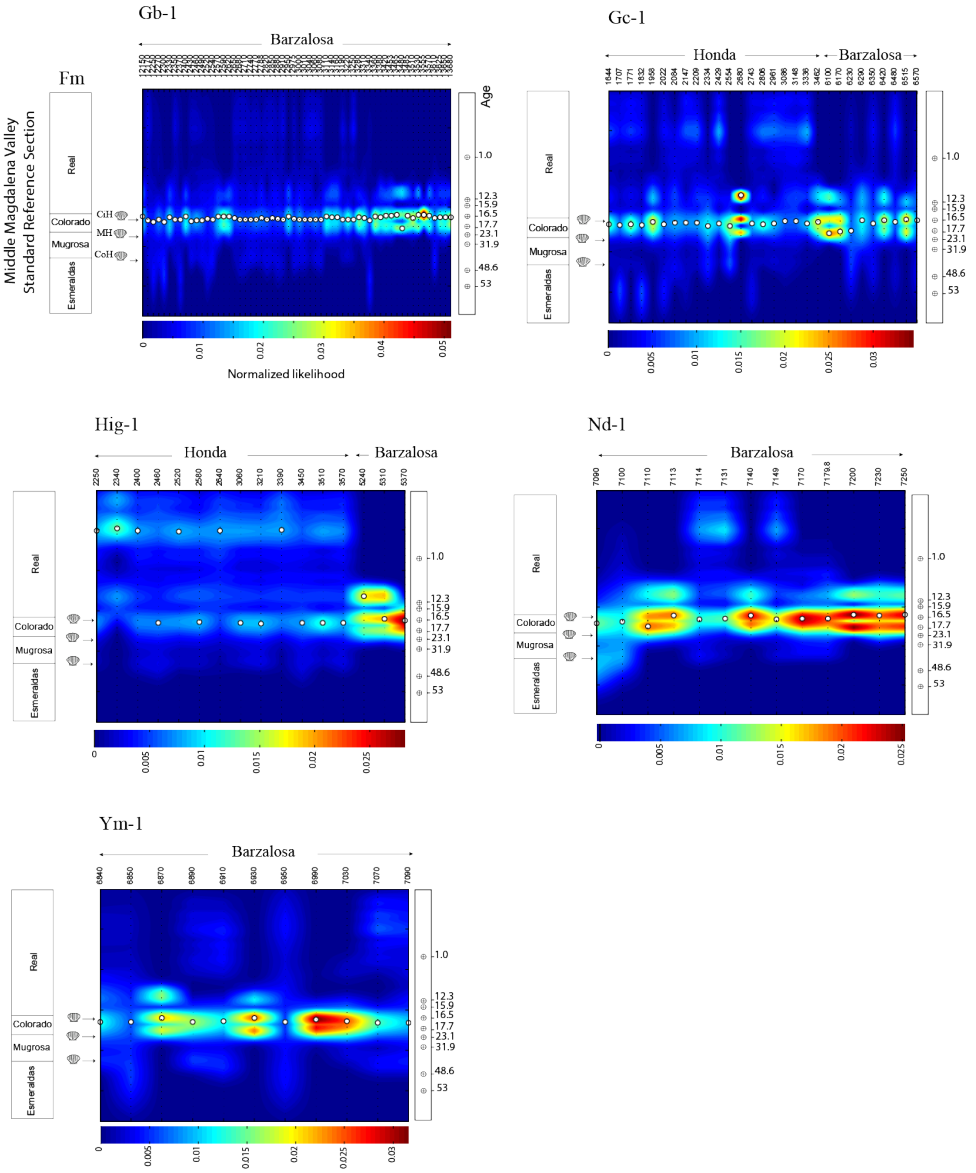

Figure 3.6: Age estimates for 198 samples distributed in five wells drilled in the Upper Magdalena Valley (UMV). Normalized likelihood values are represented by color, with higher and lower likelihood values represented by red and blue, respectively. Maximum likelihood estimates are denoted by white circles.

losa Formation show high probabilities of correlation with the interval of the SRS interpreted as deposited between 17.5 and 16 Ma approximately. This interval corresponds to the La Cira Fossiliferous Horizon. The probability values in the samples from these two wells are higher than those in Gb-1 (Figure 3.6). In Hig-1, two samples from the Barzalosa Formation show high probabilities of correlation with the interval at 16.5 Ma while the sample at 5240 feet, also from the Barzalosa Formation, exhibit a higher probability of correlation with ages younger than 12 Ma (Figure 3.6). Finally, the samples related to the Barzalosa Formation in Gc-1 exhibit high probability of correlation with the interval between 17.5 Ma and 16.5 Ma (Figure 3.6).

On the other hand, the samples from the Honda Group in the well Hig-1 exhibit in general low probability values. Some of the samples correlate with the interval associated to the La Cira Fossiliferous Horizon while other samples seems to correlate with ages younger than 1 Ma (Figure 3.6). In Gc-1, the samples from the Honda Group also exhibit low probability values that correlate with the interval between 17.5 and 16.5 Ma. However, the sample at 2860 feet exhibits a high probability of correlation with younger ages (12 Ma) (Figure 3.6).

In terms of the lacustrine-related palynomorphs the five wells from the UMV exhibit elevated abundances of algae. Figure 3.7 shows the proportion of *Botryococcus* and *Pediastrum* with respect to the total number palynomorphs (pollen and spores) for samples with counts higher than 50 palynomorphs.

The Honda Group in wells Gc-1 and Hig-1 exhibits high abundances of *Pediastrum* (Figure 3.7). In Hig-1 high abundances are specially restricted to the upper segment while in Gc-1 the high abundances are distributed through the entire interval (Figure 3.7). The Barzalosa Formation also exhibits elevated proportion of algae in the five wells (Figure 3.7). Because Gb-1 present the most complete record of the Barzalosa Formation, more than 2400 feet thick and 94 palynological samples, this well was analyzed in detail. By using the proportions of *Botryococcus* and *Pediastrum* is possible to separate three intervals in Gb-1 (Figure 3.8). The samples between 13700 and 13500 feet (Interval 1) exhibit a low proportion of lacustrine palynomorphs. *Pediastrum* dominate the association, although low proportions of *Botryococcus* are observed in some samples (Figure 3.8). The samples between 13500 and 12750 feet (Interval 2) exhibit a greater proportion of lacustrine palynomorphs and opposite to the previous interval the association was dominated almost exclusively by *Botryococcus* with sporadic occurrences of *Pediastrum* (Figure 3.8). The lacustrine proportion in samples between 12750 and 12150 feet (Interval 3) show from base to top an increasing trend with a decline toward the end of the interval (Figure 3.8).*Botryococcus* and *Pediastrum* contribute

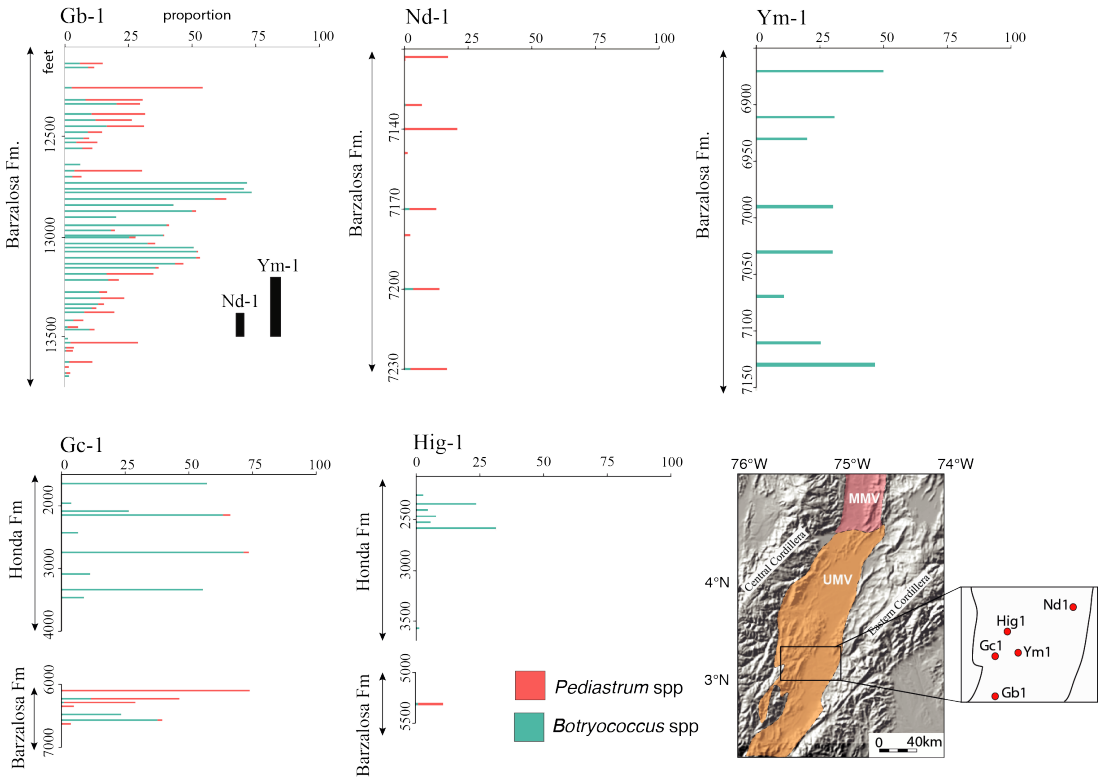

Figure 3.7: Proportion of *Botryococcus* and *Pediastrum* with respect to the total count of terrestrial palynomorphs (pollen and spores) in segments of the Barzalosa Formation and Honda Group in wells drilled in the Upper Magdalena Valley. Only samples with counts greater than 50 palynomorphs were used in the analysis. To highlight the differences in scale, Nd-1 and Ym-1 are shown at the same scale in the panel of Gb-1.

to the lacustrine component during in this interval (Figure 3.8).

The terrestrial palynological association (pollen and spores) of the three intervals in Gb-1 was determined using an indicator species analysis (De Caceres and Legendre, 2009). This analysis estimates the relationship between the species occurrence or abundance values from a set of sites or samples and the classification of the same site or samples into site groups (De Caceres and Legendre, 2012). In the case of the Gb-1, the abundance of terrestrial palynomorphs in samples with counts higher than 50 palynomorphs was used while the classification of the samples correspond to the three intervals interpreted based on the proportions of algae (Figure 3.8). A total of 72 species distributed in a 50 samples (eight samples from interval 1; 27 samples from interval 2; 15 samples from interval 3) were used in the analysis, which was

executed in the R package indicspecies (De Caceres and Legendre 2009). The results suggest that the indicator species for the interval 1 are *Rhoipites guianensis*, *Malvacipolloides maristellae*, *Echitriporites sp.*, and *Malvacidites sp.* (Figure 3.8). Although *M. maristellae* and *Malvacidites sp.* are also recorded in samples from the intervals 2 and 3, is clear that its greatest abundances occurred during the interval 1 (Figure 3.8). The intervals 2 and 3 share the indicator species *Psilatriletes < 25* and *Retitricolpites simplex var. minor.*

The abundance of these two species is very low in comparison with the indicator species of the interval 1 but they are stratigraphically restricted to the intervals 2 and 3 (Figure 3.8). The algae *Azolla* sp. is an indicator species of the interval 3, although its abundance is very low (< 10 individuals) and is also reported in one sample from the interval 2 (Figure 3.8). Other abundant terrestrial palynomorphs distributed throughout the three intervals correspond to *Laevigatosporites tibuensis*, *Magnastriatites grandiosus*, *Mauritiidites fransicoi var. minutus*, *Psilamonocolpites medius*, *Psilatriletes 25-50*, *Retitricolpites simplex*, and *Verrucatosporites usmensis* (Figure 3.8).

A transition matrix method based on Markov chain was used to analyse the depositional sequence of the three intervals of the Barzalosa Formation in Gb-1. The three intervals were defined based on the proportions of algae (Figure 3.8). The interval 1 between 14295 and 13480 feet includes the base of the formation, which does not present palynological analysis and therefore is not shown in the figure 3.8. The intervals two and three were interpreted between 13480 and 12750 feet and between 12750 and 12060 feet respectively (Figure 3.8). The three transitions matrices were tested for randomness using the quasi-independence model implemented in the software Strati-Signal (Ndiaye, 2007). The computed chi-square from the intervals one and three exceeds the critical chi square suggesting that the data do not appear to be random. The data from the interval two do not exceed the critical value suggesting therefore randomness (interval 1: critical X2 at 95% confidence level: 11.07, computed X2: 19.0; interval 2: critical X2 at 95% confidence level: 11.07, computed X2: 1.6; interval 3: critical X2 at 95% confidence level: 3.8, computed X2: 4.7). The significant transitions for the three intervals were obtained using the Walker method (Walker, 1979) at the 99% confidence level. The probability, random and walker matrices are presented in the Tables 3.1, 3.2, and 3.3, while the results are shown as lithology relationships diagrams (LRD) in the Figure 3.8. In the LRD, two given lithologies are linked with an arrow showing the probability, greater than random, to pass from one lithology to another. When transitions are simultaneously from A to B and from B to A, we say that A-B transition is cyclical. When transitions only go from A to B, the transition is referred as simple.

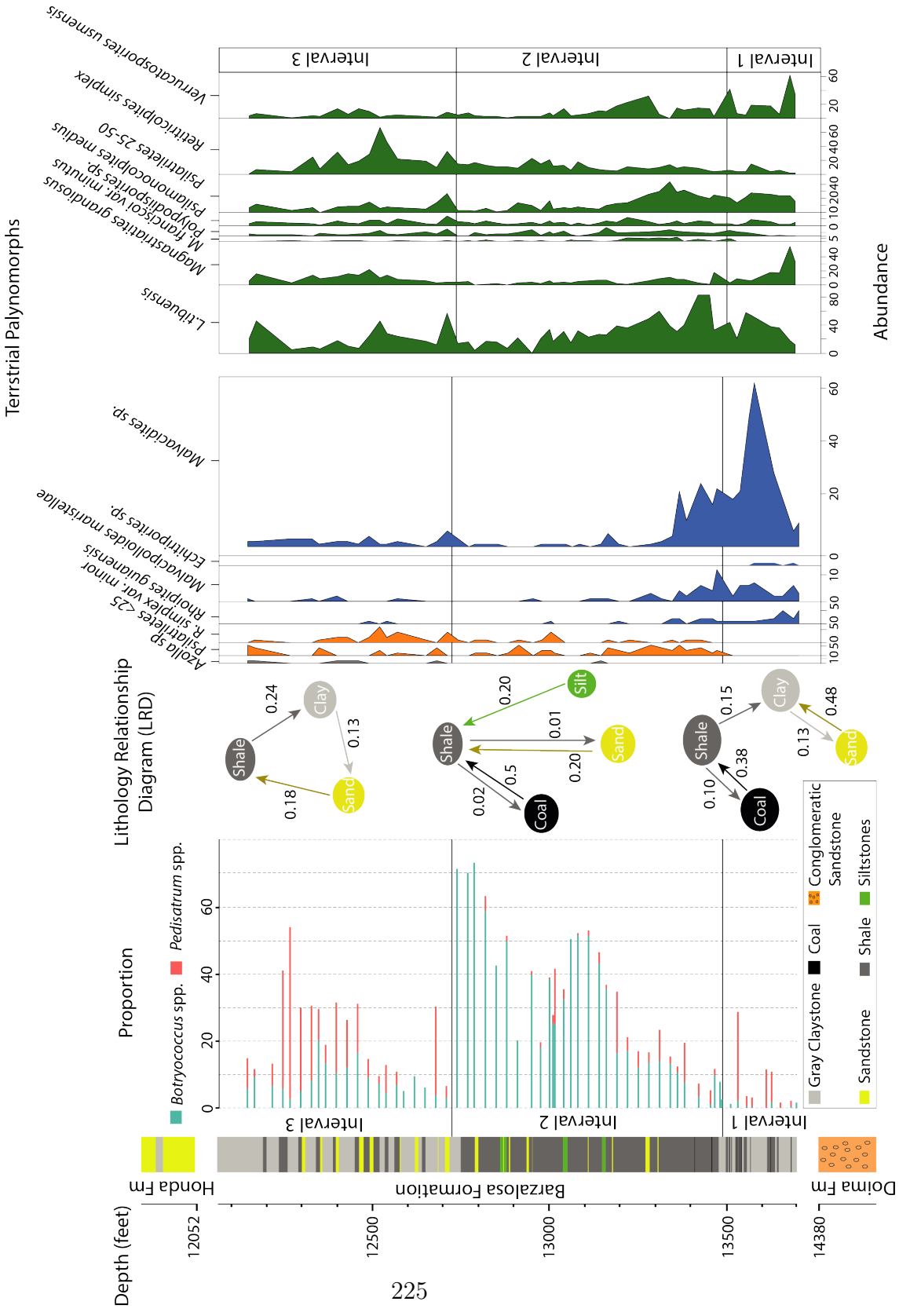

Figure 3.8: Subdivision of the Barzalosa Formation in Gb-1 based on the proportion of algae, lithology and palynological composition (see text for explanation).

Table 3.1: Probability, Random and Walker matrices for the interval 1 (14295-13480 feet) of the Barzalosa Formation in Gb-1 (GC: Gray Claystone; Sd: Sandstone).

Litho	**Probability Matrix**				**Random Matrix**				**Walker Matrix**			
	GC	Shale	Coal	Sd	GC	Shale	Coal	Sd	Gc	Shale	Coal	Sd
GC	0	0.35	0.17	0.47	0	0.41	0.25	0.33	0	-0.63	-0.073	0.13
Shale	0.7	0	0.3	0	0.54	0	0.19	0.25	0.15	0	0.10	-0.25
Coal	0.33	0.66	0	0	0.48	0.28	0	0.22	-0.15	0.38	0	-0.22
St	1	0	0	0	0.51	0.30	0.18	0	0.48	-0.30	-0.18	0

Table 3.2: Probability, random and Walker matrices for the interval 2 (13480-12750 feet) of the Barzalosa Formation in Gb-1 (GC: Gray Claystone; Sd:Sandstone).

Litho	**Probability Matrix**				**Random Matrix**				**Walker Matrix**			
	Shale	Coal	Sd	St	Shale	Coal	Sd	St	Shale	Coal	Sd	St
Shale	0	0.15	0.61	0.23	0	0.13	0.6	0.26	0	0.02	0.01	-0.03
Coal	1	0	0	0	0.5	0	0.3	0.15	0.5	0	-0.34	-0.15
Sd	0.88	0	0	0.11	0.68	0.1	0	0.21	0.20	-0.10	0	-0.09
St	0.75	0	0.25	0	0.54	0.08	0.37	0	0.20	-0.08	-0.12	0

Table 3.3: Probability, random and Walker matrices for the interval 3 (12750-12060 feet) of the Barzalosa Formation in Gb-1 (GC: Gray Claystone; Sd:Sandstone).

Litho	**Probability Matrix**			**Random Matrix**			**Walker Matrix**		
	GC	Shale	Sd	GC	Shale	Sd	GC	Shale	Sd
Gray Clay	0	0.41	0.58	0	0.55	0.45	0	-0.13	0.13
Shale	0.81	0	0.18	0.57	0	0.42	0.24	0	-0.24
Sd	0.33	0.66	0	0.52	0.47	0	-0.18	0.18	0

For the interval 1, the LRD shows two cyclical transitions (Shale-Coal and Gray claystone -Sand) and one simple transition (Shale-Clay) (Figure 3.8). The transitions with the highest probability of occurrence are sandstone to gray claystones and shale to coal. The sandstone and coal are not shown in the stratigraphic column of the Figure 3.8 because they occur below the interval with palynological analysis, which was not included in the figure. In terms of thickness and number of layers, the dominant lithology in the interval 1 is gray claystone (Table 3.5). For the interval 2, the LRD suggest two cyclical transitions (Shale-Coal, Shale-Sandstone) and one simple transition (Silt-Shale) (Figure 3.8). These transitions are random according with chi-square test. The transitions with the highest probability of occurrence are coal to shale, silt to shale and sandstone to shale. In terms of thickness and number of layers, the dominant lithology in this interval is shale (Table 3.6). For the interval 3, the LRD suggest a single transition sequence (Shale-Clay-Sandstone-Shale) (Figure 3.8). The transition with the highest probability of occurrence is shale to clay followed by sandstone to shale and clay to sandstone. In terms of thickness and number of layers, the dominant lithology in this interval is Gray Claystone (Table 3.7).

3.3.2 Flooding events during the Cenozoic

To facilitate the interpretation of the flooding events and explore their geographic distribution, each site and therefore their correspondent samples were assigned to specific geographic regions (Figure 3.3). The indices estimated for each individual sample were plotted against geological time with the colors representing the geographic areas (Figure 3.9, 3.14, 3.20). To further explore the spatial distribution of the floods, each geographic area was plotted individually (Figures 3.10 and 3.15 and 3.21). In this case the colors represent the age interval of the samples. The results are presented first for each index and subsequently a comparison is made between them.

3.3.2.1 Marine Events

The salinity index (SI) estimated for all the samples indicates the influence of marine conditions in specific intervals of time (Figure 3.9). The colors also reveal that the high SI values are concentrated in specific geographic areas (Figures 3.9, 3.10). The interpreted marine incursions, labelled with the letter **m** followed by a number (e.g.: event m1), are discussed below.

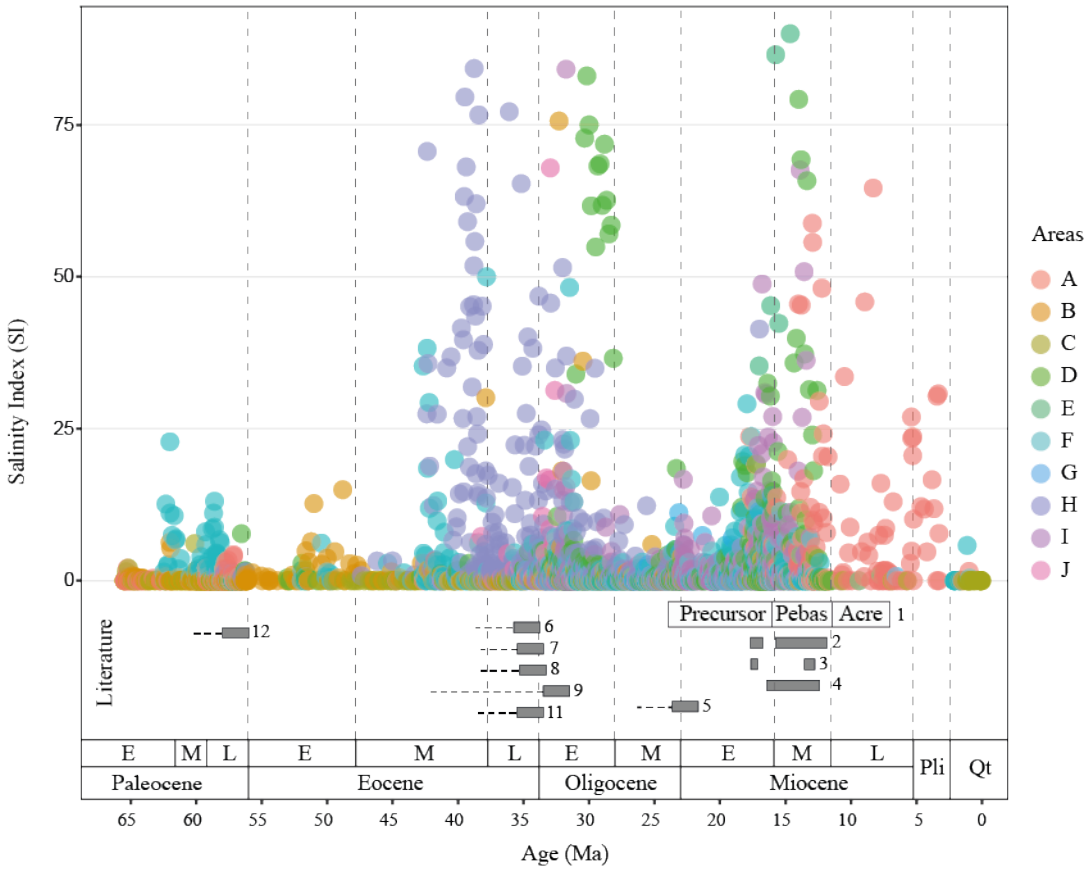

Figure 3.9: Salinity index (SI) during the Cenozoic. Each circle represents a single sample with the colors indicating the geographic areas (A to J) where the samples were taken (the location of the areas is presented in Figure 3.3) The lower panel show the most relevant marine-lacustrine episodes in northern South America described in the literature ((1) Wesselingh et al. (2010), Hoorn et al. (2010c) showing the three precursor, the Pebas and the Acre phases; (2) (3) Jaramillo et al. (2017); (4) Olaya (1997), Ramirez (1998); (5) Gomez et al. (2005); (6) Rodriguez et al. (2012); (7) Cooper et al. (1995); (8) Villamil (1999); (9) Jaramillo and Dilcher (2001); (10) Ochoa et al. (2012); (11) Louterbach et al. (2014)).

Paleogene Events

Event m1: The oldest of the incursions seems to have occurred during the middle Paleocene (Figure 3.9; Figure 3.10 event m1). This event is mainly detected in the area F where two distinct episodes can be interpreted (Figure 3.10). The first occurred approximately between 63 and 61 Ma and

the second between 59.5 and 58 Ma. Both episodes are characterized by relatively low SI values and are almost exclusively represented by samples belonging to a single well located in the area F (Bue-H15, Annex 3.1). Samples from this age located in the area H show no evidence of marine influence while only a few samples from the areas A, B, C, and D reveal very low SI values (Figure 3.10). The marine contribution to the samples from BueH15 comes mainly from moderate to low abundances of dinocysts belonging to the genera *Achomosphaera*, *Spiniferites*, *Hystrichosphaeridium*, *Circulodinium*, *Leptodinium*, *Cribroperidinium*, *Albertidinium*, *Cleistosphaeridium* and *Impletosphaeridium* (Jaramillo et al., 2011). When it is compared with information from the literature, the event m1 shows a good chronostratigraphic correspondence with the marine incursion in the Madre de Dios basin of Peru described by Louterbach et al. (2014) (Figure 3.1).

Event m2: From the early to the mid part of the middle Eocene most of the samples exhibit SI values equal to zero with exception of a short time interval between 52.5 and 48.5 Ma where a few samples (approximately 10) exhibit low SI values (2.5 to 15) (Figure 3.10, event m2). Most of these samples are located in the area B (Figure 3.10) where the marine contribution comes from microforaminifera and dinocysts of the genus *Homotryblium*, *Lingulodinium*, and *Hystrichokolpoma*. Other areas with samples from this age (C and H) present SI values equal to zero, suggest the absence of marine influence (Figure 3.10). However the number of samples in these areas is very low preventing a more accurate interpretation.

Event m3: The interval between the middle Eocene (approx. 43.5 Ma) and the early Oligocene (approx. 28 Ma) exhibits a high proportion of samples with elevated SI values (Figure 3.9). A closer inspection of the geographic areas allows the interpretation of two episodes of marine influence (events m3 and m4, Figure 3.10) that are separated by the interval between 38 and 35 Ma, where the marine influence is subtle and apparently restricted to the area H (Figure 3.10). The SI pattern of the area H suggests that the event m3 occurred between 43.5 and 38 Ma approximately. A close inspection of this interval (Figure 3.11) reveals that the marine influence was especially strong and constant in the area H while in the area F was restricted to the interval between 43.5 and 42 Ma. The areas B, C, D shows no evidence of marine influence during the entire interval (Figure 3.11). For the event m3, the sections with the highest SI values correspond to Cano Sagu and Cano las Blancas for the area H and Medina, Bue-3Cor and RiCh-1 for the area F (Table 3.4). The marine component of the event m3 is the result of the

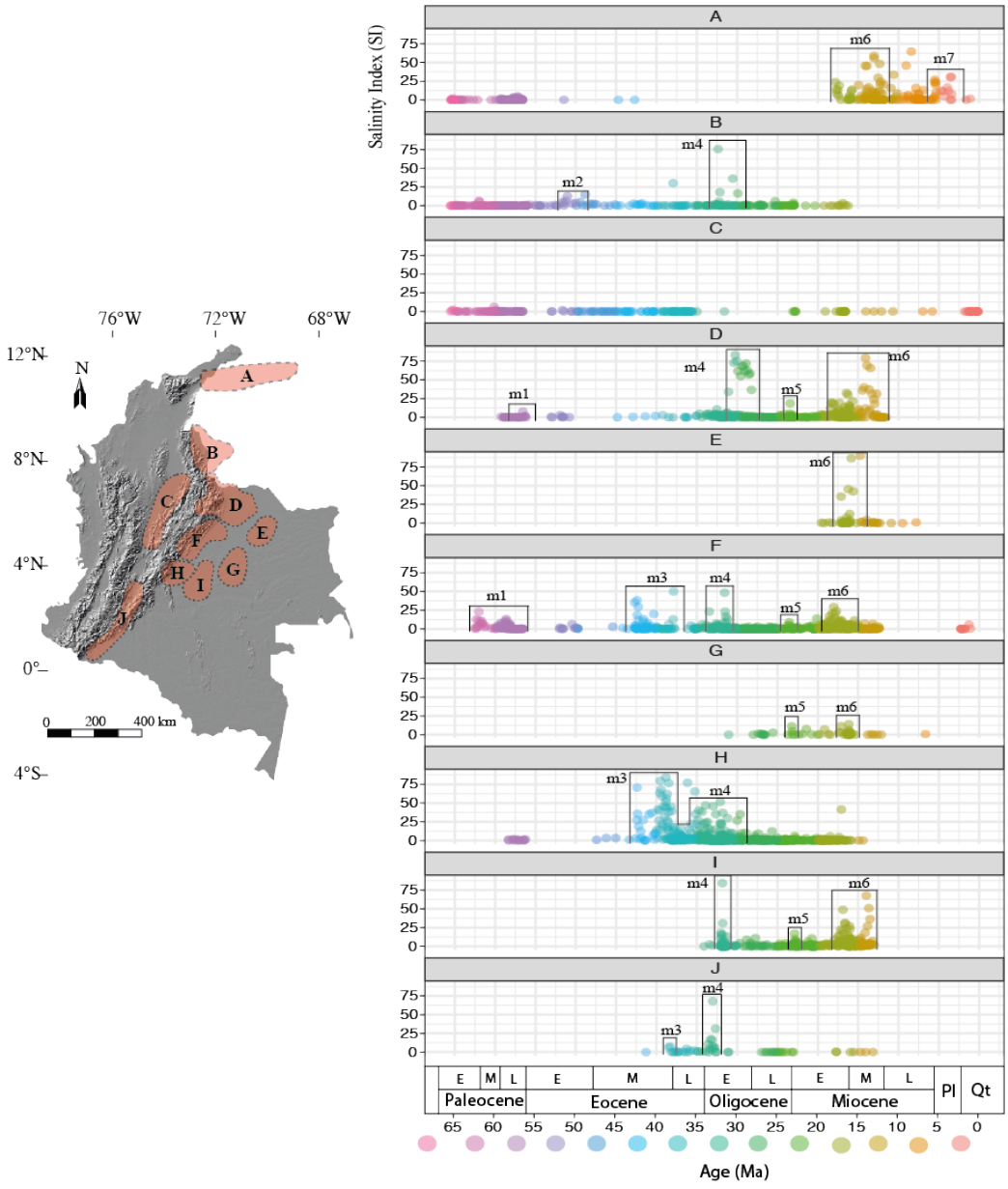

Figure 3.10: Salinity index (SI) during the Cenozoic discriminated by the geographic areas shown in the map. The intervals interpreted as marine incursions are labelled with the letter m (marine) and a number (e.g: m1). The colors of the circles represent the age interval of the samples.

contribution of a diverse association of dinocysts (approx. 36 species) and abundant microforaminifera. The most abundant dinocysts includes species of the genus *Homotryblium*, *Polysphaeridium*, *Cleistosphaeridium*, *Achomo-*

sphaera, *Cordosphaeridium*, *Hystrichokolpoma*, *Operculodinium*, *Glaphyrocysta*, *Dyphyes*, and *Dapsilidinium* that are accompanied by less abundant individuals of the species *Apteodinium* sp., *Cordosphaeridium fibrospinosum*, *Hystrichokolpoma rigaudiae*, *Lejeunecysta hyaline*, *Impagidinium* sp., *Lingulodinium machaerophorum*, and *Polysphaeridium zoharyi*.

Event m4: Event m4, also well evidenced in the area H, is interpreted to have occurred between 35 and 28 Ma approximately (Figure 3.10). Apart from the area H, this event is also well recorded in the areas B, D, I, F and H. The temporal distribution of the samples showing marine influence in the different areas suggests that the beginning and end of this episode could be either diachronous or that the south and north areas were affected by different incursions (Figure 3.11). The samples from the area H show signals of marine influence from 35 to 31 Ma while the samples from the area D show absence of marine influence during this interval but a clear increase in the SI between 30.5 and 28 Ma (Figure 3.11). The SI pattern observed in the areas B, F, I and J and F corroborate that the younger incursion occupied the south and central regions while that the second pulse apparently was restricted to the northern region (Figure 3.11). The summary of the sections discriminated by regions indicates that in the area H, the highest SI values are found in the wells Chac-1, Nines-1, Cus-2 and Fon-1 (Annex 3.3). The other sites exhibit in general low SI mean values with exception of the sites Mag-1 and Os-1 in the areas D and I with means of 33.64% and 18.38% respectively (Annex 3.3). The marine component of the oldest pulse (35 to 31 Ma) is the result of the contribution of dinocysts belonging to the genus *Achomosphaera*, *Polysphaeridium*, *Nematosphaeropsis*, *Lingulodinium*, *Operculodinium*, *Spiniferites* and *Hystrichokolpoma* and moderate abundances of microforaminifera. The marine component in the younger pulse (30.5 to 28 Ma) is the result of the contribution of abundant microforaminifera mainly and sporadic occurrences of dinocysts of the genus *Achomosphera*, *Polysphaeridium*, *Tuberculodinium*, and *Operculodinium*.

Neogene Events

Event m5: A short and almost imperceptible increase in SI is observed near the Oligocene-Miocene boundary (event m5, Figure 3.10). A close inspection of the areas B, D, F, G and H reveals low SI values prior to the end of the Oligocene (Figure 3.12). During the early Miocene (23-19 Ma) the SI values are in general very low with a subtle increase toward the end of the interval (Figure 3.12). The low number of samples does not allow a more precise interpretation for this event.

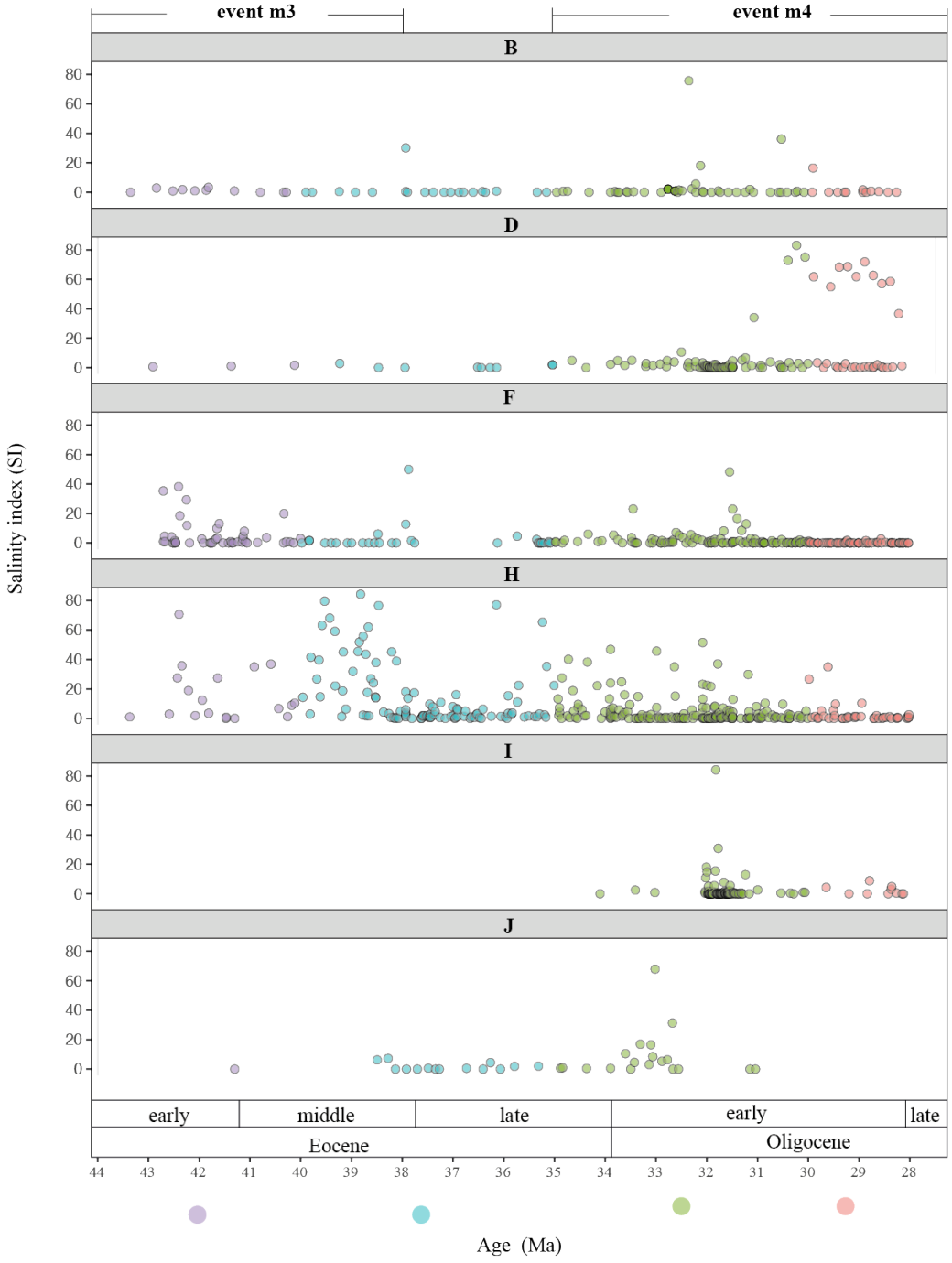

Figure 3.11: Salinity index (SI) for the event m3 in selected areas. The location of the areas is presented in Figure 3.3.

Table 3.4: Salinity index summary for the sections (wells and outcrops) located in the areas F and G for the interval between 43.5 and 38 Ma (Max SI = maximum SI value; Min Si = minimum SI value; Mean SI = mean SI value; SD SI = standard deviation of the SI).

Name	Area	# Samples	Max SI	Min SI	Mean SI	SD SI
Bue-3Cor	F	26	38.2	0	3.7	8
Cus-5	F	2	4.5	0.7	2.6	2.6
Medina	F	15	35.3	0	4.7	9.8
RiocCh-1	F	17	29.3	0	3.52	8
Cano las Blancas	H	16	70.6	4.2	30.6	18.6
Cano Sagu	H	22	84.2	3.1	42.3	23.1
Chac-1	H	5	0.59	0	0.2	0.2
Cor-1	H	1	1.8	1.8	1.8	NA
Cris-1	H	1	2.9	2.9	2.9	NA
Fon-1	H	3	14.6	2.2	8.5	6.1
Nuesp-1	H	5	3.4	0.9	2	1
Past-4	H	4	1.1	0	0.4	0.5
S-17	H	2	4.8	1.7	3.2	2.2
SanJ-1	H	2	13.9	6.2	10.1	5.3

Event m6: A very important and widely distributed marine incursion event (or events) occurred between 20 and 12 Ma (event m6, Figure 3.10). During this period, several authors have suggested the occurrence of marine incursions and/or development of lacustrine systems (Hoorn et al., 2010 and references there in). Jaramillo et al. (2017) studying a sediment-core called Saltarin, proposed the occurrence of two separate marine episodes, which are illustrated for comparison purposes at the bottom of the Figure 3.13. The first incursion occurred between 18.1 and 17.2 Ma and the second between 16.1 and 12.4 Ma (Jaramillo et al., 2017) (Figure 3.13). They are separated by a 1.1 Ma interval (between 17.2 and 16.1 Ma) where no marine influence was reported (Jaramillo et al., 2017). The results of the present study suggest that the first marine incursion (MMI) interpreted from Saltarin (Jaramillo et al 2017) started approximately 0.5 Ma earlier (18.5 Ma) in the areas D and F (Figure 3.13). The end of the MMI incursion in Saltarin is characterized by sustained low SI values lasting for approximately 1.1 Ma. The areas F and H support the lack of marine influence while oppositely elevated SI values in D, I, and E suggest the persistence of the marine influence in these areas (Figure 3.13). The marine component of the areas D, E, and I, comes mainly from the contribution of abundant microforaminifera and sporadic low abundances of dinocysts belonging to the genus *Operculodinium*, *Spiniferites*, *Polysphaeridium*, *Lejeunecysta*, and *Selenopemphix* among others. The second marine

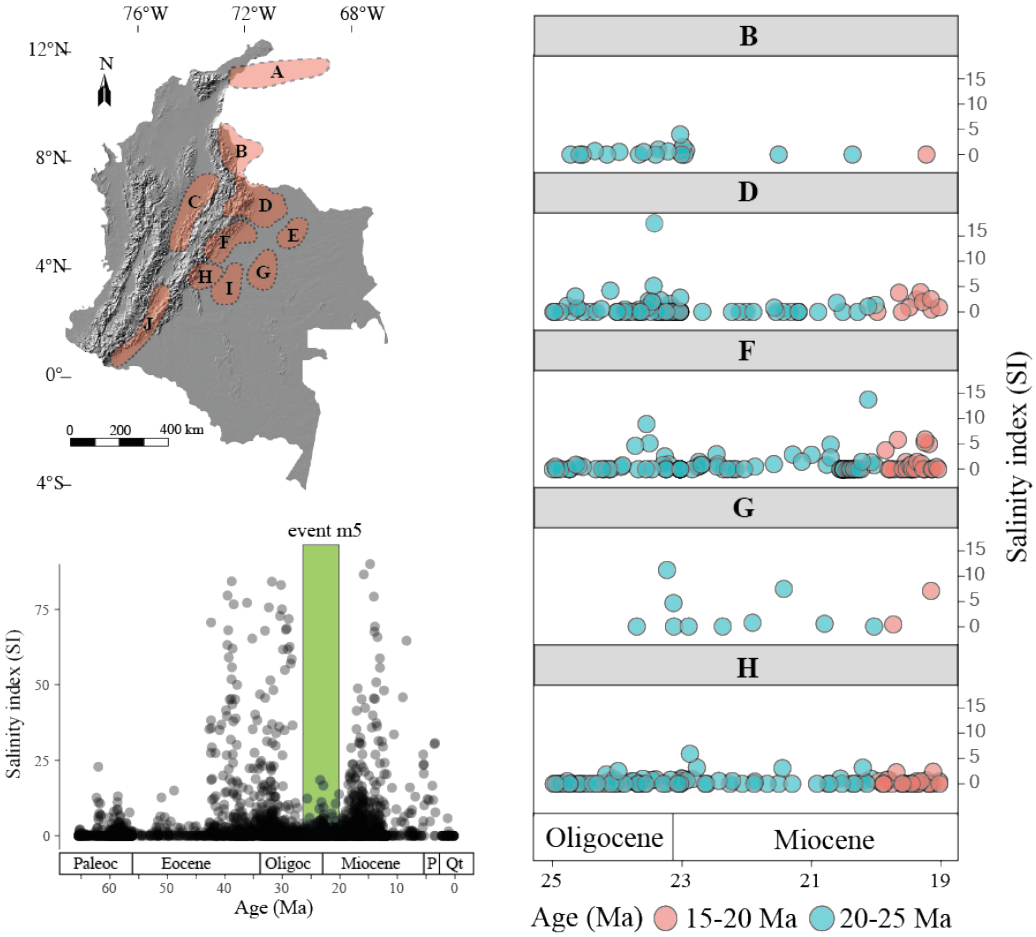

Figure 3.12: Salinity index (SI) for the event m5 in selected areas.

incursion (EMI) interpreted from Saltarin (16.1 to 12.4 Ma) (Jaramillo et al., 2017) is well evidenced in most of the areas of the present study (Figure 3.13). The most noticeable differences are the beginning of the incursion, which is younger in the areas A, I, and D and the absence of marine influence in the areas E and F (Figure 3.13). The marine component in the areas A, I and D comes mainly from the contribution of abundant microforaminifera and low abundances of dinocysts species of the genus *Achomosphaera*, *Lejeunecysta*, *Lingulodinium*, *Operculodinium*, *Polysphaeridium*, *Quadrina*, *Selenopemphix*, *Spiniferites*, and *Tuberculodinium*.

Event m7: Another marine incursion occurred during the Pliocene and is recorded by several samples in the area A (event m7, Figure 3.10). These samples correspond exclusively to two sections (Urumaco West and Uru-

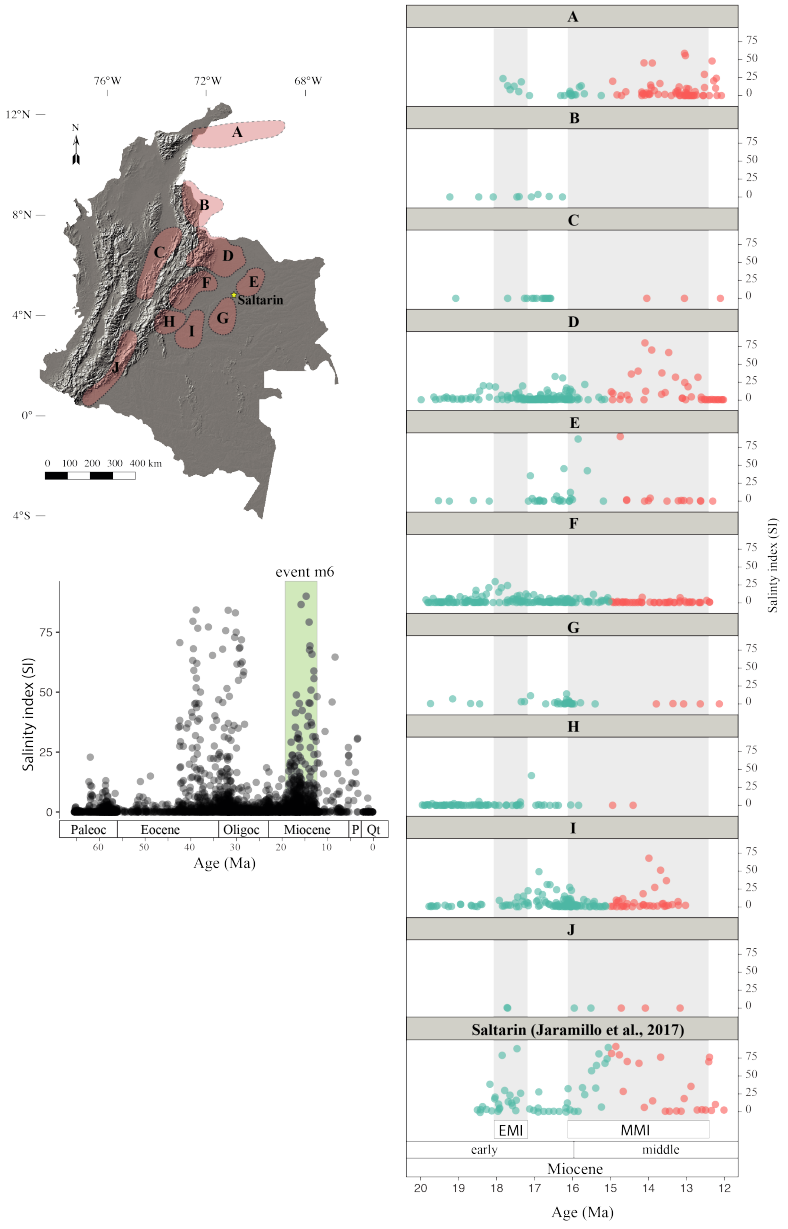

Figure 3.13: Salinity index (SI) for the event m6 in all the areas. For comparison the two marine excursions (EMI: Early Miocene Incursion and MMI: Middle Miocene Incursion) interpreted in Saltarin by Jaramillo et al. (2017) are indicated. The colors of the points indicate the age range of the samples (blue: 19 to 15 Ma; red: 15 to 12 Ma).

maco East) studied by Jaramillo et al. (2011). The marine component in these samples comes from the contribution of abundant microforaminifera

and low abundances of dinocysts abundances of the genus *Tubercolodinium*, *Selenopemphix*, *Operculodinium*, *Trinovantedinium*, *Polysphaeridium*, and *Spinifertites* among others. The low number of samples in the other areas prevents to establish the occurrence of marine conditions outside the area A (Figure 3.10).

3.3.2.2 Lacustrine Events

The lacustrine index (LI) estimated for all the samples indicates the influence of lacustrine-brackish conditions in specific time intervals (Figure 3.14). The colors of the circles reveal that the highest LI values are concentrated in specific geographic areas (Figure 3.14, 3.15). Because the lacustrine events are in general locally restricted, for their interpretation they were not separated in Paleogene and Neogene events. The lacustrine events were labelled with the letter **l** followed by a number (e.g.: event l1) as discussed below.

Event l1: The youngest lacustrine event is interpreted to have occurred during the Paleocene (event l1, Figure 3.15). Unfortunately, the low number of samples in most of the areas during this interval produces a patchy record, which makes reliable interpretation difficult. The most complete record, observed in area B, suggests the occurrence of two possible events that are separated by an interval (between 61.5 and 59.5 Ma) where no lacustrine influence is detected in any of the areas (Figure 3.16). The first lacustrine episode occurred between 65.5 and 62 Ma and the second between 59.5 and 56 Ma (Figure 3.16). The lacustrine component in the area B for the two intervals comes mainly from elevated abundances of the alga *Pediastrum* and very limited and sporadic contributions of *Botryococcus*. The second episode (59.5 -56 Ma) is well evidenced in the area H where, similar to the area B, the algal association is mostly dominated by *Pediastrum*.

Event l2: A very short lacustrine event seems to have occurred during the early Eocene (between 50 and 52.5 Ma approximately) (event l2, Figure 3.15). This event is mainly evidenced in the area D, where *Pediastrum* dominates the lacustrine association. The presence of moderate abundances of *Pediastrum* is common in samples of the areas B and C (Figure 3.15). During the early and middle part of middle Eocene, the number of samples is relatively low, with exception of the areas B and C where the LI indicates very poor to null influence of lacustrine conditions (Figure 3.15).

From the upper part of the middle Eocene to the late Miocene (40 Ma to 10 Ma) the LI pattern (Figure 3.17) suggests that in general the lacustrine

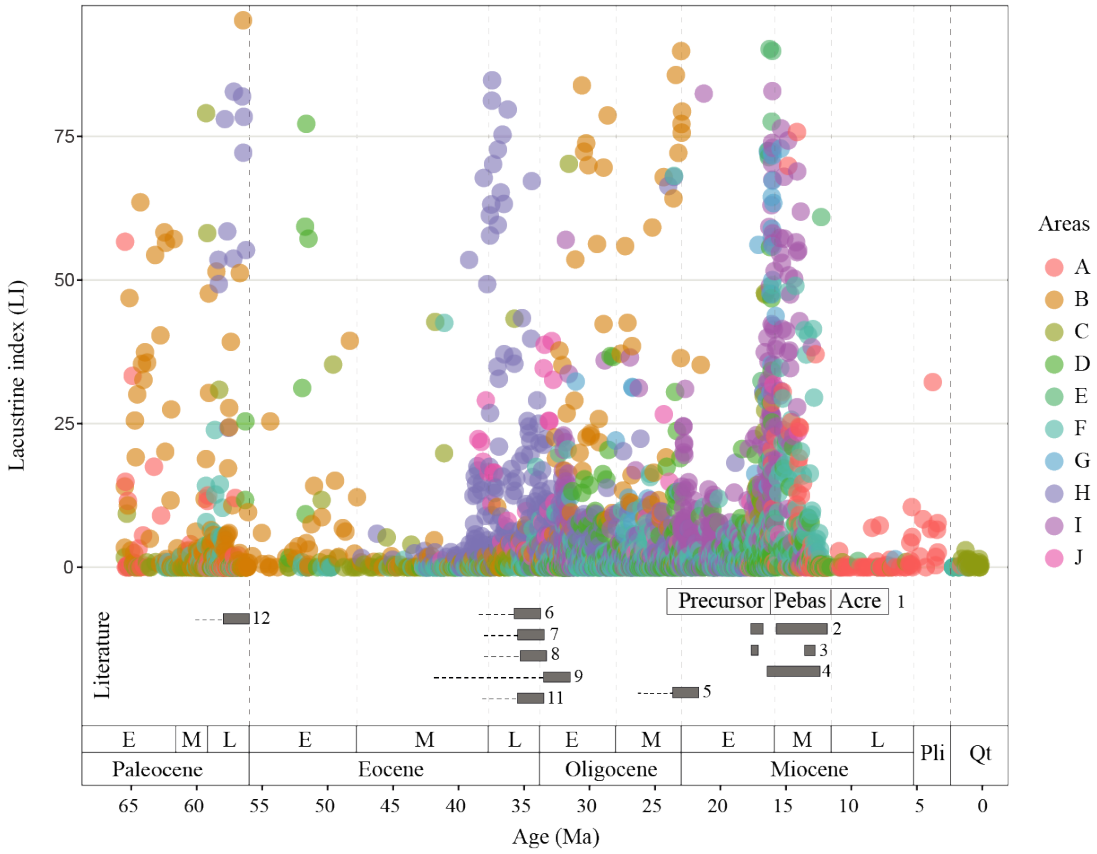

Figure 3.14: Lacustrine index (LI) during the Cenozoic. Each circle represents a single sample with the colors indicating the geographic areas where the samples were taken. The lower panel show the most relevant marine-lacustrine episodes in northern South America described in the literature ((1) Wesselingh et al. (2010), Hoorn et al. (2010c) showing the three precursor, the Pebas and the Acre phases; (2) (3) Jaramillo et al. (2017); (4) Olaya (1997), Ramirez (1998); (5) Gomez et al. (2005); (6) Rodriguez et al. (2012); (7) Cooper et al. (1995); (8) Villamil (1999); (9) Jaramillo and Dilcher (2001); (10) Ochoa et al. (2012); (11) Louterbach et al. (2014)).

events were local rather than regionally distributed. Nonetheless it is possible to differentiate at least three wide intervals in which different lacustrine events can be interpreted (Figure 3.17).

Event l3: During the first interval, between 39 and 32 Ma (Figure 3.17), the area H presents elevated SI values, especially between 38 and 36 Ma (event l3, Figures 3.15 and 3.17). In spite of their low number of samples,

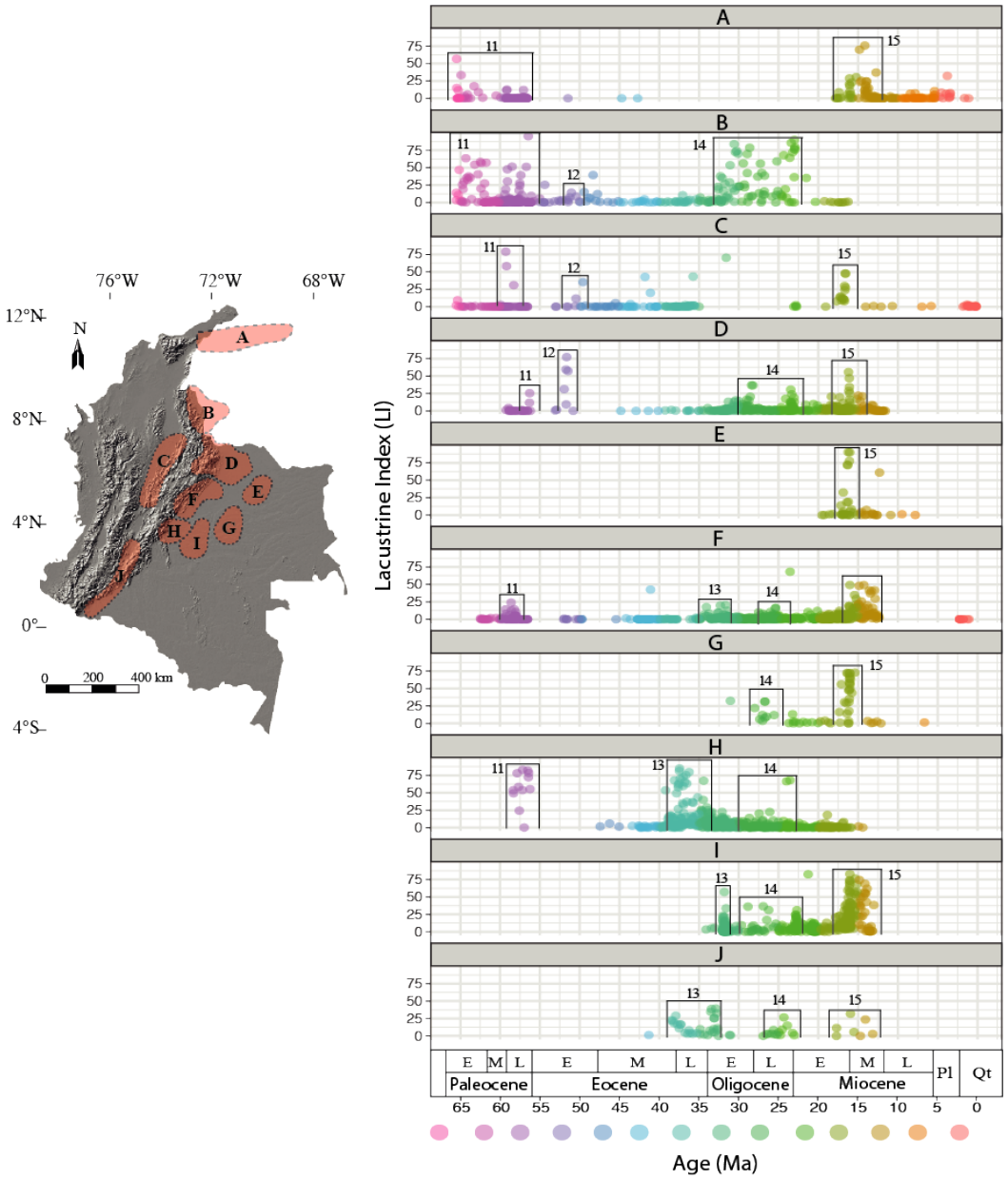

Figure 3.15: Lacustrine index (LI) during the Cenozoic discriminated by geographic areas. The intervals interpreted as influenced by lacustrine conditions are labelled with the letter l (lacustrine) and a number. The colors of the circles represent the age interval of the samples.

the areas F, I, and J, seem to indicate the influence of lacustrine conditions toward the south. On the other hand the areas located toward the north

(B, C, and D) show no evidence of lacustrine influence during this interval (Figure 3.17). The main contributor of the lacustrine component in most of the samples in the area H corresponds to *Botryococcus* with only a few samples exhibiting low proportions of *Pediastrum* (Figure 3.18). Botryooccus is also the most abundant algae in samples from the areas J and I. On the other hand, the lacustrine influence is evident in those areas located toward the north, especially in B where most of the samples exhibit very high SI values during the entire interval (Figures 3.15 and 3.17). The area D also shows evidence of lacustrine influence but it is especially concentrated at the beginning and end of the interval l4 (Figure 3.17). Interestingly, the areas B and D did not show evidence of lacustrine influence during the previous interval (event l3, Figure 3.17). Unfortunately, the lack of samples in the areas A, C, and E prevent to establish the regional extension of the lacustrine influence toward the north. The lacustrine component in area B comes mainly from the high abundance of *Botryococcus*.

Event l4: During the second interval, between 32 and 22.5 Ma (event l4, Figure 3.17), the areas located toward the center and south (F, G, H, I and J) shows a clear decrease in the SI, although a moderate to low lacustrine influence is still detected in short and specific intervals (Figures 3.15 and 3.17).

Event l5: During the third interval, between 18 and 12.5 Ma (event l5, Figures 3.15 and 3.17), most of the areas exhibit elevated SI values. However a close inspection of the figure 3.9, reveal subtle differences in the intensity and duration of the lacustrine influence between the areas (Figure 3.17). The beginning of the influence is well recorded in the area I, where outstanding SI values are observed from 18 Ma and the highest values are detected between 16 and 14 Ma (Figure 3.17). The same pattern is observed in the areas F and A, where the elevated number of samples allows having a complete record for this interval. On the other hand, the areas with low numbers of samples partially corroborate the lacustrine influence. It is difficult to test whether these areas were either under prolonged lacustrine influence like in I, F, and A, or if the influence was restricted to short periods of time, due to the low number of samples. The lacustrine component of the areas A, F, G, and I come mainly from the abundances of *Botryococcus*, although in some samples *Pediastrum* seems to dominate the lacustrine association (Figure 3.19). Finally, between 12.5 and 0 Ma most of the areas are characterized by an absence of samples. The exception is the area A in which the SI of a couple of samples suggests subtle lacustrine influence during the Pliocene

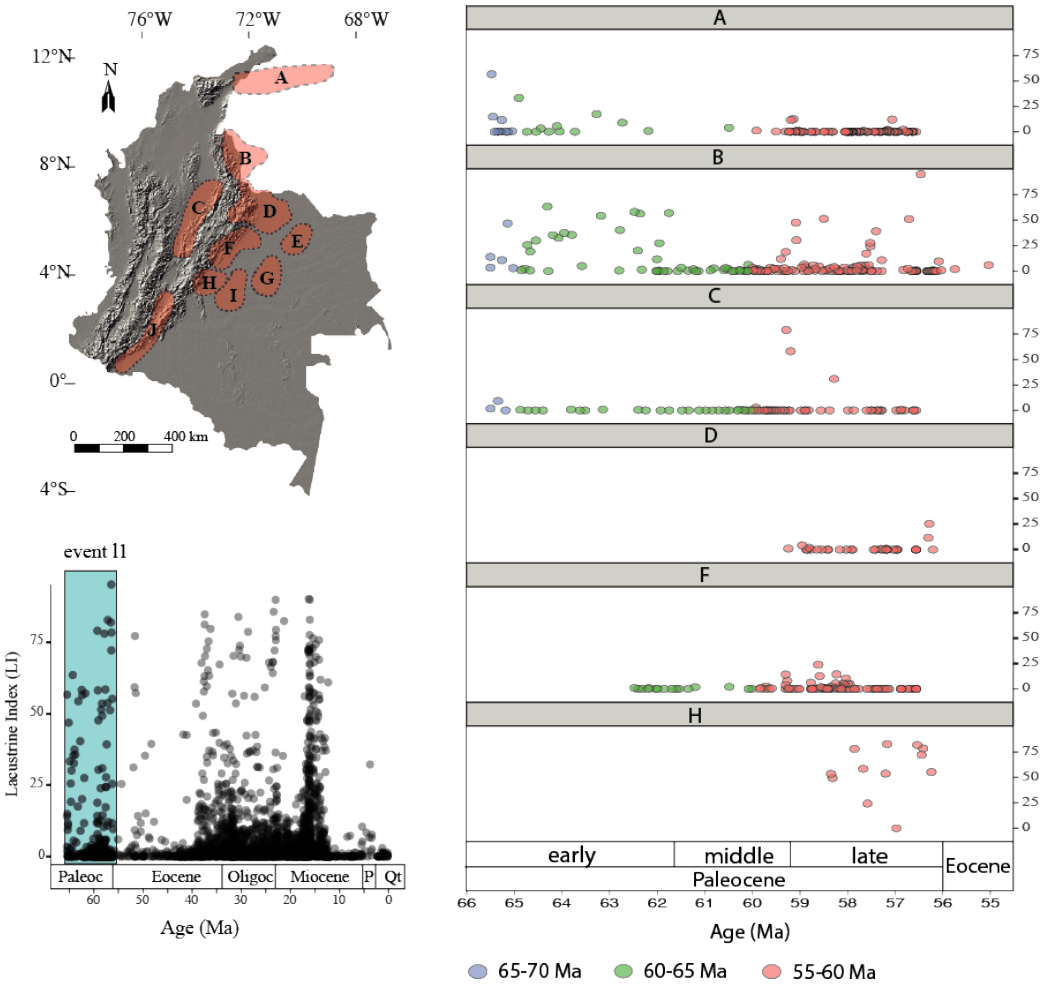

Figure 3.16: Lacustrine index (LI) for the event l1 in selected areas.

(Figure 3.15).

3.3.2.3 Mangrove Forest

The mangrove index (MI) indicates the development of mangrove vegetation in specific areas and during relatively short intervals of time (Figure 3.20). The areas C, E, G, I, and J present in general very low MI values (< 3) (Figure 3.20) suggesting the absence of mangrove forests in these areas. However, the reduced number of samples in some intervals may be affecting their detection. The areas with elevated MI indicate at least four intervals of mangrove development. These intervals are denoted with the letters **mg** (mangrove) and a number (e.g. mg1) (Figure 3.21).

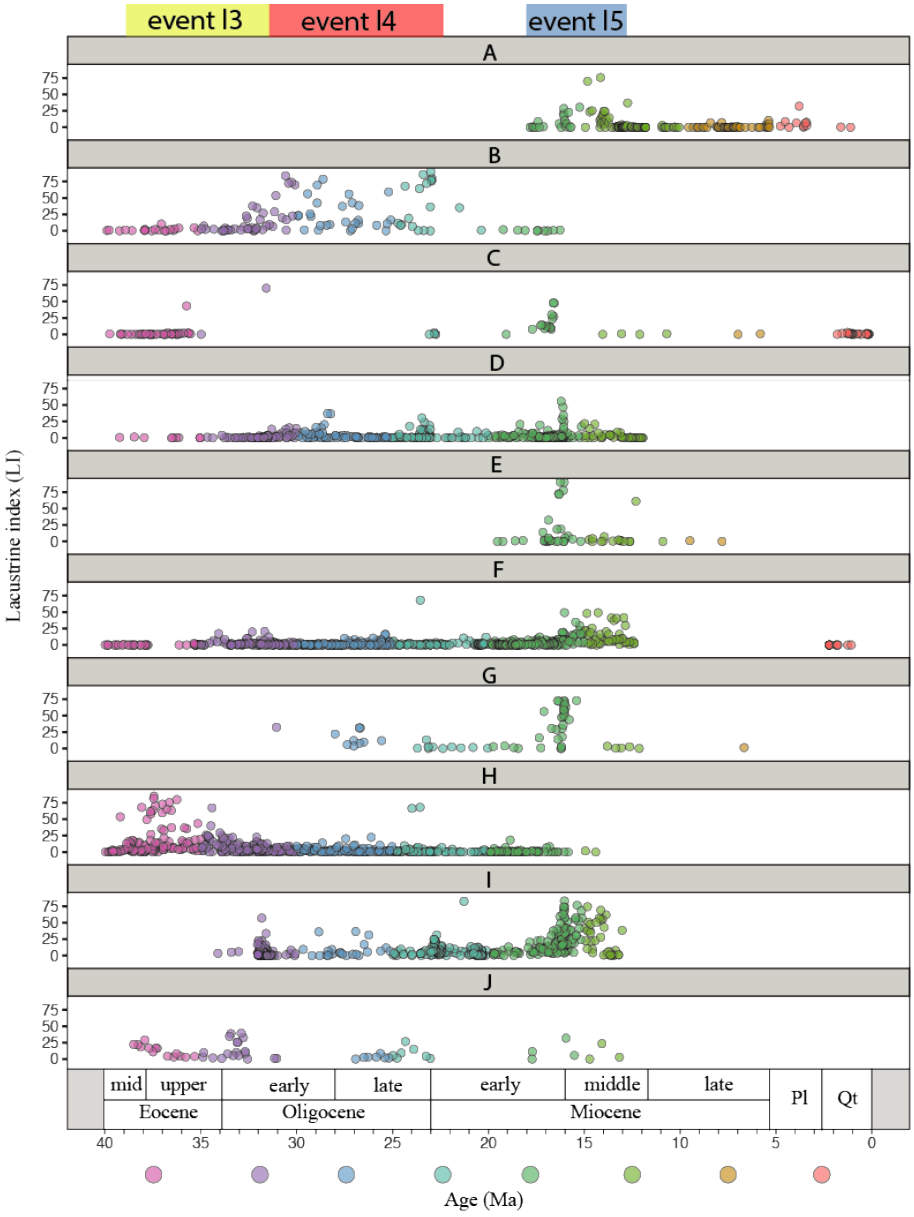

Figure 3.17: Lacustrine index (LI) for the interval between 40 Ma and Present showing the events l3, l4, and l5. The location of the areas is presented in Figure 3.3.

Event mg1: The first interval (mg1) occurred between the early to middle Paleocene and is recorded in area B (Figure 3.21). The samples from this area show moderate MGI values (< 10) with a sample reaching a maximum value of 20. The mangrove association is composed exclusively by species of

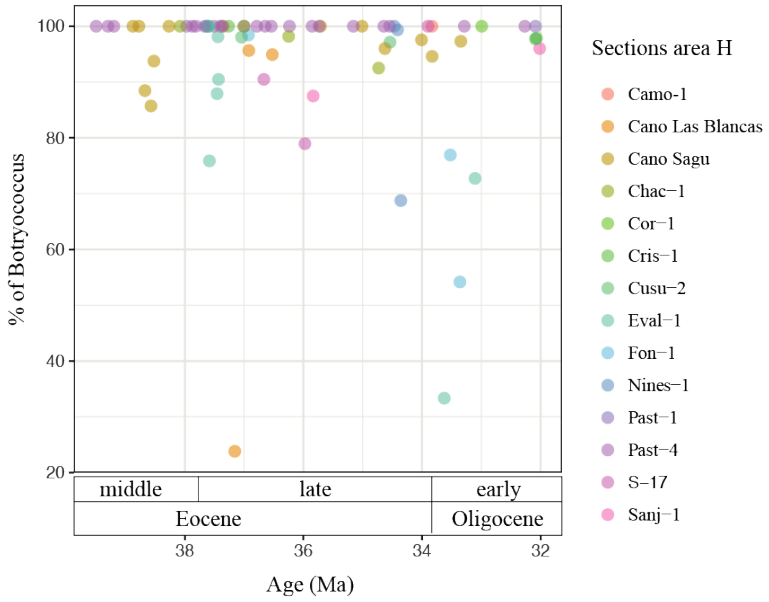

Figure 3.18: Proportion of *Botryococcus* abundance with respect to the total abundance of lacustrine elements (*Pediastrum* + *Botryococcus*) for the interval between 39 and 32 Ma, discriminated by sections of the area H. Only samples with counts higher than 20 lacustrine palynomorphs were used in the analysis.

the genus *Spinizonocolpites*.

Event mg2: The second interval (mg2) occurred at the end of the middle Eocene, approximately between 43 and 37.5 Ma (Figure 3.21). This interval is evidenced in the areas F and H with samples reaching moderate MGI values (< 20). The mangrove component in these two areas corresponds mainly to the contribution of species of the genus *Spinizonocolpites* and *Lanagiopollis* and sporadic low abundances of species of the genus *Zonocostites*.

Event mg3: The interval mg3, between 34 and 30 Ma (Figure 3.21), is well evidenced in the area D and partially in the area B (Figure 3.21). In these two areas, the mangrove association correspond almost completely to species of the genus *Lanagiopollis*.

Event mg4: Finally, during the late early Miocene and middle Miocene the areas F and A show evidences of mangrove vegetation (mg4). The evidence in the area F is very subtle and is apparently restricted to the interval between 19 and 16 Ma (Figure 3.21). In this area, species of the genus *Lanagiopollis*

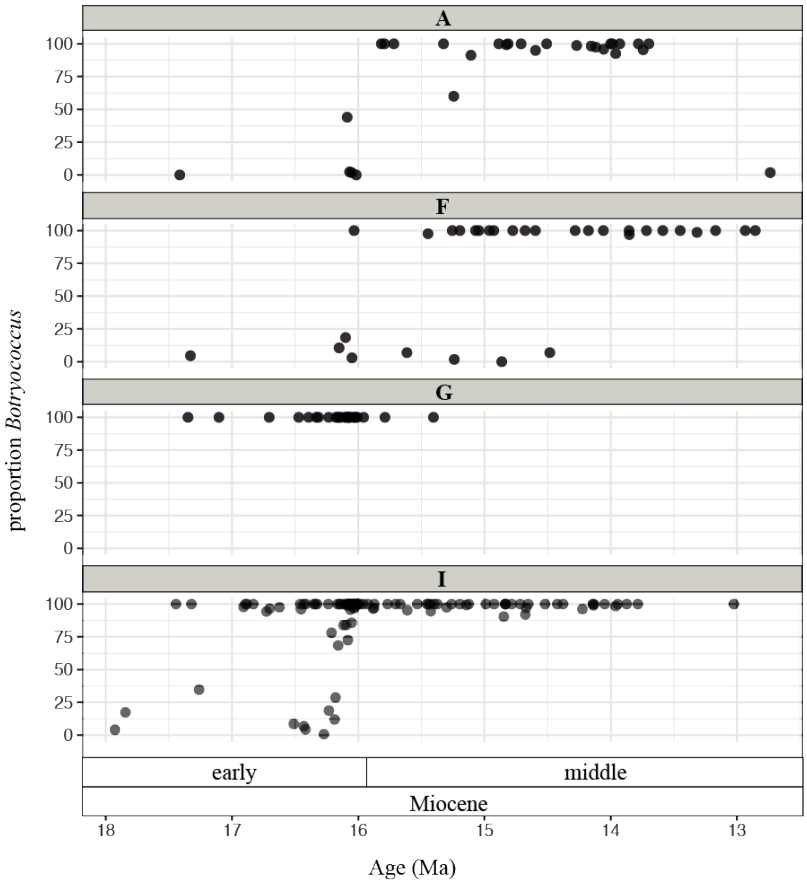

Figure 3.19: Proportion of *Botryococcus* abundance with respect to the total abundance of lacustrine elements (*Pediastrum* + *Botryococcus*) for the interval between 18 and 13 Ma, discriminated by geographic areas. Only samples with counts higher than 20 lacustrine palynomorphs were used in the analysis.

and *Zonocosites* dominate the mangrove association. On the other hand, a few samples in the area A exhibit MGI values between 20 and 80 in the interval between 14 and 10 Ma (Figure 3.21).The mangrove association in this area is dominated by species of the genus *Zonocostites* and spontaneous occurrences of species belonging to the genus *Lanagiopillis*.

3.4 Discussion

The palynological record of northern South America reveals the occurrence of several flooding episodes during the Cenozoic. The abundance of paly-

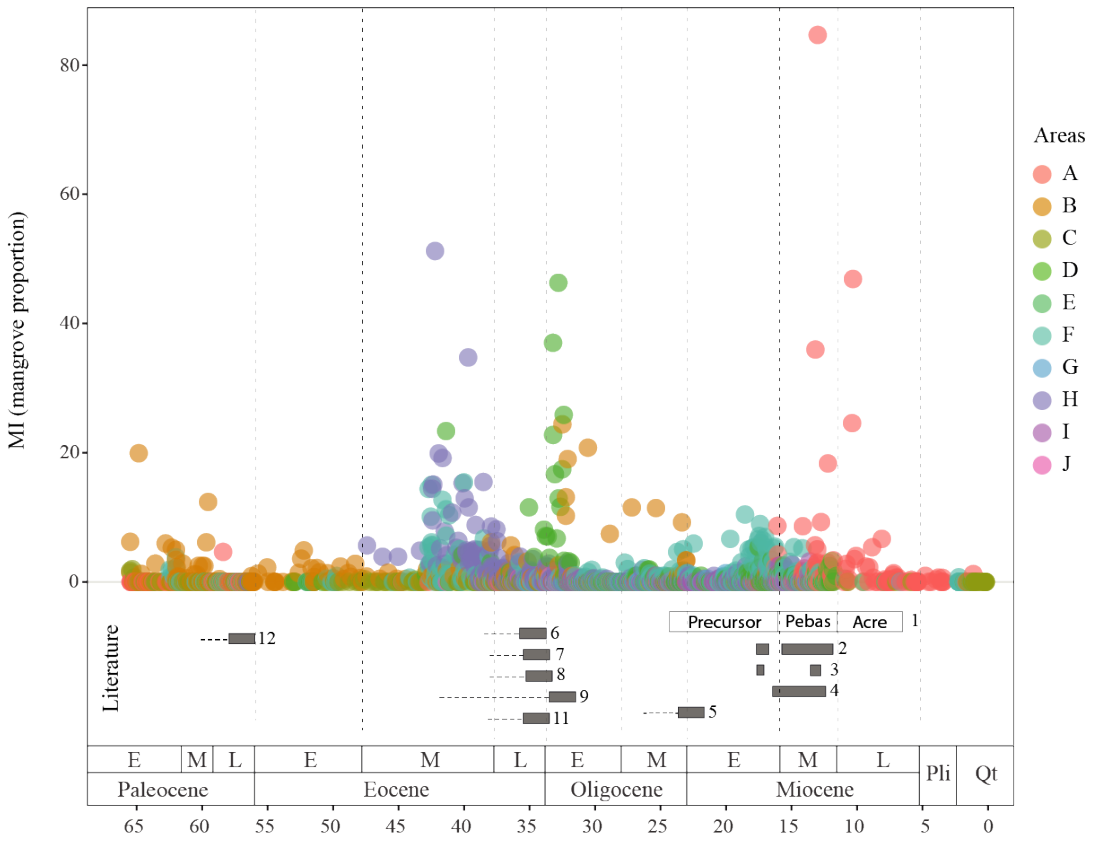

Figure 3.20: Mangrove vegetation index (MGI) during the Cenozoic. Each circle represents a single sample with the colors indicating the geographic areas where the samples were taken. The lower panel show the most relevant marine-lacustrine episodes in northern South America described in the literature ((1) Wesselingh et al. (2010), Hoorn et al. (2010); (2) (3) Jaramillo et al. (2017); (4) Olaya (1997), Ramirez (1998); (5) Gomez et al. (2005); (6) Rodriguez et al. (2012); (7) Cooper et al. (1995); (8) Villamil (1999); (9) Jaramillo and Dilcher (2001); (10) Ochoa et al. (2012); (11) Louterbach et al. (2014)).

nomorphs characteristic of specific environments of deposition (dinoflagellates, microforaminifera, algae and pollen and spores) allows differentiation between marine incursions, intervals of lacustrine/brackish influence and the development of mangrove forests. The results reveal that the different floods are not only temporal but also spatially restricted. The nature of these restrictions may be imposed by the sampling coverage, which is poor in some geographic areas and intervals, and so did not always allow us to establish the temporal and geographic range of the events with certainty. This uncertainty

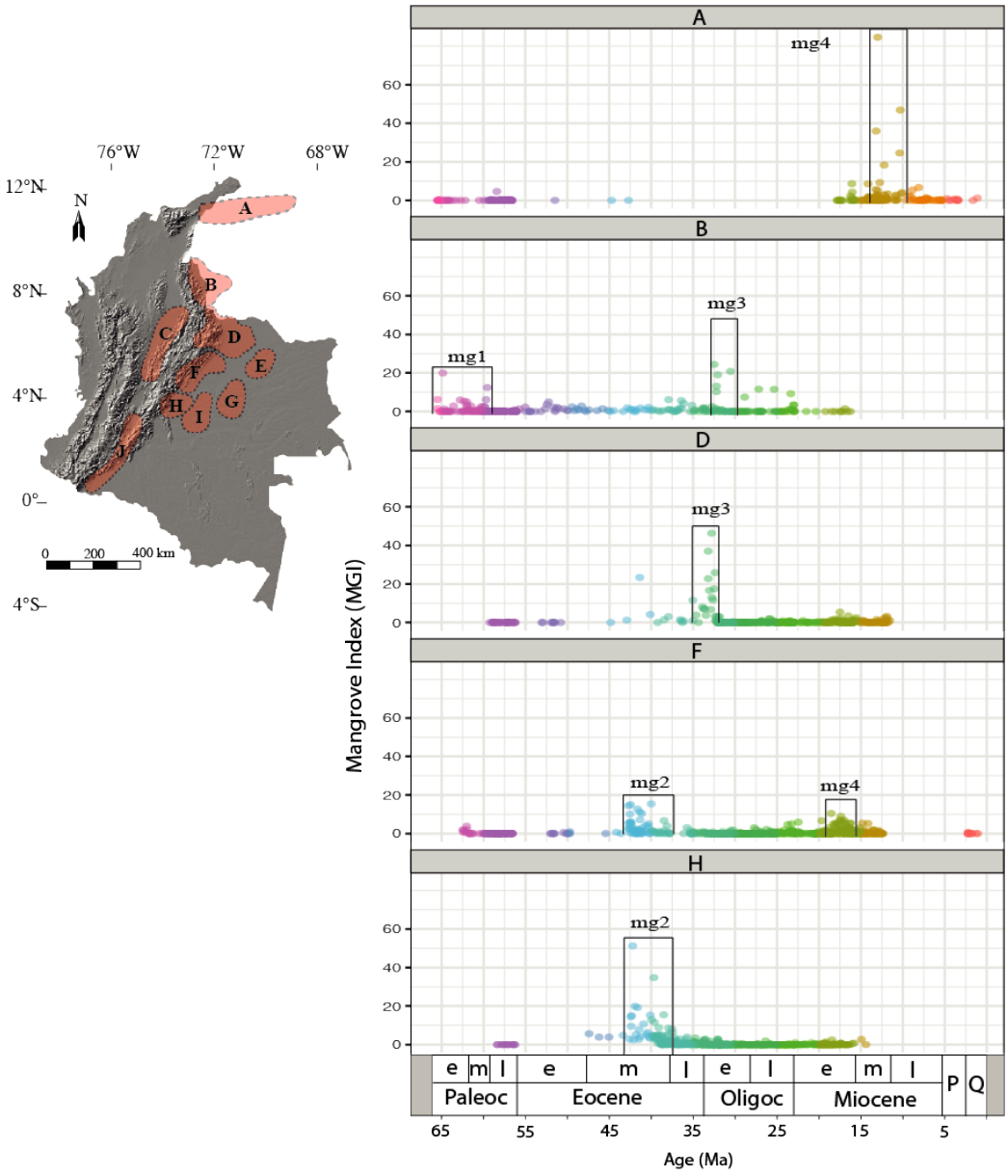

Figure 3.21: Mangrove vegetation index during the Cenozoic discriminated by geographic areas. The intervals interpreted as mangrove vegetation are labelled with the letters mg (mangrove) and a number. The colors of the circles represent the age interval of the samples.

can only be solved by the inclusion of new samples in those intervals and areas with poor sampling coverage. The results also show an important variability of the salinity, lacustrine and mangrove index (SI, LI, and MGI respectively)

in samples of similar age and from same geographic region. This variability makes it difficult to interpret some of the floods, because not always the samples in a flooding interval preserve palynomorphs indicative of the event. On the other hand it suggests that the over short intervals of time, the environmental conditions responsible of the floods were intermittent rather than continuous. This interpretation has at least two practical implications. First, it shows that in order to increase the chance of identifying flooding events using palynology it is necessary to analyse a considerable number of samples distributed, if possible, over small geographic areas (similar to the geographic areas defined in the present work, e.g. A, B, C, etc.). Second, a complete understanding of the paleogeography of the floods requires an adequate geographical coverage with enough palynological information. In this way it is possible to establish with certainty if two areas were influenced by similar environmental conditions. Other geological information, like seismic interpretation, geochemistry, and well logs among others, has been widely used in the study of the marine-lacustrine incursions (Reyes-Harker et al., 2015; Jaramillo et al., 2017; Duarte et al., 2017; Caycedo et al., 2017), especially to delimit their geographical extent. Although this information is very useful and should be incorporated whenever it is possible, it should be interpreted with caution when no paleontological information is available. The reason is that different environmental conditions (e.g. lacustrine, brackish, marine) are able produce similar sedimentological patterns that could be difficult to distinguish by methods that rely in the contrast between lithologies.

3.4.1 Flooding events during the Cenozoic

The salinity index (SI) suggests the occurrence of at least seven episodes of marine incursion during the Cenozoic (Figure 3.10). The regional coverage and temporal duration of some of these incursions are difficult to assess due to poor sampling coverage. The marine incursions m1, m2, m5, and m7 (Figure 3.10) are a good example of this difficulty. They were detected in only few areas and in general they are characterized by low SI values (between 10 and 25). Although the present evidence suggests that the events m1, m2, m5, and m7 were short in duration and spatially restricted, they also seem to be independent events rather than the continuation of the more regionally distributed events (m3, m4 and m6). With the incorporation of new information, the distribution and duration of these events will be better understood and with this knowledge they potentially can become recognized intervals for regional correlations.

The lacustrine index (LI) suggests the occurrence of at least five intervals during the Cenozoic in which lacustrine conditions were established in several

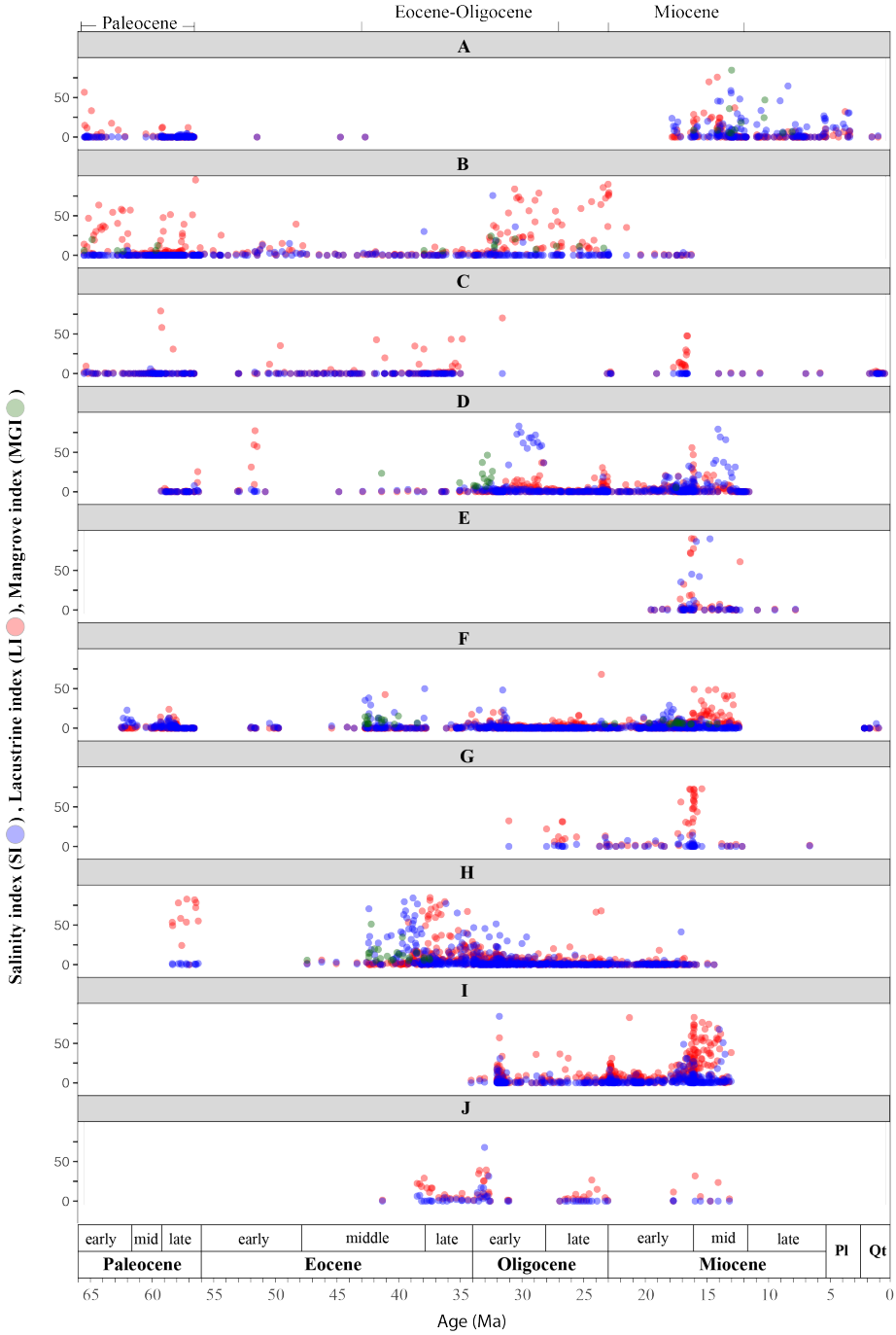

Figure 3.22: Salinity (blue), Lacustrine (red) and Mangrove (green) indices during the Cenozoic discriminated by geographic areas. The location of the areas is presented in Figure 3.3.

geographic areas (Figure 3.15). Similar to the marine incursions, the temporal and geographic distribution of the lacustrine influence is sometimes difficult to establish due to the poor sampling coverage that characterizes some of the intervals. When the SI and LI are compared (Figure 3.22) most of the lacustrine events show a close relationship with the marine incursions. Episodes of marine influence seem to be followed by episodes on lacustrine influence. Interestingly whenever this is the case, the lacustrine association is almost dominated by *Botryococcus*. This relationship is very clear for example in the area H in which the two marine incursions of the middle-late Eocene and early Oligocene (events m3 and m4, Figure 3.10) are separated by an interval of marked lacustrine influence (Figure 3.22). This relationship is also very evident during the Miocene. The two episodes of marine influence occurred at the late early Miocene and middle Miocene, are clearly separated by a period of lacustrine influence in the area I (Figure 3.22). The same lacustrine influence is well evidenced in the areas G, F, E, D, C, and A. An exception to the relationship between the marine and lacustrine events is detected during the Paleocene, in which the influence was essentially lacustrine (Figure 3.22). Interestingly and opposite to those intervals with close marine-lacustrine relationships in which *Botryococcus* dominated the lacustrine association, during the Paleocene, *Pediastrum* was the dominant alga. Although the marine events m1, m2, m5, and m7 are geographically and temporal restricted, they also show the influence of lacustrine conditions (Figure 3.22).

Finally, the mangrove index (MGI) suggests the occurrence of four intervals during the Cenozoic in which mangrove forests were established (Figure 3.21). Each of these intervals is evidenced in one or maximum two sites suggesting a geographic restriction to the development of this type of vegetation. When compared with the SI and LI, the MI is also closely related to the marine and lacustrine events.

The integration of the three indices (SI, MI, and MGI) suggest than rather than isolated events, the intervals exhibiting marine, lacustrine and mangrove influence (with exception of the Paleocene event) are closely related and therefore they can be interpreted as phases of the same process that caused the floods. According to this reasoning, the main episodes are interpreted below.

3.4.1.1 Paleocene

The palynological record of the Paleocene toward the north (especially in area B) (Figure 3.22) suggests the occurrence of two intervals with intense lacustrine influence. These two intervals lasted for the entire early Pale-

ocene and late Paleocene (Figure 3.22). A detailed taxonomical study by Pinzon (2011) based on samples from sections of the areas A and B, indicate that the lacustrine association is dominated by elevated abundances of *Pediastrum boryanum var. boryanum* and low abundances of *Pediastrum duplex var. duplex* (Pinzon 2011). At present these two species are cosmopolitan and dominate eutrophic reservoirs of temperate zones (Komarek and Jankovska, 2001). The Paleocene record in the areas located in East of the Llanos Foothills (J, H, F, and D, Figure 3.22) is patchy and incomplete because of a regional unconformity that separates different parts of the Paleocene and early Eocene (Reyes-Harker et al., 2015). On the other hand, the areas I, G and E (Figure 3.22) are geographically located toward the east of the stratigraphic pinchout or erosional truncation interpreted by Reyes et al. (2015) for the Paleocene and therefore they do not preserve sediments of this age. However, the area H and to a lesser extent the areas D and F show evidence of lacustrine influence during the late Paleocene toward the south (Figure 3.22). Louterbach et al. (2014), by studying several outcrops located in the Madre de Dios sub- Andean zone of Peru (Figure 3.1), used evidence based on facies analysis, organic geochemistry and Nd-Sr isotopic to suggest the presence of a tide-dominated shallow marine environment during the Paleocene in the western Amazonian foreland basin. The authors suggest three facies associations related to a tide-dominated estuary debouching into a shallow marine bay or lagoon. The first facies corresponds to the filling of a tide-influenced meandering channel formed in the fluvial-tidal transition zone. The second facies is related to more distal tidal-flats and saltmarsh deposits and the third facies correspond to a stressed shallow marine environment such as a bay or lagoon (Louterbach et al., 2014). Although the age of this marine incursion is not completely solved, the authors suggested either a Danian (lower Paleocene) or more likely a Thanetian (late Paleocene) age. In this sense, the marine event reported in the south of Peru is correlative with at least one of lacustrine episodes reported in the present study. The pathway of this marine incursion is still unclear. Louterbach et al. (2014) suggested a southern connection with the Atlantic Ocean (Bolivia-Argentina). However, this interpretation was mainly based on the information available at the time that suggested an absence of marine deposits in North-western South America during the Paleocene. The data from the present work indicates that this assumption is not completely true, and that lacustrine-brackish deposits were in fact widely distributed in the northern Andes during most of the Paleocene. In this sense, a new paleogeographic model explaining the differences in environments of deposition and their geographic distribution is necessary to understand the flooding episodes occurred during the Paleocene.

3.4.1.2 Eocene to Oligocene

The palynological record and specifically the Salinity, Lacustrine and Mangrove indices (SI, LI and MGI) suggest the occurrence of two flood events between the mid middle Eocene and early Oligocene (43.5 to 28 Ma) (Figure 3.22). During the first event (m3, Figure 3.10), occurred between 43.5 and 38 Ma, the areas located toward the south (areas F and H) show elevated SI values and the development of mangrove vegetation specifically in the younger part of the interval (Figure 3.22). The lacustrine influence is null. In contrast, the areas located toward the north (areas B, C, and D) show no evidence of any type of flooding during this interval (Figure 3.22). The second event (m4, Figure 3.10) is interpreted to have occurred between 35 and 28 Ma. During this interval, both the south (F and H) and north (B and D) show evidences of marine influence (Figure 3.22). An important difference between the events m3 and m4 is the lacustrine influence in m4, which is especially clear in areas to the north (areas B and D) (Figure 3.22). The pattern exhibited by the events m3 and m4 could be explained by a long-term regional event that lasted from the middle Eocene to the early Oligocene and involves two separated transgression-regression cycles that occurred at different times in the north and the south.

The first episode of this regional event is related to the event m3 (Figure 3.10) and corresponds to a marine incursion that probably came from the south and flood areas as far away as F (Figure 3.22). The second episode, between 38 and 35 Ma, is interpreted as a marine regression, which is evidenced by the low SI values in the areas H and J. It is however very important to note that during the marine withdrawal, the area H remained under lacustrine influence as indicated by the elevated LI values (Figure 3.22). The lacustrine influence is the result of elevated abundances of *Botryococcus*. In spite of the low number of samples, the area J also shows evidence of lacustrine conditions during this interval (Figure 3.22). The third episode corresponds to the event m4 (Figure 3.10) and is interpreted as two floods that affected the south and north at close but different times. The flood that affected the south (areas H, I, and J) occurred between the upper late Eocene and mid early Oligocene and it is characterized by relatively high SI values that suggest a predominance of marine conditions. On the other hand, the flood that affected the north (areas B and D) occurred between the mid early Oligocene and the end of the early Oligocene and is characterized by high LI and SI values in the areas B and D respectively, which suggest a combination of marine and lacustrine conditions (Figure 3.22). The ecological differences between the south and the north as well as the clear differences in the temporality between the two events are used here as an evidence of the occurrence of two

separate events.

The events m3 and m4 coincide with the marine influence interpreted by Ochoa et al. (2012) in samples from the Concentration and Usme Formations respectively. In spite of the low number of samples used by Ochoa et al. (2012) they fall within the range of marine influence defined in the present study (Figure 3.9). On the other hand, Cooper et al. (1995) and Villamil (1999) suggested a paleogeographic model in which a marine incursion coming from Lake Maracaibo (Venezuela) flooded the Llanos foothills and Llanos basins during the late Eocene. These paleogeographic models were however rejected by Santos et al. (2008) because they did not find evidence of marine influence in the Catatumbo and northern Llanos basins that were the communication pathways to the Caribbean Sea during the late Eocene.

Instead, Santos et al. (2008) proposed the existence of two separate corridors to explain the paleogeography of the marine incursion occurred during the late Eocene. A corridor located toward the Ecuadorian coast that was responsible of the marine incursion interpreted in the Putumayo basin, and a second corridor formed as a consequence of the separation of the Central Cordillera and the Santa Marta massif (Montes et al., 2005) that was responsible of the marine incursion observed in the central Llanos foothills. The study by Santos et al. (2008) was restricted to the upper part of the palynological zone T-07 (late Eocene) and therefore only represent the lower part of the event m4 defined in the present work. A closer inspection of the figure 3.11, support the results by Santos et al. (2008) in the sense that the during the upper late Eocene (35-34 Ma) the marine influence was concentrated toward the south and the central areas of the Llanos basin while the areas toward the north apparently had no of marine influence. However, the complete record of the event m4 reveals two important things. First, that the marine influence in the Central Llanos was not restricted to the late Eocene but lasted until the early Oligocene and second that the northern Llanos (areas B and D) was under marine-lacustrine influence during the early Oligocene (Figure 3.22). The last observation would suggest that the paleogeographic interpretation by Cooper et al. (1995) and Villamil (1999) with regard to the existence of a marine corridor through the Maracaibo Lake (Venezuela) could be valid, except that the flood in the northern areas occurred during the early Oligocene rather than in the late Eocene.

Area C, which geographically corresponds to the Middle Magdalena Valley (MMV), shows evidence of lacustrine influence during the late Eocene (Figure 3.22). The late Eocene is the most accepted age for the Los Corros horizon (Rodriguez et al., 2012), which is a fossil horizon comprising freshwater bivalves and gastropods (Pilsbry and Olsson, 1995; Nuttall 1990). The palynological record of the Los Corros horizon is challenging because the sec-

tions and wells where it has been identified usually exhibit a patchy record of the palynological associations indicative of lacustrine conditions. For example, from the five late Eocene sections studied by Rodriguez et al. (2012) in the Nuevo Mundo Syncline a unique sample located at the top of the Esmeraldas Formation exhibited elevated abundances of *Botryococcus* (116 individuals). This is one of the samples from the late Eocene with a SI value of 50 in the area C (Figure 3.22). The palynological interpretation of the los Corros horizon is usually more complex in wells drilled in the MMV (area C) because of the effect of borehole caving and the differences in the recovery of algae, which may vary according to the processing protocol. Samples that are prepared during onsite operations are more likely to present a low recovery than those processed for research purposes. This implies that even a section in which the Los Corros horizon has been identified can present a null recovery of palynomorphs indicative of lacustrine conditions. In the wells Reg-1 and Tem-1 a large number of samples were analyzed through the Los Corros horizon, which was identified by the presence of mollusc in Reg-1. However just some samples showed moderate abundances of algae (area C, Figure 3.22). Additionally when the lacustrine influence is detected, the association is dominated by *Pediastrum* in some sections (e.g. Tem-1) and by *Botryococcus* in others (e.g. Reg-1 and Nuevo Mundo). These differences suggest that rather than an extensive lacustrine system as suggested by Rodriguez et al. (2012) the MMV during the late Eocene was covered by restricted and small lacustrine systems with different ecological conditions. In contrast, a lacustrine influence in the UMV (area J) is evidenced in the early Oligocene but not during the late Eocene (Figure 3.22). This would suggest that the development of the lacustrine systems during the late Eocene was restricted to the MMV and the Llanos basin. However, to support the hypothesis of small lacustrine systems restricted to the MMV, it is necessary to analyse a major number of sites in both the MMV and UMV.

Finally, Rodriguez et al. (2012) suggest that the Los Corros horizon is time correlative with marine incursion of the late Eocene proposed by Santos et al. (2008). However, from the information compiled in this study it seems that the Los Corros horizon is more time correlative with the lacustrine event that precedes the marine incursion of the upper late Eocene and that is very evident in the area H (Figure 3.22).

3.4.1.3 Miocene to Present

Several authors have suggested the occurrence of marine incursions and/or the development of lacustrine systems in the Neotropics during the Miocene (Wesselingh et al., 2006; Hoorn, 1993, 1994; Hoorn et al., 2010c; Jaramillo

et al., 2017; Hovikoski et al., 2010). These episodes have received great attention from researchers in different disciplines because of their possible relationship with the origin and maintenance of the mega diversity observed today in the Amazon basin (Hoorn et al., 2010 and references there in).

The most popular hypothesis suggests the development of a long-lived aquatic system or mega wetland, known as the Pebas System, which covered western Amazonia between 24 and 7 Ma (Wesselingh et al., 2001; Wesselingh et al., 2006; Hoorn et al., 2010c). The debate about the salinity and temporal duration of the Pebas system has intensified during the last decade. Paleontological and geochemical evidence suggest that most of western Amazonia during the Miocene was dominated by freshwater settings at sea level. The strontium and oxygen isotopes and the common occurrence of freshwater taxa point to predominantly freshwater settings (Wesselingh et al., 2001; Kaandorp et al., 2006). Additionally, the stratigraphic continuity of these species and lineages indicates that lakes continuously occupied the system and were never entirely replaced by rivers or the sea (Wesselingh et al., 2006). In contrast, studies based on ichnofossils (marine ichnofauna), sedimentology (tidal deposits), palaeontology (marine rays) and micropaleontology (microforaminifera, dinoflagellates and mangrove pollen) have argued for the presence of mesohaline and higher salinities conditions during the Miocene (Hoviskoski et al., 2005; Rebata et al., 2006). Jaramillo et al. (2017) used the palynological and sedimentological record of two rock cores drilled in the Llanos (Saltarin) and Solimoes (105-AM) basins to propose two marine incursions during the Miocene (MMI and EMI). The two incursions occurred between 18.1 and 17.2 Ma and 16.1 and 12.4 Ma in the Llanos basin and between 18 and 17.8 Ma and 14.1 and 13.7 Ma in the Solimoes basin (Figure 3.23) (Jaramillo et al., 2017). Jaramillo et al. (2017) used seismic information to geographically extrapolate the two incursions and to propose that shallow marine waters covered western Amazonia twice during the Miocene.

The palynological record used in the present study supports the occurrence of several floods during the Miocene. The salinity index (SI) suggests a minor episode of marine influence during the early Miocene (event m5, Figure 3.10) and a major episode between the late early Miocene and middle Miocene (event m6, Figure 3.10). The lacustrine index (LI) suggests the influence of lacustrine conditions between the late early Miocene and the early middle Miocene (event l5, Figure 3.15) and the Mangrove index (MGI) suggests the development of mangrove vegetation during the late early Miocene and early middle Miocene (event mg4, Figure 3.21).

The first evidence of flooding during the Miocene is observed at the Oligocene-Miocene boundary (23 Ma) (Figure 3.23). All the areas except

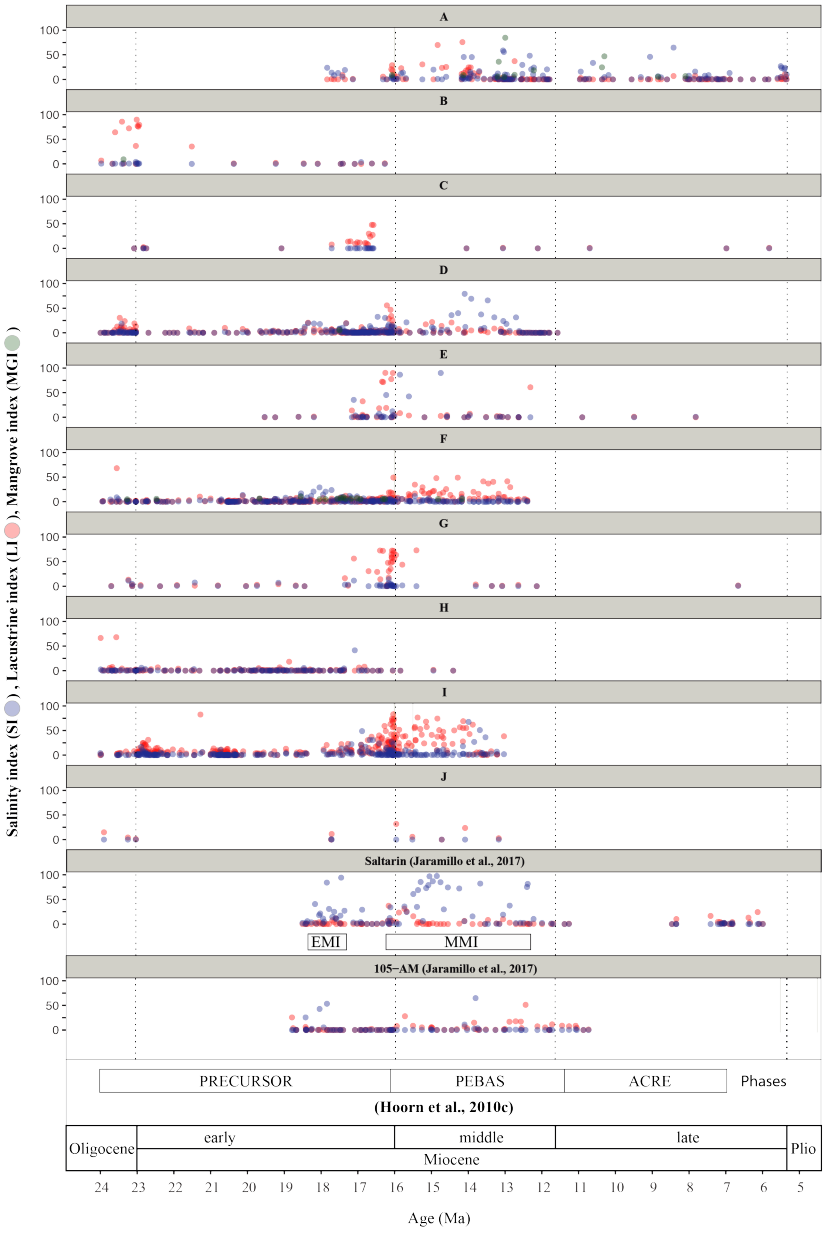

Figure 3.23: Salinity, Lacustrine and Mangrove indices during the Miocene discriminated by geographic areas. The location of the areas is shown in Figure 3.3. The three phases of the Pebas system (Hoorn et al., 2010c) and the two marine incursions (EMI, MMI) (Jaramillo et al., 2017) are included for comparison.

those with null or low number the samples, present moderately SI and LI values indicating a mixture of marine and lacustrine conditions. This mixture

suggests that this episode would correspond to the precursor phase proposed by Hoorn et al. (2010c). During this phase, lacustrine conditions alternated with episodes of Andean and cratonic fluvial drainage as well as marginal marine influence. The record presented in this study shows that the duration of this event did not exceed two million years (Figure 3.23). This contrasts with Hoorn et al. (2010c) interpretation in which the precursor phase occurred between 24 and 16 Ma.

Interestingly, this event in the area B seems to be a prolongation of a flood that started in the upper early Oligocene, which is characterized by high LI values. In this sense, the onset of the early Miocene flooding event occurred earlier in the north and progressively reached areas located toward the south. This geographic pattern seems to support the hypothesis that the flood progressed from the Caribbean into western Amazonia as suggested by several authors (Hoorn, 1993; Rasanen et al., 1995; Hovikoski et al., 2007; Wesselingh et al., 2010; Villegas et al., 2016).

The palynological record from 22 to 18.5 Ma show no evidence of marine or lacustrine influence while a strong influence is again detected between 18 .5 and 12 Ma (Figure 3.23). For this interval, Jaramillo et al. (2017) proposed two separate marine incursions that covered the entire Llanos and western Amazonia during (EMI: early Miocene incursion and MMI: middle Miocene Incursion (Jaramillo et al., 2017)). On the other hand, Hoorn et al. (2010c) proposed the Pebas Phase (16 to 11.3 Ma), which correspond to the maximum expansion of the lacustrine conditions with marginal marine influence (Figure 3.23). The EMI and MMI events and their relationship with the Pebas phase is discussed below.

The Early Miocene Incursion (EMI)

The EMI was the result of a combination of tectonic subsidence and a global rise of sea level in the early Miocene that create accommodation space that overwhelmed the rate of sedimentation allowing the marine incursion inland (Boonstra et al., 2015). In spite of the low number of samples analyzed in this interval, some of them in the areas D and F exhibit moderate SI values testing the occurrence of the marine influence. These samples are restricted to the interval between 17.2 and 8.1 Ma supporting therefore the duration of the EMI proposed by Jaramillo et al. (2017).

According to the paleogeographic interpretation by Jaramillo et al. (2017, supplemental material), during the late early Miocene (17.8 to 16.3 Ma) the marine conditions retreated northward and the filling of subaqueous basin with lake, swamp and alluvial deposits initiated. Amalgamated channels sandstones accumulated in the Llanos basin, whereas floodplain and channel-

fill deposits accumulated in the Amazonas/Solimoes basin (Jaramillo et al., 2017). In Saltarin, this interval is lithostratigraphically related to the member C1 of the Carbonera Formation (Figure 3.24). This unit corresponds to massive conglomeratic sandstones grading to medium/fine-grained sandstone accumulated in fluvial channels (Jaramillo et al., 2017). The low SI and LI values in Saltarin (Figure 3.24) suggest the absence of marine or lacustrine conditions during this interval, which would prove the retreat of the marine conditions northward. However, the Figure 3.23 reveals the influence of marine and lacustrine conditions in some areas. To explore this interval in detail, the lithology and flooding indices (SI and LI) of specific wells were compared with those of Saltarin (Figure 3.24). The lithological information was extracted from well logs and for Saltarin from the supplemental material in Jaramillo et al. (2017). The comparison clearly shows the influence of lacustrine (and to a lesser extent marine) conditions during the interval (member C1 of the Carbonera Formation) in which the deposition in Saltarin is interpreted as continental (Jaramillo et al., 2017). The lacustrine-marine influence affected areas located to the south of Saltarin, as evidenced by Ma-1, Ret-1, and Tras-1, as well as areas to the north as evidenced by Con-1 (Figure 3.24). The samples from three wells (Ret-1, Tras-1, and M-1) correspond to ditch cuttings, which could make interpreting this level as the result of contamination by caving. However, it would be suspicious that the three wells were affected by caving in the same interval. On the other hand, the samples from the well Con -1 correspond to sidewall cores, a type of sample that usually is not affected by caving. Interestingly in the four sections, the interval between 17.5 and 16.2 Ma lithologically corresponds to a series of sandstones intercalated with thin layers of mudstones overlayed by a thick sequence of mudstones (Figure 3.24). This lithological sequence clearly correlates with the member C1 of the Carbonera Formation and the Leon Formation as interpreted in Saltarin (Jaramillo et al., 2017). This lithological pattern reinforces the temporal correlation between the intervals but also suggest important lateral facies changes during the deposition of the member C1 of the Carbonera Formation. These changes are especially reflected in the salinity and lacustrine indices (Figure 3.24). Unfortunately the only information that can be extracted from the well logs is the lithology (e.g. sandstones, mudstone, limestone), which prevents a detailed facies analysis and therefore a reliable comparison with Saltarin.

The evidence suggest that from 17.8 to 16.3 Ma the areas toward the south and north of Saltarin were under lacustrine-marine influence (Figure 3.24). This indicates that the marine conditions did not retreat as far as north as suggested by Jaramillo et al. (2017). The elevated LI values during this interval could suggest environments of deposition similar to that described

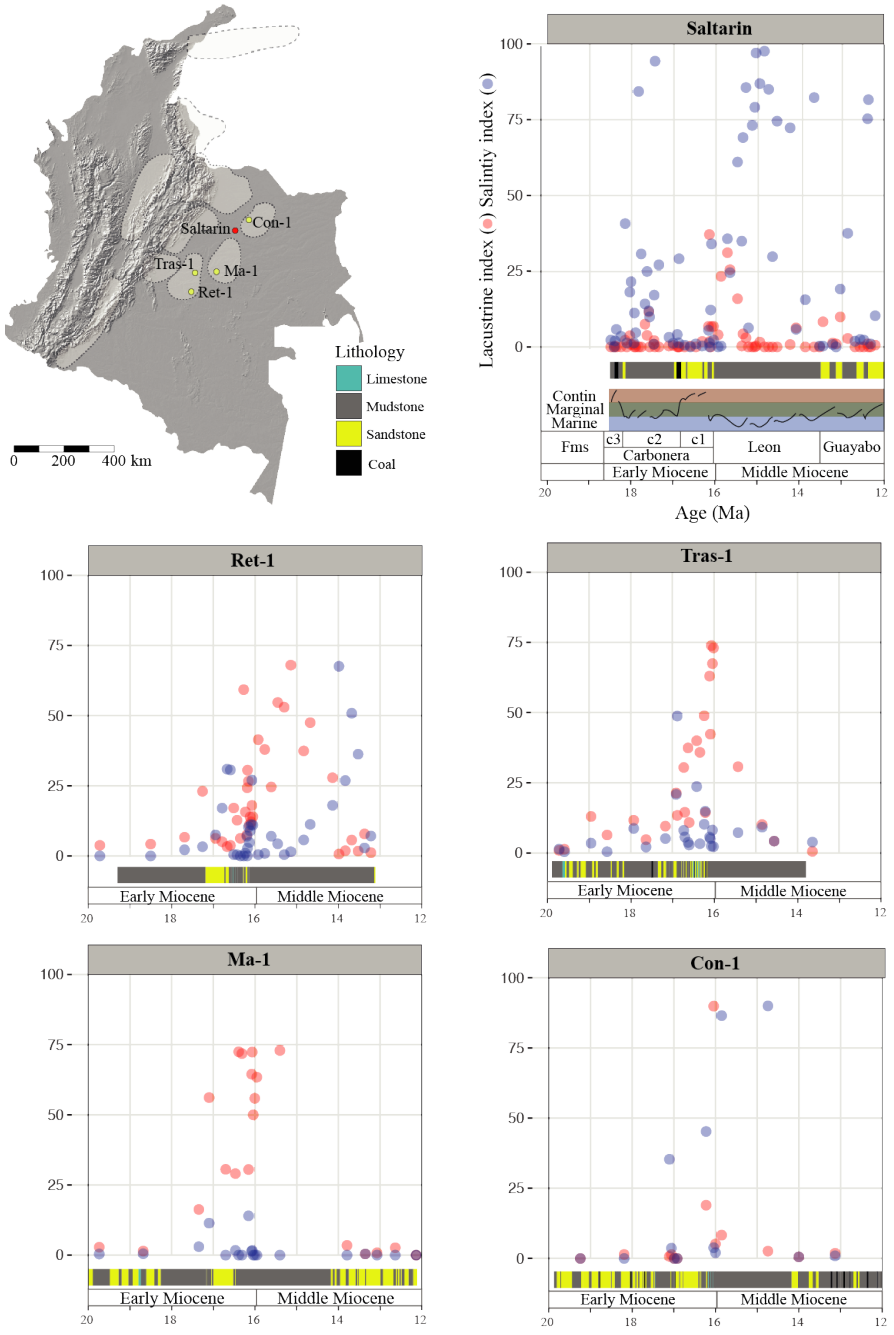

Figure 3.24: Lacustrine index (red circles), Salinity index (blue circles), and lithology of Saltarin (Jaramillo et al., 2017) and four wells (Ret-1, Tras-1, Ma-1, Con-1) drilled in the Llanos basin for the early to middle Miocene interval.

by Jaramillo et al. (2017) as marginal. The association of lithofacies in this environment represents accumulation on deltaic plains, low energy wetlands with swamps, ponds and channels, and shallow fresh water lacustrine systems (Jaramillo et al., 2017). Interestingly, this is the depositional environment interpreted for the interval in the core 105-AM drilled in the Solimoes basin that is the temporal equivalent of the member C1 of the Carbonera Formation in Saltarin (Jaramillo et al., 2017). A very important difference is the absence of lacustrine or marine influence in the core 105-AM as reflected by the low SI and LI values (Figure 3.23). This may be a consequence of the low number of samples analyzed in this interval or differences in the environment of deposition.

Finally, the results obtained from the comparison between the MMV and UMV indicate that these two basins were under lacustrine influence between 17 and 16 Ma. In the MMV this interval is associated with the La Cira Fossiliferous Horizon, which is palynologically characterized by elevated abundances of *Pediastrum* and *Botryococcus* (area C in Figure 3.22 and Figure 3.5). In the UMV the Barzalosa Formation that according with the results of the present work is time correlative with the La Cira Fossiliferous Horizon is also characterized by elevated abundances of *Pediastrum* and *Botryococcus* (Figure 3.7).

The Middle Miocene Incursion (MMI)

The MMI (Jaramillo et al., 2017) partially coincides with the Pebas phase (Hoorn et al., 2010) (Figure 3.23). The palynological record of Saltarin and to a less extent 105-AM show elevated SI values and low LI values (Figure 3.23) supporting therefore the two marine incursions interpreted by Jaramillo et al. (2017). However, an inspection of the figure 3.23 also reveals that not all the areas were under marine influence but in fact some of them were more influenced by lacustrine conditions. A good example correspond to the areas F and I. These two areas exhibit elevated LI values between 16.1 and 12.4 Ma, which is the interval in Saltarin with the highest SI values (Figure 3.23). Other areas like D and A seem to support the occurrence of marine conditions during this interval.

The differences between the areas show that this interval was not exclusively under marine influence as suggested by Jaramillo et al. (2017) and resembles more the paleogeographic interpretation of the Pebas phase proposed by Hoorn (1993, 1994, 2010c). During this phase a wetland system developed, which was composed by a highly dynamic mosaic of lakes, embayments, swamps, rivers and fluvio-tidal environments that from time to time were exposed to marine influence. Hoorn et al. (2010) suggest that during

the Pebas phase, the foreland basins situated parallel to the Andes received the bulk of the sediments through fluvial input from the emerging Eastern Cordillera. The elevated LI values observed in area I would suggest that this was not the case (Figure 3.23) and that lacustrine influence dominated over fluvial conditions even in areas located in the proximity of the Andes Cordillera.

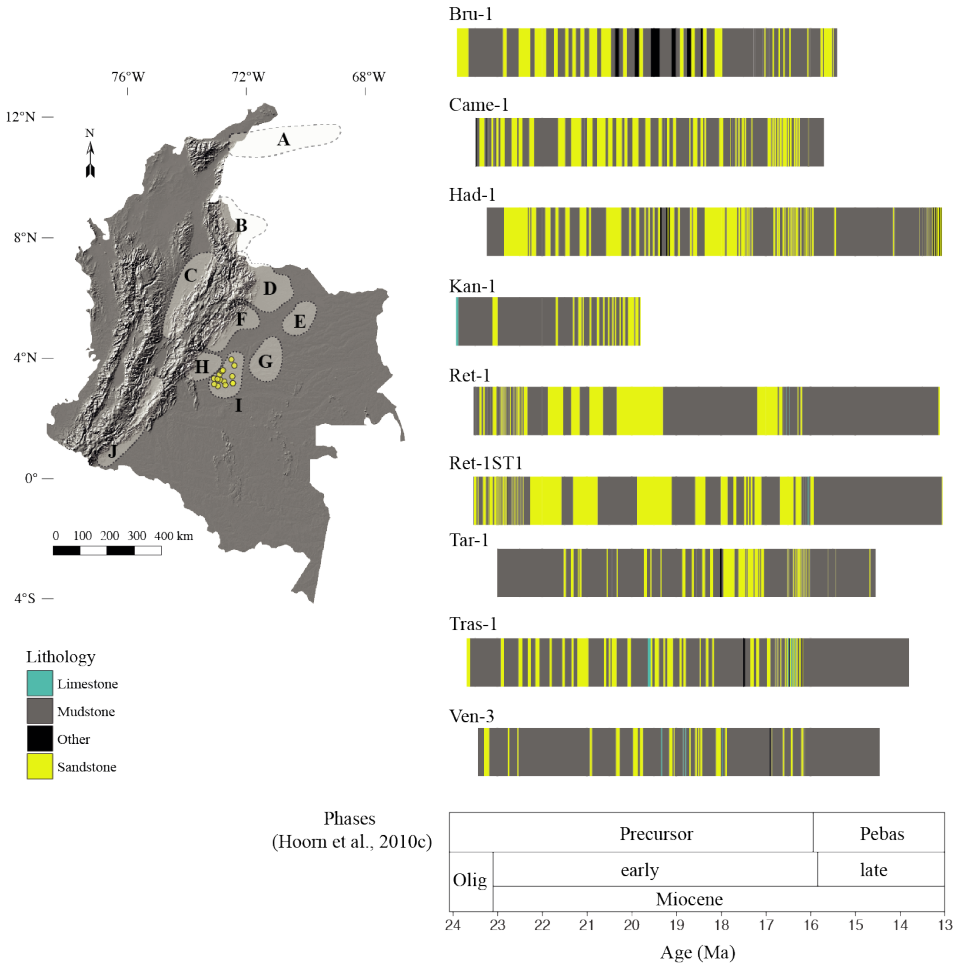

Figure 3.25: Lithology during the Precursor and Pebas phases (Hoorn, et al., 2010c) in selected wells from the area I.

The lithological pattern obtained for selected wells (Figure 3.25) also point to a prevalence of lacustrine conditions during the Pebas phase in the area I. Between 16 and 13 Ma all the sections are dominated almost exclusively by fine-grained lithologies with scarce to null presence of sandstone or any other lithology (Figure 3.25). In contrast, the precursor phase (between

24 and 16 Ma) is lithologically characterized by intercalations of sandstones and fine-grained lithologies that suggest the occurrence of fluvial channels during this interval.

Finally, the low number of samples during the Acre phase (Hoorn et al., 2010c) (Figure 3.23) prevents an accurate reconstruction of the palaeoenvironmental conditions during this interval. In the area A, a few samples exhibit relatively high SI values that suggest marine influence. The proximity of this area with the Caribbean Sea could indicate that this was a local rather than a regionally widespread event. Information from the other areas is necessary to test this idea.

3.4.2 Flooding events in the Magdalena Valleys

The age of the Barzalosa Formation has been deduced from its stratigraphic position (De Porta 1974). Isolated outcrops with presence of fossil molluscs suggest this unit correlate with the Colorado Formation in the Middle Magdalena Valley and more specifically with the La Cira Fossiliferous Horizon. The results presented in this study show that the Barzalosa Formation and the La Cira Fossiliferous Horizon share a similar palynological composition. The occurrence of elevated abundances of the algae *Pediastrum* and *Botryococcus* also supports the correlation between these two units and additionally indicates the occurrence of lacustrine systems in the Middle and Upper Magdalena Valleys during the deposition of these units.

The results of the maximum likelihood analysis show a high probability of correlation between the samples from the Barzalosa Formation and the La Cira Fossiliferous Horizon (Figure 3.6). The La Cira Fossiliferous Horizon was interpreted from a composite section in which not only the La Cira Fossiliferous Horizon but also the Mugrosa and the los Corros fossil horizons were identified by the occurrence of shell fragments. The approach of including the three fossiliferous horizons in the analysis opened the opportunity to compare the Barzalosa Formation with all their possible correlative deposits. According with the palynological zonation by Jaramillo et al. (2011), the LCH, and by association the Barzalosa Formation, were deposited during the palynological zone T13-Echitricolporites maristellae (17.7 to 16.1 Ma). This zone is delimited at the base and top by the first appearance datum (FAD) of *Malvacipolloides maristellae* and *Grimsdalea magnaclavata* respectively. Biostratigraphic key taxa with FADs within this zone include *Bombacacidites baculatus* and *Echitricolporites spinosus*, while *Rugotricolporites intensus*, *Retistephanoporites minutiporus*, *Cyclusphaera scabrata*, and *Echinatisporis brevispinosus* show their last appearance datum (LAD) during this interval (Jaramillo et al., 2011). Of those taxa mentioned above, only

M. maristellae and *E. spinosus* were reported in the wells from the Upper Magdalena Valley. This corroborates that the deposition of the Barzalosa Formation is not older that the base of the palynological zone T-13 (17.7) (Jaramillo et al., 2013) and also highlights the difficulty of correlating only based on the occurrence of biostratigraphic marker species. As shown, this difficulty can be overcome by using of quantitative methods like the maximum likelihood approach that use the relative abundance of the species.

Of the five wells analyzed in this study, Gb-1 shows the most complete record of the Barzalosa Formation. The palynological analysis, and specifically the proportions of *Botryococcus* and *Pediastrum*, allows division of this unit into three intervals (Figure 3.8). The basal interval is characterized by relatively low SI values with *Pediastrum* dominating the lacustrine association. The middle interval exhibits an increasing trend in SI that in contrast with the basal interval is almost entirely dominated by *Botryococcus*. The upper interval shows a decline with a posterior increase in SI with *Pediastrum* and *Botryococcus* alternating the dominance of the association (Figure 3.8).

Pediastrum and *Botryococcus* often occur together in the same sediments, but they are not simultaneously abundant, suggesting that they have somewhat different ecological preferences (Tyson 1995). Changes in the trophic state of a lake from oligotrophic to eutrophic a usually results in a decrease in the *Botryococcus*:*Pediastrum* ratio (BP ratio) (Pollingher, 1986). Salinity also seems to be a significant factor, with *Botryococcus* being euryhaline and *Pediastrum* stenohaline (Tyson, 1995).The changes in the relative abundance between the *Botryococcus* and *Pediastrum* have been therefore considered to be a consequence of the ecological and climatic conditions of the lacustrine systems where they live (Tyson 1995; Medeanic 2006).The changes in BP ratio observed in Gb-1, which allowed separating the Barzalosa Formation into three intervals (Figure 3.8), suggest the occurrence of important ecological and climatic changes during the deposition of this unit.

Interestingly, the three intervals previously defined based on the proportion of algae (Figure 3.8) also show marked differences in their depositional sequences, which were explored using a Markov chain approach. Although the three intervals present similar lithologies, their thickness, number of layers and distribution vary (Tables 3.5, 3.6, and 3.7). More important, the lithology relationship diagram (Figure 3.8) indicates that the three intervals are characterized by different and specific lithological transitions. It is noteworthy that the few studies from the literature (Scheibe 1934; Caceres and Etayo, 1969; De Porta 1974; Acosta 2002) have also divided the Barzalosa Formation, based on lithology, into three units or intervals (Figure 3.2). A lower segment that comprises thick layers of conglomerates intercalated

with siltstones and fine-grained sandstones. A middle segment composed by a monotonous sequence of thick layers of siltstones and claystones presenting gypsum veins intercalated with sporadic medium thickness layers of fine to medium-grained sandstones. An upper segment that corresponds to thick layers of oligomictic conglomerates intercalated with claystones and siltstones showing sporadic gypsum veins. Unfortunately, the lithological information that can be extracted from a well log is restricted almost exclusively to the general type of lithology, which prevents an accurate sedimentological interpretation. However, the lithology of Gb-1 shows in general a good concordance with the lithology of the three intervals described in the literature. There is an apparently absence of gypsum veins in the middle and upper intervals of Gb-1, which are reported in the literature. This absence could be explained by differences in the environment of deposition or what is more plausible by the difficulty of identifying minerals in ditch cutting samples. However, from the lithological analysis obtained through the Markov chain analysis and the descriptions from the literature it is possible to suggest for the Barzalosa Formation the occurrence of at least three depositional systems.

Table 3.5: Summary of the lithology for the interval 3 (14295-13480 feet) of the Barzalosa Formation in Gb-1 (GC:Gray Claystone; Sd:Sandstone; SD:Standard deviation).

Litho	**# Layers**	**Total Thickness**	**Mean Thickness**	**SD**
GC	18	1173	65	115
Coal	6	7	1.1	0.4
Sd	8	21	2.6	3.1
Shale	10	64	6.4	3.3
Total	42	1265		

Table 3.6: Summary of the lithology for the interval 2 (13480-12750 feet) of the Barzalosa Formation in Gb-1 (GC:Gray Claystone; SD:Sandstone; SD:Standard deviation).

Litho	**# Layers**	**Total Thickness**	**Mean Thickness**	**SD**
Shale	14	643	45	30.9
Sd	9	44	4.8	3.8
St	4	40	10	2.1
Coal	2	3	1.5	0.7
Total	29	730		

To summarize, based on the integration of the palynological and sedimentological information from Gb-1 it is confident to suggest that important

Table 3.7: Summary of the lithology for the interval 1 (14295-13480 feet) of the Barzalosa Formation in Gb-1 (GC:Gray Claystone,Sd:Sandstone,SD:Standard deviation).

Litho	# Layers	Total Thickness	Mean Thickness	SD
GC	13	467	35.9	30
Sd	9	77	8.5	4
Shale	11	146	13.2	4.9
Total	33	690		

ecological, climatic and geological changes occurred during the deposit of the Barzalosa Formation. The sedimentological and palynological record produced by those changes show that this unit is the result of the evolution of a lacustrine system. It is well established that due to changes in climate and/or tectonic subsidence, nonmarine basins commonly evolve from one lake type to another (Lambiase, 1990). In fact, most basin fills contain a predictable evolution between lacustrine facies associations (Neal et al., 1997). For example the Green River Formation in Wyoming (USA) records a complete gradational cycle of lake basin types from overfilled, through balanced fill and underfilled, then back through balanced fill and overfilled (Carroll et al., 1999). Is the Barzalosa Formation recording a lacustrine gradational cycle like those observed for the Green River Formation? With the information presented in this study is risky to answer this question. Detailed sedimentological analyses in sections distributed along the basin are necessary to test this hypothesis. With the information from the present study it is possible to interpret the three intervals of the Barzalosa Formation as follow.

The basal interval (interval 1) is characterized by a low BP ratio that suggests lacustrine conditions with high nutrient content. During this interval, and the lowest part of the interval 2, *Malvacipolloides maristellae* and *Malvacipolloides* sp. reach their maximum abundances (Figure 3.8). *M. maristellae* is a key taxon to identify the palynological zone T-13 (16.1-17.7 Ma) (Jaramillo et al., 2011), that is the zone associated to the deposition of the Barzalosa Formation and the la Cira Fossiliferous Horizon. As shown by the record in Gb-1, *M. maristellae* exhibit a marked facies control. This would imply a restriction on its usefulness as a biostratigraphic marker but at the same time it would be increase its use as an ecological indicator. Evidently, this interpretation is based on information from one single section and more sections are needed to test this idea. The low LI values during this interval suggest that the lacustrine system was relatively small and surrounded by vegetation, which is the main component (pollen and spores) of the palynological association (Figure 3.8).

The middle interval (interval 2) shows a continuous increasing trend of the BP ratio (Figure 3.8). The dominance of *Botryococcus* suggests a decrease of both the biological activity and the amount of nutrients. During this interval, the fine lithologies (shale, siltstone) predominate and sandstones represent only 6% of the total thickness (Table 3.6). The low representation of sandstones could be indicative of a very scarce occurrence of fluvial systems capable of delivering sediments into the lake, which would explain the low nutrient content suggested by BP ratio. The information from outcrops indicates the occurrence of gypsum veins in the middle interval of the Barzalosa Formation (Caceres and Etayo, 1969; De Porta 1974). Gypsum was not reported in Gb-1 but its absence could be explained by the difficulty of identifying minerals from well ditch cutting samples. Elevated abundances of *Botryococcus* accompanied by gypsum have been associated with periodic deposition of gypsiferous or other shallow water evaporitic facies (Nagappa 1957). This could correspond to the environment of deposition of the middle member of the Barzalosa Formation. The increasing trend in BP during this interval is indicative of the progressive geographic expansion of the lacustrine system. This expansion moved the shoreline to areas previously occupied by land, decreasing therefore the contribution of terrestrial palynomorphs that previously were closer to the lacustrine system. This is reflected in the lacustrine index that show a low contribution of terrestrial palynomorphs (pollen and spores) (Fig. 7). The decrease in the amount of nutrients is explained by the retrogradation of the discharge zones due to the expansion of the lacustrine system.

Finally, the upper interval (interval 3) exhibits fluctuations of the BP ratio with *Botryococcus* and *Pediastrum* alternating the dominance of the association (Figure 3.8). The lithological relationship diagram indicates a cyclic sedimentary sequence that involves the transition from shale to clay, from clay to sandstone, and from sandstone to shale (Figure 3.8). The thickness of these lithologies (Table 3.7) suggests either variability in the duration of the cycles or changes in the sedimentation rates or a combination of both. Unfortunately, with the available information it is not possible to discard any of them. However, the cyclic sedimentation suggests variability in the sediment discharge and therefore intermittency in the amount of nutrients that reached the lacustrine system. Climatic fluctuations cannot be discarded either, which could be the factor controlling sedimentation. During this interval the lacustrine system contracted again resembling the conditions of the interval 1.

It is now well established that the interaction between rates of sediment + water supply and accommodation space controls lakes occurrences, distribution of their strata and the character of their organic and inorganic

components (Bohacs et al., 2000). Sediment and water supply are controlled by climate while accommodation is a tectonic process. In this sense, it is possible that a combination of climate and tectonics were the mechanisms controlling the expansion and contraction of the lacustrine system of the Barzalosa Formation. The contribution of each component is still unclear

The exclusively occurrence of lacustrine-related algae and absence of marine palynomorphs (dinoflagellates and microforaminifera) found in the present study indicates that lacustrine to swamps environments prevailed in the middle and upper Magdalena valleys. This resembles the Pebas phase of the Pebas system in which lacustrine conditions expanded reaching their maximum extension (Hoorn et al., 2010). In terms of paleogeography, the single foreland basin that encompassed the middle Magdalena valley, the upper Magdalena valley, the Eastern Cordillera and the Llanos basin was disrupted at least since the late Eocene to earliest Oligocene prior to the onset of the major late Neogene exhumation pulses of the Andes (Nie et al., 2010; Moreno et al., 2011; Ochoa et al., 2012). During Miocene times, the Eastern Cordillera already separated the middle Magdalena valley from the Llanos basin (Parra et al., 2009; Caballero et al., 2010). The timing of isolation of the UMV from the Llanos basin is less clear. Using sedimentological information and apatite fission tracks, Guerrero (1997) estimated that the initial phase of uplift of the Eastern Cordillera at the latitude of the UMV occurred approximately at 12.9 Ma. Other studies however have suggested a positive relief for the Eastern Cordillera at least since approximately 22 Ma (Farris et al., 2011; Horton et al., 2010; Mora et al., 2010a; Moreno et al., 2011). The correlation and paleoenvironmental similarities between the Barzalosa Formation and the "Pebas phase" suggest that the UMV and western Amazonia were geographically connected. This implies that 16.5 Ma ago, the Eastern range of the Andes Cordillera at the latitude of the UMV still did not form enough relief to separate the two basins.

3.4.3 Macroevolution and Flooding Events

The occurrence of marine-lacustrine incursions has been associated with environmental and ecological changes that are believed have helped to modulate biological diversity. Large-scale inundations have the ability to create islands on high ground, which may be capable of isolating fauna and flora and so propitiate allopatric speciation (Nores 2004). In particular, it has been proposed that the marine/lacustrine incursion(s) occurred during the Miocene in the Amazon basin played an important role in the biodiversity dynamic of the Amazon by favouring biogeographical isolation and promoting allopatric speciation (Webb 1995; Rasanen et al., 1995; Lovejoy et al.,

1998). In the specific case of the Miocene, the direct relationship between Amazonian diversity and the floods have been particularly difficult to test despite the great attention it has received from researchers in several disciplines. This is because the floods were not the only event occurred during the Miocene. The intensification of the Andean uplift (Horton et al., 2010; Hoorn et al., 2010b), important global climate changes like the mid Miocene Climatic optimum (Zachos et al., 2001), and the onset of the Amazon River (Hoorn et al., 2017) also occurred during this period. The concurrence and complexity of these events has made it very difficult to disentangle the specific influence that each one has had on the diversity of the Amazon basin. It is very possible that a combination of events rather than isolated effects exerted the main control in shaping the macroevolutionary history of the Amazon basin. On the other hand, the relationship between diversity and other floods occurred during the Cenozoic has been poorly explored. The difficulty of finding outcrops with sediments older than the Miocene in the Amazon basin could to some extent explain the lack of studies.

Following the discussion that has been given throughout this chapter it is now clear that different areas of the Neotropics were flooded during the Cenozoic. The palynological evidence presented here allowed differentiation between lacustrine and marine events, which are nevertheless often closely related. The Figure 3.26 integrates the SQS diversity curve and the turnover rates estimated in the second chapter of this work with the global climatic curve proposed by Zachos et al. (2008) and the flooding events interpreted in this chapter separated by marine, lacustrine and mangrove influence. The interval covered by each flood corresponds to an estimation based on the maximum temporal range observed in at least one of the areas. As an example, this means that the lacustrine event l4 interpreted between 32 and 23 Ma in the Figure 3.26, is the result of the total range observed in the area B (Figure 3.15) even other areas like D and F show a shorter duration for this event. Establishing the geographic coverage of the different flooding events is difficult. It is feasible that some of them correspond to local events or that the lack of samples in other areas restricts to make an accurate interpretation of their geographical distribution. In this sense, establishing the relationship between the floods and diversity is not a trivial task because the diversity curve represents a regional estimate while some of the flooding events apparently represent local events.

In addition, a rough estimation of the accumulative duration of the floods indicates that the areas were under marine and/or lacustrine influence at different times for at least 30 Ma (Figure 3.26). This represents almost half of the Cenozoic. This estimate could be even greater taking into account the scarce information from 10 Ma to the present. The extended total temporal

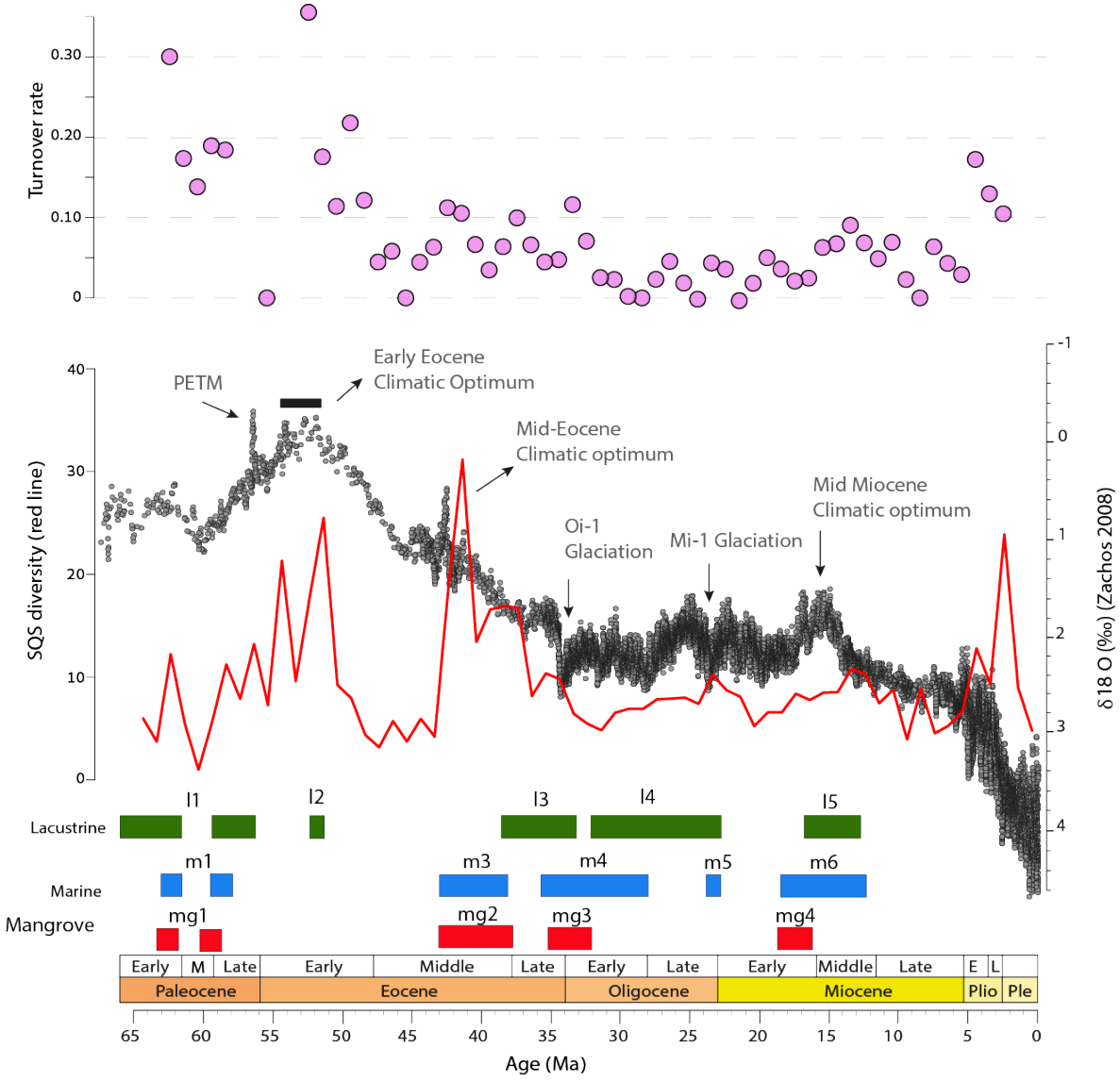

Figure 3.26: Integration of macroevolutionary estimates (SQS diversity curve and turnover rates), global climatic curve (Zachos et al., 2008) and temporal distribution of flooding events during the Cenozoic in the Neotropics.

distribution of the floods makes it difficult to find a unique relationship with the diversity and the global climatic curves. In fact, a visual comparison with the SQS diversity curve shows that episodes of marine/lacustrine influence can be related to intervals showing either an increase or decline in diversity (Figure 3.26). A good example corresponds to the Paleocene in which the diversity curve during the marine and lacustrine events shows high amplitude

fluctuations imposed over a general increasing trend (Figure 3.26). Also, at first sight the increase in regional diversity observed during the early to late Oligocene could be associated to the lacustrine event l4 (Figure 3.26). However, a close inspection of the Figure 3.22 reveals that although some areas show signals of lacustrine influence, the area B is the one exhibiting the most complete and prominent record. In fact, the record of B was used to represent the duration of this event in Figure 3.26. In this sense, it is difficult to find a mechanism that could explain how the lacustrine conditions in a specific area can exert a control over regional diversity.

In a scenario in which the geographic coverage of the events cannot be fully established, an approach to understand the relationship between diversity and the occurrence floods is to restrict the analysis to those localities showing a good record of the flooding episodes. For example, Villegas et al. (2016) used a combination of palynological and geochemical analysis from an outcrop section located along the Caqueta River (Colombia) to suggest that in the early Miocene succession (17-16 Ma) the palynological diversity does not significantly vary through the section, but changes in palynological composition are dependent on sample provenance, whereas marine influence neither dramatically alters the composition nor the palynological diversity. Similarly, D'Apolito (2016) used the palynological record of a rock-core drilled in the Solimoes basin, ranging in age between 18.7 and 10.7 Ma, to test the possible effects of inundations (freshwater/brackish or marine) on the vegetation. By using a Canonical Correspondence Analysis (CCA), D'Apolito (2016) found nearly no effect on the abundance distribution or composition of the plant communities explained by the inundations. The section Reg-1 located in area I (Figure 3.3) presents a very complete palynological record from 19.7 to 13.2 Ma showing intervals of marine and lacustrine influence. A CCA analysis of this section, using as environmental variables the influence of lacustrine, marine or marine-lacustrine conditions, indicates that only 22% of the variation in the palynological association is explained by the environmental variables. The ANOVA test also indicates no significant differences in SQS diversity between environments ($p=0.5$).

The examples above show that even for an event as well studied as the early to middle Miocene incursion, it is difficult to establish the relationship between diversity and floods. On a regional scale, this relationship is even more difficult to clarify because at least two important factors. First, some of the events show palaeoecological differences between the areas. For example, during the mid Miocene incursion the areas D and I shows lacustrine and marine influence respectively. In the middle to late Eocene episode, the area I show a complex mixture of lacustrine and marine influence while the area B show neither marine nor lacustrine influence. Evidently, this is largely the

result of the scarce information in some areas that prevent to establish the geographic distribution of the floods and therefore its relationship with diversity. The second factor makes reference to the fact that important paleogeographic and global climatic changes occurred simultaneously with the floods. As found in the chapter two of this work, climate exerted a very important control on diversity and taxonomic rates. However, it was not possible to establish a direct relationship between climate and the occurrence of floods (Figure 3.26). Although some episodes seem to show a correspondence with specific climatic events, the evidence is not overwhelming and again this can largely be attributed to the scarce information in some areas. It is expected that with the incorporation of new information these knowledge gaps will be filled and a better understanding of the temporal and geographic distribution of the flooding events will be achieved.

3.5 Conclusions

- The Neotropics experienced several flooding episodes during the Cenozoic. The palynological evidence indicates the occurrence of closely related marine, lacustrine and mangrove conditions, distributed over different geographic areas at different time intervals.

- During the Paleocene at least two flooding episodes were identified. The two episodes were recognized in the central part of the Llanos Foothills and northern Colombia. Palynologically they are characterized by the dominance of *Pediastrum* and the absence of marine palynomorphs. One of these episodes is apparently correlative with a marine incursion reported in southern Peru (Louterbach et al., 2014). The paleogeography during this interval is unknown but if the events in Peru and Colombia were coetaneous it would imply the existence of a continental scale mega system during the Paleocene.

- Two separate flooding events were interpreted between the middle Eocene and early Oligocene. The oldest event is evident in areas to the south while the youngest event is more evident in areas to the north. Although the two episodes can be part of a unique regional event, more evidence is necessary to test this hypothesis.

- During the Miocene at least three intervals of marine/lacustrine influence were identified. They partially correspond with the Pebas system phases proposed by Hoorn et al. (2010c) and the marine incursions

(EMI and MMI) proposed by Jaramillo et al. (2017). Important differences with previous interpretations include the lack of marine-lacustrine evidence during part of the precursor phase and the occurrence of lacustrine and marine conditions during the MMI.

- The Barzalosa Formation is correlative with the la Cira Fossiliferous Horizon, which is stratigraphically associated to the top of the Colorado Formation (16.5 Ma). In the well Gb-1, the Barzalosa Formation can be separated into three distinct units based on the proportion of algae (*Botryococcus* vs. *Pediastrum*), palynological composition and depositional sequence. The evidence is interpreted as the occurrence of three phases related to the development of a lacustrine system during the deposition of the Barzalosa Formation. The correlative deposits of the La Cira Fossil Horizon in the Middle Magdalena Valley and the deposits related to the palynological zone T13-E. Maristellae (Jaramillo et al., 2011) are also characterized by the occurrence of marine and lacustrine conditions. This implies that the marine and lacustrine influence was not restricted to the Llanos basin but also reached the intra montane Middle and Upper Magdalena Valleys.

- New analyses concentrated in specific areas are necessary to fully understand the relationship between floods and the macroevolutionary estimates. Ideally these analyses should ideally conclude in detailed paleogeographic reconstructions, produced not only from palynological but also all sort of geological information (e.g. sedimentology, geochemistry, seismic, etc.). These paleogeographic reconstructions can later be compared with diversity maps (like the maps presented in the chapter two of this chapter) to establish specific relationships between the floods (lacustrine vs. marine) and diversity.

Chapter 4

Synthesis

The macroevolutionary history of the Neotropical biota has been very difficult to capture because of the difficulty of finding complete and accessible geological records in this part of the world. Amazonia and the sedimentary basins that surround it are usually covered by dense vegetation or simply lack outcrops (e.g. Llanos basin in Colombia), which makes extremely difficult to find fossils. In addition, there is a substantial temporal and spatial bias in the fossil record of angiosperms, with a more complete record in the northern hemisphere and a patchy and incomplete record in the tropics (Antonelli et al., 2015). Resolving this problem is of great importance because of considerable attention and interest in Neotropical diversification.

This interest is largely due to the importance of the Neotropics for global biodiversity. It is well known, that this region maintains the highest biodiversity of the planet (Gentry 1992; Kricher 199), exerts control in global climate (Mora et al., 2008; Hubert et al., 2010) and play an important role in the dynamics of our planet. Researchers from a wide range of disciplines are now very interested (in fact this interest go back to the times of Humboldt and Darwin) in understanding how biodiversity in the Neotropics was produced and how it is maintained through time. The integration of multiple areas of research in biology (e.g. phylogeography, ecology, systematics, genetics) and Earth and physical sciences (e.g. geology, palaeontology, climatology) into the new concept of trans-disciplinary biogeography (Antonelli et al., 2018) have emerged as an important methodological approach to reconstruct the puzzle of Neotropical biodiversity and evolution in space and time. Despite important advances in our understanding of the origin and diversification of Neotropical biota, we still do not have a clear idea about the patterns of diversification through deep time. This presents a significant knowledge-gap that needs to be filled. The present thesis represents one steep towards this goal.

Palaeontology plays an important role in trans-disciplinary biogeography. Fossils are necessary to understand the history of the Neotropical biota in deep time. From the perspective of plants, palynology represents the best proxy to study the macroevolution of vegetation. Pollen and spores are fossilize readily, they are produced in large amounts (due to their role in reproduction), they are found in a widely variety of sedimentary environments, and they are recovered from small rock fragments (centimetres) like those recovered during oil drilling operations. All these characteristics make palynology a powerful proxy of vegetation in the geological past. Other microfossils obtained from palynological preparations (especially dinoflagellates, microforaminifera and alga) are excellent palaeoenvironmental indicators. Dinoflagellates and microforaminifera are associated to marine conditions while algae are usually associated to lacustrine to brackish environments. Palynology is therefore useful to reconstruct macroevolution and paleoenvironments.

In this work, I used the most complete compilation of palynological information from the Neotropics to date to explore macroevolutionary patterns of plant diversification and species richness (Chapter 2), to reconstruct several flooding events that occurred in northern South America during the Cenozoic (Chapter 3). These events include marine incursions and lacustrine-brackish systems. A rigorous biostratigraphic framework was central to this work. I achieved this using Graphic Correlation, which is presented in Chapter two, which also includes the morphological description of 34 new palynomorphs (Annex 1.7). A graphic summary of the most relevant results obtained in this work is presented at the end of the chapter as Figure 4.1.

Because most of the samples used in the analyses come from oil drilling operations (ditch cutting samples), the first occurrence datum (FAD) of the species is susceptible to be artificially increased by the undesirable effect of caving. To evaluate the effect of caving I used two versions of the composite section. One version included all the species regardless of whether their FADs were interpreted based on ditch cutting samples. The second version includes only those taxa whose FADs were estimated from rock-core or outcrop samples. The results obtained from both versions were compared. Also, because of the differences in the number of samples between regions and time intervals as well as in the number of palynomorphs counted by sample it was necessary to use several techniques of sample standardization. The results obtained from the different techniques and its subsequent integration allowed establishing the patterns of diversification of Neotropical vegetation during the Cenozoic. These patterns were then compared with a global climatic curve as well as with the flooding events to establish possible relationships (Chapters two and three).

It is well established that the history of Neotropical vegetation is closely linked to both regional and global changes in environment that occurred throughout the entire Cenozoic (Jaramillo et al., 2006; Hoorn et al., 2010 and references there in; Hoorn et al., 2018 and references there in; Antonelli, 2018). The Cenozoic experienced several transient global climate events (Paleocene-Eocene Thermal Maximum, Early Eocene Climatic Optimum, Middle Eocene Climatic Optimum, Oi-1 Glaciation, Mi-1 Glaciation, and Mid Miocene Climatic Optimum) (Figure 3.36) imposed over two major climatic sceneries: a greenhouse world during the Paleocene to middle Eocene and an icehouse world during the late Eocene to Present.

In the Chapter two, I find that the patterns of Neotropical plant diversity and taxonomic rates (origination and extinction) show a very close correspondence with the greenhouse and icehouse climates. In general, warmer climates correspond to high plant diversity and fluctuating turnover rates while cooler climates correspond to low diversity and static turnover rates. The amplitude of the fluctuations of the diversity curve and taxonomic rates also show a strong correspondence with the amplitude of the temperature curve, which was higher in the early Cenozoic greenhouse phase that in the later Cenozoic icehouse phase. The transient climatic events also played an important role in the macroevolutionary pattern of plants, particularly as drivers of extinction (Figure 3.26). Origination shows a strong correlation with the extinction in the previous 1 Ma interval indicating that when species become extinct in the Neotropics, they are replaced very rapidly. Therefore, transient climatic events of the Cenozoic played an important role in driving pulses of turnover among Neotropical plants.

In the greenhouse world of the Paleocene to early Eocene, the climatic conditions were in general much warmer than those of the Recent (Humber et al., 2009). After the asteroid impact and subsequent mass extinction of many groups at the CretaceousPaleocene boundary (K-Pg boundary) at 65.5 Ma, the world may have cooled for a few millennia (Nichols et al., 2008). However, conditions changed soon after this, in the early Paleocene. In the first 10 Ma after the K-Pg boundary, the world followed a warming trend to finally reach the maximum temperatures of the Cenozoic between 56 and 50 Ma (Figure 3.26). The palynological record of the Neotropics shows an increasing trend in diversity during this period with two very prominent peaks matching with the PETM (Paleocene-Eocene Thermal Maximum) and the EECO (Early Eocene Climatic Optimum) events. Extinction, origination and turnover rates are elevated and highly fluctuating during this period (Figure 3.26).

It is interesting to note that during most of the Paleocene the diversity was in general low. Only close to the Paleocene-Eocene boundary the diversity curve shows an increasing trend (Figure 3.26). The low diversity and

volatility of the taxonomic rates during the Paleocene is a direct consequence of the effect of the K-Pg event in Neotropical vegetation. A palynological study by de la Parra (de la Parra 2009), in a rock core drilled in northern Colombia, indicates that between 47 and 69% of the palynomorphs species disappeared below or at the K-Pg boundary. In comparison, estimates from temperate latitudes suggest extinction levels between 17 and 30% (Wolfe and Upchurch, 1986; Wilf and Johnosn, 2004; Hotton 2002). Extinction levels over the K-Pg boundary were extremely high in the Neotropics, and this resulted in dramatic differences in palynological composition between the Cretaceous and Paleocene (de la Parra 2009). The landscape went from being dominated by gymnosperms and ferns during the Cenozoic (Crane and Lidgar 1989) to completely be dominated by angiosperms in the Paleocene (Wing et al., 2009). Elevated K-Pg extinction in the Neotropics left several niches available. These niches were completely occupied approximately 10 Ma later, after which diversity reached similar values to those detected in the late Cretaceous (de la Parra, 2009). A good explanation of why it took so long to the vegetation to recover can be found in the climatic curve and paleogeography. Relatively low and fluctuating temperatures accompanied by extensive lacustrine systems and marine incursions in the recovery phase inhibited the full development of vegetation. In contrast, the constant and continuous increase in temperature with geographic areas devoid of barriers like lakes during the early Eocene, promoted diversification.

One of the most intriguing results of the present study is the abrupt decline in diversity observed during the early to middle Eocene (Figure 3.26). The low diversity is detected only in the shareholder quorum (SQS) results. On the contrary, estimates using boundary crossers and the range through assumption show a continuous increase in diversity during this interval (Figure 2.12). The discrepancy between the two estimates is well explained by range shifts and local extirpations rather than global extinctions. Studies using large phylogenies of extant plant species find that the Paleocene and Eocene correspond to the periods with the highest rates of emigration from the Neotropics during the entire Cenozoic (Morley 2000; Romero, 1993, Wilf et al., 2005, Antonelli et al., 2015) (Figure 2.81). Emigration was not compensated by immigrations, which in general were very low during the Cenozoic (Antonelli et al., 2015). My results are consistent with this finding, and suggest that an important proportion of plants species emigrated from the Neotropics during the middle Eocene, resulting in a decrease in regional richness that is evident in the SQS results (Figure 3.26). However, these species did not become extinct, and re-appear in the study region during the late Eocene. Therefore, range-through species richness estimates remain high during the middle Eocene (Figure 2.12).

The emigration of species out of the tropics during the early Eocene was triggered and facilitated by the geographical expansion of the Neotropics during the early Eocene Climatic Optimum (Jaramillo et al., 2015) and the absence of physical barriers, like marine corridors or lacustrine systems (Figure 3.26). In the upper part of the middle Eocene, the global temperature abruptly falls and this explains the low diversity. Although a diverse pool of species existed during this interval, the decline in temperature inhibited diversification and only when temperature abruptly increased during the mid Eocene Climatic Optimum MECO event, diversity reached values comparable to those of the early Eocene Climatic Optimum (Figure 3.26).

The interval between the Oligocene and Present is very interesting because approximately during the Eocene-Oligocene boundary the planet changed from a warm, ice-free greenhouse to a glacial Antarctic icehouse world (Francis et al., 2009). In the Neotropics, this change was accompanied by important regional events like the increase in orogenic activity of the Andes Cordillera (Mora et al., 2010), the onset of the Amazon River (Hoorn et al., 2017) and the occurrence of several flooding events (discussed in Chapter 3 of this work). It is believed that all these events helped to modulate the mega diversity of the Neotropics. In general, the fluctuations of the climatic curve during this period are lower in amplitude than those during the greenhouse world (Figure 3.26). The diversity curve and the taxonomic rates still show a close correspondence with the climatic curve. However, because of the low amplitude fluctuations in temperature, the response of the vegetation to the climatic changes was more accented. With respect to the transient events, the Oi-1 and Mi-1 glaciations are characterized by subtle falls in diversity while the warming event of the Mid Miocene Climatic Optimum shows an increase in diversity and fluctuating taxonomic rates (Figure 3.26).

From the middle Eocene to the middle Miocene, several marine incursions and lacustrine systems invaded and occupied extensive areas of the Neotropics (Figures 3.22 and 3.26). Previous studies suggested the occurrence of a marine incursion at the end of Eocene (Cooper et al., 1995; Villamil 1999; Santos et al., 2008). The evidence presented in Chapter three, indicates that the late Eocene marine incursion is just a continuation of a major regional flooding event that started at the end of the middle Eocene and ended approximately at the end of the late Oligocene. In fact, the palynological evidence shows that this was a complex event involving both marine incursions and lacustrine systems distributed over extensive regions (Figure 3.22). The geographic distribution of the floods suggests two phases. The first phase affected mainly southern Colombia and included a complete transgressive-regressive cycle during the middle to late Eocene. The final regressive cycle left a lacustrine system that extended from the south of the Llanos basin

to the Middle Magdalena Valley (Figure 3.22). The second phase, occurring during the early to late Oligocene, affected northern Colombia and is characterized by a mixture of marine and lacustrine conditions. The diversity curve and taxonomic rates exhibit an abrupt decline and intense fluctuations during the first phase, while the second phase is characterized by a subtle increasing trend of diversity and low amplitude fluctuations of the taxonomic rates. This pattern shows a good correspondence with global climatic curve (Figure 3.26) suggesting that, at least for this interval, climate exerted a major control in the macroevolutionary pattern of plants than flooding events.

From the Miocene to Present the Neotropics experienced several flooding episodes (Figure 3.23) and intense orogenic activity of the Andes Cordillera (Mora et al., 2010). With respect to the floods, these were temporally restricted from the early to late Miocene. However, the information compiled in this work is scarce for the late Miocene, which prevent a reliable interpretation for this interval. Hoorn et al. (1993, 1994, 2010c) proposed the development of a long-lived aquatic or mega wetland system, known as the Pebas system, which covered western Amazonia between 24 and 7 Ma (Wesselingh et al., 2001; Wesselingh et al., 2006) (Figure 3.1). The evolution of the Pebas system corresponds to three phases (Precursor, Pebas, and Acre), which differ in their predominance and alternation of fluvial, marine or lacustrine conditions (Hoorn et al. 2010c). On the other hand, Jaramillo et al. (2017), using palynological information and seismic interpretation, suggested two separate marine incursions (early Miocene Incursion (EMI) and middle Miocene Incursion (MMI)) that partially correspond to the Precursor and Pebas phases of Hoorn et al. (2010c) (Figure 3.23), which also covered western Amazonia. The evidence presented in the Chapter three, support the findings of Hoorn et al. (2010c) in the sense that the Precursor and Pebas phases correspond to a single event characterized by alternation of marine, fluvial and lacustrine conditions and not to the two separate and exclusively marine incursion interpreted by Jaramillo et al. (2017). Although it is important to notice that the evidence for the Precursor phase is scarce and difficult to interpret (Figure 3.23).

Previous evidence of the Miocene floods came mainly from studies of the Llanos basin and western Amazonia (Jaramillo et al., 2017 and references there in; Hoorn et al., 2010 and references there in). For this reason, it was not clear if the geographic distribution of the floods was in fact restricted to those areas or if they correspond to a bias imposed by the concentration of studies there. The analysis and comparison of the Middle and Upper Magdalena Valleys presented here (Chapter three) indicates that during the upper early Miocene (approximately 16.5 Ma) these two basins were covered by lacustrine systems. A detailed analysis of well Gb-1 located in the Up-

per Magdalena Valley showed that the deposits of the Barzalosa Formation correspond to a complex lacustrine system in which three phases were identified (Figure 3.8). The three proposed phases show marked differences in the proportion of algae (Botryococcus and Pediastrum), palynological composition and pattern of sediment accumulation (Figure 3.8). These changes were controlled by climate and geologic factors mainly related to the input of nutrients.

I find that the Barzalosa Formation in the Upper Magdalena Valley corresponds stratigraphically to the Colorado Formation and specifically to the La Cira fossiliferous horizon of the Middle Magdalena Valley. Although the Colorado Formation was not analyzed in detail, previous paleontological (Pilsbry and Olson, 1935) and palynological analysis indicates the influence of lacustrine conditions during the deposition of this unit. This evidence therefore shows that the Miocene floods were not restricted to the Llanos basin and western Amazonia, but also reached the intramontane basins of the Middle and Upper Magdalena Valleys. It is hypothesized that the emergence of the eastern Cordillera acted as an effective orographic barrier creating aridification in the Magdalena Valleys by middle Miocene times (Horton et al., 2010). This aridification and the influx of sediments were responsible of the culmination of these systems. When compared with the diversity curve and taxonomic rates, the Miocene floods seem to have had only a minor effect on vegetation (Figure 3.26). Again, climate exerted a major control with a peak in diversity and increasing taxonomic rates during the global warming event of the Mid Miocene Climatic Optimum.

With respect to the Andes uplift, apatite fission track analysis suggests that the most intense peaks or orogenic activity occurred at the end of the middle Miocene (12.4 Ma) and early Pliocene (4.4 Ma) (Hoorn et al., 2010b). Several studies have emphasized the pivotal role of the Andes uplift in the evolution of Amazonia ecosystems (Hoorn et al., 2018). It is now clear that this event changed the neotropics landscapes by reconfiguring drainage patterns and creating vast influx of sediments that produced a wide mosaic of edaphic conditions in the region (Hoorn et al., 2010b). The edaphic changes and new niches promoted diversification in Amazonia.

I find that the interval with the most intense orogenic activity (12.4 to 4.4 Ma) is in turn characterized by a continuous declining trend in global temperature that started at the end of the Mid Miocene Climatic Optimum and ended at the early Pliocene (Figure 3.26). This interval is characterized by a low diversity and taxonomic rates showing a declining trend (Figure 3.26). These findings are well supported by information from literature analysed in Chapter two corresponding to localities in Panama and Amazonia (Figure 2.35). Because both the Andes uplift and climate change occurred

contemporaneously, it is difficult to distangle the role played for each one in producing low diversity and declining taxonomic rates. However, it is reasonable to think that in addition to the cooling conditions, during the reconfiguration of the landscape the vegetation did not adjust immediately and only when the intense orogenic activity ceased and the new niches were completely established the vegetation strengthened and diversity increased reaching the values observed at the end of the Pliocene (Figure 3.26). It is also not possible to rule out a preservation bias produced by the reconfiguration of the drainage patterns. The influx of sediments from the Andes Cordillera produced alluvial deposits and scarce fine grained deposits, which are those that preserve palynomorphs. The low number of samples analyzed during this interval gives support to this interpretation. The dominance of alluvial deposits also helps to explain the absence of lacustrine deposits during this interval (Figure 3.26).

Finally, the Pleistocene show an outstanding peak in diversity as well as relatively elevated taxonomic rates (Figure 3.26). A close inspection of the diversity estimates for the individual samples reveals that in fact this peak is the result of the contribution of a single sample from the area G (Figure 2.49). This sample inflates diversity to levels not reached when the curve is estimated using the mean of the samples (Figure 2.30). However, both curves show that diversity is higher in the Pliocene and Pleistocene than in the late Miocene. This increase in diversity coincides with the last peak of orogenic activity at 4.4 Ma. Orogenic activity then declines until Present (Hoorn et al., 2010b). The correspondence between an increasing diversity and declining orogenic activity corroborates that only when the new niches were fully established vegetation diversified. The process of diversification does not exclusively correspond to in situ diversification but it is becoming clearer that immigrant lineages from both the north (Sklenar et al., 2011) and south (Bacon et al., 2018) played a very important role in the historic assembly of the Amazon flora (Hoorn et al., 2010b). The recent and rapid diversification of Andes lineages could be explained by the massive increase in the area of suitable habitats and opportunities for allopatric speciation, as a consequence of the Andean uplift and late Neogene climatic changes (Mora, 2008; Bacon et al., 2018).

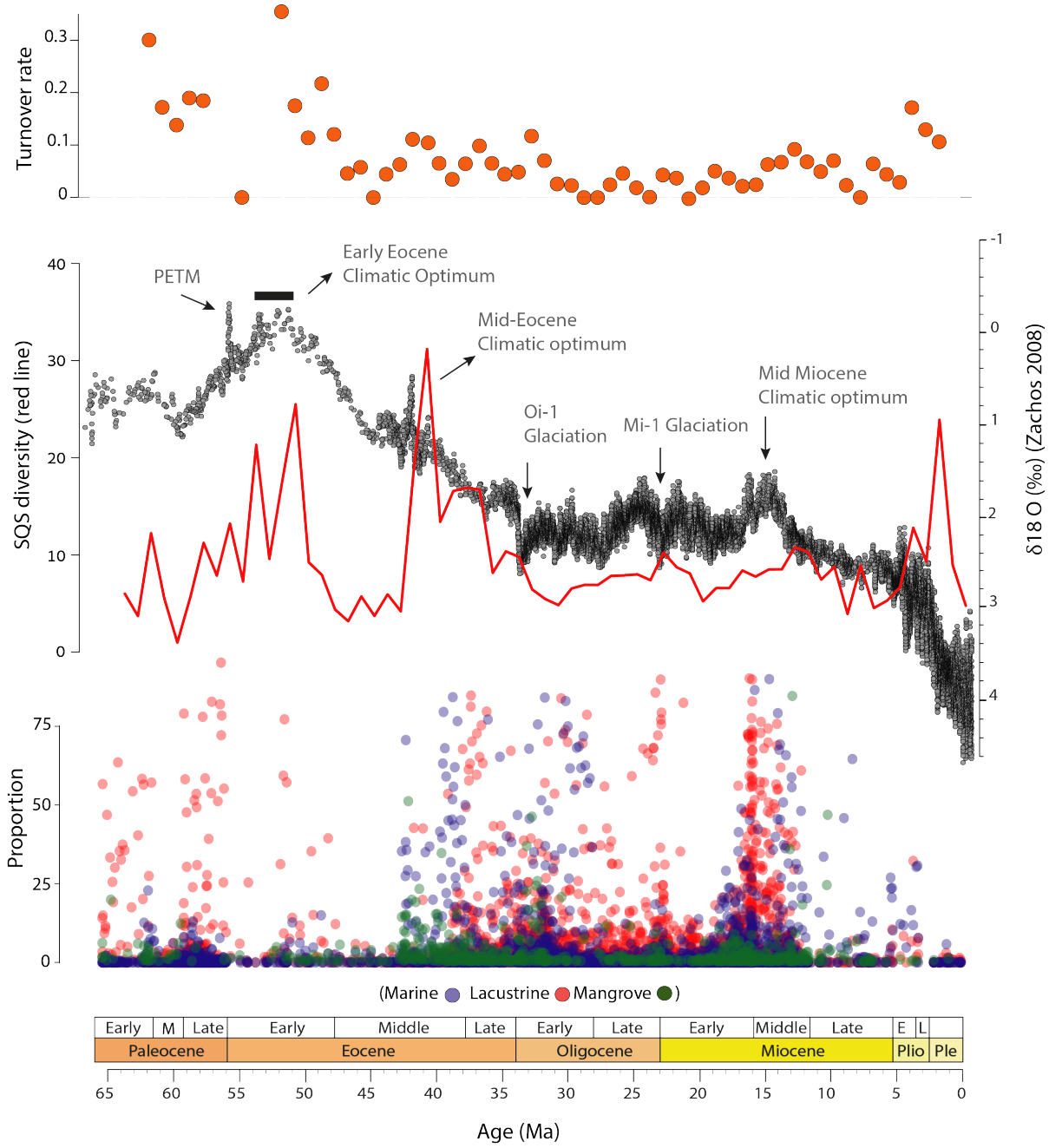

Figure 4.1: Synthesis of the macroevolutionary history of Neotropical vegetation during the Cenozoic showing turnover rates, SQS diversity, global temperature and floods.

Chapter 5

Annexes

- Chapter-1
  - **1.1** Sites used in the graphic correlation project.
  - **1.2** Lines of correlation the for sections used in this study.
  - **1.3** Final Sequence of Biostratigraphic events.
  - **1.4** List of Biostratigraphic events, Composite units, age (Ma),number of sites, spreading parameters, and biozone.
  - **1.5** List of species and sites (This annex need to be requested from the author)
  - **1.6** Association rules statistics.
  - **1.7** Systematic Palynology.
- Chapter-2
  - **2.1** Sections used in the Macroevolutionary analysis.
  - **2.2** Lines of correlation for new sections.
  - **2.3** Information of the sections from the literature used in the comparisons of diversity.
  - **2.4** SQS diversity of samples from literature and internal reports of Ecopetrol S.A.
  - **2.5** Codes of the sections used in the diversity choroplet maps.
  - **2.6** Information of the sections that compose each time interval.
  - **2.8 - 2.17** Differences in SQS diversity among sites according to Tukey's test.
  - **2.18** Benthic formainifera delta O18 data.

  - **2.19** Summary of the pairwise test correlation over the entire Cenozoic.
  - **2.20** Summary of the pairwise test correlation for the intervals 5 to 40 Ma and 51.5 to 66.5 Ma.
  - **2.21** Summary of the Generalized least square regression model for the interval 5-40 Ma.
  - **2.22** Summary of the Generalized least square regression model for the interval 51.5 -64.5 Ma.

- Chapter-3
  - **3.1** Sites and areas used in this study.
  - **3.2** Lithological information of the well Gb-1 for the Barzalosa Formation.
  - **3.3**Salinity index summary for the section located in the areas B, D, F, H, and I for the interval between 35 and 28 Ma.

References

Aaronson, S., T. Berner, K. Gold, L. Kushner, N. Patni, A. Repak, and D. Rubin. 1983. Some observations on the green planktonic alga, *Botryococcus braunii* and its bloom form. Journal of Plankton Research 5(5).

Acosta, J., R. Guatame, J. Caicedo, and J. Cardenas. 2002. Mapa Geologico de Colombia. Plancha 245 Girardot, Escala 1:10000. Memoria Explicativa. Ingeominas.

Antoine, P.-O., M. A. Abello, S. Adnet, A. J. Altamirano Sierra, P. Baby, G. Billet, M. Boivin, Y. Caldern, A. Candela, J. Chabain, F. Corfu, D. A. Croft, M. Ganerd, C. Jaramillo, S. Klaus, L. Marivaux, R. E. Navarrete, M. J. Orliac, F. Parra, M. E. Prez, F. Pujos, J.-C. Rage, A. Ravel, C. Robinet, M. Roddaz, J. V. Tejada-Lara, J. Vlez-Juarbe, F. P. Wesselingh, and R. Salas-Gismondi, 2016, A 60-million-year Cenozoic history of western Amazonian ecosystems in Contamana, eastern Peru: Gondwana Research 31, p. 30-59.

Antonelli, A., and I. Sanmartin. 2011. Why are there so many plant species in the Neotropics? Taxon 60(2):403-414.

Agrawal, R., Srikant, R. 1994. Fast Algorithms for Mining Association Rules. Pp. 487-499. In M. J. JB Bocca, C Zaniolo (eds), ed. Proc 20th Int. Conf, Very Large Data Bases, VLD. Morgan Kaufmann.

Agterberg, F. P., and F. M. Gradstein. 1999. The RASC method for ranking and scaling of biostratigraphic events. Earth-Science Reviews 46(1-4):1-25.

Agterberg, F. P., F. M. Gradstein, Q. Cheng, and G. Liu. 2013. The RASC and CASC programs for ranking, scaling and correlation of biostratigraphic events. Computers and Geosciences 54:279-292.

Alroy, J. 1996. Constant extinction, constrained diversification, and uncoordinated stasis in North American mammals. Palaeogeography, Palaeoclimatology, Palaeoecology 127:285-311.

Alroy, J. 1998. Equilibrial diversity dynamics in North American mammals. In M. L. M. a. J.Drake, ed. Bodiversity dynamics: turnover of populations, taxa and communities. Columbia University Press, New York.

Alroy, J. 1999. The fossil record of North American mammals: evidence

for a Paleocene evolutionary radiation. Systematic Biology 48(1):107-118.

Alroy, J. 1999. Putting North America's end Pleistocene megafaunal extinction in context: large scale analyses of spatial patterns, extinction rates , and size distributions. In R. MacPhee, ed. Extinctions in near time: causes, contexts, and consequences. Plenum, New York.

Alroy, J. 2000. Succesive approximations of diversity curves: Ten more years in the library Geology 28(11):1023-1026.

Alroy, J. 2008. Dynamics of Origination and extinction in the marine fossil record. PNAS 105(1):11536-11542.

Alroy, J. 2008. Phanerozoic Trends in the Global Diversity of Marine Invertebrates. Science 321.

Alroy, J. 2009. Speciation and extinction in the fossil record of North American mammals. In J. R. B. a. D. S. Roger K. Butlin, ed. Speciation and Patterns of Diversity. Cambridge University Press, British Ecological Society.

Alroy, J. 2010. Geographical, Environmental and Intrinsic Biotic Controls on Phanerozoic Marine Diversification. Palaeontology 53(6):1211-1235.

Alroy, J. 2010. Fair Sampling of Taxonomic Richness and Unbiased Estimation of Origination and extinction Rates. Pp. 55-80. In J. Alroy and G. Hunt eds. Quantitative Methods in Paleontology. Paleontological Society Short Course, The Paleontological Society.

Alroy, J. 2010b. The shifting balance of diversity among major marine animal groups. Science 329(5996):1191-4.

Alroy, J. 2014. Accurate and precise estimates of origination and extinction rates. Paleobiology 40(03):374-397.

Alroy, J., C. R. Marshall, R. K. Bambach, K. Bezusko, M. Foote, F. T. Fursich, T. A. Hansen, S. M. Holland, L. C. Ivany, D. Jablonski, D. K. Jacobs, D. C. Jones, M. A. Kosnik, S. Lidgard, S. Low, A. I. Miller, P. M. Novack-Gottshall, T. D. Olszewski, M. E. Patzkowsky, D. M. Raup, K. Roy, J. J. Sepkoski, Jr., M. G. Sommers, P. J. Wagner, and A. Webber. 2001. Effects of sampling standardization on estimates of Phanerozoic marine diversification. Proc Natl Acad Sci U S A 98(11):6261-6.

Antonelli, A., A. Zizka, D. Silvestro, R. Scharn, B. Cascales-Minana, and C. Bacon. 2015. An engine for global plant diversity: highest evolutionary turnover and emigration in the American tropics. Front Genet 6:130.

Arnold, A., Parker, W, Hansard, S. 1995. Aspect of the post-Cretaceous recovery of the Cenozoic planktic foraminifera. Marine Micropaleontology 26:319-327.

Arouri, K., P. Conaghan, M. Walter, G. Bischoff, and K. Grey. 2000. Reconnaissance sedimentology and hydrocarbon biomarkers of Ediacarian

microbial mats and acritarchs, lower Ungoolya group, officer basin. Precambrian Research 100.

Bacon, C., F. Velasquez-Puentes, and L. Hinojosa. 2018. Evolutionary persistence in Gunnera and the contribution of southern plant groups to the tropical Andes biodiversity hotspot. PeerJ.

Batten, D. 1982. Palynofacies, palaeoenvironments and petroleum. Journal of Micropaleontology 1.

Bayona, G., C. Jaramillo, M. Rueda, A. Reyes-Harker, V. Torres. 2007. Paleocene-Middle Miocene Flexural-Margin Migration of the nonmarine Llanos Foreland Basin of Colombia. CT and F Ciencia, Tecnologia y Futuro 3(3).

Bayona, G., M. Cortez, C. Jaramillo, G. Ojeda, J. Ariztizabal, A. Reyes-Harker. 2008. An integrated analysis of an orogensedimentary basin pair: Latest CretaceousCenozoic evolution of the linked Eastern Cordillera orogen and the Llanos foreland basin of Colombia. Geological Society of America Bulletin 120.

Bayona, G., A. Cardona, C. Jaramillo, A. Mora, C. Montes, V. Caballero, H. Mahecha, F. Lamus, O. Montenegro, G. Jimenez, A. Mesa, and A. Valencia. 2013. Onset of fault reactivation in the Eastern Cordillera of Colombia and proximal Llanos Basin; response to CaribbeanSouth American convergence in early Palaeogene time. In M. Nemcok, A. Mora, and J. Cosgrove, eds. Thick-Skin-Dominated Orogens: From Initial Inversion to Full Accretion. Geological Society, London, Special Publications, 377.

Bayona, G., A. Valencia, A. Mora, M. Rueda, J. Ortiz, and O. Montenegro. 2008b. Estratigrafia y procedencia de las rocas del Miocene en la parte distal de la cuenca de antepais de los Llanos de Colombia. Geologia Colombiana 33.

Bennet, K., S. Bhagwat, and K. Willis. 2012. Neotropical refugia. The Holocene 22(11):1207-1214.

Benson, R., and R. Butler. 2011. Uncovering the diversification history of marine tetrapods: ecology influences the effect og geological sampling biases. In A. S. McGowan, A.B ed. Comparing the Geological and Fossil Records: Implications for biodiversity Studies. Geological Society, London, Special Publication 358.

Benson, R. B., R. J. Butler, J. Alroy, P. D. Mannion, M. T. Carrano, and G. T. Lloyd. 2016. Near-Stasis in the Long-Term Diversification of Mesozoic Tetrapods. PLoS Biology 14(1):e1002359.

Benson, R. B., and P. D. Mannion. 2011. Multivariate models are essential for understanding vertebrate diversification in deep time. Biolology Letters 8:127-130.

Benton, M. 1995. Diversification and Extinction in the history of Life. Science 268.

Bermudez, H., J. Garcia, W. Stinnesbeck, G. Keller, J. Rodriguez, M. Hanel, J. Hopp, W. Schwarz, M. Trieloff, L. Bolivar, and F. Vega. 2015. The CretaceousPalaeogene boundary at Gorgonilla Island, Colombia, South America. Terranova 28(1).

Bijl, P., A. Houben, S. Schouten, S. Bohaty, A. Sluijs, G. Reichart, S. Damste, and H. Brinkhuis. 2010. Transient Middle Eocene Atmospheric CO2 and Temperature Variations. Science 330.

Birks, H. J. B., V. A. Felde, A. E. Bjune, J.-A. Grytnes, H. Sepp, and T. Giesecke. 2016. Does pollen-assemblage richness reflect floristic richness? A review of recent developments and future challenges. Review of Palaeobotany and Palynology 228:1-25.

Boessenkool, K., M. Van Gelder, H. Brinkhuis, and S. Troelstra. 2001. Distribution of organic-walled dinoflagellate cysts in surface sediments from transects across the Polar Front offshore southeast Greenland. Journal of Quaternary Science 16(7).

Bohacs, K., A. Carroll, J. Neal,P. Mankiewicz. 2000. Lake-Basin Type, Source Potential, and Hydrocarbon Character: An integrated Sequence-Stratigraphic-Geochemica, Framework. In E. H. Gierlowski and K. Kelts, eds, Lake basins through space and time: AAPG Studies in Geology. 46.

Bohaty, S., and J. Zachos. 2003. Significant Southern Ocean warming event in the late middle Eocene. Geology 31(11).

Bohaty, S., J. Zachos, F. Florindo, and M. Delaney. 2009. Coupled greenhouse warming and deep-sea acidification in the middle Eocene. Paleoceanography 24.

Boltovskoy, D. 1988. The range-through method and first-last appearance data in paleontological surveys. Journal of Paleontology 62:157-159.

Boonstra, M., M. Ramos, E. Lammertsma, P. Antoine, C. Hoorn. 2015. Marine connections of Amazonia: Evidence from a foraminifera and dinoflagellate cysts (early to middle Miocene, Colombia/Peru). Palaeogeography, Palaeoclimatology, Palaeoecology 417:176-194.

Boyd, J., J. Riding, M. Pound, S. De Schepper, R. Ivanovic, A. Haywood, and S. Wood. 2018. The relationship between Neogene dinoflagellate cysts and global climate dynamics. Earth Sciences Reviews 177.

Bradshaw, E., P. Rasmussen, H. Nielsen, and N. Anderson. 2005. Mid- to late-Holocene land-use change and lake develop- ment at Dallund So, Denmark: trends in lake primary production as reflected by algal and macrophyte remains. The Holocene 15.

Brasier, M. 1985. Fossil indicators of nutrient levels. 1: eutrophication and climate change. In D. Bosence, and P. Allison, eds. Marine Palaeoenvironmental Analysis from Fossils. Geological Society, Special Publication.

Brenner, W., and C. Foster. 1994. Chlorophycean algae from the Triassic of Australia. Review of Palaeobotany and Palynology 80.

Bueno, M., R. Pennington, Lavin, M., Sarkinen, T., Lewis, G., Klitgaard, B., Hughes, C, K. Dexter, L. Kamino, V. Pontara, D. Neves, J. Retter, and A. Oliveira. 2017. Effects of Quaternary climatic fluctuations on the distribution of Neotropical savanna tree species. Ecography 40:403-414.

Bush, A., M. Markey, and C. Marshall. 2004. Removing bias from diversity curves: the effect of spatially organized biodiversity on sampling standardization. Paleobiology 30:666-686.

Bush, M., M. Miller, and P. de Oliveira. 2002. Orbital forcing signal on sediments of two Amazonina lakes. Journal of Paleolimnology 27:341-352.

Buzas, M., Culver, S. 1998. Assembly, disassembly, and balance in marine communities. Palaios 13:263-275.

Caballero, M., S. Lozano, B. Ortega, J. Urrutia, and J. Macias. 1999. Environmental characteristics of Lake Tecocomulco, northern basin of Mexico, for the last 50,000 years. Journal of Paleolimnology 22.

Caballero, V., M. Parra, and A. Mora. 2010. Levantamiento de la Cordillera Oriental de Colombia durante el Eoceno tardo-Oligoceno temprano: proveniencia sedimentaria en el Sinclinal de Nuevo Mundo, cuenca Valle Medio del Magdalena. Boletin de Geologia UIS 32:45-77.

Caceres, C., and F. Etayo-Serna. 1969. Memoria Cuadrangulo L-10 Fusagasuga. Inedito.

Campbell, K., C. Frailey, and L. Pittman. 2006. The Pan-Amazonian Ucayali Peneplain, late Neogene sedimentation in Amazonia, and the birth of the modern Amazon River system. Palaeogeography, Palaeoclimatology, Palaeoecology 239.

Cardenas, D., S. Gonzales-Caro, J. Duivenvoorden, and K. Feeley. 2017. Assymetrical niche determinism across geological units shapes phylogenetic tree communities in the Colombian Amazonia. Perspectives in Plant Ecology, Evolution and Systematics 28:1-9.

Carr, D., D. White, and A. MacEachren. 2005. Conditioned Choropleth Maps and Hypothesis Generation. Annals of the Association of American Geographers 95(1):32-53.

Carroll, A., K. Bohacs. 1999. Stratigraphic classification of ancient lakes: Balancing tectonic and climatic controls. Geology 27.

Carvajal, H., G. Mora, and C. Jaramillo. 2009. A molecular evaluation of bulk organic carbon-isotope chemostratigraphy for terrestrial correlations: An example from two PaleoceneEocene tropical sequences. Palaeogeography, Palaeoclimatology, Palaeoecology 277.

Caycedo, H., and O. Catuneanu, 2018, Stratigraphic architecture of incised valleys and unincised channel systems in the Carbonera Formation (C6-

C1 members: Upper Oligocene Lower Miocene), Llanos basin, Colombia: Journal of Geodynamics.

Cazier, E., A. Hayward, G. Espinoza, J. Velandia, J. Mugniot, and W. Leel. 1995. Petroleum geology of the Cusiana Field, Llanos Basin Foothills, Colombia. APPG Bulletin 79(10).

Chao, A., C. Chiu, and L. Jost. 2014. Unifying species diversity, phylogenetic diversity, functional diversity, and related similarity/differentiation measures through Hill numbers. Annual Reviews of Ecology, Evolution, and Systematics 45.

Chao, A., and L. Jost. 2015. Estimating diversity and entropy profiles via discovery rates of new species. Methods in Ecology and Evolution 6.

Chatfield, C. 2003. The Analysis of Time Series: An Introduction. Chapman and Hall, London.

Cheetham, A., Deboo, P. 1963. A numerical index for biostratigraphic zonation in the mid-Tertiary of the eastern Gulf. Gulf Coast Association of Geological Societies Transactions 13:139-147.

Cheng, H., A. Sinha, F. W. Cruz, X. Wang, R. L. Edwards, F. M. d'Horta, C. C. Ribas, M. Vuille, L. D. Stott, and A. S. Auler. 2013. Climate change patterns in Amazonia and biodiversity. Nat Commun 4:1411.

Chrisophel, D. 1995. The Impact of climatic changes on the development of the Australian flora. In N. R. Council, ed. Effects of past global change on Life. National Academy Press, Washington, D.C.

Christopoul, F., P. Baby, and C. Davila. 2002. Stratigraphic response to a major tectonic event in a foreland basin: the Ecuadorian Oriente Basin from Eocene to Oligocene times. Tectonophysics 345.

Chu, S. 1943. The influence of mineral composition of the medium on the growth of planktonic algae. Part II. The influence of the concentration of inorganic nitrogen and phosphate phosphorous. Journal of Ecology 31.

Close, R., S. Evers, J. Alroy, and R. J. Butler. 2018. How should we estimate diversity in the fossil record? Testing richness estimators using sampling-standardised discovery curves. Methods in Ecology and Evolution 9.

Colinvaux, P., and P. de Oliveira. 2001. Amazon plant diversity and climate through the Cenozoic. Palaeogeography, Palaeoclimatology, Palaeoecology 166.

Colinvaux, P., and P. de Oliveira, 2001, Amazon plant diversity and climate through the Cenozoic: Palaeogeography, Palaeoclimatology, Palaeoecology, v. 166.

Cooper, M., F. Addison, R. Alvarez, A. Hayward, S. Howe, A. Pulham, and A. Taborda. 1995. Basin development and tecnotic history of the Llanos

Basin, Colombia. In J. Tankard, R. Suarez, and H. Welsink, eds. Petroleum basins of South America. AAPG Memoir 62.

Crame, A. 2001. Taxonomic diversity gradients through geological time. Diversity and Distributions 7:175-189.

Crane. P, S. Lidgard. 1989. Angiosperm diversification and paleolatitudinal gradients in Cretaceous floristic diversity. Science, 246

Cromley, R., and E. Cromley. 2009. Chloroplet map legend design for visualizing community health disparities. International Journal of Health Geographics 8(52).

Cross, A., G. Thompson, and J. Zaitzeff. 1996. Source and distribution of palynomorphs in bottom sediments, southern part of Gulf of California. Marine Geology 4.

D' Apolito, C. 2016.Landscape Evolution in Western Amazonia: Palynostratigraphy, Palaeoenvironments and Diversity of the Miocene Solimoes Formation, Brazil. PhD Thesis. University of Birmingham.

Danielsen, R. 2010. Dissimilarities in the recent histories of two lakes in Portugal explained by local scale environmental processes. Journal of Paleolimnology 43.

Davis, J. 2002. Statistics and Data Analysis in Geology. John Wiley and Sons.

De Caceres, M., and L. Legendre. 2009. Association between species and group of sites: indices and statistical inference. Ecology 90(12).

De Caceres, M., P. Legendre, S. Wiser, and L. Brotons. 2012. Using species combinations in indicator value analysis. Methods in Ecology and Evolution 3.

De Deckker, P. 1988. Large Australian lakes during the last 20 million years: site for petroleum source rock or metal ore deposition, or both? In A. Fleet, K. Kelts, and M. Talbot, eds. Lacustrine petroleum source rocks. Geological Society London. Spl. Publ 40, London.

De la Parra, F., A. Mora, M. Rueda, and I. Quintero. 2015. Temporal and spatial distribution of tectonic events as deduced from reworked palynomorphs in the eastern Northern Andes. AAPG Bulletin 99(8):1455-1472.

De la Parra, F., G. Rodriguez, C. Vargas, O. Bedoya, and M. Rueda. 2018. GeoPanTro: a database of palynological data from Northern South America. Instituto Colombiano del Petroleo Bucaramanga-Colombia.

de Porta, J. 1962. Edentata Xenarthra del Mioceno de La Venta (Colombia), 1: Dasypodoidea y Glyptodontoidea. Boletin de Geologia UIS 22.

De Porta, J. 1974. Lxique Stratigraphique International. Amerique Latine, Colombie (deuxieme partie), Terciario y Cuaternario. Centro. Nat. Rech. Sci 5 (4b).

Decommer, H. 1982. Etude palynoplanctologique et cadre sedimentologique du Jurassique et du Cretace du nord de. Annales de la Societe Geologique du 101.

Dengo, C. A., and M. C. Covey. 1993. Structure and of the Eastern of Colombia: Impications for trap styles and regional tectonics. AAPG Bulletin 77:1315-1337.

Dexter, K., M. Lavin, B. Torke, A. Twyford, T. Kursar, P. Coley, C. Drake, R. Hollands, and T. Pennington. 2017. Dispersal assembly of rain forest tree communities across the Amazon Basin. PNAS 114(10):2645-2650.

Dickens, G., J. O'Neil, D. Rea, and R. Owen. 1995. Dissociation of oceanic methane hydrate as a cause of the carbon isotope excursion at the end of the Paleocene. Paleoceanography 10.

Dino, R., E. Soares, L. Antonioli, C. Riccomini, and A. Nogueira. 2012. Palynostratigraphy and sedimentary facies of Middle Miocene fluvial deposits of the Amazonas Basin, Brazil. Journal of South American Earth Sciences 34.

Duarte, E., G. Bayona, C. Jaramillo, M. Parra, I. Romero, and A. Mora. 2017. Identificacion de los maximos eventos de inundacion marina Miocenos y su uso en la correlacion y analisis de la cuenca de antepais de los Llanos Orientales de Colombia. Boletin de Geologia UIS 39.

Dubreuil, C., S. Derenne, S. Largeau, C. Berkaloff, and B. Rousseau. 1989. Mechanism of formation and chemical structure of CoorongiteI. Role of the resistant biopolymer and of the hydrocarbons of *Botryococcus braunii*. Ultrastructure of Coorongite and its relationship with Torbanite. Organic Geochemistry 14(5).

Duque, A., M. Sanchez, J. Cavelier, and J. Duivenvoorden, 2002, Different floristic patterns of woody understory and canopy plants in Colombian Amazonia: Journal of Tropical Ecology, v. 18.

Echeverri, A., and V. Gallo. 2015. Historical relationship of the Caribbean and Amazonian Miocene ichthyofaunas: A hypothesis reviewed under a biogeographical approach. Geobios 48.

Ecopetrol-ICP, and STRI. 2011. Proyecto Cronologia de las Secuencias Bioestratigraficas del Cretacico. Fase II. Internal Report.

Ediger, V., and Z. Bati. 1988. Morphological examination of *Pediastrum* (Chlorophyta) from the tertiary strata of the Thrace Basin (NW Turkey). Pollen et Spores XXX(2).

Edwards, L. 1984. Insights on Why Graphic Correlation (Shaw's Method) Works. The Journal of Geology 92(5).

Edwards, L. 1995. Graphic Correlation: Some Guidelines on Theory and Practice and how they related to reality. Pp. 45-50. In K. O. Mann, and Lane, H.R, ed. Graphic Correlation. SEPM Special Publication.

Fajardo, A., L. Rojas, and J. Cristancho, 2000, Definicion del modelo estratigrafico en el intervalo Cretaceo a Mioceno medio en la cuenca de los Llanos Orientales y Piedemonte Llanero: Bucaramanga, Instituto Colombiano del Petroleo, Internal Report.

Farris, D., C. Jaramillo, G. Bayona, S. Restrepo, C. Montes, A. Cardona, A. Mora, R. Speakman, M. Glasscock, M. Reiners, and A. Valencia. 2011. Fracturing of the Panamanian Isthmus during initial collision with South America. Geology 39.

Felde, V., S. Peglar, A. Bjune, A. Grytnes, and H. Birks. 2016. Modern pollen-plant richness and diversity relationships exist along a vegetational gradient in southern Norway. The Holocene 26:163-175.

Fine, P. V., R. Ree, and R. J. Burnham. 2008. Disparity in tree species richness between tropical, temperate and boreal biones: the geographic area and age hypothesis. In W. Carson and S. Schnizer eds. Tropical Forest Community Ecology. London: Blackwell.

Foote, M. 1988. Survivorship Analysis of Cambrian and Ordovician Trilobites. Paleobiology 14(3):258-271.

Foote, M. 1993. Discordance and Concordance between Morphological and Taxonomic Diversity Paleobiology 19(2):185-204.

Foote, M., Sepkoski Jr. 1999. Absolute measures of the completeness of the fossil record. Nature 398:415-417.

Foote, M., and A. Miller. 2006. Principles of Paleontology-Third edition. W. H. Freeman.

Fortunel, C., P. Timothy, P. Fine, N. Kraft, and C. Baraloto, 2014, Environmental factors predict community functional composition in Amazonian forests: Journal of Ecology, v. 102.

Foster, G., C. Lear, and J. Rae. 2012. The evolution of pCO2, ice volume and climate during the middle Miocene. Earth and Palnetary Science Letters 341-344:243-254.

Francis. J, S. Marensi, R. Levy, Hambrey. M, V. Thorn, B. Mohr, H. Brinkhuis, J. Warnaar, J. Zachos, S. Bohat, R. DeConto. 2009. Form Greenhouse to Icehouse The Eocene Oligocene in Antarctica. Developments in Earth and Environmental Sciences.8

Fraass, A. J., D. C. Kelly, and S. E. Peters. 2015. Macroevolutionary History of the Planktic Foraminifera. Annual Review of Earth and Planetary Sciences 43(1):139-166.

Frailey, C., E. Lavina, A. Rancy, and J. Souza-Filho. 1998. A proposed Pleistocene/Holcene lae in the Amazon basin and its significance to Amazonian Geology and biogeography. Acta Amazonica 18.

Galazzo, F., E. Thomas, M. Pagani, C. Warren, V. Lucani, and L. Giusberti. 2014. The middle Eocene climatic optimum (MECO): A multiproxy

record of paleoceanographic changes in the southeast Atlantic. Paleoceanography 29.

Gee, C. 2001. The mangrove palm *Nypa* in the geologic past of the New world. Wetlands Ecology and Management 9.

Gentry, A. 1992. Tropical Forest Biodiversity: Distributional Patterns and their Conservational Significance. Oikos 63:19-28.

Germeraad J., H. C., Muller J. 1968. Palynology of Tertiary sediments from tropical areas. Palaeobotany and Palynology 6:189-348.

Glikson, M., K. Lindsay, and J. Saxby. 1989. *Botryococcus*: A planktonic green alga, the source of petroleum through the ages: Transmission electron microscopical studies of oil shales and petroleum source rocks.Organic Geochemistry 14(6).

Goldner, A., N. Herold, and M. Huber. 2014. The challenge of simulating the warmth of the mid-Miocene climatic optimum in CESM1. Climate of the Past 10(2):523-536.

Gomez, A., C. Jaramillo, M. Parra, and A. Mora. 2009. Huesser Horizon: A Lake and a Marine Incursion in Northwestern South America during the Early Miocene. Palaios 24(3-4):199-210.

Gonzales, A. 1967. A palynological study on the upper Los Cuervos and Mirador formations (lower and middle Eocene), Tibu Area, Colombia. Leiden: E.J. Brill.

Gorini, C., B. Haq, A. dos Reis, A. Silva, A. Cruz, E. Soares, and D. Grangeon. 2013. Late Neogene sequence stratigraphy evolution of the Foz do Amazonas Basin, Brazil Terra Nova 26(3).

Gosling, W., M. Bush, J. Hanselman, and A. Chepstow. 2008. Glacial-interglacial changes in moisture balance and the impact on vegetation in the southern hemisphere tropical Andes (Bolivia/Peru). Palaeogeography, Palaeoclimatology, Palaeoecology 259.

Gosling, W. D., F. E. Mayle, N. J. Tate, and T. J. Killeen. 2009. Differentiation between Neotropical rainforest, dry forest, and savannah ecosystems by their modern pollen spectra and implications for the fossil pollen record. Review of Palaeobotany and Palynology 153(1-2):70-85.

Gradstein, F. 2004. Quantitative Methods for Applied Microfossil Biostratigraphy.In E. Koutsoukos ed. Applied Stratigraphy. Topics in Geobiology. v23. Springer, Dordrecht.

Gradstein F.M., J. Ogg, A.Smith. 2012. A geologic time scale. New York: Cambridge University Press.

Graham, A. 1988a. Studies in Neotropical paleobotany. V. The Lower Miocene communities of Panama-The Culebra Formation. Ann. Missouri Bot. Gard. 75:1440-1466.

Graham, A. 1988b. Studies in Neotropical paleobotany. VI. The Lower Miocene communities of Panama- The Cucaracha Formation. Ann. Missouri Bot. Gard. 75:1467-1479.

Graham, A. 1991a. Studies in Neotropical paleobotany. VIII. The Pliocene communities of Panama- Introduction and frens, gymnosperms, angiosperms (monocots). Ann. Missouri Bot. Gard. 78:190-200.

Graham, A. 1991b. Studies in Neotropical paleobotany. IX. The Pliocene communities of Panama-Angiosperms (dicots). Ann. Missouri Bot. Gard. 78:201-223.

Graham, A. 1995. Diversification of Gulf/Caribbean Mangrove Communities through Cenozoic time. Biotropica 27(1).

Guerrero, J. 1997. Stratigraphy, sedimentary environments, and the Miocene uplift of the Colombian Andes. In F. Kay, R. Madden, R. Cifelli, and J. Flynn, eds. Vertebrate Paleontology in the Neotropics. The Miocene Fauna of La Venta, Colombia. Smithsonian Institution Press.

Guerrero, J. 1997 (b). Geochronology of the Honda Group. In F. Kay, R. Madden, R. Cifelli, and J. Flynn, eds. Vertebrate Paleontology in the Neotropics. The Miocene Fauna of La Venta, Colombia. Smithsonian Institution Press.

Guex, F. 1991. Biochronological correlations. Springer-Verlag (New York).

Gutjahr, M., A. Ridgwell, P. F. Sexton, E. Anagnostou, P. N. Pearson, H. Plike, R. D. Norris, E. Thomas, and G. L. Foster. 2017. Very large release of mostly volcanic carbon during the PalaeoceneEocene Thermal Maximum. Nature 548(7669):573-577.

Guy-Ohlson, D. 1992. *Botryococcus* as an aid in the interpretation of palaeoenvironment and depositional processes. Review of Palaeobotany and Palynology 71.

Guy-Ohlson, D. 1998. The use of the microalga *Botryococcus* in the interpretation of lacustrine environments at the JurassicCretaceous transition in Sweden. Palaeogeography, Palaeoclimatology, Palaeoecology 140.

Haffer, J. 1969. Speciation in Amazonian forest birds. Science 165:131-137.

Hahsler, M. C., S., Hornik, K., Butcha, C. 2011. The arules R-package ecosystem: Analyzing interesting patterns from large transaction datasets. Journal of Machine Learning Research 12:1977-1981.

Hahsler, M. G., B; Hornik, K. 2005. arules-A Computational Environment for mining Association Rules and Frequent Itemsets. Journal of Statistical Software 14(15):1-25.

Han, J., M. Kamber, J. Pei. 2012. Data Mining Concepts and Techniques. Morgan Kaufmann Series in Data Management Systems

Harper, C. 1984. Facies Models Revisited: An Examination of Quantitative Methods. Geosciences Canada 11.

Hayek, L., and M. Buzas. 1997. Surveying Natural Populations. Columbia University Press.

Hazel, J. 1970. Binary coeficients and clustering in stratigraphy. Geological Society of America Bulletin 81:3237-3252.

Head, M. 1996. Modern dinoflagellate cysts and their biological affinities. In J. Jansonious, and J. McGregor, eds. Palynology: Principles and Applications. American Association of Stratigraphic Palynologists Foundations, Dallas, TX.

Herrmann, M. 2010. Palaeoecological reconstruction of the late Oligocene Maar Lake of Enspel, Germany using lacustrine organic walled algae. Palaeobio Palaeoenv 90.

Higgins, M. A., K. Ruokolainen, H. Tuomisto, N. Llerena, G. Cardenas, O. L. Phillips, R. Vasquez, and M. Rasanen. 2011. Geological control of floristic composition in Amazonia forests. Journal of Biogeography 38:2136-2149.

Higgs, R. 1997. Basin development and tectonic history of the Llanos Basin, Eastern Cordillera, and Middle Magdalena Valley, Colombia: discussion. AAPG Bulletin 81(8).

Hillebrand, H. 2004. On the Generality of the Latitudinal Diversity Gradiente. American Naturalist 163(2).

Hood, K. 1986. GraphCor-Interactive Graphic Correlation Software. Hood, K.C, Houston.

Hoorn, C. 1993. Marine Incursions and the Influence of Andean Tectonics on the Miocene Depositional History of Northwestern Amazonia - Results of a Palynostratigraphic Study. Palaeogeography Palaeoclimatology Palaeoecology 105(3-4):267-309.

Hoorn, C. 1994. Fluvial palaeoenvironments in the intracratonic Amazonas Basin (Early Miocene-early Middle Miocene, Colombia). Palaeogeography,Palaeoclimatology,Palaeoecology 109:1-54.

Hoorn, C. 1994. An Environmental Reconstruction of the Palaeo-Amazon River System (Middle-Late Miocene, NW Amazonia). Palaeogeography Palaeoclimatology Palaeoecology 112(3-4):187-238.

Hoorn, C. 2006. Mangrove Forests and Marine Incursions in the Neogene Amazonia (Lower Apaporis River, Colombia). Palaios 21(2):197-209.

Hoorn, C., G. R. Bogot-A, M. Romero-Baez, E. I. Lammertsma, S. G. A. Flantua, E. L. Dantas, R. Dino, D. A. do Carmo, and F. Chemale. 2017. The Amazon at sea: Onset and stages of the Amazon River from a marine record, with special reference to Neogene plant turnover in the drainage basin. Global and Planetary Change 153:51-65.

Hoorn, C., A. Perrigo, and A. Antonelli. 2018. Mountains, Climate and Biodiversity: An Introduction. In C Hoorn, A Perrigon, and A. Anotnelli, eds. Mountains, Climate and Biodiversity. John Wiley and Sons Ltd.

Hoorn, C., and F. Wesselingh. 2010a. Amazonia: Landscape and Species Evolution: A look into the past. Wiley-Blackwell.

Hoorn, C., F. P. Wesselingh, H. ter Steege, M. A. Bermudez, A. Mora, J. Sevink, I. Sanmartin, A. Sanchez-Meseguer, C. L. Anderson, J. P. Figueiredo, C. Jaramillo, D. Riff, F. R. Negri, H. Hooghiemstra, J. Lundberg, T. Stadler, T. Sarkinen, and A. Antonelli. 2010b. Amazonia Through Time: Andean Uplift, Climate Change, Landscape Evolution, and Biodiversity. Science 330(6006):927-931.

Hoorn, C., F. Wesselingh, J. Hovikoski, and J. Guerrero. 2010c. The development of the Amazonian mega-wetland (Miocene; Brazil, Colombia, Peru, Bolivia). In C. Hoorn, and C. H. a. F. P. Wesselingh, eds. Amazonia, Landscape and Species Evolution: A look into the past. Blackwell Publishing.

Horton, B., M. Parra, J. Saylor, J. Nie, A. Mora, V. Torres, D. Stockli, and M. Strecker. 2010. Resolving uplift of the northern Andes using detrital zircon age signatures. GSA Today:4-10.

Hotton, C. 2002. Palynology of the Cretaceous-Tertiary boundary in central Montana: evidence for extra terrestrial impact as a cause of the terminal Cretaceous extinctions. In. J.H Hartman, Johnson, K., Nichols, D, ed. The Hell Creek Formation and the Cretaceous-Tertiary boundary in the northern Great Plains: An integrated continental record of the end of the Cretaceous. Geological Society of America.

Hou, L., H. Park, S. Okada, and T. Ohama. 2014. Release of single cells from the colonial oil-producing alga *Botryococcus braunii* by chemical treatments. Protoplasma 251.

Hovikoski, J., M. Gingras, M. Rasanen, L. Rebata, J. Guerrero, A. Ranzi, J. Melo, L. Romero, H. del Prado, F. Jaimes, and S. Lopez. 2007. The nature of Miocene Amazonian epicontinental embayment: High-frequency shifts of the low-gradient coastline. GSA Bulletin 119.

Hovikoski, J., M. Rasanen, M. Gingras, M. Roddaz, S. Brusset, W. Hermoza, L. Romero, and K. Lertola. 2005. Miocene semidiurnal tidal rhytmites in Madre de Dios, Peru. Geology 33.

Hovikoski, J., F. Wesselingh, M. Rasanen, M. Gingras, and H. Vonhof. 2010. Marine influence in Amazonia: evidence from the geological record. In C. Hoorn, and F. Wesselingh, eds. Amazonia, Landscape and Species Evolution: A look into the past. Blackwell Publishing.

Hughes, G., F. De la Parra, C. Vargas, and G. Suarez. 2014. A Biostratigraphic Investigation of the Proterozoic and lower Palaeozoic of Colombia:

Palynological analyses of six wells from the northern Llanos Basin. 4 International Palaeontological Congress. Mendoza, Argentina.

Humber, M., E. Thomas. 2009. Paleoceanography: The Greenhouse World. In. J Stelle, ed. Encyclopedia of Ocean Sciences. Academic Press

Humboldt, A. 1820. Voyage aux regions equinoxiales du Nouveau Continent. Paris. N.Maze.

Hunt, G., T. Cronin, and K. Roy. 2005. Species-energy relationship in the deep sea: a test using the Quaternary fossil record. Ecology Letters 8:739-747.

Jablonski, D., Roy, K., Valentine J. 2006. Out of the Tropics: Evolutionary Dynamics of the Latitudinal Diversity Gradient. Science 314.

Jankovska, V., and J. Komarek. 2000. Indicative value of *Pedisatrum* and other Coccal Green Algae in Palaeoecology. Folia Geobotanica et Phytotaxonomica 35.

Jankovska, V., and J. Pokorny. 2002. Palaeoecology of a medieval fishpond system (Vajgar, Czech Republic). Folia Geobotanica et Phytotaxonomica 37.

Jantz, N., J. Homeier, S. Len-Ynez, A. Moscoso, and H. Behling. 2013. Trapping pollen in the tropics Comparing modern pollen rain spectra of different pollen traps and surface samples across Andean vegetation zones. Review of Palaeobotany and Palynology 193:57-69.

Jaramillo, C. 2002. Response of tropical vegetation to Paleogene warming. Paleobiology 28(2).

Jaramillo, C., Rueda, M., Bayona, G., Santos, C., Florez, P., De la Parra, F. 2009. Biostratigraphy Breaking Paradigms: Dating the Mirador Formation in the Llanos Basin of Colombia. Geologic Problem Solving with Microfossils: A Volume in Honor of Garry D. Jones. SEPM (Society for Sedimentary Geology).

Jaramillo, C., E. Moreno, V. Ramirez, S. da Silva, A. Barrera, A. C. Barrera, S. Moron, F. Herrera, J. Escobar, R. Koll, S. Manchester, and N. Hoyos. 2014. Palynological record of the last 20 Million years in Panama. Pp. 134-251. In W. D. Stevens, Montiel, O. M. and Raven, P.,, ed. Paleobotany and Biogeography: A Festschrift for Alan Graham in his 80th Year. St. Louis: Missouri Botanical Garden Press.

Jaramillo, C., D. Ochoa, L. Contreras, M. Pagani, H. Carvajal-Ortiz, L. M. Pratt, S. Krishnan, A. Cardona, M. Romero, L. Quiroz, G. Rodriguez, M. J. Rueda, F. de la Parra, S. Moron, W. Green, G. Bayona, C. Montes, O. Quintero, R. Ramirez, G. Mora, S. Schouten, H. Bermudez, R. Navarrete, F. Parra, M. Alvaran, J. Osorno, J. L. Crowley, V. Valencia, and J. Vervoort. 2010. Effects of Rapid Global Warming at the Paleocene-Eocene Boundary on Neotropical Vegetation. Science 330(6006):957-961.

Jaramillo, C., I. Romero, C. D'Apolito, G. Bayona, E. Duarte, S. Louwye, J. Escobar, J. Luque, J. D. Carrillo-Briceno, V. Zapata, A. Mora, S. Schouten, M. Zavada, G. Harrington, J. Ortiz, and F. P. Wesselingh. 2017. Miocene flooding events of western Amazonia. Sci Adv 3(5):e1601693.

Jaramillo, C., M. J. Rueda, and G. Mora. 2006. Cenozoic plant diversity in the neotropics. Science 311(5769):1893-6.

Jaramillo, C., M. Zavada, J. Ortiz, A. Pardo, and D. Ochoa. 2013. The Biogeography of the Araucarian dispersed pollen Cyclusphaera. Int. J. Plant Sci 174(3):489-498.

Jaramillo C., D., D. 2001. Middle Paleogene palynology of central Colombia, South America: a study of pollen and spores from tropical latitudes. Palaeontographica, Abteilung B. 258.

Jaramillo C., M. F., Cogollo M., Parra F. 2005. Quantitative biostratigraphy for the Paleocene of the Llanos Foothills, Colombia: Improving palynological resolution for oil exploration. In R. J. Powell A.J., ed. Recent developments in applied biostratigraphy. Bath (UK): Geological Society Publishing House (The Micro- paleontological Society Special Publication TMS001).

Jaramillo C., R., M. 2004. Impact of biostratigraphy on oil exploration. 3ra Convencion Tecnica de la ACGGP.

Jaramillo, C. A., M. Rueda, and V. Torres. 2011. A palynological zonation for the Cenozoic of the Llanos and Llanos Foothills of Colombia. Palynology 35(1):46-84.

Ji, L., K. Yan, F. Meng, and M. Zhao. 2010. The oleaginous *Botryococcus* from the Triassic Yanchang Formation in Ordos Basin, Northwestern China: Morphology and its paleoenvironmental significance. Journal of Asian Earth Sciences 38.

Jimenez, J. 1984. A hypothesis to explain the reduced distribution of the mangrove Pelliciera rizophorae Tr and Pl. Biotropica 16.

Jones, D., Nicol, D. 1986. Origination, Survivorship, and Extinction of Rudist Taxa. Jounal of Paleontology 60(1):107-115.

Julier, A., P. Jardine, S. Adu-Bredu, A. Coe, A. Duah-Gyamfi, W. Fraser, B. Lomax, Y. Malhi, S. Moore, K. Owusu-Afriyie, and W. Gosling. 2017. The modern pollen-vegetation relationships of a tropical forest-savannah mosaic landscape, Ghana, West Africa. Palynology.

Kaandorp, R., F. Wesselingh, and H. Vonhof. 2006. Ecological implications from stable isotope records of Miocene western Amazonian bivalves. Journal of South American Earth Sciences 21.

Kay, F., R. Madden, R. Cifelli, and J. Flynn, 1997, Vertebrate Paleontology in the Neotropics. The Miocene Fauna of La Venta, Colombia, Smithsonian Institution Press.

Kawachi, M., T. Tanoi, M. Demura, K. Kaya, and M. Watanabe. 2012.

Relationship between hydrocarbons and molecular phylogeny of *Botryococcus braunii*. Algal Research 1.

Kemple, W., Sadler, P., Strauss, D. 1995. Extending graphic correlation to many dimensions: Stratigraphic correlation as constrained optimization Pp. 65-82. In K. O. Mann, and Lane, H.R, ed. Graphic Correlation. SEPM Special Publication.

Komarek, J., and V. Jankovska. 2001. Review of the Green Algal Genus *Pediastrum*; implication for pollen analytical Research. Bibliotheca Phycologica, Berlin.

Komarek, J., and P. Marvan, 1992, Morphological differences in natural populations of the Genus *Botryococcus* (Chlorophyaceae): Archiv fur Protistenkunde, v. 141.

Kovach, W., Batten, D. 1994. Association of palynomorphs and palynodebris with depositional environments: quatitative approaches. Cambridge University Press, Cambridge.

Kowalewski, M., Novack-Gottshall, P. 2010. Resampling Methods in Paleontology. Pp. 19-54. Quantitative Methods in Paleobiology. The Palentological Society Papers.

Kricher, J. 1999. A neotropical companion: An introduction to the animals, plants and ecosystems of the New World tropics. Princeton University Press.

Kuetzing, F. 1849. Species algarum. Leipzig 922.

Kumar, M., Monga, P., Shukla, A., Mehrotra, R. 2016. *Botryococcus* from the early Eocene lignite mines of western India: inferences on morphology, taphonomy and palaeoenvironment. Palynology.

Kurten, B. 1954. Population synamics-a new method in paleontology. Jounal of Paleontologya 28(286-292).

Lamb, H., N. Roberts, M. Leng, P. Barker, A. Benkaddour, and S. van der Kaars. 1999. Lake evolution in a semi-arid montane environment: response to catchment change and hydrocli- matic variation. Journal of Paleolimnology 21.

Lambiase, J. 1990. A model for tectonic control of lacustrine stratigraphic sequences in continental rift basins. In B. Kats, ed. Lacustrine Basin Exploration, Case Studies and Modern Analogues. APPG Memoir 50.

Latrubesse, E., S. da Silva, M. Cozzuol, and M. Absy. 2007. Late Miocene continental sedimentation in southwestern Amazonia and its regional significance: Biotic and geological evidence. Journal of South American Earth Sciences 23.

Lazarus, D., J. Barron, J. Renaudie, P. Diver, and A. Turke. 2014. Cenozoic planktonic marine diatom diversity and correlation to climate change. Plos One 9(1):e84857.

Legendre, P., and L. Legendre. 1988. Numerical Ecology.

Lehtonen, S., D. Silvestro, D. N. Karger, C. Scotese, H. Tuomisto, M. Kessler, C. Pena, N. Wahlberg, and A. Antonelli. 2017. Environmentally driven extinction and opportunistic origination explain fern diversification patterns. Sci Rep 7(1):4831.

Leite, F., Paz, J., do Carmo, D., Silva-Caminha, S. 2016. The effects of the inception of Amazonian transcontinental drainage during the Neogene on the landscape and vegetation of the Solimoes Basin, Brazil. Palynology.

Leliaert, F. D. Smith, H. Moreau, M. Herron, H. Verbruggen, C. Delwiche, O. Clerck. 2012. Phylogeny and Molecular Evolution of the Green Algae. Critical Reviews in Plant Sciences. 31

Leskovec, J. R., A; Ullman, J. 2014. Mining of Massive datasets. Cambridge University Press.

Levinton, J. 1974. Trophic group and evolution in bivalve molluscs. Paleontology 17:579-585.

Li-Ming, J., Y. Kui, M. Fan-Wei, and Z. Min, 2010, The oleaginous *Botryococcus* from the Triassic Yanchang Formation in Ordos Basin, Northwestern China: Morphology and its paleoenvironmental significance: Jounal of Asian Earth Sciences, v. 5.

Linhares, A. P., V. d. C. d. S. Gaia, and M. I. F. Ramos. 2017. The significance of marine microfossils for paleoenvironmental reconstruction of the Solimes Formation (Miocene), western Amazonia, Brazil. Journal of South American Earth Sciences 79:57-66.

Lloyd, G. T., A. B. Smith, and J. R. Young. 2011. Quantifying the deep-sea rock and fossil record bias using coccolithophores. In A. J. M. a. A. B. Smith, ed. Comparing the Geological and Fossil record. The Geological Society London, Geological Society, Special Publication 358.

Lorente, M. 1986. Palynology and Palynofacies of the Upper Tertiary in Venezuela.

Louterbach, M., M. Roddaz, J. Bailleul, P. O. Antoine, S. Adnet, J. H. Kim, E. van Soelen, F. Parra, J. Grard, Y. Calderon, C. Gagnaison, J. S. Sinninghe Damst, and P. Baby. 2014. Evidences for a Paleocene marine incursion in southern Amazonia (Madre de Dios Sub-Andean Zone, Peru). Palaeogeography, Palaeoclimatology, Palaeoecology 414:451-471.

Lovejoy, N., A. Bermingham, and A. Martin. 1998. Marine Incursions into South America. Nature 396.

Lovejoy, N., S. Willis, and J. Albert. 2010. Molecular signatures of Neogene biogeographical events in the Amazon fish fauna. In C. Hoorn, and F. Wesselingh, eds. Amazonia, Landscape and Species Evolution: A look into the past. Blackwell Publishing.

Madden, R., D. Savage, and R. Fields. 1997. A History of Vertebrate

Paleontology in the Magdalena Valley. In R. Kary, R. Madden, R. Cifelli, and J. Flynn, eds. Vertebrate Paleontology in the Neotropics. The Miocene Fauna of La Venta, Colombia. Smithsonian Institution Press.

Magurran, A. 2003. Measuring Biological Diversity. Blackwell Publishing.

Mannion, P. D., P. Upchurch, R. B. Benson, and A. Goswami. 2014. The latitudinal biodiversity gradient through deep time. Trends in Ecology and Evolution 29(1):42-50.

Marcot, J. D., D. L. Fox, and S. R. Niebuhr. 2016. Late Cenozoic onset of the latitudinal diversity gradient of North American mammals. Proc Natl Acad Sci U S A 113(26):7189-94.

Marx, F., and M. Uhen. 2010. Climate, Critters, and Cetaceans: Cenozoic Drivers of the Evolution of the Modern Whales. Science 327.

Matthias, I., M. S. S. Semmler, T. Giesecke, and M. McGlone. 2015. Pollen diversity captures landscape structure and diversity. Journal of Ecology 103(4):880-890.

Matthiesen, J., M. Kunz, and P. Mudie. 2000. Freshwater chlorophycean algae in recent marine sediments of the Beaufort, Laptev and Kara Seas (Artic Ocean) as indicators of river runoff. International Journal of Earth Sciences 89.

McIneney, F., and S. Wing. 2011. The Paleocene-Eocene Thermal Maximum: a perturbation of carbon cycle, climate, and biosphere with implications for the future. Annu. Rev. Earth. Planet. Sci 39.

McKinney, M. 1990. Classifying and analyzing evolutionary trends. In K. J. McNamara, ed. Evolutionary trends. Univ. of Arizona Press, Tucson, AZ.

Medeanic, S. 2006. Freshwater algal palynomorph records from Holocene deposits in the coastal plain of Rio Grande do Sul, Brazil. Review of Palaeobotany and Palynology 141.

Melia, M. 1984. The distribution and relationship between palynomorphs in aerosols and deep-sea sediments off the coast of Northwest Africa. Marine Geology 58.

Metzger, P., and C. Largeau. 2005. *Botryococcus braunii*: a rich source for hydrocarbons and related ether lipids. Applied Microbiology and Biotechnology 66.

Miller, K., R. Fairbanks, and G. S. Mountain. 1987. Tertiary oxygen isotope synthesis, sea level history, and continental margin erosion. Paleoceanography 2.

Mittelbach, G. G., D. W. Schemske, H. V. Cornell, A. P. Allen, J. M. Brown, M. B. Bush, S. P. Harrison, A. H. Hurlbert, N. Knowlton, H. A. Lessios, C. M. McCain, A. R. McCune, L. A. McDade, M. A. McPeek, T.

J. Near, T. D. Price, R. E. Ricklefs, K. Roy, D. F. Sax, D. Schluter, J. M. Sobel, and M. Turelli. 2007. Evolution and the latitudinal diversity gradient: speciation, extinction and biogeography. Ecology Letters 10(4):315-31.

Montes, C., A. Cardona, J. C., A. Pardo, J. Silva, V. Valencia, L. Ayala, A. Perez, L. Rodriguez-Parra, V. Ramirez, and H. Nio. 2015. Middle Miocene closure of the Central American Seaway. Science 348(6231).

Montes, C., R. Hatcher, and P. Restrepo-Pace. 2005. Tectonic reconstruction of the northern Andean blocks: Oblique convergence and rotations derived from the kinematics of the PiedrasGirardot area, Colombia. Tectonophysics 399.

Moore, P. 1994. Pollen Analysis. Wiley, 2 edition.

Mora, A., P. Baby, M. Rodazz, M. Parra, S. Brusset, W. Hemorza, and N. Espurt. 2010. Tectonic history of the Andes and sun-Andean zones: implications for the development of the Amazon drainage basin. In C. H. F. Wesselingh, ed. Amazonia: landscape and species evolution. Wiley-Blackwell.

Mora, A., M. Parra, M. Strecker, and E. R. Sobel. 2008. Climatic forcing of assymmetric orogenic evolution in the Eastern Cordillera of Colombia. GSA Bulletin 120(7/8):930-949.

Mora, A., M. Parra, M. R. Strecker, E. R. Sobel, G. Zeilinger, C. Jaramillo, S. F. Da Silva, and M. Blanco. 2010a. The eastern foothills of the Eastern Cordillera of Colombia: An example of multiple factors controlling structural styles and active tectonics. Geological Society of America Bulletin 122(11-12):1846-1864.

Mora, A., A. Reyes-Harker, G. Rodriguez, E. Teson, J. Ramires, M. Parra, V. Caballer, J. Mora, I. Quintero, V. Valencia, M. Ibanez, B. Horton, and D. Stockli, 2013, Inversion tectonics under increasing rates of shortening and sedimentation: Cenozoic example from the Eastern Cordillera of Colombia: Geological Society, London, Special Publications, v. 377.

Moreno, C., B. Horton, V. Caballero, A. Mora, M. Parra, and J. Sierra. 2011. Depositional and provenance record of the Paleogene transition from foreland to hinterland basin evolution during Andean orogenesis, northern Middle Magdalena Valley Basin, Colombia. Journal of South American Earth Sciences 32.

Morley, R. 2000. Origin and Evolution of Tropical rain forest. New York: Wiley.

Muller J., E. Di Giacomo, A. van Erve. 1987. A palynological zonation for the Cretaceous, Tertiary and Quaternary of Northern South America. American Association of Stratigraphic Palynologists Contribution Series 19:7-76.

Murphy, M., and A. Salvador. 1999. International Stratigraphic Guide-An abridged version. Episodes 22(4):255-272.

Nagappa, Y. 1957. Further occurrence of *Botryococcus* in western Pakistan. Micropaleontology.

Ndiaye, M. 2007. A multipurpose software for stratigraphic signal analysis. PhD. Universite de Geneve.

Neal, J., K. Bohacs, D. Reynolds, C. Scholz. 1997. Sequence stratigraphy of lacustrine rift basins: critical linkage of changing lake level, sediment supply, and tectonics: Abstracts with programs. Geological Society of America. 29.

Nelson, B., C. Ferreira, M. da Silva, and M. Kawasaki. 1990. Endemism centres, refugia and botanical collection density in Brazilian Amazon. Nature 345:714-716.

Nichols. D, K. Johnson. 2008. Plants at the K-T boundary. Cambridge University Press.

Nie, J., B. Horton, A. Mora, J. Saylor, T. Bush, J. Rubiano, J. Naranjo. 2010. Tracking exhumation of Andean ranges bounding the Middle Magdalena Valley Basin, Colombia. Geology.v38. 5.

Nie, J., B. Horton, J. Saylo, A. Mora, M. Mange, C. Garzione, A. Basu, C. Moreno, C. Caballero, M. Parra. 2012. Integrated provenance analysis of a convergent retroarc foreland system: U-Pb ages, heavy minerals, Nd Isotopes, and sandstone compositions of the Middle Magdalena Valley basin, northern Andes, Colombia. Earth Science Reviews. 110.

Nielsen, H., and I. Sorensen. 1992. Taxonomy and stratigraphy of late-glacial *Pediastrum* taxa from Lysmosen, Denmark- a preliminary study. Review of Palaeobotany and Palynology 74.

Niklas, K. J., Tiffney, B., Knoll,A. 1983. Patterns in vascular plant diversification. Nature 303(16).

Nogueira, A., R. Silveira, and J. Guimaraes. 2013. Neogene-Quaternary sedimentary and paleovegetation history of the eastern Solimes Basin, central Amazon region. Journal of South American Earth Sciences 46.

Nores, M. 2004. The implications of Tertiary and Quaternary sea level rise events for avian distribution patterns in the lowlands of northen South America. Global Ecology and Biogeography 13.

Nutall, C., 1990, A review of the Tertiary non-marine molluscan faunas of the Pebasian and other islands basins of north-western South America: Bulletin of the British Museum (Natural History), Geological Series, v. 45, p. 165-371.

O'Dea, A., H. A. Lessios, A. G. Coates, R. I. Eytan, S. A. Restrepo-Moreno, A. L. Cione, L. S. Collins, A. de Queiroz, D. W. Farris, R. D. Norris, R. F. Stallard, M. O. Woodburne, O. Aguilera, M. P. Aubry, W. A. Berggren, A. F. Budd, M. A. Cozzuol, S. E. Coppard, H. Duque-Caro, S. Finnegan, G. M. Gasparini, E. L. Grossman, K. G. Johnson, L. D. Keigwin,

N. Knowlton, E. G. Leigh, J. S. Leonard-Pingel, P. B. Marko, N. D. Pyenson, P. G. Rachello-Dolmen, E. Soibelzon, L. Soibelzon, J. A. Todd, G. J. Vermeij, and J. B. Jackson. 2016. Formation of the Isthmus of Panama. Sci Adv 2(8):e1600883.

Ochoa, D., C. Hoorn, C. Jaramillo, G. Bayona, M. Parra, and F. De la Parra. 2012. The final phase of tropical lowland conditions in the axial zone of the Eastern Cordillera of Colombia: Evidence from three palynological records. Journal of South American Earth Sciences 39:157-169.

Olaya, I. D. 1997. Seismic stratigraphic characterization of the Lower tertiary in the Cachira Paleohigh, Middle Magdalena Basin, Colombia [M.S. Thesis]. Colorado School of Mines.

Osorio, C., D. Michoux, and G. Tellez. 2002. Stratigraphy of the Tertiary sequences Upper Magdalena and the Putumayo basins, a different point of view for hydrocarbon exploration. Memorias de la Segunda Convencin tcnica de la Asociacin Colombiana de Gelogos y Geofsicos del Petrleo. Bogota, Colombia.

Pardo, A., Jaramillo, C., Oboh-Ikuenobe, F. 2003. Paleogene Palynostratigraphy of the Eastern Middle Magdalena Valley, Colombia. Palynology 27:155-178.

Parra, M. 2008. Cenozoic foreland-basin evolution in the northern Andes: insights from thermochronology and basin analysis in the Eastern Cordillera, Colombia. Universitt Potsdam.

Parra, M., A. Mora, C. Jaramillo, M. R. Strecker, E. R. Sobel, L. Quiroz, M. Rueda, and V. Torres. 2009. Orogenic wedge advance in the northern Andes: Evidence from the Oligocene-Miocene sedimentary record of the Medina Basin, Eastern Cordillera, Colombia. Geological Society of America Bulletin 121(5-6):780-800.

Pawlowski, J., and A. Gooday. 1993. Microforaminifera - Perspective on a Neglected Group of Foraminifera. Arch. Protistenkd 143.

Pennington, R., Lavin, M., Sarkinen, T., Lewis, G., Klitgaard, B., Hughes, C. 2010. Contrasting plant diversification histories within the Andean biodiversity hotspot. PNAS 107(31):13783-13787.

Pennington, R., and C. Dick. 2004. The role of immigrants in the assembly of the South American rainforest tree flora. Phil. Trans. R. Soc. Lond B 359:1611-1622.

Pilsbry, H., and A. Olsson. 1935. Tertiary Fresh-Water Mollusks of the Magdalena Embayment, Colombia. Proceedings of the Academy of Natural Sciences of Philadelphia 87:7-39.

Pindell, J., J. Cristancho, and R. Higgs. 1997. Clarification of the Late CretaceousPaleogene Evolution of Colombia. VI Simposio Bolivariano de Exploracin en las Cuencas Subandinas. Asociacin Colombiana de Gelogos y

Geofsicos del Petrleo, Bogota, Colombia.

Pinheiro, J., D. Bates, S. Debroy, and D. Sarkar. 2009. nlme: Linear and nonlinear Mixed effects models. R. package version 3.1-93 http://CRAN.R-project.org/package=nlme.

Pinzon, D. 2011. ACME de *Pediastrum* spp. e implicaciones Paleoecologicas despues del Limite Cretacico-Paleogeno en el norte de Sur America. Universidad Industrial de Santander, Unpublished Undergraduate Thesis.

Pitman, N. C. A., H. Mogollon, N. Davila, M. Ros, R. Garcia-Villacorta, J. Guevara, T. R. Baker, A. Monteagudo, O. L. Phillips, R. Vasquez-Martinez, M. Ahuite, M. Aulestia, D. Cardenas, C. E. Ceron, P. A. Loizeau, D. A. Neill, V. P. Nunez, W. A. Palacios, R. Spichiger, and E. Valderrama. 2008. Tree community change across 700 km of lowland Amazonian forest from the Andean foothills to Brazil. Biotropica 40:525-535.

Plain, N., C. Largeau, S. Derenne, and A. Coute. 1993. Variabilit morphologique de *Botryococcus braunii* (Chlorococcales, Chlorophyta): corrlations avec les conditions de croissance et la teneur en lipides. Phycologia 32.

Pollingher, U. 1986. Non-siliceous algae in a five meters core from Lake Kinneret. Hydrobiologia 143.

Pound, M., and U. Zalzmann. 2017. Heterogeneity in global vegetation and terrestrial climate change during the late Eocene to early Oligocene transition. Scientific Reports 7.

Powers, D., and R. Easterling. 1982. Improved methodology for using embedded markov chains to describe cyclical sediments. Journal of Sedimentary Petrology 52(3).

Prasad, V., and D. Sarkar. 2000. Palaeoenvironmental significance of *Botryococcus* (Chlorococcales) in the Subathu Formation of Jammu and Kashmir, India. Curr Sci India 78(6).

Prothero, D. 1999. Does climatic change drive mammalian evolution? GSA Today 9(9).

Punt, W., P. Hoen, S. Blackmore, S. Nilsson, and A. Thomas, 2007, Glossary of pollen and spore terminology: Review of Palaeobotany and Palynology, v. 143, p. 1-81.

Punyasena, S. W., C. Jaramillo, F. de la Parra, and Y. L. Du. 2012. Probabilistic correlation of single stratigraphic samples: A generalized approach for biostratigraphic data. AAPG Bulletin 96(2):235-244.

Quental, T., Marshall, C. 2010. Diversity dynamics: molecular phylogenies need the fossil record. Trends in Ecology and Evolution 25:434-441.

Ramirez, R. E. 1998. Stratigraphy of the Tertiary of the Middle Magdalena basin (Colombia), central and northern parts [M.S. Thesis]. University of Texas.

Rasanen, M., A. Linna, J. Santos, and F. Negri. 1995. Late Miocene Tidal Deposits in the Amazonian Foreland Basin. Science 269.

Raup, D. 1972. Taxonomic Diversity during the Phanerozoic. Science 177.

Raup, D. 1975. Taxonomic Survivorship Curves and Van Valen's LAw. Paleobiology 1(1):82-96.

Raup, D., 1977, Chapter 3. Stochastic Models in Evolutionary Palaeontology: Developments in Palaeontology and Stratigraphy, v. 5, p. 59-78.

Raup, D. 1978. Cohort Analysis of Generic Survivorship. Paleobiology 4(1):1-15.

Raup, D. 1979. Biases in the fossil record of species and genera. Bull. Carnegie Mus. Nat. Hist 13:85-91.

Raven, P., and D. Axelrod. 1974. Angiosperm biogeography and past continental movements. Ann. Missouri Bot. Gard. 61:539-673.

Rebata, L., M. Rsnen, M. K. Gingras, V. Vieira, M. Barberi, and G. Irion. 2006. Sedimentology and ichnology of tide-influenced Late Miocene successions in western Amazonia: the gradational transition between the Pebas and Nauta formations. Journal of South American Earth Sciences 21.

Renner, S. 2004. Plant dispersal across the tropical Atlantic by wind and sea currents. Int. J. Plant Sci 165.

Renner, S., G. Clausing, and K. Meyer. 2001. Historical biogeography of Melastomataceae: the roles of Tertiary migration and long-distance dispersal. International Journal of Plant Sciences 165(4):23-33.

Reyes-Harker, A., C. F. Ruiz-Valdivieso, A. Mora, J. C. Ramirez-Arias, G. Rodriguez, F. de la Parra, V. Caballero, M. Parra, N. Moreno, B. K. Horton, J. E. Saylor, A. Silva, V. Valencia, D. Stockli, and V. Blanco. 2015. Cenozoic paleogeography of the Andean foreland and retroarc hinterland of Colombia. AAPG Bulletin 99(8):1407-1453.

Reynolds, C. 1984. The ecology of freshwater Phytoplankton. Cambridge University Press.

Roddaz, M., Hermoza, W., Mora, A., Baby,P., Parra, M., Christophoul,F., Brusset,S., Espurt, N. 2010. Cenozoic sedimentary evolution of the Amazonian foreland basin system. In C. Hoorn, Wesselingh, F. P, ed. Amazonia, Landscape and Species Evolution: A look into the past. Blackwell Pusblishing.

Roddaz, M., S. Brusset, P. Baby, and G. Herail. 2006. Miocene tidal-influenced sedimentation to continental Pliocene sedimentation in the forebulgebackbulge depozones of the BeniMamore foreland Basin (northern Bolivia). Journal of South American Earth Sciences 20.

Roddaz, M., J. Viers, S. Brusset, P. Baby, and G. Herail. 2005. Sediment provenances and drainage evolution of the Neogene Amazonian foreland

basin. Earth and Planetary Science Letters 239.

Rodriguez-Forero, G., Oboh-Ikuenobe,F., Jaramillo, C., Cadena, E. 2012. Palynology of the Eocene Esemeraldas Formation, Middle Magdalena Valley Basin, Colombia. Palynology. 36.

Romero, E. 1993. South American Paleofloras. In Biological relationships between Africa and South America. Ed. P Goldblatt. New Haven, CT: Yale Univ Press.

Rull, V. 1997. Sequence analysis of western Venezuelan Cretaceous to Eocene sediments using Palynology: Chrono-Paleoenvironmental and Paleovegetational approaches. Palynology 21.

Rull, V. 1998. Middle Eocene Mangroves and vegetation changes in the Maracaibo Basin, Venezuela. Palaios 13(3).

Rull, V. 1999. Palaeofloristic and palaeovegetational changes across the Paleocene/Eocene boundary in northern South America. Review of Palaeobotany and Palynology 107.

Rull, V., J. Lopez, and T. Vegas. 2008. Contribution of non-pollen palynomorphs to the paleolimnological study of a high-altitude Andean lake (Laguna Verde Alta, Venezuela). Journal of Paleolimnology 40.

Sadler, P. 2003. Constrained optimization approaches to the paleobiologic correlation and seriation problems: a users guide and reference manual to the CONOP program family, Version 6.5.

Salamanca, S., E. van Soelen, M. Teunissen, S. Flantua, R. Santos, M. Rodazz, L. Dantas, E. van Loon, J. S. Sinninghe Damst, J. H. Kim, and C. Hoorn. 2016. Amazon forest dynamics under changing abiotic conditions in the early Miocene (Colombia Amazonia). Journal of Biogeography 43:2424-2437.

Sanchez, N., A. Mora, M. Parra, D. Garcia, M. Cortes, T. M. Shanahan, R. Ramirez, O. Llamosa, and M. Guzman. 2015. Petroleum system modeling in the Eastern Cordillera of Colombia using geochemistry and timing of thrusting and deformation. AAPG Bulletin 99(8):1537-1556.

Sangiorgi, F., L. Capotondi, and H. Brinkhuis. 2002. A centennial scale organic-walled dinoflagellate cyst record of the last deglaciation in the South Adriatic Sea (central Mediterranean). Palaeogeography, Palaeoclimatology, Palaeoecology 186(3-4).

Santos, C., C. Jaramillo, G. Bayona, M. Rueda, and V. Torres. 2008. Late Eocene marine incursion in the north-western South America. Palaeogeography, Palaeoclimatology, Palaeoecology 264:140-146.

Srkinen, T., R. T. Pennington, M. Lavin, M. F. Simon, and C. E. Hughes. 2012. Evolutionary islands in the Andes: persistence and isolation explain high endemism in Andean dry tropical forests. Journal of Biogeography 39(5):884-900.

Sarmaja-Korjonen, K., A. Seppanen, and O. Bennike. 2006. *Pediastrum* algae from a classic late glacial Blling S site, Denmark: response of aquatic biota to climate change. Review of Palaeobotany and Palynology 138.

Scheibe, R. 1934. Las relaciones entre los pisos de Honda, Gualanday y Barzalosa. CEGOC 1:63:96.

Scotese, C. 2016. Some Thoughts on Global Climate Change: the transition for Icehouse to Hothouse, in the earth history: the evolution og the Earth system https://www.academia.edu/12082909/. Paleomap Project, Evanston, IL.

Sepkoski, J. 1978. A Kinetic model of Phanerozoic Taxonomic Diversity I. Analysis of Marine Orders. Paleobiology 4(3):223-251.

Sepkoski, J. 1979. A kinetic model of Phanerozoic taxonomic diversity. II Early Paleozoic families and multiple equilibira. Paleobiology 5.

Sepkoski, J. 1996. Biodiversity: Past, Present, and Future. Journal of Paleontology 71:533-539.

Sepkoski, J. 2002. A compendium of fossil marine animal genera Bulletins of American Paleontology 363.

Sepksoki, J. J., R. Bambach, D. Raup, and J. Valentine. 1981. Phanerozoic marine diversity and the fossil record. Nature 293:435-437.

Shaw, A. 1964. Time in Stratigraphy. New York: McGraw Hill. 365 p.

Signor, P., and J. Lipps. 1982. Sampling bias, gradual extinction patterns and catastrophes in the fossil record. Pp. 219-296. In L. T. S. a. P. H. Schultz, ed. Geological Implications of impacts of large asteroids and comets on the Earth. Geological Society of America Special Publication 190.

Silva-Caminha, S., C. Jaramillo, M. Absy. 2009. Neogene palynology of the Solimoes Basin, Brazilian Amazonia. Paleontographica: Abteilung B: Paleobotany-Paleophytology 283(1-3):1-67.

Silvestro, D., Zizka, A., Bacon, C., Cascales-Minana, B., Salamin, N., Anotnelli, A. 2016. Fossil biogeography: a new model to infer dispersal, extinction and sampling from palaeontological data. Philosophical Transactions of the Royal Society of London, Series B: Biological Sciences 371.

Silvestro, D., B. Cascales-Minana, C. D. Bacon, and A. Antonelli. 2015. Revisiting the origin and diversification of vascular plants through a comprehensive Bayesian analysis of the fossil record. New Phytologist 207(2):425-36.

Sklenar. P, E. Duskova, H. Balslev. H. 2011. Tropical and temperate: evolutionary history of Paramo Flora. The Botanical Review. 77.

Sluijs, A., J. Pross, and H. Brinkhuis. 2005. From greenhouse to icehouse; organic-walled dinoflagellate cysts as paleoenvironmental indicators in the Paleogene. Earth-Science Reviews 68.

Smith, A., and A. McGowan. 2007. The shape of the Phanerozoic marine paleodiversity curve: How much can be predicted from the sedimentary rock

record of western Europe? Palaeontology 50:765-774.

Soares, E., C. D'Apolito, J. C., G. Harrington, M. Caputo, R. Barbosa, E. dos Santos, R. Dino, and A. Goncalves. 2017. Sedimentology and Palynostratigraphy of a Pliocene-Pleistocene (Piacenzian to Gelasian) deposit in the lower Negro River: Implications for the establishment of large rivers in Central Amazonia. Journal of South American Earth Sciences 79.

Srivastava, J., and V. Prasad. 2015. Effect of global warming on diversity pattern in Nypa mangroves across PaleoceneEocene transition in the paleoequatorial region of the Indian sub-continent. Palaeogeography, Palaeoclimatology, Palaeoecology 429.

Stancliffe, R. 1989. Microforaminiferal Linings: Their Classification, Biostratigraphy and Paleoecology, with Special Reference to Specimens from British Oxfordian Sediments. Micropaleontology 35(4).

Stebbins, G. L. 1974. Flowering plants: evolution above above the the species level. Harvard University Press.

Tahoun, S., A. Deaf, and A. Mansour. 2017. Palynological, palaeoenvironmental and sequence stratigraphical analyses of a Turonian-Coniacian sequence, Beni Suef Basin, Eastern Desert, Egypt: Implication of *Pediastrum* rhythmic signature. Marine and Petroleum Geology 88.

Tan, P. S., M; Kumar, V. 2014. Introduction to Data Mining. Pearson ed.

Tappan, H., and A. Loeblich. 1965. Foraminiferal remains in palynological preparations. Revue de Micropaleontologie 8(2).

Tell, G. 2004. Recent and fossil species of the genus *Pediastrum Meyen* (Chlorococcales) from Argentina and their geographical distribution. Arch. Hydrob./Algol. Stud 112.

Tell, G., and M. Zamaloa. 2004. A Miocene algal assemblage dominated by *Pediastrum leonensis* n. sp. (Chlorophyceae) from Patagonia, Argentina: paleoenvironmental implications. Journal of Paleolimnology 32.

ter Steege, H., N. C. Pitman, O. L. Phillips, J. Chave, D. Sabatier, A. Duque, J. F. Molino, M. F. Prevost, R. Spichiger, H. Castellanos, P. von Hildebrand, and R. Vasquez. 2006. Continental-scale patterns of canopy tree composition and function across Amazonia. Nature 443(7110):444-7.

Tomlinson, P. 1986. The Botany of Mangroves. Cambridge University Press, Cambridge.

Traverse, A. 2007. Paleopalynology. 2nd ed. Dordrecht: Springer. 813 p.

Turk, G. 1979. Transition Analysis of Structural sequences: Discussion. Geological Society of America Bulletin 90(10).

Tyson, R. 1995. Sedimentary Organic Matter: Organic Facies and Palynofacies. Springer-Science+Business Media.

Ulloa, C., P. Acevedo, S. Beck, M. Belgrano, R. Bernal, P. Berry, L. Brako, M. Celis, G. Davidse, R. Forzza, R. Gradstein, O. Hokche, B. Leon, S. Leon, R. Magill, D. Neill, M. Nee, P. Raven, H. Stimeel, M. Strong, J. Villaseor, J. Zarucchi, F. Zuloaga, and P. Jorgensen. 2017. An integrated assessment of the vascular plant species of the Americas. Science 358:1614-1617.

Van der Hammen, T. 1957a. Climatic periodicity and evolution of South American Maestrichtian and Tertiary Floras: a study based on pollen analysis in Colombia. Boletin Geologico 5:49-91.

Van der Hammen, T. 1957b. Palynologic stratigraphy of the Sabana de Bogota (East Cordillera of Colombia). Boletin Geologico 5:187-203.

Van der Hammen, T. 1958. Estratigrafia del Terciario y Maestrichtiano continentales y Tectonogenesis de los Andes Colombianos. Boletin Geologico 6:67-128.

Van Geel, V., 2002, Non-Pollen Palynomorphs, in J. P. Smiol, H. Birks, W. Last, R. Bradley, and K. Alverson, eds., Tracking Environmental Change using Lake sediments. Developments in Paleoenvironmental Research, Springer, Dordrecht.

Van Valen, L. 1973. A new evolutionary Law. Evol. Theory 1:1-30.

Villamil, T. 1999. CampanianMiocene tectonostratigraphy, depocenter evolution and basin development of Colombia and western Venezuela. Palaeogeography, Palaeoclimatology, Palaeoecology 153.

Villamil, T., J. Muoz, J. Sanchez, J. Aristizabal, J. Velasco, P. Luna, A. Mantilla, A. Farjardo, L. Pea, M. Paz, O. Silva, O. Sanchez, and N. Meza. 2004. The Gibraltar discovery, Northern Llanos Foothills, Colombia: Case History of an exploration Success in a frontier area. Journal of Petroleum Geology 27(4).

Villaroel, C. 2000. Un nuevo *Mylodontinae* (Xenarthra, Tardigrada) en la Fauna de La Venta, Mioceno de Colombia: estado actual de la Familia Orophodontidae. Revista Academia Colombiana de Ciencias Exactas, Fisicas y Naturales 24.

Vonhof. H, R. Kaandorp. 2010. Climate variation in Amazonia during the Neogene and the Quaternary. In C. Hoorn and F. Wesselingh, ed. Amazonia, Landscape and Species Evolution. Oxford: Blackwell Publishing

Walker, R. 1979. Facies and Facies Models: General Introduction. In R. Walker, ed. Facies Models. Geological Association of Canada.

Webb, S. 1995. Biological Implicationsofthe Middle Miocene Amazon Seaway. Science 269.

Weckstrom, K., J. Weckstrom, L. Yliniemi, and A. Korhola. 2010. The ecology of *Pediastrum* (Chlorophyceae) in subarctic lakes and their potential as paleobioindicators. Journal of Paleolimnology 43.

Weng, C., H. Hooghiemstra, and J. Duivenvoorden. 2006. Response of polen diversity to the climate-driven altitudinal shift of vegetation in the Colombian Andes. Philos Trans R Soc Lond B Biol Sci 362:253-262.

Wesselingh, F. 2006. Miocene long-lived lake Pebas as a stage of mollusc radiations, with implications for landscape evolution in western Amazonia. Scripta Geologica 133.

Wesselingh, F. 2006c. Molluscs from the Miocene Pebas Formation of Peruvian and Colombian Amazonia. Scripta Geologica 133.

Wesselingh, F., C. Hoorn, S. Kroonenberg, A. Antonelli, J. Lundberg, H. Vonhof, and H. Hooghiemstra. 2010. On the origin of Amazonian landscapes and biodiversity: a synthesis. In C. H. a. F. P. Wesselingh, ed. Amazonia, Landscape and Species Evolution. Oxford: Blackwell publishing.

Wesselingh, F., and M. Ramos. 2010b. Amazonian aquatic invertebrate faunas (Mollusca, Ostracoda) and their development over the past 30 million years. In C. Hoorn, and F. Wesselingh, eds. Amazonia, Landscape and Species Evolution: A look into the past. Blackwell Publishing.

Wetzel, A. 1983. Limnology. Saunders College Publishing, Philadelphia.

Whiteside, M. 1965. On the Occurrence of *Pediastrum* in Lake Sediments. Journal of the Arizona academy of Science 3.

Whitney, B., and F. Mayle. 2012. *Pediastrum* species as potential indicators of lake-level change in tropical South America. Journal of Paleolimnology 47.

Wiens, J., and M. Donoghue. 2004. Historical biogeography, ecology and species richness. Trends Ecol. Evol 19(12).

Wiens, J. 2007. Global patterns of diversification and species richness. Trends Ecol. Evol 19:639-644.

Wilf. P, K. Johnson. 2004. Land plant extinction at the end of the Cretaceous: a quantitative analysis of the North Dakota megafloral record. Paleobiology. 30

Wilf. P, K. Johnson, N. Cuneo, M. Smith, B. Singer, M. Gandolfo. 2005. Eocene plant diversity at Laguna del Hunco and Rio Pichilleufu, Patagonia, Argentina. Am. Nat. 165.

Wing, S., J. Alroy, and L. Hickey. 1995. Plant and mammal diversity in the Paleocene to early Eocene of the Bighorn Basin. Palaeogeography, Palaeoclimatology, Palaeoecology 115.

Wing, S., and G. Harrington. 2001. Floral response to rapid warming at the Paleocene/Eocene boundary and implications for concurrent faunal changes. Paleobiology 27.

Wing, S., F. Herrera, C. Jaramillo, C. Gomez-Navarro, P. Wilf, and C. Labandeira. 2009. Late Paleocene fossils from the Cerrejon Formation, Colom-

bia, are the earliest record of Neotropical rainforest. PNAS 196(44):18627-18632.

Wolfe. J, G. Upchurch. 1986. Vegetation, climatic and floral changes at the Cretaceous-Tertiary boundary. Nature. 324

Woods, M., T. Vandebroucke, M. Williams, J. riding, S. De Schepper, and K. Sabbe. 2014. Complex response of dinoflagellate cysts distribution patterns to cooler early Oligocene oceans. Earth Science Reviews 138.

Young, K., C. Ulloa, J. Luteyn, and S. Knapp. 2002. Plant evolution and endemism in Andean South America: an introduction. Botanical Review 68:4-21.

Zachos, J., G. Dickens, and R. Zeebe. 2008. An early Cenozoic perspective on greenhouse warming and carbon-cycle dynamics. Nature 451.

Zachos, J., M. Pagani, L. Sloan, E. Thomas, and K. Billups. 2001. Trends, Rhythms and Aberrations in Global Climate 65 Ma to Present. Science 292.

Zamaloa, M., and G. Tell. 2005. The fossil record of freshwater microalgae *Pediastrum Meyen* (Chlorophyceae) in southern South America. Journal of Paleolimnology 34.

Zhang, T. 2000. Artificial intelligence models for Quantitative Biostratigraphy. PhD Thesis. University of Illinios at Chicago.

Zhang, T., Plotnick, R. 2007. Graphic Correlation Using Genetic Algorithms. Mathematical Geology 38(781-800).

Zonneveld, K. A. F., F. Marret, G. J. M. Versteegh, K. Bogus, S. Bonnet, I. Bouimetarhan, E. Crouch, A. de Vernal, R. Elshanawany, L. Edwards, O. Esper, S. Forke, K. Grosfjeld, M. Henry, U. Holzwarth, J. F. Kielt, S. Y. Kim, S. Ladouceur, D. Ledu, L. Chen, A. Limoges, L. Londeix, S. H. Lu, M. S. Mahmoud, G. Marino, K. Matsouka, J. Matthiessen, D. C. Mildenhal, P. Mudie, H. L. Neil, V. Pospelova, Y. Z. Qi, T. Radi, T. Richerol, A. Rochon, F. Sangiorgi, S. Solignac, J. L. Turon, T. Verleye, Y. Wang, Z. H. Wang, and M. Young. 2013. Atlas of modern dinoflagellate cyst distribution based on 2405 data points. Review of Palaeobotany and Palynology 191:1-197.

Zurita, A., L. Gonzales, A. Gomez, and J. Arenas. 2013. The Most Complete Known Neogene *Glyptodontidae* (Mammalia, Xenarthra, Cingulata) from Northern South America: Taxonomic, Paleobiogeographic, and Phylogenetic Implications.Journal of Vertebrate Paleontology 33(3).

Annexes Chapter-1.

Annex-1.1. List of sites used in the graphic correlation project.

Project	Site	Latitude	Longitude	Type of Sample	# Samples
this work	Av-1	3,68	-73,44	dc	110
this work	Came-1	3,18	-72,90	dc, swc,cch,co	104
this work	Camo-1	3,64	-73,40	dc	17
this work	Caño Las Blancas	4,01	-73,82	oc	25
this work	Caño Sagu	4,08	-73,78	oc	94
this work	Canoe-1	3,61	-73,51	dc	84
this work	Casc-1	6,10	-71,82	dc	19
this work	Chac-1	3,60	-73,39	dc,swc	28
this work	Cosw-1	4,34	-71,38	dc	16
this work	Con-1	5,43	-70,44	swc	53
this work	CPE2-1	5,55	-70,19	swc	9
this work	Cris-1	3,55	-73,95	dc	65
this work	Cse-08	3,44	-71,45	dc	34
this work	Cusu-1	3,81	-73,19	dc	7
this work	Cusu-2	3,84	-73,16	dc	13
this work	Eval-1	3,46	-73,35	dc,co	25
this work	Fon-1	3,46	-73,60	dc	13
this work	Fue182	3,49	-73,61	dc	90
this work	Gua-1	4,26	-73,35	dc	139
this work	Had-1	3,24	-73,04	dc	50
this work	Kan-1	3,71	-72,56	dc,co	20
this work	Bru-1	3,03	-73,11	dc,swc	19
this work	Luro-1	3,86	-73,50	dc	44
this work	Maga-1	7,04	-72,20	dc	69
this work	Ma-1	3,72	-71,74	dc,swc,co	85
this work	Moc-1	5,15	-70,55	swc	43
this work	Mues-1	5,79	-71,9	dc	55
this work	Nac-1	5,29	-70,3	swc	20
this work	Nines-1	3,42	-73,43	dc	12
this work	Nuesp-1	3,88	-73,75	dc	96
this work	Past-1	3,80	-73,14	dc	30
this work	Past-4	3,74	-73,25	dc,cch,co	119
this work	Ret-1	3,12	-72,61	dc,swc,co	75
this work	Ret-1ST1	3,12	-72,61	dc	72
this work	Ros-1	7,86	-72,49	dc	29
this work	Rub-2	3,80	-71,51	dc,swc	29
this work	Rub-79	3,76	-71,40	dc,swc	16
this work	S-10	3,06	-72,86	dc	34
this work	S-14	3,41	-73,06	dc	47
this work	S-17	3,36	-73,93	dc,co	40
this work	S-5	3,28	-73,24	dc	48
this work	S-7	3,09	-73,23	dc	40

Annex 1.1 (continuation)

Project	Site	Latitude	Longitude	Type of Sample	# Samples
this work	Tar-1	3,26	-73,12	dc	90
this work	Tras-1	3,35	-72,63	dc,swc,co	91
this work	Val-1	3,91	-72,66	dc,swc	34
this work	Ven-2	3,52	-72,97	dc	9
this work	Ven-3	3,55	-72,94	dc,cch,co	134
Jaramillo et al 2011	Aga-1	5,83	-74,32	dc	214
Jaramillo et al 2011	Ara-2	6,95	-71,84	dc	137
Jaramillo et al 2011	Ara-3	6,98	-71,82	dc	61
Jaramillo et al 2011	Ara-4	6,98	-71,84	dc	52
Jaramillo et al 2011	Buc-1	5,61	-71,36	dc	19
Jaramillo et al 2011	Bue-3Carb	4,98	-72,74	dc	76
Jaramillo et al 2011	Bue-3Cor	4,98	-72,74	co	144
Jaramillo et al 2011	Bue-H15	4,95	-72,73	co	30
Jaramillo et al 2011	Cas-1	6,76	-73,57	dc	122
Jaramillo et al 2011	Cerrejon	11,07	-72,69	co	278
Jaramillo et al 2011	Cer-3	8,21	-72,74	dc	90
Jaramillo et al 2011	Chi-1	6,57	-70,92	dc	19
Jaramillo et al 2011	Colorado	4,84	-73,22	oc	62
Jaramillo et al 2011	Concentracion	6,03	-72,76	oc	37
Jaramillo et al 2011	Cop-1	4,44	-73,28	dc	33
Jaramillo et al 2011	Cor-1	3,77	-73,73	dc	100
Jaramillo et al 2011	Cus-5	5,11	-72,66	co	111
Jaramillo et al 2011	Din-K12	3,09	-75,30	co	48
Jaramillo et al 2011	Flo-C3	5,49	-72,42	dc	61
Jaramillo et al 2011	Gib	7,04	-72,17	oc	251
Jaramillo et al 2011	Gig-1	2,28	-75,56	dc	22
Jaramillo et al 2011	Gon-1	8,28	-72,58	dc	199
Jaramillo et al 2011	Gonzales	8,60	-72,70	dc	26
Jaramillo et al 2011	GonOut	8,28	-72,58	oc	39
Jaramillo et al 2011	Gua-1	4,74	-73,13	co	13
Jaramillo et al 2011	Gua-2	4,70	-73,16	dc	110
Jaramillo et al 2011	Hig-1	3,10	-75,27	dc	59
Jaramillo et al 2011	Jor-1	6,07	-71,24	dc	30
Jaramillo et al 2011	Jub-1	6,99	-71,53	dc	29
Jaramillo et al 2011	LaHe-1	6,25	-71,00	dc	25
Jaramillo et al 2011	LaMar-1	5,07	-72,51	dc	128
Jaramillo et al 2011	Las-1	5,38	-71,97	dc	17
Jaramillo et al 2011	Lis-1	7,10	-73,53	dc	41
Jaramillo et al 2011	Medina	4,50	-73,10	oc	678
Jaramillo et al 2011	Mol-1	11,30	-72,50	dc	87
Jaramillo et al 2011	Mon-1A	6,83	-74,04	dc	207
Jaramillo et al 2011	Muc-3	8,10	-72,52	dc	79
Jaramillo et al 2011	Nis-E1	5,62	-72,31	dc	141

Annex 1.1 (continuation)

Project	Site	Latitude	Longitude	Type of Sample	# Samples
Jaramillo et al 2011	Ori-1	0,57	-76,89	dc	88
Jaramillo et al 2011	Pac-1	3,98	-73,51	dc	18
Jaramillo et al 2011	Pal-1	4,43	-73,36	dc	216
Jaramillo et al 2011	Pau-C2FZ	5,44	-72,46	dc	21
Jaramillo et al 2011	Pij-1	3,00	-75,27	dc	46
Jaramillo et al 2011	Pum-1	0,57	-76,88	dc	185
Jaramillo et al 2011	Regadera	7,40	-72,40	oc	100
Jaramillo et al 2011	Reg-1	6,88	-73,55	dc	205
Jaramillo et al 2011	RieMacheRull	10,92	-72,26	oc	21
Jaramillo et al 2011	Rio de Oro-14	9,10	-72,90	dc	77
Jaramillo et al 2011	Rio Loro	8,40	-71,80	oc	57
Jaramillo et al 2011	Rio Molino	10,68	-72,94	oc	20
Jaramillo et al 2011	RioCh-1	4,93	-72,73	dc	184
Jaramillo et al 2011	SanFel-1	5,13	-71,85	dc	28
Jaramillo et al 2011	SanJRS	4,86	-74,63	oc	49
Jaramillo et al 2011	SanJ-1	3,38	-73,86	dc	105
Jaramillo et al 2011	SanMar-1	6,01	-71,65	dc	52
Jaramillo et al 2011	Sutatauza	5,13	-73,50	oc	69
Jaramillo et al 2011	Tam-2	6,57	-71,76	dc	96
Jaramillo et al 2011	Tib-182/187	8,59	-72,67	dc	172
Jaramillo et al 2011	Toc-1	6,28	-71,80	dc	150
Jaramillo et al 2011	Uribe	7,25	-73,37	oc	62
Jaramillo et al 2011	UrumacoEast	11,47	-69,55	oc	31
Jaramillo et al 2011	UrumacoWest	11,18	-70,26	oc	293
Jaramillo et al 2011	Zul-1	8,20	-72,45	dc	127

Annex 1.2. Lines of Correlation (LOC) for every section used in this study. Each pair of points corresponds to the endpoints of a segment of the LOC. The first column corresponds to individual sections and the second column corresponds to the composite section.

Aga-1	
14880.68	17003.06
10070	10419.29
5810	2721.73

Ara-3	
19686.52	20908.24
19165	20496
18420	19842
17940	18143
17656	17463
17656	14674
17515	14377
16240	5243
15045	4495
14309.69	4268.77

Bue-3Carb	
14050	15694
13825	14964
12870	14377
11730	9091
9390	3962

Bue-H15	
15336	19525
15267	19379
15045	18916
14982	18767
14771	18143
14162	17452

Buc-1	
7440	22000
7440	15256
7305	14377

Ara-2	
20621.40	21538,89746
20215	21148
19615	20496
19375	20218
18895	19842
18258	18143.08
17930	17560.94
17930	15329
17680	14377
16115	9091
13574.09	3759.4

Ara-4	
19230.75	20350.36
19005	19842
17865	18143
17789	18046.06
17789	14480
17589	14377

Bue-3Cor	
16921.66	21684,43219
16662	21148
16320	20496
16285	20423.1
16285	19501.41
16248	19379
16114	18916
16112	18751
16022	18585
15510	17452
15386	16849
15150	16669

Annex 1.2 (continuation)

Cer-3	
3712.82	21441.87
1040	19842
160	19379
52.13	19355.87

Concentracion	
4599	16849
4348	16426
2319	16068
2021	15816
750.32	14465.04

Las-1	
10973	21740
10973	14795
10855	14377

Mon-1A	
10317.92	11730.76
7870	9091
7220	6877
6250	5001
6000	3962
2310	789
0	0

Nis-E1	
4499.92	16251.15
3940	16068
2710	15694
1120	14964
250	14377

Pac-1	
9519	21975.50
9519	16493
9424	16426
9050	16068
8859	15864

Cas-1	
5688.31	21781.45
3530	20496
2330	19842
1450	19234
1450	16809.01

Chi-1	
6850	21781.45
6850	15353
6522.96	14383.43

Cop-1	
17032.44	19137.57
16950	18916
16645	18143
16240	16669

Mol-1	
8930	10419
7460	9091
3370	4411
3130	4157
1169.52	771.55

Muc-3	
5428.13	20010.78
5210	19842
4550	19379
3270	18767
2700	18143
2640	17995
1830	16426
1510	16068
900	14476
710	14377

Annex 1.2 (continuation)

Pau-C2FZ	
3510	16978.83
3510	16162
3420	16032
3210	15759
2910	14377
1620	10562

Pum-1	
10330	21611.66
10330	18652
6890	18123
4000	16278
3880	16068
870	14377

RioCh-1	
15999.85	21393.36
15855	21148
15544,9	20496
15544,5	20494
15544,5	19382
15496	19379
14950	17452
14785	16808
14574	16426
10868	14377
9904	9728
7940	4408

Flo-C3	
15978.71	21078.03
15575	20496
15295	20218
15250	20156
15250	19234
14695	18767
14415	18143
14405	17995
13790	17452
13295	16868
12381.65	15790.27

Ori-1	
7650	21854.22
7650	18797
3750	16068
3479.49	15863.04

Pal-1	
16560.88	16348.15
14370	16068
10500	14377
3754	5453
2850	4411
2550	4157
0	0

Pij-1	
8009	21148
7860	20496
7780	20218
7200	20100
7200	9338
7140	9091
6660	4157

Cus-5	
18399.97	21635.92
18160	21148
17846	20496
17776	20350.36
17776	19355
17526	19017
17067	17452
16810	16849
16697	16669

Din-K12	
7271.54	20630.45
7155	20496
6958	20218
6425	19873

Annex 1.2 (continuation)

Gig-1	
13375	20416
13140	19873
10930	19781
7350	16068
5350	14377

Gonzales	
1124	18144
1003	17995
69	16468
0.01	16348.15

Gua-2	
9150	19379
8110	18143
7425	16669
6920	16068
210	14377

Hig-1	
5435	21999.75
5435	9119
5310	9091
2580	5001
2250	4157

Jub-1	
11900.12	21781.45
11705	21148
11345	20218
11290	20132
11290	15741
11005	14377

Lis-1	
7099.38	20204.82
5815	19842
5035	19379
4655	18916
3685	18767
1055	18143

Gib	
10102.59	19889,50386
9936	19842
8992	18767
8600	18143
7987	17995
6700	16868
5990	16068
5600	15786
5060	15694
4300	14964
3240	14377
2010	9728
1770	9091
350	3962

Gua-1	
10299.29	21247.82
10217	21148
9893	20714
9893	19792
9696	19379
8140	17452
7735	16669

LaHe-1	
7000	21999.75
7000	16251
6500	14377

Jor-1	
8655	21999.75
8655	14989
8495	14964
7875	14377
7400	10834

Medina	
22857.73	22857.73
1088.46	1088.46

Annex 1.2 (continuation)

Colorado	
4470.5	21781.45
3281	21531
2075	20889
1633	20496
1152	20132
836	19938
807	19477
318	18916
3	18895.01

Gon-1	
5530.08	20471.64
2300	19842
2060	19023
1280	18143
810	17995
600	17708
383.64	16647.13

Reg-1	
8897.07	20059.29
8780	19842
8755	19800
8755	17720
8660	17708
7850	17372
6340	16032
4630	15765
3200	14393
980	8663

RioOro-14	
6037	20132
3497	19897
2700	19842
2655	19373
2415	18916
2252.77	18603.94

LaMar-1	
16538.20	21975.50
16149	21369
16149	18895
16095	18767
15885	18143
15825	17995
15805	17372
15605	16068
15525	15793.97
14605	14377
13312	9728
11650	4157
10025.97	3783.66

Cerrejon	
3402.87	20107.80
2754	19842
2609	19794
2298.84	19475.70
2137.33	19178.57
2043.15	18895.76
64	18143

Cor-1	
6916.67	21999.75
6880	21531
6820	21148
6745	20908
6745	17439
6740	17372
6560	16426
6320	16068
6200	15786
4110	14377
1330	5001
0	0

Annex 1.2 (continuation)

RioMolino	
794.76	20595.21
716	20496
399	20009
0	19886

SanJ-1	
6304	21902.73
6304	16590
6210	16426
5960	16068
5940	15786
5360	15694
4800	14964
4200	14377
2760	9841
2640	7184
1980	5001
1260	4032
0	0

Sutatauza	
3760	20225
3273	20160
1230	19842
769.91	19792.48

Tib-182/187	
4964.75	20622.34
4775	19918
4580	19113
4380	18901
3710	18143
3290	17995
2015	16068
280	14377
0	14165.13

Regadera	
2002.57	18992.03
1929	18900
1247	18143
902	17708
729	17625
140	17372
49	16868
0.5	16731

RieMacheRull	
3862	18900
2930	18143
2133	17589
1615	16849
143.49	16323.90

RioLoro	
3993.40	20180.57
876	19842
798	19755
342	18916.34
86.9	18361.38
86.9	16566.41
0	16275.39

SanFel-1	
8780	21999.75
8780	15887
8531.45	15571.97

SanJRS	
2356.8	15014.09
31.28	14068.11

Annex 1.2 (continuation)

Toc-1	
18370	21975.50
18265	21148
17350	20835
17350	16205
16505	14377
15830	10294
15435	7184
14020	4126
13265	3852
0	0

UrumacoEast	
4183.07	2087
1515	1332
0	0

Zul-1	
8893.14	19198.21
8870	19113
8810	18901
8030	18143
7970	17995
7800.92	17682.22
6453.45	16857.53

Sutatauza	
4557.23	21999.98
4411.09	21531.82
4285.43	21148
3989.5	20497.08
3887.96	20426.76
3641.73	20160.04
1200	19842
1003.94	19755.25
804.54	19701.18

Came-1	
2679.21	14451.94
2553.22	14381.27
2028.29	9116.25
1535.37	5246.66
796	4911.3

SanMar-1	
11385	21999.75
11385	15620
10675	14377
10015	9091
9915	4411
9105	3962
7755	3812
0	0

Tam-2	
15363.73	21994.98
15035	20496
14895	19887
14495	18901
14420	18770
14420	15741
13605	14377
12805	9841
12655	9091
12505	7184
11715	4411
10485	3852
0	0

Uribe	
10210.26	19186.08
9815	19113
8546	18901
7906	18143
6450	17708
5856	17625
5246	17589
2175	16849
17.97	16122.80

Caño Las Blancas	
520	16830
113.34	16441.3
4.15	16285.83

Annex 1.2 (continuation)

Canoe-1	
7090	16068
6940	15694
6520	14964
5700	14377
4205	7300
3800	5250

Chac-1	
6994.2	16678.1
6731.46	16430.74
6673.72	15653.35

Con-1	
3300	12300
2900	9091
2470	5243
2170	4411
2000	4039
1250	2661
940	2155

Cse-08	
3261	15724.02
2967.1	14964.6
2663.9	14381.27
2516.9	7526.14
2350.5	5369.4
1460.5	4345.9

Cusu-2	
7142.5	16402.43
7000.76	16052.61
6810	15786
6570	15600

Fon-1	
6630	16700
6520	16426
6400	16068
6295	15980

UrumacoWest	
29999.51	9362.49
28513	9091
26322	8663
22060	5243
20554	5001
19051	4411
15206	4126
9796	3852
3334	1894
0	0

GonzOut	
499.77	18143.75
490.12	18143
236.55	18077.19
224.08	17941.7
58.4	17818.7
42.02	17805.92

Av-1	
7320	15858.2
6676.9	14964.2
5831.8	14342.36
3994.5	4586.18

Camo-1	
6900	16068
6540	15694
6365	15549

Caño Sagu	
1216.23	18656.85
716.49	17996.07
602.58	16830
176.34	16441.3
139.59	16169.22
0	15974.87

Annex 1.2 (continuation)

Gua-1	
12820	16425
12780	16068
11760	15694
10560	14964
10210	14375
7965	7035
4300	3800

Kan-1	
4280.29	15702.79
3933.83	14381.23
3606.27	10999.6

Luro-1	
8995	16130
8910	16068
8440	15694
8140	14964
7100	14377

Ma-1	
3215.13	15724
2976.28	14964.64
2654.76	14381.27
2415.91	8126.85
2131.14	5229.32
1625.89	4416.6
303.05	2013.78

Mues-1	
12620	15786
12510	15694
12230	14964
12020	14377
11360	9091
10850	5245
9290	4040

Casc-1	
15010	15765
14970	15694
14730	14964
14420	14377

Cosw-1	
4013.06	15197.49
3805.19	14381.23
3522.25	9095.01
3152.69	5246.96
2869.75	5013.74

CPE2-1	
2425	7300
2150	5243
1945	4500

Cris-1	
3545	16600
3420	16426
3060	16068
2910	15786
1900	15694
50	14377

Cusu-1	
7403.11	16402.43
7270	16068
7005	15740

Eval-1	
5660	16402.43
5025	14692.19

Annex 1.2 (continuation)

Nines-1	
5942	16120
5910	16068
5870	15786
5749	15710

Past-1	
6880	16430
6800	15786
6290	14964
5763.73	13798.2

Ret-1	
2037.2	14458.97
1486.03	13759.32
1370.5	9095
1323.3	7190.42
1160.5	5519
562.15	4430.7
320.68	4119.75

Ros-1	
3010	18500
2280	18190
1732	18112
1330	17327
1110	16426
920	16068
490	15786

Rub-79	
2472.39	14381.27
2249.82	6006.71
1829.87	5264.66

S-14	
4003.84	15780.53
3801.74	15663.92
3324	13448.37
2901.48	9095.01
2341.11	5246.96
1890.98	4430.7
1045.83	4119.75

Fue-182	
6870	16430
6630	16068
6030	15694
5120	14377
2250	5245
1500	4125

Had-1	
3232.2	15780.53
3082.59	15702.79
2586.53	14381.23
1717.75	5246.96
1203.32	4430.7
642.95	4119.75

Bru-1	
2558.97	15780.53
2488.11	15702.79
2157.4	14381.23
1110.15	5246.96
747.95	4780.53

Maga-1	
2375	16414
1966	16068
1350	15786
945	15694
320	15150

Moc-1	
3180	12220
2833	7580
2447	5830
2050	4411
1850	4039
1050	2661
300	1710

Annex 1.2 (continuation)

S-5	
4614	16289.39
4306.96	16077.38
4047.12	15688.69
3515.6	14381.27
2393.5	5264.66
2051.06	4805.3
1106.18	3992.57

Tar-1	
3537,95	15780,53
3443,46	15702,79
3285,98	14964,27
2855,53	14381,23
2410,66	9056,14
1960,53	5246,96
1289,93	4547,31
986,78	4508,44

Val-1	
6177	15780.5
5326.69	15702.79
4759.76	14381.23
4350.31	11310.56

Ven-3	
4051.1	15780.53
3988.11	15702.79
3767.63	14964.27
3499.9	13798.19
2524.84	5480.17
2175.76	4897.13
1679.69	4430.7

S-7	
3153.46	15702.79
2633.77	14381.23
2153.46	9095
1712.51	5246.96
1350.31	4897.13

Nac-1	
2680	10900
2490	8006
2100	5245
1850	4411
1650	4039
900	2660
695	2370

Nuesp-1	
10520	17000
10270	16426
9700	16068
8410	15694
6790	14965
5185	14377

Past-4	
6950	16800
6804	16068
6597	15702.79
5736.11	14381.23
4707.24	9095

Ret-1ST1	
2944.8	14458.97
1582.59	13759.32
1488.1	9133.88
1244	5130.35
779.44	4430.7
377.87	4119.75

Rub-2	
2921.16	14769.92
2673.13	14381.23
2342.42	5674.5
2204.6	5402.43

Annex 1.2 (continuation)

Tras-1	
2861.35	15780.5
2729	15702.79
2590.48	14964.27
2388.91	14381.23
1973.16	9095
1903.87	7384.7
1582.61	5246.96
719	4275.22

Ven-2	
4079.49	15780.53
4053.51	15702.79
4018.86	15702.79
3796.55	14964.27

S-10	
2495.98	14614.45
1850.31	13759.32
1732.2	9095
1700.7	7229.29
1409.37	5246.96
960.5	4430.7
519.6	4119.7

S-17	
2147	16700
1850	16426
1500	16068
1300	15694
105	14377

Annex 1.3: Final sequence of biostratigraphic events separated by three categories. The first category refers to events already included in Jaramillo et al. (2011) zonation. The second category contains information about new informal taxa. The third category includes information about formal species included in this work.

Category 1. Taxa already present in Jaramillo's zonation									
Taxon	Event	Composite Units		Age (my)		Number of Sites		Spreading Parameter	
		Jaramillo et al. 2011	this work	Jaramillo et al. 2011	this Work	Jaramillo et al. 2011	this work	Jaramillo et al. 2011	this work
Adnatosphaeridium multispinosum	LAD	8170,4	8170,4	17,22		3	3	173	173
Adnatosphaeridium multispinosum	FAD	16823,1	16823,1	42,41		1	1	incierto	Incierto
Aglaoreidia? foveolata	LAD	17995,0	17995,0	55,70		6	7	17	17
Aglaoreidia? foveolata	FAD	18859,2	18859,2	58,97		4	4	9	9
Alterbidinium spp.	LAD	18649,0	18649,0	58,12		23	23	41	41
Andalusiella gabonensis	LAD	19843,2	19843,2	65,52		12	12	13	13
Andalusiella mauthei	LAD	19803,1	19803,1	65,21		20	20	35	35
Andalusiella polymorpha	LAD	19379,0	19379,0	62,00		19	19	32	32
Andalusiella spp.	LAD	19379,0	19379,0	62,00		23	23	41	41
Annutriporites iversenii	LAD	15627,6	15627,6	31,07		18	18	85	85
Apiculatasporites? cingulatus	LAD	16100,1	16100,1	34,26		3	3	30	30
Apiculatasporites? cingulatus	FAD	17708,6	17708,6	52,75		3	3	22	22
Araucariacites australis	LAD	18607,5	18607,5	57,95		26	26	68	68
Araucariacites spp.	LAD	16407,3	16407,3	37,72		24	24	112	112
Arecipites regio	LAD	16131,0	16131,0	34,61		14	14	77	77
Areoligera senonensis	LAD	19862,0	19862,0	65,82		5	5	11	11
Areoligera spp.	LAD	18546,2	18546,2	57,70		14	14	48	48
Ariadnaesporites spinosus	LAD	19821,3	19821,3	65,34		8	8	19	19
Baculamonocolpites hammenii	LAD	16300,2	16300,2	36,52		4	4	26	26
Baculamonocolpites hammenii	FAD	17625,0	17625,0	51,72		4	4	26	26
Bacumorphomonocolpites tausae	LAD	19755,2	19755,2	64,84		13	13	6	6
Bombacacidites annae	LAD	17995,0	17995,0	55,70		28	30	29	29
Bombacacidites annae	FAD	19126,0	19126,0	60,09		11	12	20	20
Bombacacidites baculatus	LAD	817,3	817,3	1,11		10	26	116	129
Bombacacidites baculatus	FAD	8492,0	8492,0	17,35		4	8	129	129
Bombacacidites baumfalki	LAD	3812,0	3812,0	11,57		9	10	214	214
Bombacacidites brevis	LAD	204,9	204,9	0,28		38	79	352	352
Bombacacidites brevis	FAD	18009,4	18009,4	55,72		10	12	321	321
Bombacacidites echinatus	LAD	15807,7	15858,1	32,23		4	5	9	9
Bombacacidites echinatus	FAD	16265,8	16572,2	36,13	39,58	2	3	7	7
Bombacacidites fossureticulatus	LAD	16068,0	16068,0	33,90		3	8	15	15
Bombacacidites fossureticulatus	FAD	16755,3	16755,3	41,65		2	3	3	3
Bombacacidites foveoreticulatus	LAD	15807,7	15807,7	32,23		17	35	25	25
Bombacacidites foveoreticulatus	FAD	17480,8	17480,8	49,94		7	9	24	24
Bombacacidites gonzalezii	LAD	11137,8	11137,8	19,77		11	17	128	128
Bombacacidites gonzalezii	FAD	17606,1	17606,1	51,49		4	6	31	31
Bombacacidites muinaneorum	LAD	717,3	717,3	0,97		11	25	280	292
Bombacacidites muinaneorum	FAD	14393,6	14393,6	23,14		4	5	189	189
Bombacacidites nacimientoensis	LAD	4127,8	4127,8	13,05		14	15	290	290
Bombacacidites nacimientoensis	FAD	18335,1	18335,1	56,85		5	5	284	284

Annex 1.3 (continuation)

Bombacacidites protofoveoreticulatus	LAD	18349,7	18349,7	56,90		3	3	7	7
Bombacacidites protofoveoreticulatus	FAD	19095,1	19095,1	59,92		3	3	8	8
Bombacacidites simplireticulatus	LAD	16068,0	16068,0	33,90		5	5	35	35
Bombacacidites simplireticulatus	FAD	17810,8	17810,8	54,01		4	4	21	21
Bombacacidites soleaformis	LAD	15807,7	15807,7	32,23		8	11	35	35
Bombacacidites soleaformis	FAD	17563,8	17563,8	50,97		4	4	22	22
Bombacacidites zuatensis	LAD	5518,6	5518,6	16,19		5	8	90	124
Bombacacidites zuatensis	FAD	10647,3	10647,3	19,27		1	1	incierto	incierto
Brevitricolpites macroexinatus	LAD	16442,3	16442,3	38,12		3	3	23	23
Brevitricolpites macroexinatus	FAD	17625,1	17625,1	51,72		3	3	22	22
Brevitricolpites microechinatus	LAD	15024,1	15024,1	27,19		13	23	67	67
Brevitricolpites microechinatus	FAD	18346,0	18346,0	56,89		5	7	44	44
Buttinia andreevi	LAD	19842,0	19842,0	65,50		14	14	9	9
Catostemma type	LAD	215,2	215,2	0,29		30	62	325	325
Catostemma type	FAD	16068,0	16068,0	33,90		4	4	281	281
Cerodinium diebelii	LAD	19833,1	19833,1	65,43		8	8	20	20
Cerodinium spp.	LAD	19372,6	19372,6	61,95		13	13	216	216
Cicatricosisporites baculatus	LAD	4104,2	4104,2	12,96		3	6	6	6
Cicatricosisporites baculatus	FAD	4228,0	4228,0	13,45		1	1	incierto	incierto
Cicatricosisporites dorogensis	LAD	14377,0	14197,0	23,03	22,85	43	77	60	60
Cicatricosisporites dorogensis	FAD	17372,7	17372,7	48,61		7	7	19	19
Cicatricososporites eocenicus	LAD	16442,3	16113,5	38,12	34,41	2	4	3	6
Cicatricososporites eocenicus	FAD	16755,3	16755,3	41,65		2	2	3	3
Clavainaperturites microclavatus	LAD	102,5	102,5	0,14		14	34	320	320
Clavainaperturites microclavatus	FAD	11226,7	11226,7	19,86		4	4	183	183
Clavatisporites mutisii	LAD	18509,2	18509,2	57,55		9	9	37	37
Clavatricolpites densiclavatus	LAD	10548,9	10548,9	19,18		20	35	160	160
Colombipollis tropicalis	LAD	18397,6	18397,6	57,10		16	16	30	30
Concavissimisporites fossulatus	LAD	4098,4	4098,4	12,93		17	37	248	248
Concavissimisporites fossulatus	FAD	16046,3	16336,0	33,76	36,92	3	4	33	39
Cordosphaeridium inodes	LAD	15851,1	15851,1	32,51		5	5	87	87
Corsinipollenites psilatus	LAD	8440,8	8440,8	17,33		13	13	239	239
Corsinipollenites sp.	LAD	112,7	112,7	0,15		41	83	381	381
Corsinipollenites undulatus	LAD	15285,0	14964,0	28,87	26,80	8	18	45	51
Corsinipollenites undulatus	FAD	17604,0	17604,0	51,46		3	4	30	30
Crassiectoapertites columbianus	LAD	316,9	316,9	0,43		28	58	323	323
Crassiectoapertites columbianus	FAD	15916,2	15916,2	32,92		4	5	279	279
Crassoretitriletes vanraadshooveni	LAD	1874,4	1874,4	3,40		13	31	52	52
Crassoretitriletes vanraadshooveni	FAD	4411,3	4411,3	14,18		3	4	51	51
Cribroperidinium edwardsii	LAD	14576,0	14576,0	24,31		1	1	incierto	incierto
Cribroperidinium spp.	LAD	9391,7	9391,7	18,01		7	7	203	203
Cribroperidinium tenuitabulatum	LAD	8828,0	8828,0	17,48		4	4	20	20
Cricotriporites guianensis	LAD	15878,6	15878,6	32,68		7	7	79	79
Cricotriporites macroporus	LAD	12096,5	12096,5	20,73		4	5	112	112
Cricotriporites macroporus	FAD	17708,6	17708,6	52,75		3	3	16	16
Cricotriporites minutiporus	LAD	16669,3	16669,3	40,68		3	3	47	47
Cricotriporites minutiporus	FAD	19028,5	19028,5	59,65		3	3	47	47
Crototricolpites annemariae	LAD	4093,5	4093,5	12,91		5	5	272	272
Crototricolpites annemariae	FAD	17687,5	17687,5	52,49		3	3	3	3
Crototricolpites protoannemariae	LAD	17816,1	17816,1	54,08		7	7	41	41
Crototricolpites protoannemariae	FAD	19013,8	19013,8	59,60		4	4	19	19
Crusafontites grandiosus	LAD	19858,9	19858,9	65,77		13	13	7	7
Crusafontites megagemmatus	LAD	16609,9	16609,9	40,01		2	2	20	20
Crusafontites megagemmatus	FAD	17590,7	17590,7	51,30		2	2	20	20
Ctenolophonidites cruciatus	LAD	15377,0	15377,0	29,46		2	2	28	28
Ctenolophonidites cruciatus	FAD	16755,3	16755,3	41,65		2	2	28	28

Annex 1.3 (continuation)

Ctenolophonidites lisamae	LAD	18010,7	18010,7	55,72		12	12	38	38
Ctenolophonidites lisamae	FAD	19475,3	19475,3	62,73		2	2	7	7
Curvimonocolpites inornatus	LAD	18167,6	18167,6	56,17		8	9	23	23
Cyatheacidites annulatus	LAD	82,0	82,0	0,11		5	9	286	286
Cyatheacidites annulatus	FAD	2661,2	2661,2	7,15		2	2	12	12
Cyclusphaera scabrata	LAD	7393,4	6826,6	16,92	16,70	36	79	211	210
Cyclusphaera scabrata	FAD	18077,2	18077,2	55,80		5	7	23	23
dinocyst acme C2	LAD	7184,0	7122,3	16,84	16,82	6	22	38	39
dinocyst acme C2	FAD	9841,4	9841,4	18,46		1	1	incierto	incierto
dinocyst acme lowermost C8	LAD	15464,9	15464,9	30,02		3	3	23	23
dinocyst acme lowermost C8	FAD	16638,8	16638,8	40,33		1	1	incierto	incierto
dinocyst acme middle shale Mirador	LAD	16808,2	16808,2	42,24		3	3	1	1
dinocyst acme middle shale Mirador	FAD	16849,7	16849,7	42,71		2	2	1	1
Dinogymnium spp.	LAD	19848,1	19848,1	65,60		25	25	35	35
Diporoconia cf. Iszkaszentgyoergyi	LAD	19177,8	19177,8	60,48		2	2	13	13
Diporopollis assamica	LAD	17995,0	17995,0	55,70		8	9	39	39
Diporopollis assamica	FAD	19080,8	19080,8	59,87		3	3	10	10
Disphaerogena carposphaeropsis	LAD	19855,5	19855,5	65,71		3	3	1	1
Duplotriporites ariani	LAD	19790,1	19790,1	65,11		15	15	20	20
Echimonocolpites densus	LAD	16450,0	16450,0	38,21		6	6	83	83
Echimonocolpites densus	FAD	17513,2	17513,2	50,34		2	2	8	8
Echimonocolpites protofranciscoi	LAD	19842,0	19842,0	65,50		20	20	8	8
Echimorphomonocolpites gracilis	LAD	16490,6	16490,6	38,66		3	3	23	23
Echimorphomonocolpites gracilis	FAD	16849,4	16849,4	42,71		1	1	incierto	incierto
Echimorphomonocolpites solitarius	LAD	16450,0	16450,0	38,21		5	5	24	24
Echimorphomonocolpites solitarius	FAD	17496,1	17496,1	50,13		2	2	13	13
Echinatisporis brevispinosus	LAD	5984,7	5984,7	16,38		5	5	233	233
Echinatisporis brevispinosus	FAD	19092,7	19092,7	59,91		4	4	63	63
Echiperiporites akanthos	LAD	102,5	102,5	0,14		32	70	347	347
Echiperiporites akanthos	FAD	16427,3	16427,3	37,95		6	7	287	287
Echiperiporites estelae	LAD	1161,1	1161,1	1,58		29	44	312	312
Echiperiporites estelae	FAD	17606,1	17606,1	51,49		9	9	310	310
Echiperiporites scabrannulatus	LAD	1968,2	1968,2	4,53		3	3	54	54
Echiperiporites scabrannulatus	FAD	4908,5	4908,5	15,69		2	2	57	57
Echitetracolpites? tenuiexinatus	LAD	16068,0	16068,0	33,90		10	15	18	18
Echitetracolpites? tenuiexinatus	FAD	16867,7	16867,7	42,92		5	5	11	11
Echitricolporites maristellae	LAD	651,9	651,9	0,89		16	38	248	277
Echitricolporites maristellae	FAD	9091,9	9091,9	17,71		4	4	140	140
Echitricolporites mcneillyi	LAD	573,8	573,8	0,78		2	2	162	162
Echitricolporites mcneillyi	FAD	1150,1	1150,1	1,56		1	1	incierto	incierto
Echitricolporites spinosus	LAD	102,5	102,5	0,14		9	12	171	171
Echitricolporites spinosus	FAD	8663,7	8663,7	17,41		3	4	132	132
Echitriletes "acanthotriletoides"	LAD	4385,3	4385,3	14,07		3	3	202	202
Echitriletes "acanthotriletoides"	FAD	14764,6	14764,6	25,52		1	1	incierto	incierto
Echitriletes intercolensis	LAD	19453,4	19453,4	62,57		8	8	34	34
Echitriletes muelleri	LAD	817,3	817,3	1,11		33	33	381	381
Echitriletes muelleri	FAD	17465,6	17465,6	49,76		7	7	308	308
Echitriporites "pseudotrianguliformis"	LAD	15916,2	15916,2	32,92		1	1	incierto	incierto
Echitriporites "pseudotrianguliformis"	FAD	15959,5	15959,5	33,20		1	1	incierto	incierto
Echitriporites "scabrabaculomorphis"	FAD	16575,0	16575,0	39,62		1	1	incierto	incierto
Echitriporites "scabrabaculomorphis"	LAD	16575,0	16575,0	39,62		2	2	0	0
Echitriporites cricotriporatiformis	LAD	1951,5	1951,5	3,94		4	7	51	72
Echitriporites cricotriporatiformis	FAD	7176,7	7176,7	16,84		3	3	105	105
Echitriporites suescae	LAD	19087,4	19087,4	59,89		19	19	47	47
Echitriporites trianguliformis	LAD	16068,0	16046,0	33,90	33,76	19	19	80	80
Echitriporites trianguliformis orbicularis	LAD	16068,0	16068,0	33,90		23	43	31	31

Annex 1.3 (continuation)

Echitriporites trianguliformis orbicularis	FAD	17598,0	17598,0	51,39		7	9	21	21
Echitriporites variabilis	LAD	16383,0	16383,0	37,45		3	8	24	24
Echitriporites variabilis	FAD	17603,8	17603,8	51,46		2	4	15	15
Ephedripites "afropollensis"	LAD	19857,5	19857,5	65,75		2	2	0	0
Etm dc13spike	LAD	17810,0	17810,0	54,00		1	1	incierto	incierto
Etm dc13spike	FAD	17818,7	17818,7	54,11		4	4	16	16
Fenestrites longispinosus	LAD	866,4	866,4	1,18		3	4	60	60
Fenestrites longispinosus	FAD	3537,0	3537,0	10,06		1	1	incierto	incierto
Fenestrites spinosus	LAD	174,2	174,2	0,24		4	9	78	83
Fenestrites spinosus	FAD	4039,3	4392,4	12,70	14,10	2	3	39	39
Foveomonoporites variabilis	LAD	18347,1	18347,1	56,89		1	1	incierto	incierto
Foveotricolpites perforatus	LAD	18143,0	18143,0	56,07		25	27	15	15
Foveotricolpites perforatus	FAD	18917,8	18917,8	59,21		10	11	15	15
Foveotricolporites etayoi	LAD	10819,2	9572,4	19,45	18,19	27	59	113	132
Foveotricolporites etayoi	FAD	15780,9	15780,9	32,05		2	2	0	0
Foveotricolporites fossulatus	LAD	15816,3	15816,3	32,28		2	2	24	24
Foveotricolporites fossulatus	FAD	16755,3	16755,3	41,65		1	1	incierto	incierto
Foveotricolporites rugulatus	LAD	11669,6	11669,6	20,30		13	22	148	13
Foveotricolporites rugulatus	FAD	18077,2	18077,2	55,80		4	5	44	44
Foveotriletes margaritae	LAD	18143,4	18143,4	56,07		30	30	66	66
Foveotriletes ornatus	LAD	61,5	61,5	0,08		10	25	289	289
Foveotriletes ornatus	FAD	15599,7	15599,7	30,89		4	5	270	270
Foveotriporites hammenii	LAD	15964,7	15964,7	33,24		16	23	30	30
Foveotriporites hammenii	FAD	17604,0	17604,0	51,46		8	10	27	27
Gabonisporis spp.	LAD	19842,0	19842,0	65,50		5	5	0	0
Gabonisporites vigourouxii	LAD	19836,0	19836,0	65,45		17	17	16	16
Gemmamonocolpites gemmatus	LAD	18138,8	18138,8	56,05		12	12	36	6
Gemmamonocolpites macrogemmatus	LAD	18916,0	18916,0	59,20		3	3	9	9
Gemmamonocolpites macrogemmatus	FAD	19432,6	19432,6	62,41		2	2	0	0
Gemmastephanoporites breviculus	LAD	16175,1	16175,1	35,11		5	6	27	27
Gemmastephanoporites breviculus	FAD	16973,9	16973,9	44,11		2	2	4	4
Gemmastephanoporites polymorphus	LAD	14727,9	14727,9	25,29		4	4	42	42
Gemmastephanoporites polymorphus	FAD	16847,7	16847,7	42,69		2	2	1	1
Glaphyrocysta perforata	LAD	19842,0	19842,0	65,50		2	2	1	1
Grimsdalea magnaclavata	LAD	1874,4	1874,4	3,40		10	28	60	96
Grimsdalea magnaclavata	FAD	5243,4	5243,4	16,09		3	3	65	65
Grimsdalea polygonalis	LAD	16474,6	16474,6	38,48		2	2	5	5
Grimsdalea polygonalis	FAD	16717,8	16717,8	41,23		1	1	incierto	incierto
Hamulatisporis caperatus	LAD	19453,4	19453,4	62,57		14	15	44	44
Heterocolpites palaeocenica	LAD	18031,9	18031,9	55,74		3	3	13	13
Heterocolpites palaeocenica	FAD	19441,9	19441,9	62,48		2	2	6	6
Homotryblium floripes	LAD	16068,0	16068,0	33,90		4	6	15	15
Homotryblium floripes	FAD	16849,4	16849,4	42,71		2	3	2	2
Horniella lunarensis	LAD	10294,0	6800,1	18,92	16,69	16	43	158	227
Horniella lunarensis	FAD	18498,1	18498,1	57,51		6	6	53	53
Hystrichosphaeropsis obscura	LAD	8606,6	8606,6	17,39		1	1	incierto	incierto
Ischyosporites problematicus	LAD	16364,7	16364,7	37,24		6	6	41	41
Ischyosporites problematicus	FAD	19129,5	19129,5	60,12		5	5	15	15
Jandufouria "minutus"	LAD	14437,4	14437,4	23,42		4	4	41	41
Jandufouria "minutus"	FAD	15750,4	15750,4	31,86		1	1	incierto	incierto
Jandufouria minor	LAD	4399,6	4399,6	14,13		12	32	241	245
Jandufouria minor	FAD	16778,9	16778,9	41,91		4	2	241	241
Jandufouria seamrogiformis	LAD	1471,1	1471,1	2,22		36	74	305	305
Jandufouria seamrogiformis	FAD	16808,2	16808,2	42,24		6	7	294	294

Annex 1.3 (continuation)

L. proxapertitoides proxapertitoides	LAD	15785,1	15785,1	32,08		13	13	78	78
L. proxapertitoides reticuloides	LAD	1945,5	1945,5	3,72		14	14	358	358
Ladakhipollenites rubinii	LAD	16594,8	16594,8	39,84		2	2	20	20
Ladakhipollenites rubinii	FAD	17606,1	17606,1	51,49		2	2	19	19
Ladakhipollenites simplex	LAD	4082,0	4082,0	12,87		11	12	281	281
Ladakhipollenites simplex	FAD	19095,1	19095,1	59,92		8	8	299	299
Laevigatosporites catanejensis	LAD	1962,4	1962,4	4,32		23	23	369	369
Laevigatosporites catanejensis	FAD	16833,4	16833,4	42,53		4	4	158	158
Laevigatosporites granulatus	LAD	727,5	727,5	0,99		22	58	349	349
Laevigatosporites granulatus	FAD	19177,8	19177,8	60,48		7	7	343	343
Lanagiopollis crassa	LAD	1975,1	1975,1	4,77		35	68	312	312
Lanagiopollis crassa	FAD	17590,7	17590,7	51,30		10	13	312	312
Lingulodinium cf. sicula	LAD	16609,9	16609,9	40,01		1	1	incierto	incierto
Lingulodinium cf. sicula	FAD	16711,0	16711,0	41,15		1	1	incierto	incierto
Lingulodinium machaerophorum	LAD	3502,3	3502,3	9,87		5	5	278	278
Lingulodinium machaerophorum	FAD	16835,3	16835,3	42,55		2	2	246	246
Longapertites microfoveolatus	LAD	15999,2	15999,2	33,46		10	10	97	97
Longapertites proxapertitoides	LAD	16720,0	16720,0	41,25		9	9	53	53
Longapertites proxapertitoides	FAD	18143,1	18143,1	56,07		3	3	19	19
Longapertites sp. 1	LAD	15917,0	15917,0	32,93		5	5	43	43
Longapertites sp. 1	FAD	19177,8	19177,8	60,48		3	3	48	48
Longapertites vaneendenburgi	LAD	17038,0	16754,7	44,83	41,64	19	20	60	60
Loranthacitoides "magnopolaris"	LAD	4082,0	4082,0	12,87		1	1	incierto	incierto
Loranthacitoides "magnopolaris"	FAD	4399,6	4399,6	14,13		1	1	incierto	incierto
Luminidites colombianensis	LAD	16194,0	16084,5	35,32	34,09	4	8	7	9
Luminidites colombianensis	FAD	16755,3	16825,0	41,65	42,43	3	5	4	14
M. franciscoi pachyexinatus	LAD	3995,9	3995,9	12,53		50	82	308	308
M. franciscoi pachyexinatus	FAD	19482,1	19482,1	62,78		11	13	310	310
Magnaperiporites spinosus	LAD	4111,0	4111,0	12,98		26	48	239	239
Magnaperiporites spinosus	FAD	15765,6	15765,6	31,96		4	4	27	27
Magnastriatites grandiosus	LAD	174,2	174,2	0,24		34	69	326	326
Magnastriatites grandiosus	FAD	16032,8	16032,8	33,67		6	6	279	279
Magnotetradites magnus	LAD	18031,9	18031,9	55,74		12	12	52	52
Margocolporites vanwijhei	LAD	1471,1	1471,1	2,22		29	55	323	323
Margocolporites vanwijhei	FAD	17708,6	17708,6	52,75		7	7	255	255
Mauritiidites crassibaculatus	LAD	3862,7	3862,7	11,85		5	5	295	295
Mauritiidites crassibaculatus	FAD	19441,9	19441,9	62,48		2	2	306	306
Mauritiidites franciscoi franciscoi	LAD	286,8	286,8	0,39		57	96	391	391
Mauritiidites franciscoi franciscoi	FAD	19482,1	19482,1	62,78		16	16	348	348
Mauritiidites franciscoi minutus	LAD	286,9	286,9	0,39		34	57	388	388
Mauritiidites franciscoi minutus	FAD	18917,8	18917,8	59,21		12	12	339	339
MgrandiosusMfranciscoiJseamrogiformis ACME Ca5	LAD	14964,0	14964,0	26,80		3	3	17	17
MgrandiosusMfranciscoiJseamrogiformis ACME Ca5	FAD	15694,6	15694,6	31,50		19	19	64	64
Momipites africanus	LAD	15336,0	15336,0	29,19		5	5	71	71
Momipites africanus	FAD	18916,7	18916,7	59,20		3	3	72	72
Monocolpopollenites ovatus	LAD	14429,1	14429,1	23,36		10	17	95	95
Monocolpopollenites ovatus	FAD	19198,6	19198,6	60,64		7	7	25	25
Monocolpopollenites spheroidites	FAD	19379,0	19379,0	62,00		1	1	incierto	incierto
Monocolpopollenites spheroidites	LAD	19379,0	19379,0	62,00		5	5	41	41
Monoporopollenites annulatus	LAD	71,7	71,7	0,10		44	85	382	382
Multimarginites vanderhammenii	LAD	789,0	789,0	1,07		11	23	136	136
Multimarginites vanderhammenii	FAD	5001,3	5021,1	15,95	16,00	3	3	59	59
Multiporopollenites pauciporatus	LAD	14377,0	14377,0	23,03		15	28	57	57
Multiporopollenites pauciporatus	FAD	16849,7	16849,7	42,71		2	3	14	14
Nijssenosporites fossulatus	LAD	758,3	758,3	1,03		9	22	267	267
Nijssenosporites fossulatus	FAD	10419,3	10419,3	19,05		2	3	115	115

Annex 1.3 (continuation)

Nothofagidites huertasii	LAD	15786,0	15774,8	32,09	32,02	13	28	32	32
Nothofagidites huertasii	FAD	17372,2	17372,2	48,60		4	5	21	21
Operculodinium centrocarpum	LAD	4225,0	4225,0	13,44		3	3	321	321
P. operculatus acme lower Cuervos	LAD	17995,0	17995,0	55,70		6	6	14	14
P. operculatus acme lower Cuervos	FAD	19482,1	19482,1	62,78		5	5	14	14
Palaeocystodinium australinum	LAD	19326,1	19326,1	61,60		12	12	30	30
Palaeocystodinium golzowense	LAD	18907,8	18907,8	59,17		11	11	31	31
Palaeocystodinium spp.	LAD	18151,2	18151,2	56,10		2	2	0	0
Palaeosantalaceaepites cingulatus	LAD	1945,5	1945,5	3,72		2	7	0	270
Palaeosantalaceaepites cingulatus	FAD	3905,4	3905,4	12,08		2	2	37	37
Perfotricolpites digitatus	LAD	924,7	924,7	1,26		37	79	331	331
Perfotricolpites digitatus	FAD	17454,6	17454,6	49,62		9	11	310	310
Periretisyncolpites giganteus	LAD	19179,6	19179,6	60,50		13	13	21	21
Periretisyncolpites magnosagenatus	LAD	18178,0	18178,0	56,21		6	6	39	39
Periretisyncolpites magnosagenatus	FAD	19403,8	19403,8	62,19		2	2	11	11
Perisyncolporites pokornyi	LAD	174,2	174,2	0,24		43	79	337	337
Perisyncolporites pokornyi	FAD	17038,0	17038,0	44,83		9	9	299	299
Petm dc13spike	LAD	17941,7	17941,7	55,63		1	1	incierto	incierto
Petm dc13spike	FAD	18077,2	18077,2	55,80		49	49	386	386
Phelodinium tricuspe	LAD	19755,7	19755,7	64,85		2	2	3	3
Poloretitricolpites absolutus	LAD	16383,0	16383,0	37,45		4	4	41	41
Poloretitricolpites absolutus	FAD	18441,7	18441,7	57,28		2	2	37	37
Polotricolporites versabilis	LAD	16287,1	16287,1	36,37		4	4	17	17
Polotricolporites versabilis	FAD	17594,9	17594,9	51,35		2	2	9	9
Polypodiaceoisporites pseudopsilatus	LAD	143,5	143,5	0,19		6	13	281	281
Polypodiaceoisporites pseudopsilatus	FAD	14176,4	14176,4	22,83		4	4	242	242
Polypodiaceoisporites? fossulatus	LAD	4157,0	4157,0	13,17		9	14	312	312
Polypodiaceoisporites? fossulatus	FAD	19755,7	19755,7	64,85		5	5	24	24
Polypodiisporites aff. speciosus	LAD	1317,3	1317,3	1,79		10	10	330	330
Polypodiisporites aff. speciosus	FAD	17941,7	17941,7	55,63		4	4	22	22
Polypodiisporites echinatus	LAD	17563,8	17563,8	50,97		3	3	20	20
Polypodiisporites echinatus	FAD	18586,0	18586,0	57,86		3	3	18	18
Polypodiisporites pachyexinatus	LAD	17995,4	17995,4	55,70		5	6	5	5
Polypodiisporites pachyexinatus	FAD	18143,7	18143,7	56,07		2	2	3	3
Polypodiisporites sp.	LAD	61,5	61,5	0,08		2	2	0	0
Polysphaeridium subtile	LAD	817,3	817,3	1,11		11	11	318	318
Polysphaeridium subtile	FAD	16867,7	16867,7	42,92		4	4	153	153
Proteacidites dehaani	LAD	19732,2	19732,2	64,67		13	13	36	36
Proteacidites triangulatus	LAD	1878,1	1878,1	3,41		16	28	289	289
Proteacidites triangulatus	FAD	14548,2	14548,2	24,13		4	4	252	252
Proxapertites cursus	LAD	16711,0	16711,0	41,15		25	27	62	62
Proxapertites cursus	FAD	19788,1	19788,1	65,09		9	9	25	25
Proxapertites humbertoides	LAD	1880,9	1880,9	3,42		30	30	366	366
Proxapertites magnus	LAD	16267,2	16267,2	36,15		15	16	68	68
Proxapertites magnus	FAD	19148,7	19148,7	60,26		8	8	57	57
Proxapertites minutihumbertoides	LAD	17810,0	17810,0	54,00		4	5	7	7
Proxapertites minutihumbertoides	FAD	18143,6	18143,6	56,07		1	1	incierto	incierto
Proxapertites operculatus	LAD	817,3	817,3	1,11		43	53	380	380
Proxapertites sulcatus	LAD	19007,0	19007,0	59,57		4	4	17	17
Proxapertites tertiaria	LAD	563,6	563,6	0,77		31	49	386	386
Proxapertites verrucatus	LAD	18047,9	18047,9	55,76		14	14	37	37
Pseudostephanocolpites perfectus	LAD	15999,2	15858,1	33,46	32,55	15	28	26	29
Pseudostephanocolpites perfectus	FAD	17538,9	17538,9	50,66		6	8	25	25
Psilabrevitricolporites simpliformis	LAD	17995,0	17995,0	55,70		12	12	29	29
Psilabrevitricolporites simpliformis	FAD	19546,9	19546,9	63,27		5	5	21	21

Annex 1.3 (continuation)

Psilabrevitricolporites triangularis	LAD	1021,2	1021,2	1,39		35	73	333	333
Psilabrevitricolporites triangularis	FAD	17701,1	17701,1	52,66		8	8	314	314
Psilamonocolpites operculatus	LAD	18042,2	18042,2	55,76		8	10	36	36
Psilaperiporites "intensus"	LAD	6309,8	6309,8	16,50		7	15	203	203
Psilaperiporites "intensus"	FAD	15786,0	15786,0	32,09		2	2	14	14
Psilaperiporites minimus	LAD	420,1	420,1	0,57		13	19	326	
Psilaperiporites minimus	FAD	16849,4	16849,4	42,71		4	4	297	297
Psilaperiporites robustus	LAD	14424,2	14424,2	23,33		10	15	42	42
Psilastephanocolpites verrucosus	LAD	15836,0	15836,0	32,41		9	9	47	47
Psilastephanocolpites verrucosus	FAD	17513,2	17513,2	50,34		2	2	13	13
Psilastephanocolporites fissilis	LAD	1962,4	1962,4	4,32		28	55	327	327
Psilastephanocolporites fissilis	FAD	18404,3	18404,3	57,13		7	9	198	198
Psilastephanoporites herngreenii	LAD	3852,0	3852,0	11,79		15	31	253	253
Psilastephanoporites herngreenii	FAD	9129,3	9129,3	17,75		1	1	incierto	incierto
Psilastephanoporites tesseroporus	LAD	2045,2	2045,2	5,48		2	2	40	40
Psilastephanoporites tesseroporus	FAD	4363,2	4363,2	13,99		2	2	46	46
Psilatricolporites caribbiensis	FAD	3591,7	3591,7	10,36		1	1	incierto	incierto
Psilatricolporites caribbiensis	LAD	3591,7	3591,7	10,36		3	3	26	26
Psilatricolporites costatus	LAD	744,6	744,6	1,01		29	54	333	333
Psilatricolporites costatus	FAD	17372,7	17372,7	48,61		6	6	306	306
Psilatricolporites devriesi	LAD	1471,1	1471,1	2,22		8	18	182	285
Psilatricolporites devriesi	FAD	10181,6	11722,4	18,81	20,36	3	3	174	174
Psilatricolporites pachydermatus	LAD	1878,1	1878,1	3,41		10	30	292	292
Psilatricolporites pachydermatus	FAD	15521,1	16022,8	30,38	33,61	4	7	273	290
Racemonocolpites facilis	LAD	16278,5	16143,4	36,27	34,75	13	13	67	67
Racemonocolpites facilis	FAD	19755,3	19755,3	64,85		5	5	70	70
Racemonocolpites racematus	LAD	16414,3	16414,3	37,80		19	19	71	71
Ranunculacidites operculatus	LAD	892,2	892,2	1,21		34	59	330	330
Ranunculacidites operculatus	FAD	16685,0	16685,0	40,86		6	6	293	293
Retibrevicolpites yavarensis	LAD	3995,4	3995,4	12,52		6	8	218	218
Retibrevicolpites yavarensis	FAD	15549,9	15549,9	30,57		1	1	incierto	incierto
Retibrevitricolpites retibolus	LAD	1975,1	1975,1	4,77		15	15	360	360
Retibrevitricolpites triangulatus	LAD	15794,0	15717,9	32,14	31,65	14	15	87	87
Retibrevitricolpites triangulatus	FAD	17589,3	17589,3	51,28		4	4	17	17
Retibrevitricolporites grandis	LAD	14476,3	14476,3	23,67		13	35	51	51
Retibrevitricolporites grandis	FAD	17708,6	17708,6	52,75		5	6	26	26
Retibrevitricolporites speciosus	LAD	16609,9	16394,6	40,01	37,58	4	10	22	24
Retibrevitricolporites speciosus	FAD	17589,0	17589,0	51,28		2	2	13	13
Retidiporites elongatus	LAD	18058,0	18058,0	55,78		9	9	44	44
Retidiporites magdalenensis	LAD	18010,7	18010,7	55,72		32	33	55	55
Retimonocolpites retifossulatus	LAD	1471,8	1471,8	2,22		23	23	369	369
Retipollenites crotonicolumellatus	LAD	1926,9	1926,9	3,56		2	2	45	45
Retipollenites crotonicolumellatus	FAD	4352,1	4352,1	13,94		11	11	325	325
Retistephanocolpites angeli	LAD	16120,8	16120,8	34,50		10	12	56	56
Retistephanocolpites angeli	FAD	18900,4	18863,5	59,14		5	5	27	27
Retistephanocolpites williamsi	FAD	17625,2	17625,2	51,72		1	1	incierto	incierto
Retistephanocolpites williamsi	LAD	17625,2	17625,2	51,72		1	1	incierto	incierto
Retistephanocolporites festivus	LAD	16002,9	16002,9	33,48		17	26	32	32
Retistephanocolporites festivus	FAD	17608,2	17608,2	51,51		6	6	26	26
Retistephanoporites angelicus	LAD	14377,1	14377,1	23,03		12	13	57	57
Retistephanoporites angelicus	FAD	16867,7	16867,7	42,92		3	3	11	11
Retistephanoporites crassiannulatus	LAD	1474,1	1474,1	2,23		17	42	301	301
Retistephanoporites crassiannulatus	FAD	16711,0	16711,0	41,15		4	4	232	232
Retistephanoporites minutiporus	LAD	8769,1	8769,1	17,46		33	74	177	177
Retistephanoporites minutiporus	FAD	17606,1	17606,1	51,49		6	6	58	58

Annex 1.3 (continuation)

Retisyncolporites angularis	LAD	16068,0	16068,0	33,90		6	10	16	16
Retisyncolporites angularis	FAD	16867,7	16867,7	42,92		2	2	0	0
Retisyncolporites aureus	LAD	16639,5	16639,5	40,34		2	2	2	2
Retisyncolporites aureus	FAD	16794,4	16794,4	42,09		1	1	incierto	incierto
Retitrescolpites baculatus	LAD	15896,5	15708,2	32,80	31,59	8	17	31	35
Retitrescolpites baculatus	FAD	18586,0	18586,0	57,86		4	5	54	54
Retitrescolpites magnus	LAD	15604,0	14653,9	30,92	24,81	16	32	31	50
Retitrescolpites magnus	FAD	17497,0	17497,0	50,14		5	7	30	30
Retitrescolpites peculiaris	LAD	18143,0	18143,0	56,07		1	1	incierto	incierto
Retitrescolpites peculiaris	FAD	18751,3	18751,3	58,53		1	1	incierto	incierto
Retitrescolpites saturum	LAD	8440,8	8440,8	17,33		12	16	194	194
Retitrescolpites saturum	FAD	18595,5	18595,5	57,90		6	7	51	51
Retitrescolpites? irregularis	LAD	563,6	563,6	0,77		43	100	336	336
Retitrescolpites? irregularis	FAD	17589,3	17589,3	51,28		12	47	310	310
Retitricolpites "cacerolensis"	LAD	5692,8	5692,8	16,26		3	3	215	215
Retitricolpites "finitus"	LAD	194,7	194,7	0,26		4	4	276	276
Retitricolpites "finitus"	FAD	15878,6	15878,6	32,68		10	10	122	122
Retitricolpites lorentae	LAD	1330,7	1330,7	1,81		4	10	262	260
Retitricolpites maturus	LAD	14727,9	14727,9	25,29		4	4	45	45
Retitricolpites maturus	FAD	17594,9	17594,9	51,35		2	2	12	12
Retitricolpites simplex	LAD	543,1	543,1	0,74		43	85	351	351
Retitricolpites simplex	FAD	18077,2	18302,4	55,80	57,13	8	8	320	320
Retitricolpites wijningae	LAD	4082,5	4082,5	12,87		2	3	207	207
Retitricolporites "beccus"	LAD	817,3	817,3	1,11		2	2	25	25
Retitricolporites "beccus"	FAD	5822,5	5822,5	16,31		2	2	75	75
Retitricolporites "fragilis"	LAD	2699,0	2699,0	7,22		1	1	incierto	incierto
Retitricolporites "fragilis"	FAD	3963,8	3963,8	12,40		1	1	incierto	incierto
Retitricolporites "heterobrochatus"	LAD	2870,0	2870,0	7,53		1	1	incierto	incierto
Retitricolporites "heterobrochatus"	FAD	4647,0	4647,0	14,94		1	1	incierto	incierto
Retitriletes sommeri	LAD	604,6	604,6	0,82		12	34	310	310
Retitriletes sommeri	FAD	15729,8	15729,8	31,73		4	4	273	273
Retitriporites dubiosus	LAD	4258,1	4258,1	13,57		12	12	261	261
Retitriporites dubiosus	FAD	17604,9	17604,9	51,47		3	3	267	267
Retitriporites poricostatus	LAD	16455,7	16455,7	38,27		2	2	1	1
Retitriporites poricostatus	FAD	17458,6	17458,6	49,67		2	2	14	14
Rhoipites "gigantiporus"	LAD	1975,1	1975,1	4,77		2	2	17	17
Rhoipites "gigantiporus"	FAD	4647,0	4647,0	14,94		2	2	53	53
Rhoipites cienaguensis	LAD	8440,8	5556,5	17,33	16,21	3	3	162	162
Rhoipites cienaguensis	FAD	16711,0	16711,0	41,15		2	2	35	35
Rhoipites guianensis	LAD	1317,3	1317,3	1,79		45	84	321	321
Rhoipites guianensis	FAD	16849,7	16849,7	42,71		8	8	297	297
Rhoipites guianensis "perbonus"	LAD	11136,0	11136,0	19,77		1	1	incierto	incierto
Rhoipites guianensis "perbonus"	FAD	16849,0	16849,0	42,70		2	2	2	2
Rhoipites hispidus	LAD	1471,5	1471,5	2,22		35	61	327	327
Rhoipites hispidus	FAD	18077,2	18077,2	55,80		8	8	321	321
Rhoipites planipolaris	LAD	4126,0	4126,0	13,04		10	42	239	239
Rhoipites planipolaris	FAD	15694,0	15694,0	31,50		2	3	103	103
Rugotricolpites intensus	LAD	8404,4	5244,9	17,31	16,09	3	7	35	35
Rugotricolpites intensus	FAD	10861,9	10861,9	19,49		2	2	2	2
Rugotricolporites felix	LAD	16414,3	16414,3	37,80		3	3	12	12
Rugotricolporites felix	FAD	17038,0	17038,0	44,83		2	2	6	6
S. spiralis acme upper Mirador	LAD	16730,2	16730,2	41,36		2	2	2	2
S. spiralis acme upper Mirador	FAD	16847,7	16847,7	42,69		23	23	34	34
Scabraperiporites asymmetricus	LAD	4088,0	4088,0	12,89		2	2	235	235
Scabratricolporites planetensis	LAD	1351,1	1351,1	1,87		11	36	281	281

Annex 1.3 (continuation)

Scabratricolporites planetensis	FAD	15759,5	15759,5	31,92		2	2	13	13
Scabratriletes granularis	LAD	19842,0	19842,0	65,50		6	7	12	12
Selenopemphix nephroides	LAD	2522,1	2522,1	6,89		2	3	95	95
Selenopemphix nephroides	FAD	9212,8	9212,8	17,83		1	1	incierto	incierto
Selenopemphix selenoides	FAD	3950,2	3950,2	12,32		1	1	incierto	incierto
Selenopemphix selenoides	LAD	3950,2	3950,2	12,32		3	3	95	95
Senegalinim laevigatum	LAD	19722,8	19722,8	64,60		11	11	25	25
Senegalinium bicavatum	LAD	19813,1	19813,1	65,28		17	17	31	31
Senegalinium obscurum	LAD	19860,8	19860,8	65,80		3	3	12	12
Senegalinium spp.	LAD	19739,1	19739,1	64,72		5	5	364	364
Siltaria mariposa	LAD	16426,5	16426,5	37,94		5	5	28	28
Siltaria mariposa	FAD	18077,2	18077,2	55,80		4	4	17	17
Spathiphyllum vanegensis	LAD	17817,3	17817,3	54,09		19	19	42	42
Spinizonocolpites baculatus	LAD	19360,7	19360,7	61,87		23	23	16	16
Spinizonocolpites breviechinatus	LAD	16455,7	16455,7	38,27		4	4	34	34
Spinizonocolpites breviechinatus	FAD	19028,5	19028,5	59,65		3	3	3	3
Spinizonocolpites echinatus	LAD	15745,6	15745,6	31,83		22	24	85	85
Spinizonocolpites grandis	LAD	16426,0	16384,8	37,94	37,47	10	20	7	7
Spinizonocolpites grandis	FAD	17513,2	17513,2	50,34		4	6	22	22
Spinizonocolpites pachyexinatus	LAD	16455,7	16455,7	38,27		3	3	68	68
Spinizonocolpites pachyexinatus	FAD	19853,0	19853,0	65,68		3	3	43	43
Spirosyncolpites spiralis	LAD	1471,1	1471,1	2,22		47	89	327	327
Spirosyncolpites spiralis	FAD	17940,3	17940,3	55,61		11	2	319	319
Stephanocolpites costatus	LAD	19023,0	19023,0	59,63		9	9	19	19
Stephanocolpites evansii	LAD	2297,4	2297,4	6,26		1	1	incierto	incierto
Stephanocolpites evansii	FAD	3591,7	3591,7	10,36		1	1	incierto	incierto
Striatopollis catatumbus	LAD	789,0	789,0	1,07		37	44	351	351
Striatopollis catatumbus	FAD	17708,7	17708,7	52,75		9	9	315	315
Striatopollis? tenuistriatus	LAD	866,4	866,4	1,18		20	46	323	323
Striatopollis? tenuistriatus	FAD	18317,6	18317,6	56,77		6	7	273	272
Striatricolporites "poloreticulatus"	LAD	1874,4	1874,4	3,40		2	2	8	8
Striatricolporites "poloreticulatus"	FAD	4647,0	4647,0	14,94		2	2	54	54
Striatricolporites digitatus	LAD	15816,3	15816,3	32,28		3	3	47	47
Striatricolporites digitatus	FAD	18895,7	18895,7	59,12		3	3	26	26
Striatriletes saccolomicites	LAD	563,6	563,6	0,77		22	29	321	321
Striatriletes saccolomicites	FAD	16169,7	16169,7	35,05		5	6	240	240
Syncolporites lisamae	LAD	18026,7	18026,7	55,74		8	8	36	36
Syncolporites marginatus	LAD	16087,1	16087,1	34,12		10	10	77	77
Syncolporites poricostatus	LAD	3187,1	3187,1	8,15		5	5	337	337
Syndemicolpites typicus	LAD	19421,1	19421,1	62,32		11	11	9	9
Tercissus sp.	LAD	19657,3	19657,3	64,11		4	4	8	8
Tetracolporites pachyexinatus	LAD	16594,8	16594,8	39,84		2	2	5	5
Tetracolporites pachyexinatus	FAD	17593,9	17593,9	51,34		2	2	17	17
Tetracolporopollenites maculosus	LAD	1351,1	1351,1	1,87		31	53	313	313
Tetracolporopollenites maculosus	FAD	17625,2	17625,2	51,72		9	10	172	172
Tetracolporopollenites spongiosus	LAD	17413,8	17413,8	49,12		5	5	19	19
Tetracolporopollenites spongiosus	FAD	19129,5	19129,5	60,12		4	4	24	24
Tetracolporopollenites transversalis	LAD	727,5	727,5	0,99		42	81	342	342
Tetracolporopollenites transversalis	FAD	18249,3	18249,3	56,50		11	11	326	326
Tetradites umirensis	LAD	18182,7	18182,7	56,23		12	12	34	34
Trichotomosulcites "psilatus"	LAD	1962,4	1962,4	4,32		2	2	2	2
Trichotomosulcites "psilatus"	FAD	5243,3	5243,3	16,09		2	2	63	63
Tricolpites antonii	LAD	6585,6	6585,6	16,61		7	7	243	243
Tricolpites antonii	FAD	18799,1	18799,1	58,73		4	4	41	41
Tricolpites clarensis	LAD	275,3	275,3	0,37		12	12	348	348

Annex 1.3 (continuation)

Tricolpites clarensis	FAD	17625,1	17625,1	51,72		4	4	33	33
Tricolpites protoclarensis	LAD	18143,0	18143,0	56,07		3	3	8	8
Tricolpites protoclarensis	FAD	19095,1	19095,1	59,92		3	3	12	12
Trithyrodinium spp.	LAD	19380,5	19380,5	62,01		8	8	21	21
Tuberculodinium vancampoae	LAD	1894,3	1894,3	3,46		6	8	275	275
Tuberculodinium vancampoae	FAD	9411,4	9411,4	18,03		2	2	18	18
Tuberositriletes verrucatus	LAD	3655,3	3655,3	10,71		5	5	283	283
Tuberositriletes verrucatus	FAD	17817,3	17817,3	54,09		4	4	283	283
Ulmoideipites krempii	LAD	15976,8	15976,8	33,31		27	28	78	78
Venezuelites globoannulatus	LAD	15784,4	15784,4	32,08		2	2	6	6
Venezuelites? distinctus	LAD	14429,1	13515,5	23,36	22,16	6	16	49	67
Venezuelites? distinctus	FAD	16867,7	16867,7	42,92		2	3	5	5
Verrucatosporites usmensis	LAD	61,5	61,5	0,08		39	65	349	349
Verrucatosporites usmensis	FAD	16304,6	16304,6	36,57		6	6	284	284
Verrucatotriletes etayoi	LAD	3962,0	2426,5	12,39	6,66	15	27	241	241
Verrucatotriletes etayoi	FAD	16073,3	16073,3	33,96		4	4	233	233
Verrustephanocolpites rugulatus	LAD	10775,9	10775,9	19,40		4	7	171	171
Verrustephanocolpites rugulatus	FAD	17458,0	17458,0	49,66		1	1	incierto	incierto
Verrutricolporites reticulatus	LAD	16024,1	15927,0	33,62	32,99	7	17	19	34
Verrutricolporites reticulatus	FAD	17625,1	17625,1	51,72		4	4	24	24
Verrutricolporites rotundiporus	LAD	1317,3	1317,3	1,79		11	14	274	274
Verrutricolporites rotundiporus	FAD	14964,0	14964,0	26,80		3	3	270	270
Verrutriletes "magnoviruelensis"	LAD	789,0	789,0	1,07		29	29	387	387
Verrutriletes virueloides	LAD	789,0	789,0	1,07		11	11	18	18
Wilsonipites margocolpatus	LAD	15010,5	15010,5	27,10		4	6	51	51
Wilsonipites margocolpatus	FAD	17563,8	17563,8	50,97		2	2	34	34
Yolkinigymnium lanceolatum	LAD	19855,5	19855,5	65,71		5	5	8	8
Zlivisporis blanensis	LAD	19321,6	19321,6	61,57		17	17	31	31
Zonocostites minor	LAD	16528,2	16339,5	39,09	36,96	2	2	21	21
Zonocostites minor	FAD	17584,3	17584,3	51,22		2	2	19	19
Zonocostites ramonae	LAD	817,3	817,3	1,11		27	27	331	331
Zonocostites ramonae	FAD	17372,7	17372,7	48,61		5	5	308	308
Zonotricolpites variabilis	LAD	19013,8	19013,8	59,60		11	11	18	18

Annex 1.3 (continuation)

Category 2. New informal Taxa									
Taxon	Event	Composite Units		Age (my)		Number of Sites		Spreading Parameter	
		Jaramillo et al. 2011	this work	Jaramillo et al. 2011	this Work	Jaramillo et al. 2011	this work	Jaramillo et al. 2011	this work
Bombacacidites "concavoides"	LAD		10964,90		19,59		5		99
Bombacacidites "gemmatus"	LAD		16259,81		36,06		1		incierto
Bombacacidites "pulcherrimus"	LAD		15745,01		31,82		1		incierto
Bombacacidites "verrucatus"	LAD		14547,37		24,13		1		incierto
Brevitricolporites "uwaeorum"	FAD		17038,03		44,84		2		21
Brevitricolporites "uwaeorum"	LAD		14132,47		22,78		21		46
Chomotriletes "zenueorum"	LAD		9572,35		18,19		3		132
Cingulatisporites "lorentae"	LAD		420,12		0,57		2		33
Clavainaperturites" grimsdaleoides"	LAD		14171,90		22,82		3		81
Clavatriporites "spicatus"	LAD		16113,50		34,41		3		11
Concavissimisporites "rugulatus"	LAD		13967,14		22,62		1		incierto
Crassosporites "baculatus"	FAD		3537,05		10,06		2		30
Crassosporites "baculatus"	LAD		102,47		0,14		4		311
Echiperiporites "magnoexinatus"	LAD		3884,61		11,97		1		incierto
Echiperiporites "psilatus"	FAD		5021,10		16,00		2		116
Echiperiporites "psilatus"	LAD		4126,00		13,04		7		207
Echipollenites "magnificus"	LAD		10093,78		18,72		1		incierto
Echitricolporites "clipeoechinatus"	LAD		5511,76		16,19		1		incierto
Fossulotriletes "hermosus"	LAD		4314,63		13,79		1		incierto
Gemmaperprolatoporis "teresitae"	LAD		16151,97		34,85		5		10
Hexaporotricolpites "striatus"	LAD		14510,01		23,89		2		8
Kuylisporites? "bicostatus"	LAD		563,57		0,77		1		incierto
Liliacidites "titanicus"	LAD		3600,85		10,41		1		incierto
Polypodiaceoisporites "interruptus"	LAD		892,19		1,21		1		incierto
Polypodiaceoisporites "murilloi"	LAD		917,98		1,25		1		incierto
Polypodiaceoisporites "verrucatus"	LAD		758,26		1,03		11		279
Polypodiaceoisporites" projectoradialis"	LAD		943,78		1,28		1		incierto
Psilabrevitricolporites "hoornii"	LAD		15727,24		31,71		1		incierto
Psiladiporites "ecopetrolis"	LAD		866,39		1,18		1		incierto
Retistephanocolpites "araucaensis"	LAD		16426,51		37,94		2		40
Retistephanoporites "yariguiensis"	LAD		6979,18		16,76		1		incierto
Retitricolporites "magnificus"	FAD		16549,16		39,32		1		incierto
Retitricolporites "magnificus"	LAD		16383,04		37,45		3		4
Retitricolporites "magnoguianensis"	LAD		8404,38		17,31		5		136
Rugutricolporites "etayoi"	LAD		2930,65		7,64		1		incierto
Scabratriletes "bacataensis"	LAD		543,08		0,74		1		incierto
Tetracolpites "quadrangularis"	LAD		18005,23		55,71		1		incierto
Trichotomosulcites "clavatus"	LAD		2063,02		5,53		5		39
Trichotomosulcites "clavatus"	FAD		4243,60		13,51		2		6
Trichotomosulcites "scabrata"	LAD		4038,90		12,70		2		197
Verrustephanocolporites "pastinensis"	LAD		15189,65		28,25		1		incierto
Verrutriletes "ampullatus"	LAD		256,17		0,35		1		incierto
Zlivisporis "gibraltarensis"	LAD		8439,90		17,33		10		210

Annex 1.3 (continuation)

Category.3 New Formal Species									
Taxon	**Event**	**Composite Units**		**Age (my)**		**Number of Sites**		**Spreading Parameter**	
		Jaramillo et al. 2011	**this work**	**Jaramillo et al. 2011**	**this Work**	**Jaramillo et al. 2011**	**this work**	**Jaramillo et al. 2011**	**this work**
Bombacacaidtes araracuarensis	LAD		1471,5		2,22		7		131
Bombacacaidtes araracuarensis	FAD		8663,1		17,41		1		incierto
Cingulatisporites laevigatus	LAD		102,5		0,14		4		90
Ctenolophonidites suigeneris	FAD		16805,6		42,21		1		incierto
Ctenolophonidites suigeneris	LAD		6548,2		16,59		19		205
Margocolporites fastigiatus	LAD		204,9		0,28		1		incierto
Polypodiisporites amazonensis	LAD		71,7		0,10		7		246
Polypodiisporites planus	LAD		1878,1		3,41		10		272
Psilastephanocolporites brevicolpatus	LAD		16346,9		37,04		5		8
Psilastephanocolporites brevicolpatus	FAD		16849,7		42,71		2		5
Psilatriletes peruanus	LAD		2661,0		7,15		6		259
Psilatriletes peruanus	FAD		4148,4		13,13		1		incierto
Psilatricolporites venezuelanus	LAD		4114,9		13,00		14		239
Pteridaceoisporis gemmatus	LAD		174,2		0,24		8		304
Retitricolpites caquetanus	LAD		3973,6		12,44		17		154

Annex 1.4. List of biostratigraphic events, composite units (CU), age in million of years (Ma), number of sites, spreading parameter (SP) and biozone (Jaramillo et al., 2011) (TC: Top Cretaceous).

Taxa	Event	Composite Units	Age (Ma)	#Sites	Spreading Paramater	Zone
Foveotriletes ornatus	LAD	61,5	0,08	25	289	T18
Polypodiisporites sp.	LAD	61,5	0,08	2	0	
Verrucatosporites usmensis	LAD	61,5	0,08	65	349	
Monoporopollenites annulatus	LAD	71,7	0,10	85	382	
Polypodiisporites amazonensis (xx)	LAD	71,7	0,10	7	246	
Cyatheacidites annulatus	LAD	82,0	0,11	9	286	
Crassosporites "baculatus" (x)	LAD	102,47	0,14	4	311	
Cingulatisporites laevigatus (xx)	LAD	102,5	0,14	4	90	
Clavainaperturites microclavatus	LAD	102,5	0,14	34	320	
Echiperiporites akanthos	LAD	102,5	0,14	70	347	
Echitricolporites spinosus	LAD	102,5	0,14	12	171	
Corsinipollenites sp.	LAD	112,7	0,15	83	381	
Polypodiaceoisporites pseudopsilatus	LAD	143,5	0,19	13	281	
Fenestrites spinosus	LAD	174,2	0,24	9	83	
Magnastriatites grandiosus	LAD	174,2	0,24	69	326	
Perisyncolporites pokornyi	LAD	174,2	0,24	79	337	
Pteridaceoisporis gemmatus (xx)	LAD	174,2	0,24	8	304	
Retitricolpites "finitus"	LAD	194,7	0,26	4	276	
Bombacacidites brevis	LAD	204,9	0,28	79	352	
Margocolporites fastigiatus (xx)	LAD	204,9	0,28	1	incierto	
Catostemma type	LAD	215,2	0,29	62	325	
Verrutriletes "ampullatus" (x)	LAD	256,17	0,35	1	incierto	
Tricolpites clarensis	LAD	275,3	0,37	12	348	
Mauritiidites franciscoi franciscoi	LAD	286,8	0,39	96	391	
Mauritiidites franciscoi minutus	LAD	286,9	0,39	57	388	
Crassiectoapertites columbianus	LAD	316,9	0,43	58	323	
Psilaperiporites minimus	LAD	420,1	0,57	19		
Cingulatisporites "lorentae" (x)	LAD	420,12	0,57	2	33	
Scabratriletes "bacataensis" (x)	LAD	543,08	0,74	1	incierto	
Retitricolpites simplex	LAD	543,1	0,74	85	351	
Kuylisporites? "bicostatus" (x)	LAD	563,57	0,77	1	incierto	
Proxapertites tertiaria	LAD	563,6	0,77	49	386	
Retitrescolpites? irregularis	LAD	563,6	0,77			
Striatriletes saccolomicites	LAD	563,6	0,77	29	321	
Echitricolporites mcneillyi	LAD	573,8	0,78	2	162	
Retitriletes sommeri	LAD	604,6	0,82	34	310	
Echitricolporites maristellae	LAD	651,9	0,89	38	277	
Bombacacidites muinaneorum	LAD	717,3	0,97	25	292	
Laevigatosporites granulatus	LAD	727,5	0,99	58	349	
Tetracolporopollenites transversalis	LAD	727,5	0,99	81	342	
Psilatricolporites costatus	LAD	744,6	1,01	54	333	
Polypodiaceoisporites "verrucatus" (x)	LAD	758,26	1,03	11	279	
Nijssenosporites fossulatus	LAD	758,3	1,03	22	267	
Multimarginites vanderhammenii	LAD	789,0	1,07	23	136	
Striatopollis catatumbus	LAD	789,0	1,07	44	351	
Verrutriletes "magnoviruelensis"	LAD	789,0	1,07	29	387	
Verrutriletes virueloides	LAD	789,0	1,07	11	18	
Bombacacidites baculatus	LAD	817,3	1,11	26	129	
Echitriletes muelleri	LAD	817,3	1,11	33	381	

Annex 1.4 (continuation)

Taxa	Event	Composite Units	Age (Ma)	#Sites	Spreading Paramater	Zone
Polysphaeridium subtile	LAD	817,3	1,11	11	318	
Proxapertites operculatus	LAD	817,3	1,11	53	380	
Retitricolporites "beccus"	LAD	817,3	1,11	2	25	
Zonocostites ramonae	LAD	817,3	1,11	27	331	
Psiladiporites "ecopetrolis" (x)	LAD	866,39	1,18	1	incierto	
Fenestrites longispinosus	LAD	866,4	1,18	4	60	
Striatopollis? tenuistriatus	LAD	866,4	1,18	46	323	
Polypodiaceoisporites "interruptus" (x)	LAD	892,19	1,21	1	incierto	
Ranunculacidites operculatus	LAD	892,2	1,21	59	330	
Polypodiaceoisporites "murilloi" (x)	LAD	917,98	1,25	1	incierto	
Perfotricolpites digitatus	LAD	924,7	1,26	79	331	
Polypodiaceoisporites" projectoradialis" (x)	LAD	943,78	1,28	1	incierto	
Psilabrevitricolporites triangularis	LAD	1021,2	1,39	73	333	
Echitricolporites mcneillyi	FAD	1150,1	1,56	1	incierto	
Echiperiporites estelae	LAD	1161,1	1,58	44	312	
Polypodiisporites aff. specious	LAD	1317,3	1,79	10	330	
Rhoipites guianensis	LAD	1317,3	1,79	84	321	
Verrutricolporites rotundiporus	LAD	1317,3	1,79	14	274	
Retitricolpites lorentae	LAD	1330,7	1,81	10	260	
Scabratricolporites planetensis	LAD	1351,1	1,87	36	281	
Tetracolporopollenites maculosus	LAD	1351,1	1,87	53	313	
Jandufouria seamrogiformis	LAD	1471,1	2,22	74	305	
Margocolporites vanwijhei	LAD	1471,1	2,22	55	323	
Psilatricolporites devriesi	LAD	1471,1	2,22	18	285	
Spirosyncolpites spiralis	LAD	1471,1	2,22	89	327	
Bombacacaidtes araracuarensis (xx)	LAD	1471,5	2,22	7	131	
Rhoipites hispidus	LAD	1471,5	2,22	61	327	
Retimonocolpites retifossulatus	LAD	1471,8	2,22	23	369	
Retistephanoporites crassiannulatus	LAD	1474,1	2,23	42	301	
Crassoretitriletes vanraadshooveni	LAD	1874,4	3,40	31	52	
Grimsdalea magnaclavata	LAD	1874,4	3,40	28	96	
Striatricolporites "poloreticulatus"	LAD	1874,4	3,40	2	8	
Polypodiisporites planus (xx)	LAD	1878,1	3,41	10	272	
Proteacidites triangulatus	LAD	1878,1	3,41	28	289	
Psilatricolporites pachydermatus	LAD	1878,1	3,41	30	292	
Proxapertites humbertoides	LAD	1880,9	3,42	30	366	
Tuberculodinium vancampoae	LAD	1894,3	3,46	8	275	
Retipollenites crotonicolumellatus	LAD	1926,9	3,56	2	45	
L. proxapertitoides reticuloides	LAD	1945,5	3,72	14	358	
Palaeosantalaceaepites cingulatus	LAD	1945,5	3,72	7	270	
Echitriporites cricotriporatiformis	LAD	1951,5	3,94	7	72	
Laevigatosporites catanejensis	LAD	1962,4	4,32	23	369	
Psilastephanocolporites fissilis	LAD	1962,4	4,32	55	327	
Trichotomosulcites "psilatus"	LAD	1962,4	4,32	2	2	
Echiperiporites scabrannulatus	LAD	1968,2	4,53	3	54	
Lanagiopollis crassa	LAD	1975,1	4,77	68	312	T17
Retibrevitricolpites retibolus	LAD	1975,1	4,77	15	360	
Rhoipites "gigantiporus"	LAD	1975,1	4,77	2	17	

Annex 1.4 (continuation)

Taxa	Event	Composite Units	Age (Ma)	#Sites	Spreading Paramater	Zone
Psilastephanoporites tesseroporus	LAD	2045,2	5,48	2	40	
Trichotomosulcites "clavatus" (x)	LAD	2063,02	5,53	5	39	
Stephanocolpites evansii	LAD	2297,4	6,26	1	incierto	
Verrucatotriletes etayoi	LAD	2426,5	6,66	27	241	
Selenopemphix nephroides	LAD	2522,1	6,89	3	95	
Psilatriletes peruanus (xx)	LAD	2661,0	7,15	6	259	
Cyatheacidites annulatus	FAD	2661,2	7,15	2	12	T16
Retitricolporites "fragilis"	LAD	2699,0	7,22	1	incierto	
Retitricolporites "heterobrochatus"	LAD	2870,0	7,53	1	incierto	
Rugutricolporites "etayoi" (x)	LAD	2930,65	7,64	1	incierto	
Syncolporites poricostatus	LAD	3187,1	8,15	5	337	
Lingulodinium machaerophorum	LAD	3502,3	9,87	5	278	
Fenestrites longispinosus	FAD	3537,0	10,06	1	incierto	
Crassosporites "baculatus" (x)	FAD	3537,05	10,06	2	30	
Psilatricolporites caribbiensis	FAD	3591,7	10,36	1	incierto	
Psilatricolporites caribbiensis	LAD	3591,7	10,36	3	26	
Stephanocolpites evansii	FAD	3591,7	10,36	1	incierto	
Liliacidites "titanicus" (x)	LAD	3600,85	10,41	1	incierto	
Tuberositriletes verrucatus	LAD	3655,3	10,71	5	283	
Bombacacidites baumfalki	LAD	3812,0	11,57	10	214	
Psilastephanoporites herngreenii	LAD	3852,0	11,79	31	253	
Mauritiidites crassibaculatus	LAD	3862,7	11,85	5	295	
Echiperiporites "magnoexinatus" (x)	LAD	3884,61	11,97	1	incierto	
Palaeosantalaceaepites cingulatus	FAD	3905,4	12,08	2	37	
Selenopemphix selenoides	FAD	3950,2	12,32	1	incierto	
Selenopemphix selenoides	LAD	3950,2	12,32	3	95	
Retitricolporites "fragilis"	FAD	3963,8	12,40	1	incierto	
Retitricolpites caquetanus (xx)	LAD	3973,6	12,44	17	154	
Retibrevicolpites yavarensis	LAD	3995,4	12,52	8	218	
M. franciscoi pachyexinatus	LAD	3995,9	12,53	82	308	
Trichotomosulcites "scabrata" (x)	LAD	4038,90	12,70	2	197	T15
Ladakhipollenites simplex	LAD	4082,0	12,87	12	281	
Loranthacitoides "magnopolaris"	LAD	4082,0	12,87	1	incierto	
Retitricolpites wijningae	LAD	4082,5	12,87	3	207	
Scabraperiporites asymmetricus	LAD	4088,0	12,89	2	235	
Crototricolpites annemariae	LAD	4093,5	12,91	5	272	
Concavissimisporites fossulatus	LAD	4098,4	12,93	37	248	
Cicatricosisporites baculatus	LAD	4104,2	12,96	6	6	
Magnaperiporites spinosus	LAD	4111,0	12,98	48	239	
Psilatricolporites venezuelanus (xx)	LAD	4114,9	13,00	14	239	
Echiperiporites "psilatus" (x)	LAD	4126,00	13,04	7	207	
Rhoipites planipolaris	LAD	4126,0	13,04	42	239	
Bombacacidites nacimientoensis	LAD	4127,8	13,05	15	290	
Psilatriletes peruanus (xx)	FAD	4148,4	13,13	1	incierto	
Polypodiaceoisporites? fossulatus	LAD	4157,0	13,17	14	312	
Operculodinium centrocarpum	LAD	4225,0	13,44	3	321	
Cicatricosisporites baculatus	FAD	4228,0	13,45	1	incierto	
Trichotomosulcites "clavatus" (x)	FAD	4243,60	13,51	2	6	

Annex 1.4 (continuation)

Taxa	Event	Composite Units	Age (Ma)	#Sites	Spreading Paramater	Zone
Retitriporites dubiosus	LAD	4258,1	13,57	12	261	
Fossulotriletes "hermosus" (x)	LAD	4314,63	13,79	1	incierto	
Retipollenites crotonicolumellatus	FAD	4352,1	13,94	11	325	
Psilastephanoporites tesseroporus	FAD	4363,2	13,99	2	46	
Echitriletes "acanthotriletoides"	LAD	4385,3	14,07	3	202	
Fenestrites spinosus	FAD	4392,4	14,10	3	39	
Jandufouria minor	LAD	4399,6	14,13	32	245	
Loranthacitoides "magnopolaris"	FAD	4399,6	14,13	1	incierto	
Crassoretitriletes vanraadshooveni	FAD	4411,3	14,18	4	51	T14
Retitricolporites "heterobrochatus"	FAD	4647,0	14,94	1	incierto	
Rhoipites "gigantiporus"	FAD	4647,0	14,94	2	53	
Striatricolporites "poloreticulatus"	FAD	4647,0	14,94	2	54	
Echiperiporites scabrannulatus	FAD	4908,5	15,69	2	57	
Echiperiporites "psilatus" (x)	FAD	5021,10	16,00	2	116	
Multimarginites vanderhammenii	FAD	5021,1	16,00	3	59	
Trichotomosulcites "psilatus"	FAD	5243,3	16,09	2	63	
Grimsdalea magnaclavata	FAD	5243,4	16,09	3	65	T13
Rugotricolpites intensus	LAD	5244,9	16,09	7	35	
Echitricolporites "clipeoechinatus" (x)	LAD	5511,76	16,19	1	incierto	
Bombacacidites zuatensis	LAD	5518,6	16,19	8	124	
Rhoipites cienaguensis	LAD	5556,5	16,21	3	162	
Retitricolpites "cacerolensis"	LAD	5692,8	16,26	3	215	
Retitricolporites "beccus"	FAD	5822,5	16,31	2	75	
Echinatisporis brevispinosus	LAD	5984,7	16,38	5	233	
Psilaperiporites "intensus"	LAD	6309,8	16,50	15	203	
Ctenolophonidites suigeneris (xx)	LAD	6548,2	16,59	19	205	
Tricolpites antonii	LAD	6585,6	16,61	7	243	
Horniella lunarensis	LAD	6800,1	16,69	43	227	
Cyclusphaera scabrata	LAD	6826,6	16,70	79	210	
Retistephanoporites "yariguiensis" (x)	LAD	6979,18	16,76	1	incierto	
dinocyst acme C2	LAD	7122,3	16,82	22	39	
Echitriporites cricotriporatiformis	FAD	7176,7	16,84	3	105	
Adnatosphaeridium multispinosum	LAD	8170,4	17,22	3	173	
Retitricolporites "magnoguianensis" (x)	LAD	8404,38	17,31	5	136	
Zlivisporis "gibraltarensis" (x)	LAD	8439,90	17,33	10	210	
Corsinipollenites psilatus	LAD	8440,8	17,33	13	239	
Retitrescolpites saturum	LAD	8440,8	17,33	16	194	
Bombacacidites baculatus	FAD	8492,0	17,35	8	129	
Hystrichosphaeropsis obscura	LAD	8606,6	17,39	1	incierto	
Bombacacaidtes araracuarensis (xx)	FAD	8663,1	17,41	1	incierto	
Echitricolporites spinosus	FAD	8663,7	17,41	4	132	
Retistephanoporites minutiporus	LAD	8769,1	17,46	74	177	
Cribroperidinium tenuitabulatum	LAD	8828,0	17,48	4	20	
Echitricolporites maristellae	FAD	9091,9	17,71	4	140	T12
Psilastephanoporites herngreenii	FAD	9129,3	17,75	1	incierto	
Selenopemphix nephroides	FAD	9212,8	17,83	1	incierto	
Cribroperidinium spp.	LAD	9391,7	18,01	7	203	
Tuberculodinium vancampoae	FAD	9411,4	18,03	2	18	

Annex 1.4 (continuation)

Taxa	Event	Composite Units	Age (Ma)	#Sites	Spreading Paramater	Zone
Chomotriletes "zenueorum" (x)	LAD	9572,35	18,19	3	132	
Foveotricolporites etayoi	LAD	9572,4	18,19	59	132	
dinocyst acme C2	FAD	9841,4	18,46	1	incierto	
Echipollenites "magnificus" (x)	LAD	10093,78	18,72	1	incierto	
Nijssenosporites fossulatus	FAD	10419,3	19,05	3	115	
Clavatricolpites densiclavatus	LAD	10548,9	19,18	35	160	
Bombacacidites zuatensis	FAD	10647,3	19,27	1	incierto	
Verrustephanocolpites rugulatus	LAD	10775,9	19,40	7	171	
Rugotricolpites intensus	FAD	10861,9	19,49	2	2	
Bombacacidites "concavoides" (x)	LAD	10964,90	19,59	5	99	
Rhoipites guianensis "perbonus"	LAD	11136,0	19,77	1	incierto	
Bombacacidites gonzalezii	LAD	11137,8	19,77	17	128	
Clavainaperturites microclavatus	FAD	11226,7	19,86	4	183	
Foveotricolporites rugulatus	LAD	11669,6	20,30	22	13	
Psilatricolporites devriesi	FAD	11722,4	20,36	3	174	
Cricotriporites macroporus	LAD	12096,5	20,73	5	112	
Venezuelites? distinctus	LAD	13515,5	22,16	16	67	
Concavissimisporites "rugulatus" (x)	LAD	13967,14	22,62	1	incierto	
Brevitricolporites "uwaeorum" (x)	LAD	14132,47	22,78	21	46	
Clavainaperturites" grimsdaleoides"(x)	LAD	14171,90	22,82	3	81	
Polypodiaceoisporites pseudopsilatus	FAD	14176,4	22,83	4	242	
Cicatricosisporites dorogensis	LAD	14197,0	22,85	77	60	T11
Multiporopollenites pauciporatus	LAD	14377,0	23,03	28	57	
Retistephanoporites angelicus	LAD	14377,1	23,03	13	57	
Bombacacidites muinaneorum	FAD	14393,6	23,14	5	189	
Psilaperiporites robustus	LAD	14424,2	23,33	15	42	
Monocolpopollenites ovatus	LAD	14429,1	23,36	17	95	
Jandufouria "minutus"	LAD	14437,4	23,42	4	41	
Retibrevitricolporites grandis	LAD	14476,3	23,67	35	51	
Hexaporotricolpites "striatus" (x)	LAD	14510,01	23,89	2	8	
Bombacacidites "verrucatus" (x)	LAD	14547,37	24,13	1	incierto	
Proteacidites triangulatus	FAD	14548,2	24,13	4	252	
Cribroperidinium edwardsii	LAD	14576,0	24,31	1	incierto	
Retitrescolpites magnus	LAD	14653,9	24,81	32	50	
Gemmastephanoporites polymorphus	LAD	14727,9	25,29	4	42	
Retitricolpites maturus	LAD	14727,9	25,29	4	45	
Echitriletes "acanthotriletoides"	FAD	14764,6	25,52	1	incierto	
Corsinipollenites undulatus	LAD	14964,0	26,80	18	51	
MgrandiosusMfranciscoiJseamrogiformis ACME Ca5	LAD	14964,0	26,80	3	17	T10
Verrutricolporites rotundiporus	FAD	14964,0	26,80	3	270	
Wilsonipites margocolpatus	LAD	15010,5	27,10	6	51	
Brevitricolpites microechinatus	LAD	15024,1	27,19	23	67	
Verrustephanocolporites "pastinensis" (x)	LAD	15189,65	28,25	1	incierto	
Momipites africanus	LAD	15336,0	29,19	5	71	
Ctenolophonidites cruciatus	LAD	15377,0	29,46	2	28	
dinocyst acme lowermost C8	LAD	15464,9	30,02	3	23	
Retibrevicolpites yavarensis	FAD	15549,9	30,57	1	incierto	
Foveotriletes ornatus	FAD	15599,7	30,89	5	270	

Annex 1.4 (continuation)

Taxa	Event	Composite Units	Age (Ma)	#Sites	Spreading Paramater	Zone
Annutriporites iversenii	LAD	15627,6	31,07	18	85	
Rhoipites planipolaris	FAD	15694,0	31,50	3	103	T9
MgrandiosusMfranciscoiJseamrogiformis ACME Ca5	FAD	15694,6	31,50	19	64	
Retitrescolpites baculatus	LAD	15708,2	31,59	17	35	
Retibrevitricolpites triangulatus	LAD	15717,9	31,65	15	87	
Psilabrevitricolporites "hoornii" (x)	LAD	15727,24	31,71	1	incierto	
Retitriletes sommeri	FAD	15729,8	31,73	4	273	
Bombacacidites "pulcherrimus" (x)	LAD	15745,01	31,82	1	incierto	
Spinizonocolpites echinatus	LAD	15745,6	31,83	24	85	
Jandufouria "minutus"	FAD	15750,4	31,86	1	incierto	
Scabratricolporites planetensis	FAD	15759,5	31,92	2	13	
Magnaperiporites spinosus	FAD	15765,6	31,96	4	27	
Nothofagidites huertasii	LAD	15774,8	32,02	28	32	
Foveotricolporites etayoi	FAD	15780,9	32,05	2	0	T8
Venezuelites globoannulatus	LAD	15784,4	32,08	2	6	
L. proxapertitoides proxapertitoides	LAD	15785,1	32,08	13	78	
Psilaperiporites "intensus"	FAD	15786,0	32,09	2	14	
Bombacacidites foveoreticulatus	LAD	15807,7	32,23	35	25	
Bombacacidites soleaformis	LAD	15807,7	32,23	11	35	
Foveotricolporites fossulatus	LAD	15816,3	32,28	2	24	
Striatricolporites digitatus	LAD	15816,3	32,28	3	47	
Psilastephanocolpites verrucosus	LAD	15836,0	32,41			
Cordosphaeridium inodes	LAD	15851,1	32,51	5	87	
Bombacacidites echinatus	LAD	15858,1	32,55	5	9	
Pseudostephanocolpites perfectus	LAD	15858,1	32,55	28	29	
Cricotriporites guianensis	LAD	15878,6	32,68	7	79	
Retitricolpites "finitus"	FAD	15878,6	32,68	10	122	
Crassiectoapertites columbianus	FAD	15916,2	32,92	5	279	
Echitriporites "pseudotrianguliformis"	LAD	15916,2	32,92	1	incierto	
Longapertites sp. 1	LAD	15917,0	32,93	5	43	
Verrutricolporites reticulatus	LAD	15927,0	32,99	17	34	
Echitriporites "pseudotrianguliformis"	FAD	15959,5	33,20	1	incierto	
Foveotriporites hammenii	LAD	15964,7	33,24	23	30	
Ulmoideipites krempii	LAD	15976,8	33,31	28	78	
Longapertites microfoveolatus	LAD	15999,2	33,46	10	97	
Retistephanocolporites festivus	LAD	16002,9	33,48	26	32	
Psilatricolporites pachydermatus	FAD	16022,8	33,61	7	290	
Magnastriatites grandiosus	FAD	16032,8	33,67	6	279	
Echitriporites trianguliformis	LAD	16046,0	33,76	19	80	
Bombacacidites fossureticulatus	LAD	16068,0	33,90	8	15	
Bombacacidites simplireticulatus	LAD	16068,0	33,90	5	35	
Catostemma type	FAD	16068,0	33,90	4	281	
Echitetracolpites? tenuiexinatus	LAD	16068,0	33,90	15	18	
Echitriporites trianguliformis orbicularis	LAD	16068,0	33,90	43	31	T7
Homotryblium floripes	LAD	16068,0	33,90	6	15	
Retisyncolporites angularis	LAD	16068,0	33,90	10	16	
Verrucatotriletes etayoi	FAD	16073,3	33,96	4	233	

Annex 1.4 (continuation)

Taxa	Event	Composite Units	Age (Ma)	#Sites	Spreading Paramater	Zone
Luminidites colombianensis	LAD	16084,5	34,09	8	9	
Syncolporites marginatus	LAD	16087,1	34,12	10	77	
Apiculatasporites? cingulatus	LAD	16100,1	34,26	3	30	
Cicatricososporites eocenicus	LAD	16113,5	34,41	4	6	
Clavatriporites "spicatus" (x)	LAD	16113,50	34,41	3	11	
Retistephanocolpites angeli	LAD	16120,8	34,50	12	56	
Arecipites regio	LAD	16131,0	34,61	14	77	
Racemonocolpites facilis	LAD	16143,4	34,75	13	67	
Gemmaperprolatoporis "teresitae" (x)	LAD	16151,97	34,85	5	10	
Striatriletes saccolomicites	FAD	16169,7	35,05	6	240	
Gemmastephanoporites breviculus	LAD	16175,1	35,11	6	27	
Bombacacidites "gemmatus" (x)	LAD	16259,81	36,06	1	incierto	
Proxapertites magnus	LAD	16267,2	36,15	16	68	
Polotricolporites versabilis	LAD	16287,1	36,37	4	17	
Baculamonocolpites hammenii	LAD	16300,2	36,52	4	26	
Verrucatosporites usmensis	FAD	16304,6	36,57	6	284	
Concavissimisporites fossulatus	FAD	16336,0	36,92	4	39	
Zonocostites minor	LAD	16339,5	36,96	2	21	
Psilastephanocolporites brevicolpatus (xx)	LAD	16346,9	37,04	5	8	
Ischyosporites problematicus	LAD	16364,7	37,24	6	41	
Echitriporites variabilis	LAD	16383,0	37,45	8	24	
Poloretitricolpites absolutus	LAD	16383,0	37,45	4	41	
Retitricolporites "magnificus" (x)	LAD	16383,04	37,45	3	4	
Spinizonocolpites grandis	LAD	16384,8	37,47	20	7	T6
Retibrevitricolporites speciosus	LAD	16394,6	37,58	10	24	
Araucariacites spp.	LAD	16407,3	37,72	24	112	
Racemonocolpites racematus	LAD	16414,3	37,80	19	71	
Rugotricolporites felix	LAD	16414,3	37,80	3	12	
Siltaria mariposa	LAD	16426,5	37,94	5	28	
Retistephanocolpites "araucaensis" (x)	LAD	16426,51	37,94	2	40	
Echiperiporites akanthos	FAD	16427,3	37,95	7	287	
Brevitricolpites macroexinatus	LAD	16442,3	38,12	3	23	
Echimonocolpites densus	LAD	16450,0	38,21	6	83	
Echimorphomonocolpites solitarius	LAD	16450,0	38,21	5	24	
Retitriporites poricostatus	LAD	16455,7	38,27	2	1	
Spinizonocolpites breviechinatus	LAD	16455,7	38,27	4	34	
Spinizonocolpites pachyexinatus	LAD	16455,7	38,27	3	68	
Grimsdalea polygonalis	LAD	16474,6	38,48	2	5	
Echimorphomonocolpites gracilis	LAD	16490,6	38,66	3	23	
Retitricolporites "magnificus" (x)	FAD	16549,16	39,32	1	incierto	
Bombacacidites echinatus	FAD	16572,2	39,58	3	7	
Echitriporites "scabrabaculomorphis"	FAD	16575,0	39,62	1	incierto	
Echitriporites "scabrabaculomorphis"	LAD	16575,0	39,62	2	0	
Ladakhipollenites rubinii	LAD	16594,8	39,84	2	20	
Tetracolporites pachyexinatus	LAD	16594,8	39,84	2	5	
Crusafontites megagemmatus	LAD	16609,9	40,01	2	20	
Lingulodinium cf. sicula	LAD	16609,9	40,01	1	incierto	
dinocyst acme lowermost C8	FAD	16638,8	40,33	1	incierto	
Retisyncolporites aureus	LAD	16639,5	40,34	2	2	

Annex 1.4 (continuation)

Taxa	Event	Composite Units	Age (Ma)	#Sites	Spreading Paramater	Zone
Cricotriporites minutiporus	LAD	16669,3	40,68	3	47	
Ranunculacidites operculatus	FAD	16685,0	40,86	6	293	
Lingulodinium cf. sicula	FAD	16711,0	41,15	1	incierto	
Proxapertites cursus	LAD	16711,0	41,15	27	62	
Retistephanoporites crassiannulatus	FAD	16711,0	41,15	4	232	
Rhoipites cienaguensis	FAD	16711,0	41,15	2	35	
Grimsdalea polygonalis	FAD	16717,8	41,23	1	incierto	
Longapertites proxapertitoides	LAD	16720,0	41,25	9	53	
S. spiralis acme upper Mirador	LAD	16730,2	41,36	2	2	
Longapertites vaneendenburgi	LAD	16754,7	41,64	20	60	
Bombacacidites fossureticulatus	FAD	16755,3	41,65	3	3	
Cicatricososporites eocenicus	FAD	16755,3	41,65	2	3	
Ctenolophonidites cruciatus	FAD	16755,3	41,65	2	28	
Foveotricolporites fossulatus	FAD	16755,3	41,65	1	incierto	
Jandufouria minor	FAD	16778,9	41,91	2	241	
Retisyncolporites aureus	FAD	16794,4	42,09	1	incierto	
Ctenolophonidites suigeneris (xx)	FAD	16805,6	42,21	1	incierto	
dinocyst acme middle shale Mirador	LAD	16808,2	42,24	3	1	
Jandufouria seamrogiformis	FAD	16808,2	42,24	7	294	
Adnatosphaeridium multispinosum	FAD	16823,1	42,41	1	Incierto	
Luminidites colombianensis	FAD	16825,0	42,43	5	14	
Laevigatosporites catanejensis	FAD	16833,4	42,53	4	158	
Lingulodinium machaerophorum	FAD	16835,3	42,55	2	246	
Gemmastephanoporites polymorphus	FAD	16847,7	42,69	2	1	
S. spiralis acme upper Mirador	FAD	16847,7	42,69	23	34	
Rhoipites guianensis "perbonus"	FAD	16849,0	42,70	2	2	
Echimorphomonocolpites gracilis	FAD	16849,4	42,71	1	incierto	
Homotryblium floripes	FAD	16849,4	42,71	3	2	
Psilaperiporites minimus	FAD	16849,4	42,71	4	297	
dinocyst acme middle shale Mirador	FAD	16849,7	42,71	2	1	
Multiporopollenites pauciporatus	FAD	16849,7	42,71	3	14	
Psilastephanocolporites brevicolpatus (xx)	FAD	16849,7	42,71	2	5	
Rhoipites guianensis	FAD	16849,7	42,71	8	297	
Echitetracolpites? tenuiexinatus	FAD	16867,7	42,92	5	11	
Polysphaeridium subtile	FAD	16867,7	42,92	4	153	
Retistephanoporites angelicus	FAD	16867,7	42,92	3	11	
Retisyncolporites angularis	FAD	16867,7	42,92	2	0	
Venezuelites? distinctus	FAD	16867,7	42,92	3	5	
Gemmastephanoporites breviculus	FAD	16973,9	44,11	2	4	
Perisyncolporites pokornyi	FAD	17038,0	44,83	9	299	
Rugotricolporites felix	FAD	17038,0	44,83	2	6	
Brevitricolporites "uwaeorum" (x)	FAD	17038,03	44,84	2	21	
Nothofagidites huertasii	FAD	17372,2	48,60	5	21	
Cicatricosisporites dorogensis	FAD	17372,7	48,61	7	19	T5
Psilatricolporites costatus	FAD	17372,7	48,61	6	306	
Zonocostites ramonae	FAD	17372,7	48,61	5	308	
Tetracolporopollenites spongiosus	LAD	17413,8	49,12	5	19	
Perfotricolpites digitatus	FAD	17454,6	49,62	11	310	

Annex 1.4 (continuation)

Taxa	Event	Composite Units	Age (Ma)	#Sites	Spreading Paramater	Zone
Verrustephanocolpites rugulatus	FAD	17458,0	49,66	1	incierto	
Retitriporites poricostatus	FAD	17458,6	49,67	2	14	
Echitriletes muelleri	FAD	17465,6	49,76	7	308	
Bombacacidites foveoreticulatus	FAD	17480,8	49,94	9	24	
Echimorphomonocolpites solitarius	FAD	17496,1	50,13	2	13	
Retitrescolpites magnus	FAD	17497,0	50,14	7	30	
Echimonocolpites densus	FAD	17513,2	50,34	2	8	
Psilastephanocolpites verrucosus	FAD	17513,2	50,34	2	13	
Spinizonocolpites grandis	FAD	17513,2	50,34	6	22	
Pseudostephanocolpites perfectus	FAD	17538,9	50,66	8	25	
Bombacacidites soleaformis	FAD	17563,8	50,97	4	22	
Polypodiisporites echinatus	LAD	17563,8	50,97	3	20	
Wilsonipites margocolpatus	FAD	17563,8	50,97	2	34	
Zonocostites minor	FAD	17584,3	51,22	2	19	
Retibrevitricolporites speciosus	FAD	17589,0	51,28	2	13	
Retibrevitricolpites triangulatus	FAD	17589,3	51,28	4	17	
Retitrescolpites? irregularis	FAD	17589,3	51,28	47	310	
Crusafontites megagemmatus	FAD	17590,7	51,30	2	20	
Lanagiopollis crassa	FAD	17590,7	51,30	13	312	
Tetracolporites pachyexinatus	FAD	17593,9	51,34	2	17	
Polotricolporites versabilis	FAD	17594,9	51,35	2	9	
Retitricolpites maturus	FAD	17594,9	51,35	2	12	
Echitriporites trianguliformis orbicularis	FAD	17598,0	51,39	9	21	
Echitriporites variabilis	FAD	17603,8	51,46	4	15	
Corsinipollenites undulatus	FAD	17604,0	51,46	4	30	
Foveotriporites hammenii	FAD	17604,0	51,46	10	27	
Retitriporites dubiosus	FAD	17604,9	51,47	3	267	
Bombacacidites gonzalezii	FAD	17606,1	51,49	6	31	
Echiperiporites estelae	FAD	17606,1	51,49	9	310	
Ladakhipollenites rubinii	FAD	17606,1	51,49	2	19	
Retistephanoporites minutiporus	FAD	17606,1	51,49	6	58	
Retistephanocolporites festivus	FAD	17608,2	51,51	6	26	
Baculamonocolpites hammenii	FAD	17625,0	51,72	4	26	
Brevitricolpites macroexinatus	FAD	17625,1	51,72	3	22	
Tricolpites clarensis	FAD	17625,1	51,72	4	33	
Verrutricolporites reticulatus	FAD	17625,1	51,72	4	24	
Retistephanocolpites williamsi	FAD	17625,2	51,72	1	incierto	
Retistephanocolpites williamsi	LAD	17625,2	51,72	1	incierto	
Tetracolporopollenites maculosus	FAD	17625,2	51,72	10	172	
Crototricolpites annemariae	FAD	17687,5	52,49	3	3	
Psilabrevitricolporites triangularis	FAD	17701,1	52,66	8	314	
Apiculatasporites? cingulatus	FAD	17708,6	52,75	3	22	
Cricotriporites macroporus	FAD	17708,6	52,75	3	16	
Margocolporites vanwijhei	FAD	17708,6	52,75	7	255	
Retibrevitricolporites grandis	FAD	17708,6	52,75	6	26	
Striatopollis catatumbus	FAD	17708,7	52,75	9	315	
Etm dc13spike	LAD	17810,0	54,00	1	incierto	

Annex 1.4 (continuation)

Taxa	Event	Composite Units	Age (Ma)	#Sites	Spreading Paramater	Zone
Proxapertites minutihumbertoides	LAD	17810,0	54,00	5	7	
Bombacacidites simplireticulatus	FAD	17810,8	54,01	4	21	
Crototricolpites protoannemariae	LAD	17816,1	54,08	7	41	
Spathiphyllum vanegensis	LAD	17817,3	54,09	19	42	
Tuberositriletes verrucatus	FAD	17817,3	54,09	4	283	
Etm dc13spike	FAD	17818,7	54,11	4	16	
Spirosyncolpites spiralis	FAD	17940,3	55,61	2	319	
Petm dc13spike	LAD	17941,7	55,63	1	incierto	
Polypodiisporites aff. specious	FAD	17941,7	55,63	4	22	
Aglaoreidia? foveolata	LAD	17995,0	55,70	7	17	
Bombacacidites annae	LAD	17995,0	55,70	30	29	4b
Diporopollis assamica	LAD	17995,0	55,70	9	39	
P. operculatus acme lower Cuervos	LAD	17995,0	55,70	6	14	
Psilabrevitricolporites simpliformis	LAD	17995,0	55,70	12	29	
Polypodiisporites pachyexinatus	LAD	17995,4	55,70	6	5	
Tetracolpites "quadrangularis" (x)	LAD	18005,23	55,71	1	incierto	
Bombacacidites brevis	FAD	18009,4	55,72	12	321	
Ctenolophonidites lisamae	LAD	18010,7	55,72	12	38	
Retidiporites magdalenensis	LAD	18010,7	55,72	33	55	
Syncolporites lisamae	LAD	18026,7	55,74	8	36	
Heterocolpites palaeocenica	LAD	18031,9	55,74	3	13	
Magnotetradites magnus	LAD	18031,9	55,74	12	52	
Psilamonocolpites operculatus	LAD	18042,2	55,76	10	36	
Proxapertites verrucatus	LAD	18047,9	55,76	14	37	
Retidiporites elongatus	LAD	18058,0	55,78	9	44	
Cyclusphaera scabrata	FAD	18077,2	55,80	7	23	4a
Foveotricolporites rugulatus	FAD	18077,2	55,80	5	44	
Petm dc13spike	FAD	18077,2	55,80	49	386	
Rhoipites hispidus	FAD	18077,2	55,80	8	321	
Siltaria mariposa	FAD	18077,2	55,80	4	17	
Gemmamonocolpites gemmatus	LAD	18138,8	56,05	12	6	
Foveotricolpites perforatus	LAD	18143,0	56,07	27	15	3b
Retitrescolpites peculiaris	LAD	18143,0	56,07	1	incierto	
Tricolpites protoclarensis	LAD	18143,0	56,07	3	8	
Longapertites proxapertitoides	FAD	18143,1	56,07	3	19	
Foveotriletes margaritae	LAD	18143,4	56,07	30	66	
Proxapertites minutihumbertoides	FAD	18143,6	56,07	1	incierto	
Polypodiisporites pachyexinatus	FAD	18143,7	56,07	2	3	
Palaeocystodinium spp.	LAD	18151,2	56,10	2	0	
Curvimonocolpites inornatus	LAD	18167,6	56,17	9	23	
Periretisyncolpites magnosagenatus	LAD	18178,0	56,21	6	39	
Tetradites umirensis	LAD	18182,7	56,23	12	34	
Tetracolporopollenites transversalis	FAD	18249,3	56,50	11	326	
Striatopollis? tenuistriatus	FAD	18317,6	56,77	7	272	
Bombacacidites nacimientoensis	FAD	18335,1	56,85	5	284	
Brevitricolpites microechinatus	FAD	18346,0	56,89	7	44	
Foveomonoporites variabilis	LAD	18347,1	56,89	1	incierto	
Bombacacidites protofoveoreticulatus	LAD	18349,7	56,90	3	7	
Colombipollis tropicalis	LAD	18397,6	57,10	16	30	

Annex 1.4 (continuation)

Taxa	Event	Composite Units	Age (Ma)	#Sites	Spreading Paramater	Zone
Psilastephanocolporites fissilis	FAD	18404,3	57,13	9	198	
Retitricolpites simplex	FAD	18302,4	57,13	8	320	
Poloretitricolpites absolutus	FAD	18441,7	57,28	2	37	
Horniella lunarensis	FAD	18498,1	57,51	6	53	
Clavatisporites mutisii	LAD	18509,2	57,55	9	37	
Areoligera spp.	LAD	18546,2	57,70	14	48	
Polypodiisporites echinatus	FAD	18586,0	57,86	3	18	
Retitrescolpites baculatus	FAD	18586,0	57,86	5	54	
Retitrescolpites saturum	FAD	18595,5	57,90	7	51	
Araucariacites australis	LAD	18607,5	57,95	26	68	
Alterbidinium spp.	LAD	18649,0	58,12	23	41	
Retitrescolpites peculiaris	FAD	18751,3	58,53	1	incierto	
Tricolpites antonii	FAD	18799,1	58,73	4	41	
Aglaoreidia? foveolata	FAD	18859,2	58,97	4	9	
Retistephanocolpites angeli	FAD	18863,5	59,11	5	27	
Striatricolporites digitatus	FAD	18895,7	59,12	3	26	
Palaeocystodinium golzowense	LAD	18907,8	59,17	11	31	
Gemmamonocolpites macrogemmatus	LAD	18916,0	59,20	3	9	
Momipites africanus	FAD	18916,7	59,20	3	72	
Foveotricolpites perforatus	FAD	18917,8	59,21	11	15	3a
Mauritiidites franciscoi minutus	FAD	18917,8	59,21	12	339	
Proxapertites sulcatus	LAD	19007,0	59,57	4	17	
Crototricolpites protoannemariae	FAD	19013,8	59,60	4	19	
Zonotricolpites variabilis	LAD	19013,8	59,60	11	18	
Stephanocolpites costatus	LAD	19023,0	59,63	9	19	
Cricotriporites minutiporus	FAD	19028,5	59,65	3	47	
Spinizonocolpites breviechinatus	FAD	19028,5	59,65	3	3	
Diporopollis assamica	FAD	19080,8	59,87	3	10	
Echitriporites suescae	LAD	19087,4	59,89	19	47	
Echinatisporis brevispinosus	FAD	19092,7	59,91	4	63	
Bombacacidites protofoveoreticulatus	FAD	19095,1	59,92	3	8	
Ladakhipollenites simplex	FAD	19095,1	59,92	8	299	
Tricolpites protoclarensis	FAD	19095,1	59,92	3	12	
Bombacacidites annae	FAD	19126,0	60,09	12	20	2
Ischyosporites problematicus	FAD	19129,5	60,12	5	15	
Tetracolporopollenites spongiosus	FAD	19129,5	60,12	4	24	
Proxapertites magnus	FAD	19148,7	60,26	8	57	
Diporoconia cf. Iszkaszentgyoergyi	LAD	19177,8	60,48	2	13	
Laevigatosporites granulatus	FAD	19177,8	60,48	7	343	
Longapertites sp. 1	FAD	19177,8	60,48	3	48	
Periretisyncolpites giganteus	LAD	19179,6	60,50	13	21	
Monocolpopollenites ovatus	FAD	19198,6	60,64	7	25	
Zlivisporis blanensis	LAD	19321,6	61,57	17	31	
Palaeocystodinium australinum	LAD	19326,1	61,60	12	30	
Spinizonocolpites baculatus	LAD	19360,7	61,87	23	16	1
Cerodinium spp.	LAD	19372,6	61,95	13	216	
Andalusiella polymorpha	LAD	19379,0	62,00	19	32	
Andalusiella spp.	LAD	19379,0	62,00	23	41	

Annex 1.4 (continuation)

Taxa	Event	Composite Units	Age (Ma)	#Sites	Spreading Paramater	Zone
Monocolpopollenites spheroidites	FAD	19379,0	62,00	1	incierto	
Monocolpopollenites spheroidites	LAD	19379,0	62,00	5	41	
Trithyrodinium spp.	LAD	19380,5	62,01	8	21	
Periretisyncolpites magnosagenatus	FAD	19403,8	62,19	2	11	
Syndemicolpites typicus	LAD	19421,1	62,32	11	9	
Gemmamonocolpites macrogemmatus	FAD	19432,6	62,41	2	0	
Heterocolpites palaeocenica	FAD	19441,9	62,48	2	6	
Mauritiidites crassibaculatus	FAD	19441,9	62,48	2	306	
Echitriletes intercolensis	LAD	19453,4	62,57	8	34	
Hamulatisporis caperatus	LAD	19453,4	62,57	15	44	
Ctenolophonidites lisamae	FAD	19475,3	62,73	2	7	
M. franciscoi pachyexinatus	FAD	19482,1	62,78	13	310	
Mauritiidites franciscoi franciscoi	FAD	19482,1	62,78	16	348	
P. operculatus acme lower Cuervos	FAD	19482,1	62,78	5	14	
Psilabrevitricolporites simpliformis	FAD	19546,9	63,27	5	21	
Tercissus sp.	LAD	19657,3	64,11	4	8	
Senegalinim laevigatum	LAD	19722,8	64,60	11	25	
Proteacidites dehaani	LAD	19732,2	64,67	13	36	
Senegalinium spp.	LAD	19739,1	64,72	5	364	
Bacumorphomonocolpites tausae	LAD	19755,2	64,84	13	6	
Racemonocolpites facilis	FAD	19755,3	64,85	5	70	
Phelodinium tricuspe	LAD	19755,7	64,85	2	3	
Polypodiaceoisporites? fossulatus	FAD	19755,7	64,85	5	24	
Proxapertites cursus	FAD	19788,1	65,09	9	25	
Duplotriporites ariani	LAD	19790,1	65,11	15	20	
Andalusiella mauthei	LAD	19803,1	65,21	20	35	
Senegalinium bicavatum	LAD	19813,1	65,28	17	31	
Ariadnaesporites spinosus	LAD	19821,3	65,34	8	19	
Cerodinium diebelii	LAD	19833,1	65,43	8	20	
Gabonisporites vigourouxii	LAD	19836,0	65,45	17	16	TOP CRETACEOUS
Buttinia andreevi	LAD	19842,0	65,50	14	9	
Echimonocolpites protofranciscoi	LAD	19842,0	65,50	20	8	
Gabonisporis spp.	LAD	19842,0	65,50	5	0	
Glaphyrocysta perforata	LAD	19842,0	65,50	2	1	
Scabratriletes granularis	LAD	19842,0	65,50	7	12	
Andalusiella gabonensis	LAD	19843,2	65,52	12	13	
Dinogymnium spp.	LAD	19848,1	65,60	25	35	
Spinizonocolpites pachyexinatus	FAD	19853,0	65,68	3	43	
Disphaerogena carposphaeropsis	LAD	19855,5	65,71	3	1	
Yolkinigymnium lanceolatum	LAD	19855,5	65,71	5	8	
Ephedripites "afropollensis"	LAD	19857,5	65,75	2	0	
Crusafontites grandiosus	LAD	19858,9	65,77	13	7	
Senegalinium obscurum	LAD	19860,8	65,80	3	12	
Areoligera senonensis	LAD	19862,0	65,82	5	11	

Annex 1.6. Support, confidence and lift for association rules with a minimum support of 20% and confidence of 50%.

Rules	*support*	*confidence*	*lift*
{} => {Psilatriletes sp. 25}	0,7919	0,792	1
{} => {Polypodiisporites sp.}	0,5563	0,556	1
{Polypodiisporites sp.} => {Psilatriletes sp. 25}	0,4926	0,885	1,118
{Psilatriletes sp. 25} => {Polypodiisporites sp.}	0,4926	0,622	1,118
{Laevigatosporites tibuensis} => {Psilatriletes sp. 25}	0,4480	0,921	1,163
{Psilatriletes sp. 25} => {Laevigatosporites tibuensis}	0,4480	0,566	1,163
{Fungi} => {Psilatriletes sp. 25}	0,4246	0,926	1,169
{Psilatriletes sp. 25} => {Fungi}	0,4246	0,536	1,169
{Psilamonocolpites medius} => {Psilatriletes sp. 25}	0,4246	0,909	1,148
{Psilatriletes sp. 25} => {Psilamonocolpites medius}	0,4246	0,536	1,148
{Laevigatosporites tibuensis} => {Polypodiisporites sp.}	0,3482	0,716	1,287
{Polypodiisporites sp.} => {Laevigatosporites tibuensis}	0,3482	0,626	1,287
{Fungi} => {Laevigatosporites tibuensis}	0,3397	0,741	1,524
{Laevigatosporites tibuensis} => {Fungi}	0,3397	0,699	1,524
{Psilamonocolpites medius} => {Polypodiisporites sp.}	0,3397	0,727	1,307
{Polypodiisporites sp.} => {Psilamonocolpites medius}	0,3397	0,611	1,307
{Laevigatosporites tibuensis,Polypodiisporites sp.} => {Psilatriletes sp. 25}	0,3397	0,976	1,232
{Laevigatosporites tibuensis,Psilatriletes sp. 25} => {Polypodiisporites sp.}	0,3397	0,758	1,363
{Polypodiisporites sp.,Psilatriletes sp. 25} => {Laevigatosporites tibuensis}	0,3397	0,690	1,418
{Fungi,Laevigatosporites tibuensis} => {Psilatriletes sp. 25}	0,3291	0,969	1,223
{Fungi,Psilatriletes sp. 25} => {Laevigatosporites tibuensis}	0,3291	0,775	1,594
{Laevigatosporites tibuensis,Psilatriletes sp. 25} => {Fungi}	0,3291	0,735	1,602
{Mauritiidites franciscoi minutus} => {Psilatriletes sp. 25}	0,3142	0,980	1,238
{Fungi} => {Polypodiisporites sp.}	0,3142	0,685	1,232
{Polypodiisporites sp.} => {Fungi}	0,3142	0,565	1,232
{Polypodiisporites sp.,Psilamonocolpites medius} => {Psilatriletes sp. 25}	0,3079	0,906	1,144
{Psilamonocolpites medius,Psilatriletes sp. 25} => {Polypodiisporites sp.}	0,3079	0,725	1,303
{Polypodiisporites sp.,Psilatriletes sp. 25} => {Psilamonocolpites medius}	0,3079	0,625	1,338
{Fungi,Polypodiisporites sp.} => {Psilatriletes sp. 25}	0,3057	0,973	1,229
{Fungi,Psilatriletes sp. 25} => {Polypodiisporites sp.}	0,3057	0,720	1,294
{Polypodiisporites sp.,Psilatriletes sp. 25} => {Fungi}	0,3057	0,621	1,353
{Mauritiidites franciscoi franciscoi} => {Psilatriletes sp. 25}	0,2696	0,864	1,091
{Mauritiidites franciscoi minutus} => {Polypodiisporites sp.}	0,2675	0,834	1,500
{Fungi,Laevigatosporites tibuensis} => {Polypodiisporites sp.}	0,2675	0,788	1,416
{Fungi,Polypodiisporites sp.} => {Laevigatosporites tibuensis}	0,2675	0,851	1,751
{Laevigatosporites tibuensis,Polypodiisporites sp.} => {Fungi}	0,2675	0,768	1,675
{Fungi,Laevigatosporites tibuensis,Polypodiisporites sp.} => {Psilatriletes sp. 25}	0,2654	0,992	1,253
{Fungi,Laevigatosporites tibuensis,Psilatriletes sp. 25} => {Polypodiisporites sp.}	0,2654	0,806	1,450
{Fungi,Polypodiisporites sp.,Psilatriletes sp. 25} => {Laevigatosporites tibuensis}	0,2654	0,868	1,785
{Laevigatosporites tibuensis,Polypodiisporites sp.,Psilatriletes sp. 25} => {Fungi}	0,2654	0,781	1,704
{Mauritiidites franciscoi minutus,Polypodiisporites sp.} => {Psilatriletes sp. 25}	0,2633	0,984	1,243
{Mauritiidites franciscoi minutus,Psilatriletes sp. 25} => {Polypodiisporites sp.}	0,2633	0,838	1,506

Annex 1.6 (continuation)

Rules	*support*	*confidence*	*lift*
{Polypodiisporites sp.,Psilatriletes sp. 25} => {Mauritiidites franciscoi minutus}	0,2633	0,534	1,667
{Spirosyncolpites spiralis} => {Psilatriletes sp. 25}	0,2548	0,845	1,067
{Laevigatosporites tibuensis} => {Psilamonocolpites medius}	0,2463	0,507	1,084
{Psilamonocolpites medius} => {Laevigatosporites tibuensis}	0,2463	0,527	1,084
{Mauritiidites franciscoi minutus} => {Laevigatosporites tibuensis}	0,2442	0,762	1,566
{Laevigatosporites tibuensis} => {Mauritiidites franciscoi minutus}	0,2442	0,502	1,566
{Laevigatosporites tibuensis,Mauritiidites franciscoi minutus} => {Psilatriletes sp. 25}	0,2442	1,000	1,263
{Mauritiidites franciscoi minutus,Psilatriletes sp. 25} => {Laevigatosporites tibuensis}	0,2442	0,777	1,598
{Laevigatosporites tibuensis,Psilatriletes sp. 25} => {Mauritiidites franciscoi minutus}	0,2442	0,545	1,700
{Laevigatosporites tibuensis,Psilamonocolpites medius} => {Psilatriletes sp. 25}	0,2420	0,983	1,241
{Laevigatosporites tibuensis,Psilatriletes sp. 25} => {Psilamonocolpites medius}	0,2420	0,540	1,157
{Psilamonocolpites medius,Psilatriletes sp. 25} => {Laevigatosporites tibuensis}	0,2420	0,570	1,172
{Retistephanoporites minutiporus} => {Psilatriletes sp. 25}	0,2399	0,950	1,199
{Mauritiidites franciscoi franciscoi} => {Polypodiisporites sp.}	0,2335	0,748	1,345
{Fungi} => {Psilamonocolpites medius}	0,2293	0,500	1,070
{Fungi,Psilamonocolpites medius} => {Psilatriletes sp. 25}	0,2272	0,991	1,251
{Fungi,Psilatriletes sp. 25} => {Psilamonocolpites medius}	0,2272	0,535	1,145
{Psilamonocolpites medius,Psilatriletes sp. 25} => {Fungi}	0,2272	0,535	1,167
{Rhoipites guianensis} => {Psilatriletes sp. 25}	0,2166	0,903	1,140
{Mauritiidites franciscoi minutus} => {Fungi}	0,2144	0,669	1,459
{Mauritiidites franciscoi franciscoi,Polypodiisporites sp.} => {Psilatriletes sp. 25}	0,2144	0,918	1,159
{Mauritiidites franciscoi franciscoi,Psilatriletes sp. 25} => {Polypodiisporites sp.}	0,2144	0,795	1,430
{Fungi,Mauritiidites franciscoi minutus} => {Psilatriletes sp. 25}	0,2123	0,990	1,250
{Mauritiidites franciscoi minutus,Psilatriletes sp. 25} => {Fungi}	0,2123	0,676	1,473
{Fungi,Psilatriletes sp. 25} => {Mauritiidites franciscoi minutus}	0,2123	0,500	1,560
{Laevigatosporites tibuensis,Mauritiidites franciscoi minutus} => {Polypodiisporites sp.}	0,2102	0,861	1,548
{Mauritiidites franciscoi minutus,Polypodiisporites sp.} => {Laevigatosporites tibuensis}	0,2102	0,786	1,616
{Laevigatosporites tibuensis,Polypodiisporites sp.} => {Mauritiidites franciscoi minutus}	0,2102	0,604	1,883
{Laevigatosporites tibuensis,Mauritiidites franciscoi minutus,Polypodiisporites sp.} => {Psilatriletes sp. 25}	0,2102	1,000	1,263
{Laevigatosporites tibuensis,Mauritiidites franciscoi minutus,Psilatriletes sp. 25} => {Polypodiisporites sp.}	0,2102	0,861	1,548
{Mauritiidites franciscoi minutus,Polypodiisporites sp.,Psilatriletes sp. 25} => {Laevigatosporites tibuensis}	0,2102	0,798	1,642
{Laevigatosporites tibuensis,Polypodiisporites sp.,Psilatriletes sp. 25} => {Mauritiidites franciscoi minutus}	0,2102	0,619	1,930
{Mauritiidites franciscoi franciscoi} => {Psilamonocolpites medius}	0,2081	0,667	1,427
{Cicatricosisporites dorogensis} => {Psilatriletes sp. 25}	0,2059	0,924	1,167
{Lanagiopollis crassa} => {Psilatriletes sp. 25}	0,2038	0,932	1,177
{Retitrescolpites magnus} => {Psilatriletes sp. 25}	0,2017	0,960	1,212
{Spirosyncolpites spiralis} => {Psilamonocolpites medius}	0,2017	0,669	1,432

Annex 1.7: Systematic Palynology

In this section new palynomorphs that were found in sections and wells used in this study are described and illustrated. Description of new species were ordered by major morphological grousp (e.g. Monoletes, Triletes, Tricpolpate, etc), then alphabetical within section. The new species were erected and compared to existing species in the literatura using the morphological database of the Biostratigrapgy Team of the Instituto Colombiano del Petroleo (ECOPETROL). This electronic database host updated taxonomic information of pollen, spores and dinocysts of Paleozoic, Cretaceous and Cenozoic ages in northern South America. In total 34 different palynomorph types were described, of which eight correspond to sopres and 26 to pollen. The terminology used in descriptions follow Punt et al. (2007). All grains are located using the England Finder coordinate system (EF). All type and figured specimen in Plates-6 are stored in the palynological collection of the Biostratigraphy Team of the Instituto Colombiano del Petroleo (ECOPETROL. SA).

Pteridophyte and bryophyte spores

Trilete spores

Genus *Concavissimisporites* Delcourt & Sprumont 1955

Type Species *Concavissimisporites verrucosus* Delcourt & Sprumont 1955

Concavissimisporites rugulatus n.sp

Plate 1 figure 1
Holotype. Plate 1, figures 1, sample 5840 (1425), EF: K22-1/2
Type Locality: Well Pastinaca-1, Carbonera Formation, Middle Magdalena Valley, Colombia.
Description: Spores single, symmetry radial, amb triangular obtuse concave, trilete, curvature absent. Laesura distinct, radii mid-sized 13um, TLI 0.92, margo <0.5um wide, commissure straight, borders straight, ends rounded, sporoderm 1-layered, intexine 1.5 um thick. Sculpture rugulate in proximal and distal face, muri 1.5-2um wide, groove 0.5um wide, 4-6um long, elongated.
Dimensions. Equatorial diameter length 27um; equatorial diameter width 27um, length/width 1, nm=1, no=1.
Intraspecific variation and remarks: principal remark is the combination of shape (very concave outline) and sculpture.
Comparisons: *Concavissimisporites variverrucatus* (Couper 1958) Brenner 1963 is verrucate, *Concavissimisporites fossulatus* Dueñas 1980 is fossulate, *Cocavissimisporites punctatus* (Delcourt and Sprumont 1955) Singh 1964 is verrucate to verrruco-rugulae. *Concavissimisporites apiverrucatus* Couper 1958 is densely verrucate.

Inracrassitudisporites interruptus gen. et sp. nov

Plate 1 figure 2
Holotype. Plate 1, figure 2 , sample 2430, EF: L33-1
Type Locality: Well Montoyas-1A, Real Formation Colombia, Middle Magdalena Valley.
Description. Spores single, symmetry radial, amb triangular-obtuse-convex, trilete, curvature absent. Laesura distinct, straight, end rounded, radii long, 14um, reaching the equator, TLI: 0.97, margo indistinct, commissure distinct. Cingulum 6-7um interrupted at radial areas forming an interradial crassitude. The crassitude is equally

wide everywhere excepting in the radial regions where disappears. Sculpture laevigate. Some verrucae close to the joining area of the trilete mark.
Dimensions: Equatorial diameter length 27um; equatorial diameter width 19um, length/width 1.4, nm=1, no=1.
Intraspecific variation and remarks: interradial crassitude equally wide.
Comparisons: *Inracrassitudisporites lorenteae* has cingulum resembling three verrucae.

Inracrassitudisporites lorenteae n.sp

Plate 1, figures 3-4
Holotype. Plate 1 figure 3 sample 1230, EF: S13-4
Paratype. Plate 1, figures 4, sample 410, EF: L18-2
Type Locality: Well Montoyas-1A, Real Formation Colombia, Middle Magdalena Valley.
Description. Spores single, symmetry radial, amb triangular-obtuse-convex, trilete, curvature absent. Laesura distinct, straight, end pointed, radii long, 13um, almost reaching the equator, TLI: 0.96, margo distinct, very thin <0.5um, commissure distinct, intexine 1um. Cingulum 4-6um interrupted in the radial areas forming an interradial crassitude and given the appearance of three big verrucae in each one of the interradial zones. Sculpture verrucate-laevigate?. Verrucae sparse, rounded to irregular in shape at the proximal face, 2-5um thick. Distal face probably laevigate but the appearance is discontinuous due to poor preservation.
Dimensions. Equatorial diameter length 21-(24.6)-27um; equatorial diameter width 14-(19.6)-24um, length/width 1.25, nm=3, no=2.
Intraspecific variation and remarks: Thickness of the cingulum can vary between specimens. Sculpture in the distal face is difficult to establish due to bad preservation. The most prominent feature is the interradial crassitude resembling three big verrucae.
Comparison: The genus *Crassitudisporites* Hiltman 1967 accommodates to trilete spores where in the equatorial region the exine is thickened into a crassitude which is equally wide everywhere and not wider than 1/5 of the spore radius. *Cingulatisporites* Thomson in Thomson & Pflug 1953 accommodates to trilete spores characterized by a narrow cingulum. Spores with a crassitude or a zona therefore should not be assigned to this genus (Jansonius and Hills 1976). *Polypodiaceoisporites* Potonie 1951 ex Potonie 1956 accommodates to trilete spores where the exine in the equatorial region is thickened into a crassitude that is equally wide every where but no wider than 1/5 of the spore radius.

Derivation of the name: Genus named from the term 'interrradial crassitude' and species after

Inracrassitudisporites projectoradialis n.sp

Plate 1 figures 5
Holotype. Plate 1, figure 5, sample 2490, EF: Q51/1-2
Type Locality: Well Montoyas-1A, Real Formation Colombia, Middle Magdalena Valley.
Description: Spores single, symmetry radial, amb convex subtriangular, trilete, curvature absent. Laesura distinct, straight, raddi 10um, TLI 0.7, margo distinct formed by verrucae, commissure distinct. Cingulum 5-6um wide, decreasing toward the radial regions, forming an interradial crassitude, radial zone with big verrucae. Sculpture verrucae in proximal and distal face. In proximal face, verrucae concentrated around the commissure, circular-elongated, sometimes fused. Toward the equator verrucae small, circular, generally isolated. Distal face with concave faceta triangular, surrounded by verrucae producing a 2um wide ring, verrucae circular-elliptic, decreasing in size toward the equator, sometimes fused.
Dimensions: Equatorial diameter length 29um; equatorial diameter width 24um, length/width 1.20, nm=1, no=1.
Intraspecific variation and remarks: interradial crassitude, margo surrounded by verrucae, pattern formed by the sculpture.
Comparisons: *Inracrassitudisporites lorenteae* has cingulum resembling three verrucae; *Inracrassitudisporites interruptus* is laevigate.

Genus *Polypodiaceoisporites* Potonie 1951 ex Potonie 1956

Type Species. *Polypodiaceoisporites speciosus* (Pot.) ex Pot. 1956

Polypodiaceoisporites? murilloi n.sp

Plate 1 figures 6-7
Holotype. Plate 1, figure 6, sample 2490, EF: R26
Paratype. Plate 1, figure 7, sample 2460, EF: Y18-3
Type Locality: Well Montoyas-1A, Real Formation, Middle Magdalena Valley, Colombia.
Description: Spores single, symmetry radial, amb triangular obtuse convex, trilete, curvature absent. Laesura distinct, end pointed, radii long 13um, TLI 0.96, margo

distinct, <0.5um, commissure straight, end pointed, sporoderm 1-layered, intexine 1um thick. Cingulum 4um wide at interradial region and 2um wide at radial region, laevigate. Sculpture striate in both proximal and distal face, striae thin, <0.5um thick, 1-1.5 um apart, arranged parallel to laesura.
Dimensions. Equatorial diameter length 31-(31.5)-32um; equatorial diameter width 24-(25)-26um, length/width 1.2, nm=2, no=2.
Intraspecific variation and remarks: cingulum equally wide everywhere, sculpture striate.
Comparisons: *Striatriletes elegantis* Jaramillo et al 2007 lacks cingulum.

Polypodiaceoisporites? verrucatus n.sp

Plate 1 figures 8-9
Holotype. Plate 1, figures 8, sample 4630, EF: K10-1
Paratype. Plate #, figures 9, sample 2200, EF: N19-4
Type Locality: Well Molino del Viento-1, Guajira, Colombia.
Description: Spores single, symmetry radial, amb triangular obtuse convex, trilete, curvature absent. Laesura distinct, straight, end pointed, radii 10um, TLI 0.76, margo distinct, 2um, formed by verrucae, commissure distinct, intexine 1um. Cingulum 4-4.5um thick, equally wide everywhere, laevigate. Sculpture verrucate in proximal and distal face. In proximal face, verrucae restricted to the laesura, circular to elliptic, 1-2 um wide, <0.5 apart, sporadic small scabrae on the surface. Distal face verrucae, circular to elliptic, verrucae 1-1.5 wide, isolated or fusing each other, densely and homogeneously distributed.
Dimensions. Equatorial diameter length 24-(24.3)-25um; equatorial diameter width 17-(18.3)-20um, length/width 1.3, nm=3, no=3.
Intraspecific variation and remarks: cingulum equally wide everywhere, verrucae restricted to laesura in proximal face.
Comparisons: These specimens cannot be placed in any existing genus. They are provisionally placed in the genus *Polypodiaceoisporites* Potonie 1951 ex Potonie 1956 that is very similar but has reticulate distal face (Jansonius & Hills 1976). The genus *Cingulatisporites* Thomson in Thomson and Pflug 1953 exclude specimens with cingulum surpassing 1/5 of the spore diameter sculpture verrucate to corrugate. *Polypodiaceoisporites? fossulatus* Jaramillo et al 2001 is fossulate on distal face. *Polypodiaceoisporites pseudopsilatus* Lorente 1986 is regulate on distal face. *Polypodiaceoisporites? amazonensis* Silva-Caminha et al 2010 is fossulate on distal face and laevigate in proximal face.

Genus *Scabratriletes* Potonie 1956

Type Species *Scabratriletes cristatus* Potonie 1956

Scabratriletes bacataensis n.sp

Plate 1 figures 10-11
Holotype. Plate 1, figure 10, Montoyas 2430 (908), EF: K37-4
Paratype. Plate 1, figure 11, Montoyas 1590 (901), EF: X26-2
Type Locality: Well Montoyas-1A, Real Formation, Middle Magdalena Valley, Colombia.
Description: Spores single, symmetry radial, amb circular to triangular-obtuse-convex, trilete, curvature absent, radii long reaching the equator, TL=1, commissure straight, ends pointed, sporoderm 2-layered, nexine 0.5um, sexine 1.0um, sculpture scabrate, rounded in plant view, 0.5-1um diameter, 0.5-1.0um apart, densely and evenly distributed over the entire body, sculpture interscabrae psilate, provided with one central and 6 concentrical thinned areas (pseudopores), diameter of the pseudopores 5-7um, provided with an annular thickening of 1.5-2um thick.
Dimensions: equatorial diameter 49um, nm=1,no=4.
Intraspecific variation and remarks: variation in shape and size of the sculpture, principal remark presence of a central and 6 concentrical pseudopores.
Botanical affinity: *Phaeoceros* (Anthocerotaceae, Anthocerotae).

Genus *Verrucatotriletes* Van Hoeken-Klinkenberg 1964

Type Species *Verrucatotriletes bullatus* Van Hoeken-Klinkenberg 1964

Verrucatotriletes ampullatus n.sp

Plate 1 figures 12-14
Holotype. Plate 1, figures 14, sample 1500 (900), EF: F8-3
Paratype. Plate 1, figures 12, sample 2400 (740, EF: B23-3/4
Type Locality: Well Montoyas-1A, Real Formation, Middle Magdalena Valley, Colombia.
Description: Spores single, symmetry radial, amb triangular obtuse straight, trilete, curvature absent, radii long reaching almost the equator 15um, TLI 1, commissure straight, ends pointed, sporoderm 1-layered, intexine <0.5um. Sculpture verrucate in proximal and distal face, verrucae 10-20um wide, 3-5um long, rounded to elongated with vertices rounded, shaped irregulary, distributed irregulary, heterogeneous in size in shape, sculpture interverrucae laevigate.
Dimensions. Equatorial diameter length 26-(27)-30um; equatorial diameter width

23-(26.5)-30um; length/width 1, nm=4, no=4.
Intraspecific variation and remarks: This group has a large intraspecific variation mainly in the size and distribution of the sculptural elements.
Comparisons: *Verrucatotriletes bullatus* van Hoeken-Klinkenberg is bigger.

Anteturma Pollenites

Diploporate

Genus Hexaporotricolpites Boltenhagen 1967

Type Species *Hexaporotricolpites emelianovii*

Hexaporotricolpites striatus n.sp

Plate 2 figures 1-2
Holotype. Plate 2, figure 1, sample outcrop Cristal (605), EF: M12-4
Paratype. Plate 2, figure 2, sample 4740 (672), EF: V54-4
Type Locality: Cristales Outcrop, Carbonera Formation, Llanos, Colombia.
Description: Monad, radial, isopolar, prolate, polar area small, diploporate, colpi very long, almost reaching the polar area, straight, end pointed, slightly marginate, colpus length 28um, colpus width 1um, pori circular, 3.5um diameter, annulate, annulus 1um wide, two pores located near the extremities of each furrow, semitectate, exine ~1um thick, columellae distinct, sculpture striato-reticulate, striae parallel to the colpi, <1um wide, muri 0.5um wide, 0.5um long, striae reticulate, lumina 0.5um wide, rounded, heterobrochate.
Dimensions: Polar diameter length 38, polar diameter width 25, length/width 1.52;nm=1, no=2.
Intraspecific variation and remarks: hexaporotricolpate form with striate-reticulate sculpture.
Comparisons: *Hexaporotricolpites muelleri* Herngreen, 1975 is psilate.

Diporate

Genus Psiladiporites Varma & Rawat 1963 in van der Hammen & Wijmmstra 1964

Psiladiporites ecopetrolis n.sp

Plate 2 figures 3-4
Holotype. Plate 2, figures 3, sample Montoyas1- 2400(609), EF: M13
Type Locality: Well Montoyas A1, Real Formation, Middle Magdalena Valley, Colombia
Description: Monad, bilateral, isopolar, elliptic, diporate, pori circular, 10um diameter, vestibulate, tectate, exine 2um thick, columellae indistinct, sculpture psilate-scabrate, difficult to establish due to poor preservation.
Dimensions: equatorial diameter 46um; polar diameter 32um; polar/equatorial 0.7; nm=1,no=1.
Comparisons: *Psiladiporites minimus* Van der Hammen & Wymstra 1964 has smaller pores; *Psiladiporites reduntantis* Gonzales 1967 has smaller pores.

Inaperturate

Genus *Clavainaperturites* Van der Hammen & Wijmstra 1964

Type Species Clavainaperturites clavatus Van der Hammen & Wijmstra 1964

Clavainaperturites grimsdaleoides n.sp

Plate #2 figures 5-6
Holotype. Plate 2, figure 5, sample Arauca2 -18293.2 (23), EF: K7-4
Paratype. Plate 2, figures 6, sample San Juan Rio Seco 632.7 (703), EF: F-35
Type Locality: Well Arauca-2, Llanos, Colombia.
Description: Monad, bilateral, isopolar, elliptic, inaperturate, intectate, exine 1.5um thick, increasing to 2.5um beneath the sculptural elements, sculpture clavate, clavae 6um long, 3-4um wide, 5-12um apart, head of the clavae 3um wide, 2um long, in plain view circular to slightly elliptical, evenly distributed over the entire grain, deeply rooted sunking the exine, surface interclavae echinate, spines very small, 0.5-1um long, 0.5um apart, densely distributed over the entire grain.
Dimensions: polar diameter 50-(51.7)-53.5um; nm=2, no=3.
Intraspecific variation and remarks: variation in the size of the clavae.
Comparisons: *Grimsdalea magnaclavata* Germeraad et al 1968 has a thinner exine, surface interclavae scabrate to baculate; *Grimsdalea minor* Dueñas 1980 is smaller.

Echipollenites magnificus gen. et sp. nov

Plate 2 figure 7-8
Holotype. Plate 2, figures 7-8, sample 8930 (458), EF: T46
Type Locality: Well Molino del Viento, Guajira, Colombia.
Description: Monad, radial, isopolar, circular, inaperturate, semitectate, nexine 4um thick, sexine 1um thick, sculpture echinate, spines very long, conical, distributed over the entire grain, 4um wide at the base tapering to 2um at the top, 9-10um high, tips rounded, 7um apart, sculpture intespines micropitted.
Dimensions: Polar diameter length 42, polar diameter width 42, length/width 1;nm=1, no=1.
Intraspecific variation and remarks: combination of inaperturate, thickness of the exine and big size of the echinae.

Monosulcate

Genus *Liliacidites* Couper 1953

Type Species *Liliacidites kaitangataensis* **Couper 1953**

Liliacidites titanicus n.sp

Plate 2 figure 9
Holotype. Plate 2, figures 9, sample 5580 (750), EF: G4
Type Locality: Well Montoyas A1, Middle Magdalena Valley, Colombia.
Description: Monad, bilateral, anisopolar, amb elliptic, monosulcate, sulcus simple, long, borders straight, ends pointed, semitectate, exine 4-5um thick, columellae 2.0um thick, 2um wide, some columellae fussing together forming a septum, 1.5um wide, 5-6um long, sculpture reticulate, heterobrochate, lumina 5-12um long, 3-5um wide, elongated-ellipsoidal, muri 2um wide.
Dimensions: equatorial diameter 82um, polar diameter 55um, polar/equatorial 0.7; nm=1, no=1.
Intraspecific variation and remarks: big size, lumina heterobrochate and formation of septum.
Comparisons: *Retimonocolpites nigeriensis* Van Hoeken-Klinkenberg 1966 has lumina decreasing toward the extremes of the grain; *Retimonocolpites retifossulatus* Lorente 1986 is foveoreticulate; *Retimonocolpites tertiarius* Gonzales 1967 is homobrochate; *Liliacidites variegatus* Cooper 1953 is smaller.

Genus *Retimonocolpites* Pierce 1961

Type Species *Retimonocolpites dividuus* Pierce 1953

Retimonocolpites interceptoclavatus n.sp

Plate 2 figure 10
Holotype. Plate 2, figure 10, sample Garzas-1 8050 (1242), EF: M37
Type Locality: Well Garzas-1, Middle Magdalena Valley, Colombia.
Description: Monad, bilateral, anisopolar, prolate, monosulcate, sulcus simple, long, borders straight, ends rounded, 50um long, 3um wide, semitectate, exine 1.5um thick, sculpture reticulate-clavate, reticulate, polygonal, vertices angular to rounded, duplicolumellate, heterobrochate, lumina 2-5um diameter, muri 1.0um wide, clavae when present located at the intersection of murii, 3-5um long, 2um wide, caput 1.5-3um diameter.
Dimensions: equatorial diameter 47um, polar diameter 33um, polar/equatorial 0.7; nm=1, no=1.
Intraspecific variation and remarks: monosulcate, duplicolumellate, sporadic clavae at the interception of muri.

Pantoporate

Genus *Echiperiporites* Van der Hammen & Wymstra 1964 emend. Anzotegui 1996

Type Species Echiperiporites akanthos Van der Hammen & Wymstra 1964

Echiperiporites magnoexinatus n.sp

Plate 3 figure 1
Holotype. Plate 3, figure 1, sample 5910 (752), EF: K-34
Type Locality: Well Montoyas-1, Middle Magdalena Valley, Colombia.
Description: Monad, radial, isopolar, spherical, pantoporate, ~34 pores, pori circular, 2-3um diameter, pori annulate, 2um wide, intectate, nexine 4um thick, decreasing 2um near the pores, sculpture echinate, spines with bottle shape, distributed over the entire grain, 3um wide at the base, tapering to 2um at the top, 10-11um high, tips rounded, 5-7um apart, sculpture interspines psilate.
Dimensions: Polar diameter length 43, polar diameter width 43, length/width 1; nm=1, no=1.
Intraspecific variation and remarks: pantoporate with spines.
Comparisons: *Echiperiporites estelae* Germeraad et al 1968 is tectate, *Magnaperiporites spinosus* Gonzales 1967 has more than 50 pores, *Echiperiporites psilatus* Jaramillo et al 2010 has a thinner exine.

Echiperiporites psilatus n.sp

Plate 3 figures 2-5
Holotype. Plate 3, figure 4, sample 15200 (75), EF: J21-3
Paratype. Plate 3, figure 2 , sample 14230 (61), EF: E16-3
Type Locality: Well Arauca-2, Carbonera Formation, Llanos, Colombia.
Description: Monad, radial, isopolar, circular, pantoporate, pori circular, 4um diameter, annulate, annulus 3um wide, intectate, nexine 1-2um thick, sculpture echinate, spines very long, distributed over the entire grain, spines 2.5um wide at the base tapering to 1um at the top, 5-6um high, tips rounded, 5-6um apart, sculpture interspines psilate.
Dimensions: Polar diameter length 43.5, polar diameter width 43.5, length/width 1;nm=1, no=2.
Intraspecific variation and remarks: variation in the size of the spines and thickness of the nexine.
Comparisons: *Echiperiporites cricotriporatiformis* Jaramillo et al 2010 is triporate and spines are shorter (verrucae-like), *Echiperiporites akanthos* van der Hammen & Wymstra 1964, is smaller, tectate and spines are shorter; *Echiperiporites estelae* Germeraad et al 1968 is tectate and surface interspines is micropitted; *Echiperiporites lophatus* Silva-Caminha et al 2010 is tectate, has endospores simple, echinae restricted to the tectum surrounding the pores resembling a lophate ornamentation; *Echiperiporites intectatus* Silva-Caminha et al 2010 is smaller, has spines showing two distribution patterns and interspine surface is slightly scabrate.

Genus *Psilaperiporites* Regali 1974

Type Species *Psilaperiporites robustus* Regali 1974

Psilaperiporiporites intensus nov.sp

Plate 4 figures 1-2
Holotype. Plate 4, figure 1, sample Gibraltar -4690 (246), EF: P19-3
Paratype. Plate 4, figure 2, sample Volcanera -13100 (90), EF: J18-4
Type Locality: Well Gibraltar, Llanos foothills, Colombia.
Description: Monad, radial, isopolar, amb circular, pantoporate, ~36 pores, 3-4um apart, pori simple, circular, 3um wide, 3um long, tectate, exine 1um thick, nexine <0.5um thick, columellae distinct, sculpture psilate.
Dimensions: equatorial diameter 23 (25) 28; polar diameter 28 (33) 37
Comparisons: *Psilaperiporites multiporatus* Hoorn 1994 is bigger and has 9-16 annulate pores, *P.suarezi* Vajda-Sanvanez 1999 has 16-34 pores, *P. brenacii* Silva-

Caminha et al 2010 has 10 pores, *Parsonidites?* sp.2 Jaramillo & Dilcher 2001 has 12 pores, *Multiporopollenites pauciporatus* Jaramillo & Dilcher 2001 has 18-23 pores.

Stephanocolpate

Genus *Clavastephanocolpites* van der Hammen & Wijmstra 1964

Type Species *Clavastephanocolpites crotonoides* van der Hammen & Wijmstra 1964

Clavastephanocolpites bariorum nov.sp

Plate 4 figures 3
Holotype. Plate 4, figure 3, sample Mucurera3-2670 (398), EF: O15-3
Type Locality: Well Mucurera-3, Catatumbo, Colombia.
Description: Monad, radial, isopolar, amb circular, stephanocolpate, five colpate, colpi simple, mid sized, borders straight, end pointed, polar area large, 15um wide, intectate, nexine 1um thick, sculpture clavate, clavae 1.0-1.5um long, 0.5um wide, 0.5um apart, densely an evenly distributed over the entire grain, circular in plain view.
Dimensions: equatorial diameter 32um, nm=1, no=1.
Comparisons: *Clavastephanocolpites crotonoides* van der Hammen & Wymstra 1964 has croton pattern.

Genus *Retistephanocolpites* Leidelmeyer 1966

Type Species *Retistephanocolpites angelii* Leidenmeyer 1966

Retistephanocolpites timizaensis n.sp

Plate 4 figures 4-5
Holotype. Plate #4 figure 4, sample Guarumo1 -5170 (956), EF: R23-4
Paratype. Plate 4, figure 5, sample Higueron1 -5760 (555), EF: M-15
Type Locality: Well Guarumo-1, Middle Magdalena Valley, Colombia.
Description: Monad, radial, isopolar, circular, stephanocolpate, five colpate, ectocolpi costate, colpi short, borders straight, ends pointed, 10um long, slightly protuding, polar area very large, 25um wide, semitectate, exine 2.5um thick, nexine 1.5um thick, increasing to 1.5um near colpi, columellae distinct, 1um thick, 1.5um wide, 1um apart, tectum restricted to the muri, sculpture reticulate, heterobrochate, lumina 4-6um wide, strongly muricurvate, muri 0.5um wide, pluricolumellate, tip of columellae visible in plant view, given perforate aspect to the muri.
Dimensions: equatorial diameter 34 (35) 37, nm=3, no=3.

Intraspecific variation and remarks: stephanocolpate, muricurvate, columellae visible given a perforate aspect to the muri.
Comparisons: *Stephanocolpites costatus* van der Hammen 1954 has a zonate endocingulum, *Retistephanocolpites tropicalis* Dueñas 1980 has smaller lumina (0.5um wide), *Retistephanocolpites* sp.2 Jaramillo & Dilcher 2001 is simplicolumellate and lumina is polygonal.

Stephanocolporate

Genus *Verrustephanocolporites* Salard-Cheboldaeff 1978

Type Species: *Verrustephanocolporites complanatus* Salard-Cheboldaeff 1978

Verrustephanocolporites pastinensis n.sp

Plate 4 figure 6
Holotype. Plate 4, figure 6, sample Pastinaca-6430 (1427), EF: E41-1/2
Type Locality: Well Pastinaca-1, Llanos, Colombia.
Description: Monad, radial, isopolar, amb circular, stephanocolporate, four colporate, ectocolpi very short, borders straight, ends pointed, endospores costate, lalongate, 5um long, 2um wide, costae 3.5um wide, 2um thick, slightly protruding, tectate, exine 1.5um thick, columellae indistinct, sculpture verrucate, verrucae 1um wide, <0.5 long, distributed densely, rounded to elongated.
Dimensions: equatorial diameter 26um.
Intraspecific variation and remarks: combination of stephanocolporate and verrucae.

Stephanoporate

Genus *Retistephanoporites* Gonzales 1967

Type Species *Retistephanoporites angelicus* Gonzales 1967

Retistephanoporites yariguensis n.sp

Plate 4 figures 7-9
Holotype. Plate 4, figure 7, sample Montoyas 7390 (762), EF: K45-4
Paratype. Plate 4, figure 9, sample Montoyas 7250 (761), EF: R12-4
Type Locality: Well Montoyas A1, Real Formation, Middle Magdalena Valley, Colombia.

Description: Monad, radial, isopolar, amb circular, stephanoporate, 4-5 porate, pori distinct, circular, 3um wide, 3um long, pori costate, costae 5um wide, 2.5um thick, slightly protruding, tectate, exine 2um thick, nexine 0.5um thick, columellae <1um thick, tectum 0.5um thick, columellae distinct, <1um wide, 1-1.5 apart, sculpture foveoreticulate, homobrochate, lumina 1-2um wide, 1-2um long, elongate to subrounded to polygonal, muri 1-1.5um wide, pluricolumellate.
Dimensions: equatorial diameter 28-(29)-30um; nm=2,no=2.
Comparisons: *Retistephanoporites crassiannulatus* Lorente 1986 is reticulate and pori annulate.

Trichotomosulcate

Genus *Trichotomosulcites* Couper 1953

Type Species *Trichotomosulcites subgranulatus* Couper 1953

Trichotomosulcites clavatus n.sp

Plate 5 figures 1-2
Holotype. Plate 5, figures 2, sample Cumarito1- 2340(609), EF: C17-1
Paratype. Plate 5, figures 1, sample Tocoragua-14320 (868), EF: N14
Type Locality: Well Cumarito, Llanos, Colombia.
Description: Monad, radial, anisopolar, amb triangular obtuse convex, trichotomosulcate, colpus long, almost reaching equator, ends open to rounded, semitectate, exine 1.5-2um thick, columellae distinct, sculpture clavate, clavae variable in shape and size, 1-5um wide, 2-6 long, in plan view circular, densely and distributed all over the grain, caput flat or rounded, sculpture interclavae psilate.
Intraspecific variation and remarks: trichotomosulcate, clavate. Variation in the size and density of clavae.
Dimensions: equatorial diameter 43-(45.5)-48um; nm:4, no=4.
Comparisons: *Trichotomosulcites laevigatus* Boltenhagen 1976 is psilate; *Trichotomosulcites ornatus* Boltenhagen 1976 is reticulate.

Tricolporate

Genus *Bombacacidites* Couper 1960

Type species Bombacacidites bombaxoides Couper 1960

Bombacacidites apocolpicus n.sp

Plate 5 figures 3-4

Holotype. Plate 5, figure 3, sample 12636.3 (623), EF: R25-2
Paratype. Plate 5, figure 4, sample 5330 (138), EF: G44-1
Type Locality: Well La Gloria-2, Llanos, Colombia.
Description: Monad, radial, isopolar, amb triangular obtuse straight, tricolporate, planaperturate, colpi very long, ends pointed, reaching the border of the apocolpia, ectocolpi marginate, 2um wide, 2um thick, surrounding the entire colpi, pori indistinct, lalongate 5X3 um, tectate, exine 1.5um thick, nexine 0.5um thick, columellae distinct, <0.5 thick, 0.5-1um apart, tectum <0.5um thick, tectum thickness increases slightly around the colpi, exine with a very distinct thickening at apocolpia forming a very distinctive circular dark area, of 5um wide. Sculpture reticulate, homobrochate, simplicollumelate, lumina 0.5-1um wide, circular, muri 0.5um wide, reticula absent in the margin of the colpi and in the circular dark area where is psilate.
Dimensions: Polar diameter length 25-(25)-25, polar diameter width 25-(25)-25, length/width 1; nm=2, no=2.
Intraspecific variation and remarks: distinct thickening at apocolpia.
Comparisons: *Bombacacidites poloanularis* Jaramillo et al 2007 is costate, triangular obtuse convex, has shorter colpi and lumina is smaller. *Bombacacidites pulcherrimus* n.sp has shorter colpi and has a distinctive Y shape mark at apocolpia.

Bombacacidites concavoides n.sp

Plate 5 figures 5-7
Holotype. Plate 5, figure 5, sample 3195 (562), EF: U9-3
Paratype. Plate 5, figure 7, sample 1330 (122), EF: E16-3
Type Locality: Well Arama-1, Carbonera Formation, Llanos, Colombia.
Description: Monad, radial, isopolar, amb triangular obtuse concave, tricolporate, planaperturate, colpi short 4um, ends rounded, costae distinct 2um wide, pori indistinct, circular 3X3um, tectate, exine 1.5um thick, nexine 0.5um thick increasing around the colpi, columellae distinct 0.5um thick, 0.5um wide, 0.5-1 apart, tectum 0.5um thick. Sculpture reticulate-foveolate, reticulate at apocolpia and equatorial areas surrounding the colpi, lumina heterobrochate, 1.5-2um wide, subpolygonal, muri 0.5um wide, simplicolumellate, reticulum changes abruptly to foveolae at mesocolpia, foveola ~1um wide, circular, 0.5um apart, densely and homogeneously distributed.
Dimensions: Polar diameter length 29-(35.6)-43, polar diameter width 28-(36)-43, length/width 1; nm=3, no=4.

Intraspecific variation and remarks: this group has variation in the size of the lumina, principal remark is the concave outline.
Comparisons: *Bombacacidites annae* (van der Hammen 1954) Leidelmeyer 1966 is circular, *Bombacacidites soleaformis* Muller et al 1987 is homobrochate.

Bombacacidites gemmatus n.sp

Plate 5 figure 8
Holotype. Plate 5, figure 8, sample 5220 (1547), EF: M13-3
Type Locality: Well Yoli-1, Llanos, Colombia.
Description: Monad, radial, isopolar, amb triangular obtuse convex, tricolporate, planaperturate, colpi short, ectocolpi costate, colpi slightly protruding, costae 3um wide, endopori lalongate, tectate, exine 1.5um thick, nexine <0.5um thick, columellae distinct 1um thick, tectum <0.5um thick. Sculpture gemmate-microreticulate, gemmae distributed sparsely, 1.5um long, 2um wide, circular in plane and cross view, surface intergemmae microreticulate, brochi homobrochate, lumina <1um wide, rounded, distributed densely and homogeneously, muri <0.5um wide.
Dimensions: Polar diameter length 56, polar diameter width 53, length/width 1; nm=1, no=1.
Intraspecific variation and remarks: combination of *Bombacacidites*-type and gemmate sculpture.

Bombacacidites inversus n.sp

Plate 6 figure 1
Holotype. Plate 6, figure 1, sample 2280 (392), EF: F26
Type Locality: Mucurera-3, Catatumbo, Colombia.
Description: Monad, radial isopolar, amb circular, tricolporate, planaperturate, colpi simple, short, ends rounded, pori distinct, lalongate, 5X9um, costate, semitectate, exine 2um thick, columellae distinct, 1um thick, 4-5um apart at mesocolpia, tectum continuous at apocolpia and almost absent at mesocolpia. Sculpture reticulate, heterobrochate, at apocolpia reticula confined to a circular area of 13um in diameter, lumina 2-3um wide, elongated to sub-rounded, muri 1um wide, reticula at mesocolpia markedly different, tectum is almost absent, curvimurate, lumina 5-9um wide, muri 0.5um wide, nexine slightly scabrate at mesocolpia.
Dimensions: Polar diameter length 52, polar diameter width 52, length/width 1; nm=1, no=1.
Intraspecific variation and remarks: *Bombacacidites* type with unique pattern of lumina, larger at mesocolpia than at apocolpia.

Bombacacidites pulcherrimus n.sp

Plate 6 figure 2

Holotype. Plate 6, figure 2, sample 9121 (1471), EF: P17-1

Type Locality: Well Akacias-11, Llanos, Colombia.

Description: Monad, radial, anisopolar, amb triangular obtuse straight, tricolporate, planaperturate, colpi short 5um length, 1um wide, narrow, end pointed, ectocolpi costate, costae 2-2.5um wide, endopores indistinct, semitectate, exine 1.5um thick, exine thinner toward vertices of the grain, columellae distinct, thickening of the exine at proximal face forming a very distinctive Y shape. Sculpture reticulate-fossulate, fossuloreticulate at apocolpia and colpi margins gradually changing to reticulate at mesocolpia, heterobrochate, 1.5um wide, microreticulate at vertices of the grain, homobrochate, < 1um wide.

Dimensions: Polar diameter length 37, polar diameter width 36, length/width 1; nm=1, no=1.

Intraspecific variation and remarks: distinctive Y shape at apocolpia.

Comparisons: Differs from other Bombacacidites in the distinctive Y shape mark at apocolpia.

Bombacacidites verrucatus n.sp

Plate 6 figure 3-4

Holotype. Plate 6, figures 4, sample 3502.8 (1549), EF: N19

Paratype. Plate 6, figures 3, sample 7331.3 (1548), EF: F46-4

Type Locality: Well Caño Sur Este-6, Llanos, Colombia.

Description: Monad, radial, isopolar, amb triangular obtuse convex, tricolporate, planaperturate, colpi short, ends pointed, costate, pori indistinct, semitectate, exine 1.5um thick, nexine <0.5um thick, columellae distinct, <1um thick, <0.5um apart. Sculpture reticulate-verrucate, heterobrochate, lumina circular, 1um wide, muri <0.5 thick, verrucae over entire surface, circular in plain view, +- densely distributed, homogeneous in size and shape, 1-2um wide, 0.8um height.

Dimensions:

Intraspecific variation and remarks: combination of Bombacacidtes-type and verrucate sculpture.

Comparisons: *Bombacacidites gemmatus* n.sp is bigger and sculpture is gemmate.

Genus *Rugutricolporites* Gonzales Guzman 1967

Type Species *Rugutricolporites felix* Gonzales Guzman 1967

Rugutricolpites etayoi nov.sp

Plate 6 figure 5
Holotype. Plate 6, figure 5, sample Mucurera3-2670 (398), EF: O15-3
Type Locality: Well Tocoragua-1, Llanos, Colombia.
Description: Monad, radial, isopolar, amb triangular-obtuse-convex, tricolporate, apocolpial area small, 5um wide, colpi long, ectocolpi simple, endocolpi costate, borders straight, end rounded pori lalongate, intectate, sculpture rugulate, rugulae long, curved, <1um wide.
Dimensions: equatorial diameter 26um, nm=1, no=1.
Comparisons: *Rugutricolporites felix* Gonzales 1967 is tectate and has short rugulae.

Triporate

Clavatriporites dispersiclavatus gen. et sp. nov

Plate 6 figure 6
Holotype. Plate 6, figures 6, sample Gibraltar 5720 (144), EF: N19
Type Locality: Well Gibraltar-1, Piedemonte Llanero, Colombia.
Description: Monad, radial isopolar, amb circular, triporate, pori very large and distinct, lalongate, 7X13um, slightly annulate, intectate, nexine 1um thick increasing to 2um near the pores, sculpture clavate, clavae, 1-2um high, 1um wide, 1-2 um apart, densely and evenly distributed over the entire grain, in plain view clavae circular, surface interclavae psilate.
Dimensions: equatorial diameter 38um; nm=1,no=1.
Comparisons: *Clavatricolpites densiclavatus* Jaramillo & Dilcher 2001 is tricolpate; *Crototricolpites finitus* Silva-Caminha et al 2010 is tricolpate and clavae densely distributed.

Clavatriporites spicatus n.sp

Plate 6 figures 7-8
Holotype. Plate 6, figures 7, sample 10261.5 (1551), EF: K20-4
Paratype. Plate 6, figures 8, sample 6874.4 (1573), EF: O51-2
Type Locality: Well Apiay-22, Carbonera Formation, Llanos, Colombia.
Description: Monad, radial, isopolar, amb circular, triporate, pori lalongate, 17X7um, intectate. Sculpture clavate-baculate, clavae 2-2.5um high, 1-1.5um wide, 1-2um apart, densely and evenly distributed over the entire grain, head of the clavae circular in

plant view, ovoid in cross section, surface interclavae psilate-baculate, baculae 1um high, 0.5um wide, 0.5um apart.
Dimensions: Polar diameter length 42-(46)-50, polar diameter width 42-(46)-50, length/width 1; nm=3, no=4.
Intraspecific variation and remarks: principal remark is the combination of aperture and sculpture and the size of the pori, instraspecific variation in size of clavae.
Comparisons: *Bacutriporites echinatus* Jaramillo et al 2001 is tectate, baculate-echinate.

Fossutriporites cerebriformis gen. et sp. nov

Plate 6 figure 9
Holotype. Plate 6, figure 9, sample San Juan-1 6270(588), EF: R25
Type Locality: Well San Juan-1, Llanos, Colombia.
Description: Monad, radial, isopolar, amb triangular-obtuse-convex, triporate, planaperturate, costate, pori lalongate, tectate, nexine 0.5um thick, columellae distinct, 0.5um thick, tectum 0.5um, nexine increasing to 1um toward the pore, sculpture fossulate, fossulae 0.5um wide, 3-5um long, pattern resembling the convolutions of a brain, muri 0.5um wide, fossulae evenly and uniformly distributed over the entire grain.
Dimensions: equatorial diameter 47um; nm=1,no=1.
Intraspecific variation and remarks: combination of triporate aperture and fossulae.
Comparisons: *Florschuetzia meridionalis* Germeraad 1968 has thicker exine (3um).

Genus *Foveotriporites* Gonzales 1967

Type Species *Foveotriporites hammenii* Gonzales 1967

Foveotriporites motiloneorum n.sp

Plate 6 figures 10
Holotype. Plate 6, figure 10, sample Arauca-2 18322.8 (30), EF: L51
Type Locality: Well Arauca-2, Llanos Basin, Colombia.
Description: Monad, radial, isopolar, amb triangular-obtuse-convex, triporate, pori distinct, costate, circular, 10um long, slightly protruding, costae 4um wide, tectate, exine 3-5um thick, nexine 1um thick, nexine increasing near the pore to 2um, columellae indistinct, 0.5um thick, tectum 0.5-1um thick, sculpture foveolate,

homobrochate, foveolae 1um long, 0.5-1um wide, slightly elongated, 1.0-1.5um apart, densely and evenly distributed over the entire grain.
Dimensions: equatorial diameter 37um, nm=1, no=1.
Comparisons: *Foveotriporites hammenii* Gonzales 1967 is bigger (54um), columellae distinct and lumina wider (1.5-3.5um), *Foveotriporites* sp.1 Jaramillo & Dilcher 2001 is bigger (50um) and tectum is thinner.

Genus *Gemmatriporites* Meon 1991

Type Species *Gemmatriporites harianensis* Meon 1991

Gemmatriporites duquei n.sp

Plate 6 figures 1
Holotype. Plate 6, figures 11, sample Arauca-2 -14560 (69), EF: S59-2
Type Locality: Well Arauca-2, Llanos, Colombia.
Description: Monad, radial, isopolar, amb triangular-obtuse-convex, triporate, pori distinct, costate, circular, 5um long, slightly protruding, costae 2um wide, tectate, exine 1.5um thick, nexine 1um thick increasing 2um near pore, columellae indistinct, sculpture gemmate, gemmae 1.0-1.5um high, 1.0-2.0um wide, circular in plain view, 3-5um apart, sparsely and evenly distributed over the entire grain, surface intergemmae micropitted.
Dimensions: equatorial diameter 36um, nm=1, no=1.
Comparisons: *Crassitriapertites gemmatus* Herngreen 1975 has a thicker exine.

Plate 1

1. *Concavissimisporites rugulatus* sp. nov (Holotype).
2. *Inracrassitudisporites interruptus* sp.nov (Holotype).
3. *Inracrassitudisporites lorenteae* sp.nov (Holotype).
4. *Inracrassitudisporites lorenteae* sp.nov (Paratype).
5. *Inracrassitudisporites projectoradialis* sp.nov (Holotype).
6. *Polypodiaceoisporites? murilloi* sp.nov (Holotype).
7. *Polypodiaceoisporites? murilloi* sp.nov (Paratype).
8. *Polypodiaceoisporites? verrucatus* sp.nov (Holotype).
9. *Polypodiaceoisporites? verrucatus* sp.nov (Paratype).
10. *Scabratriletes bacataensis* sp.nov (Holotype).
11. *Scabratriletes bacatensis* sp.nov (Paratype).
12. *Verrucatotriletes ampullatus* sp.nov (Paratype).
13. *Verrucatotriletes ampullatus* sp.nov
14. *Verrucatotriletes ampullatus* sp.nov (Holotype).

Plate 2

1. *Hexaporotricolpites striatus* sp. nov (Holotype).
2. *Hexaporotricolpites striatus* sp. nov (Paratype).
3. *Psiladiporites ecopetrolis* sp.nov (Holotype).
4. *Psiladiporites ecopetrolis* sp.nov.
5. *Clavainaperturites grimsdaleoides* sp.nov (Holotype).
6. *Clavainaperturites grimsdaleoides* sp.nov (Paratype).
7. *Echipollenites magnificus* sp.nov (Holotype).
8. *Echipollenites magnificus* sp.nov.
9. *Liliacidites titanicus* sp.nov (Holotype).
10. *Retimonocolpites interceptoclavatus* sp.nov (Holotype).

Plate 3

1. *Echiperoporites magnoexinatus* sp.nov. (Holotype).
2. *Echiperiporites psilatus* sp.nov. (Paratype).
3. *Echiperiporites psilatus* sp.nov.
4. *Echiperiporites psilatus* sp.nov (Holotype)
5. *Echiperiporites psilatus* sp.nov.

Plate 4

1. *Psilaperiporites intensus* sp.nov. (Holotype).
2. *Psilaperiporites intensus* sp.nov. (Paratype).
3. *Clavastephanocolpites bariorum* sp.nov (Holotype).
4. *Retistephanocolpites timizaensis* sp.nov (Holotype).
5. *Retistephanocolpites timizaensis* sp.nov (Paratype).
6. *Verrustephanocolporites pastinensis* sp.nov (Holotype).
7. *Retistephanoporites yariguensis* sp.nov (Holotype).
8. *Retistephanoporites yariguensis* sp.nov
9. *Retistephanoporites yariguensis* sp.nov (Paratype)

Plate 5

1. *Trichotomosulcites clavatus* sp.nov. (Paratype)
2. *Trichotomosulcites clavatus* sp.nov. (Holotype)
3. *Bombacacidites apocolpicus* sp.nov. (Holotype)
4. *Bombacacidites apocolpicus* sp.nov. (Paratype)
5. *Bombacacidites concavoides* sp.nov. (Holotype).
6. *Bombacacidites concavoides* sp.nov.
7. *Bombacacidites concavoides* sp.nov. (Paratype).
8. *Bombacacidites gemmatus* sp.nov. (Holotype).

Plate 6

1. *Bombacacidites inversus* sp. nov (Holotype).
2. *Bombacacidites pulcherrimus* sp.nov. (Holotype).
3. *Bombacacidites verrucatus* sp. nov (Paratype).
4. *Bombacidites verrucatus* sp.nov. (Holotype).
5. *Rugutricolpites etayoi* sp.nov. (Holotype).
6. *Clavatricolpites dispersiclavatus* sp.nov. (Holotype).
7. *Clavatriporites spicatus* sp.nov (Holotype).
8. *Clavatriporites spicatus* sp.nov (Paratype).
9. *Fossutriporites cerebriformis* sp.nov (Holotype).
10. *Foveotriporites motiloneorum* sp.nov. (Holotype).
11. *Gemmatriporites duquei* sp.nov. (Holotype).

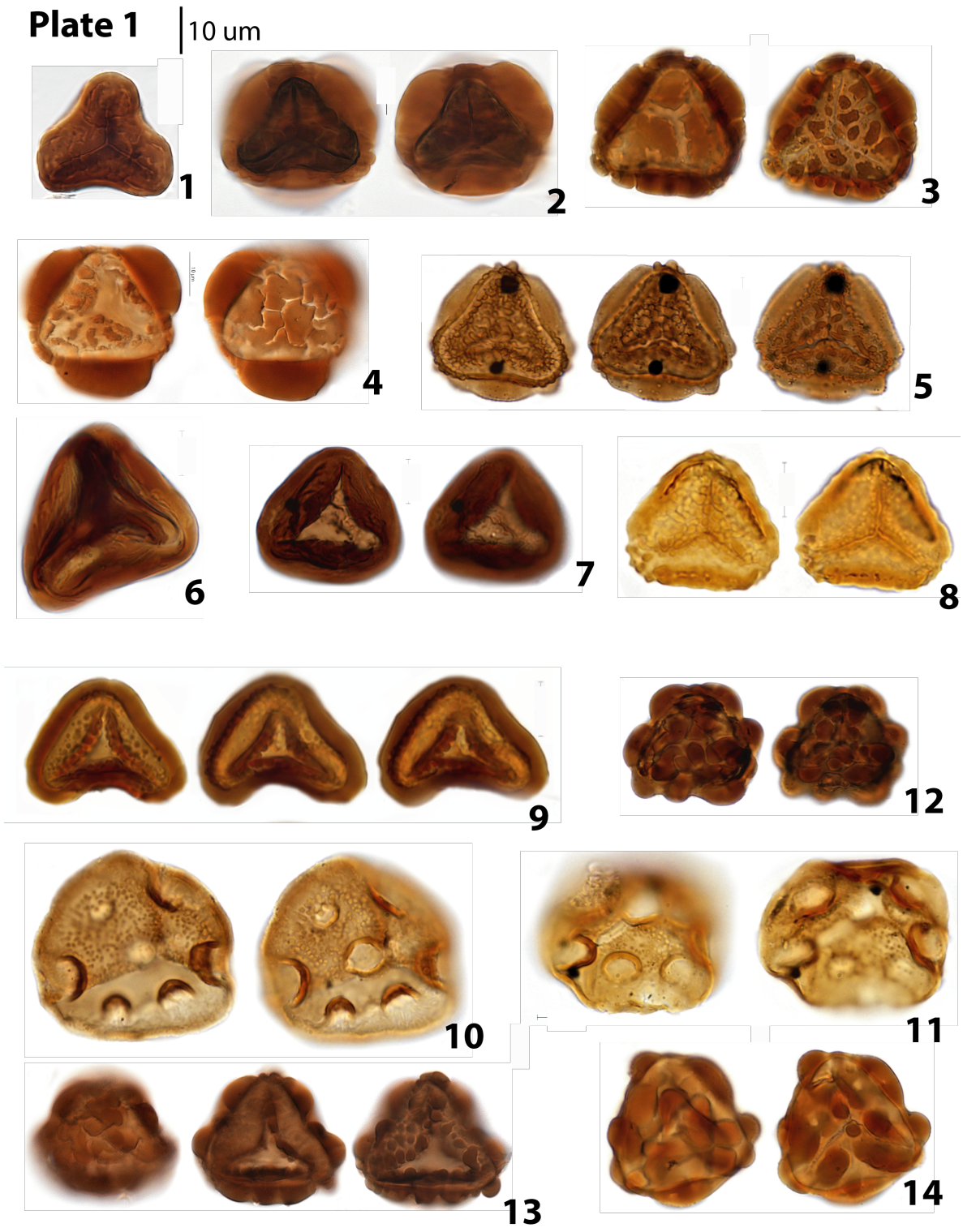

Plate 1. (**1**) *Concavissimisporites rugulatus* sp. nov; **(2)** *Intracrassitudisporites interruptus* sp.nov**; (3,4)** *Intracrassitudisporites lorentae* sp.nov; **(5)** *Intracrassitudisporites projectoradialis* sp.nov; **(6,7)** *Polypodiaceoisporites? murilloi* sp.nov; **(8,9)** *Polypodiaceoisporites? verrucatus* sp.nov; **(10,11)** *Scabratriletes bacatensis* sp.nov; **(12,13,14)** *Verrucatotriletes ampullatus* sp.nov;

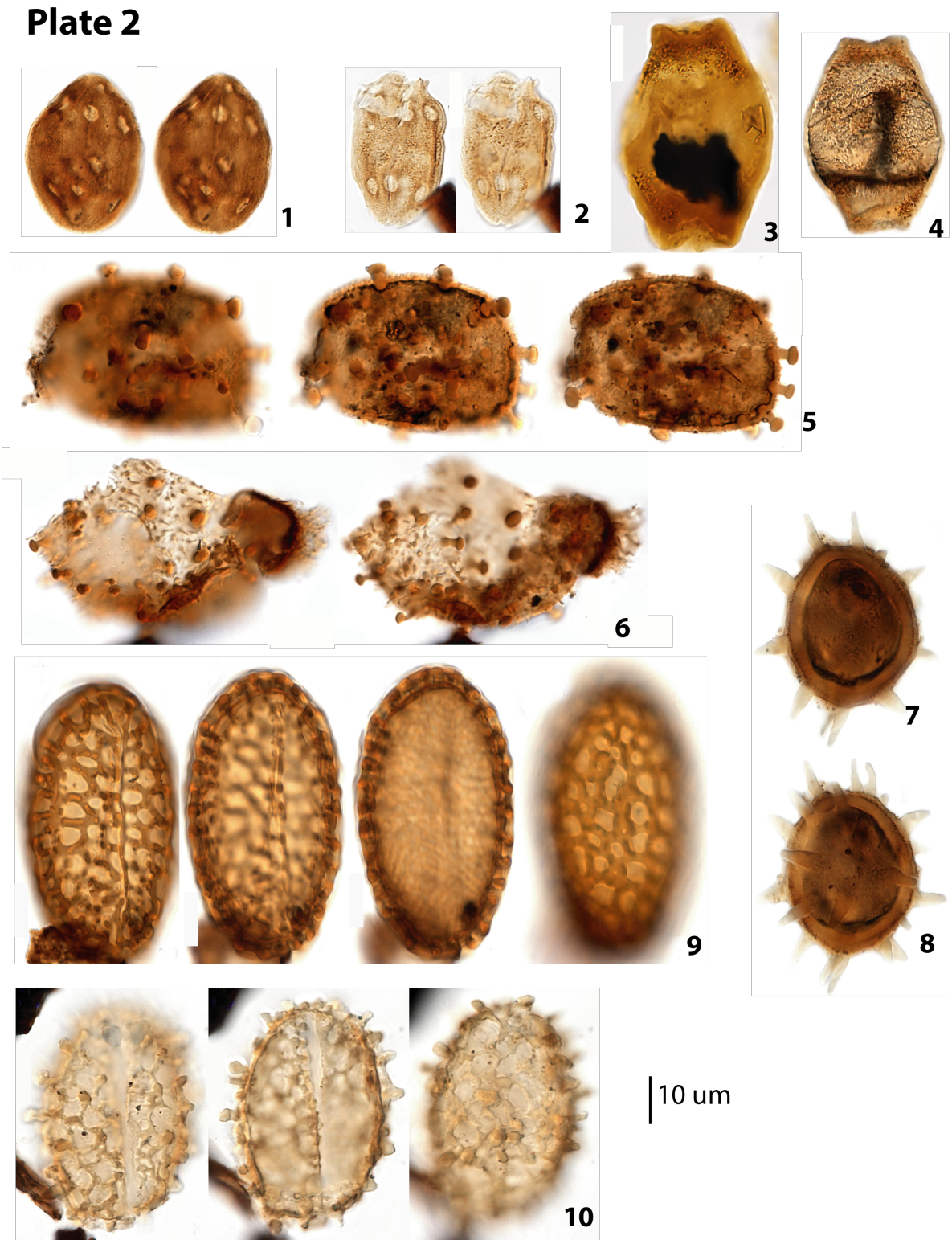

Plate 2. (1,2) *Hexaporotricolpites striatus* sp.nov; **(3,4)** *Psiladiporites ecopetrolis* sp. nov; **(5,6)** *Clavainaperturites grimsdaleoides* sp.nov; **(7,8)** *Echipollenites magnificus* sp.nov**; (9)** *Liliacidites titanicus* sp.nov; **(10)** *Retimonocolpites interceptoclavatus* sp.nov.

Plate 3

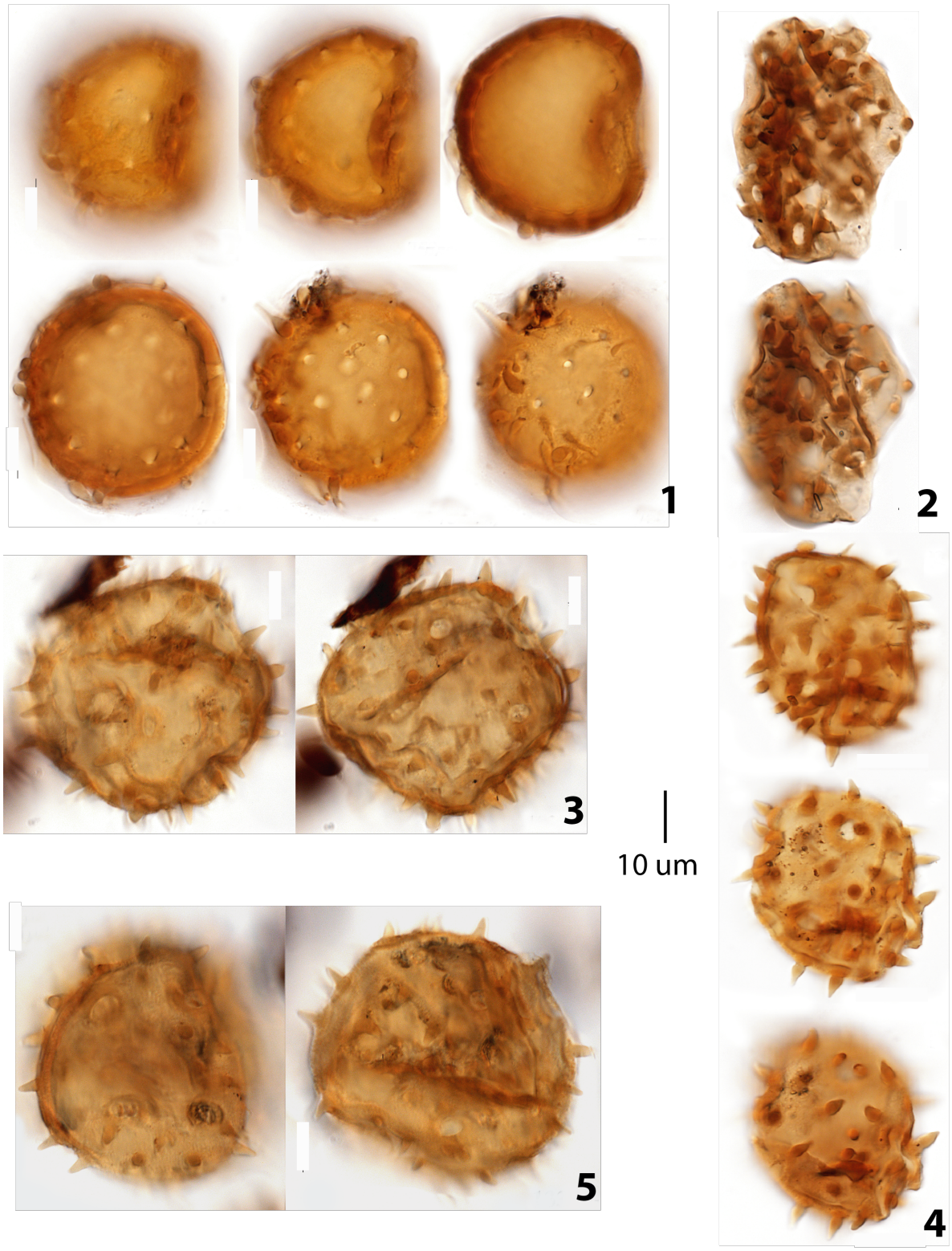

Plate 3. (1) *Echiperiporites magnoexinatus* sp.nov; **(2,3,4,5)** *Echiperiporites psilatus* sp.nov

Plate 4

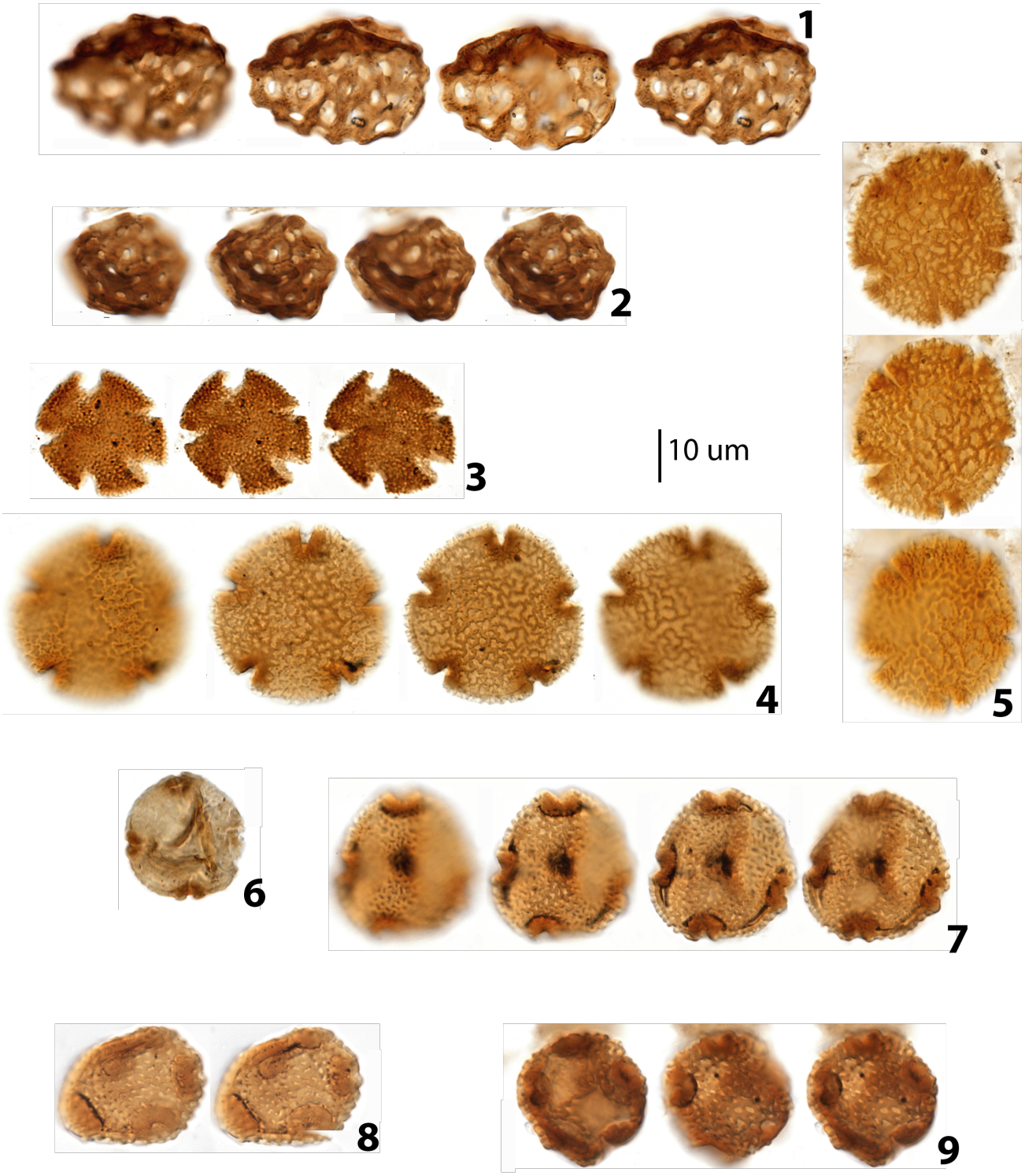

Plate 4. (1,2) *Psilaperiporites intensus* sp.nov; **(3)** *Clavastephanocolpotes bariorum* sp.nov; **(4,5)** *Retistephanocolpites timizaensis* sp.nov; **(6)** *Verrustephanocolporites pastinensis* sp.nov; **(7,8,9)** *Retistephanoporites yariguensis* sp.nov.

Plate 5

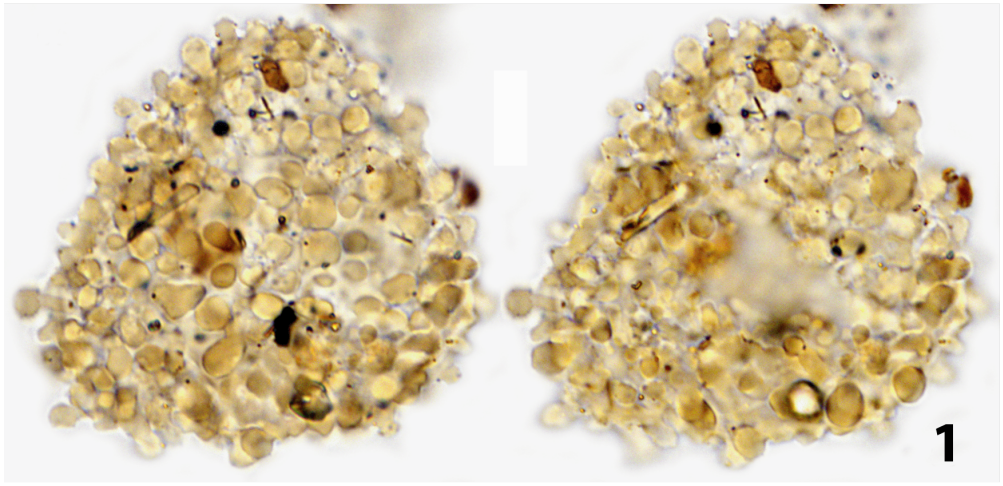

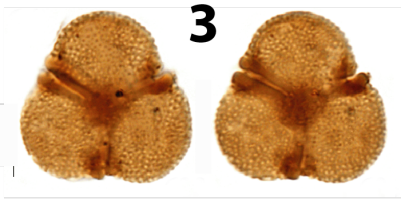

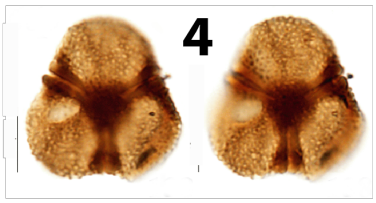

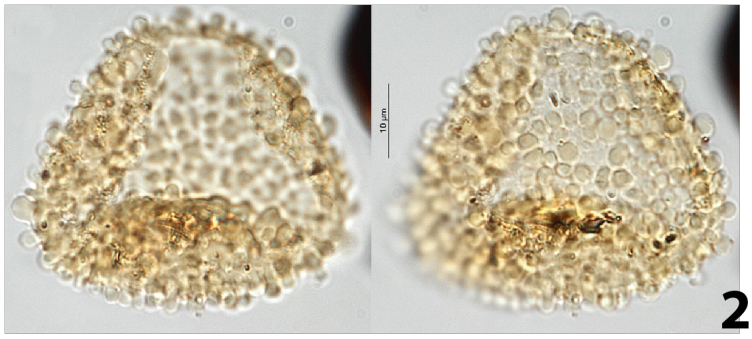

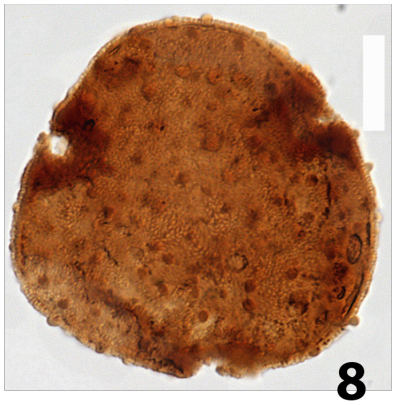

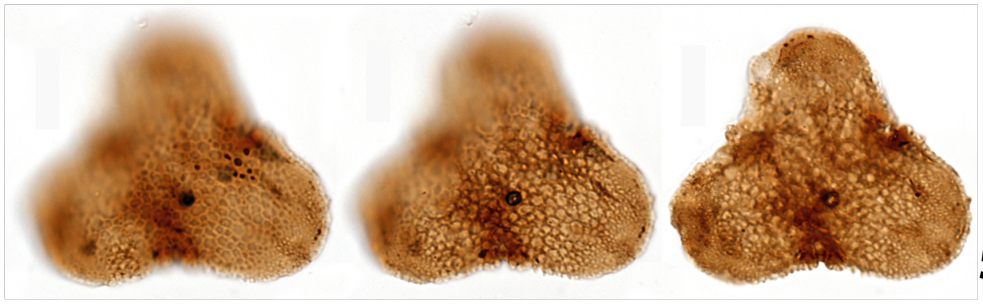

10 um

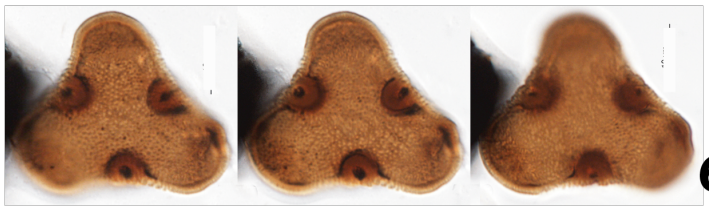

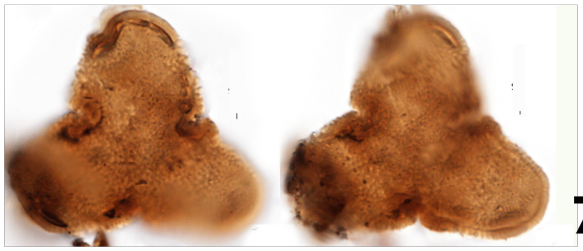

Plate 5. (1,2) *Trichotomosulcites clavatus* sp.nov; **(3,4)** *Bomobacacidites apocolpicus* sp.nov; **(5,6,7)** *Bombacacidites concavoides* sp.nov; **(8)** *Bombacacidites gemmatus* sp.nov.

Plate 6

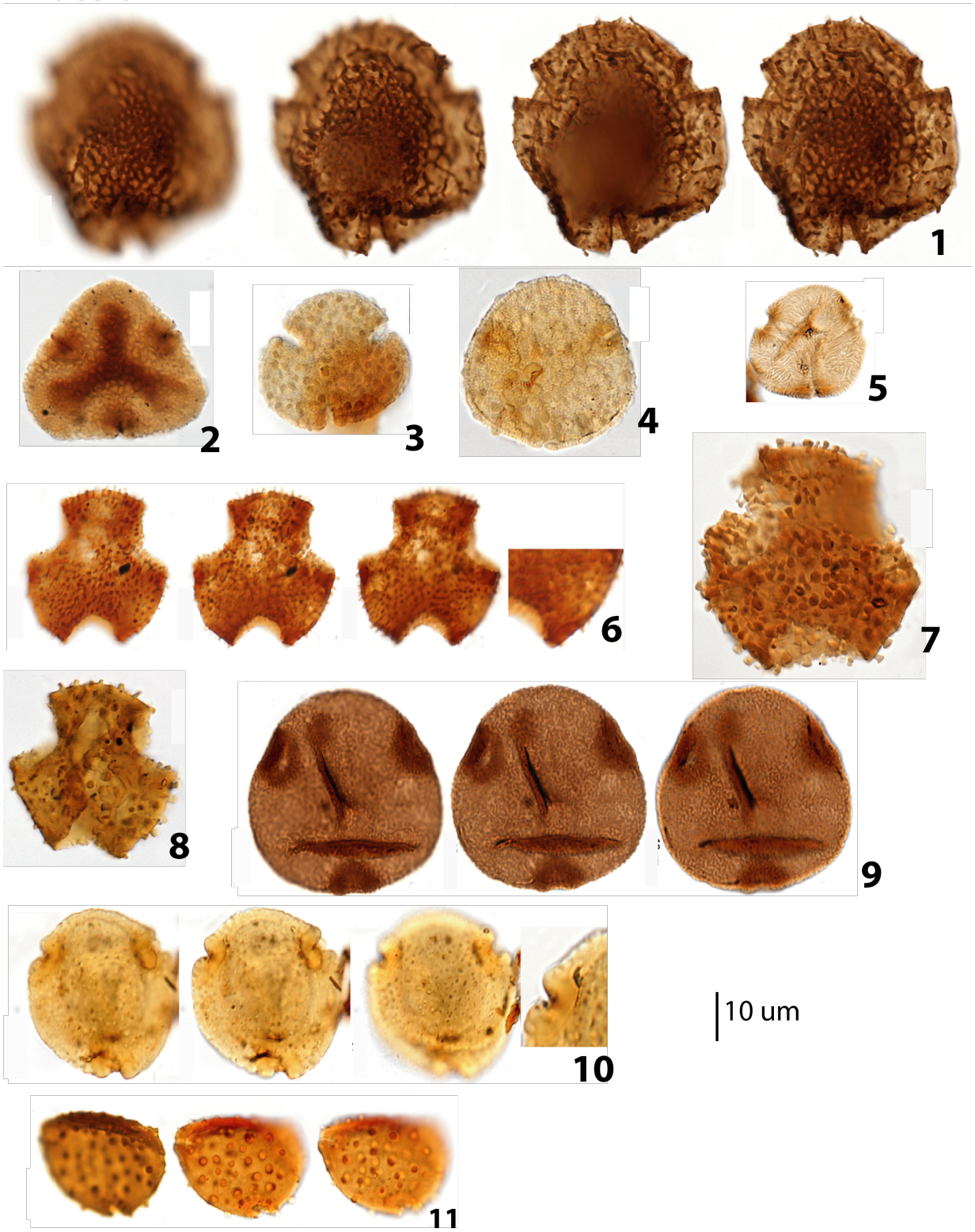

Plate 6. (1) *Bombacacidites inversus* sp.nov; **(2)** *Bombacacidites pulcherrimus* sp.nov; **(3,4)** *Bomobacacidites verrucatus* sp.nov; **(5)** *Rugutricolpites etayoi* sp.nov; **(6)** *Clavatricolpites dispersiclavatus* sp.nov; **(7,8)** *Clavatriporites spicatus* sp.nov; **(9)** *Fossutriporites cerebriformis* sp.nov; **(10)** *Foveotriporites motiloneorum* sp.nov; **(11)** *Gemmatriporites duquei* sp.nov.

Annexes Chapter-2

Annex 2.1: Sections, including wells and outcrops, used in this study. Of these, 106 correspond to sections previously analyzed on the first chapter of this work. The remaining 7 correspond to 5 and 2 wells drilled in the Middle Magdalena Valley and Catatumbo basins respectively and are identified with an asterisk.

Code	Source	Latitude	Longitude
Aga-1	Jaramillo et al 2011	5,83	-74,32
Ara-2	Jaramillo et al 2011	6,95	-71,84
Ara-3	Jaramillo et al 2011	6,98	-71,82
Ara-4	Jaramillo et al 2011	6,98	-71,84
Av-1	This work (Chapter-1)	3,68	-73,44
Buc-1	Jaramillo et al 2011	5,61	-71,36
Bue-3Carb	Jaramillo et al 2011	4,98	-72,74
Bue-3Cor	Jaramillo et al 2011	4,98	-72,74
Bue-H15	Jaramillo et al 2011	4,95	-72,73
Came-1	This work (Chapter-1)	3,18	-72,90
Camo-1	This work (Chapter-1)	3,64	-73,40
Caño Las Blancas	This work (Chapter-1)	4,01	-73,82
Caño Sagu	This work (Chapter-1)	4,08	-73,78
Canoe-1	This work (Chapter-1)	3,61	-73,51
Casc-1	This work (Chapter-1)	6,10	-71,82
Cas-1	Jaramillo et al 2011	6,76	-73,57
Cerrejon	Jaramillo et al 2011	11,07	-72,69
Cer-3	Jaramillo et al 2011	8,21	-72,74
Chac-1	This work (Chapter-1)	3,60	-73,39
Cosw-1	This work (Chapter-1)	4,34	-71,38
Colorado	Jaramillo et al 2011	4,84	-73,22
Concentracion	Jaramillo et al 2011	6,03	-72,76
Con16 *	This work (new)	7,32	-73,46
Con-1	This work (Chapter-1)	5,43	-70,44
Cop-1	Jaramillo et al 2011	4,44	-73,28
Cor-1	Jaramillo et al 2011	3,77	-73,73
CPE2-1	This work (Chapter-1)	5,55	-70,19
Cris-1	This work (Chapter-1)	3,55	-73,95
Cse-08	This work (Chapter-1)	3,44	-71,45
Cus-5	Jaramillo et al 2011	5,11	-72,66
Cusu-1	This work (Chapter-1)	3,81	-73,19
Cusu-2	This work (Chapter-1)	3,84	-73,16
Eval-1	This work (Chapter-1)	3,46	-73,35
Flo-C3	Jaramillo et al 2011	5,49	-72,42
Fon-1	This work (Chapter-1)	3,46	-73,60
Fue182	This work (Chapter-1)	3,49	-73,61
Gib	Jaramillo et al 2011	7,04	-72,17
Gig-1	Jaramillo et al 2011	2,28	-75,56
Gon-1	Jaramillo et al 2011	8,28	-72,58

Annex 2.1 (continuation)

Code	Source	Latitude	Longitude
Gonzales	Jaramillo et al 2011	8,6	-72,7
GonOut	Jaramillo et al 2011	8,28	-72,58
Gua-1	This work (Chapter-1)	4,26	-73,35
Gua-1	Jaramillo et al 2011	4,74	-73,13
Gua-2	Jaramillo et al 2011	4,70	-73,16
Had-1	This work (Chapter-1)	3,24	-73,04
Hig-1	Jaramillo et al 2011	3,10	-75,27
Jor-1	Jaramillo et al 2011	6,07	-71,24
Jub-1	Jaramillo et al 2011	6,99	-71,53
Kan-1	This work (Chapter-1)	3,71	-72,56
LaHe-1	Jaramillo et al 2011	6,25	-71,00
LaMar-1	Jaramillo et al 2011	5,07	-72,51
Bru-1	This work (Chapter-1)	3,03	-73,11
Las-1	Jaramillo et al 2011	5,38	-71,97
Lis-1	Jaramillo et al 2011	7,10	-73,53
LiNo1 *	This work (new)	7,14	-73,54
Li158-2 *	This work (new)	7,14	-73,55
Li4 *	This work (new)	7,14	-73,54
Luro-1	This work (Chapter-1)	3,86	-73,50
Maga-1	This work (Chapter-1)	7,04	-72,20
Ma-1	This work (Chapter-1)	3,72	-71,74
Medina	Jaramillo et al 2011	4,5	-73,1
Moc-1	This work (Chapter-1)	5,15	-70,55
Mol-1	Jaramillo et al 2011	11,30	-72,50
Mon-1A	Jaramillo et al 2011	6,83	-74,04
Muc-3	Jaramillo et al 2011	8,10	-72,52
Mues-1	This work (Chapter-1)	5,79	-71,9
Nac-1	This work (Chapter-1)	5,29	-70,31
Nines-1	This work (Chapter-1)	3,42	-73,43
Nis-E1	Jaramillo et al 2011	5,62	-72,31
Nuesp-1	This work (Chapter-1)	3,88	-73,75
Nuevo Mundo *	This work (new)	7,23	-73,33
Ori-1	Jaramillo et al 2011	0,57	-76,89
Pac-1	Jaramillo et al 2011	3,98	-73,51
Pal-1	Jaramillo et al 2011	4,43	-73,36
Past-1	This work (Chapter-1)	3,80	-73,14
Past-4	This work (Chapter-1)	3,74	-73,25
Pau-C2FZ	Jaramillo et al 2011	5,44	-72,46
Pij-1	Jaramillo et al 2011	3,00	-75,27
Pum-1	Jaramillo et al 2011	0,57	-76,88
Regadera	Jaramillo et al 2011	7,4	-72,4
Reg-1	Jaramillo et al 2011	6,88	-73,55

Annex 2.1 (continuation)

Code	Source	Latitude	Longitude
Ret-1	This work (Chapter-1)	3,12	-72,61
Ret-1ST1	This work (Chapter-1)	3,12	-72,61
RieMacheRull	Jaramillo et al 2011	10,92	-72,26
RioCh-1	Jaramillo et al 2011	4,94	-72,74
Rio de Oro-14	Jaramillo et al 2011	9,10	-72,90
Rio Loro	Jaramillo et al 2011	8,4	-71,8
ZuW2 *	This work (new)	8,23	-72,46
Zul-1	Jaramillo et al 2011	8,20	-72,45
Ros1 *	This work (new)	7,86	-72,49
Rub-2	This work (Chapter-1)	3,80	-71,51
Rub-79	This work (Chapter-1)	3,76	-71,40
S-10	This work (Chapter-1)	3,06	-72,86
S-14	This work (Chapter-1)	3,41	-73,06
S-17	This work (Chapter-1)	3,36	-73,93
S-5	This work (Chapter-1)	3,28	-73,24
S-7	This work (Chapter-1)	3,09	-73,23
SanFel-1	Jaramillo et al 2011	5,13	-71,85
SanJRS	Jaramillo et al 2011	4,86	-74,63
SanJ-1	Jaramillo et al 2011	3,38	-73,86
SanMar-1	Jaramillo et al 2011	6,01	-71,65
Tam-2	Jaramillo et al 2011	6,57	-71,76
Tar-1	This work (Chapter-1)	3,26	-73,12
Tib-182/187	Jaramillo et al 2011	8,6	-72,67
Toc-1	Jaramillo et al 2011	6,3	-71,80
Tras-1	This work (Chapter-1)	3,4	-72,63
Uribe	Jaramillo et al 2011	7,2	-73,37
UrumacoEast	Jaramillo et al 2011	11,5	-69,55
UrumacoWest	Jaramillo et al 2011	11,2	-70,26
Val-1	This work (Chapter-1)	3,9	-72,66
Ven-2	This work (Chapter-1)	3,5	-72,97
Ven-3	This work (Chapter-1)	3,6	-72,94
Zul-1	Jaramillo et al 2011	8,2	-72,45

Annex_2.2: Lines of correlation (LOC) for the new sections. Each pair of points corresponds to the endpoints of a segment of the LOC. The first column corresponds to the individual section and the second column to the composite section. LiNo1, Li158-2, Li4, Con16, and Nuevo Mundo are located in the Middle Magdalena Valley basin and ZuW2 and Ros1 in the Catatumbo basin.

LiNo1	
9460	18338,9
11300	19434,3

Li158-2	
7600	18268,2
9490	19893

Li4	
9000	16068
11380	17350
11380	18143
13185,9	19363,6
15300	19800

Con16	
8400	16300
9930	17031

Ros1	
3010	18500
2280	18190
1732	18112
1330	17327
1110	16426
920	16068
490	15786

Nuevo Mundo	
0	16164
124,64	16231
212,48	16278,5
700,48	16427,3
1695,76	16669,3
2665,66	17038
2899,52	17372,2
3237,36	17590,7

ZuW2	
2590	5245
4120	9091
4960	14377
6710	15786
7510	16068
8110	16594
8110	18143
9450	19380

Annex 2.3 Information of the areas, sections and number of samples extracted from the literature and wells used to compare the diversity obtained in this work. The geographic location is presented in figure 2.8. (oc: outcrop; rc: rock core; cu: ditch cuttings).

Source	Number Fig 2.8	Country	Region	Section name	Type of Sample	Latitude	Longitude	# Samples
Jaramillo, 2014	1	Panama	Bocas del Toro	10-North Coast	outcrop	9,10	-81,56	10
		Panama	Bocas del Toro	11-South Coast	outcrop	9,09	-81,54	5
		Panama	Bocas del Toro	12-North Valiente	outcrop	9,07	-81,81	5
		Panama	Bocas del Toro	15-South Valiente	outcrop	9,14	-81,94	5
		Panama	Bocas del Toro	16-North Point West	outcrop	9,18	-82,06	5
		Panama	Bocas del Toro	17-Piedra Roja Point West	outcrop	9,15	-82,01	4
		Panama	Bocas del Toro	19-North Point-Tiburon Point	outcrop	9,155	-82,02	10
		Panama	Bocas del Toro	20-Nispero Point South	outcrop	9,17	-82,02	2
		Panama	Bocas del Toro	22-Bastimentos Island	outcrop	9,32	-82,11	3
		Panama	Bocas del Toro	24-Solarte Cay	outcrop	9,14	-82,01	4
	3	Panama	Darien	Rio Chico	outcrop	8,22	-77,59	2
		Panama	Darien	Rio Chucunaque	outcrop	8,33	-77,76	1
		Panama	Darien	Rio Icuanati	outcrop	8,41	-77,64	1
		Panama	Darien	Rio Tupisa	outcrop	8,33	-77,61	3
		Panama	Darien	Rio Turquesa	outcrop	8,47	-77,71	5
	2	Panama	Panama Central	01-Sabanita to Payardi	outcrop	9,35	-79,81	7
		Panama	Panama Central	02-Margarita to Gatun	outcrop	9,30	-79,91	10
		Panama	Panama Central	05-Rio Indio	outcrop	9,19	-80,19	2
		Panama	Panama Central	Empire Section La Boca	outcrop	9,08	-79,68	14
		Panama	Panama Central	GH9	outcrop	9,03	79,63	11
		Panama	Panama Central	Hodges Hill Section	outcrop	9,05	-79,65	24
		Panama	Panama Central	Roadside K2	outcrop	9,05	-79,6	7
Pierre-Olivero,2016	9	Peru	Contamana	Contamana	outcrop	7,33	74,951	4
Leite, 2016	8	Brazil	Brazil	1AS-19-AM	rock-core	-5,25	-71,55	32
ICP_Internal reports	4	Colombia	Sinu-San Jacinto	SSJ-3	rock-core	9,43	-75,43	25
		Colombia	Sinu-San Jacinto	SSJ-15	rock-core	8,60	-75,57	13
		Colombia	Sinu-San Jacinto	SSJ-4	rock-core	9,50	-75,25	3
		Colombia	Sinu-San Jacinto	SSJ-8	rock-core	9,63	-75,29	5
	6	Colombia	Catatumbo	In1	cutting	8,64	-72,88	8
		Colombia	Catatumbo	Ti	cutting	8,72	-72,71	15
		Colombia	Catatumbo	Tr1	cutting	8,15	-72,47	27
	5	Colombia	VMM	Bo3	cutting	7,32	-73,76	6
		Colombia	VMM	Cr7	cutting	7,53	-73,69	92
Jaramillo, 2017	7	Colombia	Llanos	Saltarin	rock-core	5,02	-70,83	112
	12	Brazil	Brazil	1AS-105-AM	rock-core	-4,41	-70,55	91
Hoorn,2006	7	Colombia	Apaporis	Apaporis		0,28	-70,2	25
Salamanca, 2016	9	Colombia	Llanos	Mariname	outcrop	-0,08	-71,99	47
Silva-Caminha,2009	11	Brazil	Brazil	1AS-19-AM	rock-core	-4,55	-67,92	33
	10	Brazil	Brazil	1AS-27-AM	rock-core	-4,28	-69,17	8

Annex 2.4 SQS diversity of samples from the literature and internal reports of Ecopetrol SA.

1AS-105-AM/ Saltarin (Jaramillo et al 2017)

Source	Basin	section	Age	sqs=0.6
Jaramillo_2017	Amazonas	1AS-105-AM	10,72	3,92
Jaramillo_2017	Amazonas	1AS-105-AM	10,86	3,37
Jaramillo_2017	Amazonas	1AS-105-AM	11,04	9,63
Jaramillo_2017	Amazonas	1AS-105-AM	11,07	10,56
Jaramillo_2017	Amazonas	1AS-105-AM	11,25	2,89
Jaramillo_2017	Amazonas	1AS-105-AM	11,44	2,77
Jaramillo_2017	Amazonas	1AS-105-AM	11,71	2,13
Jaramillo_2017	Amazonas	1AS-105-AM	11,78	2,26
Jaramillo_2017	Amazonas	1AS-105-AM	11,79	2,83
Jaramillo_2017	Amazonas	1AS-105-AM	11,9	4,54
Jaramillo_2017	Amazonas	1AS-105-AM	12,11	5,84
Jaramillo_2017	Amazonas	1AS-105-AM	12,43	3,30
Jaramillo_2017	Amazonas	1AS-105-AM	12,54	8,06
Jaramillo_2017	Amazonas	1AS-105-AM	12,56	4,91
Jaramillo_2017	Amazonas	1AS-105-AM	12,7	7,68
Jaramillo_2017	Amazonas	1AS-105-AM	12,87	7,54
Jaramillo_2017	Amazonas	1AS-105-AM	12,99	5,35
Jaramillo_2017	Amazonas	1AS-105-AM	13,02	6,90
Jaramillo_2017	Amazonas	1AS-105-AM	13,25	2,11
Jaramillo_2017	Amazonas	1AS-105-AM	13,51	6,80
Jaramillo_2017	Amazonas	1AS-105-AM	13,69	4,40
Jaramillo_2017	Amazonas	1AS-105-AM	13,73	5,15
Jaramillo_2017	Amazonas	1AS-105-AM	13,79	2,66
Jaramillo_2017	Amazonas	1AS-105-AM	13,83	3,00
Jaramillo_2017	Amazonas	1AS-105-AM	14,02	6,12
Jaramillo_2017	Amazonas	1AS-105-AM	14,09	6,34
Jaramillo_2017	Amazonas	1AS-105-AM	14,3	5,14
Jaramillo_2017	Amazonas	1AS-105-AM	14,44	0,96
Jaramillo_2017	Amazonas	1AS-105-AM	14,64	2,69
Jaramillo_2017	Amazonas	1AS-105-AM	14,84	3,21
Jaramillo_2017	Amazonas	1AS-105-AM	14,97	3,71
Jaramillo_2017	Amazonas	1AS-105-AM	14,99	6,49
Jaramillo_2017	Amazonas	1AS-105-AM	15	5,27
Jaramillo_2017	Amazonas	1AS-105-AM	15,25	10,02
Jaramillo_2017	Amazonas	1AS-105-AM	15,49	6,72
Jaramillo_2017	Amazonas	1AS-105-AM	15,71	2,62
Jaramillo_2017	Amazonas	1AS-105-AM	15,93	6,76
Jaramillo_2017	Amazonas	1AS-105-AM	16,03	10,52
Jaramillo_2017	Amazonas	1AS-105-AM	16,04	6,49
Jaramillo_2017	Amazonas	1AS-105-AM	16,07	8,50
Jaramillo_2017	Amazonas	1AS-105-AM	16,09	1,90

Annex 2.4
(continuation)

Jaramillo_2017	Amazonas	1AS-105-AM	16,11	5,15
Jaramillo_2017	Amazonas	1AS-105-AM	16,13	2,62
Jaramillo_2017	Amazonas	1AS-105-AM	16,21	1,06
Jaramillo_2017	Amazonas	1AS-105-AM	16,34	2,88
Jaramillo_2017	Amazonas	1AS-105-AM	16,41	1,82
Jaramillo_2017	Amazonas	1AS-105-AM	16,48	2,30
Jaramillo_2017	Amazonas	1AS-105-AM	16,61	2,83
Jaramillo_2017	Amazonas	1AS-105-AM	16,67	2,02
Jaramillo_2017	Amazonas	1AS-105-AM	16,77	2,95
Jaramillo_2017	Amazonas	1AS-105-AM	16,79	4,01
Jaramillo_2017	Amazonas	1AS-105-AM	16,86	6,39
Jaramillo_2017	Amazonas	1AS-105-AM	16,89	4,02
Jaramillo_2017	Amazonas	1AS-105-AM	16,93	5,32
Jaramillo_2017	Amazonas	1AS-105-AM	17,07	4,06
Jaramillo_2017	Amazonas	1AS-105-AM	17,25	1,45
Jaramillo_2017	Amazonas	1AS-105-AM	17,39	4,59
Jaramillo_2017	Amazonas	1AS-105-AM	17,46	1,73
Jaramillo_2017	Amazonas	1AS-105-AM	17,48	3,97
Jaramillo_2017	Amazonas	1AS-105-AM	17,56	3,56
Jaramillo_2017	Amazonas	1AS-105-AM	17,63	1,55
Jaramillo_2017	Amazonas	1AS-105-AM	17,68	0,96
Jaramillo_2017	Amazonas	1AS-105-AM	17,75	3,02
Jaramillo_2017	Amazonas	1AS-105-AM	17,82	3,61
Jaramillo_2017	Amazonas	1AS-105-AM	17,83	2,30
Jaramillo_2017	Amazonas	1AS-105-AM	17,92	3,08
Jaramillo_2017	Amazonas	1AS-105-AM	18,03	1,89
Jaramillo_2017	Amazonas	1AS-105-AM	18,07	2,03
Jaramillo_2017	Amazonas	1AS-105-AM	18,24	5,07
Jaramillo_2017	Amazonas	1AS-105-AM	18,26	2,42
Jaramillo_2017	Amazonas	1AS-105-AM	18,28	2,60
Jaramillo_2017	Amazonas	1AS-105-AM	18,37	2,01
Jaramillo_2017	Amazonas	1AS-105-AM	18,38	0,98
Jaramillo_2017	Amazonas	1AS-105-AM	18,401	3,99
Jaramillo_2017	Amazonas	1AS-105-AM	18,402	7,13
Jaramillo_2017	Amazonas	1AS-105-AM	18,403	3,76
Jaramillo_2017	Amazonas	1AS-105-AM	18,404	4,38
Jaramillo_2017	Amazonas	1AS-105-AM	18,41	8,27
Jaramillo_2017	Amazonas	1AS-105-AM	18,66	1,06
Jaramillo_2017	Amazonas	1AS-105-AM	18,67	4,48
Jaramillo_2017	Amazonas	1AS-105-AM	18,75	13,36
Jaramillo_2017	Amazonas	1AS-105-AM	18,78	12,95
Jaramillo_2017	Llanos	Saltarin	5,48	NA
Jaramillo_2017	Llanos	Saltarin	5,99	16,59

Annex 2.4
(continuation)

Jaramillo_2017	Llanos	Saltarin	6,09	9,11
Jaramillo_2017	Llanos	Saltarin	6,13	11,31
Jaramillo_2017	Llanos	Saltarin	6,16	NA
Jaramillo_2017	Llanos	Saltarin	6,34	3,24
Jaramillo_2017	Llanos	Saltarin	6,38	8,46
Jaramillo_2017	Llanos	Saltarin	6,81	20,95
Jaramillo_2017	Llanos	Saltarin	6,82	21,92
Jaramillo_2017	Llanos	Saltarin	6,84	12,76
Jaramillo_2017	Llanos	Saltarin	6,87	4,11
Jaramillo_2017	Llanos	Saltarin	6,89	13,26
Jaramillo_2017	Llanos	Saltarin	6,9	24,94
Jaramillo_2017	Llanos	Saltarin	7,02	NA
Jaramillo_2017	Llanos	Saltarin	7,03	14,06
Jaramillo_2017	Llanos	Saltarin	7,04	18,43
Jaramillo_2017	Llanos	Saltarin	7,045	20,23
Jaramillo_2017	Llanos	Saltarin	7,06	31,84
Jaramillo_2017	Llanos	Saltarin	7,09	14,75
Jaramillo_2017	Llanos	Saltarin	7,11	5,37
Jaramillo_2017	Llanos	Saltarin	7,15	19,67
Jaramillo_2017	Llanos	Saltarin	7,21	15,48
Jaramillo_2017	Llanos	Saltarin	7,41	12,05
Jaramillo_2017	Llanos	Saltarin	7,49	NA
Jaramillo_2017	Llanos	Saltarin	7,51	NA
Jaramillo_2017	Llanos	Saltarin	7,7	1,00
Jaramillo_2017	Llanos	Saltarin	7,9	NA
Jaramillo_2017	Llanos	Saltarin	8,34	1,04
Jaramillo_2017	Llanos	Saltarin	8,35	6,23
Jaramillo_2017	Llanos	Saltarin	8,39	3,78
Jaramillo_2017	Llanos	Saltarin	8,46	6,49
Jaramillo_2017	Llanos	Saltarin	11,26	16,33
Jaramillo_2017	Llanos	Saltarin	11,38	1,07
Jaramillo_2017	Llanos	Saltarin	11,69	1,00
Jaramillo_2017	Llanos	Saltarin	11,74	4,41
Jaramillo_2017	Llanos	Saltarin	11,99	12,38
Jaramillo_2017	Llanos	Saltarin	12,22	5,78
Jaramillo_2017	Llanos	Saltarin	12,33	8,91
Jaramillo_2017	Llanos	Saltarin	12,38	1,84
Jaramillo_2017	Llanos	Saltarin	12,4	5,70
Jaramillo_2017	Llanos	Saltarin	12,49	2,12
Jaramillo_2017	Llanos	Saltarin	12,58	8,96
Jaramillo_2017	Llanos	Saltarin	12,7	2,25
Jaramillo_2017	Llanos	Saltarin	12,87	6,19
Jaramillo_2017	Llanos	Saltarin	13,05	12,01

Annex 2.4
(continuation)

Jaramillo_2017	Llanos	Saltarin	13,15	7,16
Jaramillo_2017	Llanos	Saltarin	13,23	1,20
Jaramillo_2017	Llanos	Saltarin	13,46	10,69
Jaramillo_2017	Llanos	Saltarin	13,54	6,47
Jaramillo_2017	Llanos	Saltarin	13,67	5,94
Jaramillo_2017	Llanos	Saltarin	13,88	5,78
Jaramillo_2017	Llanos	Saltarin	14,1	7,76
Jaramillo_2017	Llanos	Saltarin	14,24	8,51
Jaramillo_2017	Llanos	Saltarin	14,44	4,59
Jaramillo_2017	Llanos	Saltarin	14,55	2,32
Jaramillo_2017	Llanos	Saltarin	14,66	5,52
Jaramillo_2017	Llanos	Saltarin	14,75	2,11
Jaramillo_2017	Llanos	Saltarin	14,85	2,15
Jaramillo_2017	Llanos	Saltarin	14,96	13,67
Jaramillo_2017	Llanos	Saltarin	15,05	NA
Jaramillo_2017	Llanos	Saltarin	15,08	8,17
Jaramillo_2017	Llanos	Saltarin	15,14	7,31
Jaramillo_2017	Llanos	Saltarin	15,23	8,25
Jaramillo_2017	Llanos	Saltarin	15,29	3,67
Jaramillo_2017	Llanos	Saltarin	15,36	2,50
Jaramillo_2017	Llanos	Saltarin	15,39	3,12
Jaramillo_2017	Llanos	Saltarin	15,49	12,64
Jaramillo_2017	Llanos	Saltarin	15,67	NA
Jaramillo_2017	Llanos	Saltarin	15,73	10,77
Jaramillo_2017	Llanos	Saltarin	15,82	5,75
Jaramillo_2017	Llanos	Saltarin	15,88	10,83
Jaramillo_2017	Llanos	Saltarin	15,95	9,34
Jaramillo_2017	Llanos	Saltarin	16,06	4,97
Jaramillo_2017	Llanos	Saltarin	16,11	6,62
Jaramillo_2017	Llanos	Saltarin	16,13	8,59
Jaramillo_2017	Llanos	Saltarin	16,15	6,82
Jaramillo_2017	Llanos	Saltarin	16,16	4,11
Jaramillo_2017	Llanos	Saltarin	16,18	8,73
Jaramillo_2017	Llanos	Saltarin	16,33	6,67
Jaramillo_2017	Llanos	Saltarin	16,48	3,35
Jaramillo_2017	Llanos	Saltarin	16,61	32,17
Jaramillo_2017	Llanos	Saltarin	16,65	3,96
Jaramillo_2017	Llanos	Saltarin	16,75	2,20
Jaramillo_2017	Llanos	Saltarin	16,88	9,63
Jaramillo_2017	Llanos	Saltarin	16,89	3,58
Jaramillo_2017	Llanos	Saltarin	16,92	4,49
Jaramillo_2017	Llanos	Saltarin	17,02	8,14
Jaramillo_2017	Llanos	Saltarin	17,12	5,61

Annex 2.4
(continuation)

Jaramillo_2017	Llanos	Saltarin	17,36	9,29
Jaramillo_2017	Llanos	Saltarin	17,45	4,39
Jaramillo_2017	Llanos	Saltarin	17,47	7,16
Jaramillo_2017	Llanos	Saltarin	17,48	5,40
Jaramillo_2017	Llanos	Saltarin	17,51	NA
Jaramillo_2017	Llanos	Saltarin	17,58	5,13
Jaramillo_2017	Llanos	Saltarin	17,6	9,57
Jaramillo_2017	Llanos	Saltarin	17,64	4,00
Jaramillo_2017	Llanos	Saltarin	17,69	8,66
Jaramillo_2017	Llanos	Saltarin	17,78	8,07
Jaramillo_2017	Llanos	Saltarin	17,84	4,82
Jaramillo_2017	Llanos	Saltarin	17,91	3,41
Jaramillo_2017	Llanos	Saltarin	17,94	1,96
Jaramillo_2017	Llanos	Saltarin	17,95	18,14
Jaramillo_2017	Llanos	Saltarin	18,02	6,49
Jaramillo_2017	Llanos	Saltarin	18,05	12,98
Jaramillo_2017	Llanos	Saltarin	18,12	7,08
Jaramillo_2017	Llanos	Saltarin	18,16	11,56
Jaramillo_2017	Llanos	Saltarin	18,26	11,48
Jaramillo_2017	Llanos	Saltarin	18,35	NA
Jaramillo_2017	Llanos	Saltarin	18,37	13,94
Jaramillo_2017	Llanos	Saltarin	18,4	10,89
Jaramillo_2017	Llanos	Saltarin	18,42	7,39
Jaramillo_2017	Llanos	Saltarin	18,5	1,98

Annex 2.4
(continuation)

Contamana (Pierre et al 2016)				
Source	**Basin**	**section**	**Age**	**sqs=0.6**
Pierre_2016	Contamana	Contamana	42,5	12,87
Pierre_2016	Contamana	Contamana	41	27,37
Pierre_2016	Contamana	Contamana	11,6	18,98
Pierre_2016	Contamana	Contamana	11	1,78

Apaporis (Hoorn 2006)				
Source	**Basin**	**section**	**Age**	**sqs=0.6**
Hoorn_2006	Amazonas	Apaporis_4	15	9,60
Hoorn_2006	Amazonas	Apaporis_4	14,92	5,97
Hoorn_2006	Amazonas	Apaporis_4	14,84	4,55
Hoorn_2006	Amazonas	Apaporis_4	14,77	7,04
Hoorn_2006	Amazonas	Apaporis_4	14,73	8,04
Hoorn_2006	Amazonas	Apaporis_4	14,61	3,05
Hoorn_2006	Amazonas	Apaporis_4	14,58	13,20
Hoorn_2006	Amazonas	Apaporis_4	14,52	5,02
Hoorn_2006	Amazonas	Apaporis_4	14,45	6,01
Hoorn_2006	Amazonas	Apaporis_4	14,39	8,29
Hoorn_2006	Amazonas	Apaporis_4	14,31	7,43
Hoorn_2006	Amazonas	Apaporis_4	14,23	11,61
Hoorn_2006	Amazonas	Apaporis_4	14,16	13,05
Hoorn_2006	Amazonas	Apaporis_4	12,74	2,59
Hoorn_2006	Amazonas	Apaporis_4	12,68	1,14
Hoorn_2006	Amazonas	Apaporis_4	12,61	1,26
Hoorn_2006	Amazonas	Apaporis_4	12,53	2,47
Hoorn_2006	Amazonas	Apaporis_4	12,47	4,37
Hoorn_2006	Amazonas	Apaporis_4	12,42	2,90
Hoorn_2006	Amazonas	Apaporis_4	12,37	3,99
Hoorn_2006	Amazonas	Apaporis_4	12,31	10,47
Hoorn_2006	Amazonas	Apaporis_4	12,19	14,72
Hoorn_2006	Amazonas	Apaporis_4	12,16	11,50
Hoorn_2006	Amazonas	Apaporis_4	12,06	4,27
Hoorn_2006	Amazonas	Apaporis_4	12,03	6,01

Ecopetrol Sections				
Source	**Basin**	**section**	**Age**	**sqs=0.6**
Ecopetrol	Catatumbo	In	58	1,71
Ecopetrol	Catatumbo	In	58,1	1,71
Ecopetrol	Catatumbo	In	58,2	1,73
Ecopetrol	Catatumbo	In	58,25	0,94
Ecopetrol	Catatumbo	In	58,3	1,67

Annex 2.4
(continuation)

Ecopetrol	Catatumbo	In	58,31	1,57
Ecopetrol	Catatumbo	In	58,34	1,61
Ecopetrol	Catatumbo	In	58,9	1,07
Ecopetrol	Catatumbo	Ti	58,5	1,10
Ecopetrol	Catatumbo	Ti	58,76	1,00
Ecopetrol	Catatumbo	Ti	58,77	2,28
Ecopetrol	Catatumbo	Ti	58,85	2,53
Ecopetrol	Catatumbo	Ti	58,86	1,99
Ecopetrol	Catatumbo	Ti	59,01	2,94
Ecopetrol	Catatumbo	Ti	59,24	2,72
Ecopetrol	Catatumbo	Ti	59,26	4,61
Ecopetrol	Catatumbo	Ti	59,48	2,01
Ecopetrol	Catatumbo	Ti	59,5	1,00
Ecopetrol	Catatumbo	Ti	59,58	NA
Ecopetrol	Catatumbo	Ti	59,6	1,804
Ecopetrol	Catatumbo	Ti	59,76	2,696
Ecopetrol	Catatumbo	Ti	59,89	1,132
Ecopetrol	Catatumbo	Ti	59,97	1,728
Ecopetrol	Catatumbo	Tr	58,8	0,997
Ecopetrol	Catatumbo	Tr	58,93	0,882
Ecopetrol	Catatumbo	Tr	59	0,945
Ecopetrol	Catatumbo	Tr	59,11	0,865
Ecopetrol	Catatumbo	Tr	59,29	0,910
Ecopetrol	Catatumbo	Tr	59,43	1,473
Ecopetrol	Catatumbo	Tr	59,56	1,005
Ecopetrol	Catatumbo	Tr	59,7	2,742
Ecopetrol	Catatumbo	Tr	59,83	1,010
Ecopetrol	Catatumbo	Tr	59,97	NA
Ecopetrol	Catatumbo	Tr	60,1	1,778
Ecopetrol	Catatumbo	Tr	60,24	1,824
Ecopetrol	Catatumbo	Tr	60,37	0,860
Ecopetrol	Catatumbo	Tr	60,51	0,955
Ecopetrol	Catatumbo	Tr	60,64	1,008
Ecopetrol	Catatumbo	Tr	60,73	0,996
Ecopetrol	Catatumbo	Tr	60,78	0,954
Ecopetrol	Catatumbo	Tr	60,88	0,919
Ecopetrol	Catatumbo	Tr	60,91	1,004
Ecopetrol	Catatumbo	Tr	61,05	1,478
Ecopetrol	Catatumbo	Tr	61,18	0,997
Ecopetrol	Catatumbo	Tr	61,32	1,060
Ecopetrol	Catatumbo	Tr	61,45	0,950
Ecopetrol	Catatumbo	Tr	61,59	0,951
Ecopetrol	Catatumbo	Tr	61,72	0,949

Annex 2.4
(continuation)

Ecopetrol	Catatumbo	Tr	61,86	0,901
Ecopetrol	Catatumbo	Tr	62	0,994
Ecopetrol	SanJacinto	P3	30,01	8,364
Ecopetrol	SanJacinto	P3	30,49	6,511
Ecopetrol	SanJacinto	P3	31,07	5,425
Ecopetrol	SanJacinto	P3	31,73	2,500
Ecopetrol	SanJacinto	P3	33,48	4,523
Ecopetrol	SanJacinto	P3	33,66	4,662
Ecopetrol	SanJacinto	P3	34	3,728
Ecopetrol	SanJacinto	P3	38,86	10,471
Ecopetrol	SanJacinto	P3	39,44	6,128
Ecopetrol	SanJacinto	P3	39,74	6,289
Ecopetrol	SanJacinto	P3	40,65	2,271
Ecopetrol	SanJacinto	P3	41,03	5,429
Ecopetrol	SanJacinto	P3	46,31	NA
Ecopetrol	SanJacinto	P3	47,42	5,97
Ecopetrol	SanJacinto	P3	47,69	2,10
Ecopetrol	SanJacinto	P3	49,00	10,03
Ecopetrol	SanJacinto	P3	49,45	NA
Ecopetrol	SanJacinto	P3	50,28	5,62
Ecopetrol	SanJacinto	P3	50,45	NA
Ecopetrol	SanJacinto	P3	50,94	12,413
Ecopetrol	SanJacinto	P3	51,51	NA
Ecopetrol	SanJacinto	P3	52,08	4,92
Ecopetrol	SanJacinto	P3	52,79	7,10
Ecopetrol	SanJacinto	P3	54,34	3,36
Ecopetrol	SanJacinto	P3	55,30	NA
Ecopetrol	SanJacinto	P4	19,4	8,01
Ecopetrol	SanJacinto	P4	20,5	8,17
Ecopetrol	SanJacinto	P4	19,2	2,18
Ecopetrol	SanJacinto	P8	31	6,66
Ecopetrol	SanJacinto	P8	32	5,54
Ecopetrol	SanJacinto	P8	37,9	7,67
Ecopetrol	SanJacinto	P8	38,3	5,46
Ecopetrol	SanJacinto	P8	39,5	8,97
Ecopetrol	SanJacinto	P15	19,01	7,78
Ecopetrol	SanJacinto	P15	19,12	5,54
Ecopetrol	SanJacinto	P15	19,35	9,90
Ecopetrol	SanJacinto	P15	19,38	5,21
Ecopetrol	SanJacinto	P15	20,61	4,99
Ecopetrol	SanJacinto	P15	20,76	7,95
Ecopetrol	SanJacinto	P15	21,81	8,59
Ecopetrol	SanJacinto	P15	21,85	4,05

Annex 2.4
(continuation)

Ecopetrol	SanJacinto	P15	22,02	9,09
Ecopetrol	SanJacinto	P15	22,14	7,04
Ecopetrol	SanJacinto	P15	22,25	9,52
Ecopetrol	SanJacinto	P15	22,91	8,72
Ecopetrol	SanJacinto	P15	22,98	6,46
Ecopetrol	VMM	Bo3	46	1,06
Ecopetrol	VMM	Bo3	46,2	1,24
Ecopetrol	VMM	Bo3	46,4	1,01
Ecopetrol	VMM	Bo3	46,8	1,84
Ecopetrol	VMM	Bo3	46,9	1,11
Ecopetrol	VMM	Bo3	47	3,37
Ecopetrol	VMM	CR7	16,59	NA
Ecopetrol	VMM	CR7	16,611	10,075
Ecopetrol	VMM	CR7	16,63	7,838
Ecopetrol	VMM	CR7	16,65	7,390
Ecopetrol	VMM	CR7	16,67	8,204
Ecopetrol	VMM	CR7	16,69	8,546
Ecopetrol	VMM	CR7	16,71	8,232
Ecopetrol	VMM	CR7	16,74	2,296
Ecopetrol	VMM	CR7	16,76	5,239
Ecopetrol	VMM	CR7	16,78	3,624
Ecopetrol	VMM	CR7	16,8	3,297
Ecopetrol	VMM	CR7	16,82	2,556
Ecopetrol	VMM	CR7	16,84	4,179
Ecopetrol	VMM	CR7	16,87	4,165
Ecopetrol	VMM	CR7	16,89	4,217
Ecopetrol	VMM	CR7	16,91	3,880
Ecopetrol	VMM	CR7	16,93	8,155
Ecopetrol	VMM	CR7	16,95	4,004
Ecopetrol	VMM	CR7	16,97	3,103
Ecopetrol	VMM	CR7	17	2,557
Ecopetrol	VMM	CR7	23	5,618
Ecopetrol	VMM	CR7	23,45	2,205
Ecopetrol	VMM	CR7	23,675	3,201
Ecopetrol	VMM	CR7	23,9	3,551
Ecopetrol	VMM	CR7	24,125	1,995
Ecopetrol	VMM	CR7	24,35	4,229
Ecopetrol	VMM	CR7	24,575	1,583
Ecopetrol	VMM	CR7	24,8	2,089
Ecopetrol	VMM	CR7	25,025	2,441
Ecopetrol	VMM	CR7	25,25	1,779
Ecopetrol	VMM	CR7	25,475	2,956
Ecopetrol	VMM	CR7	25,7	0,984

Annex 2.4
(continuation)

Ecopetrol	VMM	CR7	25,925	5,468
Ecopetrol	VMM	CR7	26,15	2,994
Ecopetrol	VMM	CR7	26,375	1,018
Ecopetrol	VMM	CR7	26,6	5,684
Ecopetrol	VMM	CR7	26,825	7,938
Ecopetrol	VMM	CR7	27,05	2,657
Ecopetrol	VMM	CR7	27,275	6,233
Ecopetrol	VMM	CR7	27,5	1,478
Ecopetrol	VMM	CR7	27,725	2,350
Ecopetrol	VMM	CR7	28,025	4,163
Ecopetrol	VMM	CR7	28,25	0,873
Ecopetrol	VMM	CR7	28,475	0,963
Ecopetrol	VMM	CR7	28,7	4,255
Ecopetrol	VMM	CR7	28,925	3,221
Ecopetrol	VMM	CR7	29,15	2,106
Ecopetrol	VMM	CR7	29,375	6,380
Ecopetrol	VMM	CR7	29,6	3,614
Ecopetrol	VMM	CR7	29,825	2,127
Ecopetrol	VMM	CR7	30,05	3,064
Ecopetrol	VMM	CR7	30,5	3,691
Ecopetrol	VMM	CR7	30,725	1,069
Ecopetrol	VMM	CR7	30,95	6,520
Ecopetrol	VMM	CR7	31,175	3,239
Ecopetrol	VMM	CR7	31,475	2,018
Ecopetrol	VMM	CR7	31,71	4,590
Ecopetrol	VMM	CR7	31,7	3,434
Ecopetrol	VMM	CR7	31,775	2,277
Ecopetrol	VMM	CR7	31,85	2,100
Ecopetrol	VMM	CR7	31,925	3,348
Ecopetrol	VMM	CR7	32	6,310
Ecopetrol	VMM	CR7	32,075	1,448
Ecopetrol	VMM	CR7	32,15	1,887
Ecopetrol	VMM	CR7	32,225	2,068
Ecopetrol	VMM	CR7	32,3	1,894
Ecopetrol	VMM	CR7	32,375	2,965
Ecopetrol	VMM	CR7	32,45	1,955
Ecopetrol	VMM	CR7	32,525	4,646
Ecopetrol	VMM	CR7	32,6	2,142
Ecopetrol	VMM	CR7	32,675	3,011
Ecopetrol	VMM	CR7	32,75	3,183
Ecopetrol	VMM	CR7	32,825	1,700
Ecopetrol	VMM	CR7	32,9	1,912
Ecopetrol	VMM	CR7	32,975	NA

Annex 2.4
(continuation)

Ecopetrol	VMM	CR7	33,05	2,21
Ecopetrol	VMM	CR7	33,125	3,68
Ecopetrol	VMM	CR7	33,2	2,79
Ecopetrol	VMM	CR7	33,275	3,23
Ecopetrol	VMM	CR7	33,35	2,72
Ecopetrol	VMM	CR7	33,425	1,98
Ecopetrol	VMM	CR7	33,5	4,22
Ecopetrol	VMM	CR7	56,7	5,52
Ecopetrol	VMM	CR7	56,75	5,53
Ecopetrol	VMM	CR7	56,81	1,52
Ecopetrol	VMM	CR7	56,87	0,97
Ecopetrol	VMM	CR7	56,98	0,94
Ecopetrol	VMM	CR7	57,09	2,65
Ecopetrol	VMM	CR7	57,18	1,64
Ecopetrol	VMM	CR7	57,32	1,81
Ecopetrol	VMM	CR7	57,43	2,91
Ecopetrol	VMM	CR7	57,5	3,08

1AS-33M (Leite et al 2016)

Source	Basin	section	Age	sqs=0.6
Leite_206	Amazonas	1AS-33-M	2,6	11,890
Leite_206	Amazonas	1AS-33-M	3,326	1,144
Leite_206	Amazonas	1AS-33-M	3,484	8,657
Leite_206	Amazonas	1AS-33-M	3,876	8,804
Leite_206	Amazonas	1AS-33-M	4,117	1,462
Leite_206	Amazonas	1AS-33-M	4,514	3,438
Leite_206	Amazonas	1AS-33-M	4,637	6,132
Leite_206	Amazonas	1AS-33-M	4,646	1,143
Leite_206	Amazonas	1AS-33-M	4,702	11,761
Leite_206	Amazonas	1AS-33-M	4,705	1,156
Leite_206	Amazonas	1AS-33-M	4,736	8,944
Leite_206	Amazonas	1AS-33-M	4,739	11,519
Leite_206	Amazonas	1AS-33-M	4,756	9,052
Leite_206	Amazonas	1AS-33-M	5,042	4,054
Leite_206	Amazonas	1AS-33-M	5,086	7,124
Leite_206	Amazonas	1AS-33-M	5,115	4,512
Leite_206	Amazonas	1AS-33-M	5,169	9,710
Leite_206	Amazonas	1AS-33-M	5,218	8,132
Leite_206	Amazonas	1AS-33-M	5,319	7,925
Leite_206	Amazonas	1AS-33-M	5,527	11,483
Leite_206	Amazonas	1AS-33-M	5,593	2,389
Leite_206	Amazonas	1AS-33-M	5,695	3,840
Leite_206	Amazonas	1AS-33-M	8,040	1,803

Annex 2.4
(continuation)

Leite_206	Amazonas	1AS-33-M	9,6	0,871
Leite_206	Amazonas	1AS-33-M	9,81	1,135
Leite_206	Amazonas	1AS-33-M	10,40	1,029
Leite_206	Amazonas	1AS-33-M	10,59	6,272
Leite_206	Amazonas	1AS-33-M	11,15	2,360
Leite_206	Amazonas	1AS-33-M	11,37	2,748
Leite_206	Amazonas	1AS-33-M	12,04	3,032
Leite_206	Amazonas	1AS-33-M	12,44	1,782
Leite_206	Amazonas	1AS-33-M	13,97	6,979

Panama Sections (Jaramillo et al 2014)

Source	Basin	section	Age	sqs=0.6
Jaramillo_2014	Bocas	Bocas	1,81	13,732
Jaramillo_2014	Bocas	Bocas	1,82	12,407
Jaramillo_2014	Bocas	Bocas	2	3,836
Jaramillo_2014	Bocas	Bocas	2,051	4,846
Jaramillo_2014	Bocas	Bocas	2,052	12,690
Jaramillo_2014	Bocas	Bocas	2,053	9,682
Jaramillo_2014	Bocas	Bocas	2,054	6,769
Jaramillo_2014	Bocas	Bocas	2,055	11,110
Jaramillo_2014	Bocas	Bocas	2,4	3,299
Jaramillo_2014	Bocas	Bocas	2,651	9,724
Jaramillo_2014	Bocas	Bocas	2,652	2,264
Jaramillo_2014	Bocas	Bocas	2,653	1,894
Jaramillo_2014	Bocas	Bocas	2,752	2,102
Jaramillo_2014	Bocas	Bocas	2,754	4,429
Jaramillo_2014	Bocas	Bocas	3,45	4,907
Jaramillo_2014	Bocas	Bocas	3,551	5,228
Jaramillo_2014	Bocas	Bocas	3,55	4,855
Jaramillo_2014	Bocas	Bocas	3,55	15,086
Jaramillo_2014	Bocas	Bocas	3,55	12,055
Jaramillo_2014	Bocas	Bocas	3,55	1,137
Jaramillo_2014	Bocas	Bocas	3,55	6,687
Jaramillo_2014	Bocas	Bocas	3,552	5,967
Jaramillo_2014	Bocas	Bocas	3,552	16,268
Jaramillo_2014	Bocas	Bocas	3,552	6,797
Jaramillo_2014	Bocas	Bocas	3,552	9,163
Jaramillo_2014	Bocas	Bocas	3,553	10,345
Jaramillo_2014	Bocas	Bocas	3,553	3,046
Jaramillo_2014	Bocas	Bocas	3,553	1,912
Jaramillo_2014	Bocas	Bocas	3,553	9,844
Jaramillo_2014	Bocas	Bocas	3,553	7,051

Annex 2.4
(continuation)

Jaramillo_2014	Bocas	Bocas	3,553	4,066
Jaramillo_2014	Bocas	Bocas	3,554	5,574
Jaramillo_2014	Bocas	Bocas	3,554	5,674
Jaramillo_2014	Bocas	Bocas	3,554	8,702
Jaramillo_2014	Bocas	Bocas	4	8,971
Jaramillo_2014	Bocas	Bocas	4,250	6,804
Jaramillo_2014	Bocas	Bocas	4,251	11,747
Jaramillo_2014	Bocas	Bocas	4,252	7,934
Jaramillo_2014	Bocas	Bocas	4,252	11,846
Jaramillo_2014	Bocas	Bocas	4,252	9,563
Jaramillo_2014	Bocas	Bocas	4,252	5,638
Jaramillo_2014	Bocas	Bocas	4,252	8,914
Jaramillo_2014	Bocas	Bocas	4,252	1,114
Jaramillo_2014	Bocas	Bocas	4,252	11,755
Jaramillo_2014	Bocas	Bocas	4,253	4,675
Jaramillo_2014	Bocas	Bocas	4,253	2,849
Jaramillo_2014	Bocas	Bocas	4,253	3,909
Jaramillo_2014	Bocas	Bocas	4,253	8,455
Jaramillo_2014	Bocas	Bocas	4,253	9,606
Jaramillo_2014	Bocas	Bocas	4,62	12,217
Jaramillo_2014	Bocas	Bocas	4,63	8,282
Jaramillo_2014	Bocas	Bocas	5,65	5,557
Jaramillo_2014	Bocas	Bocas	6,4	6,779
Jaramillo_2014	Darien	Darien	6,951	5,013
Jaramillo_2014	Darien	Darien	6,951	5,633
Jaramillo_2014	Darien	Darien	6,952	5,139
Jaramillo_2014	Darien	Darien	6,952	2,035
Jaramillo_2014	Darien	Darien	6,952	3,823
Jaramillo_2014	Darien	Darien	6,952	6,830
Jaramillo_2014	Darien	Darien	6,952	1,624
Jaramillo_2014	Darien	Darien	6,953	7,082
Jaramillo_2014	Darien	Darien	6,953	7,109
Jaramillo_2014	Darien	Darien	6,953	7,361
Jaramillo_2014	Darien	Darien	6,953	4,275
Jaramillo_2014	Darien	Darien	7,05	4,777
Jaramillo_2014	Panama_Central	Panama_Central	6,01	6,586
Jaramillo_2014	Panama_Central	Panama_Central	6,02	6,057
Jaramillo_2014	Panama_Central	Panama_Central	8,3	5,227
Jaramillo_2014	Panama_Central	Panama_Central	8,726	4,054
Jaramillo_2014	Panama_Central	Panama_Central	8,753	6,303
Jaramillo_2014	Panama_Central	Panama_Central	8,754	7,662
Jaramillo_2014	Panama_Central	Panama_Central	8,754	6,105
Jaramillo_2014	Panama_Central	Panama_Central	8,770	9,159

Annex 2.4
(continuation)

Jaramillo_2014	Panama_Central	Panama_Central	8,773	6,760
Jaramillo_2014	Panama_Central	Panama_Central	9,412	2,368
Jaramillo_2014	Panama_Central	Panama_Central	9,424	2,997
Jaramillo_2014	Panama_Central	Panama_Central	9,464	4,829
Jaramillo_2014	Panama_Central	Panama_Central	9,737	9,452
Jaramillo_2014	Panama_Central	Panama_Central	10,143	5,150
Jaramillo_2014	Panama_Central	Panama_Central	10,874	4,830
Jaramillo_2014	Panama_Central	Panama_Central	10,881	3,348
Jaramillo_2014	Panama_Central	Panama_Central	10,883	5,518
Jaramillo_2014	Panama_Central	Panama_Central	11,553	13,890
Jaramillo_2014	Panama_Central	Panama_Central	11,674	7,752
Jaramillo_2014	Panama_Central	Panama_Central	18,915	2,740
Jaramillo_2014	Panama_Central	Panama_Central	18,928	2,844
Jaramillo_2014	Panama_Central	Panama_Central	18,931	5,174
Jaramillo_2014	Panama_Central	Panama_Central	18,935	4,428
Jaramillo_2014	Panama_Central	Panama_Central	18,948	12,080
Jaramillo_2014	Panama_Central	Panama_Central	18,953	4,484
Jaramillo_2014	Panama_Central	Panama_Central	18,954	12,493
Jaramillo_2014	Panama_Central	Panama_Central	18,961	8,160
Jaramillo_2014	Panama_Central	Panama_Central	18,962	6,069
Jaramillo_2014	Panama_Central	Panama_Central	18,962	3,483
Jaramillo_2014	Panama_Central	Panama_Central	18,962	5,272
Jaramillo_2014	Panama_Central	Panama_Central	18,974	1,879
Jaramillo_2014	Panama_Central	Panama_Central	18,981	1,132
Jaramillo_2014	Panama_Central	Panama_Central	19,086	2,016
Jaramillo_2014	Panama_Central	Panama_Central	19,173	2,242
Jaramillo_2014	Panama_Central	Panama_Central	19,175	3,158
Jaramillo_2014	Panama_Central	Panama_Central	19,201	5,684
Jaramillo_2014	Panama_Central	Panama_Central	19,215	5,429
Jaramillo_2014	Panama_Central	Panama_Central	19,241	5,057
Jaramillo_2014	Panama_Central	Panama_Central	19,254	5,013
Jaramillo_2014	Panama_Central	Panama_Central	19,264	1,718
Jaramillo_2014	Panama_Central	Panama_Central	19,268	5,499
Jaramillo_2014	Panama_Central	Panama_Central	19,269	2,375
Jaramillo_2014	Panama_Central	Panama_Central	19,278	4,640
Jaramillo_2014	Panama_Central	Panama_Central	19,281	5,052
Jaramillo_2014	Panama_Central	Panama_Central	19,290	4,600
Jaramillo_2014	Panama_Central	Panama_Central	19,308	3,937
Jaramillo_2014	Panama_Central	Panama_Central	19,311	4,395
Jaramillo_2014	Panama_Central	Panama_Central	19,321	4,610
Jaramillo_2014	Panama_Central	Panama_Central	19,327	4,201
Jaramillo_2014	Panama_Central	Panama_Central	19,334	8,280
Jaramillo_2014	Panama_Central	Panama_Central	19,347	4,287

Annex 2.4
(continuation)

Jaramillo_2014	Panama_Central	Panama_Central	19,374	3,523
Jaramillo_2014	Panama_Central	Panama_Central	19,381	3,906
Jaramillo_2014	Panama_Central	Panama_Central	19,398	5,831
Jaramillo_2014	Panama_Central	Panama_Central	19,407	5,654
Jaramillo_2014	Panama_Central	Panama_Central	19,409	4,445
Jaramillo_2014	Panama_Central	Panama_Central	19,416	4,571
Jaramillo_2014	Panama_Central	Panama_Central	19,425	5,087
Jaramillo_2014	Panama_Central	Panama_Central	19,433	5,080
Jaramillo_2014	Panama_Central	Panama_Central	19,434	6,284
Jaramillo_2014	Panama_Central	Panama_Central	19,444	4,879
Jaramillo_2014	Panama_Central	Panama_Central	19,454	4,203
Jaramillo_2014	Panama_Central	Panama_Central	19,462	3,701
Jaramillo_2014	Panama_Central	Panama_Central	19,463	3,327
Jaramillo_2014	Panama_Central	Panama_Central	19,470	5,199
Jaramillo_2014	Panama_Central	Panama_Central	19,478	4,185
Jaramillo_2014	Panama_Central	Panama_Central	19,479	3,119
Jaramillo_2014	Panama_Central	Panama_Central	19,480	1,005
Jaramillo_2014	Panama_Central	Panama_Central	19,480	0,950
Jaramillo_2014	Panama_Central	Panama_Central	19,481	1,003
Jaramillo_2014	Panama_Central	Panama_Central	19,485	3,619
Jaramillo_2014	Panama_Central	Panama_Central	19,493	4,344
Jaramillo_2014	Panama_Central	Panama_Central	19,525	1,220
Jaramillo_2014	Panama_Central	Panama_Central	19,527	0,981
Jaramillo_2014	Panama_Central	Panama_Central	19,528	0,980

1AS-19-AM (Silva et al 2010)

Source	Basin	section	Age	sqs=0.6
Silva_2010	Amazonas	1AS-19-AM	3,7	1,08
Silva_2010	Amazonas	1AS-19-AM	4,498	1,90
Silva_2010	Amazonas	1AS-19-AM	4,56	10,39
Silva_2010	Amazonas	1AS-19-AM	4,729	5,16
Silva_2010	Amazonas	1AS-19-AM	5,032	5,02
Silva_2010	Amazonas	1AS-19-AM	5,361	1,16
Silva_2010	Amazonas	1AS-19-AM	5,44	2,64
Silva_2010	Amazonas	1AS-19-AM	5,6	1,04
Silva_2010	Amazonas	1AS-27-AM	3,7	5,94
Silva_2010	Amazonas	1AS-27-AM	3,802	7,33
Silva_2010	Amazonas	1AS-27-AM	3,833	1,76
Silva_2010	Amazonas	1AS-27-AM	3,855	5,98
Silva_2010	Amazonas	1AS-27-AM	3,859	5,31
Silva_2010	Amazonas	1AS-27-AM	3,878	6,35
Silva_2010	Amazonas	1AS-27-AM	3,908	7,10
Silva_2010	Amazonas	1AS-27-AM	3,912	2,38

Annex 2.4
(continuation)

Silva_2010	Amazonas	1AS-27-AM	3,928	7,08
Silva_2010	Amazonas	1AS-27-AM	3,931	3,03
Silva_2010	Amazonas	1AS-27-AM	3,944	0,99
Silva_2010	Amazonas	1AS-27-AM	4,087	3,00
Silva_2010	Amazonas	1AS-27-AM	4,090	5,04
Silva_2010	Amazonas	1AS-27-AM	4,118	3,04
Silva_2010	Amazonas	1AS-27-AM	4,133	4,00
Silva_2010	Amazonas	1AS-27-AM	4,174	4,18
Silva_2010	Amazonas	1AS-27-AM	4,186	6,75
Silva_2010	Amazonas	1AS-27-AM	4,296	6,19
Silva_2010	Amazonas	1AS-27-AM	4,298	7,10
Silva_2010	Amazonas	1AS-27-AM	4,331	2,54
Silva_2010	Amazonas	1AS-27-AM	4,371	5,91
Silva_2010	Amazonas	1AS-27-AM	4,427	9,15
Silva_2010	Amazonas	1AS-27-AM	4,591	8,63
Silva_2010	Amazonas	1AS-27-AM	4,719	4,51
Silva_2010	Amazonas	1AS-27-AM	4,745	2,36
Silva_2010	Amazonas	1AS-27-AM	4,810	8,09
Silva_2010	Amazonas	1AS-27-AM	4,976	1,90
Silva_2010	Amazonas	1AS-27-AM	5,060	5,42
Silva_2010	Amazonas	1AS-27-AM	5,083	3,73
Silva_2010	Amazonas	1AS-27-AM	5,175	7,46
Silva_2010	Amazonas	1AS-27-AM	5,181	5,01
Silva_2010	Amazonas	1AS-27-AM	5,455	3,45
Silva_2010	Amazonas	1AS-27-AM	5,6	2,04

Mariname (Salamanca et al 2016)

Source	Basin	section	Age	sqs=0.6
Salamanca_2016	Amazonas	Mariname	16,1	16,78
Salamanca_2016	Amazonas	Mariname	16,107	15,07
Salamanca_2016	Amazonas	Mariname	16,114	12,04
Salamanca_2016	Amazonas	Mariname	16,121	13,40
Salamanca_2016	Amazonas	Mariname	16,128	17,63
Salamanca_2016	Amazonas	Mariname	16,131	15,41
Salamanca_2016	Amazonas	Mariname	16,135	10,18
Salamanca_2016	Amazonas	Mariname	16,550	10,78
Salamanca_2016	Amazonas	Mariname	16,557	9,54
Salamanca_2016	Amazonas	Mariname	16,564	8,34
Salamanca_2016	Amazonas	Mariname	16,570	16,21
Salamanca_2016	Amazonas	Mariname	17,363	10,96
Salamanca_2016	Amazonas	Mariname	17,377	9,94
Salamanca_2016	Amazonas	Mariname	17,390	6,47
Salamanca_2016	Amazonas	Mariname	17,404	7,73

Annex 2.4
(continuation)

Salamanca_2016	Amazonas	Mariname	17,425	8,54
Salamanca_2016	Amazonas	Mariname	17,439	8,78
Salamanca_2016	Amazonas	Mariname	17,456	5,58
Salamanca_2016	Amazonas	Mariname	17,473	5,12
Salamanca_2016	Amazonas	Mariname	17,487	7,30
Salamanca_2016	Amazonas	Mariname	17,501	6,18
Salamanca_2016	Amazonas	Mariname	17,508	6,99
Salamanca_2016	Amazonas	Mariname	17,518	6,91
Salamanca_2016	Amazonas	Mariname	17,529	6,59
Salamanca_2016	Amazonas	Mariname	17,546	8,46
Salamanca_2016	Amazonas	Mariname	17,553	7,07
Salamanca_2016	Amazonas	Mariname	17,563	7,42
Salamanca_2016	Amazonas	Mariname	17,570	6,35
Salamanca_2016	Amazonas	Mariname	17,581	4,84
Salamanca_2016	Amazonas	Mariname	17,584	4,59
Salamanca_2016	Amazonas	Mariname	17,588	5,69
Salamanca_2016	Amazonas	Mariname	17,591	7,02
Salamanca_2016	Amazonas	Mariname	17,594	9,28
Salamanca_2016	Amazonas	Mariname	17,598	7,77
Salamanca_2016	Amazonas	Mariname	17,608	8,68
Salamanca_2016	Amazonas	Mariname	17,612	8,86
Salamanca_2016	Amazonas	Mariname	17,626	12,22
Salamanca_2016	Amazonas	Mariname	17,636	13,33
Salamanca_2016	Amazonas	Mariname	17,672	15,92
Salamanca_2016	Amazonas	Mariname	17,676	15,86
Salamanca_2016	Amazonas	Mariname	17,679	13,85
Salamanca_2016	Amazonas	Mariname	17,683	22,96
Salamanca_2016	Amazonas	Mariname	17,686	13,80
Salamanca_2016	Amazonas	Mariname	17,690	13,89
Salamanca_2016	Amazonas	Mariname	17,693	17,34
Salamanca_2016	Amazonas	Mariname	17,697	14,85
Salamanca_2016	Amazonas	Mariname	17,7	16,78

Annex 2.5: Codes of the sections used in the choroplet maps and geographic locations assigned according to the map in Figure 2.48.

Section	Code	Geographic Area
Aga-1	1	C
Ara-2	2	D
Ara-3	3	D
Ara-4	4	D
Av-1	5	H
Buc-1	6	H
Bue-3Carb	7	F
Bue-3Cor	8	F
Bue-H15	9	F
Came-1	10	I
Camo-1	11	H
Caño Las Blancas	12	H
Caño Sagu	13	H
Canoe-1	14	H
Casc-1	15	D
Cas-1	16	C
Cerrejon	17	A
Cer-3	18	B
Chac-1	19	H
Chig-1	20	D
Cosw-1	21	G
ConcentracionPazRio	23	D
Con16	24	C
Con-1	25	E
Cop-1	26	F
Cor-1	27	H
CPE2-1	28	E
Cris-1	29	H
Cse-08	30	G
Cus-5	31	F
Cusu-1	32	H
Cusu-2	33	H
Eval-1	34	H
Flo-C3	35	F
Fon-1	36	H
Fue182	37	H
Gib	38	D
Gon-1	40	B

Annex 2.5 (continuation)

Section	Code	Geographic Area
GonOut	42	B
Gua-1	43	F
Gua-1	44	F
Gua-2	45	F
Had-1	46	I
Hig-1	47	J
Jor-1	48	D
Jub-1	49	D
Kan-1	50	I
LaHe-1	51	D
LaMar-1	52	F
Bru-1	53	I
Las-1	54	F
Lis-1	55	C
LiNo1	56	C
Li158-2	57	C
Li4	58	C
Luro-1	59	H
Mag-1	60	D
Ma-1	61	G
Medina	62	F
Moc-1	63	E
Mon-1A	65	C
Muc-3	66	B
Mues-1	67	D
Nac-1	68	E
Nines-1	69	H
Nis-E1	70	F
Nuesp-1	71	H
Nuevo Mundo	72	C
Pac-1	74	H
Pal-1	75	F
Past-1	76	H
Past-4	77	H
Pau-C2FZ	78	F
Pij-1	79	J
Pum-1	80	J
Regadera	81	D

Annex 2.5 (continuation)

Section	Code	Geographic Area
Reg-1	82	C
Ret-1	83	I
Ret-1ST1	84	I
RieMacheRull	85	A
RioCh-1	86	F
Rio de Oro-14	87	B
Rio Loro	88	B
ZuW2	89	B
Zul-1	90	B
Ros1	91	B
Rub-2	92	G
Rub-79	93	G
S-10	94	I
S-14	95	I
S-17	96	I
S-5	97	I
S-7	98	I
SanFel-1	99	F
SanJRS	100	C
SanJ-1	101	H
SanMar-1	102	D
Tam-2	103	D
Tar-1	104	I
Tib-182/187	105	B
Toc-1	106	D
Tras-1	107	I
Uribe	108	C
Val-1	111	I
Ven-2	112	I
Ven-3	113	I
Zul-1	115	B

Annex 2.6: Information about the sections that compose each time interval. The name of the sections is presented in Annex 2.5. Diversity was estimated using a composite sample (sqs_06) and as the mean of the SQS diversity estimated for each individual sample. #N/A indicates that all the samples for that specific section show counts lower than 50 palynomorphs.

Bin 5 -10 Ma

code_section	Diversity sqs_06	Diversity mean_samples	# Samples
1	2,25		#N/A
25	5,34		1
61	16,56	9,78	4
62	3,67		1
63	9,50		2
65	6,54	5,18	4
68	8,13	6,84	4

Bin 10 -15 Ma

code_section	Diversity sqs_06	Diversity mean_samples	# Samples
1	1,55		#N/A
2	4,33		2
3	9,97		#N/A
7	5,09	4,66	6
25	5,71		2
27	2,35		#N/A
28	8,71		1
30	2,13		1
37	10,51		2
38	6,98	7,16	4
43	6,03	5,43	16
46	7,55	6,60	6
47	6,92		3
52	9,96		#N/A
61	7,66	5,48	6
62	7,51	6,67	19
63	3,64	3,15	6
65	7,12	7,55	6
67	4,49		1
68	7,79	5,89	8
75	3,78	3,89	8

Annex 2.6
(continuation)

79	6,66		3
83	5,68	5,79	8
84	2,35	3,40	7
86	5,17		2
94	6,39		#N/A
95	7,49	7,80	9
97	3,94		2
101	4,74		#N/A
102	3,63	3,50	15
103	3,51	3,31	7
104	7,58		#N/A
106	6,55	5,78	25
107	2,43	2,50	4
113	4,25		1

Bin 15 -20 Ma

code_section	Diversity		# Samples
	sqs_06	mean_samples	
1	6,56		#N/A
2	5,015	4,46	36
3	9,569		#N/A
5	2,196	2,33	18
7	5,796	5,20	38
10	4,491	3,89	14
14	1,942	1,68	11
21	7,282		1
25	5,762		7
27	3,653	3,37	12
28	9,31		5
30	3,835		3
37	3,627	3,44	23
38	6,493	5,46	54
43	5,015	4,54	40
46	6,202	5,30	11
47	8,142		7
50	2,211		1
52	11,3		#N/A
53	7,504		2
61	10,59	6,75	11
62	6,972	5,09	70

Annex 2.6
(continuation)

63	6,653	6,70	11
65	3,701	3,61	17
67	4,806	3,85	16
68	11,63		6
75	4,791	4,48	15
77	1,939		8
78	3,14		3
79	5,495		3
82	0,87		#N/A
83	6,787	5,76	28
84	5,22	4,49	14
86	6,452	6,01	28
89	4,94	4,24	15
92	8,539		7
93	5,254		8
94	5,496		2
95	6,606	6,42	13
97	4,691	4,91	10
98	7,897	6,44	14
101	4,013		9
102	3,911		2
103	3,777	3,59	12
104	6,105		8
106	7,502	6,73	38
107	4,951	4,96	22
113	3,135		4

Bin 20-25

code_section	Diversity sqs_06	Diversity mean_samples	# Samples
1	9,03		#N/A
2	5,933	4,97	8
3	6,41		1
4	6,557	5,21	22
5	3,889	4,33	19
6	8,721		1
7	6,917	6,46	18
10	3,77		4
14	3,04	2,36	7
15	5,916		4
20	7,071		#N/A

Annex 2.6
(continuation)

21	7,337		2
25	7,701		1
27	4,274	3,70	7
29	5,883		2
30	9,707	8,43	5
37	6,639	5,77	18
38	2,54	2,53	24
43	4,744	4,13	11
45	11,37		2
46	3,957		4
48	5,92		3
49	2,256		#N/A
50	9,03		3
51	6,171		1
52	9,99		#N/A
53	7,686		#N/A
54	6,056		#N/A
59	3,27		1
61	9,297		4
62	7,505	6,27	47
66	2,424		3
67	4,824	4,60	7
70	16,31	14,60	5
71	3,838	2,81	8
75	7,828	9,33	11
76	6,381	6,25	6
77	3,362	2,85	9
78	2,452	2,36	5
82	5,877		#N/A
83	9,395	4,98	20
84	5,97	5,30	37
86	4,63	4,01	31
89	8,23	5,60	5
92	6,65	4,43	5
93	7,444		2
94	8,572	4,26	8
95	5,304	5,06	7
96	2,447		3
97	4,587	4,95	8
98	4,03	3,96	15

Annex 2.6
(continuation)

100	8,235	6,60	6
101	5,223	4,04	16
102	4,004	4,08	5
103	4,219	3,75	6
104	5,749	3,31	8
105	8,534	8,14	11
106	4,902	4,57	11
107	4,081	3,49	38
111	3,322	2,99	8
113	2,375	2,41	6

Bin 25 - 30 Ma

code_section	Diversity		# Samples
	sqs_06	mean_samples	
1	8,69		#N/A
2	6,12	5,45	5
5	2,22	2,36	21
6	7,67		1
7	8,49	7,89	9
14	4,11	2,63	9
15	6,38	6,07	8
20	13,99		#N/A
21	8,95		1
23	5,009		3
27	4,23	3,72	14
29	7,821		3
30	8,409		4
34	3,30	2,70	9
37	3,72	3,94	9
38	4,40	3,93	33
43	5,26	4,44	13
45	4,15	3,82	20
46	9,28		1
48	8,34		2
49	3,38		2
50	2,50		4
51	5,78		#N/A
52	15,19		#N/A
53	5,164		#N/A
54	6,183		1

Annex 2.6
(continuation)

59	5,107	4,61	6
60	3,321		#N/A
61	7,926	6,32	8
62	6,87	4,83	32
66	2,441		3
67	6,361	5,39	10
70	5,836	5,70	44
71	4,245	3,38	23
75	5,258	4,86	21
76	3,983	3,58	7
77	2,953	2,56	8
78	3,03		1
82	3,721		1
86	5,316	4,32	22
89	8,205	7,86	9
92	6,176		#N/A
95	4,939		2
96	3,848	3,80	11
97	5,91	5,64	5
100	6,826		#N/A
101	6,12	5,47	8
102	7,622		2
103	3,465	3,50	6
104	5,198	7,66	5
105	2,352	3,43	21
106	4,239	4,06	11
107	5,612		4
111	4,774		4
112	7,394		4
113	3,538	2,51	5

Bin 30 - 35 Ma

code_section	Diversity		# Samples
	sqs_06	mean_samples	
1	8,9		#N/A
5	3,576	3,21	6
7	5,468		2
11	4,459	4,12	11
13	4,277	3,54	19
14	2,344	2,48	10

Annex 2.6
(continuation)

15	4,946	4,99	6
19	2,145		2
23	4,743	6,29	7
27	5,759	5,27	11
29	5,82	3,96	17
32	6,386	5,19	5
33	7,612	7,19	7
34	2,969	3,00	6
35	3,86		2
36	3,974	4,48	5
37	4,575	3,99	14
38	3,122	3,11	51
43	5,645	4,64	17
45	4,557	3,13	20
46	11,05	6,33	5
52	26,3		#N/A
53	3,535	2,94	5
58	4,109		#N/A
59	7,532	3,61	11
60	2,136	2,08	20
62	17,91	7,12	16
66	2,976		3
67	5,211		3
69	4,761	6,05	12
70	7,142	6,47	45
71	3,848	3,72	34
74	42,2		#N/A
75	6,355	5,70	43
76	4,488	4,10	5
77	3,925	3,33	13
78	2,946		3
82	3,26		1
86	3,313		2
89	3,965	3,92	15
91	2,208	2,18	7
95	4,594	4,14	5
96	3,58	3,78	8
97	5,385	5,15	7
98	4,353		3
99	6,274	6,24	5

Annex 2.6
(continuation)

101	5,77	4,69	16
103	7,837		2
104	2,389	2,36	7
105	6,406	7,81	19
106	5,966	5,04	12
111	5,802	4,76	18
112	6,054	5,56	5
113	3,423	2,96	57

Bin 35 - 40 Ma

code_section	Diversity sqs_06	mean_samples	# Samples
1	12,6		#N/A
12	9	7,86	16
13	4,8	3,89	23
19	10,3	6,29	7
23	15,13	7,17	6
24	2,04	1,98	11
27	8,97		3
29	12,18		4
32	12,51		2
33	20,47		2
34	14,06	9,12	5
35	2,92		#N/A
36	6,66	6,46	5
37	14,61		3
38	4,58	4,65	9
43	12,61		2
45	10,13		3
58	4,64		1
60	3,6		2
62	19,62	11,48	10
66	1,45	1,56	9
70	8,45		3
71	9,67	9,21	10
72	3,46	3,42	22
74	12,36	9,78	8
75	5,17	6,87	19
76	10,91		3
77	13,41	10,6	18

Annex 2.6
(continuation)

82	1,79	1,39	6
86	29,96	21,14	14
88	12		1
89	9,47		#N/A
91	2,65		2
96	10,18	9,67	6
97	5,68		2
101	13,21	10,87	9
105	5,93	5,84	13
108	3,98		2

Bin 40 - 45 Ma

code_section	Diversity		# Samples
	sqs_06	mean_samples	
1	14,4		#N/A
8	24,73	19,7	27
12	7,144	5,76	5
13	9,858	9,37	4
19	5,782		#N/A
24	1,812	1,68	10
27	6,925		1
31	19,5		2
35	1,718		#N/A
36	2,351		2
38	9,514		3
40	14,89		#N/A
45	10,43		#N/A
58	2,322	2,13	10
62	15,18	15,28	9
66	1,628	1,9	6
71	10,34	9,06	5
72	1,971	2,43	8
77	11,15	7,17	5
78	7,942		1
81	9,895		3
82	1,666	1,51	5
86	25,45	18,43	9
91	1,866		2
96	7,737		1
105	5,502	5,33	10

Annex 2.6
(continuation)

108	5,913		2

Bin 45 - 50 Ma

code_section	Diversity		# Samples
	sqs_06	mean_samples	
3	2,68		#N/A
8	9,816		2
26	5,875		#N/A
27	9,479		3
31	15,19		2
38	0,936		#N/A
40	23,16		1
44	9,496		#N/A
58	2,345	1,95	11
62	1,504		1
66	1,825	1,72	6
72	3,624		1
81	51,11		1
82	1,605	1,46	9
86	1,18		#N/A
91	2,365		2
105	5,472	6,03	8
108	2,224		2
115	5,903		#N/A

Bin 50 - 55 Ma

code_section	Diversity		# Samples
	sqs_06	mean_samples	
3	1,34		#N/A
8	12,84	8	8
26	1,764		1
31	8,903		1
35	2,031		#N/A
38	1		#N/A
42	24,91	13,8	6
62	9,718		#N/A
66	0,922		1
81	22,76	16,3	12
82	1,733	1,69	6

Annex 2.6
(continuation)

86	4,973	7,07	1
91	2,082		1
105	6,951		13
108	14,9	5,59	9
115	3,865		3

Bin 55 - 60 Ma

code_section	Diversity		# Samples
	sqs_06	mean_samples	
2	13,36	7,1	14
3	4,16		#N/A
4	16,85	9,13	11
8	4,534	3,35	15
9	0,874	1,83	20
13	1,064	1,18	10
26	9,371	3,32	14
35	4,711	2,36	5
38	1,154		3
40	1,094	1,34	6
42	3,892		2
45	13,71	10,58	29
55	4,053		3
56	3,591	3,28	29
57	4,161		1
58	0,973	1,02	7
62	2,451	2,14	8
66	1,724		4
81	2,466	2,05	17
87	9,717	6,73	26
88	4,188	2,92	22
89	1,646	1,71	9
90	2,064	1,68	8
91	1,011	1,38	28
105	4,052	2,25	27
108	9,794	3,95	15
115	1,077	1,2	13

Annex 2.6
(continuation)

Bin 60 - 65 Ma

code_section	Diversity		#
	sqs_06	mean_samples	Samples
2	1,94		#N/A
4	4,836		#N/A
8	5,234	4,6	11
9	4,936	3	4
16	13,85		#N/A
18	3,957	4,88	11
40	1,117	1,99	6
44	3,409		#N/A
56	1,039	1,18	16
57	2,415		#N/A
58	2,386	1,74	13
62	15,8		2
66	1,991	2,5	11
86	16,04	16,1	7
87	1,836		3
88	7,66	2,72	4
89	5,598		1
90	1,037	1,4	9
105	4,974	4,32	5
108	1,921		2
115	1,028		1

Annex 2.8: ANOVA Table for the choroplet maps.

Bin 5 - 10 Ma

	Df	Sum Sq	Mean Sq	F-value	Pr (> F)
Site	3	59,4	19,8	3,318	0,061
Residuals	14	83,55	5,96		

Bin 10 - 15 Ma

	Df	Sum Sq	Mean Sq	F-value	Pr (> F)
Site	16	333,9	20,87	3,598	1.8 e-05
Residuals	142	823,6	5,8		

Bin 15 - 20 Ma

	Df	Sum Sq	Mean Sq	F-value	Pr (> F)
Site	26	759	29,187	4,422	8.41 e-12
Residuals	583	3848	6,601		

Bin 20 - 25 Ma

	Df	Sum Sq	Mean Sq	F-value	Pr (> F)
Site	37	1594	43,08	6,949	2,00E-16
Residuals	458	2840	6,2		

Bin 25 - 30 Ma

	Df	Sum Sq	Mean Sq	F-value	Pr (> F)
Site	30	708,7	23,625	4,458	1,54E-12
Residuals	388	2056	5,299		

Bin 30 - 35 Ma

	Df	Sum Sq	Mean Sq	F-value	Pr (> F)
Site	42	1333	31,73	5,314	2,00E-16
Residuals	587	3505	5,97		

Bin 35 - 40 Ma

	Df	Sum Sq	Mean Sq	F-value	Pr (> F)
Site	21	4807	228,88	9,61	2,00E-16
Residuals	225	5359	23,82		

Bin 40 - 45 Ma

	Df	Sum Sq	Mean Sq	F-value	Pr (> F)
Site	12	6330	527,5	11,76	1,98E-14
Residuals	100	4485	44,9		

Annex 2.8 (continuation)

Bin 45 - 50 Ma

	Df	Sum Sq	Mean Sq	F-value	Pr (> F)
Site	3	114,48	38,16	21,41	1,31E-07
Residuals	30	53,47	1,78		

Bin 50 - 55 Ma

	Df	Sum Sq	Mean Sq	F-value	Pr (> F)
Site	5	1240	248	9,966	1,52E-06
Residuals	47	1170	24,88		

Bin 55 - 60 Ma

	Df	Sum Sq	Mean Sq	F-value	Pr (> F)
Site	21	2792	132,95	26,6	2,00E-16
Residuals	326	1628	4,99		

Bin 60 - 65 Ma

	Df	Sum Sq	Mean Sq	F-value	Pr (> F)
Site	11	1372,5	124,77	12,89	8,89E-15
Residuals	98	948,4	9,68		

Annexes 2.7 - 2.17: Differences in SQS diversity among sites in different times intervals according to Tukey's test.

Annex 2.7

Interval 60-65 Ma	
section	86
8	x
9	x
17	x
18	x
40	x
56	x
58	x
66	x
88	x
90	x
105	x

Annex 2.9

Interval 55-60 Ma				
section	**8**	**9**	**13**	**62**
2	x	x	x	x
4	x	x	x	x
26	x	x	x	x
38	x	x	x	x
40	x	x	x	x
42	x	x	x	x
55	x	x	x	x
56	x	x	x	x
58	x	x	x	x
66	x	x	x	x
81	x	x	x	x
88	x	x	x	x
89	x	x	x	x
90	x	x	x	x
91	x	x	x	x
105	x	x	x	x
108	x	x	x	x
115	x	x	x	x

Annex 2.10

Annex 2.14

Interval 25-30 Ma		
section	**89**	**7**
5	x	x
14	x	x
27	x	x
34	x	x
38	x	x
45	x	x
71	x	x
77	x	x
86	x	x
96	x	x
105	x	x
113	x	x

Annex 2.15

Interval 20-25 Ma			
section	**70**	**75**	**105**
2	x		
4	x	x	
5	x	x	x
7	x		
14	x	x	x
27	x	x	
30	x	x	
37	x		
38	x	x	x
43	x	x	
62	x		
67	x	x	
71	x	x	x
75	x		
76	x		
77	x	x	x
78	x	x	x
80	x	x	

Interval 50-55 Ma	
section	**81**
8	x
82	x
105	x
108	x

Annex 2.11

Interval 40-45 Ma			
section	**86**	**8**	**62**
12		x	
24	x	x	x
58	x	x	x
62			x
66	x	x	
72	x	x	x
77		x	
82	x	x	x
105	x	x	

Annex 2.12

Interval 35-40 Ma					
section	**86**	**77**	**80**	**62**	**101**
12	x				
13	x	x	x	x	
19	x				
23	x				
24	x	x	x	x	x
34	x				
36	x				
38	x				
62	x				
66	x	x	x	x	x
71	x				
72	x	x	x	x	x
117	x				
74	x				
75	x				
77	x				
80	x				
83	x	x			
84	x	x			
86	x	x	x		
89	x				
92	x				
94	x	x			
95	x				
97	x				
98	x	x	x		
100	x				
101	x	x	x		
102	x	x			
103	x	x			
104	x	x	x		
105	x				
106	x	x			
107	x	x	x		
111	x	x	x		
113	x	x	x		

Annex 2.16

Interval 15-20 Ma	
section	**106**
2	x
5	x
14	x
27	x
37	x
43	x
65	x
67	x

Annex 2.17

Interval 10-15 Ma	
section	**95**
63	x
84	x
103	x
107	x

82	x	x	x	x	x
96	x				
101	x				
105	x				

Annex 2.13					
Interval 30-35					
section	**105**	**70**	**62**	**33**	**75**
5	x				
11	x				
13	x	x	x		
14	x	x	x		
29	x				
34	x				
37	x				
38	x	x	x	x	x
45	x	x	x		
53	x				
59	x				
60	x	x	x	x	x
71	x	x	x		
77	x	x	x		
80	x				
89	x				
91	x	x	x		
104	x	x	x		
113	x	x	x	x	x

Annex 2.18: Benthic foraminifera $\delta^{18}O$ data for 1.0 Ma intervals. *n*= number of samples falling in each bin; *midpoint :* estimated $\delta^{18}O$ mean at each interval; *Change:* difference between current $\delta^{18}O$ midpoint value and preceding one; *SD*: Standard deviation.

Interval (Ma)	n	Midpoint	Change	SD
64.5	13	0.578	NA	0.3674
63.5	13	0.768	0.19	0.3425
62.5	7	0.619	-0.149	0.2569
61.5	17	0.579	-0.04	0.2431
60.5	13	0.568	-0.011	0.2846
59.5	13	0.744	0.176	0.3221
58.5	26	0.925	0.181	0.1922
57.5	33	0.766	-0.159	0.1848
56.5	30	0.574	-0.192	0.1871
55.5	58	0.375	-0.199	0.2321
54.5	61	0.13	-0.245	0.3470
53.5	36	0.183	0.053	0.2766
52.5	31	-0.024	-0.207	0.2620
51.5	12	-0.09	-0.066	0.2484
50.5	12	-0.124	-0.034	0.2628
49.5	12	0.088	0.212	0.3224
48.5	16	0.128	0.04	0.2692
47.5	18	0.322	0.194	0.1491
46.5	19	0.579	0.257	0.1985
45.5	12	0.858	0.279	0.2408
44.5	18	1.048	0.19	0.1625
43.5	58	0.959	-0.089	0.2600
42.5	124	1.081	0.122	0.2185
41.5	202	1.001	-0.08	0.2668
40.5	93	1.211	0.21	0.2245
39.5	38	1.233	0.022	0.2259
38.5	43	1.42	0.187	0.1577
37.5	28	1.58	0.16	0.1588
36.5	43	1.686	0.106	0.2602
35.5	52	1.734	0.048	0.2252
34.5	196	1.723	-0.011	0.2244
33.5	496	2.304	0.581	0.4370
32.5	498	2.271	-0.033	0.3157
31.5	522	2.191	-0.08	0.2888
30.5	530	2.304	0.113	0.2899
29.5	342	2.235	-0.069	0.3020
28.5	340	2.327	0.092	0.3088

Annex 2.18
(continuation)

27.5	321	2.409	0.082	0.2908
26.5	625	2.13	-0.279	0.3478
25.5	606	1.976	-0.154	0.2559
24.5	550	1.843	-0.133	0.2666
23.5	729	2.115	0.272	0.3820
22.5	646	2.15	0.035	0.3516
21.5	436	2.032	-0.118	0.3628
20.5	438	2.108	0.076	0.3072
19.5	485	2.296	0.188	0.2968
18.5	502	2.228	-0.068	0.2528
17.5	272	2.244	0.016	0.2966
16.5	227	1.898	-0.346	0.3393
15.5	137	1.759	-0.139	0.2492
14.5	211	1.793	0.034	0.2631
13.5	379	2.215	0.422	0.2550
12.5	315	2.435	0.22	0.2388
11.5	179	2.539	0.104	0.2421
10.5	88	2.603	0.064	0.2000
9.5	202	2.732	0.129	0.1940
8.5	93	2.845	0.113	0.1997
7.5	118	2.79	-0.055	0.2398
6.5	330	2.85	0.06	0.2172
5.5	838	2.953	0.103	0.2324
4.5	922	3.036	0.083	0.2044
3.5	924	3.13	0.094	0.2280
2.5	1204	3.551	0.421	0.3078
1.5	864	3.775	0.224	0.3236
0.5	933	4.06	0.285	0.4582

Annex 2.19: Summary of the pairwise tests of correlation over the entire Cenozoic. The mean value of the intervals and the rates of change (first difference) were used for the comparisons.

Mean SQS_Diversity	Mean Isotopes			
	Pearson		Spearman	
	cor	p	cor	p
SQS_diversity_t	0.154	0.218	0.08	0.507
SQS_diversity_t1	0.158	0.210	0.08	0.51
SQS_diversity_t2	0.162	0.203	0.09	0.46
SQS_diversity_t3	0.125	0.33	0.02	0.81

Change SQS_Diversity	Change Isotopes			
	Pearson		Spearman	
	cor	p	cor	p
SQS_Diversity_t	0.085	0.50	0.047	0.70
SQS_diversity_t1	0.052	0.68	0.05	0.68
SQS_diversity_t2	0.070	0.58	0.151	0.23
SQS_diversity_t3	0.018	0.89	0.007	0.95

Annex 2.20: Summary of the pairwise comparison for the two intervals in which the Cenozoic was divided (5 to 40 Ma and 51.5 to 66.5 Ma). The mean value of the intervals and the rate of change of the climatic curve (first difference) were used for the comparisons.

Interval 4.5 Ma - 40 Ma									
Mean SQS_Diversity	Mean Isotopes				Change SQS_Diversity	Change Isotopes			
	Pearson		Spearman			Pearson		Spearman	
	cor	p	cor	p		cor	p	cor	p
SQS_diversity_t	0.66	1.1e-05*	0.53	0.001*	**SQS_Diversity_t**	0.003	0.98	0.15	0.36
SQS_diversity_t1	0.52	1.14e-03*	0.42	0.011*	**SQS_diversity_t1**	0.14	0.40	0.18	0.28
SQS_diversity_t2	0.38	2.2e-02*	0.27	0.10	**SQS_diversity_t2**	0.22	0.19	0.25	0.13
SQS_diversity_t3	0.21	2.1e-01	0.03	0.82	**SQS_diversity_t3**	0.031	0.85	0.008	0.95

Interval 51.5 Ma - 66.5 Ma									
Mean SQS_Diversity	Mean Isotopes				Change SQS_Diversity	Change Isotopes			
	Pearson		Spearman			Pearson		Spearman	
	cor	p	cor	p		cor	p	cor	p
SQS_diversity_t	0.58	0.04 *	0.413	0.1826	**SQS_Diversity_t**	0.25	0.44	0.32	0.24
SQS_diversity_t1	0.33	0.31	0.11	0.72	**SQS_diversity_t1**	0.33	0.32	0.40	0.223
SQS_diversity_t2	0.35	0.30	0.41	0.22	**SQS_diversity_t2**	0.13	0.71	0.176	0.627
SQS_diversity_t3	0.26	0.49	0.33	0.38	**SQS_diversity_t3**	0.29	0.43	0.40	0.286

Annex 2.21: Summary of the Generalized least squares (GLS) regression model for the interval between 5 and 40 Ma. The mean value of the intervals and the rate of change of the climatic curve (first difference) were used for the comparisons.

	ARMA (p)	t-value	R^2	p-value	AIC	log-likelihood	Phi1	Phi2	Phi3
Turnover	1	2.89	-0.176	0.006 *	-140	74.06	0.38		
	2	2.88	-0.18	0.0069 *	-138.16	74.08	0.38	-0.027	
	3	2.88	-0.124	0.0068 *	-138.72	75.36	0.41	-0.15	0.31
Diversification	1	-1.63	-0.26	0.11	-128	68.29	0.063		
	2	-1.49	-0.30	0.14	-127.66	68.83	0.099	-0.245	
	3	-1.84	-0.22	0.07	-127.53	69.76	0.15	-0.277	0.31

Annex 2.22: Summary of the Generalized least squares (GLS) regression model for the interval between 51.5 Ma and 64.5 Ma. The mean value of the intervals and the rate of change of the climatic curve (first difference) were used for the comparisons.

Interval 51.5 - 64.5 Ma									
	Mean_Climate values								
	ARMA (p)	t-value	R^2	p-value	AIC	log-likelihood	Phi1	Phi2	Phi3
SQS_diversity	1	-3.5	-0.84	0.0043*	83.91	-37.95	0.0056		
	2	-3.91	-0.85	0.0021*	85.78	-37.89	-0.026	-0.113	
	3	-4.33	-0.87	0.001*	87.69	-37.8	-0.04	-0.14	-0.10

Interval 51.5 - 64.5 Ma									
first-difference Climatic values									
	ARMA (p)	t-value	R^2	p-value	AIC	log-likelihood	Phi1	Phi2	Phi3
Turnover	1	-0.62	0.10	0.55	-1.46	4.73	-0.35		
	2	-1.32	0.10	0.23	-0,81	5.40	-0.8	-0.5	
	3	-1.30	0.10	0.23	1.16	5.41	-0.7	-0.5	0.07
Diversification	1	-1.18	0.14	0.28	2.0	2.98	-0.10		
	2	-7.72	0.24	0.04 *	-0.47	5.23	0.57	-0.96	
	3	-10.17	0.24	0.0004 *	-1.26	6.63	-0.23	-0.47	-0.84

Annexes Chapter-3

Annex 3.1: Sections (outcrops and wells) and correspondent areas used in the analysis of the flooding events.

Code	Area	Lat	Lon
Aga-1	C	5.83	-74.32
Ara-2	D	6.95	-71.84
Ara-3	D	6.98	-71.82
Ara-4	D	6.98	-71.84
Av-1	H	3.68	-73.44
Buc-1	D	5.61	-71.36
Bue-3Carb	F	4.98	-72.74
Bue-3Cor	F	4.98	-72.74
Bue-H15	F	4.95	-72.73
Came-1	I	3.18	-72.90
Camo-1	H	3.64	-73.40
Caño Las Blancas	H	4.0	-73.81
Caño Sagu	H	4.0	-73.78
Canoe-1	H	3.61	-73.51
Casc-1	D	6.10	-71.82
Cas-1	C	6.76	-73.57
Cerrejon	A	11.07	-72.69
Cer-3	B	8.21	-72.74
Chac-1	H	3.60	-73.39
Chig-1	D	6.56	-70.91
Cosw-1	G	4.34	-71.38
Colorada Sarmiento	H	4.84	-73.22
ConcentracionPaz de Rio	D	6.03	-72.76
Con16	C	7.31	-73.46
Con-1	E	5.43	-70.44
Cop-1	F	4.44	-73.28
Cor-1	H	3.77	-73.73
CPE2-1	E	5.55	-70.19
Cris-1	H	3.55	-73.95
Cse-08	G	3.44	-71.45
Cus-5	F	5.11	-72.66
Cusu-1	H	3.81	-73.19
Cusu-2	H	3.84	-73.16
Eval-1	H	3.46	-73.35
Flo-C3	F	5.49	-72.42
Fon-1	H	3.46	-73.60
Fue182	H	3.49	-73.61
Gib	D	7.04	-72.17

Annex 3.1 (continuation)

Code	Area	Lat	Lon
Gi-1	J	2.27	-75.55
Gon-1	B	8.28	-72.58
Gonzales1967	B	8.6	-72.7
GonOut	B	8.28	-72.58
Gua-1	F	4.26	-73.35
Gc1	J	3.09	-75.2752
Gb1	J	2.82	-75.35
Gu-1	F	4.74	-73.13
Gua-2	F	4.70	-73.16
Had-1	I	3.24	-73.04
Hig-1	J	3.10	-75.27
Jor-1	D	6.07	-71.24
Jub-1	D	6.99	-71.53
Kan-1	I	3.71	-72.56
LaHe-1	D	6.25	-71.00
LaMar-1	F	5.07	-72.51
Bru-1	I	3.03	-73.11
Las-1	F	5.38	-71.97
Lis-1	C	7.10	-73.53
LNP	C	7.13	-73.54
L15	C	7.14	-73.54
L4	C	7.13	-73.54
Luro-1	H	3.86	-73.50
Maga-1	D	7.04	-72.20
Ma-1	G	3.72	-71.74
Medina	F	4.50	-73.10
Moc-1	E	5.15	-70.55
MV-1	A	11.29	-72.50
Mon-1A	C	6.83	-74.04
Muc-3	B	8.10	-72.52
Mues-1	D	5.79	-71.9
Nac-1	E	5.29	-70.3
Nines-1	H	3.42	-73.43
Nis-E1	F	5.62	-72.31
Nuesp-1	H	3.88	-73.75
Nuevo Mundo	C	7.22	-73.32
Nd1	J	3.10	-75.21
Os-1	J	0.56	-76.89
Pac-1	H	3.98	-73.51
Pal-1	F	4.43	-73.36
Past-1	H	3.80	-73.14

Annex 3.1 (continuation)

Code	Area	Lat	Lon
Past-4	H	3.74	-73.25
Pau-C2FZ	F	5.44	-72.46
Pij-1	J	3.00	-75.27
Pum-1	J	0.57	-76.88
Regadera	D	7.40	-72.40
Reg-1	C	6.88	-73.55
Ret-1	I	3.12	-72.61
Ret-1ST1	I	3.12	-72.61
RieMacheRull	A	10.92	-72.26
RioCh-1	F	4.93	-72.73
Rio de Oro-14	B	9.10	-72.90
Rio Loro	B	8.40	-71.80
RZ2	B	8.23	-72.46
Zul-1	B	8.20	-72.45
R-1	B	7.86	-72.49
Rub-2	G	3.80	-71.51
Rub-79	G	3.76	-71.40
S-10	I	3.06	-72.86
S-14	I	3.41	-73.06
S-17	I	3.36	-73.93
S-5	I	3.28	-73.24
S-7	I	3.09	-73.23
SanFel-1	F	5.13	-71.85
SanJRS	C	4.86	-74.63
SanJ-1	H	3.38	-73.86
SanMar-1	D	6.01	-71.65
Tam-2	D	6.57	-71.76
Tar-1	I	3.26	-73.12
Tib-182/187	B	8.59	-72.67
Toc-1	D	6.28	-71.80
Tras-1	I	3.35	-72.63
Uribe	C	7.25	-73.37
Urumaco East	A	11.4	-69.54
Urumaco West	A	11.18	-70.25
Val-1	I	3.91	-72.66
Ven-2	I	3.52	-72.97
Ven-3	I	3.55	-72.94
Ym1	J	3.09	-75.27
Y-1	D	6.13	-70.76
Zul-1	B	8.20	-72.45

Annex 3.2: Lithological information from the well log of the well Gb-1 for the Barzalosa Formation.

from	to	Lithology	Interval
12060	12190	Claystone_gray	Interval_3
12190	12200	Shale	Interval_3
12200	12235	Claystone_gray	Interval_3
12235	12260	Shale	Interval_3
12260	12290	Claystone_gray	Interval_3
12290	12300	Shale	Interval_3
12300	12310	Sandstone	Interval_3
12310	12340	Claystone_gray	Interval_3
12340	12352	Shale	Interval_3
12352	12358	Sandstone	Interval_3
12358	12388	Claystone_gray	Interval_3
12388	12396	Shale	Interval_3
12396	12405	Sandstone	Interval_3
12405	12450	Claystone_gray	Interval_3
12450	12462	Shale	Interval_3
12462	12475	Sandstone	Interval_3
12475	12492	Shale	Interval_3
12492	12503	Sandstone	Interval_3
12503	12520	Shale	Interval_3
12520	12535	Claystone_gray	Interval_3
12535	12545	Shale	Interval_3
12545	12562	Claystone_gray	Interval_3
12562	12577	Shale	Interval_3
12577	12580	Sandstone	Interval_3
12580	12620	Claystone_gray	Interval_3
12620	12630	Sandstone	Interval_3
12630	12640	Claystone_gray	Interval_3
12640	12650	Shale	Interval_3
12650	12685	Claystone_gray	Interval_3
12685	12687	Sandstone	Interval_3
12687	12705	Claystone_gray	Interval_3
12705	12718	Sandstone	Interval_3
12718	12750	Claystone_gray	Interval_3
12750	12790	Shale	Interval_2
12790	12800	Sandstone	Interval_2
12800	12861	Shale	Interval_2
12861	12870	Siltstone	Interval_2
12870	12872	Sandstone	Interval_2

Annex 3.2 (continuation)

from	to	Lithology	Interval
12872	12880	Siltstone	Interval_2
12880	12886	Shale	Interval_2
12886	12890	Sandstone	Interval_2
12890	12936	Shale	Interval_2
12936	12943	Sandstone	Interval_2
12943	12952	Shale	Interval_2
12952	12953	Sandstone	Interval_2
12953	13039	Shale	Interval_2
13039	13052	Siltstone	Interval_2
13052	13110	Shale	Interval_2
13110	13112	Sandstone	Interval_2
13112	13150	Shale	Interval_2
13150	13160	Siltstone	Interval_2
13160	13178	Shale	Interval_2
13178	13181	Sandstone	Interval_2
13181	13273	Shale	Interval_2
13273	13285	Sandstone	Interval_2
13285	13307	Shale	Interval_2
13307	13310	Sandstone	Interval_2
13310	13412	Shale	Interval_2
13412	13413	Coal	Interval_2
13413	13460	Shale	Interval_2
13460	13462	Coal	Interval_2
13462	13480	Shale	Interval_2
13480	13500	Claystone_gray	Interval_1
13500	13507	Shale	Interval_1
13507	13510	Claystone_gray	Interval_1
13510	13512	Coal	Interval_1
13512	13515	Claystone_gray	Interval_1
13515	13518	Shale	Interval_1
13518	13527	Claystone_gray	Interval_1
13527	13531	Shale	Interval_1
13531	13532	Coal	Interval_1
13532	13540	Shale	Interval_1
13540	13541	Coal	Interval_1
13541	13545	Shale	Interval_1
13545	13546	Coal	Interval_1
13546	13551	Claystone_gray	Interval_1

Annex 3.2 (continuation)

from	to	Lithology	Interval
13551	13560	Shale	Interval_1
13560	13569	Claystone_gray	Interval_1
13569	13571	Shale	Interval_1
13571	13617	Claystone_gray	Interval_1
13617	13627	Shale	Interval_1
13627	13628	Coal	Interval_1
13628	13640	Shale	Interval_1
13640	13645	Claystone_gray	Interval_1
13645	13650	Shale	Interval_1
13650	13685	Claystone_gray	Interval_1
13685	13686	Coal	Interval_1
13686	13887	Claystone_gray	Interval_1
13887	13897	Sandstone	Interval_1
13897	13947	Claystone_gray	Interval_1
13947	13948	Sandstone	Interval_1
13498	13957	Claystone_gray	Interval_1
13957	13960	Sandstone	Interval_1
13960	14024	Claystone_gray	Interval_1
14024	14025	Sandstone	Interval_1
14025	14070	Claystone_gray	Interval_1
14070	14071	Sandstone	Interval_1
14071	14077	Claystone_gray	Interval_1
14077	14080	Sandstone	Interval_1
14080	14081	Claystone_gray	Interval_1
14081	14082	Sandstone	Interval_1
14082	14091	Claystone_gray	Interval_1
14091	14092	Sandstone	Interval_1
14092	14295	Claystone_gray	Interval_1

Annex 3.3: Summary of Salinity index for sections (wells and outcrops) located in the areas B, D, F, H, I and J for the interval between 35 and 28 Ma (max_si = maximum SI value; min_si = minimum SI value; mean_si = mean SI value calculated for all the samples; sd_si = standard deviation of the SI).

Interval 28 - 35 Ma					
Name	**# samples**	**max_si**	**min_si**	**mean_si**	**sd_si**
Area F					
Nis-E1	53	48.25	0	3.1	7.79
Medina	18	23.13	0	1.48	5.42
Pal-1	35	3.79	0	1.08	1.05
Bue-3Carb	2	0.99	0.93	0.96	0.04
RioCh-1	4	1.99	0	0.74	0.87
Gua-1	17	2.86	0	0.48	0.98
Gua-2	22	1.9	0	0.22	0.52
Flo-C3	1	0	0	0	NA
Pau-C2FZ	3	0	0	0	0
Area H					
Chac-1	2	40.13	35	37.56	3.63
Nines-1	12	51.52	1.72	21.51	19.09
Cusu-2	7	36.97	3.43	18.69	11.86
Fon-1	5	24.79	7.25	16.02	8.13
Eval-1	9	26.67	0.89	9.73	7.85
Luro-1	5	34.95	0	8.83	14.93
Caño Sagu	12	27.52	0	6.7	9.35
Past-4	15	18.8	0	3.86	5.57
Camo-1	9	10.3	0	3.32	3.42
Cor-1	17	7.53	0	2.8	2.58
SanJ-1	15	13.17	0	2.14	3.55
S-17	13	5.42	0	1.48	1.64
Fue182	17	3.07	0	1.13	1.14
Cris-1	12	5.61	0	0.74	1.58
Past-1	5	1.45	0	0.62	0.53
Canoe-1	11	4.67	0	0.61	1.38
Nuesp-1	35	4.61	0	0.61	1.04
Av-1	11	1.43	0	0.37	0.55
Cusu-1	3	0.71	0	0.24	0.41

Annex 3.3 (continuation)

Interval 28 - 35 Ma					
Name	**# samples**	**max_si**	**min_si**	**mean_si**	**sd_si**
Area B					
RZ2	19	75.63	0	7.6	18.62
R-1	7	18.05	0	3.29	6.56
Tib-182/187	24	0.74	0	0.06	0.19
Muc-3	4	0	0	0	0
Area D					
Maga-1	26	83.05	0	33.64	32.67
Gib	59	10.55	0	1.86	1.98
CPZ	4	0.99	0	0.61	0.43
Mues-1	6	1.98	0	0.57	0.78
Casc-1	7	0.58	0	0.08	0.22
Tam-2	1	0	0	0	NA
Toc-1	12	0	0	0	0
Area I					
Os-1	7	67.91	0.47	18.38	24.59
Pum-1	12	16.55	0	3.74	5.01
Tras-1	7	12.98	0	3.67	5.15
Ven-3	55	84.16	0	3.43	12.43
Kan-1	2	5.56	0.91	3.23	3.29
Ven-2	6	8.8	0	3.03	3.29
S-5	5	2.52	0	1.18	0.95
Val-1	14	2.63	0	0.6	0.81
S-14	6	0.51	0	0.39	0.19
Tar-1	9	1.63	0	0.34	0.53
S-7	2	0.65	0	0.32	0.46
Had-1	3	0	0	0	0
Bru-1	4	0	0	0	0